

Hygrothermal performance of different wood-frame wall assemblies wetted by simulated
rain infiltration

Anik Teasdale St-Hilaire

A thesis
in the
Department
of
Building, Civil and Environmental Engineering

Presented in partial fulfillment of the requirements
for the degree of Doctor of Philosophy
at
Concordia University
Montreal, Québec, Canada

January 2006

©Anik Teasdale St-Hilaire, 2006



Library and
Archives Canada

Bibliothèque et
Archives Canada

Published Heritage
Branch

Direction du
Patrimoine de l'édition

395 Wellington Street
Ottawa ON K1A 0N4
Canada

395, rue Wellington
Ottawa ON K1A 0N4
Canada

Your file Votre référence

ISBN: 978-0-494-16282-8

Our file Notre référence

ISBN: 978-0-494-16282-8

NOTICE:

The author has granted a non-exclusive license allowing Library and Archives Canada to reproduce, publish, archive, preserve, conserve, communicate to the public by telecommunication or on the Internet, loan, distribute and sell theses worldwide, for commercial or non-commercial purposes, in microform, paper, electronic and/or any other formats.

The author retains copyright ownership and moral rights in this thesis. Neither the thesis nor substantial extracts from it may be printed or otherwise reproduced without the author's permission.

AVIS:

L'auteur a accordé une licence non exclusive permettant à la Bibliothèque et Archives Canada de reproduire, publier, archiver, sauvegarder, conserver, transmettre au public par télécommunication ou par l'Internet, prêter, distribuer et vendre des thèses partout dans le monde, à des fins commerciales ou autres, sur support microforme, papier, électronique et/ou autres formats.

L'auteur conserve la propriété du droit d'auteur et des droits moraux qui protègent cette thèse. Ni la thèse ni des extraits substantiels de celle-ci ne doivent être imprimés ou autrement reproduits sans son autorisation.

In compliance with the Canadian Privacy Act some supporting forms may have been removed from this thesis.

Conformément à la loi canadienne sur la protection de la vie privée, quelques formulaires secondaires ont été enlevés de cette thèse.

While these forms may be included in the document page count, their removal does not represent any loss of content from the thesis.

Bien que ces formulaires aient inclus dans la pagination, il n'y aura aucun contenu manquant.


Canada

ABSTRACT

Hygrothermal performance of different wood-frame wall assemblies wetted by simulated rain infiltration

Anik Teasdale St-Hilaire
Concordia University, 2006

The infiltration of rainwater can result from envelope defects that allow water to infiltrate into the stud cavity behind the exterior sheathing, i.e. the back wall. Once rainwater migrates into the stud space, it cannot easily evacuate and is thus likely to accumulate, leading to potential degradation of the wood studs and exterior sheathing, depending on the temperature conditions. Therefore, studying the drying potential of wood-frame wall assemblies that have been subjected to a moisture load like rain infiltration can provide valuable information with respect to the assembly's hygrothermal performance.

The primary objectives of the research project were:

- To evaluate the wetting and drying performance of hygroscopic components in wood-frame wall assemblies wetted by rain infiltration;
- To investigate the impact of several parameters on the hygrothermal response of the various monitored components such as the sheathing material, the type of vapor retarder, and the presence of foam insulation on the exterior side of the assembly;
- To develop a framework for large-scale envelope testing of wall assemblies subjected to wind-driven rain infiltration.

The role of the vapor retarder, the exterior insulation, an added exterior insulation, the wall height, the presence of hygroscopic cladding was studied and the effect of varying the moisture load was also investigated. The research was primarily experimental but also included some simulation work. The experimental methodology comprised the determination of:

- Two wetting protocols which simulated wetting of the wall assemblies due to rain infiltration;
- The experimental protocol, including the indoor and outdoor environmental conditions, the assembly construction, the parameters to be varied, and instrumentation for the monitoring of temperature, relative humidity and moisture content for each wall assembly.

The first of the two wetting methodologies consisted of introducing water in a drop-by-drop fashion on the interior surface of the sheathing. The rate, frequency and duration of the water insertion was rationalized based on a statistical analysis of a Montreal weather database, determination of impinging wind-driven rain on a building façade, and estimation of the ratio of water infiltration through an example of an envelope defect. The second protocol involved pre-wetting one of the envelope components, the bottom plate, prior to its installation in the wall assemblies at the test's start.

The drop-by-drop rain infiltration loading resulted, in some cases, in lateral moisture migration and moisture distribution patterns that were not repeated from one wetting event to another. Despite these variations, most moisture accumulation occurred at the bottom of the wall in the bottom plate and in the sheathing, following similar patterns. The greatest and lowest moisture contents were experienced in the plywood and asphalt-coated sheathings, respectively.

The moisture content results from the experiments show that the sheathing material had the most significant impact on the drying response of the wall components, with the lowest and highest drying rate occurring when OSB and fiberboard sheathings were employed, respectively. Increasing the vapor permeability of the vapor retarder within the range allowed by the National Building Code of Canada increased the drying rate of the wetted components within the walls when OSB sheathing was employed. Comparison of the experimental and numerical results highlighted the difficulties in simulating a three-dimensional problem in a two-dimensional domain, the need for accurate and complete material properties, and the need to include of all relevant transport phenomena like air transport in hygrothermal envelope models to increase the accuracy of the simulation results.

ACKNOWLEDGEMENTS

First and foremost, my supervisors, Dr. Dominique Derome, and Dr. Paul Fazio, must be thanked. This thesis would not have been possible without their academic, moral and financial support. Dominique, with her broad knowledge of both architecture and building engineering, pushed me to focus on the details and go deeper into the analysis while keeping sight of the problem at hand. This thesis would likely have been a Master's rather than a Ph.D. thesis if she had not urged me to apply for accelerated admittance into the doctorate program. Dr. Fazio helped me to keep in mind the bigger picture and the needs of the building science and the building envelope community.

Many students have contributed to the work in this thesis. Eric Turcotte helped a great deal with the labor-intensive task of building a test hut and 19 test wall assemblies over the course of a summer. Un gros merci, Eric! Luis Candanedo spent a countless hours during his first semester at Concordia in the lab with me, repeatedly weighing gravimetric samples. Luis, no lo hubiera podido hacer sin ti! Thanks also Nicolas Dauphant, Evelien Pegge, Jacelyn Daigle, Nicolas Godat, Daphné Cachot, and Florian Bouju.

Experimental work is not always easy. The development and execution of the experiments generated many questions and necessitated specialized equipment. I could always count on Jiwu Rao's technical wisdom and experience for the programming of the data acquisition system, amongst other things. The technical support and advice given by Jacques Payer, Joe Hrib, Dorina Banu, and Luc Demers in particular, who spent a lot of time teaching me about electronics and instrumentation – is also very gratefully acknowledged. When it comes to solving computer-related problems, Sylvain Bélanger and François Carrière were indispensable and deserve a sincere thank you! My appreciation also goes to Olga Soares, Nella Fiorentino, Sheila Anderson, Kathy McAleese, Debbie Walker, Linda Swinden, Betty Bondo and Gloria Miller, who were always there to answer my administrative questions.

The years I've spent as a graduate student at Concordia would have been as special to

me had it not been for the terrific group of friends that I've made in and outside of the BCEE Department. There exists within the department, faculty, and university, a richness of cultures from all corners of the globe that have allowed me to better understand and appreciate ethnic diversity. I will not give any names because I could go on for pages and pages. You know who you are.

When life gets tough, family is always there to lend a sympathetic ear. I'd like to thank my siblings, Mary, Carl and Ian for being patient and understanding. Mom and Dad, thank you for encouraging me to pursue graduate studies, and for being there when I needed to talk and bounce ideas around. I know how proud you are of this achievement! To my whole family, thanks for all the laughs we've shared over the years, they definitely make life more enjoyable!

To my future husband, Wayne Haughton, I appreciate your patience and your sense of humor, and the sacrifices you have made in the last three years and will continue to make, as the partner of a professional woman. Thanks for being so considerate of my needs and happiness as well as your own.

TABLE OF CONTENTS

| | |
|--|-------------|
| LIST OF FIGURES | xii |
| LIST OF TABLES | xxvi |
| NOMENCLATURE | xxxi |
| 1. INTRODUCTION | 1 |
| 1.1 Context of the Research Project | 1 |
| 1.2 Problem | 3 |
| 1.3 Objectives and Approach | 4 |
| 2. LITERATURE REVIEW | 7 |
| 2.1 Function of the building envelope and the role of wall components | 7 |
| 2.2 Moisture management in the building envelope | 14 |
| 2.2.1 Rain | 14 |
| 2.2.2 Water vapor transport by diffusion | 16 |
| 2.2.3 Water vapor transport by convection | 17 |
| 2.2.4 Moisture transport by capillarity | 17 |
| 2.2.5 Moisture in hygroscopic materials, the sorption isotherm and mold growth | 18 |
| 2.3 Previous experimental works on the role of exterior sheathing in the hygrothermal performance of wall assemblies | 22 |
| 2.4 Previously established experimental rain simulation and wetting methodologies | 33 |
| 2.4.1 Methods simulating rain impinging onto building surface | 34 |
| 2.4.2 Wetting methods by direct insertion of water into assemblies | 40 |
| 2.5 Previous studies on wind-driven rain, wind-driven rain impinging the building envelope, and wind-driven rain infiltration into the building envelope | 51 |
| 2.5.1 Wind-driven rain | 52 |
| 2.5.2 Wind-driven rain on building façades | 54 |
| 2.5.3 Rain infiltration | 64 |

| | |
|---|------------|
| 2.6 Review of work on representative climate data for building envelope testing | 73 |
| 2.6.1 Construction-independent methods for selection of reference years | 74 |
| 2.6.2 Construction-dependent methods for selection of reference years | 80 |
| 2.6.3 Deterministic and quasi-stochastic loading | 84 |
| 2.6.4 Duration of wetting load application | 85 |
| 2.7 Summary | 87 |
| 3. METHODOLOGY FOR THE DEVELOPMENT OF THE WETTING PROTOCOL | 89 |
| 3.1 Methodology for simulation of wind-driven rain infiltration – tests 1 and 2 | 89 |
| 3.1.1 Methodology to determine the rate of water infiltration | 90 |
| 3.1.2 Duration and frequency of wet and dry days during the experiment | 106 |
| 3.1.3 Location and method of water introduction in test assemblies | 106 |
| 3.2 Methodology for wetting by partial immersion method – test 3 | 107 |
| 3.3 Conclusion | 111 |
| 4. EXPERIMENTAL PROTOCOL | 112 |
| 4.1 Scope and objective of the experimental work | 112 |
| 4.2 Testing facility | 114 |
| 4.3 Description of the test setup | 116 |
| 4.3.1 Description of test hut | 116 |
| 4.3.2 Composition of the assemblies | 118 |
| 4.3.3 Parameters and testing conditions evaluated and experimental hypotheses | 121 |
| 4.4 Monitoring protocol | 126 |
| 4.4.1 Temperature | 126 |
| 4.4.2 Relative humidity | 127 |
| 4.4.3 Moisture content | 131 |
| 4.4.4 Air pressure | 141 |
| 4.4.5 Construction and instrumentation | 142 |
| 4.5 Test climate loading | 142 |
| 4.5.1 Pre-conditioning phase | 143 |

| | |
|---|------------|
| 4.5.2 Wetting phase | 145 |
| 4.5.3 Drying phase | 145 |
| 4.6 Experimental history | 146 |
| 4.6.1 Climatic conditions | 147 |
| 4.6.2 Observations during wetting phase | 151 |
| 4.7 Test 2 | 152 |
| 4.7.1 Composition of the assemblies and testing parameters | 153 |
| 4.7.2 Monitoring protocol | 155 |
| 4.7.3 Wetting methodology and test climate loading | 158 |
| 4.7.4 Experimental history | 158 |
| 4.8 Test 3 | 163 |
| 4.8.1 Composition of the assemblies | 164 |
| 4.8.2 Monitoring protocol | 164 |
| 4.8.3 Testing climate loading | 167 |
| 4.8.4 Experimental history | 168 |
| 4.9 Summary and Conclusion | 171 |
| 5. HYGROTHERMAL PERFORMANCE OF ASSEMBLIES TESTED | 172 |
| 5.1 Assembly Response to Moisture Load - Tests 1 and 2 | 173 |
| 5.1.1 General wetting pattern | 173 |
| 5.1.2 General wetting trends in the sheathings | 175 |
| 5.1.3 General wetting trends in the bottom plate | 180 |
| 5.1.4 Lateral migration of water. | 181 |
| 5.1.5 Rapid increase in moisture content due to the wetting events | 182 |
| 5.1.6 Moisture accumulation from week to week | 184 |
| 5.1.7 Repeatability of wetting pattern during the course of the tests | 186 |
| 5.1.8 Adsorption of water by the insulation | 186 |
| 5.1.9 Water leakage | 187 |
| 5.1.10 Summary of wetting behavior | 189 |
| 5.2 Role of Wall Components on the Drying Behavior - Tests 1 and 2 | 197 |
| 5.2.1 Role of the sheathing on the drying performance | 200 |
| 5.2.2 Role of the vapor retarder on the drying performance | 202 |

| | |
|---|------------|
| 5.2.3 Role of the exterior insulation on the drying performance | 203 |
| 5.2.4 Role of the cladding on the drying performance | 204 |
| 5.2.5 Role of the assembly height on the drying performance | 206 |
| 5.3 Global Wetting and Drying Performance in Tests 1 and 2 | 208 |
| 5.4 Role of Wall Components on the Drying Behavior – Test 3 | 212 |
| 5.4.1 Role of the exterior sheathing | 212 |
| 5.4.2 Role of the vapor retarder | 246 |
| 5.5 Summary and Conclusions | 255 |
| 6. HYGROTHERMAL SIMULATIONS AND PARAMETRIC ANALYSES | 259 |
| 6.1 Overview of Heat, Air and Moisture Modeling | 259 |
| 6.2 Numerical Simulation of Test 3 using WUFI 2D | 261 |
| 6.2.1 Governing heat and moisture transport equations in WUFI-2D | 262 |
| 6.2.2 Description of the assemblies | 264 |
| 6.2.3 Output data | 265 |
| 6.2.4 Climate loading, surface transfer and initial conditions | 266 |
| 6.2.5. Simulation results | 272 |
| 6.3 Comparison of simulation results and results from test 3 | 278 |
| 6.4 Parametric Analyses and Effect of Duration of Exposure | 282 |
| 6.4.1 Description of test set-up | 283 |
| 6.4.2 Description of the assemblies | 283 |
| 6.4.3 Wetting method and schedule | 283 |
| 6.4.4 Climate loading, surface transfer and initial conditions | 284 |
| 6.4.5 Role of exterior insulation on the hygrothermal performance | 286 |
| 6.4.6 Effect of stud cavity height on the hygrothermal performance | 291 |
| 6.4.7 Impact of wind-driven rain infiltration loading on hygrothermal performance | 292 |
| 6.4.8 Effect of Duration of Exposure on hygrothermal performance | 297 |
| 6.5 Summary and Conclusions | 300 |
| 7. CONCLUSION | 304 |
| 7.1 Summary | 304 |
| 7.2 Scope and Limitations of the Work | 307 |

| | |
|---|------------|
| 7.3 Summary of experimental and Simulation Findings | 309 |
| 7.4 Contributions of the research | 312 |
| 7.5 Suggestions to Improve the Experimental Protocol and Recommendations for Future Work | 313 |
| 7.6 Related Publications | 315 |
| REFERENCES | 316 |
| APPENDIX A. STATISTICAL ANALYSIS OF TRUDEAU INTERNATIONAL AIRPORT WEATHER STATION PRECIPITATION DATA FOR EXPERIMENTAL PROTOCOL | 332 |
| APPENDIX B. DETERMINATION OF WATER IMPINGING THE TOP CORNER OF A LOW-RISE BUILDING | 335 |
| APPENDIX C. TRANSPORT MECHANISMS AND MATERIAL PROPERTIES AS USED IN FOUR HYGROTHERMAL MODELS | 340 |
| APPENDIX D. BASIC MATERIAL PROPERTIES AND MATERIAL PROPERTY FUNCTIONS AS USED IN THE WUFI SIMULATIONS | 345 |
| APPENDIX E. APPROXIMATION OF THE MOISTURE CONTENT DISTRIBUTION IN THE BOTTOM PLATE INSERTS IN WALLS 1 TO 6 | 354 |

LIST OF FIGURES

| Figure no. | Title | Page |
|---------------|---|------|
| 2.1 | Typical sorption isotherms for wood, concrete and gypsum. | 20 |
| 2.2 | Conditions required for mold growth based on measurements with wood. | 21 |
| 2.3 | Permeability of plywood and oriented strand board as a function of relative humidity. | 23 |
| 2.4 | Measured and predicted moisture content of wall specimen 5 built with fiberboard sheathing. | 25 |
| 2.5 | Measured and predicted moisture content of wall specimen 6 built with plywood sheathing. | 26 |
| 2.6 | Principle of Holmgren's testing apparatus. | 36 |
| 2.7 | EIFS detail testing at Warnock Hersey, Vancouver, using a DC3 airplane engine. | 39 |
| 2.8 | Schematic picture of a stud/bottom plate element. | 40 |
| 2.9 | Stucco wall drying experiment. | 42 |
| 2.10 | Plan view of building, showing the angle θ . | 61 |
| 2.11 | Typical measured rain admittance functions for simple buildings for buildings with different height/width (H/W) factors | 62 |
| 2.12 | Numerical results of specific catch ratio as a function of wind speed at 10 m height and horizontal rainfall intensity. | 64 |
| 2.13 | Water entry under static pressure difference through deficiency above electrical outlet in EIFS-clad wall assemblies no. 7 and 9 at given spray rates. | 68 |
| 2.14 | Water entry through the deficiency above the electrical outlet in the stucco-clad walls in relation to static pressure differential at different spray rates. | 69 |

| Figure no. | Title | Page |
|-------------------|---|-------------|
| 2.15 | Percentage of water entry through deficiency above ventilation duct in stucco-clad walls. | 69 |
| 2.16 | Water entry into deficiency above ventilation duct as a function of static pressure and spray rate for an EIFS-clad wall no. 10. | 70 |
| 2.17 | Notional path of water entry at wall-window interface about deficiency for the stucco-clad walls. | 72 |
| 2.18 | Plot of DI versus WI for 40 North-American candidate cities from the MEWS project. | 79 |
| 3.1 | Frequency distribution of horizontal rainfall in August for three years: 1996, 1998 and 1988, the years with the minimum, average and maximum monthly rainfall, respectively, over 1981-2001. | 94 |
| 3.2 | Frequency distribution of hourly wind speed during rainfall in August (1981-2001). | 95 |
| 3.3 | Window detail in EIFS wall. | 98 |
| 3.4 | Schematic section of the mock test wall/window assembly simulating a perimeter sealant defect at the windowsill used in the water infiltration test. | 100 |
| 3.5 | Schematic section drawing of mock test wall/window assembly simulating a perimeter sealant defect at the windowsill used in the water leakage test. | 101 |
| 3.6 | Photo of the calibration set-up for the Rain Penetration Chamber from inside the Chamber. | 102 |
| 3.7 | Photo of the set-up for the rain infiltration test including the plastic funnel sheet and bucket used to collect the leakage water. | 103 |
| 4.1 | Schematic representation of the Environmental Chamber. | 115 |
| 4.2 | Environmental Chamber Facility in the climatic chamber mode. | 115 |
| 4.3 | Plan view of the test hut. | 117 |
| 4.4 | Elevation of the test hut. | 118 |
| 4.5 | Schematic elevation of a typical test wall. | 119 |

| Figure no. | Title | Page |
|-------------------|---|-------------|
| 4.6 | Plan view of base case wall assembly. | 120 |
| 4.7 | Plan view of base case wall assembly. | 120 |
| 4.8 | Elevation and plan views of the moisture content measurement monitoring protocol in the framing and sheathing of assembly 1 to 12 and 14 to 16. | 128 |
| 4.9 | Elevation and plan views of the moisture content measurement monitoring protocol in the framing and sheathing of assembly 13. | 129 |
| 4.10 | Elevation and plan views of the moisture content measurement monitoring protocol in the framing and sheathing of assembly 17. | 130 |
| 4.11 | Elevation and plan views of the moisture and content measurement monitoring protocol in the framing and sheathing of assemblies 18 and 19. | 131 |
| 4.12 | Section view showing the expected water flow path at the bottom of the test wall during wetting phase. | 133 |
| 4.13 | Photo of the interior finish of a typical wall assembly showing the three gypsum access doors. | 135 |
| 4.14 | A hole for a sheathing gravimetric sample at the bottom center of the sheathing was used as an access panel to reach the sample in the bottom plate. | 136 |
| 4.15 | Photo from the exterior of assembly 12 showing the access door within the sheathing membrane and exterior insulation, as well a hole made for a sheathing gravimetric sample that enabled access to the bottom plate sample beyond. | 136 |
| 4.16 | Schematic (not to scale) showing the painted surfaces of the gravimetric sample and how it sat within the bottom plate. | 138 |
| 4.17 | Photo of the junction between the wood stud and bottom plate in a typical wall assembly with their gravimetric samples and the dental floss to ease their removal. | 138 |
| 4.18 | Calibration of data points at 17oC for asphalt-coated fiberboard. | 141 |

| Figure no. | Title | Page |
|-------------------|--|-------------|
| 4.19 | Adsorption curve for white spruce at 21°C. | 144 |
| 4.20 | Hourly temperature profiles for wetting phase of test 1 showing the average temperatures reproduced in the hot box and cold box of the environmental chamber and inside the test hut vs. the planned temperatures. | 148 |
| 4.21 | Hourly temperature profiles for first drying phase of test 1 showing the average temperatures reproduced in the hot box and cold box of the environmental chamber and inside the test hut vs. the planned temperatures. | 148 |
| 4.22 | Hourly temperature profiles for second drying phase of test 1 showing the average temperatures reproduced in the hot box and cold box of the environmental chamber and inside the test hut vs. the planned temperatures. | 149 |
| 4.23 | Hourly relative humidity profiles for wetting phase of test 1 showing the average relative humidities reproduced in the hot box and cold box of the environmental chamber and inside the test hut vs. the planned relative humidities. | 150 |
| 4.24 | Hourly relative humidity profiles for first drying phase of test 1 showing the average temperatures reproduced in the hot box and cold box of the environmental chamber and inside the test hut vs. the planned relative humidities. | 150 |
| 4.25 | Hourly relative humidity profiles for second drying phase of test 1 showing the average relative humidities reproduced in the hot box and cold box of the environmental chamber and inside the test hut vs. the planned relative humidities. | 151 |
| 4.26 | Schematic showing path of path of water runoff on the plywood sheathing. | 152 |
| 4.27 | Elevation and plan views of the moisture content measurement monitoring protocol in the framing and sheathing of walls 2, 5, 8, 11, | |

| Figure no. | Title | Page |
|-----------------------|---|-------------|
| | 14, 15 and 16 for test 2. | 155 |
| 4.28 | Elevation and plan views of the moisture content measurement monitoring protocol in the framing and sheathing of walls 13 for test 2. | 156 |
| 4.29 | Elevation and plan views of the moisture content measurement monitoring protocol in the framing and sheathing of wall 17 for test 2. | 157 |
| 4.30 | Hourly temperature profiles for wetting phase of test 2 showing the average temperatures reproduced in the hot box and cold box of the environmental chamber and inside the test hut vs. the planned temperatures. | 159 |
| 4.31 | Hourly temperature profiles for first drying phase of test 2 showing the average temperatures reproduced in the hot box and cold box of the environmental chamber and inside the test hut vs. the planned temperatures. | 160 |
| 4.32 | Hourly temperature profiles for second drying phase of test 2 showing the average temperatures reproduced in the hot box and cold box of the environmental chamber and inside the test hut vs. the planned temperatures. | 160 |
| 4.33 | Hourly relative humidity profiles for wetting phase of test 2 showing the average relative humidities reproduced in the hot box and cold box of the environmental chamber and inside the test hut vs. the planned relative humidities. | 161 |
| 4.34 | Hourly relative humidity profiles for first drying phase of test 2 showing the average relative humidities reproduced in the hot box and cold box of the environmental chamber and inside the test hut vs. the planned relative humidities. | 162 |
| 4.35 | Hourly relative humidity profiles for second drying phase of test 2 showing the average relative humidities reproduced in the hot box and cold box of the environmental chamber and inside the test hut vs. the | |

| Figure no. | Title | Page |
|-----------------------|--|-------------|
| | planned relative humidities. | 162 |
| 4.36 | Elevation and plan views of the moisture content measurement monitoring protocol in the framing of assemblies 1 to 6 of test 3. | 166 |
| 4.37 | Elevation and plan views of the moisture content measurement monitoring protocol in the sheathing of assemblies 1 to 6 for test 3. | 167 |
| 4.38 | Hourly temperature profiles for first drying phase of test 3 showing the average temperatures reproduced in the hot box and cold box of the environmental chamber and inside the test hut vs. the planned temperatures. | 169 |
| 4.39 | Hourly temperature profiles for second drying phase of test 3 showing the average temperatures reproduced in the hot box and cold box of the environmental chamber and inside the test hut vs. the planned temperatures. | 170 |
| 4.40 | Relative humidity profiles for first and second drying phases of test 3 showing the average relative humidities reproduced in the hot box and cold box of the environmental chamber and inside the test hut vs. the planned relative humidities. | 170 |
| 5.1 | Measured moisture content with time at various locations within the studs and bottom plate of OSB-sheathed wall 1, test 2. | 174 |
| 5.2 | Measured moisture content with time at various locations in the OSB sheathing of wall 1 in test 2. | 174 |
| 5.3 | Measured moisture content with time at various heights of the spruce stud of wall 17 during the wetting phase of test 1. | 175 |
| 5.4 | Moisture migration path in the plywood gravimetric samples in test 1 which resulted in high moisture accumulation in these gravimetric samples at the top of the walls. | 176 |
| 5.5 | Measured moisture content with time at various locations in the plywood sheathing of wall 2 in test 1. | 177 |
| 5.6 | Measured moisture content with time at various locations in the | |

| Figure no. | Title | Page |
|-------------------|---|-------------|
| | plywood sheathing of wall 2 during the wetting phase of test 2. | 178 |
| 5.7 | Measured moisture content with time at various locations in the fiberboard sheathing of wall 3 during the wetting phase of test 2. | 179 |
| 5.8 | Measured moisture content with time at various locations in the fiberboard sheathing of wall 6 during the wetting phase of test 2. | 179 |
| 5.9 | Measured moisture content with time at various locations in the bottom plate of the fiberboard-sheathed wall 3 during the wetting phase of test 2. | 181 |
| 5.10 | a) Bottom plate gravimetric sample showing the painted and the unpainted surfaces. b) Section view of the center horizontal or right horizontal bottom plate gravimetric samples nestled within the bottom plate, showing the direction of moisture flow into the sample. | 183 |
| 5.11 | Measured moisture content with time in the center horizontal and right horizontal gravimetric specimens of the bottom plate in wall 1, and at the location of the left horizontal electric resistance sensor in wall 10 during the wetting phase of test 2. | 185 |
| 5.12 | Measured moisture content with time at various locations in the plywood sheathings of various wall assemblies during the wetting phase of test 2. | 185 |
| 5.13 | Photograph of the test set-up of the wetting pattern obtained on the surface of two plywood sheathings during a separate water infiltration test where, as in tests 1 and 2, water was introduced on the top surface of the sheathing. | 188 |
| 5.14 | Photographs of the wetting pattern obtained on the surface of two plywood sheathings, shown in a) and b), during a separate water infiltration test where, as in tests 1 and 2, water was introduced on the top surface of the sheathing. | 189 |
| 5.15 | Average of peak moisture contents at each location in a) OSB walls 1, 4, 7 and 10; b) plywood-sheathed walls 2, 5 8 11 and 14, and; c) | |

| Figure no. | Title | Page |
|-------------------|--|-------------|
| | fiberboard-sheathed walls 3, 6, 9 and 12. | 194 |
| 5.16 | Average of peak moisture contents at each location in a) 1-m high plywood-sheathed walls 2, 5 8 11 and 14, and; b) 2-m high plywood-sheathed wall 13. | 195 |
| 5.17 | Average of peak moisture contents in plywood walls: a) walls 2, 5 8 11 and 14 with the base load; b) wall 15 with half the base load and; c) wall 16 with one and a half times the base load. | 196 |
| 5.18 | Average of peak moisture contents at each location in a) plywood-sheathed walls 2, 5 8 11 and 14, and; b) plywood-sheathed wall 17, where water was inserted at the top of the sheathing next to the stud on the right-hand side of the center cavity. | 197 |
| 5.19 | Moisture content with time measurements in the center vertical “CV” gravimetric sample in OSB wall 1, plywood wall 2 and fiberboard wall 3 during the wetting phase of test 2. | 199 |
| 5.20 | Moisture content measured at the start and end of the four-day “dry” period in the center vertical “CV” gravimetric sample in OSB wall 1, plywood wall 2 and fiberboard wall 3 in test 2. | 199 |
| 5.21 | Relative moisture content at the beginning and end of the four-day “dry” period, calculated relative to the initial moisture content at the beginning of the same period in the center vertical “CV” gravimetric sample in OSB wall 1, plywood wall 2 and fiberboard wall 3 in test 2. | 200 |
| 5.22 | Moisture content versus time in the plywood sheathing at row “A” center measured by electrical resistance probes in wall 2 and wall 14 in test 2. | 205 |
| 5.23 | Moisture content versus time in the plywood sheathing at row “D” center measured by electrical resistance probes in wall 2 and wall 14 in test 2. | 206 |

| Figure no. | Title | Page |
|-------------------|--|-------------|
| 5.24 | Moisture content in time in the plywood sheathing at row “A” center measured by electrical resistance probes in wall 2 and wall 13 in test 2. | 207 |
| 5.25 | Maximum moisture content versus time exposed to moisture content greater or equal to 20% in the OSB, plywood and fiberboard sheathings of walls 1 to 12 in test 1. | 209 |
| 5.26 | Maximum moisture content versus time exposed to moisture content greater or equal to 20% in the OSB, plywood and fiberboard sheathings of walls 1 to 12 in test 2. | 209 |
| 5.27 | Maximum moisture content versus time exposed to moisture content greater or equal to 20% in the bottom plates of walls 1 to 12 of test 1, grouped with respect to the sheathing materials used in each wall. | 211 |
| 5.28 | Maximum moisture content versus time exposed to moisture content greater or equal to 20% in the bottom plates of walls 1 to 12 of test 1, grouped with respect to the sheathing materials used in each wall. | 211 |
| 5.29 | Moisture content in the bottom plate inserts versus time for walls 1, 2 and 3 in test 3. | 216 |
| 5.30 | Curves of normalized cumulative mass losses with time for the bottom plate inserts in walls 1, 2 and 3 in test 3. | 216 |
| 5.31 | Schematic showing the determination of the derivative at point mt using the moving window approach. | 217 |
| 5.32 | Drying rate in the bottom plate inserts versus time for walls 1, 2 and 3 in test 3, found using the moving window technique. | 217 |
| 5.33 | Moisture content in the bottom plate inserts versus time for walls 4, 5 and 6 in test 3. | 219 |
| 5.34 | Curves of normalized cumulative mass losses with time for the bottom plate inserts in walls 4, 5 and 6 in test 3. | 219 |
| 5.35 | Moisture content drying rate in the bottom plate inserts versus time for walls 4, 5 and 6, found using the moving window technique in test 3. | 220 |

| Figure no. | Title | Page |
|-------------------|---|-------------|
| 5.36 | Moisture content with time of samples CH1 in OSB-sheathed walls 1, 2 and 3 in test 3. The figure also shows the fitted lines during the first stage of drying, indicating the rates of constant decreasing moisture content for each data series. | 224 |
| 5.37 | Vapor pressure with time in the stud cavity of walls 1, 2 and 3 at approximately 150 mm above the bottom plate inserts in test 3. | 225 |
| 5.38 | Rate of change of moisture content for samples CH1 in walls 1, 2 and 3 in test 3, found using the moving window technique. | 225 |
| 5.39 | Moisture content with time of samples CH1 in walls 4, 5 and 6 in test 3. | 227 |
| 5.40 | Rate of change of moisture content for samples CH1 in walls 4, 5 and 6 in test 3. | 228 |
| 5.41 | Moisture content with time of samples CH2 in walls 1, 2 and 3 in test 3. | 231 |
| 5.42 | Measured relative humidity in the stud cavity of walls 1, 2 and 3 from test 3 at approximately 50 mm above the center of the bottom plate insert. | 231 |
| 5.43 | Calculated relative humidity in the stud cavity of walls 1, 2 and 3 from test 3 on the interior surface of the sheathing at approximately 50 mm above the center of the bottom plate insert. | 232 |
| 5.44 | Rate of change of moisture content for samples CH2 in OSB wall 1, plywood wall 2 and fiberboard wall 3 in test 3 found using the moving window technique. | 232 |
| 5.45 | Moisture content with time of samples CH2 in OSB-sheathed wall 4, plywood-sheathed wall 5 and fiberboard-sheathed wall 6 in test 3. | 234 |
| 5.46 | Rate of change of moisture content for samples CH2 in walls 4, 5 and 6 from test 3, found using the moving window technique. | 234 |
| 5.47 | Water vapor permeance in OSB, plywood and asphalt-coated fiberboard. | 235 |

| Figure no. | Title | Page |
|-----------------------|---|-------------|
| 5.48 | Moisture content with time of samples CV in walls 1, 2 and 3 from test 3. | 237 |
| 5.49 | Rate of change of moisture content for samples CV in walls 1, 2 and 3 in test 3, found using the moving window technique. | 238 |
| 5.50 | Moisture content with time of samples CV in OSB-sheathed walls 4, 5 and 6 from test 3. | 239 |
| 5.51 | Rate of change of moisture content for samples CV in walls 4, 5 and 6 in test 3, found using the moving window technique. | 240 |
| 5.52 | Moisture content with time of sheathing samples DR1 in walls 1, 2 and 3 from test 3. | 242 |
| 5.53 | Moisture content with time of sheathing samples DR1 in wall 4, 5 and 6 from test 3. | 243 |
| 5.54 | Moisture content in the bottom plate inserts versus time for walls 1 and 4 in test 3. | 248 |
| 5.55 | Normalized cumulative moisture loss in the bottom plate inserts versus time for walls 1 and 4 in test 3. | 249 |
| 5.56 | Rate of change of moisture content for bottom plate inserts in walls 1 and 4 in test 3, found using the moving window technique. | 249 |
| 5.57 | Moisture content in the bottom plate inserts versus time for walls 2 and 5 in test 3. | 250 |
| 5.58 | Normalized cumulative moisture loss in the bottom plate inserts versus time for walls 2 and 5 in test 3. | 251 |
| 5.59 | Rate of change of moisture content for bottom plate inserts in wall 2 and 5 from test 3, found using the moving window technique. | 251 |
| 5.60 | Moisture content in the bottom plate inserts versus time for walls 3 and 6 in test 3. | 253 |
| 5.61 | Normalized cumulative moisture loss in the bottom plate inserts versus time for walls 3 and 6 in test 3. | 253 |
| 5.62 | Rate of change of moisture content for bottom plate insets in walls 3 | |

| Figure no. | Title | Page |
|-------------------|--|-------------|
| | and 6 in test 3 using the moving window technique. | 254 |
| 6.1 | Section view of the wall assemblies 1 to 6. | 265 |
| 6.2 | Horizontal wall cross section (a) and vertical wall cross-section for the middle (b) and end (c) sections (see Figure 6.2 c) for at the level of the bottom plate for a wall with a polyethylene vapor retarder. | 271 |
| 6.3 | Moisture content in the bottom plate inserts in walls 1 to 6 from the first 28 days of the third experiment and from the simulations. | 275 |
| 6.4 | Vapor permeance of OSB, plywood and fiberboard. | 276 |
| 6.5 | Liquid diffusivity of OSB, plywood and fiberboard. | 276 |
| 6.6 | Moisture content in the bottom plate inserts in wall 1 for the base case, when the OSB permeance is increased by a factor of 100, and when the OSB liquid diffusivity is increased by a factor of 100. | 277 |
| 6.7 | Sorption curves for OSB, plywood and fiberboard based on volumetric moisture content. | 277 |
| 6.8 | Schematic showing the moisture laden air convection loop within an insulated stud cavity. | 279 |
| 6.9 | Vertical section view of the bottom of the wall assembly insert showing the areas in the sheathing and in the bottom depth that are saturated at each wetting event. | 284 |
| 6.10 | Total moisture content simulation results for the bottom plate of OSB-sheathed walls 1 and 10. | 288 |
| 6.11 | Moisture content simulation results in the saturated exterior and saturated exterior corner zones of the bottom plate for OSB-sheathed walls 1 and 10. | 288 |
| 6.12 | Temperature simulation results at the geometric center of the saturated exterior zone of the bottom plate OSB-sheathed walls 1 and 10. | 289 |
| 6.13 | Relative humidity simulation results in the insulated stud space above the bottom plate in OSB-sheathed walls 1 and 10. | 289 |
| 6.14 | Total moisture content simulation results in the OSB sheathing for | |

| Figure no. | Title | Page |
|-------------------|---|-------------|
| | OSB-sheathed walls 1 and 10. | 290 |
| 6.15 | Moisture content simulation results in the saturated zone of the OSB sheathing for OSB-sheathed walls 1 and 10. | 290 |
| 6.16 | Global moisture content simulation results in the bottom plate and the OSB sheathing for walls 1 and 13, with a 1000-mm and 2000-mm high stud cavity, respectively. | 292 |
| 6.17 | Vertical section view of the bottom of the wall assembly bottom plate showing the areas in the sheathing and in the bottom depth that are saturated at each wetting event. | 294 |
| 6.18 | Global moisture content simulation results in the bottom plate and in the sheathing of the two OSB-sheathed walls, one with a bottom plate wetted width of 20 mm and the other with a width of 40 mm. | 294 |
| 6.19 | Moisture content simulation results in the bottom plate of two OSB-sheathed walls, one which is wetted once a week, and the other three times a week. | 296 |
| 6.20 | Moisture content simulation results in the saturated center and (non-saturated) center zones of the bottom plate for two OSB-sheathed walls, one which is wetted once a week, and the other three times a week. | 296 |
| 6.21 | Moisture content simulation results in the sheathing as a whole and in the saturated zone of the sheathing for two OSB-sheathed walls, one which is wetted once a week, and the other three times a week. | 297 |
| 6.22 | Global moisture content simulation results in the bottom plate and in the sheathing of OSB-sheathed wall 1. | 299 |
| 6.23 | Relative humidity simulation results at the center of the insulated stud cavity above the bottom plate in OSB-sheathed wall 1. | 299 |
| 6.24 | Global moisture content simulation results in the OSB-sheathed and in the saturated sheathing zone of wall 1. | 300 |
| B.1 | Numerical results of specific catch ratio as a function of wind speed at | |

| Figure no. | Title | Page |
|-----------------------|--|-------------|
| | 10 m height and horizontal rainfall intensity. | 336 |
| B.2 | Test building: north-west and south-west facades and position of driving rain gauges 1 to 9 at the façade. | 336 |
| B.3 | Frequency distribution of hourly wind speed during rainfall in August (1981-2001). | 339 |
| E.1 | Plan view of the bottom plate insert showing the depth of the water penetration at the height of the pool of water, and wetted surfaces in the “middle section” and the “end section”. | 357 |
| E.2 | Bottom plate insert showing the wetted surfaces during the partial immersion. | 358 |

LIST OF TABLES

| Table no. | Title | Page |
|--------------|--|------|
| 2.1 | Summary of work done on hygrothermal performance of wall panels constructed with various types of exterior sheathings. | 31 |
| 2.2 | Static and dynamic pressures for the water entry tests for wall assemblies with intentional deficiencies. | 38 |
| 2.3 | Comparison of various laboratory methods for wetting of envelope assemblies. | 45 |
| 2.4 | Comparison of direct water insertion methods to recreate moisture distribution patterns. | 49 |
| 2.5 | Water penetration standard tests used to test the water penetration resistance of envelope components themselves, or of installed components. | 65 |
| 2.6 | Deficiencies introduced in the stucco-clad wall for the MEWS project. | 67 |
| 3.1 | 50-year mean climatic data for Montreal, Trudeau International Airport weather station for years 1941 to 1990. | 93 |
| 3.2 | Data showing the calculated average hourly horizontal rainfall, average daily number of hours of rain, the average number of rainy days and the average total amount of rain over the month, for the months from April to October for the Trudeau airport climatic station for the years 1981 to 2001. | 94 |
| 3.3 | Average ratio of water infiltration to water impinging on window surface as a function of defect size. | 104 |
| 3.4 | Mass and apparent moisture content change with time for full and partial immersion trial of two wood specimens taken from the same timber piece. One of the specimens was fully immersed in water while the second was partially immersed. | 109 |

| Table no. | Title | Page |
|------------------|---|-------------|
| 3.5 | The initial moisture content, final moisture content after 31 days of partial immersion, and the moisture content gained in the immersion process. | 110 |
| 3.6 | Maximum and minimum initial and final moisture contents after 26 days of partial immersion in gravimetric specimens CH1, CH2 and CV in walls 1 to 6. | 111 |
| 4.1 | Wall testing parameters. | 124 |
| 4.2 | Testing condition variables. | 124 |
| 4.3 | Test wall configurations and testing parameters for test 1. | 125 |
| 4.4 | Location and number of gravimetric samples and moisture content probes within each wall assembly. | 134 |
| 4.5 | Planned indoor and outdoor temperature and relativity conditions for the wetting and drying phases of the experiment. | 146 |
| 4.6 | Test wall configuration and testing parameters for test 2. | 154 |
| 4.7 | Types of sheathings and vapor retarders in walls 1 to 6 in test 3. | 164 |
| 4.8 | Planned indoor and outdoor temperature and relativity conditions for the wetting and drying phases of test 3. | 168 |
| 5.1 | Examples of walls where an increase in moisture content was found at the location of sheathing and bottom plate gravimetric samples due to lateral migration of water. | 182 |
| 5.2 | Relative moisture content at the end of the four-day “dry” period, calculated relative to the initial moisture content at the beginning of the same four-day period at various locations in the bottom plate and the sheathing in walls 1 to 7 of test 2. | 200 |
| 5.3 | Relative moisture content at the end of the four-day “dry” period, calculated relative to the initial moisture content at the beginning of the same four-day period at various locations in the bottom plate and the sheathing in walls 1 to 7 of test 2. | 203 |
| 5.4 | Relative moisture content at the end of the four-day “dry” period, | |

| Table no. | Title | Page |
|------------------|---|-------------|
| | calculated relative to the initial moisture content at the beginning of the same period in two gravimetric specimens in row “D” right 2 in plywood walls 2 and 11, test 2. | 204 |
| 5.5 | Initial and final moisture content and moisture content lost in the drying process for the bottom plate inserts of walls 1 to 3 in test 3. | 214 |
| 5.6 | Initial and final moisture content and moisture content lost in the drying process for the bottom plate inserts of walls 4 to 6 in test 3. | 218 |
| 5.7 | Initial and final moisture contents, drying rate during the period of constant drying, and peak drying rate in the center horizontal 1 (CH1) specimens in walls 1, 2 and 3 in test 3. | 224 |
| 5.8 | Initial and final moisture contents, drying rate during the period of constant drying, and peak drying rate in the center horizontal 1 (CH1) specimens in walls 4, 5 and 6 in test 3. | 227 |
| 5.9 | Initial and final moisture contents, drying rate during the period of constant drying, and peak drying rate in the center horizontal 2 (CH2) specimens in walls 1, 2 and 3 in test 3. | 230 |
| 5.10 | Water absorption coefficients across the major surface for three OSB samples, three plywood samples, and one asphalt-coated wood fiberboard sample. | 230 |
| 5.11 | Initial and final moisture contents, drying rate during the period of constant drying, and peak drying rate in the center horizontal 2 (CH2) specimens in walls 4, 5 and 6 in test 3. | 233 |
| 5.12 | Initial and final moisture contents, drying rate during the period of constant drying, and peak drying rate in the center vertical (CV) specimens in walls 1, 2 and 3 from test 3. | 237 |
| 5.13 | Initial and final moisture contents, drying rate during the period of constant drying, and peak drying rate in the center vertical (CV) specimens in walls 4, 5 and 6 from test 3. | 239 |
| 5.14 | Initial and final moisture content and drying rate in the sheathing DR1 | |

| Table no. | Title | Page |
|------------------|---|-------------|
| | specimens in walls 1, 2 and 3 from test 3. | 241 |
| 5.15 | Constant rates and peak rates of change of moisture content for samples CH1 and CH2 in walls 1 to 6 in test 3, sorted in terms of the level of drying – low, medium and high. | 244 |
| 5.16 | Final moisture content in samples CH1 and CH2 from walls 1 to 6 in test 3. | 245 |
| 5.17 | Initial and final moisture content and moisture content lost in the drying process for the bottom plate inserts of walls 1 to 6 in test 3. | 248 |
| 6.1 | Interior and exterior conditions set in test no. 3 and in the WUFI2D simulations. | 266 |
| 6.2 | Surface transfer conditions for wall assemblies. | 268 |
| 6.3 | The initial temperature assigned to each wall component. | 270 |
| 6.4 | The initial moisture content assigned to each wall component. | 270 |
| 6.5 | Average drying rate of the bottom plate inserts, calculated from the results of experiment 3 and the WUFI 2D simulations. | 275 |
| 6.6 | Interior and exterior conditions set in test no. 3 and in the WUFI2D simulations. | 285 |
| 6.7 | The initial temperature assigned to each wall component. | 286 |
| 6.8 | The initial moisture content assigned to each wall component. | 286 |
| 6.9 | Final moisture content simulation results in the bottom plate zones for two wall systems, one which is wetted once a week, and the other three times a week. | 297 |
| B.1 | Mean precipitation data for Montreal’s Trudeau International Airport weather station for years 1941 to 1990. | 337 |
| B.2 | Data showing the average horizontal hourly rainfall and total rainfall for the months from April to October, for the Trudeau International Airport climatic station for the years 1981 to 2001. | 337 |
| C.1 | Material parameters and material functions used in hygrothermal models. | 342 |

| Table no. | Title | Page |
|----------------------|---|-------------|
| C.2 | Transport mechanisms considered by hygrothermal models. | 343 |
| C.3 | Moisture and thermal potentials used in several hygrothermal models. | 344 |
| D.1 | Materials and basic material properties used in the simulations. | 345 |
| D.2 | Material functions for OSB. | 347 |
| D.3 | Material functions of plywood. | 348 |
| D.4 | Material functions of asphalt-coated fiberboard. | 350 |
| D.5 | Material functions of spruce. | 351 |
| D.6 | Material functions of interior gypsum. | 352 |
| E.1 | Measured dry density and mass measurements of the bottom plate inserts, and calculations for determination of the initial average moisture content of the wood within the bottom plate. | 358 |

NOMENCLATURE

| Symbol | Parameter | Units |
|-----------------|--|------------------------------------|
| a | diameter, of raindrop | mm |
| A | area | m ² |
| A _c | capillary water absorption coefficient | kg/m ² s ^{1/2} |
| B | water penetration coefficient | m/s ^{1/2} |
| d | height | m |
| D _{vl} | binary diffusion coefficient between water vapor and air | m ² /s |
| D _w | capillary transport coefficient, also called liquid diffusivity | m ² /s |
| D _φ | liquid conduction coefficient | kg/ms |
| \bar{E} | mean error | - |
| f _h | probability-density function of raindrop size as a flux through a horizontal plane | m ⁻¹ |
| F | cumulative frequency distribution | - |
| g | mass flow rate per unit area | kg/m ² ·s |
| G | mass transfer | ng/s or kg/s |
| h | heat transfer film coefficient | W/m ² ·K |
| h _v | latent heat of phase change | J/kg |
| H | total enthalpy | J/m ³ |
| I | global radiation | W/m ² |
| j | counting index, e.g. number of hours in a year | - |
| k | thermal conductivity | W/m ² K |
| k _m | moisture-dependent conductivity, used in numerical simulations | W/m |
| l | length (of flow path) | m |
| M | permeance | ng/m ² sPa |

| | | |
|----------------|--|--|
| M | molecular mass | g/mol |
| MC | moisture content | %-mass |
| n | counting index, e.g. number of years | - |
| p | partial pressure | Pa |
| P | total pressure | Pa |
| q | heat flux density | W/m ² |
| r | radius | m |
| R | rainfall intensity | l/m ² h (= mm/h) |
| R _v | gas constant for water vapor | J/kg·K |
| s _d | equivalent diffusion air layer thickness | m |
| S _h | heat source or sink | W/m ³ |
| S _m | moisture source or sink | kg/m ³ s |
| t | time | s |
| T | temperature | °C |
| w | volumetric moisture content | kg/m ³ |
| w | moisture content of the air | kg _{water vapor} /kg _{dry air} |
| v | volumetric humidity content of air | g/m ³ |
| V _T | terminal velocity of raindrop | cm/s |
| V | wind speed | m/s |
| x | distance | m |
| x _t | water penetration depth | m |
| z | height above ground | m |

Greek alphabet symbols

| | | |
|----------------|--------------------------|-----------|
| α | power law exponent | - |
| β | azimuth angle | degree |
| δ | water vapor permeability | ng/Pa·s·m |
| δ | boundary layer thickness | m |
| η _a | specific catch ratio | - |
| η | catch ratio | - |

| | | |
|----------|--|-------------------|
| μ | vapor diffusion resistance factor | - |
| θ | in plan view, angle between the normal to the building façade and the wind | degree |
| ρ | density | kg/m ³ |
| σ | surface tension of water | N/m |
| ϕ | relative humidity | % |
| Φ | temperature | K |

Subscripts

| | |
|---------|---------------------------------------|
| a | air, atmosphere |
| bv | vertical surface on a building façade |
| conv | convective |
| dm | dry material |
| D | day |
| e, ext | exterior |
| g | gradient, as in gradient wind speed |
| h | heat |
| h | horizontal surface |
| H | hour |
| int | interior |
| l | liquid |
| meas | measured |
| M | month |
| o | Saturation |
| oc | open country |
| sim | simulated |
| sub | suburban |
| S, surf | surface |
| v | vertical surface |
| v | vapor |
| va | ambient vapor |

| | |
|--------|--------------------------------|
| vm | vapor above capillary meniscus |
| vo | vapor, at saturation |
| w | moisture |
| z1, z2 | height above ground of z1, z2 |

Abbreviations

| | |
|-----------|---|
| aDRI | annual driving rain index |
| CMHC | Canada Mortgage and Housing Corporation |
| CWEC | Canadian Weather Year for Energy Calculations |
| DEFS | direct-applied exterior finish system |
| DI | drying index |
| DRF | driving rain factor |
| DRI | driving rain index |
| EDRA | Envelope Drying Rates Analysis experiment |
| EIFS | exterior insulation and finish system |
| EMC | equilibrium moisture content |
| FSP | fiber saturation point |
| HAM | heat, air and moisture |
| IEA | International Energy Annex |
| IRC | Institute for Research in Construction |
| MEWS | Moisture Management in Exterior Walls Systems project |
| MDRY | moisture durability reference year |
| MI | moisture index |
| MRY | moisture reference year |
| NBCC | National Building Code of Canada |
| NRCC | National Research Council, Canada |
| OSB | oriented strand board |
| RAF | rain attenuation factor |
| RH | relative humidity |
| RHT index | relative humidity temperature index |
| RTD | resistance temperature device |

| | |
|-------|--|
| TMY | typical meteorological year |
| TRY | typical reference year |
| WI | wetting index |
| WYEC2 | Weather Year for Energy Calculations version 2 |

1. INTRODUCTION

1.1 Context of the Research Project

Moisture can pose a serious threat to the integrity and durability of the building envelope. Indeed, it is said to account for up to 80% of the damage in building envelopes (Bomberg and Brown, 1993). The accumulation of moisture within hygroscopic materials such as wood can, if temperature conditions are appropriate, produce a breeding ground for decay fungi, leading to the deterioration of building envelope components. For example, field investigations following the building envelope failure disaster that hit homes in the lower mainland of British Columbia commonly documented cases where the accumulation of moisture within wall assemblies caused rotting of wood framing members and wood-based exterior sheathing (Edgar, 1998; Lang *et al.*, 1999).

Rain may be an important source of moisture in the building envelope. Field studies show that rain tends to penetrate not through the main fabric of envelopes but rather to infiltrate through defects at envelope junctions such as the interface between walls and windows, deck perimeters, balconies and walkways (Marsh, 1977; Addleson, 1972; Beers and Smith, 1998; Ricketts and Lovatt, 1996; Lies and Faith, 1998; Zwyer *et al.*, 1998). However, understanding the nature of rain and its infiltration into the building envelope is difficult because of the many factors to take into account. The characteristics of rain as well the deposition of rain water on a building envelope must be identified both qualitatively and quantitatively. Research has shown that impinging wind-driven rain on a building façade, or driving rain falling onto a building façade, is a function of many parameters including the rainfall intensity and the raindrop size distribution, the wind speed and direction, the duration and frequency of rainstorms, local topography, sheltering by surrounding trees and buildings, the orientation of the building façade, the building's geometry, and the location on the building. Recent advances in driving rain

characterization (Blocken and Carmeliet, 2000, 2002a, 2005) make it possible to take into account realistic rain loads in hygrothermal studies.

Experimental studies on the impact of rain infiltration tend to either use a spray rack or similar apparatus to simulate water impinging on a building façade (Edgar, 1998; Tsongas *et al.*, 1998; Poirier *et al.*, 1997; Brown *et al.*, 1997) or to simply introduce water directly into the test panel (Lang *et al.*, 1999; Tsongas *et al.*, 1998; Hens and Fatin, 1995; Desjarlais *et al.*, 1993; Korsgaard and Rode, 1992; and Onysko and Jones, 1989). The former method is commonly used to test the rain penetration resistance of wall systems. However, the direct introduction of water into panels is preferred for hygrothermal testing as it allows control over the amount and/or rate of water insertion into the test assemblies.

The building envelope is comprised of various components that work together to separate the indoor environment from that outdoors. Components like the sheathing and the vapor barrier play a significant role in controlling heat, air and moisture transfer across the envelope. In the event of incidental moisture leakage into the building envelope due to a faulty window, for example, envelope components play a role not only in moisture absorption and distribution within the envelope, but also in the drying capability of the system. Utilization of materials that enhance the drying is desired because it reduces the risk of moisture-induced decay. For example, wood and wood-based sheathing materials are commonly used in North America because of their structural strength and relatively low cost. Each of these materials has different moisture absorption properties and air and vapor permeances, and therefore behaves differently when exposed to wetting and drying conditions.

Despite continuous advances, hygrothermal modeling of the building envelope is still bounded by limitations that may restrict the type of problems that can be studied. For example, modeling tools require accurate material properties which depend on temperature, moisture content and moisture history but which have not been fully characterized. Although three-dimensional modeling of the heat and moisture transfers is possible, most current models are limited to one or two-dimensions. Numerical tools have difficulty dealing with the complex geometry of liquid moisture insertion and runoff and do not include material properties regarding liquid uptake and redistribution. Hence,

while time-consuming and costly, experimental testing in a laboratory and/or a field setting remains a primary method for the advancement of knowledge in the field of building envelope.

1.2 Problem

Good building practices and detailing exist to prevent rain infiltration-induced building envelope failures, such as providing walls with a capillary break and allowing air pressure equilibrium with the introduction of rain screen cladding, or with a second line of defense against water infiltration such as flashing around openings and through-flashing below window frames. However, instances of improper design, inadequate training, poor workmanship, and inadequate supervision and site inspection can result in improper building practices, leading to rain infiltration failures.

Such failures are owed to the fact that rain can be a significant source of moisture when it is allowed to infiltrate within the building envelope. Recent computational and field studies including those of Choi (1994; 1999; 2000), Blocken and Carmeliet (2000; 2001a; 2001b; 2002a), and Straube and Burnett (1998a; 2000a) have advanced the state of knowledge with respect to linking the effect of the rate of horizontal rainfall (the rain falling on a horizontal plane, in a location undisturbed by buildings and other obstacles) and wind speed to wind-driven rain on building facades. However, few experimental studies consider rain as a source of moisture in hygrothermal testing, perhaps because of the complex nature of the rain infiltration process. In fact, there exists no standard methodology for experimentally reproducing rain infiltration, taking into account actual climatic loads such as rainfall, wind speed and wind orientation. Such a methodology is needed to set boundary conditions for experimental or numerical building envelope tests that consider rain as a source of moisture.

While building envelope failures in the field show evidence of decaying wood components resulting in building envelope failures, little information is available on the drying capacity of wood-frame walls built with wood-frame sheathing. It will be shown

that of those hygrothermal studies that have been done, none have established the role of various wood-based sheathing and other envelope components in the hygrothermal performance of wall systems. Wood sheathings like oriented strand board, (OSB), plywood and fiberboard have different moisture absorption capacities and water vapor permeabilities, which affect the assemblies' ability to manage moisture. Also, few experimental works involve large-scale assemblies exposed to realistic daily temperature and relative humidity levels found in the field.

Due to the limitations of numerical modeling, large-scale testing is an important method of evaluating the performance of envelope assemblies. Such experimental studies are fundamental in assessing performance of the assembly as a whole with respect to heat performance, water vapor retarding capacity, air barrier rating, rain penetration resistance, etc. Therefore, there is a need to establish a framework for large-scale envelope testing with respect to designing test panels, setting environmental conditions for indoor and outdoor conditions and determining monitoring protocols.

1.3 Objectives and Approach

The primary objectives of the research project were:

- To investigate the wetting and drying performance of hygroscopic components in wood-frame wall systems wetted by simulated rain infiltration through a building envelope defect;
- To develop a framework for large-scale testing of wall assemblies subjected to rain infiltration;
- To determine the locations within the wall that are most susceptible to moisture accumulation, and;
- To examine the impact of several parameters including the sheathing, the vapor retarder, and the presence of exterior foam insulation and of exterior cladding on the hygrothermal behavior of the wetted components.

To accomplish these goals, the following tasks were performed:

- The development of a rationalized wetting protocol to simulate rain water infiltration for Montreal using local climatic data;
- The development of a protocol that establishes the indoor and outdoor environmental testing conditions to which the wall assemblies were subjected, including temperature and relative humidity;
- The design of test wall assemblies, determination of the test parameters to be varied and of the experimental instrumentation for temperature, relative humidity and moisture content;
- The analysis of the experimental results, including reproduction of the behavior with modeling.

To this effect, three large-scale building envelope tests were tested in a test hut. Each of the first two tests each included 19 wall assemblies, 17 of which were wetted, while the third test involved six wall assemblies. The construction of the test walls reflected current construction practice and made use of building materials found in the field. The assemblies were subjected to simulated rainwater loads as well as temperature and relative humidity differentials, replicating actual environmental conditions found in Montreal, Québec. Two wetting methodologies were developed and applied. The first consisted of introducing water in a drop-by-drop fashion onto the interior surface of the wall sheathing at a rate, duration and frequency that was rationalized using a climatic data. This methodology was applied to the first two tests. The liquid moisture source in the second methodology was a pre-wetted wall component. In addition to the overall performance of the different assemblies, the role of several building envelope components, and in particular the sheathing, was evaluated experimentally.

This thesis is organized as follows. An extensive literature review on the current state of knowledge of building envelope testing with regards to the influence of sheathing on the performance of the envelope and previously developed liquid moisture wetting methodologies is described in detail in Chapter 2. The development of the two wetting methodologies and the experimental protocol are subsequently presented in Chapters 3 and 4, respectively. The wetting and drying results from the three tests are discussed in Chapter 5. In the following chapter, numerical simulations are conducted for the wall set-up and loading in test 3 using an existing 2-dimensional heat and moisture transport

envelope model. The simulation results are compared with the experimental work, and serve as a basis for parametric analyses. Finally, a summary of the findings, the contributions of this work and recommendations for future work are given in Chapter 7.

2. LITERATURE REVIEW

The field of heat, air and moisture performance of the building envelope has an established knowledge base. However, as the following literature review shows, much still remains to be known about the hygrothermal performance of the envelope, specifically where hygroscopic materials like wood are subjected to a moisture load in liquid form.

The literature review first presents the function of the building envelope as a whole and that of its components, as well as how the envelope manages moisture. In addition, previous works on the hygrothermal performance of walls built with different sheathing materials are presented. Then, the literature review addresses experimental wetting methods that have been developed to simulate rain, and previous numerical and field studies on wind-driven rain and rain penetration. The survey continues with a discussion on previous efforts to simulate wind-driven rain experimentally, and to understand impinging wind-driven rain on the building envelope, or rain striking the building envelope, and rain infiltration into wall systems. Finally, the chapter closes with a review of work on the selection of representative climate data for building envelope testing.

2.1 Function of the building envelope and the role of wall components

The building envelope, also called the building enclosure, consists of a system that separates the indoor and outdoor environments, comprising the walls, roof, and foundation, and all of their sub-units such as windows, doors, skylights, etc.

Straube and Burnett (2005) group the functions of the building envelope into five categories:

1. Support functions: to support and accommodate all structural loadings. Examples of loads include dead load, live load, seismic load, whole building and differential settlement, wind, creep and shrinkage.

2. Control functions: to control or moderate loads imposed by the exterior and interior environments. The building envelope must control the transfer of heat, air, water vapor, rain, light, solar and other radiation, noise, fire, smoke, chemicals (e.g. acid rain), particulates (e.g. dust, volatile organic compounds, mold spores), insects, birds and animals.
3. Finish functions: to finish exterior and interior surfaces. Finishes must protect the envelope from chemical attack, reduce wear and tear and be aesthetically pleasing.
4. Distribution functions: to distribute services and utilities. Services and utilities which may require distribution within the building envelope include water pipes, ventilation ductwork and electrical wiring.
5. Qualitative functions: to meet qualitative attributes over the envelope's life span. Qualities that may be required or desired include constructability, operability, repairability, maintainability, short or long-term economic viability, safety, aesthetics, sustainability, convertibility and disposability.

Individual components making up the envelope are interconnected and as such function as a system. A common wood-frame wall assembly for a cold climate may consist of the following components, from the outside to the inside:

- exterior cladding
- air space
- exterior sheathing membrane
- exterior sheathing
- wall framing
- thermal insulation installed between the framing members and/or on the exterior side of the exterior sheathing
- membrane
- interior sheathing and finish

Each of these components is briefly described next in terms of how it performs and examples of current materials are given.

Exterior cladding

The exterior cladding provides control over rain penetration, light, solar and other forms of radiation. In addition, the cladding must be rigid and be supported so that it can transfer wind loads to the structure. Together with the air space behind it, it forms the rain screen. Common materials used include masonry cladding such as brick, concrete block and stone; board siding in polyvinyl chloride, wood or aluminum; aluminum or steel panels, lumber planks, wood shingles, as well as stucco.

Air space

An air space is commonly provided behind many exterior claddings such as masonry and siding. In fact, the National Building Code of Canada (NBCC) (National Research Council of Canada (NRCC), 1995) requires that there be an air space at least 25 mm wide behind the masonry cladding for wood-frame assemblies (art. 9.20.6.4, sentence 2). This air space provides a capillary break between the cladding and the exterior sheathing, as well as a means of air pressure moderation across the exterior cladding. Both these measures decrease the risk of rain water penetration across the cladding and to the back wall as they minimize the capillary and air pressure forces responsible for rain infiltration. The air space also facilitates drainage of any water that may have found its way behind the cladding. In addition, the air space allows for a gap where air convection can take place. Weep holes at the bottom and the vent holes at the top of masonry walls, for example, provide the means for air to enter and exit the air space. Many researchers (Hazleden, 2001; Hens and Janssens, 1999; TenWolde and Rose, 1999; Straube and Burnett, 1998b; Rose, 1995) believe that the ventilation promotes drying of walls and roofs. However, some claddings like bevel siding have gaps between the boards that allow air to circulate behind them, and for this reason do not require a vertical air space behind them for ventilation drying (Canada Mortgage and Housing Corporation (CMHC), 1988). The need for an air space behind siding may depend on the type of siding, the siding material and the climate.

Exterior sheathing and sheathing membrane

Exterior sheathing, also called wall sheathing or simply sheathing in this thesis,

consists of rigid sheets or lumber planks that are installed on the cold side of the wall framework and are nailed directly into the wall framing members. The purpose of exterior sheathing is to brace the wall structure, thus providing resistance to wind load. It is also used as a nailing base for some types of siding and backing for others (CMHC, 1988).

The NBCC (NRCC, 1995) presents the minimum thickness for several different types of wall sheathings, some wood-based and some not: lumber, fiberboard, oriented strand board (OSB), waferboard, exterior grade plywood, rigid mineral fiberboard, exterior gypsum board, expanded polystyrene, and both faced and unfaced urethane and isocyanurate board (article 9.23.16.2). Other materials such as extruded polystyrene board, semi-rigid glass fiber panel, cement board, gypsum board faced with glass fibers are also used (CMHC, 1988). Fiberboard is usually surface-impregnated with asphalt to increase water resistance (CMHC, 1988). Wood-based exterior sheathings are commonly used in Canada and the United States because of the ready availability of wood. Three types of wood-based sheathing are commonly found in North American construction, namely plywood, OSB and wood fiberboard. The use of OSB in the Canadian residential building market has grown, partly taking over that of plywood. This is likely due to OSB's lower cost. In Québec, however, fiberboard is commonly employed. The NBCC (art. 9.23.16.5 sentence 1) (NRCC, 1995) requires that a gap of not less than 2 mm shall be left between sheets of plywood, OSB, waferboard or fiberboard to allow for thermal expansion and shrinkage of the panels. The gap also permits air movement.

It should be noted that although the structural strengths of these sheathing materials have been tested extensively by wood research institutes like Forintek Canada Corp., little work has been performed thus far to establish their role in the hygrothermal performance of wall assemblies subjected to actual climatic conditions.

A sheathing membrane is placed on the outer surface of the sheathing and should be water resistant but water vapor permeable. It acts as a second barrier to any wind and rain that might penetrate the cladding (CMHC, 1988). It also acts as a water shedding device during construction and in the event of water penetration through the cladding after completion of the envelope. It must be permeable enough to allow any water vapor in the inner wall to diffuse out of the wall. The NBCC (NRCC, 1995) requires that at

least one layer of sheathing membrane be applied beneath siding, stucco and masonry cladding unless non-wood-based rigid exterior insulating sheathing or exterior insulating sheathing with an integral membrane is installed (art. 9.23.17.3 and 9.23.17.4). Common sheathing membranes include building paper (tar-saturated felt or paper) and spun-bonded polyolefin sheets.

Wall framing

Studs are used in wood-frame residential construction of three stories and a half or less to provide structural strength to the building. Typically 38 mm by 140 mm (2" by 6" nominal) or 38 mm by 89 mm (2" by 4" nominal) studs are used (CMHC, 1988). The wider studs are typically used in cold climates because they offer additional space for more insulation but are not required for structural purposes. The NBCC (NRCC, 1995) specifies the minimum wood stud size as a function of stud spacing, the supported load and the maximum unsupported height (art. 9.23.10.1). Wood species used for wood framing in Eastern Canada and the United States are typically spruce, pine and fir, which are grouped together and designated by the abbreviation SPF in the wood industry. Steel studs are also used, although the NBCC (NRCC, 1995) does not provide recommended tabulated steel stud sizes for load bearing exterior walls.

Thermal insulation

Thermal insulation serves to reduce heat transfer across the building envelope and thus decrease the heating load in a building. Installing batt insulation in the stud space is common and provides minimal interference with electrical and mechanical services within the wall. Adding exterior insulation in new construction or retrofit to increase the thermal resistance and reduce thermal breaks, thus reduce energy consumption. In Québec, the minimum thermal resistance of envelope components such as walls, roofs, and foundations are dictated by the "Regulation respecting energy conservation in new buildings" (Regulation, 1992). For example, the minimum thermal resistance for wall assemblies above ground level for a wood-frame wall of a building in Montreal (zone A) is $3.4 \text{ m}^2 \text{ }^\circ\text{C/W}$.

Materials used as thermal insulation include, but are not limited to, glass fiber,

mineral fiber, expanded and extruded polystyrene, cellulose fiber, polyurethane, and polyisocyanurate. Depending on the material, insulation can be found in the form of batts, rigid boards, loose fill and sprayed in situ.

Membrane

In cold climates, a membrane is typically placed on the warm side of the insulation as a vapor retarder to control water vapor diffusion which can potentially cause condensation in exterior envelopes subjected to temperature differentials. As a general rule, the control layer should be located on the warm side of the insulation. The NBCC (NRCC, 1995) (art. 9.25.4.2, sentence 1) states that vapor retarders are materials with a water vapor permeance not greater than $45 \text{ ng}/(\text{Pa}\cdot\text{s}\cdot\text{m}^2)$; however, the code also expresses that where other elements in the building assembly have low vapor permeance, the permeance of the vapor retarder must be further reduced to $15 \text{ ng}/(\text{Pa}\cdot\text{s}\cdot\text{m}^2)$. This would be the case when low permeance cladding such as metal or vinyl siding with tight joints and without a vented air space or plywood sheathing is used. The NBCC (NRCC, 1995) allows that vapor retarders with a permeance of less than $60 \text{ ng}/(\text{Pa}\cdot\text{s}\cdot\text{m}^2)$ be installed within the exterior envelope assembly such that the minimum ratio of total thermal resistance of all materials outboard of its innermost impermeable surface and the total thermal resistance of all materials inboard of that surface is not less than 0.2 for a building located in a region where the heating degree days is up to 4999, as is the case for Montreal (art. 9.25.1.2). Materials typically used as vapor retarders include polyethylene, installed between the interior sheathing and the framing, and low permeance paint applied on the interior sheathing. Aluminum sheets, aluminum-faced gypsum board, and some vinyl wallpapers also serve the same purpose. It should be recognized that any material with a low water vapor permeance acts as vapor retarders.

Interior sheathing

Interior sheathing describes any material used to cover the interior wall and ceiling framing. The most common material used for this purpose is gypsum board, although others such as plaster, plywood, hardboard, simulated cladding hardboard and lumber can also be used. While 9.5 mm thick gypsum can be used on supports spaced up to 400 mm

on center, a 12.7 mm board is most typically used for its extra strength. NBCC (NRCC, 1995) requirements regarding the thickness of gypsum boards, orientation of the boards relative to the framing and maximum spacing of supports are described in article 9.29.5.9. The interior sheathing is usually painted to provide greater resistance to wear and tear, and to meet visual aesthetic appeal requirements.

Air barrier

The air barrier comprises a system of envelope components rather than one material, and is critical to the proper hygrothermal performance of envelope assemblies. The air barrier's function consists of controlling the infiltration and exfiltration of air through the building envelope. Air flow through the envelope is caused by an air pressure differential across it due to the wind, stack effect and mechanical ventilation. Air flow through the envelope is undesirable because of two reasons: 1) it can cause a sensible heat flux through the envelope, which increases heating or cooling energy demand and can cause drafts, leading to poor thermal comfort; 2) the egress of warm moist indoor air through walls can, in the winter season, cause the water vapor in the air to condense, either in liquid form or as frost, on cold surfaces within the building envelope, which can result in the deterioration of materials; conversely, in summer, the ingress of warm moist outdoor air can lead to condensation onto cold surfaces within the envelope if the building is mechanically cooled.

It has been common practice to use polyethylene sheets to perform both functions of an air and vapor barrier. However, its lack of rigidity makes other approaches like airtight drywall, blown-in polyurethane and spun-bonded polyolefin sheathing membranes to be more and more used as an air barrier. The NBCC (NRCC, 1995) requires that air barrier materials used as an air barrier have air leakage characteristics not greater than $0.02 \text{ l/(s}\cdot\text{m}^2)$ measured at an air pressure differential of 75 Pa (art. 5.4.1.2, sentence 1). The code also requires that penetrations in the air barrier system such as those created by windows, doors, electrical wiring and boxes, piping, etc., be sealed to maintain the integrity of the air barrier system (art. 5.4.1.2 sentence 7, and art. 9.25.3.3).

Whereas this section has dealt with the function of each envelope component, the

following discusses how the components function as a system to manage moisture in the building envelope.

2.2 Moisture management in the building envelope

2.2.1 Rain

Rain is an important source of moisture into the building envelope and prevention of rainwater penetration must be carefully taken into account during the design and construction stages. Water penetration requires three factors to be present concurrently: the presence of water, an opening, and a force to drive the water through the hole, which may include kinetic energy, capillarity, gravity, or an air pressure difference. The management of rainwater may be done in three ways: the mass wall approach, the face seal method and the rainscreen principle.

In the mass wall approach, the wall has sufficient moisture storage capacity that it can absorb all of the rainwater that penetrates through the exterior wall surface without permitting moisture transfer to the interior. The face seal method relies on a water-impermeable exterior face as the means of deflecting the moisture incident on them. As it relies on sealing of joints, walls making use of this method are particularly vulnerable to water leakage.

The rainscreen approach, which is more commonly used, assumes that some water will penetrate the outer layer of the envelope and therefore includes a second line of defense to ensure that any rainwater that leaks through the cladding can effectively be drained back to the outside. In typical residential buildings, the rainscreen construction makes use of a vertical drainage plane behind the cladding, flashing and weepholes to ensure water drainage. More importantly, the rainscreen approach, through the presence of openings in the cladding and of an air space, ensures that air pressure differentials across the cladding are minimized, thereby minimizing the amount of water being

induced into the assembly. Field testing by Straube (2000b) has shown that even in well-built, ventilated and tightly compartmentalized claddings, this pressure difference is seldom truly negated, and hence the use of the term pressure moderated is more appropriate.

Hazleden and Morris (1999) have summarized the requirements for the control of rainwater penetration with the 4 D's: deflection, drainage, drying and durability. Deflection is the first line of defense against water penetration and mainly involves roof overhangs, copings and other architectural features such as certain siding profiles and flashings that deflect rainwater from the building façade. It is estimated that a properly designed deflection system can deal with over 90% of the water incident on a building (Hazleden and Morris, 1999).

Drainage involves evacuating any water that traverses the cladding through the use of an air space behind the cladding, a drainage plane, flashing, weep hole, etc. In theory, this reduces the load of water penetration into the back wall to less than 1% of that on the cladding, which is deemed manageable (Hazleden and Morris, 1999).

Since, in reality, design and construction cannot achieve perfection, it may occur that rain water penetrates through the cladding and bypass the drainage systems. As well, high moisture contents can be found in the construction lumber itself. Hence, it is desirable to design wall systems that are capable of drying as quickly as possible. The risk of fungal growth is diminished by the use of materials that dry quickly, and wall systems whose configuration promotes drying, hence reducing the time exposure to moisture. Vapor diffusion is the main building envelope drying mechanism (Straube, 2001). Thus, the water vapor permeability of each building envelope component becomes important for drying.

The last "D", durability, refers to a material's ability to tolerate moisture or store water safely. Wood in its natural state has a built-in moisture tolerance which varies depending on the species as well as the location where the wood is found within the tree (sapwood versus heartwood). For example, the heartwood of a moderately durable species like Douglas fir may be able to tolerate moisture contents up to 23%, while the moisture tolerance of western red cedar, a durable wood, may be up to 35% moisture content (Hazleden and Morris, 1999).

To summarize, moisture management is enhanced when the building envelope system is well equipped for deflection, drainage, drying and durability. While deflection and drainage has been thoroughly researched and can currently be effectively achieved in practice, drying and durability of materials are more complex to attain as they are functions of the wall configuration, the material properties such as moisture absorption and adsorption, the water vapor and air permeability, as well as the exterior and interior loading. The following sections will deal with the transfer of moisture in the form of water vapor diffusion and moist air migration.

2.2.2 Water vapor transport by diffusion

The transmission of water vapor through materials is governed by Fick's Law, which is expressed as:

$$g_v = -\delta \frac{\partial p_v}{\partial x} \quad [2.1]$$

where g_v is the mass transfer rate through the cross sectional area perpendicular to the flow path over unit time [$\text{ng}/\text{m}^2 \cdot \text{s}$],

δ is the water vapor permeability of the material [$\text{ng}/(\text{Pa} \cdot \text{s} \cdot \text{m})$],

p_v is the vapor pressure [Pa]

x is the distance along the flow path [m]

dp_v/dx is the vapor pressure gradient across the specimen [Pa/m].

For steady state conditions, this relationship is expressed as follows:

$$G_v = \delta A \frac{(p_1 - p_2)}{l} \quad [2.2]$$

where G_v is the total water vapor mass flow [ng/s],

A is the cross sectional area perpendicular to the flow path [m^2],

$p_1 - p_2$ is the water vapor pressure difference across the specimen [Pa],

l is the length of the flow path [m], and

δ is the average permeability of the material [$\text{ng}/(\text{Pa} \cdot \text{s} \cdot \text{m})$].

In reality, the water vapor permeability of a material varies with relative humidity (RH)

and moisture content of a material. Often, for simplicity, the average permeability is used.

When dealing with a material of a specified thickness, it is convenient to refer to the permeance of the material, M , where $M = \delta l$, in $\text{ng}/(\text{Pa}\cdot\text{s}\cdot\text{m}^2)$. The corresponding equation is:

$$G = MA\theta(p_2 - p_1) \quad [2.3]$$

2.2.3 Water vapor transport by convection

Air flow through a building envelope can carry a great deal more moisture across the envelope than diffusion alone (Salonvaara and Karagiozis, 1998; Kumaran, 1996a; Quirouette, 1985; Handegord, 1982). For example, the exfiltration of warm, moist indoor air in the heating season can cause an important deposition of moisture on cold surfaces within the envelope, which can lead to mold growth and decay. The lack of airtightness may lead to serious building envelope problems, especially in buildings that are humidified and pressurized by a mechanical ventilation system (Ogle and O'Connor, 1995).

2.2.4 Moisture transport by capillarity

The presence of liquid water in the building envelope can be the result of the formation of condensate at interfaces within the assembly, incidental rainwater penetration through envelope defects, contact with a pool of water or even the slower process of moisture accumulation within hygroscopic materials.

When liquid transport dominates at high moisture contents, capillary pressure is the driving potential for moisture movement. Capillary movement can transport tens of times more water within materials than diffusion in stones, brick and concrete (Krus and Holm, 1999).

From a mathematical point of view, capillary water transport can be expressed as follows (Krischer and Kast, 1978):

$$g_l = -D_w(w) \frac{dw}{dx} \quad [2.4]$$

where g_l is the liquid mass flow rate per unit area [$\text{kg}/\text{m}^2\text{s}$];

$D_w(w)$ is the liquid transport coefficient, also called the liquid diffusivity [m^2/s];

w is the moisture content per volume [kg/m^3], and;

x is the distance along the flow path [m].

It has been determined that the liquid transport coefficient is dependent upon moisture content, which complicates the solution of the above equation and the experimental determination of the liquid transport coefficient (Richards, 1992).

It has also been found that liquid transport varies depending on whether it is occurring in the wetting or the drying mode. Krischer and Kast (1978)'s model assumes a bundle of interconnected cylindrical capillaries of varying diameters where the equilibrium pressure of all filled capillaries at a given cross section is assumed. The negative pressure is determined by the suction pressure of the largest filled capillary in the cross section. If the water supply is cut off, fluid movement continues: the smaller pores which are not yet filled with water suck dry the larger pores through the cross connections by virtue of their greater suction power. However, this process is much slower than the earlier absorption process, and therefore it is necessary to use a different fluid transport coefficient to account for an absorption or a drying process (Krus and Holm, 1999).

2.2.5 Moisture in hygroscopic materials, the sorption isotherm and mold growth

As was discussed in the preceding sections, moisture migration in porous building materials can occur via several mechanisms including water vapor diffusion, convection and capillary transport. Such transport mechanisms can cause moisture storage and accumulation within hygroscopic materials like wood.

The relationship between the equilibrium moisture content of a material and the relative humidity at a specific temperature can be represented by a graph called a sorption isotherm, and is shown for wood, concrete and gypsum in Figure 2.1. When the relative humidity of the surrounds increases, the material gains moisture, a process called adsorption, and when the relative humidity decreases, the material loses moisture, called

desorption. The adsorption and desorption isotherm curves are not identical for most hygroscopic materials. The difference is called hysteresis. Two explanations for hysteresis are the presence of hydroxyl groups and lignin, below the fiber saturation point, and above the fiber saturation point, the ink-bottle effect (Kollmann and Côté, 1984).

Wood and other hygroscopic materials often change in dimension with changes in moisture content. The moisture content at which the cell walls of wood are saturated yet the cell cavities contain no free water is called the fiber saturation point (FSP) of wood, and occurs, as far as it can be determined, for most species at about 28% moisture content. The FSP represents the upper limit for vapor moisture gain from the air, as well as the upper limit of swelling (ASHRAE, 2001).

The maximum moisture content is reached when all the pores of a material are filled with water. This can only occur experimentally by maintaining the material in a vacuum, by boiling the material or by keeping the material in contact with water for many years. In practice, however, the maximum moisture content of materials is lower, and is referred to as the capillary moisture content (ASHRAE, 2001).

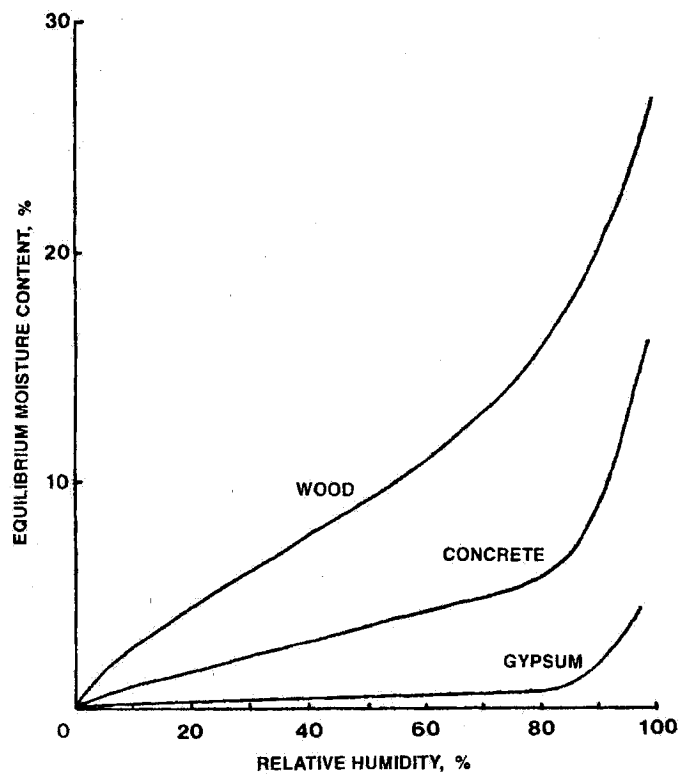


Figure 2.1. Typical sorption isotherms for wood, concrete and gypsum (hysteresis is ignored (ASHRAE, 2001)).

In residential buildings, hygroscopic materials such as wood framing members and plywood, OSB and fiberboard sheathing materials are vulnerable to mildew, mould and fungi growth when the temperature and moisture content conditions are favorable. For most wood-rotting fungi, the temperature for optimum growth lies between 25 and 30°C, although growth can occur at temperatures as low as 0°C, depending upon the specific species. On average, the optimum moisture content for fungal growth conditions lies between 35 and 50% (Viitanen, 1996). This finds the cell walls saturated with water and a layer of free water lining the cell cavities (Kollmann and Côté, 1984). Oxygen is also necessary for fungal growth and is typically readily available in building envelope applications. Favorable growth conditions can not only lead to decay of the wood components but also the production of toxic spores by mold fungi that may lead to poor indoor air quality and occupant health problems. Figure 2.2 graphically illustrates the temperature and relative humidity conditions required for mold growth based on measurements with wood.

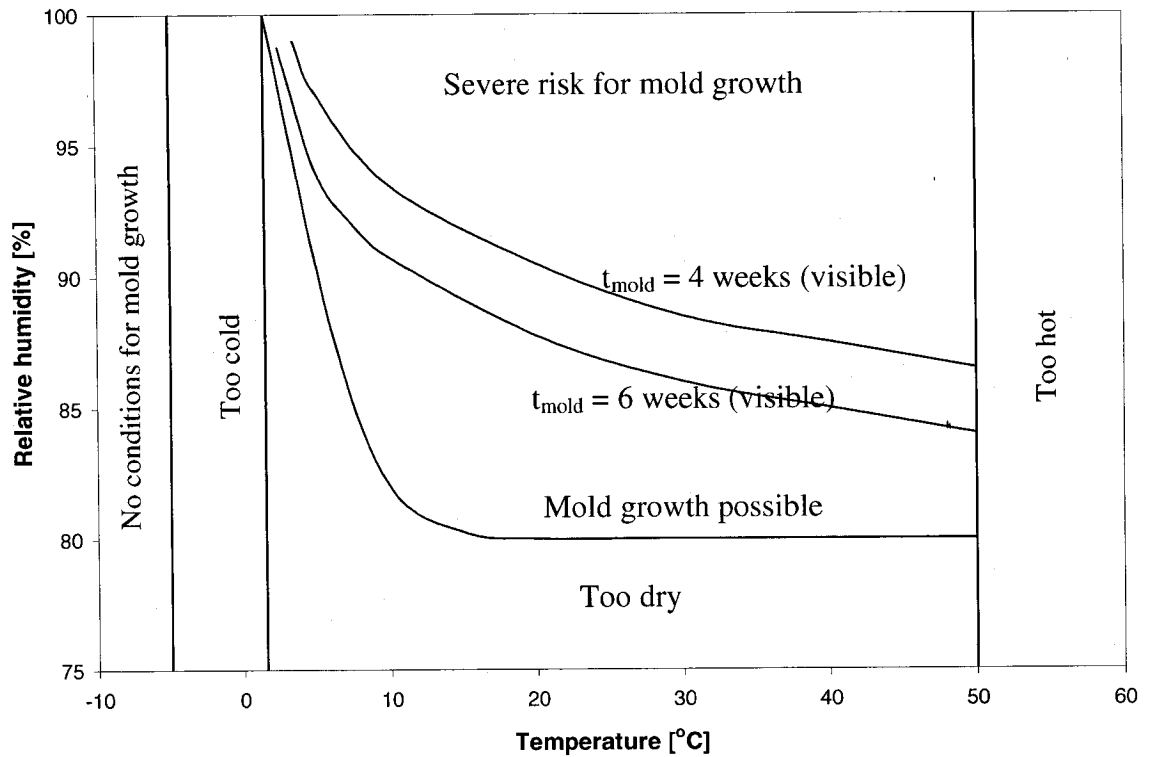


Figure 2.2. Conditions required for mold growth based on measurements with wood (as per Ojanen, 1998, taken from Viitanen, 1996).

Ideally, wood assembly components such as exterior sheathing should be maintained at conditions that prevent or minimize the risk of mould growth and decay. Many previous studies have been performed that study the role of exterior sheathing in the hygrothermal performance of wall assemblies, and these are discussed next.

2.3 Previous experimental works on the role of exterior sheathing in the hygrothermal performance of wall assemblies

Several studies have been conducted over the last decade that include the evaluation of the role of wall sheathings in the hygrothermal performance of wall assemblies. Several research teams, Salonvaara *et al.* (1998), Ojanen (1998) and Zarr *et al.* (1995), Lang *et al.* (1999) and Hazleden (2001) have conducted experiments to evaluate the role various sheathings. In addition, in a field study, Ricketts and Lovatt (1996) attempted to correlate the type of exterior sheathing with the performance of wall assemblies.

Both Salonvaara *et al.* (1998) and Lang *et al.* (1999) examined the performance of a wood-based sheathing and a non-wood sheathing. Salonvaara *et al.* conducted an experiment to study the hygrothermal performance of 12 different test panels including porous wood fiberboard, and dense mineral wool with a spun-bonded polyolefin air barrier membrane. Comparison of two walls built without framing which were identical except for the wall sheathing material showed that the moisture content of wood chips installed between the stud cavity insulation and the sheathing was lower for the wall with dense mineral wool board than for that with porous wood fiberboard. It was suggested that the lower moisture content in the mineral wool board wall was due to the lower vapor permeability of the mineral wool. Lang *et al.* (1999) performed a study comparing the drying performance of wood-frame and steel frame wall assemblies sheathed with plywood and gypsum board sheathing, respectively. While the findings show that the steel-framed wall performed marginally better than the wood-frame ones, the results were not conclusive for several reasons including different moisture loads for both types of test panels, the bottom track in the steel frame wall acting as a reservoir and limiting contact between the water and the gypsum sheathing, as well as possible measurement errors.

Ojanen (1998), Zarr *et al.* (1995) and Hazleden (2001) tested walls built with different types of wood sheathings. Ojanen (1998) performed an experiment including three test wall assemblies with different wood sheathings: plywood, OSB, and porous wood fiberboard. The panels consisted of, from the inside to the outside, glass fiber batt

or cellulose thermal insulation and a wood-based sheathing board, with or without mineral wool insulation installed on the exterior side of the sheathing. The walls were installed horizontally with the glass fiber or batt insulation at the bottom to facilitate one-dimensional heat and moisture transfer. The moisture source for each assembly was a 10 mm pool of water at bottom of a plastic box in which sat the thermal insulation.

Results show that the wall with the porous wood fiberboard experienced the highest moisture mass flow; next came the plywood, and then the OSB. The author suggests that the higher drying rates are due to the higher vapor permeability of the sheathing, as shown in the permeability curves in the figure below.

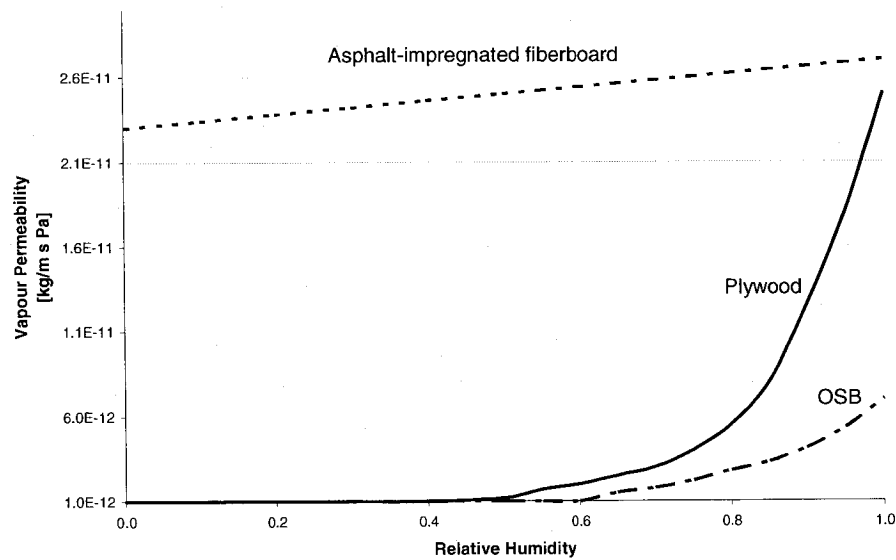


Figure 2.3. Permeability of plywood and oriented strand board as a function of relative humidity (plywood and OSB values are reported in Ojanen (1998), and asphalt-impregnated fiberboard are from Kumaran *et al.* (2002a)).

Zarr *et al.* (1995) performed an experiment that included two panels sheathed with fiberboard and plywood sheathing. Each panel was equipped with a 0.305 m diameter polycarbonate sleeve inserted around the metering area to ensure no transverse moisture movement. The panels consisted of unpainted gypsum board, glass fiber insulation, sheathing and sugar pine siding without a cavity air space behind the siding. Moisture content was measured on the interior and exterior surface of the sugar pine siding, and on the interior surface of the wood sheathing using the electrical resistance technique. The panels were subjected to a 42-day pre-conditioning period where the exterior temperature was kept steady at about 21°C, and then followed by 4 winter periods and a summer

period. The first winter period lasted only one day and was steady at 7.2°C, and was followed by a 6-day winter diurnal period where the temperature varied from about 0°C to 15°C. Then a 34-day steady winter period was performed where the exterior temperature was at about -3°C, which was followed by another diurnal period of 7 days with temperature conditions same as the first. The last period of the test was a summer drying where the exterior temperature was constant at about 33°C. The exterior relative humidity was kept low at 3 to 11% to minimize frost accumulation on the chamber's refrigeration coil. The indoor temperature and relative humidity were constant throughout the test at 21.2°C and 50%, respectively.

Figure 2.4 shows that for the panel with fiberboard sheathing, the moisture content reaches a maximum of approximately 13.5% on the inside surface of the fiberboard sheathing and 20% on the inside surface of the wood siding, which indicates that the moisture migrating from the warm, moist interior chamber to the colder exterior chamber likely condenses on the cold interface between the fiberboard sheathing and the sugar pine siding, and then quickly dries out when exposed to the summer conditions at day 48. The same wetting and drying general trends are observed in the plywood-sheathed assembly. Figure 2.5 shows that for the plywood-sheathed panel, the peak moisture content on the inside surface of the sheathing is somewhat higher than that for the fiberboard panel at about 15%. A more important difference is observed in the moisture content on the inside surface for sugar pine siding, which is only 8% for the plywood-sheathed assembly, compared to 20% for the fiberboard panel. Again, the moisture migrates from the warm, moist chamber to the exterior. However, the relatively lower water vapor permeability of the plywood sheathing compared to that of fiberboard tends to reduce the outward moisture drive, trapping moisture on the inside of the sheathing and reducing the moisture flux to the adjacent sugar pine siding, thereby decreasing the occurrence of interstitial condensation between these.

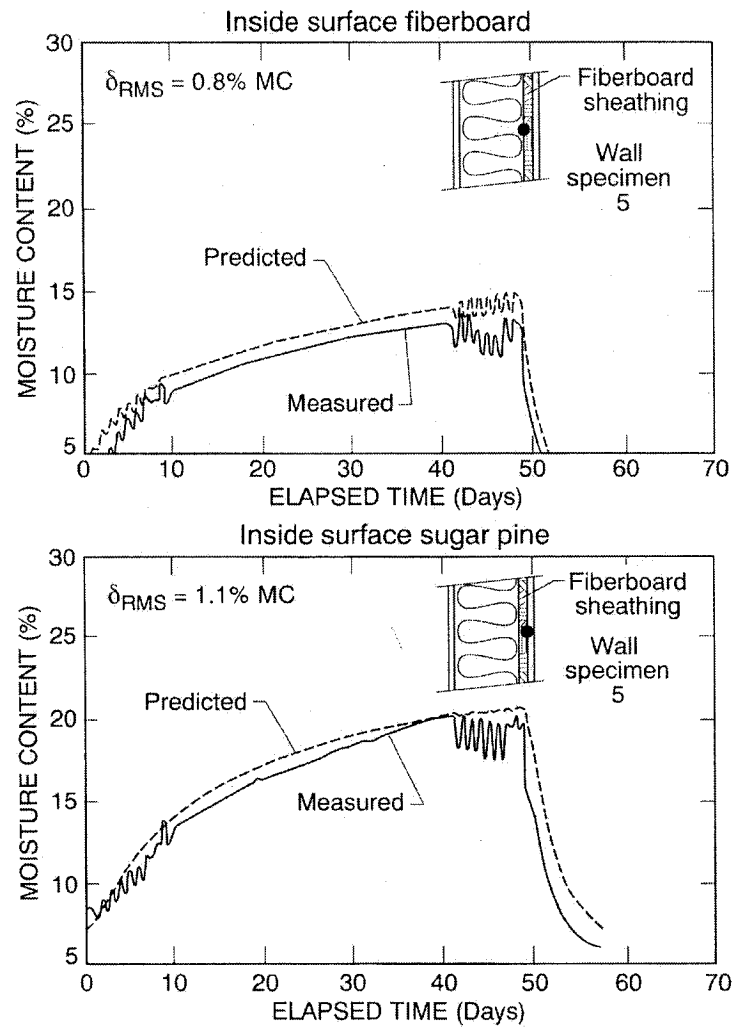


Figure 2.4. Measured and predicted moisture content of wall specimen 5 built with fiberboard sheathing (Zarr *et al.*, 1995).

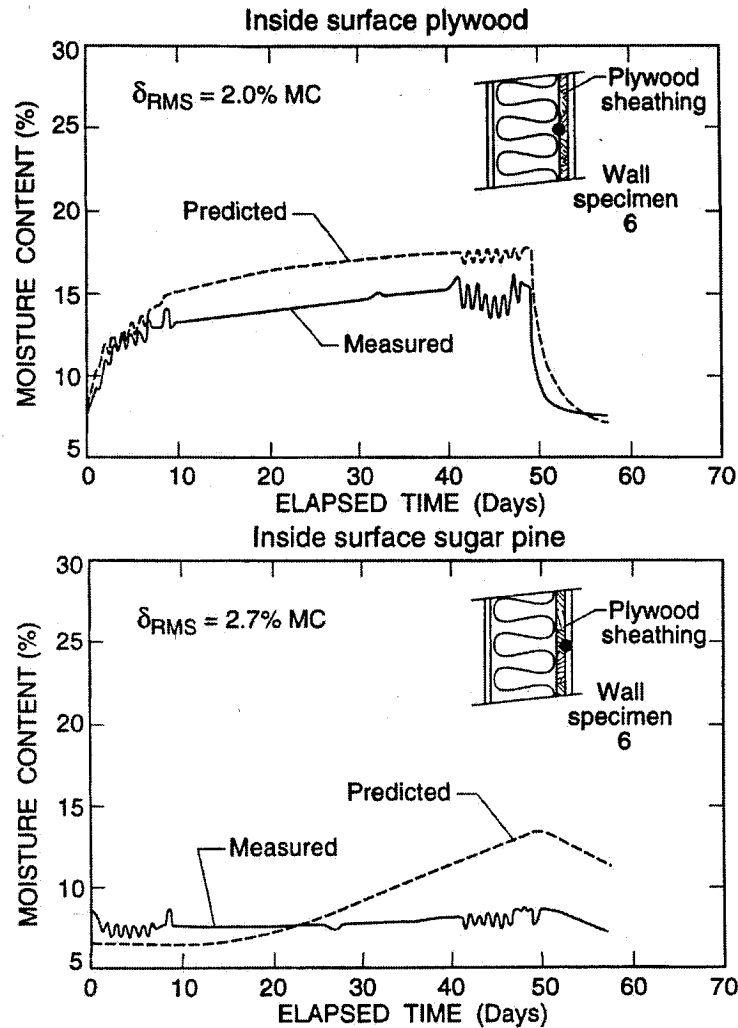


Figure 2.5. Measured and predicted moisture content of wall specimen 6 built with plywood sheathing (Zarr *et al.*, 1995).

Hazleden (2001) and Hazleden and Morris (2001) performed a large-scale experiment comprising two separate tests whose main objective was to evaluate the comparative drying rates of 12 different wall assemblies. Wetting of the wall panels was performed by placing the panels, devoid of insulation and interior sheathing, stud face down in a pool such that the water level was within 6 mm (test 1) and 18 mm (test 2) of the plywood or OSB sheathings to evenly wet the stud lumber for 10 days. The objective of the wetting procedure was to attain 25-30% moisture content in the studs and plates and 15 to 22% moisture content in the OSB and plywood sheathings. In the first test, actual initial moisture content measured varied between 21.6% and 38.5% in the wood framing, between 19.7% and 38.5% in the 9 OSB sheathing panels, and between 26.6% and 37.0%

in the three plywood sheathing panels, as measured by a hand-held electrical resistance moisture content meter (Hazleden, 2001). In both tests, panels were subjected to interior conditions of 20°C and an average of 40% RH and exterior conditions of 5°C and 70% RH. A continuous air flow of 0.86 to 4.62 m/s (at the diffuser) was applied on the cladding at a distance of 500 mm from the bottom of the panel, producing a pressure differential of 0.1 to 0.7 Pa at the bottom of the wall cladding with respect to the top, depending on the wall assembly. During the second test, the panels were subjected to heat-generating light sources providing an 8-hour solar cycle to achieve a combined ambient and sol air temperature of up to 15°C on the cladding surfaces. The drying for a panel, expressed as the percentage moisture loss, is determined as the mass of moisture lost in a panel at the end of the test relative to the mass of moisture gained during the initial wetting period. Results showed that despite the plywood-sheathed panels incurred higher moisture contents at the beginning of the drying phase, panels with plywood sheathing dried at a faster rate than comparable panels with OSB. For example, for stucco-clad panels without a venting cavity behind the stucco, the plywood-sheathed panel had a percentage moisture loss 2.7 times that of the OSB panel. For panels with a 19 mm bottom vented cavity behind the stucco cladding, plywood also had a more favorable percentage moisture loss, this time 1.8 times that of the OSB panel. For stucco-clad panels vented at the top and bottom, plywood's percentage moisture loss was essentially the same as that of OSB. It has been suggested that the differences in moisture performance were not the result of the panel design but rather the amount of water they had absorbed. However, Hazleden and Morris' (2001) analysis of the total panel moisture absorption and desorption shows that there was no correlation between moisture gained and the percentage moisture lost in both the plywood and OSB wall assemblies.

Another recent study that dealt with the hygrothermal performance of wood-based sheathing is the Moisture Management in Exterior Wall Systems project, or MEWS. The MEWS project was conducted by a consortium of researchers and members of the construction industry and executed by the National Research Council's Institute for Research in Construction (IRC) (Lacasse *et al.*, 2003; Mukhopadhyaya *et al.*, 2003; Bomberg *et al.*, 2002; Maref *et al.*, 2002a; Maref *et al.*, 2002b; Beaulieu *et al.*, 2002).

The goal of the study was primarily to predict, using the hygIRC heat, air and moisture numerical model, the hygrothermal performance of wall systems with various types of cladding that have been subjected to wetting due to simulated rainwater infiltration. Numerical testing was performed for seven different North American climates, simulating for each climate a “wet”, a “dry” and an “average” reference year. The boundary conditions, including temperature, relative humidity, horizontal rainfall, wind pressure and solar radiation for each climate were established using hourly weather data for each reference year. Horizontal rainfall is defined as the amount of rain falling on a horizontal plane, where the wind is undisturbed by building and other obstacles. The rates of water insertion were determined in a three-step process:

- 1) determine the moisture load imposed by a given climate using weather data;
- 2) determine the proportion of that load that can reach the face of the wall by utilizing Straube’s (2000) simplified driving rain prediction tool (which will be described in section 2.5.2.3), and;
- 3) for each cladding system, characterize the water loading directly into the stud cavity as a function of air pressure differential due to a given water leakage path at a through-the-wall penetration by performing water penetration tests using IRC’s Dynamic Test Wall Facility.

The MEWS project included several parametric analyses using hygIRC as the predicting tool to examine the role of various material properties on the drying response of the various types of walls. Of interest are analyses comparing the role of OSB, plywood and uncoated fiberboard in two different climates, Wilmington, North Carolina, and Ottawa, Ontario (Beaulieu *et al.*, 2002). The modeling analyses concluded that changing the type of wood sheathing had an insignificant effect on the overall moisture performance of the wall assembly.

Preliminary experimental qualitative and quantitative tests were performed to observe the water distribution and measure the water leakage from panels where such water was inserted. It was found that water introduced at the top of the panel under the top plate tends to accumulate at the bottom of the wall, with excess water leaking out through the interface between the bottom plate and the adjacent vertical sheets (Lacasse *et al.*, 2003). Beaulieu *et al.* state (2002) “flow of ‘free water’ on material surfaces” lies “outside the

current capabilities of hygIRC”. However, hygIRC has the ability to simulate injection of any quantity of moisture at any location of the wall at any time on an hourly basis (Mukhopadhyaya *et al.*, 2003). The modeling work reflects the conditions of the penetration tests by simulating wetting at a localized area at the top of bottom plate in stud cavity. Also in the validation tests, the wood framing was de-coupled from the OSB sheathing membrane by coating the wood-frame with a lacquer (Maref *et al.*, 2002b). Thus, the modeling does not simulate the presence of wood-frame studs and the moisture buffering effect caused by their moisture absorption and desorption.

Interpretation of the MEWS moisture content results, in units of mass of moisture per unit length (kg/m) of wall, is difficult because it does not allow comparison of the results with known risk thresholds, e.g. fiber saturation point, i.e. an average of 28% moisture content, for mold germination.

The Relative Humidity Temperature (RHT) index is a newly developed index proposed by the MEWS consortium that allows the comparison of the drying response of different walls. It is calculated as follows:

$$RHT(X) = \Sigma(RH - X) \cdot (T - 5) \quad [2.5]$$

where the summation indicates the number of hours where the location in the specimen is at, as per the first term bracket, at a relative humidity, RH, above $X = 95\%$ and, as per the second bracket, at a temperature, T, above 5°C (Beaulieu *et al.*, 2002). Given the hourly fluctuations in boundary conditions including rainfall, outdoor temperature, and relative humidity and the subsequent hygrothermal response of the building envelope, the data sampling interval of one hour, given its large value, may not give an accurate overall picture of the performance of the building envelope. The RHT index does not give an absolute measure of the moisture performance, i.e. the local moisture content and temperature, and is not sensitive to the level of moisture content and temperature to which the wood components are exposed. Therefore, the published MEWS results do not permit a determination of the true moisture content and the risk of moisture-related degradation of the wood components.

To summarize, the literature survey has shown that several studies have been performed to evaluate the wetting/drying performance of walls with various sheathings. Salonvaara *et al.* (1998) compare the drying potential of wall assemblies with one

permeable and one wood-based sheathing.

Ojanen's (1998) experiment, while documenting the relative effects of wood sheathing permeability on drying capacity, does not simulate actual conditions in the field because of the horizontal set-up of the wall panels and the fact that it does not consider the effects of convective flow within the wall cavity. Moreover, Ojanen's assemblies do not include any framing members and therefore do not reflect the moisture storage potential of wood studs. In addition, Ojanen's method of wetting the interior surface of the stud cavity insulation is not representative of actual field wetting.

The experimental work done by Zarr *et al.* (1995), while a major contribution for the validation of MOIST, has limited practical applications. First, the small scale of the test panels and the use of a plastic sleeve foster one-directional moisture transfer within the metering area of the test panels, which is not realistic. Second, the set-up of the panels excludes the moisture absorption capacity of wood framing members. Third, the external environmental conditions, which alternate between steady and diurnal, do not represent actual climatic conditions to which a true wall would be subjected.

Hazleden's work is one of the first that attempts to compare the drying rates of large-scale assemblies built with OSB and plywood sheathing. However, Hazleden recognizes that the wetting protocol undertaken does not simulate the wetting of walls in the field; also, the walls were subjected to steady state environmental conditions that are not representative of real weather data.

The results of the parametric analyses performed by the MEWS consortium to characterize the role of sheathing material properties offer a comparative examination for specimens that are wetted by simulated rain infiltration. However, the important limitations caused by the 2-dimensional domain of calculation and the determination of the material properties, including the assumption of perfect contact between materials, as well as the form of the results, do not permit an accurate assessment of local moisture content change with time, as well as local risks of moisture-induced degradation.

The studies above tend to demonstrate that the permeability of the sheathing influences the drying rate of the assembly. However, the limitations of the studies must be taken into account. For example, in many cases, the experimental environmental conditions created do not represent the cyclic temperature and relative humidity loads to

which actual wall assemblies are exposed to in the field. Many test assemblies do not include wood framing members, which, along with wood sheathing play a role in the overall moisture absorption/desorption of panels. In some cases, tests do not replicate three-dimensional heat, air and moisture transfer that exists in reality with wood-frame assemblies. In addition, wetting loads in most experimental works are mainly due to diffusive moisture flow, and those studies that consider water as a moisture source do not reflect field wetting conditions. Considering the limitations of previous studies, additional field and laboratory research is required to establish the appropriateness of these and other wall sheathings with respect to type of wall assembly, moisture loading and type of climate for design purposes. A summary of the above-mentioned works on the hygrothermal performance of wood exterior sheathings is presented in the table below.

Table 2.1. Summary of work done on hygrothermal performance of wall panels constructed with various types of exterior sheathings.

| Research team | Exterior sheathings tested | Panel size and types | Environmental boundary conditions – warm side | Environmental boundary conditions – cold side | Limitations |
|---------------------------------|--|----------------------|---|--|---|
| Laboratory Studies | | | | | |
| Salonvaara <i>et al.</i> (1998) | Porous wood fiberboard, dense mineral wool with SBPO | 0.46 x 1.73 m | 20°C Winter: 25%RH, spring: 50% RH | Winter: -10°C (75 days), spring: 5°C (40 days); approx. 60% RH | Only 2 sheathings compared, one wood-based, one not; frameless assemblies: hygrothermal effect of wood studs not considered |
| Ojanen (1998) | Plywood, OSB, porous wood fiberboard | 0.4 x 0.32 m | 22°C | -10°C (32 days), -5°C (29 days), +3°C (30 days) | Frameless assemblies installed horizontally; one-dimensional heat and |

| | | | | | |
|---------------------------|--------------------------|--------------------------------|--------------------|--|---|
| | | | | | moisture transfer; convective effects not considered |
| Zarr <i>et al.</i> (1995) | Plywood, wood fiberboard | 0.305 m diameter metering area | 21.2°C, 50% RH | 2 steady winter periods at 7.2°C alternating with 2 sinusoidal winter periods ranging from 1.1 to 15.6°C, followed by a steady summer period at 32°C | Frameless assemblies; temperature in winter periods do not reach freezing levels; polycarbonate sleeve framing around metering area limits moisture transfer to one-dimension |
| Hazleden (2001) | Plywood, OSB | 1.22 x 2.44 m | 20°C, 30% - 50% RH | 5°C, 70% RH | Wetting method and environmental conditions do not reflect field conditions |

All of the previously mentioned works, except for Ricketts and Lovatt's field study, have studied the performance of the exterior sheathing under controlled laboratory conditions. Various sources of moisture were used in these and other tests, including a pool of water to generate a vapor differential vapor pressure (Ojanen, 1998), and vapor transport through infiltrating or exfiltrating air (Desmarais *et al.*, 1998). A summary of these methods is found in Table 2.3 in section 2.4.2. However, wetting of the building envelope due to liquid moisture often occurs in the field due to infiltration of rain water. The EDRA project (Hazleden, 2001; Hazleden and Morris, 2001) involved impregnating materials in a water bath to set an initial moisture content. On the other hand, the 1999 study by Lang *et al.* introduced water through a perforated pipe directly into the stud cavity. This method of rain infiltration simulation as well as other previously established wetting methods are discussed in the following section.

2.4 Previously established experimental rain simulation and wetting methodologies

Rain can be a significant source of moisture within the building envelope if it penetrates at defects located on the cladding. Moisture can accumulate in hygroscopic materials such as wood and can cause the onset of decay and also potentially compromise the function of the material if conditions of temperature and time are appropriate. Steel members such as studs are also vulnerable to moisture as they are susceptible to corrosion. The potential for moisture-induced degradation of wood-based building components such as framing and sheathing has been catastrophically evidenced in the large number of residential building envelope failures in homes built between 1983 and 1997 in the lower mainland of British Columbia (Culyer and Edgar, 1998). An enquiry into the causes of the failures was conducted by the Barrett Commission (Barrett, 1998) and found that the climate of that region, characterized by mild weather and significant rainfall fostered conditions that increase the likelihood of water ingress and deterioration. The reconstruction bill to repair the damage to building construction due to accumulated rainwater leakage and other causes is estimated to cost up to \$1 billion.

To understand rainwater ingress, it is not only important to know how much water runs off a building façade, but where it is likely to penetrate. Today, most walls are designed and built using the rainscreen principle, which assumes that some rainwater will likely penetrate the cladding. Therefore, the wall is constructed such that the moisture entering into the space behind the cladding will be able to drain out via the drainage plane, flashing membranes and weep holes, for example. However, poor detail design, faulty workmanship and, sometimes, lack of adequate maintenance can result in envelope defects that allow water to infiltrate into wall assemblies. For example, water leakage in windows can be attributed to many causes such as poorly designed windows, the formation of cracks and fissures due to poor joint detailing that does not allow for structural movement, thermal stresses, and sealants that deteriorate over time. Building envelope consultants and researchers have documented many cases of rainwater leakage (Marsh, 1977; Addleson, 1972; Beers and Smith, 1998; Lies and Faith, 1998, Zwayer *et al.*, 1998) and all agree that envelope junctions, rather than the wall fabric itself, are responsible for rain water penetration. Ricketts and Lovatt (1996) conducted a study of

37 problematic and 9 control low-rise wood-frame residential buildings in the coastal climate of the British Columbia lower mainland. The survey found that rainwater ingress occurred at interface details, primarily at window details as well as deck perimeters, balconies and walkways. Because glazing is impervious to water, windows collect water at their sills. Beers and Smith (1998), glazing consultants, have witnessed and reported that many cases of wetting of the inner wall are due to punctured window sill flashing and defective corner window miter joints, for example. Lies and Faith (1998) explain that improper integration of flashing or altogether absence of flashing also lead to water leakage in buildings. These instances of water leakage show that rain leakage into the stud cavity behind the exterior sheathing, i.e. the back wall, do occur in reality and can pose a serious threat to the integrity of the building envelope.

Studies dealing with the rain infiltration of building envelopes have been performed using several methods, some simple and some more complex, to simulate wet conditions on the exterior surface and within wall assemblies. Experiments tend to either use a spray rack or similar apparatus to simulate water impinging on a building façade or to simply introduce water directly into the test panel. In the following sections, methods to simulate rain impinging onto a building surface are first discussed, followed by wetting methods by direct insertion of water into assemblies.

2.4.1 Methods simulating rain impinging onto building surface

Methods which spray water onto the exterior surface of a façade, or a portion thereof, are usually used to test building envelope junctions or entire envelope systems for water leakage defects. Svendsen (1955) reports on methodologies developed in the late 1940's to simulate wind-driven rain. In the Netherlands, a method conceived by Ratiobouw in 1947 involved projecting water in thin streams at a high rate of $700 \text{ l/m}^2\text{h}$ from a perforated container such that the entire 1.0 m^2 test panel surface was covered. Similarly, testing performed at the Building Research Station in England utilized six atomizers mounted so that the $1.25 \times 2.50 \text{ m}$ panels erected side by side were somewhat uniformly sprayed at a rate of 85 l/h . Both of these experiments lasted less than 8 hours and involved evaluating the rain penetration resistance of the test panels.

Schematics of an experimental set-up devised by Holmgren in Norway to study the tightness of wall panels are shown in Figure 2.6 (Svendsen, 1955). The test panel is installed such that its exterior side faces the inside of the chamber. From a trough on the roof, and parallel to the test panel, wicks conduct water onto a perforated pipe. A stream of air passes through the perforations and drives the water drops with high velocity against the test panel. The water drops can be distributed over the entire test panel by rotating the perforated pipe, and the water rate can be controlled. The fan, which feeds the air into the pipe, also pressurizes the chamber. Two methods are used: a standard method that lasts 192 hours, and a more severe 46-hour accelerated test.⁶ Both methods include a water delivery rate of 8 l/m²h. In the standard test, wetting periods are alternated with drying periods, and a positive pressure of 50 mm of water is maintained in the chamber. However, the accelerated test involves a 5-hour wetting period, a 5-hour drying period, followed by a 36 hour wetting period, all the while maintaining a positive 75 mm water pressure (736 Pa) within the chamber.

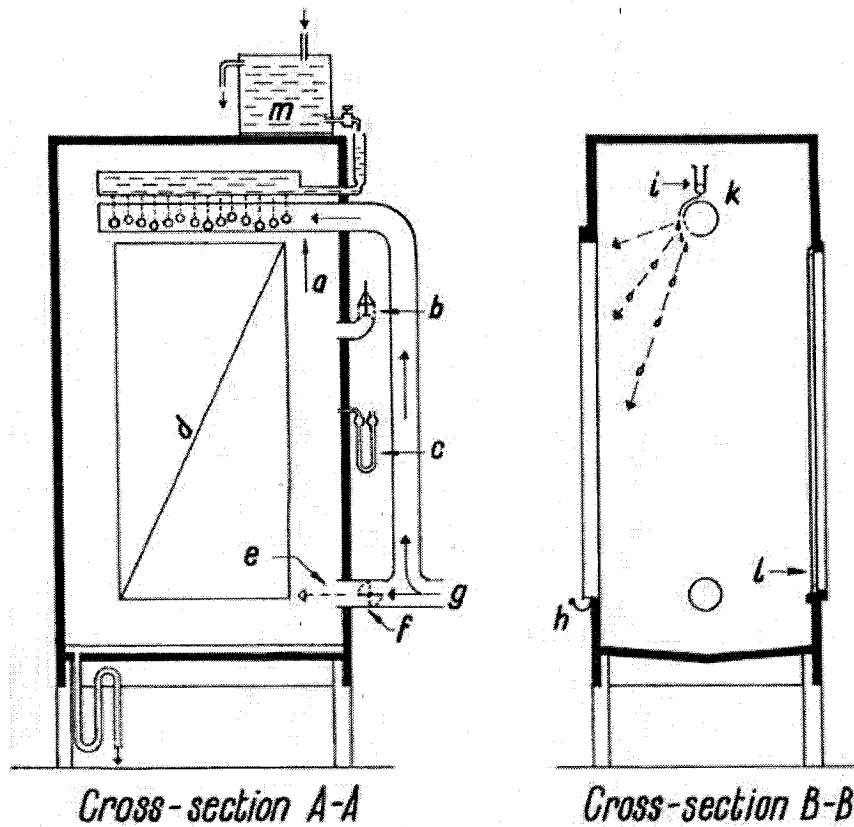


Fig. 7:
Principle of the rain test apparatus

- a. Injection of air for artificial driving rain.
- b. Automatic pressure valve.
- c. Manometer.
- d. Test panel, 61.5 x 126.5 cm.
- e. Injection of air for super-pressure.
- f. Damper.
- g. Fan.
- h. Collecting trough for penetrated water.
- i. Water trough.
- k. Wicks lead the water a-fore the air holes.
- l. Window.
- m. Water.

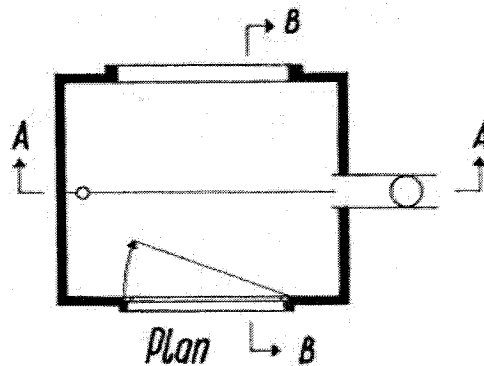


Figure 2.6. Principle of Holmgren's testing apparatus (Svendsen, 1955).

Another methodology to simulate wind-driven rain was developed by Tsongas *et al.* (1998) where the objectives included establishing the occurrence of upward wicking between horizontal lap siding boards for 2.4 x 2.4 m test walls. In these seven-day tests,

water was sprayed onto a wall once a day for 15 minutes at a rate of 0.147 m³/s (0.14 gpm) from each of two low-flow irrigation-type spray heads. The point of interest of this wetting protocol is the selection of the rate of water spray. The amount of water was chosen such that:

- 1) the highest amount of rain for a one-month period in the previous 40 years in January according to the American National Climatic Center data;
- 2) an average January wind speed of 14.5 km/h (4.0 m/s);
- 3) a raindrop terminal velocity of 145 km/h (40.3 m/s);
- 4) a maximum 1/3 of the rain hitting any given wall orientation;
- 5) an accumulation of rain at the bottom course of siding of a 9.1 m three-story wall.

The amount of water, calculated using available weather data, was assumed to be the worse case amount to spray on a wall. The authors make no mention of the temperature and relative humidity conditions or of any pressure differential generated across the test walls.

The National Research Council of Canada has also developed a rain simulation testing apparatus called the Dynamic Wall Test Facility. The apparatus includes a water spray system that simulates wind-driven rain as well as an air blower and an electronically-controlled hydraulic piston, which create a combination of static and variable pressures (Poirier, 1993). The wetting and drying performance of direct-applied exterior finish systems (DEFS) and exterior insulation and finish systems (EIFS) has been tested using the facility, with the specimens subjected to water spray and various static and dynamic air pressure differentials. While the exact set-up of the water-spraying apparatus is not explained, water was sprayed on the exterior of the specimens at a rate of 4.2 l/min·m² (Brown *et al.*, 1997). The facility has also been used in the large-scale project called MEWS mentioned above, to evaluate the rain penetration of seventeen different types of wall assemblies including face seal and rain screen EIFS, stucco, masonry, and siding-clad walls. The walls were constructed with window junctions, HVAC duct and electrical penetrations and exposed to two spray rates, 1.7 l/m²s and 3.4 l/m²s. Static and dynamic pressure differentials were used as shown in Table 2.2, where the frequency of the dynamic tests was 0.5 Hz; the pressures were determined from the literature and climate data (Cornick *et al.*, 2002; Lacasse *et al.*, 2003). The results of the

study provide measurements of quantities of water penetrating into the assemblies for various defect types for each of the seventeen types of wall systems. The study's results serve as an input of hourly data for the hygIRC heat, air and moisture numerical simulations (Beaulieu *et al*, 2002). Application of this methodology is ideal for modeling simulations because the results of the water penetration tests, in combination with hourly precipitation, wind speed and wind direction data obtained from climatological stations, can be input into a software such as hygIRC to establish the boundary conditions.

Table 2.2. Static and dynamic pressures for the water entry tests for wall assemblies with intentional deficiencies. In the table, *f* is the frequency and *t* is the time (Lacasse *et al.*, 2003)

| Static Test Conditions | | |
|-------------------------|--|---------------------|
| Step | Nominal spray rate [l/m ² ·s] | Pressure [Pa] |
| 1 | 1.7 | 0 |
| 2 | | 300 |
| 3 | | 150 |
| 4 | | 75 |
| 5 | 3.4 | 75 |
| 6 | | 150 |
| 7 | | 300 |
| Dynamic Test Conditions | | |
| Step | Nominal spray rate [l/m ² ·s] | Pressure [Pa] |
| 1 | 1.7 | 0 |
| 2 | | 75 + 40 sin(2π f t) |
| 3 | | 150 + 60 sin(2πft) |
| 4 | | 300 + 125 sin(2πft) |
| 5 | 3.4 | 75 + 40sin(2πft) |
| 6 | | 150 + 60sin(2πft) |
| 7 | | 300 + 125 sin(2πft) |

Sto Corporation has also been involved in experimental work to study the performance of EIFS-type walls. Sto Corp. built a three-story structure at Warnock Hersey in Vancouver, B.C., to evaluate the performance of 41 EIFS details. The structure was exposed to a static pressure difference up to 1 kPa and dynamic winds generated by a DC3 airplane engine producing winds of 120 km/h and a simulated rainfall of 200 mm/h, as shown in Figure 2.7 (Edgar, 1998).

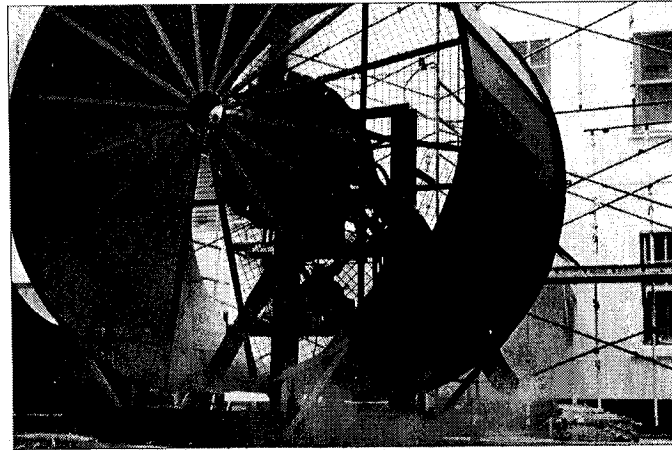


Figure 2.7. EIFS detail testing at Warnock Hersey, Vancouver, using a DC3 airplane engine (Edgar, 1998).

The methods described above all consists of subjecting a wall to some kind of water spray, and range from quite complex, where a dynamic or static pressure differential is applied across the envelope, to very simple, such as running water down a surface until the desired degree of wetting is achieved. For example, in their study evaluating the drying effectiveness of cavity ventilation, Hens and Fatin (1995) simulated wetting of the outer wythe of a masonry cavity wall by trickling water from a sparge pipe down the outer leaf until capillary saturation was reached. Whiteside *et al.* (1980) and Newman *et al.* (1982) also used a sparge pipe to simulate rain in an effort to test water penetration through masonry cavity walls with and without insulation within the cavity. These methods of introducing water on the surface of the envelope are usually used to determine the water penetration resistance of factory-built units such as window or installed units in-situ. For this purpose, several standard test methods exist and typically specify that the test can be performed with or without a static or dynamic air pressure difference. Examples of such standards are the CAN/CSA-A440-00 Windows (CAN/CSA, 2000), which rates windows for water tightness, ASTM E331-00 Standard Test Method for Water Penetration of Exterior Windows, Curtain Walls, and Doors by Uniform Static Air Pressure Difference (ASTM, 2000a), ASTM E547-00 (ASTM, 2000b) for static air pressure difference, NT BUILD 116 Windows, Window-doors, External Doors, Facades: Pulsating Air Pressure Test (Nordic Innovation Center, 1980), and DIN EN 1027 Windows and doors - Watertightness - test method (DIN, 2000).

Rain penetration tests are not, however, designed to control the amount of water that

penetrates into the building assembly. In experiments where the drying rate will be evaluated as a function of the amount of moisture load, the most suitable way to experimentally simulate wetting due to rain is to insert water directly into the wall assembly. Previous investigations that have done so are discussed next.

2.4.2 Wetting methods by direct insertion of water into assemblies

Several researchers have introduced water into exterior wall and roof assemblies as a wetting method. The simplest of the methods was one performed by Segerholm (2005) to study the influence of construction moisture on wood-frame systems, and in particular how the stud and bottom plate affect each other under wetting and drying processes, how the moisture barrier under the bottom plate influences the drying behavior of the latter, and the importance of nails in water penetration. Segerholm made use of a simple spruce stud-bottom plate assembly (see the figure below) which was wetted for 6 minutes/ hour for a total duration of 24, 48 or 96 hours, and the subsequently dried under indoor ambient conditions. The bottom plate-stud assembly was wetted by dripping water from a fine aluminum mesh mounted approximately 1 meter above the floor. This wetting method resulted in a simulated rain that was measured to be between 2 and 6 mm/h.

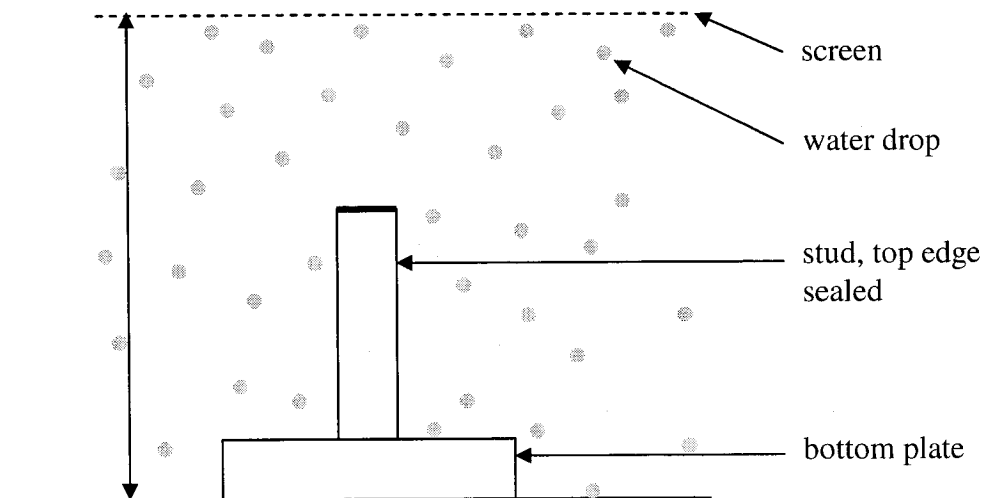


Figure 2.8. Schematic picture of a stud/bottom plate element (from Segerholm, 2005)

Several other researchers have introduced water into exterior wall and roof

assemblies as a wetting method. For example, research was undertaken by Lang *et al.* (1999) for the Envelope Drying Rates Analysis Consortium (EDRA) to examine the drying potential of stucco-clad walls involved wetting the envelope. In this particular instance, a preliminary test was performed on three wall panels to develop an understanding of the instrumentation being used and to assess the method of introducing moisture into the specimens. It was decided to increase the moisture content of the wood members within the stud cavity to 20% by weight before the drying period began, and therefore given that the specimens contained approximately 41 kg of wood, then 8.2 kg (or 8.2 l) of water was added. Once the preliminary test was concluded, however, it was resolved that only half this quantity of water should be added during the main experiment because very little moisture migrated to the upper half of the sample panels. Water was injected through an 8 mm interior diameter clear vinyl tubing with 1.6 mm holes drilled at intervals of 13 mm. The tubing was covered with an ABS pipe split in half lengthwise to direct the water onto the interior surface of the exterior sheathing and prevent backsplash, as shown in the diagram below. For the main experiment, the 4 l of water was introduced at a rate of 1 l per day for the wood-framed test walls. It was observed, however, that an undetermined quantity of water flowed out of some of the specimens.

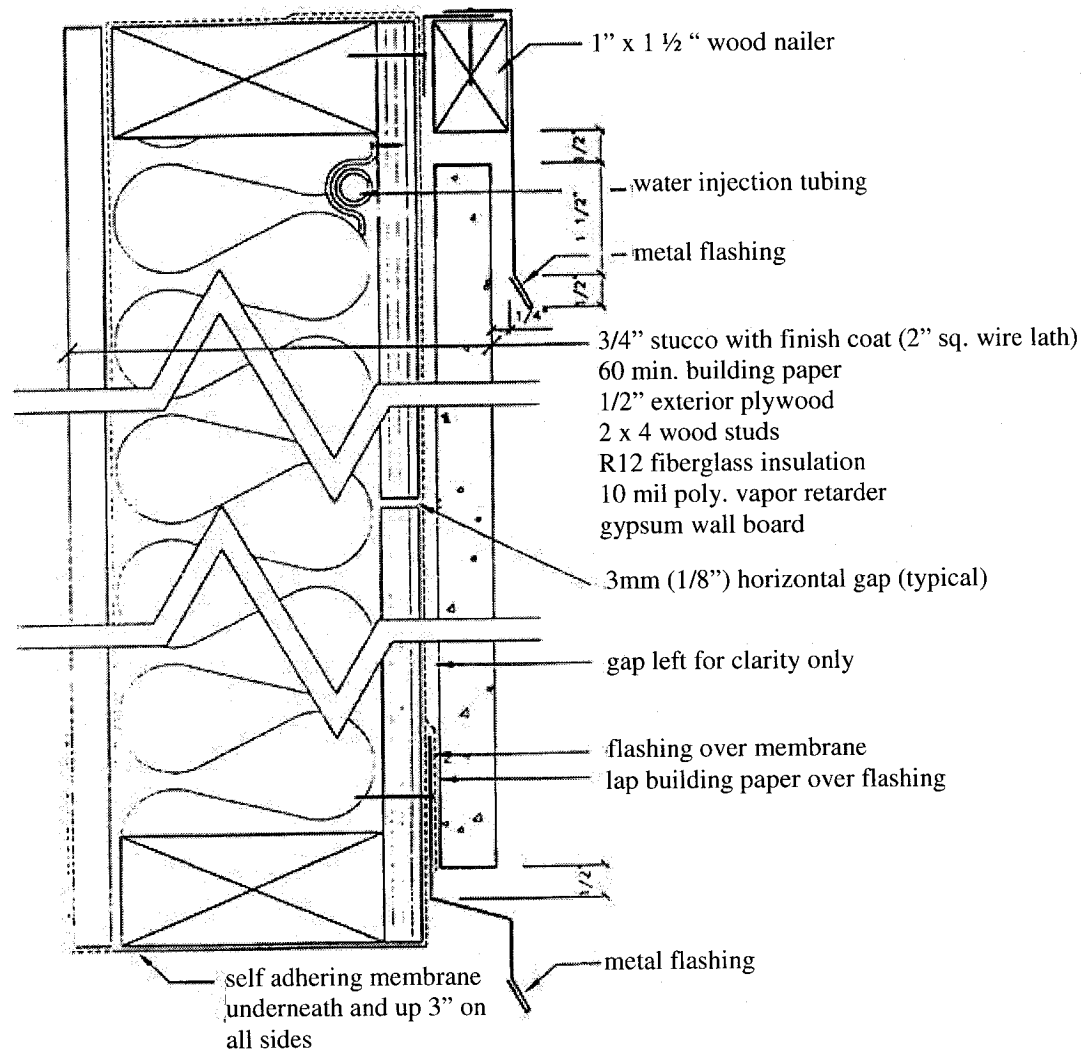


Figure 2.9. Stucco wall drying experiment. Test panel showing placement of water injection tubing (Lang *et al.*, 1999).

Tsongas *et al.* (1998) performed two experimental methodologies to introduce water between the siding and the building paper. These methodologies are the only ones found in the literature that involve a point source. The objective of both methods involved observing the extent of lateral migration of the water behind the siding. In the first method, water was inserted once at a rate of 2.1 ml/s (2 gpm) for a total of 28.4 l (7.5 gallons), and the wall was opened up after 24 hours. This amount corresponded to the amount of rainwater that was estimated to enter walls at leaks at the intersection of the siding and the concrete entryway landing. The rate was based on an assumption 76 mm (3 in.) of the rain falling upon the landing with a given size and slope over a 3-day period.

The second method involved a four-week test where the amount of water was introduced in a manner that was felt to be typical of a water leak over a month in the rainy season. Water was introduced between the siding and the building paper system through 6.4 mm (0.25 in.) diameter piece of flattened soft copper tubing at a rate of 0.03 l/min (1.0 ounce/min) for 12 hours/day for 2 days, then 0.03 l/min (1.0 ounce/min) for 2 hours every 12 hours for 2 days, and finally for one hour a day at a rate of 1.9 l/day (1.0 ounce/day) for 24 days. Some of the water drained out of the walls and was caught in a collection basin before being pumped to a drain.

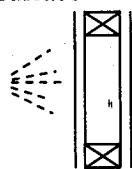
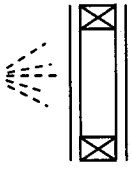
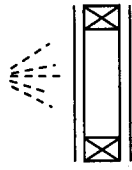
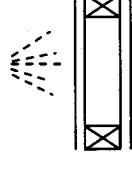
A simpler way of simulating rain penetration into envelope assemblies is to pour water directly into the panel. For instance, the wetting methodologies for low-slope roof assemblies of Desjarlais *et al.* (1993) and Korsgaard and Rode (1992) involved introducing 1 kg (1 l) of water to a sheet of blotting paper which was placed in the test assembly to improve the lateral dispersion of water. Desjarlais *et al.* (1998) wetted roof assemblies in a similar fashion, but the moisture added there varied from 2.9 to 4.4 kg. A comparable wetting procedure can be applied to walls, as was done by Onysko and Jones (1989): the test wall panel, devoid of exterior cladding, was placed horizontally face down in a 6 mm deep pool of water to simulate a condition where condensation led to a complete wetting of the waferboard sheathing. The sheathing was allowed to soak up the water overnight, with a plastic tarp placed over the entire assembly to prevent water from evaporating into the space above. The wetting method in the EDRA study (Hazleden, 2001; Hazleden and Morris, 2001) was similar, where wall assemblies devoid of interior sheathing and stud cavity insulation were placed in a shallow tank of water such that the stud side faced down and the water level did not reach the sheathing. A slightly more elaborate scheme was adopted by Schumacher *et al.* (2003), whose wetting system included 15 double sheets of a thick highly adsorptive paper installed inside of a high density fiberboard sheathing panel. The absorptive sheets are laid in an array 3 sheets wide by 5 sheets high. One side of each double sheet is stapled to the fiberboard sheathing, and the double sheet is fed by a small diameter tube which is fitted between the sheets. Wetting of the panel was achieved by introducing a total of 1350 g (1.35 l) of water through the water injection tube; the wetting was done in three doses of 450 g (0.35 l) each at 4-hour intervals to ensure there was no water leakage and even wetting of the

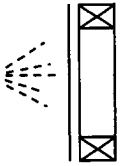
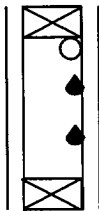
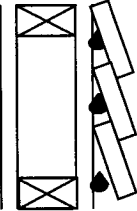
sheathing. A similar approach was used by Straube *et al.* (2004) in an ASHRAE-sponsored field study, but in this instance the wetting was performed three times in two series of walls, each series being tested for approximately seven to eight months. This experimental work was used to validate MOISTURE-EXPERT, an advanced hygrothermal building envelope model (Karagiozis, 2004b).

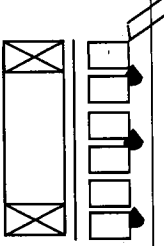
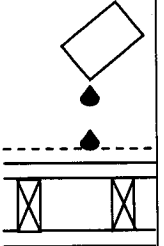
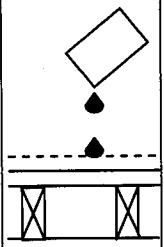
Ojanen (1998) used a different approach to simulate wetting of the envelope. His experiment consisted of wall assemblies without framing members mounted horizontally in a box where the top of the assembly is exposed to cold environment. 10 mm of free water was poured in the bottom of the box to simulate an initial moisture load in the plywood sheathing layer. The testing setup was done in this manner to facilitate the construction of a one-dimensional temperature and moisture transfer computer model, which was validated by the experimental data.

The laboratory wetting methodologies from the above-mentioned researchers are summarized in the table below. The table describes the rate of water insertion, the method of application, and the frequency and duration of wetting. As well, for the direct water insertion methods, Table 2.4 highlights the geometry of the wetting pattern, examples from literature, capacity to control patterns and moisture content, surface from which water evaporates, analysis of experimental data, data that can be used in simulation, as well as advantages and limitations.

Table 2.3. Comparison of various laboratory methods for wetting of envelope assemblies.

| Research Team, Origin | Rate of water insertion (original units) | Rate of water insertion [ℓ/m^2h] or [ℓ/h] or [ℓ/m^2] | Method of application | Frequency / duration of wetting | Location of wetting within assembly | Additional notes |
|--|--|---|---|---|---|---|
| Water Sprayed on the surface of the Assembly | | | | | | |
| Ratiobouw, the Netherlands (reported in Svendsen, 1955) | 700 ℓ/m^2h | 700 ℓ/m^2h | Projected in thin streams from perforated container | No information / less than 8 hours | Exterior surface  | Test panels 1.0 m^2 ; test performed to evaluate rain penetration resistance |
| Building Research Station, UK (reported in Svendsen, 1955) | 85 ℓ/h | 27.2 $\ell/m^2 \cdot h$ | Rack of 6 atomizers | No information / less than 8 hours | Exterior surface  | 1.25 x 2.50 m test panels; test performed to evaluate rain penetration resistance |
| Holmgren, Norway (reported in Svendsen, 1955) | 8 $\ell/m^2 \cdot h$ | 8 $\ell/m^2 \cdot h$ | Spray from pipe at top of assembly | Standard test: total of 192 hours of alternating wetting and drying periods | Exterior surface  | 0.615 x 1.265 m test panel; 50 mm water pressure maintained on exterior surface |
| Tsongas <i>et al.</i> (1998) U.S.A. | 0.147 ℓ/min | 0.18 $\ell/m^2 \cdot h$ | 2 spray heads, each covering 0.76 m diameter circular area, each at 1/3 width point at very top of wall | 15 min/day for 7 days | Exterior surface  | 2.4 x 2.4 m test wall |

| | | | | | | |
|--|---|--|--|--------|--|---|
| Brown <i>et al.</i> , (1997) Canada | 4.2 l/m ² ·min | 252 l/m ² ·h | Spray rack | - | Exterior surface  | Up to 2.4 x 2.4 m test panels; variable static and dynamic air pressure can be maintained |
| Water Inserted in the Assembly | | | | | | |
| Lang <i>et al.</i> (1999) Canada | 1 l/day (linear source) | 0.0417 l/h (linear source), or 0.014 l/m ² ·h | Spray from perforated pipe at the top of stud space | 4 days | Interior surface of exterior sheathing  | 1.22 m wide x 2.43 m high walls containing 3 stud spaces; undetermin ed quantity of water leaked out of specimens |
| Tsongas <i>et al.</i> (1998) U.S.A. | Method 1: 28.4 l /3.75 h Method 2: 0.53 ml/s for 12 hours/day for 2 days, 0.53 ml/s for 2 hours every 12 hours for 2 days, 1.9 l/h for 1 hour /day for 24 days (point source) | Method 1: 0.88 l/m ² h Method 2: 0.22 l/m ² ·h for 12 hours/day for 2 days, 0.22 l/m ² ·h for 2 hours every 12 hours for 2 days, 0.22 l/m ² ·h for 1 hour/day for 24 days (point source) | Irrigation drip system with electronic timer control, through 0.25 in. diameter piece of soft copper tubing | - | top left- hand corner of assembly, between siding and building paper  | 2.4 m high x 3.6 m wide test walls |

| | | | | | | |
|---|--------------|---------------------------------------|--|---|---|---|
| Hens and Fatin (1995) Belgium | Unknown rate | Unknown rate | Trickling water from a sparge pipe | - / Until capillary saturation of masonry is attained | Outer surface of masonry wall  | - |
| Desjarlais <i>et al.</i> (1993) U.S.A. and Denmark | 1 kg | 0.826 l/m ² (initial load) | Water placed on blotting paper to improve lateral dispersion | - | On both sides of plywood roof Sheathing  | 1.1 x 1.1 m low-slope roof assemblies |
| Korsgaard and Rode (1992) Denmark | 1 kg | 7.143 l/m ² (initial load) | Water placed on blotting paper to improve lateral dispersion | - | On interior surface of plywood roof deck or above insulation  | 0.40 x 0.35 m low-slope test roof panel |

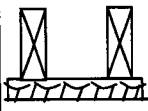

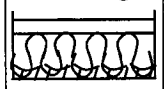
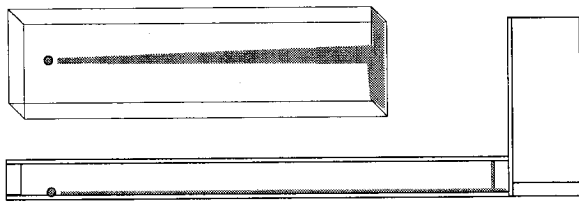
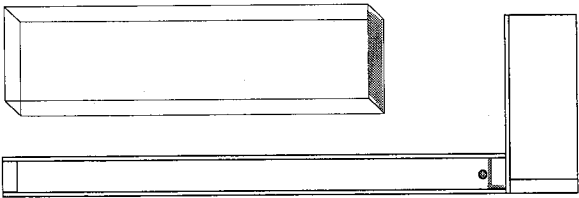
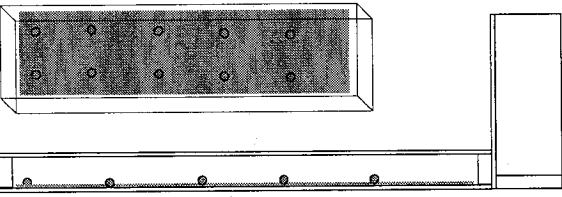
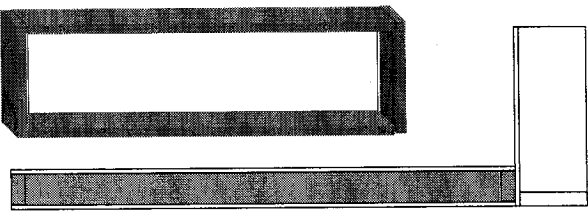
| | | | | | | |
|--------------------------------|---|---|---|-----------------------------------|--|---|
| Onysko and Jones (1989) Canada | | - | Waferboard sheathing placed face down in cell containing 6 mm of water | No information / approx. 12 hours | Exterior sheathing  | 2.4 x 3.0 m test wall panels |
| Hazleden (2001) Canada | 32 mm or 19 mm of water placed in bottom of box | - | Wood-frame wall devoid of sheathing and insulation placed stud-side down in shallow tank of water | 10 day | Wood studs (by water absorption) and sheathing (by capillarity and diffusion)  | 1.22 x 2.44 m test wall panels |
| Ojanen (1998) Finland | 10 mm of water placed in bottom of box | - | Absorption of water vapor by diffusion | - | Interior surface of sheathing  | 0.4 x 0.32 m wall sections installed horizontally |

Table 2.4. Comparison of direct water insertion methods to recreate moisture distribution patterns.

| Wetting following a schedule | | | | |
|------------------------------|---|--|--|---|
| | Patterns very close to reality (?) | Controlled patterns | Uniform water distribution | Immersion of panels |
| Geometry |  |  |  |  |
| Literature examples | <p>Lang <i>et al.</i> (1999) – use of linear rather than point load</p> <p>Variations</p> <p>Tsongas <i>et al.</i> (1998) – point load inserted between the siding and the building paper</p> | | <p>Schumacher <i>et al.</i> 2003 (Burnett/ASHRAE project) but behavior of sheathing not part of study</p> <p>Variations</p> <p>Puyallup facility – sheet on warm side of assembly- no wetting of wood components- use of line loading -</p> <p>Korsgaard and Rode 1992 – roofs wet once</p> <p>Desjarlais <i>et al.</i> 1993 and 1998 – roofs wet once</p> | <p>Hazleden and Morris 2001 (EDRA) – immersion of frame</p> |

| Description of geometry | 3-D transfer of moisture | 2-D transfer of moisture | 1-D transfer of moisture | 3-D transfer of moisture |
|---|--|--|--|---|
| Capacity to control patterns and moisture content | With or without wick Point or linear load | With the use of wick fabric Two or three insertion points to distribute water | With the use of wick fabric Array of insertion points to distribute water evenly | Depends on depth and duration of immersion |
| Surface from which water evaporates | Moisture exits from sheathing and bottom plate. Exits from wick if present | Moisture exits from bottom plate and wick fabric | Moisture exits from sheathing or directly from wick | Moisture exits from sheathing and stud frame |
| Analysis of experimental data | Data on moisture distribution, redistribution and exiting | Data on moisture redistribution and exiting | Data on moisture redistribution (not including sheathing) and exiting | Data on moisture redistribution and exiting |
| Data that can be used in simulation | Complex problem to simulate with modeling | Difficult problem to simulate with modeling | Simpler problem to simulate with modeling | Complex problem to simulate with modeling |
| Combination of wetting modes | | Can start with initially wet components | Can start with initially wet components | |
| Advantages | Similar to a concentrated source Wetting of the sheathing Analysis of sheathing absorption | Easy to control wetting pattern Similar to source leading to water accumulation at bottom of cavity | Should be easy to control wetting pattern of fabric | |
| Disadvantages | Recreates only one possible wetting pattern Difficulty in controlling wetting pattern Wall sheathing must be perfectly vertical Bottom plate must be perfectly horizontal Potential absorption of water by insulation if not prevented by design | No wetting of sheathing, except for sheathing at bottom plate Difficulty in ensuring uniformity of wetting by wick fabric from wall to wall | Difficulty in ensuring good wick fabric/sheathing contact, and wetting of sheathing, especially if gravimetry in sheathing is used Difficulty in ensuring uniformity of wetting by wick fabric from wall to wall Does not represent a real situation | Difficulties of reproducing same initial moisture content |

Methods of rain insertion have been presented. However, the amount of water to insert has to be determined.

The following section will present previous studies on atmospheric wind-driven rain, wind-driven rain impinging onto building facades, as well as rain penetration into building envelopes. This will serve as a basis for the development of a wetting methodology for the estimation of rain penetration in building envelope testing.

2.5 Previous studies on wind-driven rain, wind-driven rain impinging the building envelope, and wind-driven rain infiltration into the building envelope

Hygrothermal testing aiming to reproduce field wind-driven rain and wind-driven rain leakage wetting conditions requires that these wetting loads be understood and quantified. Field tests documenting wind-driven rain falling onto building facades has been performed by many researchers in the last decades such as Holmgren in 1937, Croiset, Lacy and other scientists at the British Research Station in the 1950's (Lacy, 1965), Henriques (1992) and Straube and Burnett (2000a, 2000b). However, there has been no case reporting the amount of wind-driven rain leakage into building envelopes due to a defect. The lack of knowledge in this area and the lack of a standardized wetting methodology have led to great variability in the development of wetting protocols for experimental testing on parameters such as the quantity of water inserted, the duration and frequency of water introduction, etc., as shown in Table 2.3. Such information is very useful for experimental research as well as in establishing the boundary conditions for building envelope numerical simulations. For example, a numerical analysis conducted by Salonvaara and Karagiozis (1998) included setting an initial moisture content of 44% for the OSB sheathing. However, while the authors do not explain the selection of such a value, they state that this represents a very wet initial moisture condition as if the OSB was wetted directly by rain.

A guideline to aid researchers with the development of a wetting methodology and, in particular, one that attempts to simulate wetting due to rain penetration as a function of location for a specific climate would need to provide the following parameters: a. the

quantity of water to introduce; b. the duration and frequency of introduction; c. the location of water insertion in the test wall assembly; and finally, d. the method of introduction during the experiment.

Simulating rainwater leakage into wall assemblies is challenging because of the many factors involved. First, rain is itself a complex phenomenon, as its speed and path is affected by drag forces and the wind. Before discussing the wind-driven rain on building facades, the nature of rain and the impact of wind will be examined.

2.5.1 Wind-driven rain

The term “wind-driven rain” describes rain with a horizontal component in its direction due to the effect of wind. There are many parameters that characterize wind-driven rain. These include the rate of horizontal rainfall, or the rate of rainfall falling on a horizontal plane, the size distribution of raindrops and the raindrop velocity. Meteorologists began studying the size distribution of raindrops in the mid 1940’s as a result of the use of radar equipment to locate precipitation. The drop size distribution can be influenced by many factors including rate of rainfall, type of rain, position relative to the center of the rainstorm, relative humidity, etc. Best (1950), one of the pioneers in this research area, estimated the cumulative probability distribution of raindrops, $F(a)$, as a function of raindrop diameter, a , in mm, and horizontal rainfall intensity, R_h , in l/m^2h or mm/h , as:

$$F\{a\} = 1 - \exp\{-(2a/1.30R_h^{0.232})^{2.245}\} \quad [2.6]$$

Other raindrop size distributions have been proposed by Waldvogel (1974) and Mualem and Assouline (1986). There has been some controversy regarding the sensitivity of the raindrop size distribution on the driving rain intensities impinging on envelopes. Choi (1994) showed that the size distribution of the raindrops has little effect. However, van Mook *et al.* (1997), using Waldvogel’s model (1974) to simulate two different size distributions, demonstrated that the raindrop size distribution does, in fact, significantly affect the driving rain intensity impinging on building envelopes. Van Mook *et al.* (1997) suggested that the shapes of the raindrop spectra used by Choi are too similar to show the differences that these may cause on the wind-driven rain on building facades.

However, irrespective of these considerations, Best's raindrop size distribution was used in this study given that numerical estimations of wind-driven rain based on this distribution have been validated with experimental data (Blocken and Carmeliet, 2001a, 2001b, 2002a).

The size of the raindrop affects the terminal velocity of the raindrops, and all but the largest of raindrops reach their terminal velocity within about 20 m of the beginning of their fall (Straube and Burnett, 2000a). Thus it can be assumed that raindrops approaching buildings have reached their terminal velocity. The terminal velocity of raindrops, V_T , studied by Dingle and Lee in 1972, can be predicted as a function of the raindrop radius, a , using a third-degree regression formula:

$$V_T = -16.6033 + 983.688a - 355.206a^2 + 43.9104a^3 \quad [2.7]$$

for $0.05 < a < 2.9$ mm, and V_T is expressed in cm/s. While Dingle and Lee (1972) have developed more accurate formula for the prediction of terminal velocities of raindrops, these are valid for a smaller range of drop radii, as it was found that a sharp physical change occurs at a radius of 0.7 mm.

As a raindrop falls through the atmosphere, it is subjected to gravity, buoyancy and drag forces. The drag force is the component of force on a raindrop that acts parallel and opposite to its direction of motion. The buoyancy force on a raindrop, defined for this case as the force of gravity on the ambient air displaced by the raindrop, is small and can be neglected. Gravity, of course, causes the drop to fall vertically towards the earth, while the wind imparts a horizontal component to the raindrop trajectory. Rain that is thus affected by the wind is often called wind-driven rain or driving rain. Straube and Burnett (2000a) define wind-driven rain as the rate of rain that passes through a vertical plane in the atmosphere, and calculate it as follows:

$$R_v = R_h \frac{V}{V_T} \quad [2.8]$$

where R_v and R_h are the driving and horizontal rain, respectively, in $l/m^2 \cdot h$ or $mm/m^2 \cdot h$, V and V_T are the average wind velocity and the raindrop terminal velocity, in m/s. Since the wind velocity significantly decreases as it approaches the ground, the trajectory of raindrops will be curved. Very close to the ground, abrupt changes in topography like hilltops and around buildings result in significant wind variations, and the raindrop's

momentum causes its velocity components to vary from that of the wind. This difference between wind and raindrop trajectory strongly depends on raindrop size (Straube and Burnett, 2000a; Choi, 1994).

2.5.2 Wind-driven rain on building façades

The impingement of wind-driven rain on the surface of a building façade involves a number of complex physical phenomena. At the local scale, these phenomena include the impact of raindrops on the façade, raindrop splashing, adsorption and absorption of the rainwater by the building materials, and evaporation of the rainwater. The work on this topic is in its infancy, and the importance of each of these phenomena on the boundary conditions for HAM building envelope testing is not yet known. Blocken *et al.* (2002b), Carmeliet and Blocken (2004, 2005) and Carmeliet *et al.* (2005) have developed simple models to study impinging wind-driven rain and surface runoff, and then applying the modeling results as boundary conditions for HAM simulations. The work is currently being pursued at the Katholieke Universiteit of Leuven, in Belgium.

At the building scale, there are also complex interactions between the wind, the rain, the building and the surroundings. Near ground level, the flow of wind around buildings and the trajectory of raindrops within the flow field is highly variable, and the impingement of wind-driven rain on building facades is affected by many parameters listed below, the first five of which are functions of the climate, and the next five vary depending on building characteristics:

- the horizontal rainfall (and hence raindrop size distribution) ;
- the wind speed;
- the wind direction;
- the duration of rainstorm;
- the frequency of rainstorm;

- the location on façade;
- the building geometry;
- the façade orientation;
- surrounding topography, and;
- sheltering affects of surrounding buildings and trees.

Horizontal rainfall (and hence drop size distribution). Horizontal rainfall is the volume of rain that falls on one square meter horizontal plane. It is typically measured on an hourly basis in open country-type terrains at meteorological stations, with units of l/m^2 , or mm. The rate of horizontal rainfall is influenced by the size distribution of raindrops. It is generally accepted that the smaller the horizontal rainfall rate, the smaller the average raindrop size in the distribution, and vice versa. Since smaller raindrops have a lower inertia, their trajectory is more influenced by the force of the wind, causing them to be swept around the building (Choi, 1993, 1994; Karagiozis and Hadjisophocleous, 1995; van Mook *et al*, 1997; Blocken and Carmeliet, 2002a). Hence, the higher the horizontal rainfall, the greater the impinging rain on the building surface (Straube and Burnett, 2000a)

Wind speed. Wind speed has great positive impact on impinging rain by increasing the horizontal component of the velocity of raindrops, more so for small than large raindrops (Choi, 1994; Karagiozis and Hadjisophocleous, 1995; Blocken and Carmeliet, 2002a). Impinging wind-driven rain increases both with increasing horizontal rainfall and wind speed. Therefore, the most severe hourly driving rain on buildings occurs during simultaneous occurrence of high horizontal rainfall rate and extreme wind speed (Blocken and Carmeliet, 2000). However, Choi (1994), using weather data from Sydney, Australia, has found that the probability of co-occurrence of high horizontal rainfall and extreme wind speed is low. This means that for a higher horizontal rainfall, the extreme wind speed will be smaller, and thus the wind-driven rain on building facades will be lower.

Wind direction. The highest rate of impinging wind-driven rain occurs when the wind acts normal to the building façade; however, when the wind direction is not normal to the surface, the impinging wind-driven rain generally decreases as the wind angle increases, the only exception being at the top upwind corner, which may experience higher impinging wind-driven rain when the wind angle is between 0 and 30 degrees (Choi, 2000)

Duration and frequency of rainstorm. The greater the duration of wind-driven rain events, the greater the absorption of water by the cladding, and with time, the cladding materials, e.g. brick, can become saturated, hence increasing the amount of runoff down

the envelope forms and increasing the amount of rain reaching a specific location on the envelope.

Location on the façade. The rate of impinging wind-driven rain is affected to a large extent by the location on the façade on which it falls, with a greater rate of impinging wind-driven rain at the top edge (when no overhang is present) (Karagiozis and Hadjisophocleous, 1995) and vertical side edges of a building façade compared to the middle (Choi, 1994; Straube and Burnett, 2000a; Blocken and Carmeliet, 2000, 2002a).

Building geometry. Tall buildings receive more wind-driven rain at the top and edges than short buildings (Straube and Burnett, 2000a) since wind speed increases with height; however, Choi (1994)'s numerical work found that the greater the width to height ratio, the smaller the impinging wind-driven rain over the entire building facades for a constant building height and depth.

Façade orientation. As mentioned before, a façade oriented in a direction normal to the wind direction is subjected to more wind-driven than one oriented at an oblique angle.

Surrounding topography. The presence of valleys and hills and mountains around the building may significantly affect the speed of the upstream wind, and therefore can impact the wind-driven rain striking buildings.

Sheltering effect of architectural elements and surrounding buildings and trees. The presence of architectural elements such as overhangs, cornices, etc., sheltering the building from wind-driven rain can reduce the amount of wind-driven rain impinging on the building envelope (van Mook *et al.*, 1997; Hangan, 1999; Straube and Burnett, 2000a; Blocken and Carmeliet, 2002a), but usually on surfaces immediately below the element. This effect is less pronounced when the wind speed is high, and less so, when the horizontal rainfall is low (Blocken and Carmeliet, 2000, 2002a). Depending on their location, surrounding buildings and trees may have various effects on the wind flow on the different building facades.

In the following sections, the driving index will be introduced, as well as methods to predict wind-driven rain on building façades.

2.5.2.1 The driving rain index

The driving rain index was developed from a correlation between driving rain,

rainfall and wind speed. The DRI indicates the severity of exposure of a site and can be used for comparison purposes when selecting a building site (Lacy, 1965). The first works on the subject were conducted in the 1950's by Hoppestad who mapped driving rain indices for Norway. In 1962, Lacy further developed the basic criteria with which driving rain indices for various countries including the United Kingdom, Canada, Denmark and Portugal were established. Lacy's driving rain index, in its simplest form, was calculated as the product of the mean annual rainfall and the mean annual wind speed, and is measured in m^2/s . However, this posed an important restriction: it did not include the importance of wind direction, and it assumed that the mean annual wind speed and the wind speed during rain periods were constant. While this constancy has been verified for the UK, there is no guarantee that it is so for other countries, notably maritime countries (Henriques, 1992).

The work of Prior, which was the basis of the British Standard Institution's Draft for Development in 1984, refined the average annual driving rain index. The average annual driving rain index was calculated for 12 directions, each covering 30 degrees, using a summation of the hourly products of the rainfall on a horizontal plane, R_h , the wind speed, V , and the cosine of the angle between the wind direction and the azimuth concerned, β , as follows:

$$DRI = \Sigma R_h \cdot V \cdot \cos \beta \quad [2.9]$$

In this application, the north direction equals 0° . Statistical evaluation of rainfall and simultaneous wind speed in downtown Montreal and at a Montreal airport has shown that local topographical features can strongly affect the directional characteristics of wind-driven rain on building facades (Fazio *et al.*, 1995). For this reason, the direction of the wind, and hence wind-driven rain, should be considered by building designers and planners.

Fazio *et al.* (1995) have also developed a methodology to quantify the rate of driving rain and precipitation amount on a building façade of given orientation. The methodology uses two methods. The first uses an empirical equation by Lacy (1965) (see section 2.5.2.2 below), while the second is based on a correlation between the driving rain index and the amount of driving rain on a wall by Henriques (1992) which states that a DRI of $1 \text{ m}^2/\text{s}$ is equivalent to 90 to 100 l/m^2 of rainwater falling on a vertical surface.

It was found that the accuracy of methods to predict wind-driven rain on building surfaces that make use of the driving rain index may be problematic because 1) the amount of rain deposited on a wall will vary depending on the exact location on the surface, and; 2) in a unit time, a high rainfall rate with a short duration can result in the same driving rain index as a low rainfall rate with a high duration. Also, the raindrop size distributions are different due to the different type of rainfall, i.e. the rainfall intensity is different, thereby changing the drop size distribution, the terminal velocity of the raindrops, their deflection pattern around a building, and the driving rainfall rate on the building façade (Fazio *et al.*, 1995). The same team has also developed a methodology to derive the driving rain index of an urban area based on climatological data from a suburban or rural meteorological station. The DRI results obtained from the methodology compare favorably with those derived from the recorded data in the urban area. The method is useful for determining the driving rain exposure for urban areas where the climatological data is not available (Zhu *et al.*, 1995).

Some numerical and field work has been done to quantify the wind-driven rain distribution on building façades. Many researchers such as Choi (1994, 2000), Sankaran and Paterson (1995), Karagiozis and Hadjisophocleous (1995, 1997), van Mook *et al.* (1997) and van Mook (1999a, 1999b), and Blocken and Carmeliet (2000, 2001a, 2001b, 2002a, 2002b) have developed or applied computational fluid dynamics (CFD) models to simulate driving rain impinging on building envelopes. Choi (1999) has developed simple correlations relating the DRI to the annual and maximum amounts of impinging wind-driven rain. The simple correlations are found rainfall and wind speed data as input and using CFD to determine the amount of wind-driven rain on a particular zone on a building façade. Good agreement was found between predicted and calculated mean and maximum impinging wind-driven rain values.

Existing CFD codes such as FLUENT (van Mook, 1997, 1999) and TASCflow (Karagiozis and Hadjisophocleous, 1995, 1997) are commonly used by many researchers and are based on the k- ϵ model from fluid dynamics. Of the above works, that of Choi (1991, 1992, 1994, and 1999) and Karagiozis and Hadjisophocleous (1995, 1997) has not been validated experimentally. The modeling study by Sankaran and Paterson, which makes use of the k- ϵ turbulence model and takes wind gusts into account, has been

validated for wind flow around buildings, but no experimental verification of the model for wind-driven rain impinging on building facades was found. Hangan (1999) and Hangan and Inculet's study (2001) compares the results of a CFD study on wind-driven rain, which makes use of the k- ϵ turbulence model, with those from a boundary layer wind tunnel (BLWT) test conducted at the University of Western Ontario. The use of a BLWT for wind-driven rain simulation presents difficulties with respect to rain drop introduction into the flow field. As well, there is poor agreement between the simulation and experimental results at different locations for both low rise and high rise buildings. Wind-driven rain on buildings was also studied numerically and experimentally using full-scale measurements of driving rain on a building at the Eindhoven University of Technology (van Mook *et al.*, 1997, van Mook, 1999a, 1999b). The modeling work makes use of the standard k- ϵ model which does not account for raindrop dispersion due to the turbulence of the wind. Important discrepancies can be seen between the measured results from a field test, and simulated results at low wind speeds, and further investigations need to take place to determine whether the discrepancy is due to the errors in the calculation in the wind velocity field, the drop trajectories or in the raindrop spectra.

In the following sections, the work of Lacy, Straube and Burnett as well as that of Blocken and Carmeliet will be presented as a basis for driving rain load estimations on building envelope facades. The three methods are relatively simple to apply and have been validated with field data.

2.5.2.2 Lacy's relation for driving rain on a vertical surface

Lacy (1965) developed a relation between the rate of water deposition on vertical surfaces, that on horizontal surfaces, as well as the wind speed:

$$R_v = (2/9) \cdot V \cdot R_h^{8/9} \quad [2.10]$$

where R is the rate of rainfall in mm/h, V is the wind speed in m/s and the suffixes v and h refer to vertical and horizontal surfaces, respectively. Lacy's calculation of driving rain on building surfaces is limited in that it assumes drops are not deflected before reaching the surface and that they are all the same size in a given storm. In addition, Lacy's model does not account for the wind direction with respect to the building façade orientation,

nor the fact that the distribution of wind-driven rain varies across a building façade due to the wind flow pattern.

2.5.2.3 Straube and Burnett's rain admittance function method

Straube and Burnett (1998a; 2003) describe a mathematical equation relating the rate of driving rain on a vertical plane undisturbed by the local effects of the building, R_v , to the wind speed, V , and the rate of horizontal rainfall, R_h :

$$R_v = DRF \cdot V \cdot R_h \quad [2.11]$$

where DRF is the driving rain factor. Straube and Burnett (2000a) show that the DRF can be calculated as the inverse of the raindrop terminal velocity V_T , and usually lies between 0.2 and 0.225. Thus, to find the DRF, the raindrop terminal velocity must be known, and can be calculated using the previously mentioned equation by Dingle and Lee (equation 2.7). However, rainstorms contain raindrops of many sizes. The empirical formula by Best (1950) (see equation 2.6) estimating the cumulative probability distribution of raindrop, $F(a)$, can be used for this purpose when the rate of horizontal rainfall intensity, R_h , is known to find the median drop size. Thus, the terminal velocity of the median drop size can be found, and then DRF can subsequently be calculated.

The driving rain, R_v , can, in turn, be used to determine the driving rain on a building façade, R_{bv} (Straube and Burnett, 2000a):

$$R_{bv} = RAF \cdot \cos(\theta) \cdot R_v = RAF \cdot \cos(\theta) \cdot DRF \cdot V(d) \cdot R_{hor} \quad [2.12]$$

where V is the wind speed at the height of interest, d , while θ , the angle in plan view between the wind and the normal to the building façade, accounts for the fact that the wind direction is not always normal to the wall (see Figure 2.10). The RAF, the rain admittance function, is a proportionality constant relating driving rain in the environment to rain deposited on the building. The RAF depends on the location on the wall façade.

Straube and Burnett (2000) have calculated the RAF over building facades for various building geometries, as can be seen in Figure 2.11. Since façades are susceptible to receive rain from angles ranging from -90° to $+90^\circ$, the total amount of rainfall striking the façade can be found by summing up the contributions of wind-driven originating from the -90° to $+90^\circ$ to the surface normal.

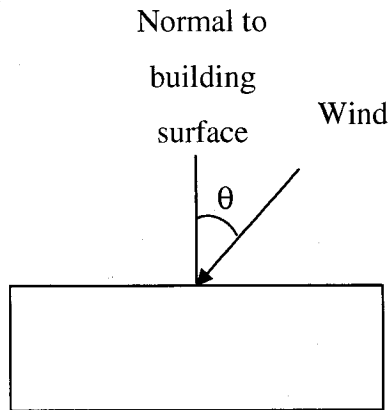


Figure 2.10. Plan view of building, showing the angle θ .

Thus, knowing the rate of horizontal rainfall, the wind speed and direction at the height of interest, and the RAF for the façade location of interest, the rate of wind-driven rain on a building facade, R_{bv} , can be calculated for each direction by determining the DRF using either the raindrop terminal velocity function and the cumulative probability function for each raindrop size, or simply by assuming a value between 0.2 and 0.225. If an average rain deposition rate is sought over a larger time span, the contribution of rain coming from each direction can be obtained by summing up the contribution of each wind direction.

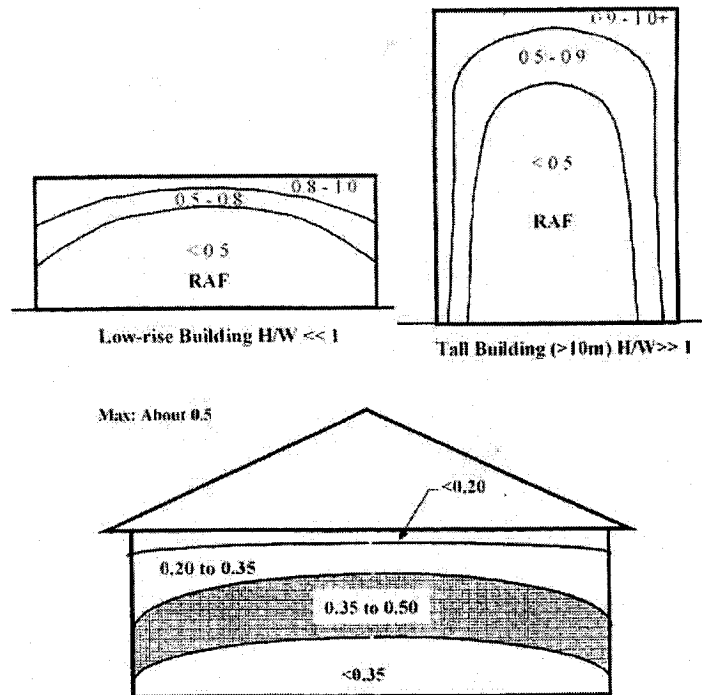


Figure 2.11. Typical measured rain admittance functions for simple buildings for buildings with different height/width (H/W) factors (Straube and Burnett, 2000a).

2.5.2.4 Blocken and Carmeliet's driving rain load estimation

The determination of wind-driven rain on building facades has also been done by Blocken and Carmeliet. This numerical model is based on the work of Choi (1991, 1992, 1994) which makes use of the standard k- ϵ model from fluid dynamics. This model solves the Navier Stokes equation. However, because the standard k- ϵ model utilized by Choi is known to provide inferior performance when dealing with separated flows, Blocken and Carmeliet use a variant developed by Shih *et al.* (1995) named the realizable k- ϵ turbulence model. It has been validated for a wide range of flows including separated flows (Shih *et al.*, 1995; Kim *et al.*, 1997). Also, the numerical model has been validated for driving rain impinging on building facades by Blocken and Carmeliet (2000, 2001a, 2001b) and good agreement has generally been found between numerical and experimental results.

In Blocken and Carmeliet's model, the wind-driven rain striking a building envelope is calculated using the realizable k- ϵ model, which determines the wind flow pattern around buildings and the raindrop trajectory in the airflow. The authors make use of the

specific catch ratio, $\eta_a(a)$, which is a function of the raindrop radius, a , and is defined as the ratio of the intensity of raindrops of radius “ a ” landing on a specific zone on the building face to the intensity of the rainfall on a horizontal plane away from the local effects of the building:

$$\eta_a(a) = \frac{R_{bv}(a)}{R_h(a)} \quad [2.13]$$

Again, R_{bv} is the rate and the amount of rain deposition on a vertical building surface and R_h is the rate of horizontal rainfall. The catch ratio for a zone, η , is the integral product of the specific catch ratio and the raindrop size distribution over all raindrop radii:

$$\eta = \int_a F(a) \eta(a) da \quad [2.14]$$

In their analysis, Blocken and Carmeliet chose the raindrop size distribution developed by Best. Best’s model has been utilized by many wind-driven rain numerical models (Choi, 1991, 1992, 1994; Blocken and Carmeliet, 2000, 2001a, 2001b; Karagiozis, and Hadjisophocleous, 1995; 1997, Hangan and Inculet, 2001).

Blocken and Carmeliet have performed numerical evaluations to determine the catch ratio at several locations on a building façade, and have validated the model using field data. An example of catch ratio results is shown graphically in Figure 2.12 for a location at approximately 1/3 of the height of a one-story building with a flat roof. The wind direction is perpendicular to the surface of the façade. Required local meteorological data for the graph are the horizontal rainfall, R_h , and the wind speed at a 10 m height above ground, V_{10} .

Three methods for estimating wind driven rain have been presented, and they agree that the rate of horizontal rainfall and the speed of the wind strongly affect the rate of impinging rain at a specific location on the building envelope surface given a wind flowing normal to the building façade. Driving rain estimations are used in the study of rain infiltration in building envelopes.

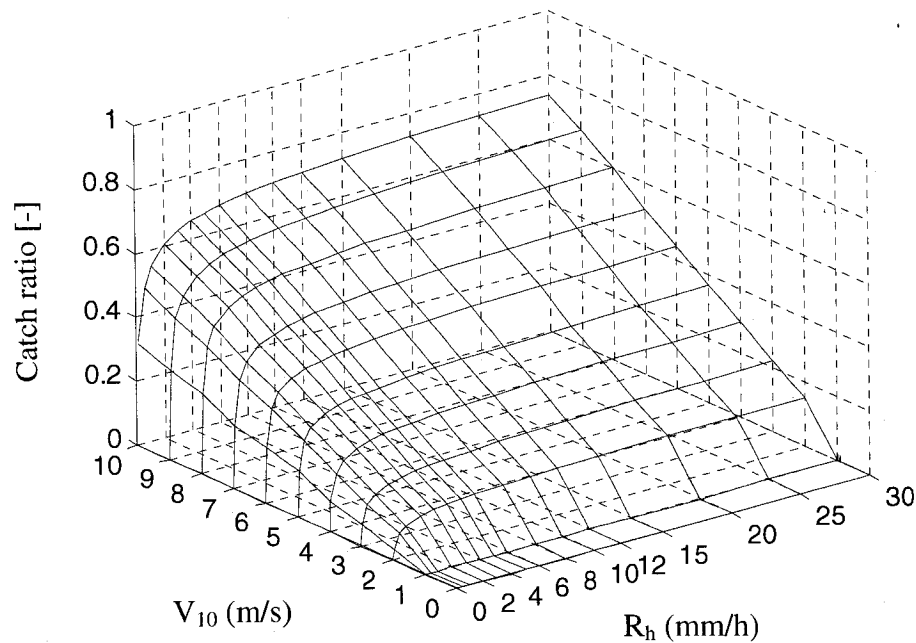


Figure 2.12. Numerical results of specific catch ratio as a function of wind speed at 10 m height and horizontal rainfall intensity (from Blocken and Carmeliet, 2001b).

2.5.3 Rain infiltration

While much numerical and experimental work has been done on the prediction of wind-driven rain onto building facades, little is known about water leakage into building envelopes. Building envelope field studies have shown that high moisture content of hygroscopic materials can result from rain leakage events. However, no field measurements of actual rain leakage into the back wall have been documented.

Most of the work that has been done on the topic of water penetration testing in building envelopes aims to determine the resistance to water penetration of exterior envelopes, and in particular windows, skylights, curtain walls and doors. A brief survey of standard test methods for water penetration resistance is presented next, followed by laboratory work on the quantification of water leakage through envelope defects.

2.5.3.1 Standard test methods for water penetration resistance

Standard test methods exist to evaluate the water penetration resistance of manufactured component, some providing a level of performance while others simply a

pass or fail rating. These are typically performed in a laboratory setting. Alternatively, the installed component such as a window can be tested for water penetration resistance in the field. With such a method, the component, the adjacent construction as well as the joint between the two is tested, and corrective measures can be undertaken if a leak is found. Several standard test methods for water penetration and the recommended exposure conditions are shown in Table 2.5.

While these tests are mainly intended to provide a pass or fail evaluation of the water leakage performance, the methodology they prescribe can also be used to measure the water leakage rate for intentional defects. For example, ASTM E331-00, the Standard Test Method for Water Penetration of Exterior Windows, Skylights, Doors and Curtain Walls by Uniform Static Pressure Difference (ASTM, 2000a), is commonly used by industry, but recommends a uniform static air pressure difference of 137 Pa, which is equivalent to a 15 m/s, or a 54 km/h wind. The appropriateness of these test methods, and in particular the water spray rates and air pressure differences recommended for the determination of water leakage rates will be reviewed at a later date.

Table 2.5. Water penetration standard tests used to test the water penetration resistance of envelope components themselves, or of installed components.

| Standard | Envelope Component Tested | Item Tested: Component (C) or Installed Component (IC), Lab (L) or Field (F) test | Water Spray Rate [l/m ² min] | Air Pressure | Static (S) or Dynamic (D), Uniform (U) or Cyclic (C) |
|------------------|--|---|---|--|--|
| ASTM E331-00 | Windows, skylights, doors, curtain walls | C, L | min. 3.4 | 137 Pa | S, U |
| ASTM 514-90 | Masonry wythe | C, L | min. 2.3 | 500 Pa | S, U |
| ASTM E547-00 | Windows, skylights, doors, curtain walls | C, L | min. 3.4 | Cycles of 0 to 137 Pa to 0 | S, C |
| CAN/CSA-A440-M90 | Windows, skylights, doors, curtain walls | C, L | min. 3.4 ¹ | 4 cycles of 137 Pa (5 min. duration) and 0 Pa (1 min. duration) ¹ | S, U |

| | | | | | |
|--|---|-------|---|---|---------------|
| NT BUILD 116 (Nordic Innovation Center, 1980) | Windows, window/doors, doors, facades | C, L | runoff: 0, 0.1, 0.2; driving rain: 1, 0.7, 1.2, 1.7 | Pulses from 0 to X; X increases from 0 to 1500 in 8 cycles | D (pulsating) |
| NT BUILD 421 (Nordic Innovation Center, 1993) | Flat and sloped roofs, roof components | C, L | runoff: 1.7; driving rain: 0.3 | varies with roof slope: pulses from 0 to X, X increases with each of 5 cycles | D (pulsating) |
| AAMA 501.2-03 (AAMA, 2003) | Storefronts, curtain walls and sloped glazing systems | IC, F | Not specified; 205 – 240 kPa nozzle pressure | - | S, U |
| AAMA 502-02 (AAMA, 2002) | Windows and sliding glass doors | IC, F | As per ASTM 1105 | Depends on product designation ² | |
| ASTM 1105-00 | Windows, skylights, doors, curtain walls | IC, F | min. 3.4 | not specified | S, U or C |

¹ Air pressure and water spray rate as specified by ASTM E547.

² The static air pressure recommended should be 2/3 of that recommended by ANSI/AAMA/NWDA 101/I.S.2 (1997) for the specified product designation.

2.5.3.2 Work on the quantification of water leakage through envelope defects

A great deal of work has been done by the MEWS consortium to characterize water leakage for wall assemblies. Water penetration tests were performed on 17 wall assemblies with different types of cladding including 5 stucco, 5 EIFS, 4 masonry and 3 siding-clad walls. The main parameters that were investigated with respect to water leakage quantification included, but were not limited to, cladding type, face seal versus rainscreen wall, the presence of a drainage plane behind the exterior insulation and material used to create the drainage plane (in EIFS-clad walls), and insulating sheathing board versus wood sheathing with sheathing membrane. Water leakage tests were performed using two water spray rates and static or dynamic pressure differential across the wall assemblies, as shown Table 2.2.

There were several deficiencies in the first and second lines of defense of the wall assemblies that were investigated for the purpose of rain penetration testing. The deficiencies in the first line of defense for the stucco-clad assemblies are shown in Table 2.6 and those for the rest of the assemblies are similar. There were many types of deficiencies explored with respect to the second line of defense, for example lack of flashing, incorrect installation of window flashing, incorrect installation of weather resistive barrier, gap in sealant beneath the duct on the indoor side, just to name a few. Details can be found in Bomberg *et al.*, 2002. Some general conclusions are highlighted here.

Table 2.6. Deficiencies introduced in the stucco-clad wall for the MEWS project (Bomberg *et al.*, 2002)

| Junction | 1st line of defense |
|---|---|
| Wall-window | Missing 90 mm of sealant length in the center of the sill and at one end of the sill Missing 90 mm of sealant length at the bottom of one jamb |
| Wall-exterior electrical outlet | Missing 50 mm of sealant length in the center of the top of the cover plate |
| Wall-ventilation duct | Missing 50 to 90 mm of sealant length in the center of the top of the cover plate |
| Two and one horizontal control joints in the cement plaster | Partial bond between the cement plaster and the preformed metal strip used for the control joints |

It was found that, as expected, while in some cases there was little effect (see Figure 2.13), the water entries generally increased with increasing spray rate applied across the wall assembly. Figure 2.14 shows the relation between percent water entry rate through a deficiency above an electrical outlet in a stucco-clad wall and the impinging water spray rate for various air pressure differences. Except for the case where no air pressure was applied, the water leakage rate was higher at the higher spray rate. Also, doubling the spray rate only increased the leakage rate by about 33%. Figure 2.15 shows the percentage of water leakage through defects above ventilation ducts in six stucco-clad walls at applied pressure differences of 0, 75, 150 and 300 Pa, respectively. The figure shows that the leakage generally increased with increasing rate of impinging water for all walls except wall no. 4 which experienced a greater percentage leakage rate at all pressure differences applied. The same general tendency for increased leakage rate with increased load application was found in EIFS, masonry and siding-clad walls with defects above the electrical outlets, above the ventilation ducts and at the bottom of windows (Lacasse *et al.*, 2003).

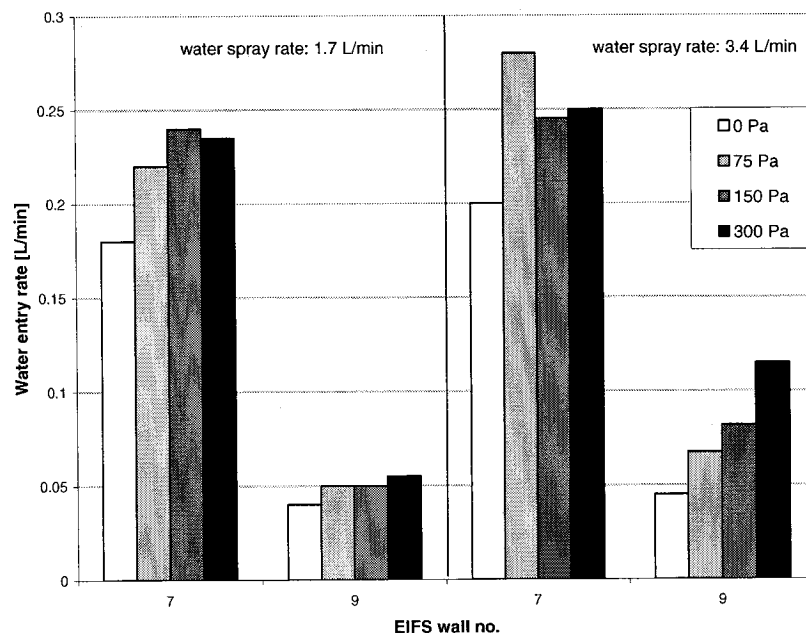


Figure 2.13. Water entry under static pressure difference through deficiency above electrical outlet in EIFS-clad wall assemblies no. 7 and 9 at given spray rates (derived from Lacasse, 2003).

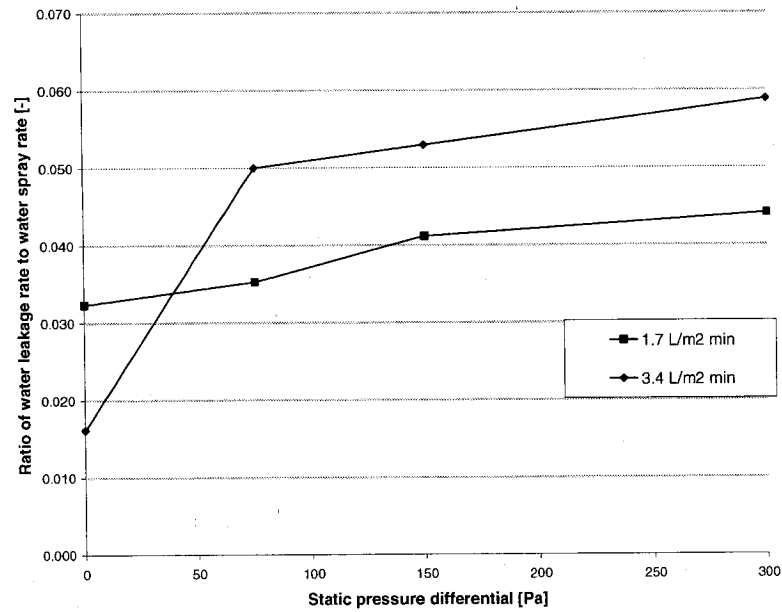


Figure 2.14. Water entry through the deficiency above the electrical outlet in the stucco-clad walls in relation to static pressure differential at different spray rates (derived from Lacasse *et al.*, 2003).

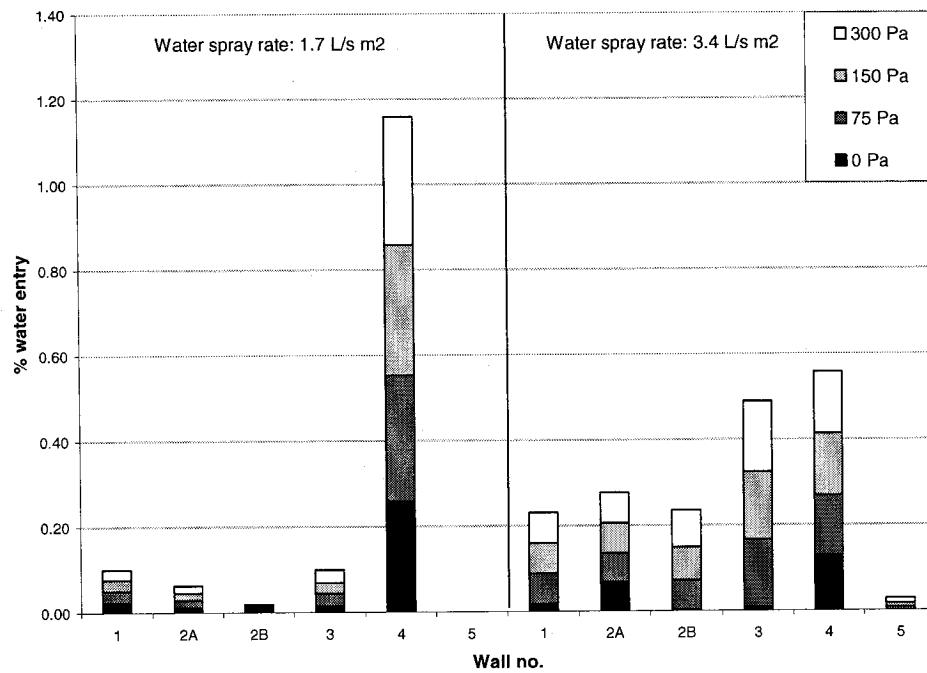


Figure 2.15. Percentage of water entry through deficiency above ventilation duct in stucco-clad walls for two impinging water spray rates and four pressure differentials ranging from 0 to 300 Pa applied across the wall assemblies (data extracted from Lacasse *et al.*, 2003).

The MEWS water leakage tests show that the correlation between leakage rate and

pressure differential is not clear. For most assemblies, there is some leakage even when no air pressure difference is applied (see Figures 2.13 to 2.15), and the leakage rate considerably increases once a pressure of 75 Pa is set. Generally, however, increasing the pressure in this test beyond 75 Pa to 150 Pa and 300 Pa does not increase the leakage rate significantly, as can be seen when comparing the proportion of leakage in walls exposed to a pressure difference of 0, 75, 150 and 300 Pa, respectively (see Figure 2.15). However, the results also show that other wall systems exhibited significant increases in water leakage when subjected to higher air pressures, as shown in Figure 2.16. The water penetration amounts shown in this figure are for an EIFS-clad wall which incorporates a drained cavity using a 3 mm nylon drainage mat.

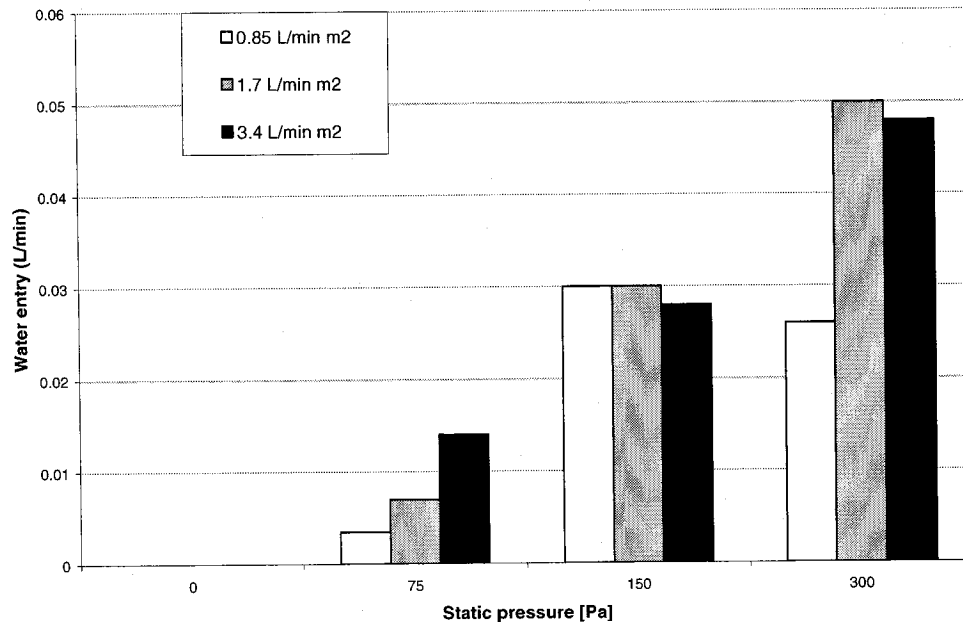


Figure 2.16. Water entry into deficiency above ventilation duct as a function of static pressure and spray rate for an EIFS-clad wall no. 10 (Lacasse *et al.*, 2003).

Walls that incorporated a vented drainage space between the cladding and the sheathing experienced little leakage, hence showing the benefits of the air cavity with respect to water penetration control, as shown in Figure 2.15: the stucco-clad wall no. 5 was the only stucco wall incorporating a drained stucco-clad system with vents at top and bottom of the cavity.

It should be noted that, due to the sprays, the water drops travel almost horizontally

onto the building surface. For this reason, in the vast majority of leakage tests performed, water entry was found in walls when no pressure difference was applied. The force caused by the air pressure difference applied across the wall specimen adds to the force driving the water into the defects. However, in actuality, raindrops fall vertically to the ground due to gravity unless wind is present to give the drops a horizontal component. With regards to wind-driven rain leakage, the wind not only gives the raindrops a horizontal momentum but the air pressure differential that the wind creates also provides a driving force that can drive the impinging rain into building envelope defects. This is an important difference between the spray test method and actual wind-driven rain penetration. This difference does not seem to have been studied. Almost all water penetration tests do not report water drop end velocities, although air velocities are sometimes measured Maerker (1983). No study has been performed on the role of kinetic energy vs. rate of water spray and air pressure differential in the wetting of surface and water penetration.

As was stated earlier, wind-driven rain generally penetrates at building envelope junctions such as wall/window and wall/balcony interfaces. However, the exact location of the deficiency with respect to the envelope junction may play a role in the leakage due to surface runoff from above. For example, a defect in the perimeter of a wall/window interface will likely pose a greater risk of rain penetration if located at the bottom of the window because of the impermeable nature of the glazing above and the high probability of water collection at the bottom of the window. The risk is lower at the top of the window since a smaller amount of rain is likely to be present there, especially if the cladding materials above the window are highly absorptive, like brick.

The amount of water that may leak through a deficiency may also depend on the lateral location of the defect with respect to the envelope component. The MEWS water penetration studies included measurements of water leakage through the perimeter joint at the windowsill, both at the bottom corner as well as at the center of the sill, as shown in Figure 2.17. Results show that very little, if any, water penetrated through the center defect, while significant quantities leaked at the corner defect (Lacasse *et al.*, 2003). This may be due to the fact that water runs down the exterior vertical jambs of the window and

collects in larger quantities at the corner of the window.

Other factors may influence the leakage rate through a building envelope defect. The orientation of defect, for example, may have some influence. Hens and Fatin (1995) state that for masonry claddings, rain infiltration occurs mainly through the vertical mortar joints, also called head joints, between the bricks. Often mentioned is the theoretical hydrostatic pressure of the film of water on the cladding, although such a film, either running down or sticking to the cladding, results in no vertical water movement at the surface of the cladding due to the no-slip condition. Hence, no pressure should be exerted on the surface. Finally, with the advent of water accumulation within bricks, it has been suggested that a hydrostatic pressure over the height of the water column can be present, with pressures of about 10 Pa per mm height (Straube and Burnett, 2000b). However, in bricks, given the small size of pores (insert range of pore size here (reference, year)) within which water movement takes place, capillarity is likely to dominate as the driving force. The gravity force also plays a role in water movement across the cladding.

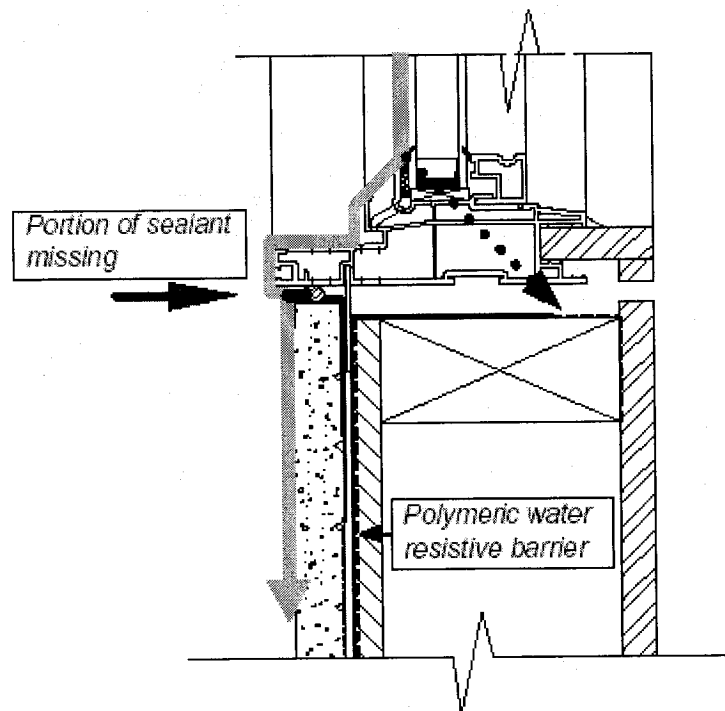


Figure 2.17. Notional path of water entry at wall-window interface about deficiency for the stucco-clad walls (Lacasse *et al.*, 2003).

The size of a defect, as well as its geometric configuration, i.e. the height:width ratio,

may also impact the rainwater leakage, although testing is required to verify this hypothesis since this aspect has not been investigated.

Overall, the findings suggest that the water entry rate is a function of the water spray rate, the air pressure difference across the wall, as well as the geometric configuration of the defect opening and the configuration of the wall assembly itself. A large number of parameters describe envelope defects and these cannot be averaged and could eventually be evaluated in a stochastic type of analysis. For the purposes of water leakage research, it is therefore difficult to reproduce a “typical” defect” and quantify the leakage characteristics. Much work remains to be done to fully characterize rainwater leakage through the building envelope and its deficiencies.

2.6 Review of work on representative climate data for building envelope testing

Heat, air and moisture building envelope evaluation, either experimental or numerical, requires setting boundary conditions or loads to which the wall or roof assemblies will be subjected. Several approaches have been developed to develop boundary conditions that reflect a specific climate. While no standard technique exists, it is generally agreed upon that, as it has been suggested for solar and energy studies that weather simulation should have three basic requirements: 1) true frequencies, where mean values and daily amplitude variations are close to the real ones and natural lower and higher daily variations; 2) true sequences, where duration and frequencies of weather sequences are similar to what occurs in reality, and; 3) true correlations between different parameters, e.g. temperature, solar radiation, cloud cover and wind (Lund and Mathis, 1991, in Geving, 1997). Methodologies have been developed for numerical modeling applications that consist of generating conditions that vary on an hourly basis in a stochastic or random fashion as are the conditions to which envelope assemblies experience in the field. To this purpose, reference years are selected to reflect a certain degree of severity for a climate. Reference years are years of hourly weather data that are selected based on statistical analysis of a large number, say 20 or more, of years of data. Examples of statistical years include the typical reference year (TRY), the typical

meteorological year (TMY) and weather years for energy calculations, WYEC2 (Weather Year for Energy Calculations version 2) and CWeC (Canadian Weather Year for Energy Calculations). These statistical years contains several climatic parameters such as maximum, minimum and mean temperature and relative humidity, maximum and mean wind speed, and daily global radiation, to characterize the climate with respect to heat and solar loads. In the context of hygrothermal testing, reference years are taken from meteorological databases and are subsequently used as input boundary conditions for numerical HAM studies. Climatic parameters should include temperature, relative humidity (alternately, dewpoint or wet bulb temperature could also be used), solar radiation, wind speed and direction, horizontal rainfall, and possibly cloud cover. Methods for determination of moisture reference years can be classified into two categories: those included in the first group are construction-independent and evaluate the reference year based on statistical manipulation of long-term weather data. Other methods, including that developed by the International Energy Agency (IEA) Annex 24 (Sanders, 1996), Geving (1997) and by the National Research Council (Djebbar, 2001) consider the effects of the envelope construction in the selection of the reference boundary conditions. Both groups can be broken down further into two types: those that take wind-driven rain into account and those that do not. These methods, as well as their applicability for stochastic, deterministic and quasi-stochastic determination of loading in numerical and experimental testing are discussed next.

2.6.1 Construction-independent methods for selection of reference years

Methods that do not consider wind-driven rain

The Π -factor method was developed by Hagentoft and Harderup (1993, 1996), and, while this method considers the material properties of the cladding, it is included in the construction-independent group because the selection of the reference year is not based on the envelope performance. It is based on wetting of the envelope on the cold plane outboard of the thermal insulation due to winter diffusion and is defined as the summation of the average hourly difference between saturation humidity of the outdoor surface temperature (T_s), $v_o(T_s)$, and the exterior humidity of the air, v_{ext} :

$$\Pi = \text{average}(v_o(T) - v_{ext}) \quad [2.15]$$

where $v_o(T_s)$ and v_{ext} are in g/m^3 . The average is taken over every hour of yearly available weather data, and the external surface temperature takes solar effects on a north-facing wall into account. The Π -factor gives a general indication for drying potential. When the outdoor relative humidity is high, the drying potential to the outdoors is reduced and the potential risk of summer condensation is high, resulting in a small Π -factor. Sanders (1996) suggests that a reference year should provide a more severe stress on the structure than the average climate with the aim of getting a factor of safety with respect to moisture damage. While structural engineering typically uses wind loads with a 50-year return period due to the risk of harm to human beings and heavy economical losses in the event of failure, lower return periods are usually recommended for moisture design. The International Energy Agency Annex 24 suggests a 10-year return period, meaning that the reference year subjects the envelope to severe hygrothermal loads that occurs once in every 10 years.

A tool developed by the NRCC/IRC called WeatherSmart makes use of a drying-out potential, called Π' -factor, that is analogous to Hagentoft and Harderup (1996)'s Π -factor. However, unlike the Π -factor, the Π' -factor does not take into account the characteristics of the wall to find the surface wall temperature, T_s . The Π' -factor is defined as the average of the difference between the absolute saturated humidity per unit volume at the outside wall surface and the absolute humidity per unit volume of the outdoor air, both in kg/m^3 :

$$\Pi' = \text{average}(v_o(T_s) - v_{out}) \quad [2.16]$$

The potential for a wet assembly to dry is small when the Π' -factor is small, and vice versa (Djebbar *et al.*, 2001).

Kalamees and Vinha (2004) have developed a construction-independent method called the saturation deficit for the selection of a moisture reference year that is very similar to the Π -factor and the DI, which will be described below. It is based on the drying potential of the outdoor air. It is determined similarly as the MEWS drying index (DI) but only takes into account the months with the lowest drying potential, determined to be December, January and February for Estonia.

The same authors have also developed a construction-independent moisture reference

year based on a different criterion: mould growth (Kalamees and Vinha, 2004). Making use of Viitanen's model, the method consists of determining the annual mould growth index using average daily temperature and relative humidity data and selecting the 10% level from a cumulative percentage of mould growth indices of 30-years. The technique takes into account the delay in mould growth due to a dry period and that the mould index remains constant when the temperature goes below freezing. Unlike other methods, Kalamees and Vinha have selected the reference year beginning in July and ending in June. It should be noted that since the method is construction-independent, outdoor temperature and relative humidity climatic data are used to evaluate the mould growth index. These conditions do not likely represent those to which the hygroscopic materials within an envelope would be subjected.

Methods that consider wind-driven rain

WeatherSmart also includes two modules for establishing a moisture reference year (MRY) that include the effect of wind-driven rain. The first deals with the exterior wetting potential of envelope assemblies. This module within WeatherSmart involves only weather analysis. It can be determined by selecting the year with the maximum amount of horizontal rainfall, R_h , or vertical rainfall, R_v . Vertical rainfall is defined as rain falling through vertical plane and is estimated based on Lacy (1965)'s correlation:

$$R_v = 0.222 \cdot V_{10} \cdot R_h^{0.88} \cos(\theta) \quad [2.17]$$

where V_{10} is the wind speed at 10 m height from grade, θ is the angle between the wind and the normal to the vertical plane, and the horizontal and vertical rainfalls are in units of $\text{kg/m}^2\text{h}$ here (Djebbar *et al.*, 2001).

The second WeatherSmart module that considers wetting by wind-driven rain makes use of the exterior wetting potential detailed above in conjunction with the modified Π' -factor method. The method combines the drying-out potential and the wetting driving rain method in finding the year that is the least forgiving in terms of both wetting of the exterior wall by wind-driven rain and the least potential for drying out. The worst year, evaluated with this method, is calculated as the one with the maximum product of the yearly vertical rain and the inverse of the Π' -factor (Djebbar *et al.*, 2001).

A method for determining the moisture reference year has also been developed by

Karagiozis (2004b) at the Oak Ridge National Laboratory (ORNL). The ORNL method bases its reference year on the modeling of wetting-drying balance of one layer of absorbent cladding exposed to the four cardinal points. The wetting of the stand-alone porous cladding includes absorption of wind-driven rain, condensation of the outdoor air and moisture deposition through air exfiltration. The drying is by diffusion through the cladding and evaporation at the exterior surface depending of the outdoor relative humidity. Specifically, the moisture absorption of the cladding is the resultant of three processes:

- the mass of wind-driven rain impinging on 1 m^2 exterior cladding (using Lacy's (1965) method), in kg/m^2 , multiplied by the brick absorption capacity; the method assumes uniform impinging wind-driven rain on the brick surface using the relation that takes into account wind directions from -90° to $+90^\circ$ to the normal of the building façade;
- condensation of the water vapor contained in 1 m^3 of outdoor air adjacent to the wall onto 1 m^2 of exterior cladding, in kg/m^2 ;
- absorption of all the water vapor in the air into the cladding due to wind-induced air infiltration or exfiltration through the exterior cladding, in kg/m^2 ; the wall is assumed to have an air permeance of $0.02 \text{ l/m}^2\cdot\text{Pa}\cdot\text{s}$; windward facades experience air infiltration, side and leeward facades experience exfiltration. Pressure differences due to stack effect are not taken into account.

The drying of the brick is taken into account:

- drying by evaporation dependent on temperature, outdoor relative humidity and solar radiation striking the façade. In determining the incident and emitted radiation, the model considers cloud cover, as well as the short and long-wave absorption and long-wave emissivity of the cladding.

Moisture content determinations in the porous cladding due to each of the three wetting processes and the drying process for a particular climate are made using a numerical HAM tool called Moisture-Expert every hour over 30 years for the cladding facing each of the four cardinal directions. Climatic data required are hourly outdoor dry bulb temperature, relative humidity, horizontal rainfall, wind speed, wind direction, solar radiation, and cloud cover. The method combines the effect of each of the three wetting

methods on the 1 m² brick cladding for each hour, and the moisture content in the brick cladding at the end of one year of simulation is recorded. The most onerous out of each of the four cardinal directions with respect to moisture absorption is selected for that particular year of weather data. The years are then ranked in terms of moisture content in the brick cladding at the end of each year. The moisture reference year is determined as the year that reached the 10% highest ranking. In other words, for 30 years of weather data with each year ranked in terms of moisture content, the moisture reference year is the third one.

The MEWS Consortium developed a Moisture Index, MI, to describe the climate and allow comparison of different climates. The MI is a function of two terms, the Wetting Index, WI, and the Drying Index, DI, describing a climate's potential to wet and to dry the envelope, respectively. The higher the MI, the more severe the moisture loading. The WI can be determined in two ways: the total annual average rainfall, or a more sophisticated measure that considers the effect of wind during rain, the annual driving rain index, aDRI (see Cornick *et al.*, 2002, for more details). Since hourly wind speed is not always reported at climatological stations, and since horizontal rainfall is readily available even for weather stations that do not report hourly data, the total annual rainfall was the preferred parameter for the MEWS study. Therefore, the WI, in mm/year, was calculated as:

$$WI = \frac{1}{n} \sum R_h \quad [2.18]$$

where the summation of the hourly horizontal rainfall, R_h , is carried out over a year and n is the number of years being considered. The drying index, DI, in kg_{water}/kg_{air}-year is a measure of the potential of a wet assembly to dry by evaporation, and is determined as:

$$DI = \frac{1}{n} \sum_{i=1}^n \sum_{h=1}^j \Delta w(t) \quad [2.19]$$

where n is the number of years being considered, j is the number of hours in a year, i.e. either 8760 or 8784, and Δw , in kg_{water}/kg_{air}, is defined as follows:

$$\Delta w(t) = w_o(t) - w(t) \quad [2.20]$$

where $w_o(t)$ is the humidity ratio at saturation at time t , and $w(t)$ is the humidity ratio at ambient conditions, both in kg_{water}/kg_{air}. w is calculated as in kg_{water}/kg_{air}:

$$w = 0.622 \left(\frac{P_{v,ext}}{P_{ext} - P_{v,ext}} \right) \quad [2.21]$$

Here, $p_{v,ext}$ is the vapor pressure of the ambient air and p_{ext} is the total pressure of the outdoor air, both in kPa.

Figure 2.18 shows the WI plotted against the DI. The location of each city's point on the graph characterizes its climate: on the upper left corner as being hot and dry, the upper right corner as being hot and wet, the lower left corner as being cold and dry, and the lower right corner as cold and wet

Ranking various cities' moisture loading is done by comparing the cities' Moisture Index, a single number that combines the effect of the wetting index and the drying index. Before the Moisture Index is determined, however, the MI and the DI are normalized to reduce the effect of variability among the various cities being compared:

$$I_{normalized} = \frac{I - I_{min}}{I_{max} - I_{min}} \quad [2.22]$$

The Moisture Index is then determined as follows:

$$MI = \left(WI_{normalized}^2 + (1 - DI_{normalized})^2 \right)^{1/2} \quad [2.23]$$

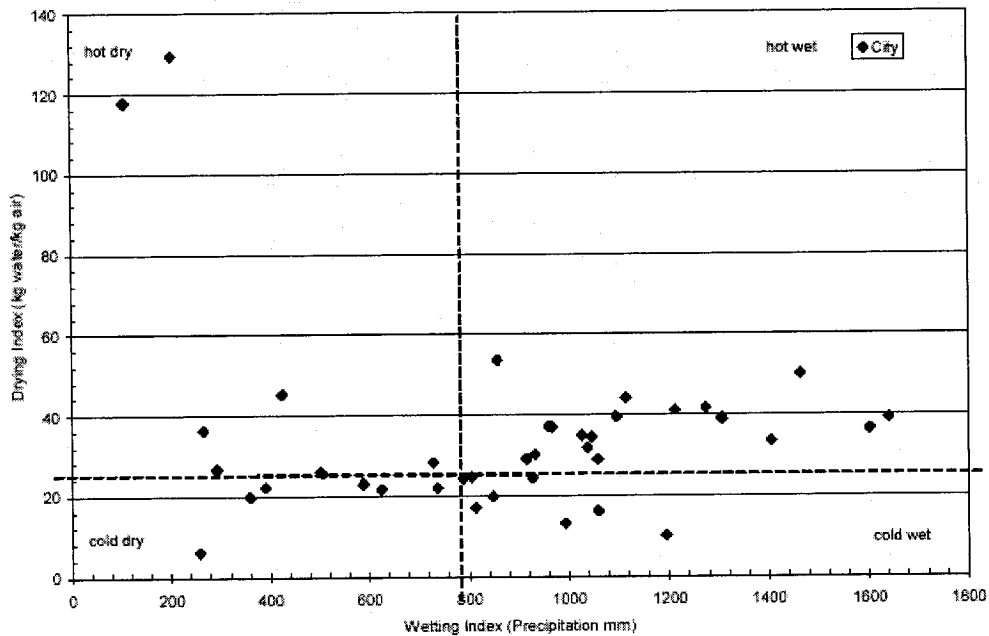


Figure 2.18. Plot of DI versus WI for 40 North-American candidate cities from the MEWS project (Cornick *et al.*, 2002).

One of the objectives of developing the MI was to designate specific years for input for the purpose of hygrothermal modeling. To this purpose, a Moisture Index was found for each year for each location, and from these years, three were classified as wet, dry or average. It has been suggested that wet and dry years could both be defined, independent of building characteristics and response, as those years that deviate more than one standard deviation from the mean, and average years as those that deviate within one standard deviation. However, for the MEWS project, a wet and a dry year for a given climate were defined as those with the highest and lowest moisture index, respectively, and the average year as the one with the moisture index closest to the average of the years (Cornick *et al.*, 2002).

2.6.2 Construction-dependent methods for selection of reference years

Three methodologies for the determination of a reference year that base the selection of the reference year on the hygrothermal response of envelope assemblies have been developed. The mechanism for wetting here is diffusive moisture transfer, a process that is very much dependent on the envelope configuration and material properties.

The first two methods, that of the IEA Annex 24 (Sanders, 1996) and of Geving (1997), do not consider moisture loading by wind-driven rain, while the one developed by the NRCC WeatherSmart tool does.

Methods that do not consider wind-driven rain

Sanders' (1996) proposed method, developed in the context of IEA Annex 24, involves finding a durability reference year (DRY) by determining the climate that causes 10% level (90th percentile) of condensation within 5 envelope assemblies as determined by a Glaser, MATCH-like tool or Π -factor method. The IEA method specifies north and south-facing walls with an impermeable façade, north and south-facing lightweight walls, and a flat roof. This method specifies that each "year" begin in October and end the following September so that winter diffusion wetting precedes summer drying. Input data include many years of monthly average values of outdoor temperature, relative humidity and solar radiation. Rode (1993), however, cautions against the use of monthly

means of climatic and suggests that it is necessary to consider the intensity and frequency of the peak values because of the non-linearity of the moisture migration processes.

Geving (1997) developed a construction-dependent reference year called Moisture Durability Reference Year (MDRY) that uses hourly weather data and is based on two evaluation criteria, MC-Avg, and MC-Max, as defined below:

- MC-Avg: the average total moisture content, in kg/m^2 , of the whole construction during the last year of the calculation period, and;
- MC-Max: the maximum moisture content, in kg/m^2 , in the hygroscopic layer just outside the insulation or the outermost part of the insulation during the last year of the calculation period.

Values for MC-Avg and MC-Max are calculated for each of the six defined construction types and for as many years available of weather data, in two ways. In the first method, called the “full method”, the two criteria are calculated by means of a one-dimensional HAM model. At least 10 years of hourly data of outdoor temperature, relative humidity and global radiation, are recommended, or daily data with the use of an expected diurnal variation. The methodology specifies the requirements of the HAM model, construction types, input parameters including materials and material properties, indoor conditions, wall orientation, simulation period and evaluation criteria. The second method, called the “simplified method,” finds the MC-Avg and MC-Max criteria by using linear regression equations that are based on the fact that strong correlations have been found between the two evaluation criteria and the average annual outdoor relative humidity. A regression equation is found for both criteria and for each of the construction types, in the following form:

$$MC_{avg} = \beta_0 + \beta_1 T_{year} + \beta_2 I_{g,year} \quad [2.24]$$

$$MC_{max} = \beta_0 + \beta_1 T_{year} + \beta_2 RH_{year} + \beta_3 I_{g,year} \quad [2.25]$$

where T_{year} , RH_{year} and $I_{g,year}$ are the annual averages for outdoor temperature ($^{\circ}\text{C}$), relative humidity (%) and global radiation (W/m^2), respectively, and β_0 , β_1 , and β_2 and β_3 are regression coefficients. Once values of MC-Avg and MC-Max are found for each year and construction type, the years are ranked in terms of the relative moisture stress on a construction. The details for selecting a single MDRY are explained in Geving (1997).

Geving's findings indicate that when the calculated values for both moisture criteria were used to select an MDRY for each construction, the MDRY's had return periods near 10 years when comparing with the MC-Avg and the MC-Max found using HAM simulations with the exception of some constructions using MC-Max.

It is highly likely that for different constructions, different MDRY's will be obtained, and the difficulty then lies in selecting one MDRY for all the given construction types. However, Geving claims that one MDRY can be found for a given climate that is independent of the type of construction, orientation, etc., and represents a varying degree of performance severity for the different constructions (Geving, 1997). Geving recommends, though, that MDRY's resulting in a probability above 50% be avoided.

Advantages of the concept of selecting a year with real climatic data includes requirements such as true sequences, true frequencies and true correlations, and the use of different construction types in the process assures that the varying climatic response of the different construction types is taken into account.

The full method is limited in the sense that it is a time-consuming and laborious process, and at least 10 years of hourly data is needed. In contrast, the simplified method is quick and easy to use, only requires annual mean climatic parameters, and gives almost the same results as the full method. However, further investigations is required to find out if regression equations developed for one climate can be used for other climates. With respect to both methods, Geving gives the following limitations:

- 1) only one-dimensional heat and mass transfer is considered;
- 2) wind-driven rain and air migration through the assembly are not taken into account;
- 3) the chosen MDRY should not be applied to constructions with a low vapor permeance outside the insulation when the determination of the MRY has been performed using a constant annual indoor relative humidity, and;
- 4) the selected MDRY may not be a critical 10% year for all types of moisture calculations and it may not be sufficiently severe for different constructions.

Methods that consider wind-driven rain

WeatherSmart includes a refined method for determination of a construction-dependent moisture reference year (MRY) analogous to the one set out by the IEA

Annex-24 (Sanders, 1996) and by Geving (1997) except that it considers wind-driven rain as a moisture source. Typical indoor boundary conditions, i.e. controlled indoor environments, are selected. WeatherSmart uses a one-dimensional HAM tool, hygIRC, to determine the moisture performance of a set of at least 5 typical building envelope designs subjected to a given climate for a prescribed time period. Then, a moisture load module identifies the worst moisture years by rank using a worst moisture year criteria as well as the 10%-level MC-Avg and MC-Max for the location. A method outlined by Djebbar *et al.* (2001) indicates how to select the moisture reference year when the various criteria produce several different critical years. However, when the analysis is run using a large bank of data of, say, 30 years, the designer must still decide whether to apply the loads of the 10%-level year considering that the moisture loads likely recur every 10 years, or select the worst moisture year for the location.

The advantages of establishing reference years are that they provide stochastic environmental boundary conditions such as temperature, rainfall and wind speed, that, with respect to wind-driven rain, incorporate Lund and Mathis' true frequencies, true sequences and true correlations. Such stochastic loading is ideal for a numerical HAM simulation study, where the climatic data from the selected reference year can be easily input. As was seen, reference years can be determined by statistical analysis of the meteorological data, or by ranking the years with respect to the severity of the performance of selected constructions. While some of the construction-dependent methods take into account wind-driven rain, none of them take into consideration driving rain *infiltration* into the back wall of building envelopes. In the presence of envelope defects, rainwater leakage can be the source of moisture several orders of magnitude greater than diffusion or moisture deposition by air convection. To be applicable for wetting by wind-driven rain penetration, the simulation tools need to take into account the complex process of intermittent impinging wind-driven rain upon the cladding surface, that being absorbed or running off, evaporating, and leaking in through cracks or defects, and also how the leakage water is then distributed within the 3-dimensional assembly. Another difficulty lies in modeling the three-dimensional absorption of leakage water in anisotropic hygroscopic materials such as wood and engineered wood

products. These important limitations restrict the use of moisture reference year selection based on the moisture performance of envelopes subjected to wind-driven rain penetration loads. Therefore, for the purposes of wetting due to driving rain infiltration, the loading can be determined by a statistical analysis of weather data.

2.6.3 Deterministic and quasi-stochastic loading

Given the limitations of numerical modeling where rainwater infiltration loads are considered, experimental testing is more suitable to evaluate certain types of hygrothermal responses. Such research has been done to date using deterministic loading methods (Lang *et al.* 1999). While stochastic boundary conditions such as that occurring in reality may be ideal, the control of space conditioning and water insertion rates required for driving rain infiltration testing is difficult and costly to achieve experimentally. Therefore, deterministic or quasi-stochastic methods may be more appropriate for experimental setups.

Deterministic climate characterization and experimental simulation

Deterministic climatic loads have long been used in HVAC design. For example, the National Building Code of Canada recommends the use of a 2.5% temperature value for design of building heating systems, which signifies the lowest temperature at or below which only the small percentage of 2.5% of hourly outdoor air temperatures in January occur (NBCC, art. 2.2.1.1.(1) (NRCC, 1995)). ASHRAE (2001), on the other hand, provides 99% and 99.6% annual cumulative frequency of occurrence temperature design conditions for sizing HVAC equipment for heating requirements. Monthly data is also used to provide additional information when solar geometry and intensity and building occupancy vary. Deterministic wind-driven rain loading conditions produce steady state or diurnally varying wetting conditions that repeat in a pattern on a daily, weekly or monthly basis, usually determined as per weather data analysis based on statistical analysis of weather database. A procedure to determine the environmental conditions and driving rain penetration loads for deterministic conditions could first select a moisture design reference year using one of the 4 previously described methods: 1)

WeatherSmart's exterior wetting potential; 2) WeatherSmart's combined exterior wetting/drying out potential; 3) ORNL-ANK method, or; 4) MEWS Moisture Index. Once the reference year would be selected with the desired criteria, e.g. a 10% return period, the climatic parameters could easily be calculated.

It has been commented that in contrast to hourly data, averaged data, i.e. daily, weekly data or monthly data, may not adequately reflect actual climatic events and hence lead to incorrect envelope performance results, especially in light constructions (Rode, 1993; Künzle, 1993; Geving, 1997). Furthermore, given the stochastic nature of rainstorms in terms of their irregular intensities and the intermittent frequencies in which they occur, hourly data are necessary.

Whereas the stochastic method implicitly includes determination of the frequency and duration of wind-driven rain, the deterministic method requires an extra step to determine these features. To meet Lund and Mathis' (1991) "true sequences" requirement, the deterministic wetting methodology should reproduce the frequency and duration of climatic events such as wind-driven rain episodes as faithfully as possible.

Quasi-stochastic climate characterization and experimental simulation

No experimental works have been found in the literature that have made use of stochastic or quasi-stochastic climatic loading because of the difficulties in programming and controlling such conditions. To simulate daily and monthly temperature variations, Derome and Fazio (2000) used a steady periodic temperature cycling over nine periods representing the Montreal climate from November to July.

In terms of wind-driven rain infiltration loading, to attain the practicality of the deterministic method, and the stochastic nature of real weather, a quasi-stochastic method is recommended. This approach method is closer to reality since a different rate of driving rain infiltration is applied for each hour. However, the approach requires a computer-controlled water loading apparatus.

2.6.4 Duration of wetting load application

Whereas numerical modeling can be performed on a long time span of one or more

years, this is not practical for experimentation. The duration of the wetting phase may need to be decreased. However, if a short or a long-term exposure duration more appropriate? The answer may depend on the objectives of experiment, i.e. to evaluate the impact of short-term wetting or long-term wetting on the hygrothermal response of the envelope. An approach similar to the environmental loading indices described by Sanders (1996) in the context of Annex 24 can be adopted. Sanders presents two wall indices that can describe wind-driven rain. The first is called a spell wall index and involves shorter term spells of heavy driving rain impacting on a façade where there are several short periods of rain separated by intervals without rain that "do not permit significant drying of the façade. It is characterized in terms of rain penetration through masonry which needs prolonged input of water. The concept of the spell index can be used for studies where the aim is to determine the drying capacity of a wall system exposed to relatively large infiltration rates. An example of the application of such a concept is an experiment carried out by Lang *et al.* (1999) to examine the drying behavior of walls subjected to water inserted through a pipe at the top of the wall assembly at a rate of 0.0417 l/h , or a total of 4 l over 4 consecutive days. The intent of the wetting process in this case was to increase the moisture content of the wood wall components to 20% moisture content. However, the relatively large load of water accumulated at the bottom of the wood-frame assemblies and took a significant amount of time to dry.

Sanders' second index, termed annual wall index, is a long-term (generally annual) average amount of driving rain impacting on a façade, and influences the average moisture content of envelope cladding. Therefore, it is more relevant to determine the risk to frost damage, fungal growth, etc. The concept of an annual wall index can be applied to evaluate the response of envelopes to more prolonged, average loads. It should be noted that when testing the hygrothermal performance of materials such as wood subjected to a water source, a relatively long time span is required for in-depth absorption given the slow absorption of water into wood, especially in the tangential and radial directions.

2.7 Summary

Hygroscopic materials such as wood, found, for example, in exterior sheathing and framing members of the building envelope, have the potential to absorb and store eventual moisture, a situation which may lead to deterioration building envelopes if temperature and time conditions are favorable. Many studies investigated the behavior of such materials in envelope assemblies subjected to different loading conditions. However, it was found that little large-scale experimental work has been performed to date to examine the role of wood-based exterior sheathing in the hygrothermal performance of the wall assemblies exposed to realistic environmental conditions, namely rain water penetration through minor defects.

Rain can be an important source of moisture, as was revealed by the British Columbia condominium building envelope failure study commissioned by David Barrett in 1998. However, few experimental research projects consider rain leakage as a source of moisture because of the complexity of the rain infiltration process. Those studies that do include rain leakage tend to either spray the exterior surface of the wall using a spray rack, or insert water directly into the assemblies. The former procedure is usually intended for rain penetration tests and is not designed to allow any control over the amount of water that leaks into the assemblies. Consequently, the latter method is deemed more appropriate for studies where the drying of the panels will be monitored and analyzed.

To accurately simulate rain penetration, it was shown that it is necessary to understand the nature of rain, wind-driven rain in the atmosphere, and driving rain deposition on building envelopes. Models developed by Blocken and Carmeliet as well as Straube and Burnett can be used to determine the impinging rain on a specific location of a building facade. Both models require inputs such as the rate or amount of horizontal rainfall, the wind speed and the wind orientation. An understanding of how and where rain infiltrates building walls is also an important key in simulating rain leakage. Studies found in literature show that envelope interfaces such as wall/window junctions are common culprits and windows are particularly vulnerable to rain water leakage since the impervious nature of glazing leads to water accumulation at the sills.

In the study of drying of wall assemblies, two issues have surfaced. The use of a vapor retarder in cold climate construction is required by the National Building Code of Canada to minimize the migration of water vapor into building envelope assemblies and the potential formation of condensation on the surfaces outboard of the thermal insulation during the heating season. However, it is argued in the literature that the presence of a vapor barrier such as the commonly used polyethylene membrane can hinder the drying of incidental moisture within the stud space when conditions favor inward vapor migration. There is a need to investigate the impact of the permeance of the vapor retarder in assemblies that have been subjected to simulated water infiltration and real climatic loading. In addition, the energy crisis of the 1970's has called for the use of thermal insulation to reduce the heat flow across the envelope, and hence the energy consumption required to maintain desired comfort levels with the building. Exterior insulation is a popular option for new and retrofit works. However, the presence of exterior insulation changes the envelope temperature distribution and also reduces the vapor permeance outboard of the wall sheathing. It was found that previous work has been done to evaluate the role of exterior insulation on hygrothermal performance; however, there is a need to investigate its effects on the drying performance for large-scale specimens subjected to important moisture loads such as simulated driving rain infiltration.

The following work deals with the development of a wetting protocol that seeks to simulate rainwater leakage through a typical building envelope detail using actual climatic data from the Montreal meteorological station at the Pierre-Elliott Trudeau International Airport, in Dorval. A series of test wall panels with various construction configurations including different exterior sheathings will be subjected to a wetting cycle and then a drying cycle representing Montreal weather conditions, during which time they will be monitored with temperature, relative humidity and moisture content sensors in order to observe their hygrothermal performance.

3. METHODOLOGY FOR THE DEVELOPMENT OF THE WETTING PROTOCOL

The objective of the wetting protocol development was to specify the set-up and procedure for the wetting of wall assemblies to realistically simulate exposure to rain infiltration through an example of a defect in a window/wall junction. Rain infiltration is defined as “a process by which water passes through a material or between materials in a system and reaches a space that is not directly or intentionally exposed to the water source” (ASTM, 2002). As was stated in the literature review, little research has been done to estimate the amount of rainwater infiltration into building envelope deficiencies. Field studies have reported moisture content accumulation leading to rotting of wood components in walls that have suffered from rainwater leakage (Ricketts and Lovatt, 1996). However, the amount or rate of rainwater infiltrating into wall assemblies in the field has not yet been documented. Hence, a wetting protocol for the Montreal climate was developed for the purpose of establishing the water infiltration load into a wood-frame wall for two large-scale building envelope hygrothermal experiments that were run in the Environmental Chamber. Based on findings from the first two tests, a second methodology was developed for a third hygrothermal experiment also performed in the Environmental Chamber. The experimental wetting methodologies are discussed here.

3.1 Methodology for simulation of wind-driven rain infiltration – tests 1 and 2

The objective of the methodology was to generate loading in the form of a liquid moisture source based on actual climate characteristics that a) produced experimentally repeatable wetting patterns; b) permitted analysis of the impact of wetting of the assemblies on their hygrothermal response, and; c) was straightforward to carry out experimentally. Hence, a deterministic methodology was developed to estimate the rate of driving rain infiltration into wall systems and was based on three steps:

1. Establishing the nature of the climate in terms of the relevant climate parameters;
2. Determining the average rate of wind-driven rain impinging at a specified location on a building façade, and;
3. Quantifying the ratio of water infiltration to impinging water through an intentional building envelope defect.

The ratio of water infiltration was determined using the results of a water leakage test. The frequency and duration of the water insertion were determined from analysis of meteorological data.

The case examined was one of a low-rise wood-frame residential building devoid of roof overhangs located in a relatively open area of suburban Montreal. The building was not sheltered from wind and rain and from surrounding buildings and trees. The wind was assumed to strike at 90° to the plane of the facade. The wall section under consideration was taken to be at mid-height of a one-story façade.

This development of the wetting protocol used in experiments 1 and 2 is presented in the following sections.

3.1.1 Methodology to determine the rate of water infiltration

The determination of the rate of water insertion first requires statistical analysis of a weather database, followed by determining the rate of water impinging on a given wall surface at a specific area on the facade. Finally the proportion of the impinging water that leaks into the building envelope through a defect must be established. These three steps are described in detail below.

3.1.1.1 Climate database analysis

The climate variables typically required to calculate impinging rates of wind-driven rain are:

1. the horizontal rainfall,
2. the wind speed, and;
3. the wind direction.

Horizontal rainfall is defined as the amount of rain falling on a horizontal plane

undisturbed by building and other effects

Before continuing, a note should be made on the severity level chosen for the climatic conditions. As was stated in the literature review, much work has been undertaken in the last 15 years or so in an attempt to set guidelines for setting boundary conditions for HAM testing, and numerical simulations in particular (see section 2.6). The studies suggest the use of boundary conditions that provide a certain level of severity, e.g. climate conditions with a return period of 10 years, i.e. conditions that have a probability of being exceeded once in 10 years. However, in this study, it was desired to set climatic conditions that are typical for the Montreal area, and hence average conditions were selected.

Since the amount of horizontal rainfall varies throughout the year, the month of the year to be simulated in the test was found first. The month selected was one with sufficient rainfall that would have the potential to produce a significant amount of water leakage and one when temperatures are greater than 0°C in order to preclude precipitation in the form of snow. Meteorological data from the Trudeau International Airport weather station in the Montreal suburb of Dorval, provided by the Environment Canada website, was examined to select the month from which precipitation data was taken. The monthly average data over the period from 1941 to 1990 was obtained from Environment Canada is shown in Table 3.1. Data indicates that August has the highest amount of rain (100.3 mm). The results of a detailed analysis of the *hourly* rain and snow data for the years between 1981 to 2001 using raw data obtained from Environment Canada are shown in seen in Table 3.2 (the computation method of the analysis is given in Appendix A). A comparison of the precipitation data in Tables 3.1 and 3.2 shows that while the average hourly precipitation rate is slightly higher in July, the average total rainfall in August is higher. The higher monthly rainfall in August occurs because both the average daily hours of rainfall and the average number of rainy days over the month days are greater during this month. Thus, an average hourly horizontal rainfall in August of 1.93 mm, or 1.93 l/m², was found. The recommendations of Sanders (1996), Künzle (1993) and Geving (1997) suggest the use of climate conditions with a 10-year return period, or a climate that subjects the envelope to severe hygrothermal loads occurring once in every 10 years. While conditions of this severity could have been applied here, the intent of the

test for which this methodology was developed was to consider commonly occurring conditions, or average, hence a 50% probability. An examination of the frequency distributions of the August hourly horizontal rainfall for years with the minimum, maximum and average monthly rainfall in August (Figure 3.1) over the 1981-2001 period confirms that the highest frequency of rainfall by far occurs at rates of less than 2.0 mm per hour. Hence, the selection of hourly horizontal rainfall of 1.93 l/m^2 ($6.06 \text{ liquid-ounces/ft}^2$) was appropriate.

Table 3.1. 50-year mean climatic data for Montreal, Trudeau International Airport weather station for years 1941 to 1990 (Environment Canada website).

| | Jan. | Feb. | Mar. | Apr. | May | June | July | Aug. | Sept. | Oct. | Nov. | Dec. |
|--------------------------------|-------|-------|------|------|------|------|------|-------|-------|------|------|------|
| Precipitation | | | | | | | | | | | | |
| Rain [mm] | 20.8 | 18.8 | 34.1 | 62.6 | 66.7 | 82.5 | 85.6 | 100.3 | 86.5 | 72.8 | 70.4 | 35.1 |
| Snow [mm] | 47.7 | 41.2 | 31.3 | 10.9 | 1.6 | 0 | 0 | 0 | 0 | 2.6 | 24.1 | 54.8 |
| Temperature | | | | | | | | | | | | |
| Daily min. [°C] | -14.9 | -13.5 | -6.9 | 0.6 | 7.3 | 12.5 | 15.4 | 14.1 | 9.3 | 3.6 | -2 | -11 |
| Daily Mean [°C] | -10.3 | -8.8 | -2.4 | 5.7 | 12.9 | 18 | 20.8 | 19.4 | 14.5 | 8.3 | 1.6 | -6.9 |
| Days with: | | | | | | | | | | | | |
| Measurable horizontal rainfall | 4 | 4 | 7 | 11 | 13 | 13 | 12 | 13 | 11 | 13 | 11 | 6 |
| Measurable horizontal snowfall | 15 | 12 | 9 | 3 | - | 0 | 0 | 0 | 0 | 1 | 6 | 14 |
| Relative humidity | | | | | | | | | | | | |
| Measured at 6:00 [%] | 75 | 75 | 75 | 75 | 75 | 78 | 82 | 86 | 87 | 84 | 82 | 78 |
| Measured at 15:00 [%] | 69 | 66 | 61 | 55 | 52 | 56 | 55 | 58 | 60 | 62 | 70 | 72 |

Table 3.2. Data showing the calculated average hourly horizontal rainfall, average daily number of hours of rain, the average number of rainy days and the average total amount of rain over the month, for the months from April to October, analysis of 20-year Environment Canada climatic data file for the Trudeau airport climatic station for the years 1981 to 2001.

| | April | May | June | July | August | Sept. | Oct.* |
|--|-------|------|------|------|--------|-------|-------|
| Average hourly horizontal rainfall over 20 years [mm] | 1.06 | 1.21 | 1.63 | 2.02 | 1.93 | 1.56 | 1.23 |
| Average daily number of hours of rain over 20 years [hrs] | 5.5 | 4.6 | 3.9 | 3.4 | 3.8 | 4.5 | 5.0 |
| Average number of rainy days in a month over 20 years [days] | 11.4 | 13.5 | 12.9 | 11.9 | 12.4 | 12.0 | 12.1 |
| Average monthly horizontal rainfall over 20 years [mm] | 66.4 | 75.4 | 82.3 | 82.0 | 89.7 | 84.4 | 74.2 |

*Data for 2001 were not available when the analysis was done.

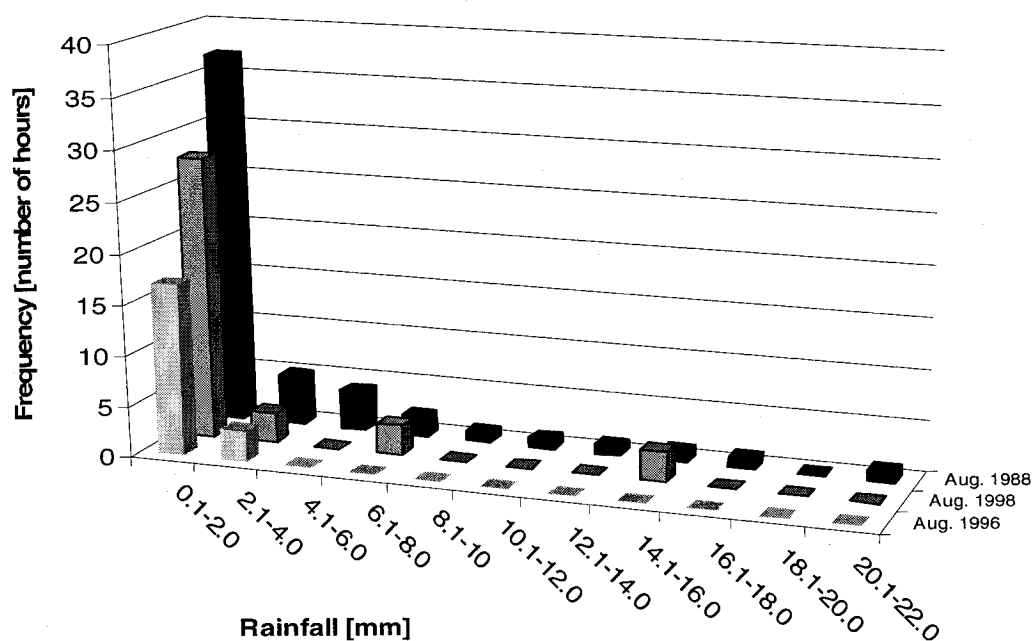


Figure 3.1. Frequency distribution of horizontal rainfall in August for three years: 1996, 1998 and 1988, the years with the minimum, average and maximum monthly rainfall, respectively, over 1981-2001.

The wind speed and wind direction must also be determined to obtain the rate of water impinging on a given wall surface. Statistical analysis of hourly wind speed data from the Montreal meteorological station at Trudeau airport for August 1981 to 2001 has

produced a wind speed frequency distribution, which can be found in the Figure 3.2. In keeping with the intent of the test to use commonly occurring wind-driven rain conditions, the most frequently occurring wind speed during rainfall was initially selected. Analysis of this data, as explained in Appendix B, shows that the most prevalent suburban wind speed for all wind directions during rainfall in August is in the 1.5 to 2.0 m/s range and occurs 13.5% of the time. To simplify the computations, it is assumed that the wind strikes in a direction perpendicular to the plane of the façade. The hourly wind speed, as well as the hourly rate of rainfall, are used to determine the rate of rainwater impinging on a given wall surface.

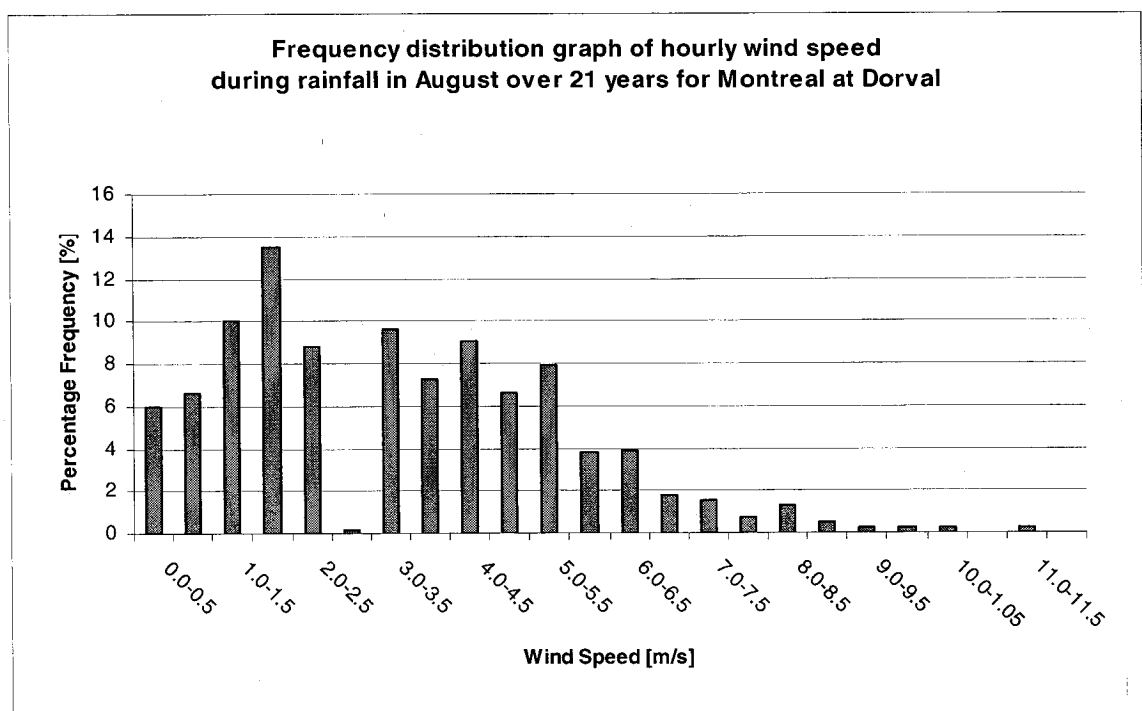


Figure 3.2. Frequency distribution of hourly wind speed during rainfall in August (1981-2001).

3.1.1.2 Determination of rate of water impinging on a given wall surface

Three methods were described in the literature survey to calculate the amount of water impinging on a given wall surface using weather data. Straube and Burnett (2000)'s empirical method, as well as Choi (1991, 1994; 1999a; 2000)'s and Blocken and Carmeliet (2000b, 2001a, 2001b)'s numerical studies require climatic data inputs such as the horizontal rainfall amount of rate, the wind speed and the wind direction. Straube and

Burnett's method involves the computation of the driving rain factor, or DRF, which is a function of the raindrop size distribution and the terminal velocity of raindrops. While the DRF value can be assumed to lie between 2.0 and 2.225, assuming an incorrect DRF value can lead to an error in estimating the driving rain on a building façade as high as 11%.

Therefore, the determination of wind-driven rain on building facades was based on the results of Blocken and Carmeliet's numerical study. It should be noted that their study did not account for wetting by water runoff, and nor did the present work. To calculate the amount of wind-driven rain impinging a zone on a wall surface, the input data required are the horizontal rainfall, the wind speed, and the wind direction. Results from Blocken and Carmeliet's CFD model at approximately one-third the height of a one-story building is shown graphically in Figure 2.12 in terms of a catch ratio. The catch ratio is defined as the ratio of the intensity of raindrops landing on a specific zone on the building face to the intensity of the horizontal rainfall. Once the rate of horizontal rainfall and the wind speed is known, the catch ratio and then the rate of driving rain onto a building surface can be found.

As was said in the literature review, Blocken and Carmeliet's model makes use of Best's raindrop size distribution. The model has been validated with field data and shown to be accurate for wind flows perpendicular to the façade surface, although further verification by these authors will take into account varying wind directions (Blocken and Carmeliet, 2002). In addition, the computational fluid dynamics model does not take into account the turbulent dispersion of raindrops that may occur when raindrops reach a turbulent region after separation, for example. Last, the model's predictions may be less accurate at locations on the building surface where there is a sweeping effect of drops, i.e. at the top and side edges of the façade, and at the transition between unsheltered and sheltered regions on the façade due to an overhang, for example, or a combination of these two phenomena.

With the hourly rate of horizontal rainfall and the 10 m suburban wind speed known (see section 3.1.1.1), the catch ratio was determined. For this purpose, the results of Blocken and Carmeliet's research (2001b), which is based on Best's raindrop size distribution, were used. Figure 2.12 shows that for an average August wind speed V_{10} of

2.0 m/s and an August hourly horizontal precipitation rate of 1.93 l/m^2 , the catch ratio is approximately 0.12 for a specific location on the building facade. This catch ratio, multiplied by the horizontal precipitation rate, resulted in 0.23 l/m^2 per hour of rain impinging at a specified location on the building envelope. It should be noted that Figure 2.12 shows a catch ratio that was generated for a specific location on a building facade, with a given distance from the roof overhang, height of wall, etc. The hourly rate of impinging rain per unit area served to determine the hourly rate of water infiltration.

3.1.1.3 Determination the fraction of impinging water infiltration into a wall assembly

A water infiltration test was performed in the Rain Penetration Chamber with the object of estimating the fraction of impinging water that infiltrates through a defect at a wall/window junction. In this test, water runoff on the exterior surface of the wall, and actual determination of water infiltration paths through envelope defects and into the stud space were not included in the study. Also, the study did not look at different detailing and junction configurations.

The chamber is 3.35 m wide by 1.30 m deep by 3.00 m high. It has a rough opening on one side that can accommodate specimens with sizes up to 2.4 m by 2.4 m. The spray rack consists of 4 horizontal pipes 610 mm apart facing the opening, each pipe fitted with up to 23 nozzles. The pipes can be set to move collectively up and down to promote a uniform spray rate throughout the opening. The water which runs off the tested specimen is collected at the bottom of the Rain Penetration Chamber and is recirculated to the tubes via a pump. The spray rate can be controlled and calibrated by adjusting a supply valve. The chamber has a small 0.44 by 0.60 m window at the back for visualization.

Wall/window junctions are found in every building and the impervious nature of glazing leads to collection of rainwater at the bottom of the window, which, in turn, increases the risk and the magnitude of rainwater infiltration if a defect is present at the sill. Thus, a window mock-up was designed and built for the purpose of the water leakage tests.

The geometry of the defect that was simulated for the water infiltration test was based on an example of a failure detail presented in a workshop sponsored by CMHC (1999). In this case, the seal between the aluminum window frame and the extruded aluminum

sill was the only line of defense against water infiltration into the EIFS back wall (see Figure 3.3). To make matters worse, any shrinkage of the wood framing due to drying of the initial construction moisture could cause the slope of the aluminum sill to reverse, thus ensuring water infiltration through gaps in the sealant.

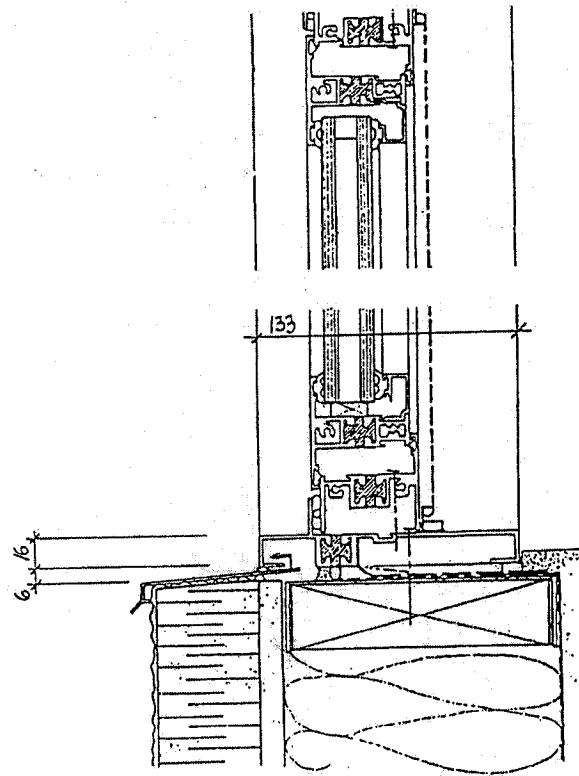


Figure 3.3. Window detail in EIFS wall (CMHC, 1999).

The amount of water that reaches a particular location on a building façade, and hence the water that can potentially leak into the envelope, depends on both the amount of rainwater that strikes the wall at that location, and the water runoff from above, and, to a lesser extent, from the sides. Field observations (Doshi, 2005) and computational field studies (Choi, 1994; Blocken and Carmeliet, 2000a) show that the top of a building façade tends to be exposed to greater amounts of impinging rain, while the lower façade sections receive less direct rain. Bell (2001) states that the water that impinges directly upon a building surface area is small compared to the water runoff from above. However, the amount of water runoff is difficult to quantify because it depends on

several parameters such as the height of the wall above the point under consideration, the moisture content and water absorption capacity of the building materials above, and the presence of water-shedding architectural details such as cornices drips and overhangs, etc. In addition, it is suggested that the proportion of water collecting at a window sill due to water running off the façade above the window is small compared to that running off the glazing itself. Because of the two aforementioned reasons, water runoff from the wall surface above the window was not considered or simulated in the water infiltration test. The mock wall/window was constructed in such a way that the any water runoff from above the window was collected and drained away by means of a gutter above the window. Thus, the fraction of rain infiltrating into a defect in the wall mockup was solely a function of the rate of impinging water on the one square meter of glass.

Thus, a perimeter seal defect was simulated during the water infiltration test. A series of four tests with different leakage areas were performed, the first with one 25 mm² gap in the sealant, the second with two 25 mm² gaps, the third with three 25 mm² gaps, and the last with one 50 mm² gap. The different defect area sizes were used in an attempt to establish a rough correlation between total leakage area and amount of water infiltration. Figure 3.4 shows a section view of the Rain Penetration Chamber and the wall/window set-up, and Figure 3.5 shows an elevation of the mock wall/window junction showing where the defect was located.

The water infiltration test was based on the methodology from ASTM E331-00 (2000a), the Standard Test Method for Water Penetration of Exterior Windows, Curtain Walls and Doors by Uniform Static Air Pressure Difference. The Standard prescribes that a spray rate of 3.4 l/m²min and a positive air pressure difference of 137 Pa be applied to the outside of the assembly with respect to the inside to simulate the effect of wind. The water spray is applied directly to the exterior face of the tested assembly, and hence simulates wind-driven rain in the field.

Before running the test, a water flow calibration procedure was run. The calibration method specified in ASTM E331-00 (2000a) was used but was slightly modified: while the Standard describes a 0.37 m² (4 sq.ft.) calibration catch box compartmentalized into 0.093 m² (1 ft²) squares, a square catch box of the same size as the 1 m² glass opening was used. The lower and upper limits of impinging water set by the Standard are:

- a minimum of 0.25 l/min in each square;
- a maximum of 0.63 l/min in each square;
- a minimum of 1.26 l/min of water in the entire 0.37 m² (4 sq. ft) catch box.

These limits are converted for a single 1 m² opening:

- a minimum of 2.69 l/min·m²;
- a maximum of 6.78 l/min·m².

The calibration was done on a wall/window mockup built without the 1 m² glass pane, and the amount of water entering the 1 m² opening was collected and then measured.

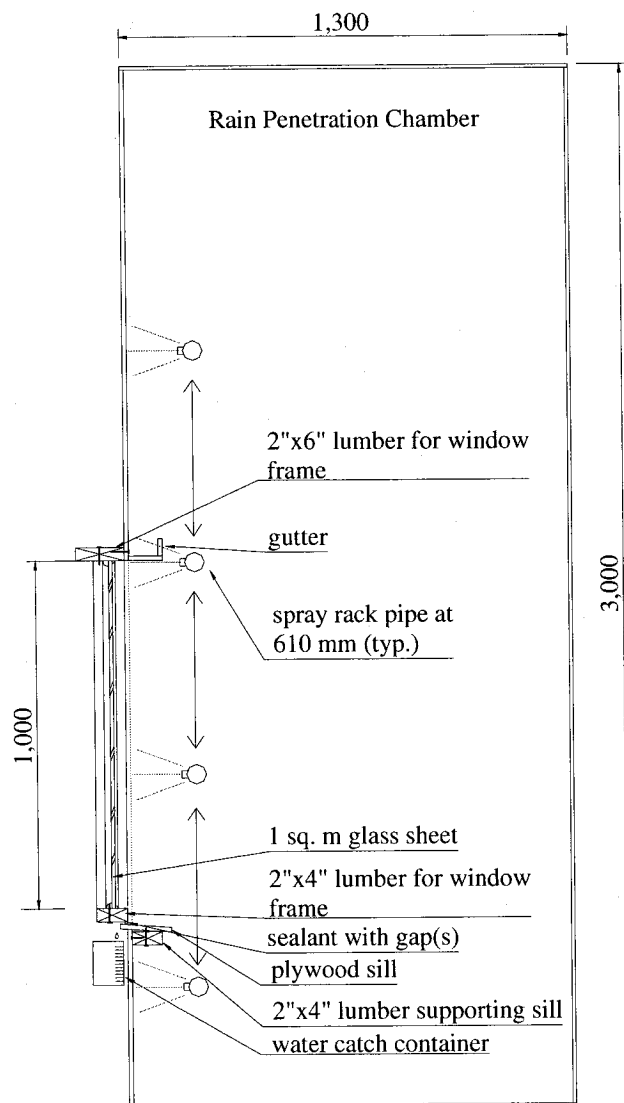


Figure 3.4. Schematic section of the mock test wall/window assembly simulating a

perimeter sealant defect at the windowsill used in the water infiltration test.

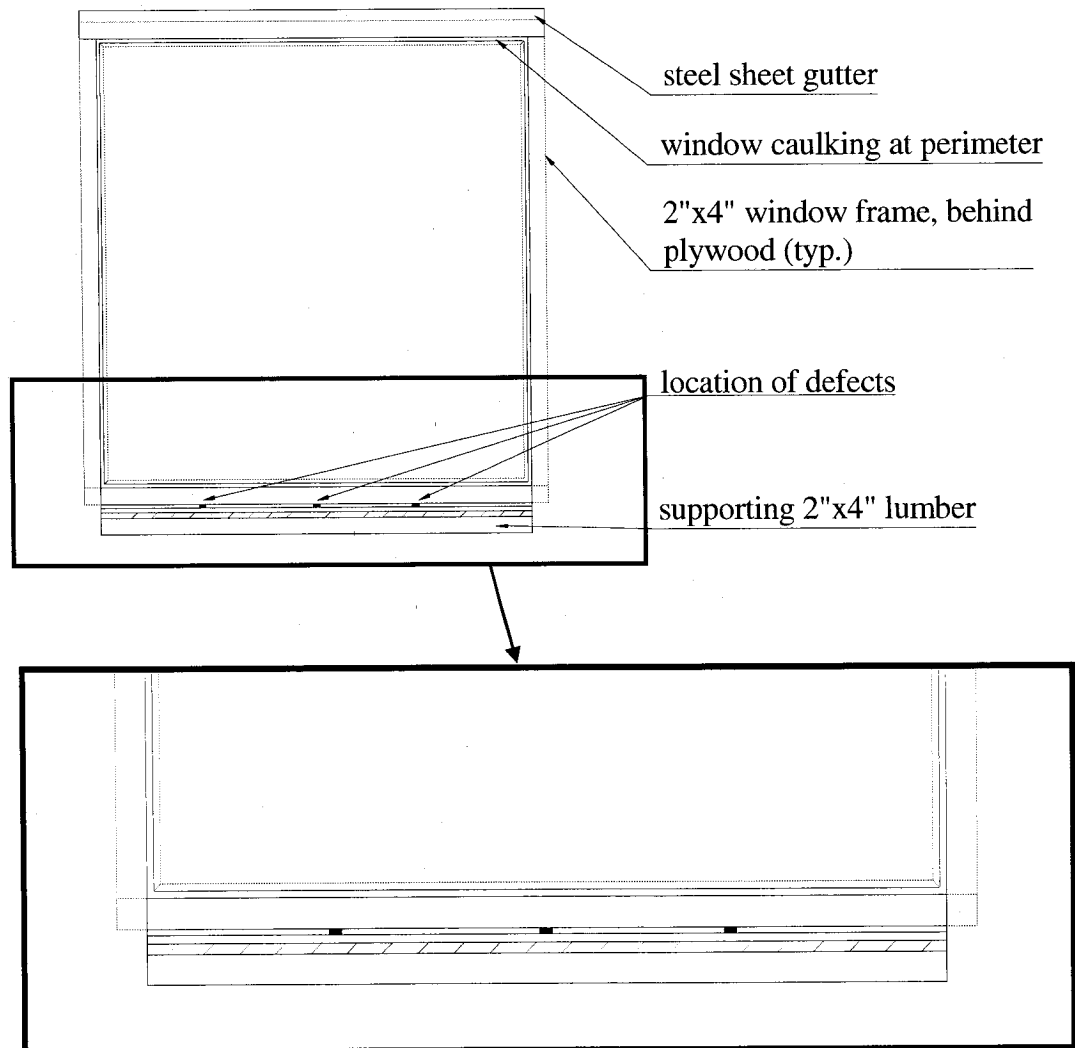


Figure 3.5. Schematic section drawing of mock test wall/window assembly simulating a perimeter sealant defect at the windowsill used in the water leakage test.

During the water infiltration test, the window and connecting wall was subjected to conditions specified in ASTM E331-00 (2000a), namely an air pressure differential of 137 Pa (2.86 lb/ft²) across the panels of the chamber, and a rate of impinging water per surface area established within a specified range, as mentioned previously.

The water infiltration tests were conducted in the Rain Penetration Chamber for the four different configurations of defects in the window sill. For each size of defect, the water leakage test was conducted for a one minute period and a 15 minute period. The water infiltrating through the window sill was collected using a graduated cylinder or a

bucket for the shorter and longer tests, respectively. In the latter case, the volume of water collected was determined by weighing the water-filled bucket. Photos of the calibration set-up taken from the interior of the Rain Penetration Chamber and of the set-up for the rain infiltration test are shown in Figures 3.6 and 3.7.

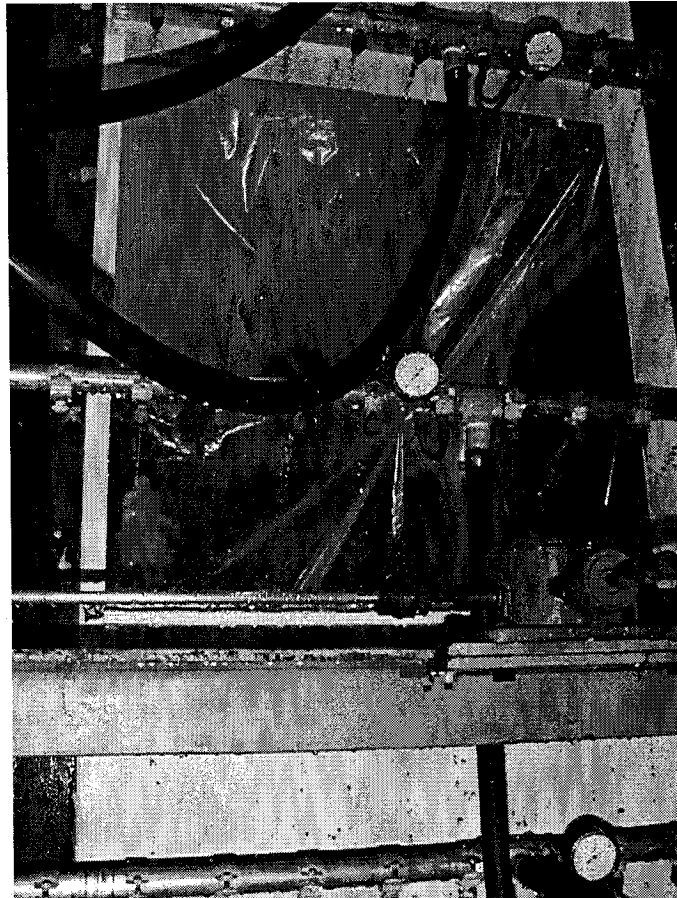


Figure 3.6. Photo of the calibration set-up for the Rain Penetration Chamber from inside the Chamber.

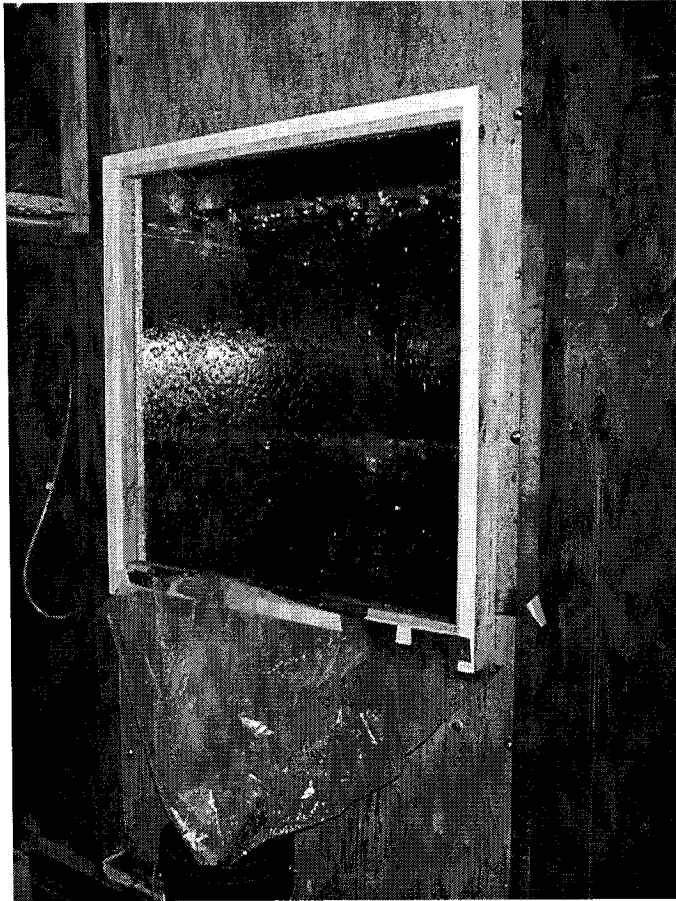


Figure 3.7. Photo of the set-up for the rain infiltration test including the plastic funnel sheet and bucket used to collect the leakage water.

The results of the water infiltration test were used to establish a relationship between the amount of water that infiltrated through the gap(s) into the assembly, with respect to the amount of water that impinges upon the window surface, for a given type of defect and known leakage areas. The ratios of the amount of leakage water to the total amount of water impinging over the 1 m² window opening, expressed as percentages, are summarized in Table 3.3. The difference between the one minute test and the 15 minute test, while not significant, can be attributed to slight variations in the flow rate as well as measurement error. The table also shows the average of the 1-minute and the 15-minute tests.

The water infiltration results show that, for gaps with the same dimension, increasing the number of gaps from one to two, or one to three approximately doubled or tripled the ratio of water infiltration, respectively. However, when the area of a single gap was increased from 25 mm² to 50 mm², the infiltration ratio did not increase in proportion to

the gap area.

Table 3.3. Average ratio of water infiltration to water impinging on window surface as a function of defect size.

| Defect Size | Average ratio of water infiltration to water impinging on window surface for 1 minute test [%] | Average ratio of water infiltration to water impinging on window surface for 15 minute test [%] | Average ratio of water infiltration to water impinging on window surface [%] | Rate of air leakage at 75 Pa [l/s] |
|-------------------------------|---|--|---|---|
| One 25 mm ² gap | 4.4 | 4.6 | 4.5 | 0.070 |
| Two 25 mm ² gaps | 10.5 | 10.4 | 10.4 | 0.513 |
| Three 25 mm ² gaps | 14.7 | 15.3 | 15.0 | 0.770 |
| One 50 mm ² gap | 4.6 | 5.9 | 5.3 | 0.256 |

It should be noted that studies by Choi (1998) and Galitz and Whitlock (1998) have demonstrated that the ASTM E331-00 does not accurately simulate local field conditions, and that the conditions prescribed by ASTM E331 are extreme. The large spray rate and air pressure differential may have produced a greater water proportion of water infiltration than a smaller rate. This would have to be verified with measurements since the openings used were quite small and saturation of the opening area may even occur at lower rates. Using a high spray rate and air pressure differential may represent an upper or maximum percentage of water infiltration. While there is a clear need to develop a standard test method for evaluating the water penetration or infiltration resistance of envelope systems that takes into consideration realistic water spray rates and air pressure differences for different climates, to do so was beyond the scope of this study.

In order to quantify the size of the defects, the flow rate of air leakage was calculated for each defect configuration using the fan pressurization method according to ASTM E283-84, the Standard Test Method for Rate of Air Leakage Through Exterior Windows, Curtain Walls, and Doors. This method involves generating a given pressure differential, in this instance 75 Pa, across the walls of Rain Penetration Chamber using a variable speed fan and measuring the air flow required to maintain this pressure differential before

and after a gap, or gaps, is made in the sill sealant. The difference between these two gives the net leakage due to the gap(s). Results of the air flow leakage tests are shown in Table 3.3 for all four geometric defect configurations. The results indicate that increasing the number of 25 mm² gaps from two to three increased the air leakage rate by 50%. However, a greater number of specimens should be studied before correlations between the number of defects, and defect area as well as the water and air leakage rates could be established.

3.1.1.4 Final determination of rate of water infiltration loading

The estimated amount of water leaking into the windowsill defect due to actual local climatic conditions can now be determined based on: (1) the estimated amount of water striking the building façade which can be calculated by the product of the average hourly rainfall in l/m² and the catch ratio, η , and, (2) the ratio of water leakage in relation to the amount of water impinging on the window surface. The rate of water entry is simply the product of these two items. For example, given an average August hourly rainfall rate of 1.93 l/m² and a catch ratio η of 0.12, then an estimate of the amount of water striking the façade is simply 1.93 l/m² x 0.12, or 0.23 l/m². Note that the value of the catch ratio is adjusted to take into consideration wind speed, the location on the building being considered (central to the façade at one-third the building height), and the orientation of the façade in relation to the prevailing winds (assumed to be normal to the façade). The amount of water leakage through a 10-mm wide windowsill defect can be determined by multiplying the water leakage ratio for that specific defect (average value, 5.3%) by the estimated hourly rate of water striking the façade (0.23 l/m²). The result suggests that approximately 12.2 ml/m²h of water infiltrate into the building envelope through the 10-mm wide defect at the windowsill.

In addition, a sensitivity analysis was performed to evaluate the impact of varied rates of water introduction into the wall assemblies on the drying capacity of the assemblies. For this purpose, two test walls were constructed with OSB exterior sheathing, a polyethylene vapor retarder and without exterior insulation. In one wall, the infiltration rate was decreased by 50%, and in another wall the rate was increased by 50% of the base case water infiltration rate. The water insertion was done for the same frequency and

duration in all the wall system.

3.1.2 Duration and frequency of wet and dry days during the experiment

Other parameters that were established for the water insertion procedure were the number of hours during which water was inserted into the assemblies each day, and the number of days during which wetting took place during the wetting phase. These two parameters were determined using hourly precipitation data from 1981 to 2001, and are shown in Table 3.2 for the months from April to October, inclusively. The statistical analysis found that on average, for the month of August, there are 3.4 hours of rain during a rainy day, and there are 12.6 rainy days over the month.

The intent of the wetting phase was to simulate field rain frequencies as closely as possible. The realistic weather pattern of rainy days followed by dry days should be used in the wetting procedure for the experiment. Houghton and Carruthers (1976) document that the large-scale movements of air masses corresponding to weather map fluctuations occur every four days or so. Thus, to approximate the pattern during the wetting phase, three days of wetting were followed alternatively with four days where no water was introduced. The cycle of wet followed by dry days was repeated four times, resulting in a total of 12 days of wetting for August.

To this point of the presentation of the methodology, the hourly amount of water insertion into the wall assemblies, the number of wetting hours per day, the number of consecutive wetting and drying days, as well as the number of wet/dry cycles have been established. The last issue to consider is the location of water insertion into the test assemblies.

3.1.3 Location and method of water introduction in test assemblies

As was shown in the literature review, walls are not designed to manage rainwater that infiltrates into the stud space of wood-frame walls. Therefore, water that enters this space cannot easily evacuate and is likely to accumulate, leading to potential degradation of the wood studs and exterior sheathing and other materials. For the test, water was thus

introduced into the stud cavity because it provided a worse-case scenario with respect to the wall assembly drying potential and enabled the evaluation of the hygrothermal performance of the wood-frame wall assemblies.

In an actual situation, water that infiltrates through a defect in the sill of a window flows downwards due to gravity. Thus, only the section of the wall beneath the window is expected to be wetted by rainwater infiltration. For this reason, the experiment was conceived with wall assemblies of only 1.0 m in height, and water was introduced into the stud space at the top center of the interior surface of the sheathing.

Water was delivered into each assembly by means of a 24-channel peristaltic pump. The pump and each of the 24 cassettes were calibrated and fine-tuned to supply the required 12 ml/h flow rate of water to each panel within a margin of error of 5%. Silicone tubing was used to transport the water from the pump to the panel at the inside surface of the sheathing, and a small shallow notch was made into the surface of the sheathing where the tip of the injection tube was fitted to ensure that water ran onto the interior surface of the sheathing.

3.2 Methodology for wetting by partial immersion method – test 3

The rationale behind the third test was to provide additional information not available from the first two tests but that, at the same time, be complementary to them. In terms of the wetting methodology, the intent was to introduce a moisture source into the wall assemblies that was uniform from wall to wall in order to facilitate analysis of the roles of sheathing and vapor retarder material on the drying of the assemblies. Several methods were considered to introduce a moisture load into the wall assemblies. There were:

1. Introducing water in a drop by drop fashion directly on a stud member;
2. Introducing water in a drop by drop fashion directly on a bottom plate;
3. Initial wetting of a stud member by full or partial immersion;
4. Initial wetting of a bottom plate member by full or partial immersion.

The first two methods were based on tests 1 and 2 and involved introducing water directly at the top inside surface of the stud member (method 1) or directly onto the top

surface of the bottom plate (method 2). While these methods attempted to correct problems of varying moisture distribution, there was no guarantee that all walls would receive and absorb the same amount of water on the stud and/or bottom plate. For instance, a slight curvature in the stud or the bottom plate could change the flow path and hence the moisture distribution in these elements at monitored locations. Hence, these methods were dismissed.

The third and fourth methods involved inserting a wet stud (method 3) or a wet bottom plate (method 4) into each wall assembly adjacent to an existing stud or bottom plate member before commencing the drying process. These members were logically called a stud and bottom plate insert, respectively. The members could be wetted by full or partial immersion in a pool of water until a given moisture content was reached. Preliminary results from the first two tests showed that water leaking into a stud space at the top of an assembly tended to fall to the bottom of the panel and collect on and around the bottom plate. Therefore, it followed that the wetting methodology for the third test should attempt to produce the same effect if it was to complement the first two tests. Therefore, the fourth wetting method was selected for the third test.

The next consideration involved determining whether full or partial immersion should be utilized in the wetting protocol. A 7-day wetting trial was performed in which two 38 mm by 140 mm by about 430 mm long pieces of dry spruce lumber were wetted. The first piece was fully immersed, and the second was partially immersed in a pool of water 13 mm deep. The samples were weighed on a daily basis and the moisture content relative to the initial mass was calculated. Visual observation showed that, for the partially immersed piece, water tended to wick up the 38 mm x 140 mm end surfaces and to wet these surfaces almost completely even though the depth of the water pool is only 13 mm.

The results from one week of full and partial immersion are shown in the table below. They indicate that, as anticipated, the moisture contents in both samples increased with time and were higher in the sample that was completely immersed. However, after a 3-day period had elapsed, the difference in apparent moisture content in both samples remained approximately constant at about 7.5%. This indicated that the difference was due to the additional surface area in the fully immersed sample that was not wetted in the

partially immersed one. Given that moisture movement in wood along the direction of the fibers occurs much more readily than in the tangential or radial directions, it also followed that the increase in moisture with time was due to water uptake at the 38 mm x 140 mm ends rather than the other surfaces. Cutting the fully immersed wood at its midpoint revealed that only the surface was wet and in fact very little liquid penetrated the wood at this section. However, cutting the wood at 10 mm from the end revealed that the entire section was wet. Thus, the hypothesis that absorption was achieved mainly through water uptake at the end surfaces was confirmed. Moisture transfer also occurred within the wood by vapor diffusion from the wetted surface of the wood towards the inside.

The intent of the wetting protocol of test 3 was to introduce a moisture load into the wall assembly stud cavity that would dry via the interior and exterior boundary materials, i.e. the interior vapor retarder and gypsum finish, and the sheathing and sheathing membrane. Since wetting the bottom plate insert produced a moisture load on its surface, then the surface was the one exposed to the stud cavity, i.e. the top surface. Thus, the partial immersion method was selected for test 3 such that the wetted surface of the bottom plate insert was installed face up into the wall assembly.

Table 3.4. Mass and apparent moisture content change with time for full and partial immersion trial of two wood specimens taken from the same timber piece. One of the specimens was fully immersed in water while the second was partially immersed.

| Time [h] | Fully immersed wood | | Partially immersed wood | | Difference in apparent MC* [%] |
|----------|---------------------|------------------|-------------------------|------------------|--------------------------------|
| | Mass [g] | Apparent MC* [%] | Mass [g] | Apparent MC* [%] | |
| 0 | 837.7 | 0 | 827.3 | 0 | 0 |
| 3 | 901.6 | 7.7 | 877.8 | 6.1 | 1.6 |
| 7 | 923.5 | 10.3 | 893.2 | 8.0 | 2.3 |
| 70 | 1058.2 | 26.4 | 981.9 | 18.7 | 7.7 |
| 96 | 1091.0 | 30.3 | 1014.6 | 22.6 | 7.7 |
| 118 | 1115.1 | 33.2 | 1040.7 | 25.8 | 7.4 |
| 141.5 | 1140.1 | 36.2 | 1066.5 | 28.9 | 7.3 |
| 165.5 | 1166.1 | 39.3 | 1087.6 | 31.5 | 7.8 |

*Relative to its “dry” mass at the beginning of the immersion.

The wetting procedure was as follows:

1. Weigh all “dry” bottom plate inserts and their gravimetric samples. The bottom plate inserts should be intact, e.g. without holes for gravimetric samples.

2. Place the bottom plate inserts and the gravimetric samples to be inserted into the top horizontal and side vertical surface of the bottom upper face down into a shallow pool of water 13 mm deep.
3. On a daily basis, remove the bottom place inserts and gravimetric samples from the pool of water, towel surface dry them and, then, weigh them.
4. Repeat steps 2 and 3 until the desired moisture content is achieved.
5. When ready, drill the holes for the gravimetric samples into each bottom plate insert and install the samples. Install a thermocouple adjacent to each gravimetric sample.
6. Install the bottom plate insert, wet surface facing upwards, into its respective wall panel and begin the drying phase.

Therefore, for the purpose of test 3, six 38 mm x 140 mm x 360 mm bottom plate inserts were wetted by partial immersion in a pool of water 13 mm deep. The initial moisture content before wetting, the final moisture content after 31 days of partial immersion, and the moisture content gained in the immersion process are shown in Table 3.5. The table shows that the average moisture content in the inserts prior to and after wetting were about 16% and 55%, an average gain of about 39% moisture content.

Table 3.5. The initial moisture content, final moisture content after 31 days of partial immersion, and the moisture content gained in the immersion process.

| Insert no. | Initial moisture content [%] | Final moisture content after 31-day partial immersion [%] | Increase in moisture content after 31-day partial immersion [%] |
|-------------------|-------------------------------------|--|--|
| 1 | 16.2 | 53.0 | 36.8 |
| 2 | 15.4 | 53.1 | 37.7 |
| 3 | 15.4 | 56.8 | 41.4 |
| 4 | 16.3 | 56.1 | 39.8 |
| 5 | 16.7 | 54.9 | 38.2 |
| 6 | 15.6 | 53.6 | 38.0 |
| Average | 15.9 | 54.6 | 38.7 |
| Variation | 1.3 | 3.8 | 4.6 |

Gravimetric samples CH1, CH2 and CV were also partially immersed in a pool of water 13 mm deep. The samples were painted with acrylic paint to limit the limit the moisture absorption during the wetting process by the curved and top surface. However,

it was found that the paint had a limited effect, and the moisture content in these samples increased significantly in the 26-day wetting process, as shown in Table 3.6. It can be seen that much greater variations in moisture content exist from one sample to another.

Table 3.6. Maximum and minimum initial and final moisture contents after 26 days of partial immersion in gravimetric specimens CH1, CH2 and CV in walls 1 to 6.

| Sample name | Number of samples | Minimum final moisture content [%] | Maximum final moisture content [%] | Variation in final moisture content [%] |
|-------------|-------------------|------------------------------------|------------------------------------|---|
| CH1 | 6 | 119.9 | 146.8 | 26.9 |
| CH2 | 6 | 112.4 | 138.0 | 25.6 |
| CV | 6 | 119.6 | 152.9 | 33.3 |

3.3 Conclusion

To summarize, two deterministic methodologies were developed to simulate wind-driven rain infiltration loading for large-scale building envelope experimental testing. The first of the two is a drop-by-drop insertion method that is based on analysis of real climatic loads, establishment of impinging wind-driven rain on a building façade, and an estimate of the proportion of water infiltration through an envelope defect. The second methodology was developed in order to provide a similar initial moisture load from wall to wall, and consisted of pre-immersing a wall component prior to its installation into each of the wall assemblies at the start of the test. The following chapter presents the remainder of the experimental protocol, including the scope and objectives of the work, the testing facility and the test set-up, the monitoring protocol, the climate loading and the experimental history of tests 1, 2 and 3. The analysis of the experimental results is presented in Chapter 5.

4. EXPERIMENTAL PROTOCOL

This chapter deals with the experimental protocol for all three tests conducted at the Building Envelope Performance Laboratory of Concordia University.

The first experiment included 19 large-scale wood-frame wall assemblies wetted by the drop-by-drop method. The second experiment makes use of the same test set-up and wetting method as that employed in test 1, except:

- the moisture content monitoring scheme was improved in the plywood-sheathed walls by replacing gravimetric samples by moisture content pins along the path of water infiltration, and;
- the OSB sheathing in seven of the 19 wall assemblies was replaced by plywood.

The third experiment was developed to provide similar moisture contents at the start of the drying phase and, hence, simplify the comparison of the moisture content results. The experimental protocol of this last test consisted of the following:

- a different wetting methodology consisting of pre-wetting bottom plate inserts was applied to generate a more uniform moisture distribution from wall to wall;
- six, rather than 19 walls were tested;
- the role of two parameters, the exterior sheathing material, and the type of vapor retarder, was examined, and;
- the monitoring protocol was modified.

Specifically, the chapter presents the scope and objectives of the experimental work, a description of the test facility and the test set-up, and the monitoring protocol, the climatic test loading, and the experimental history for each of the three experiments.

4.1 Scope and objective of the experimental work

The main objective of the experiments to investigate the role of the wall exterior sheathing, the vapor retarder, exterior insulation and exterior cladding on the drying

response of various hygroscopic wall components after a one-month rain infiltration cycle for several configurations of wood-frame wall assemblies. A total of 44 large-scale wall assemblies with different configurations housed within a test hut inside the Environmental Chamber were monitored during the three experiments. The base case test wall was a platform-type frame system with 38 mm x 140 mm wood studs and an insulated stud cavity.

In addition to the wall parameters mentioned above, four testing condition variables were also implemented. All but one of the test wall assemblies were constructed without a cladding; one wall included wood siding to evaluate the influence of the cladding on the drying performance of the assembly. Also, the experiment included two wall assemblies to evaluate the impact of varying the water infiltration load on the hygrothermal performance of the test walls. To this effect, the wetting load was increased by 50% in one test wall, and reduced by 50% in another identically-built wall. The third testing condition involved inserting water at the top of the inside surface of the sheathing adjacent to the stud rather than in the top middle of the stud space. Last, one full-height wall assembly was tested to investigate whether the height of the assembly had an impact on the wetting pattern and on the drying performance.

Specifically, the data obtained during the test allowed the determination of:

1. The amount of moisture accumulated and the moisture distribution pattern in each wall during the wetting phase;
2. The locations within the wood-frame walls that were most susceptible to moisture accumulation for the given water infiltration pattern;
3. The impact of several parameters on the hygrothermal behavior such as: type of sheathing, type of vapor retarder, the presence of foam insulation on the exterior side of the assembly, and the presence of exterior cladding.

The experiment began with a pre-conditioning phase, which was followed by a wetting phase and drying phase. During the pre-conditioning phase, climate loading was set in the Environmental Chamber to increase the moisture content in the wall assemblies' wood components to levels reflecting those found at the end of a winter wetting season in Montreal. During the following four-week wetting phase, water was

introduced into the stud space of each test assembly at a controlled rate, frequency and duration to simulate rainwater infiltration. Finally, the drying phase was performed to allow evaluation of the hygrothermal behavior of the wall specimens subjected to climatic conditions permitting drying, i.e. in the spring and summer. The climatic conditions during the drying phase were typical of Montreal and were obtained from analysis of Trudeau Airport weather station data. A description of the climatic loading is given in section 4.5

4.2 Testing facility

The Environmental Chamber is a unique research facility for the study of the building envelope in terms of the heat and moisture transfer of building envelope specimens including air infiltration, rain penetration and condensation. The large size of the Chamber permits testing of large-scale exterior wall and roof assemblies, and may include the junction between these, and windows and doors, for example. In the guarded hot box mode, the two chambers, the hot box and the cold box, represent the indoor and outdoor environments, respectively. Figure 4.1 shows a schematic diagram of the Environmental Chamber configured as a guarded hot box.

The stationary cold box is a chamber 7.5 m high by 4.4 m wide by 3.6 m deep in which temperatures ranging from -40°C to 50°C can be maintained, to simulate exterior conditions. The mechanical equipment include a 5 ton screw compressor, a 12000 cfm recirculation fan and a 25 kW re-heating heater. The hot box sits on 4 compressed air pads to move the hot box to and from the cold box. The hot box, in which the test hut was built, is 7.5 m high by 4.4 m wide by 6.1 m deep, and temperatures from 5°C to 50°C , and relative humidities ranging from 10 to 90% can be generated. The hot box is equipped with a 600 cfm air recirculation system, a fresh air supply/return damper and a humidification system. The walls of the chamber are made of 150 mm foamed polyurethane boards, laminated between 0.8 mm aluminum sheets outside and 0.8 mm stainless steel sheets inside (Fazio *et al.*, 1997). For this experiment, the facility is used in the climatic chamber mode where the hot and cold boxes are joined to form a 7.5 m

high by 4.4 m wide by 10.5 m deep climatic chamber, seen in Figure 4.2.

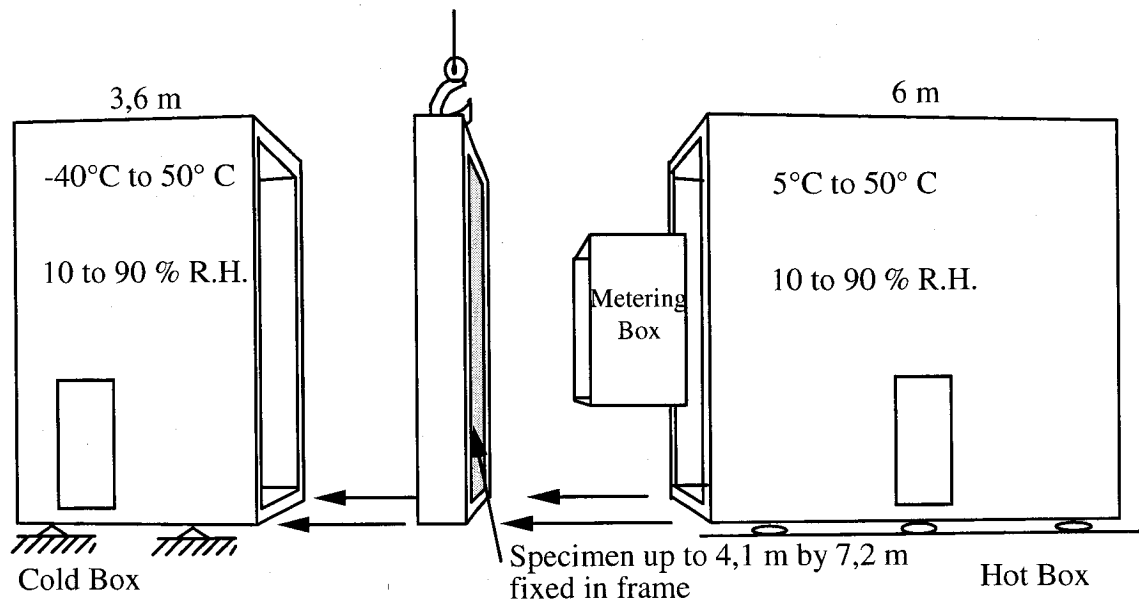


Figure 4.1. Schematic representation of the Environmental Chamber (after Fazio *et al.*, 1997).

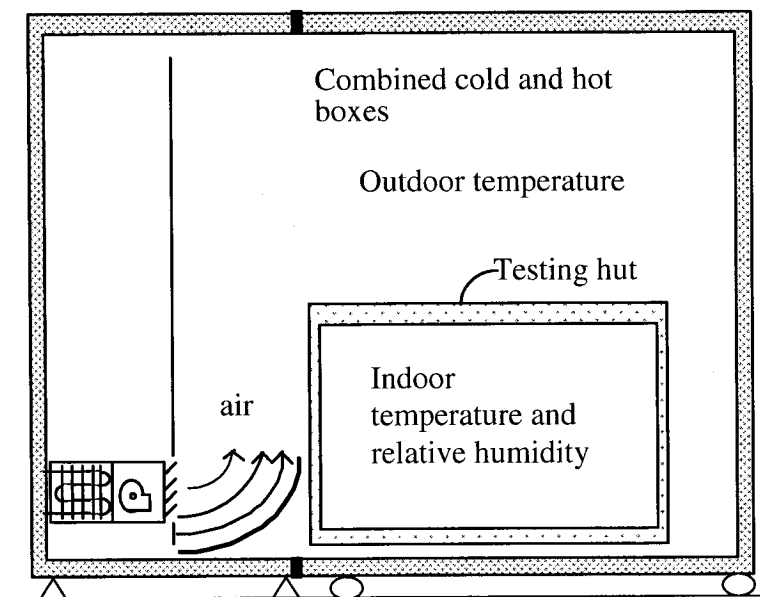


Figure 4.2. Environmental Chamber Facility in the climatic chamber mode (after Fazio *et al.*, 1997).

4.3 Description of the test setup

For the first test, 19 monitored test walls and two witness walls were constructed and installed to form the envelope of a test hut. 18 of the monitored walls and one witness wall measured 840 mm wide by 1.075 m high. The remaining monitored wall and witness walls were 840 mm wide by 2.075 m high, reflecting full-scale wall dimensions found in the field. These 2 walls were used for comparative purposes. All the walls were isolated from each other, as will be explained later.

4.3.1 Description of test hut

The test hut, which was built in the hot box of the Environmental Chamber, was 3.2 m wide, 4.2 m long and 2.8 m high, as shown in Figure 4.3. An elevation is shown in Figure 4.4. The test hut was designed to reflect the platform type of construction with assemblies found in Canadian residential buildings.

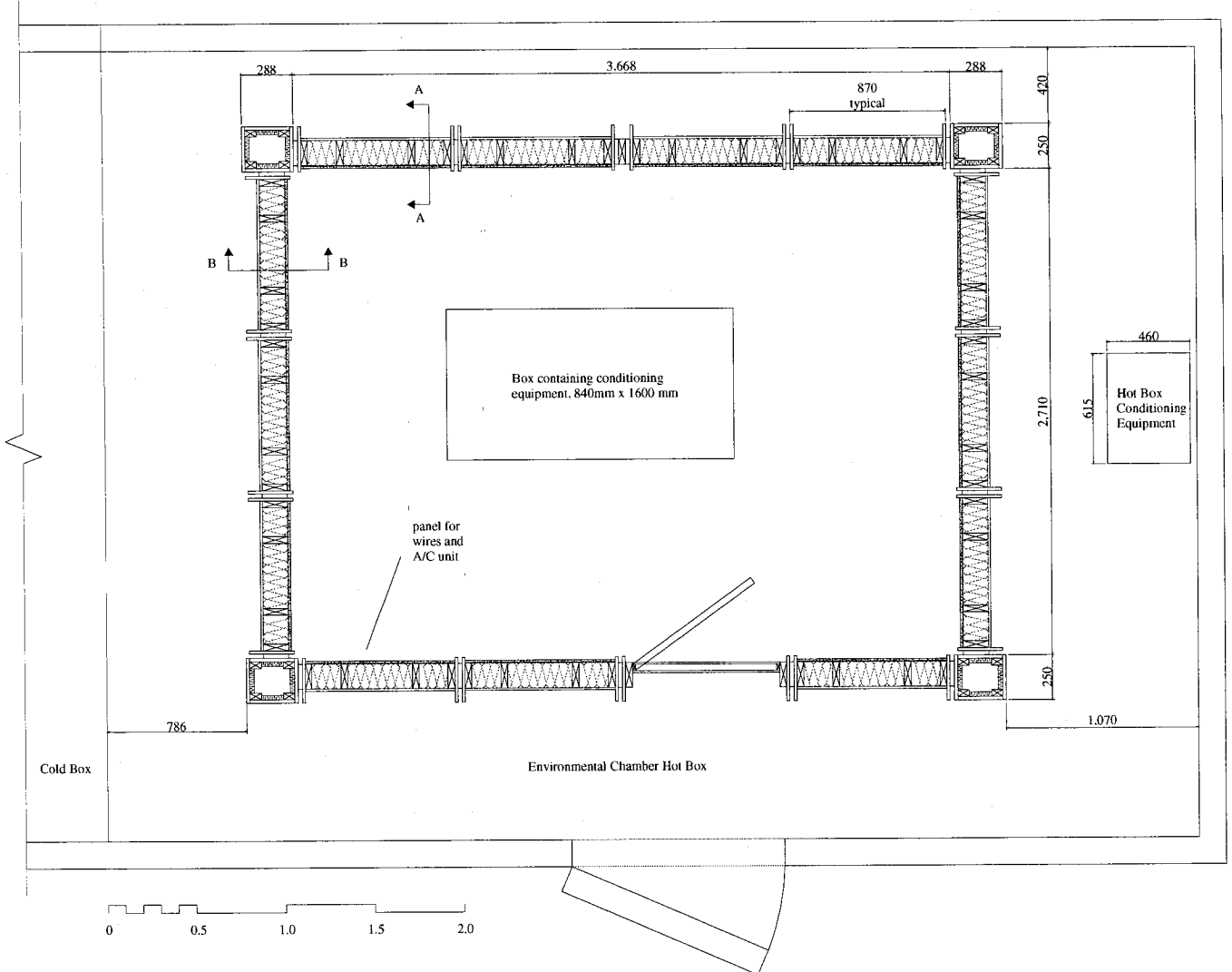


Figure 4.3. Plan view of the test hut.

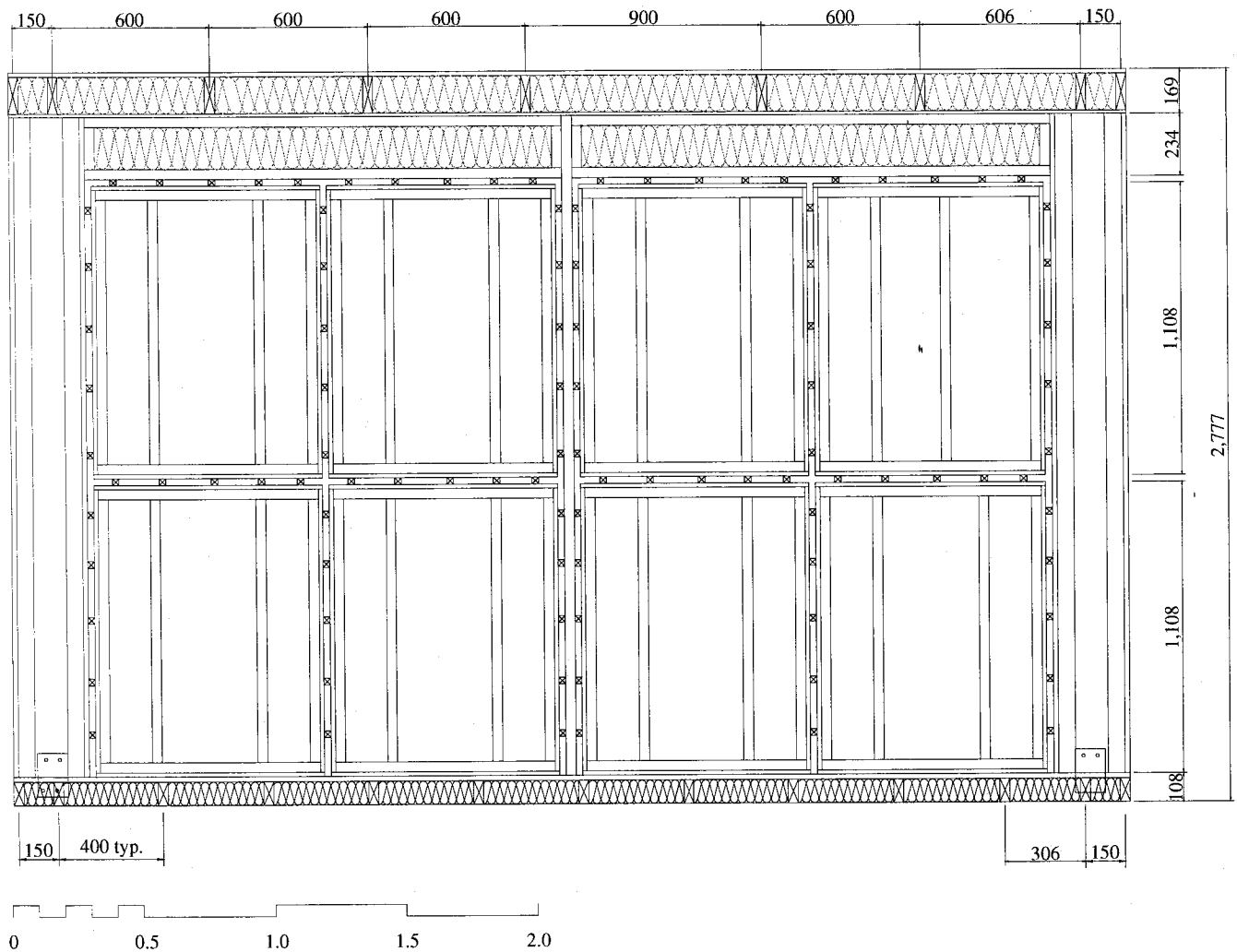


Figure 4.4. Elevation of the test hut.

4.3.2 Composition of the assemblies

The test walls were designed to reproduce current residential construction conditions. The height of the wall assemblies was set to 1.0 m, reflecting the approximate size of a wall built beneath a window. Every monitored test wall was built with two 38 mm x 140 mm wood studs spaced at 400 mm on center, plus another stud at 200 mm on each side. The resulting side spaces served as buffer zones between the test wall and the adjacent

ones, and monitoring was only done in the central stud space. The test assembly setup aimed to recreate actual site construction methods. In actual platform construction for end-wall framing, shown in Figure 4.5, the wall framing is bounded underneath by a sub-floor wood panel. In a similar fashion, the test walls were framed all sides by 16 mm thick plywood, as shown in Figure 4.6. A modified bituminous membrane was installed on the outside of the plywood framing. The plywood and bituminous membrane served to minimize moisture and air transport between adjacent test walls. For both cases of actual construction and the test assembly setup, during drying of the assemblies, vapor diffusion occurs towards the inside and outside of the assembly.

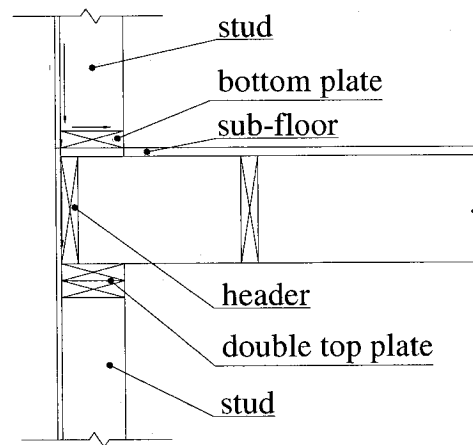


Figure 4.5 End-wall framing in platform construction method.

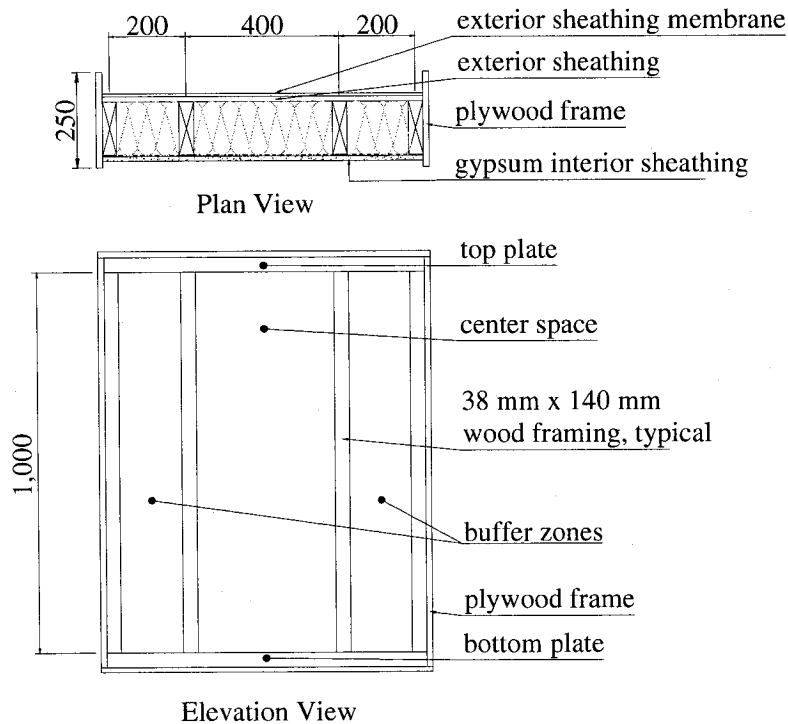


Figure 4.6. Schematic elevation of a typical test wall.

The base case test assembly, as found in typical wall construction without cladding, is shown in Figure 4.7. The case examined that of a north-facing wall with a ventilated air space behind the cladding, permitting exchange of air between the air space and the exterior environment. Therefore, all but one of the walls were constructed without exterior cladding.

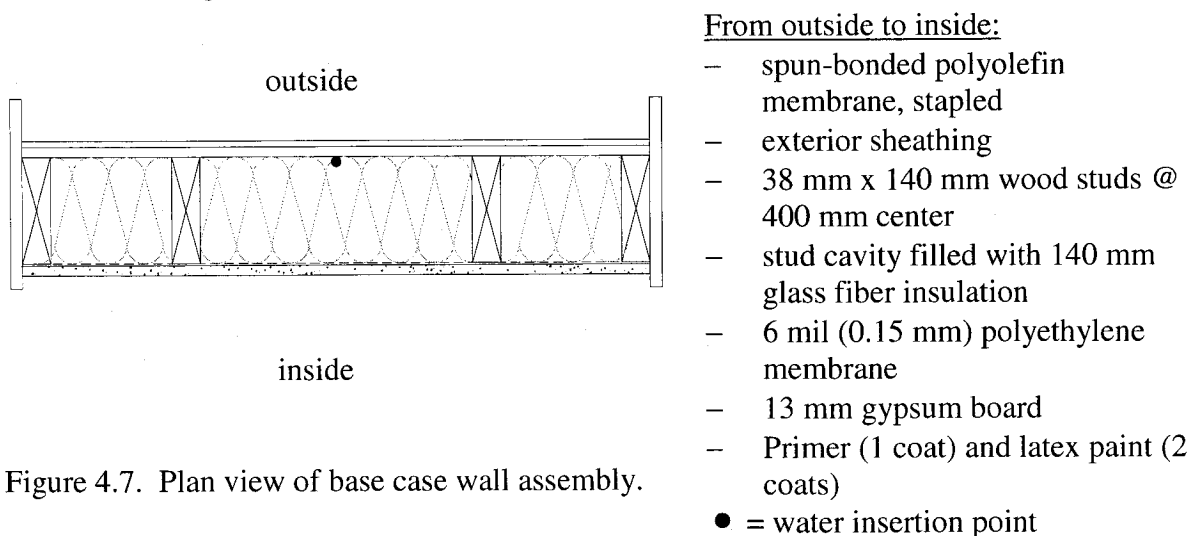


Figure 4.7. Plan view of base case wall assembly.

4.3.3 Parameters and testing conditions evaluated and experimental hypotheses

The impact of four assembly components was evaluated in the study:

- 1) the exterior sheathing;
- 2) the vapor retarder;
- 3) the exterior insulation, and;
- 4) the hygroscopic cladding.

In addition, three testing conditions were varied during the experiment:

- 5) the location of the water insertion, and;
- 6) the height of the assembly, and;
- 7) the rate of water introduction into the assemblies.

Justification for the selection of the above-mentioned parameters and testing is explained below, as well as the experimental hypotheses for each.

For the four assembly component parameters:

- 1) Regarding exterior sheathing, three wood-based types found in North American housing construction, namely plywood, oriented strand board and low density wood fiberboard coated with an asphaltic product, were integrated in the test assemblies. In the last two decades, the use of oriented strand board in the Canadian residential building market has grown, largely replacing plywood due to its lower cost. In Québec, however, fiberboard sheathing panels have long been employed as exterior sheathing. With respect to the experiment, it was expected that the sheathing materials with lower water vapor permeance, i.e. OSB and plywood, would decrease the moisture transfer between the stud space and the exterior, hence decreasing the drying rate and also leading to increased level of exposure to conditions that may lead to mold and rot growth.
- 2) Regarding the vapor retarder, three levels of permeance were examined. The vapor retardant materials were selected to study whether a higher permeance of the vapor retarder, installed on the warm side of the batt insulation, would facilitate drying to the interior. Three walls used 0.15 mm (6 mil) thick polyethylene sheet

(permeance of $3.4 \text{ ng/s m}^2 \text{ Pa}$) (ASHRAE (2001); three more walls employed vapor retardant primer paint (permeance of $34.5 \text{ ng/s m}^2 \text{ Pa}$ (ICI, 2003)), and the last set of three walls was built without a vapor retarder. It should be noted that, in accordance with standard practice, a coat of latex primer paint, with permeance of $360 \text{ ng/s m}^2 \text{ Pa}$, and two coats of latex paint with combined permeance of approximately $86 \text{ ng/s m}^2 \text{ Pa}$, were laid on the interior finish except for those walls with the low permeance primer paint, as explained above. Both the polyethylene and the low permeance primer paint have a water vapor permeability lower than the maximum value of $45 \text{ ng/Pa}\cdot\text{s}\cdot\text{m}^2$ recommended by the National Building Code of Canada (NBCC, 1995) for low-rise buildings. For buildings where high resistance to vapor movement is present, such as in a wall having cladding or exterior sheathing with low vapor permeance, the maximum vapor permeance of the vapor retarder is reduced to 15 ng/Pa s m^2 (art. 9.25.4.2). It was expected that the low vapor permeance of the polyethylene membrane, and to a lesser extent of the low permeance primer, would decrease the rate of moisture transfer from the stud space to the inside of the test hut, hence decreasing the inward drying rate for the selected climatic conditions and possibly leading to exposure to conditions that may favor mold growth.

- 3) The third parameter is the use of extruded polystyrene as exterior insulation. This parameter was adopted because it is a common strategy to improve the thermal insulation properties of new construction as well as existing construction during retrofitting works. Three walls were tested with exterior insulation, one with each type of sheathing. It was expected that in the early spring, the warmer temperatures in the sheathing and in the stud space due to the exterior insulation would increase the walls' drying capacity compared to that of the base case. In the late spring and summer, the presence of exterior insulation would have the reverse effect on the drying capacity. In addition, the decreased vapor permeance outboard of the sheathing due to the exterior insulation may decrease the drying capacity as well. Note that in actual new construction, $38 \text{ mm} \times 89 \text{ mm}$ rather than $38 \text{ mm} \times 140 \text{ mm}$ studs are used in walls designed for exterior insulation because less cavity

insulation is required. Thus in the experiment, the assemblies constructed with exterior insulation used 38 mm x 89 mm studs.

- 4) The role of the rain-screen cladding in the hygrothermal performance of the back wall is assumed here to be limited. To verify this assertion, one assembly was built with wood siding and an air space of 19 mm. Because wood is a hygroscopic material, it could be that the cladding would have a buffering effect on the wetting and drying performance of the test wall. The cladding may also act as a temperature buffer, thus reducing the temperature variations of the portion of the wall behind it.

The first two testing conditions are discussed here, while the third, the rate of water introduction into the assemblies, was presented in section 3.1.1.3 entitled “Rate of water introduction”.

- 5) Most specimens received water at the top center interior surface of the sheathing. This corresponds to a window defect located in the middle of the window sill. However, case studies in literature cite many instances where the location of the window imperfection is at the corner of the window, in the miter joint, for example. To reflect this situation, a wall specimen was tested where water was inserted at the top of the assembly, on the interior surface of the sheathing next to one of the inner studs. It was anticipated that the eccentric location of water insertion would cause water accumulation at the base of the wall assembly near the stud rather than in the middle of the assembly, and hence increase moisture levels within the stud itself.
- 6) The last testing parameter varied height of the test wall. As explained previously, one meter high walls were used because water leakage flows downward from windows. However, one full 2.0 m high wall assembly was included in the experiment to investigate the impact of the scale of the wall on the wetting distribution and drying behavior of the wall systems and also the effect of possible convection loops within the stud cavity on the drying of the wall. It was expected that increasing the magnitude of the convective loops would distribute the

evaporating moisture in the stud space and throughout the wall during the drying phase, thereby enhancing drying.

As well, two witness walls, one short 1.0 m high and one full-scale 2.0 m high, were constructed for visualization purposes. These 2 walls were devoid of insulation during the wetting phase to enable visual inspection of the wetting pattern.

The wall parameters and the testing condition variables for the walls are summarized in the Tables 4.1 and 4.2 below. Table 4.3 shows the specific configuration for each of the 19 test wall assemblies.

Table 4.1. Wall testing parameters.

| Vapor retarder* | Core | Sheathing | Exterior Insulation |
|--|--|--|---|
| <ul style="list-style-type: none"> polyethylene sheet low permeance primer paint none | <ul style="list-style-type: none"> 38 mm x 140 mm wood framing with 140 mm glass fiber batt insulation 38 mm x 89 mm wood framing with 89 mm glass fiber batt insulation** | <ul style="list-style-type: none"> OSB Plywood Fiberboard | <ul style="list-style-type: none"> none extruded polystyrene, 38 mm |

* The interior gypsum finish of all the walls are primed and painted with latex paint except for the low permeance primer paint cases.

** For assemblies with exterior extruded polystyrene insulation.

Table 4.2. Testing condition variables.

| Rate of Water Insertion | Cladding | Height |
|---|--|--|
| <ul style="list-style-type: none"> X (<i>base case</i>*) 0.5X 1.5X | <ul style="list-style-type: none"> None (<i>base case</i>) Wood siding | <ul style="list-style-type: none"> 1.0m (<i>base case</i>) 2.0 m |

* "X" denotes the base rate of water inserted into wall assemblies during the wetting phase, 12 ml/m²h.

Table 4.3. Test wall configurations and testing parameters for test 1.

| Wall no. | Type of sheathing | Type of vapor retarder | Presence of exterior extruded polystyrene insulation | Presence of wood siding | Amount of water* | Other characteristics |
|----------|-------------------|----------------------------|--|-------------------------|------------------|-----------------------------|
| 1 | OSB | polyethylene | no | no | X | - |
| 2 | plywood | polyethylene | no | no | X | - |
| 3 | wood fiberboard | polyethylene | no | no | X | - |
| 4 | OSB | low permeance primer paint | no | no | X | - |
| 5 | plywood | low permeance primer paint | no | no | X | - |
| 6 | wood fiberboard | low permeance primer paint | no | no | X | - |
| 7 | OSB | none | no | no | X | - |
| 8 | plywood | none | no | no | X | - |
| 9 | wood fiberboard | none | no | no | X | - |
| 10 | OSB | polyethylene | yes | no | X | 2"x4"studs |
| 11 | plywood | polyethylene | yes | no | X | 2"x4"studs |
| 12 | wood fiberboard | polyethylene | yes | no | X | 2"x4"studs |
| 13 | OSB | polyethylene | no | no | X | full 2.0 m height |
| 14 | OSB | polyethylene | no | yes | X | - |
| 15 | OSB | polyethylene | no | no | 0.5X | - |
| 16 | OSB | polyethylene | no | no | 1.5X | - |
| 17 | OSB | polyethylene | no | no | X | water inserted next to stud |
| 18 | OSB | polyethylene | no | no | None | - |
| 19 | OSB | none | no | no | None | - |

*X denotes the base rate of water inserted into wall assemblies during wetting phase.

4.4 Monitoring protocol

The intent of the monitoring protocol, and the moisture content monitoring in particular, was to examine the wetting and drying responses of the walls over the course of the test at locations which, according to literature, were at higher risk of moisture accumulation, and therefore susceptible to moisture-induced damage. Hence, a monitoring grid was developed in the bottom plate, the exterior sheathing and the studs to wetting, redistribution and drying patterns in terms of space and time. Greater accumulation of moisture was expected at the bottom than at the top of the assemblies, and therefore the sensor grid was tighter in these locations.

Overall, parameters monitored included moisture content, temperature, relative humidity, and air pressure. A total of 282 small material samples were periodically removed from the test walls for gravimetric moisture content measurement, in addition to 84 electrical resistance moisture content probes. As well, 157 thermocouples and 19 relative humidity sensors were used to electronically monitor temperature and relative humidity within and on the surface of the wall assemblies during the experiment.

Monitoring of moisture content, temperature and relative humidity was done in the 400 mm space between the central wood studs in each test assembly. In a symmetrical fashion, moisture contents were measured electronically using electrical resistance moisture probes on one side, and by gravimetry on the other side.

4.4.1 Temperature

Temperature measurements within the walls were conducted using thermocouples, type T, copper and constantan, 30 gauge, with $\pm 0.5^{\circ}\text{C}$ accuracy. The thermocouples measured the temperature at locations adjacent to moisture content probes in the wood framing and the exterior sheathings at a depth of 6 mm, at the locations shown in Figures 4.8 to 4.11. Thermocouples were also used to monitor the temperature on the surface of the gypsum and of the sheathing in the middle of each. In addition, three resistance temperature detectors (RTDs) were used to measure the temperature of the air both inside and outside the test house.

Thermocouple calibration was carried on a systematic basis rather than on individual sensors. For the calibration process, the temperature both inside and outside the test hut was set at a constant, and its uniformity was maintained by operating the HVAC equipment in the cold box and hot box. Additional fans were used to promote air circulation into and out of the test hut and as well as around it. Once the temperature stabilized throughout the Environmental Chamber for over 4 hours, temperature readings were taken over a period of one hour or more and then averaged. The averaged temperature reading from each thermocouple was compared to that of a “true” reading from an RTD probe. The RTD probe, calibrated to an accuracy of $\pm 0.2^{\circ}\text{C}$, was placed in the center of the test hut. The difference between each thermocouple reading and the RTD reading was obtained and used as a correction factor for each thermocouple. Subsequently, the correction factors were inputted into the data acquisition program for automatic correction of thermocouple readings used in the presented results.

4.4.2 Relative humidity

The relative humidity within the stud space at a height of approximately 150 mm from the top was monitored with capacitance type relative humidity sensors that have an accuracy of $\pm 4\%$. The relative humidity indoor and outdoor of the test hut was also measured with the same type of sensor.

Calibration of each capacitive type relative humidity sensor was performed by using a chilled mirror dewpoint hygrometer as a reference. A relative humidity simulation chamber, which was controlled by a chilled mirror hygrometer and an RTD, was alternatively set to two relative humidities, 40% and 80%, and the zero and the span of the relative humidity sensor's potentiometers are adjusted until the desired accuracy of $\pm 2\%$ was reached. Then, the setpoint of the relative humidity simulator was set to 40% relative humidity and ramped up to 90% at 10% intervals to evaluate the deviation between the relative humidity sensor readings and that of the dewpoint hygrometer.

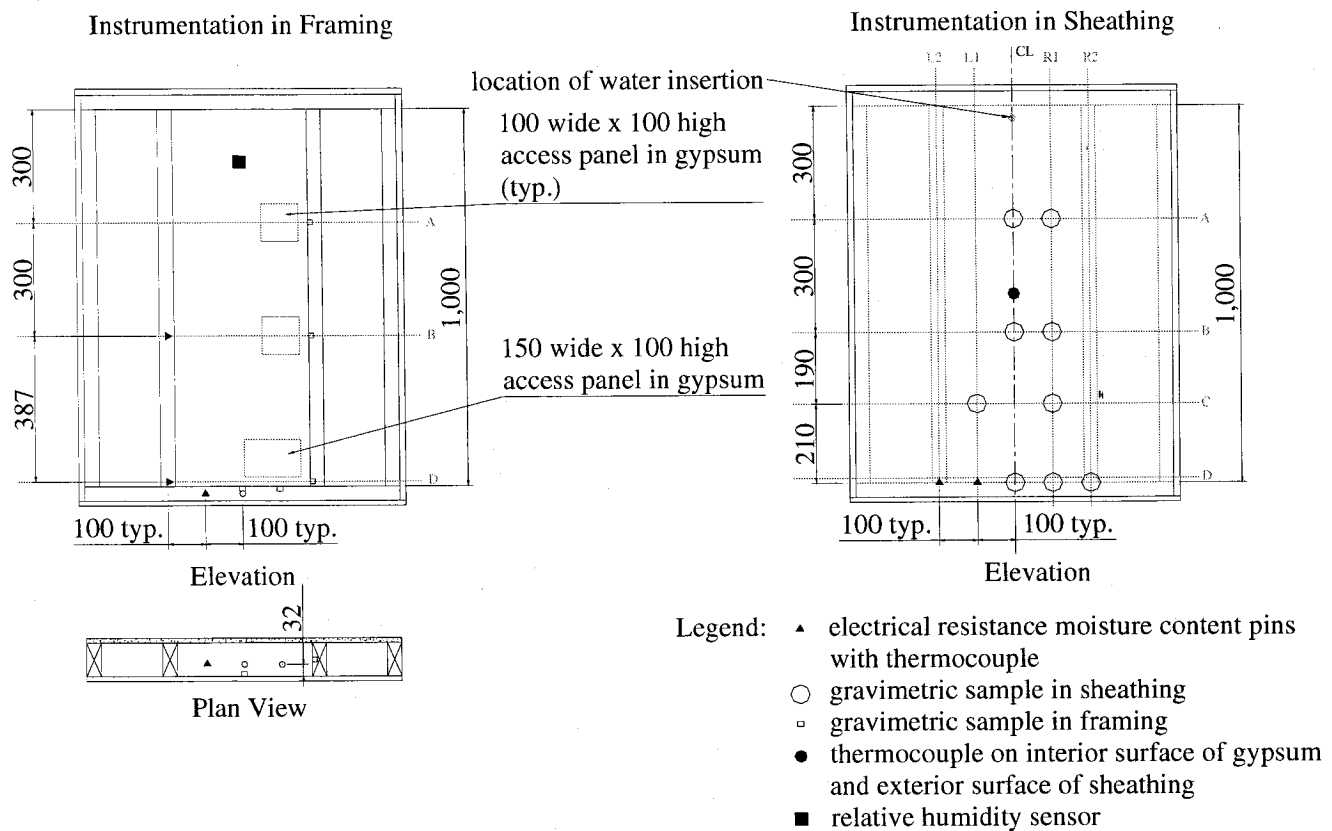


Figure 4.8. Elevation and plan views of the moisture content measurement monitoring protocol in the framing and sheathing of assembly 1 to 12 and 14 to 16. The location of the electrical resistance moisture pins with their thermocouple, the gravimetric samples in the sheathing and the framing, the thermocouple on the inside surface of the gypsum and outside surface of the sheathing, and the relative humidity sensor are shown.

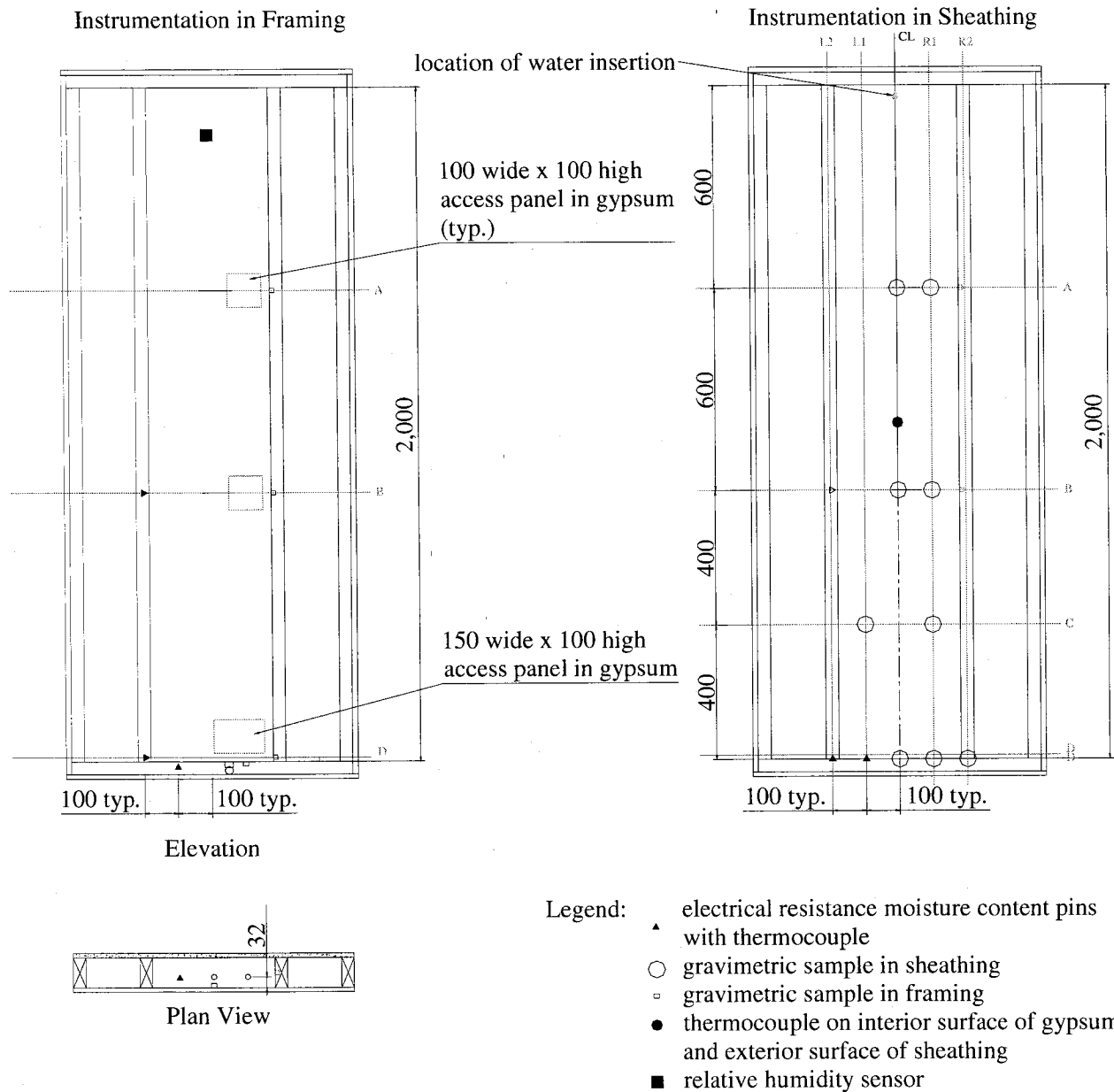


Figure 4.9. Elevation and plan views of the moisture content measurement monitoring protocol in the framing and sheathing of assembly 13. The location of the electrical resistance moisture pins with their thermocouple, the gravimetric samples in the sheathing and the framing, the thermocouple on the inside surface of the gypsum and outside surface of the sheathing, and the relative humidity sensor are shown.

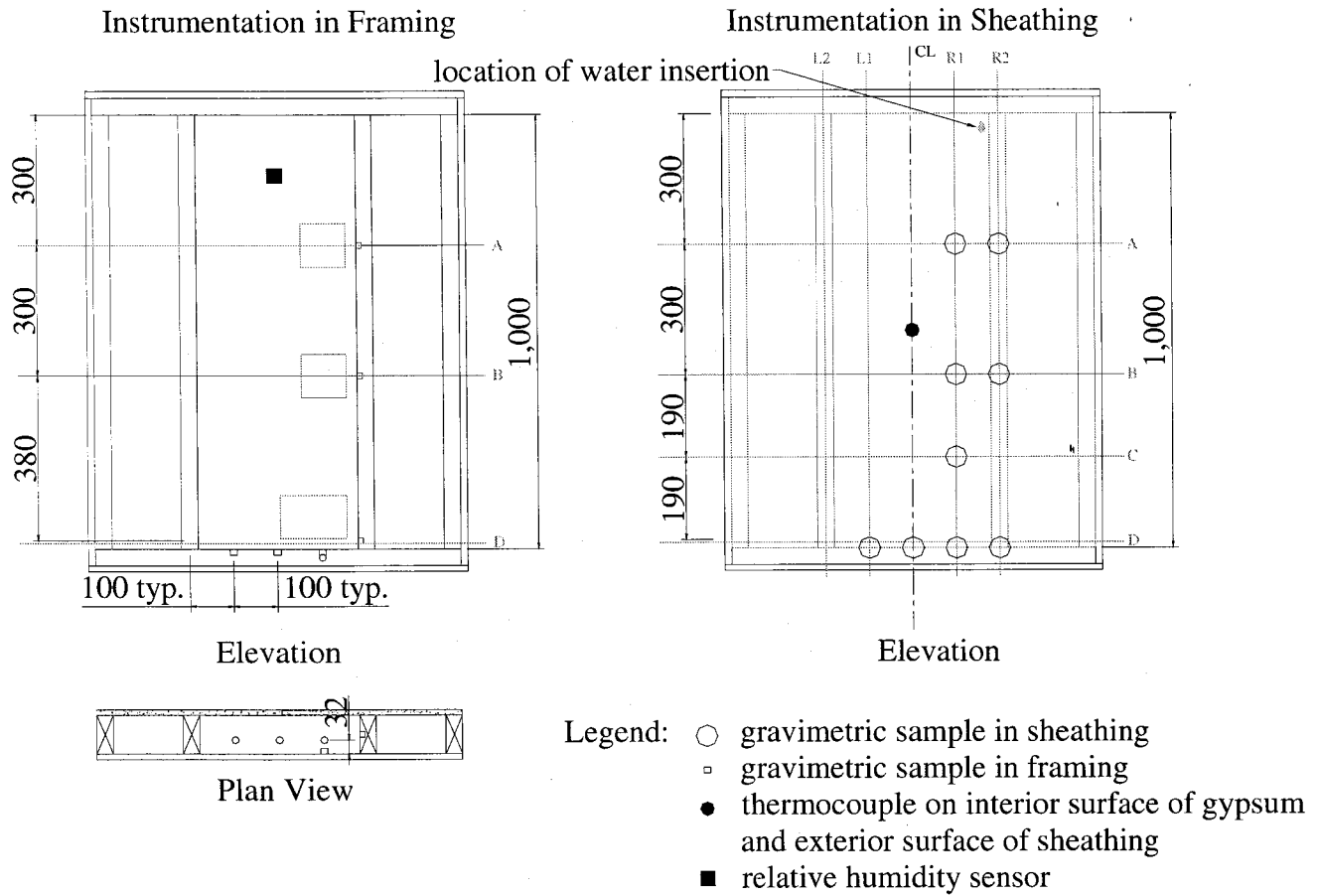


Figure 4.10. Elevation and plan views of the moisture content measurement monitoring protocol in the framing and sheathing of assembly 17. The location of the gravimetric samples in the sheathing and the framing, the thermocouple on the inside surface of the gypsum and outside surface of the sheathing, and the relative humidity sensor are shown.

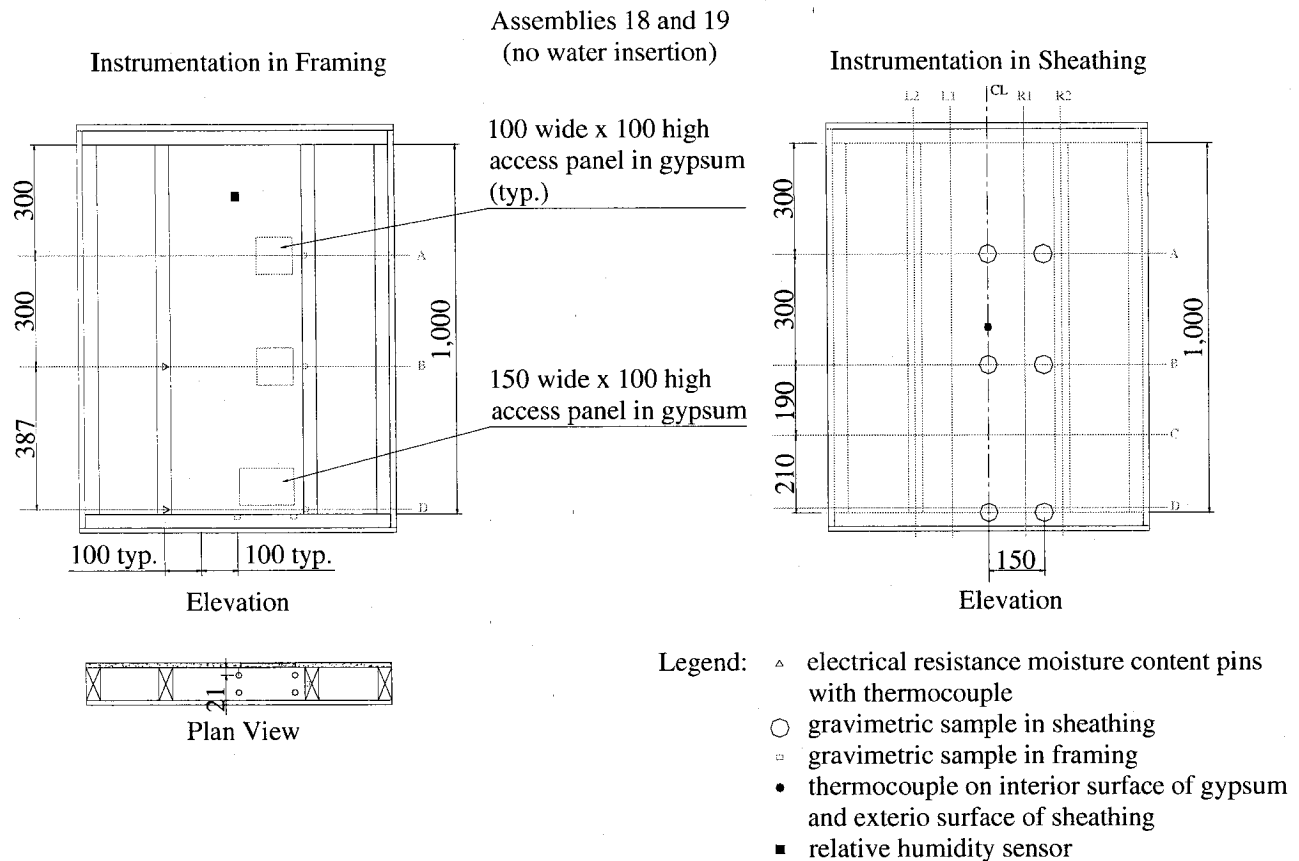


Figure 4.11. Elevation and plan views of the moisture and content measurement monitoring protocol in the framing and sheathing of assemblies 18 and 19. The location of the electrical resistance moisture pins with their thermocouple, the gravimetric samples in the sheathing and the framing, the thermocouple on the inside surface of the gypsum and outside surface of the sheathing, and the relative humidity sensor are shown.

4.4.3 Moisture content

Monitoring the moisture content of assemblies was used to evaluate the level of exposure to conditions that could lead to moisture-induced degradation in building envelopes, and thus it was essential to the monitoring protocol. In this experiment, both gravimetric samples and moisture content probes were used to monitor the moisture content of the wood sheathing and the wood studs. Gravimetry, while time consuming when large number of samples are involved, is applicable over all moisture content

ranges. However moisture content measurement using the electrical resistance technique is limited at the lower bound of 6% because of the high electrical resistance of wood at that moisture content, and at the upper bound to the fiber saturation point of wood, i.e. approximately 28% moisture content by weight. The method is more accurate in the range between 10% and 20% moisture content.

Most moisture content measurements were performed at those locations in components susceptible to moisture accumulation and mould growth. Water was inserted at the top middle of the sheathing, on the surface facing the stud cavity and flowed downwards more or less along the vertical center line of the sheathing toward the bottom plate. This wetting pattern was expected to create a moisture loading symmetry about the vertical center line of the sheathing which was taken advantage of in the moisture content monitoring protocol. To this effect, gravimetric samples and moisture content probes were installed more or less symmetrically on each side of the vertical center line of each test wall in the wood framing and sheathing, and this placement was expected to enable comparative analysis of the readings of the two moisture content measurement methods.

As the water ran down the interior surface of the sheathing, some water was expected to be absorbed by the sheathing material, and the rest was expected to continue to flow downwards. Although it was expected that the water would collect at the level of the wood bottom plate, gravimetric samples and moisture content probes were installed in the studs and the sheathing at various heights in the wood stud and sheathing to monitor the level of moisture content throughout the experiment. It was expected that there would be redistribution of moisture within the test walls during the drying phase which cause the moisture content towards the top to increase.

It was anticipated that some water would accumulate on the top surface of the bottom plate. It was also expected that some water penetrates the vertical interface between the sheathing and the bottom plate, as shown in Figure 4.12. The quantity of water that reaches this vertical space depends on the amount of water that reaches the bottom plate. Thus, the bottom of the sheathing and the bottom plate are especially vulnerable to moisture accumulation and were closely monitored. Specifically, a moisture content probe was installed in the bottom plate such that it measures the moisture content of the wood at a distance of 6 mm below the top surface. In addition, three gravimetric samples

were installed in the bottom plate, two being in the top surface, and one being on the side surface adjacent to the sheathing, as shown in Figures 4.8 to 4.11.

Water was expected to accumulate on the surfaces of the bottom plate during the wetting phase. In the case of intact wood, water would migrate from the surfaces and into the wood. However, where a gravimetric sample has been installed, water could migrate within the gap between the gravimetric sample and the surrounding wood, causing an increase in the moisture content of the specimen that would not occur if the wood were intact. To prevent the occurrence of such migration, the unexposed surfaces of the gravimetric samples in the bottom plate were painted with an acrylic paint.

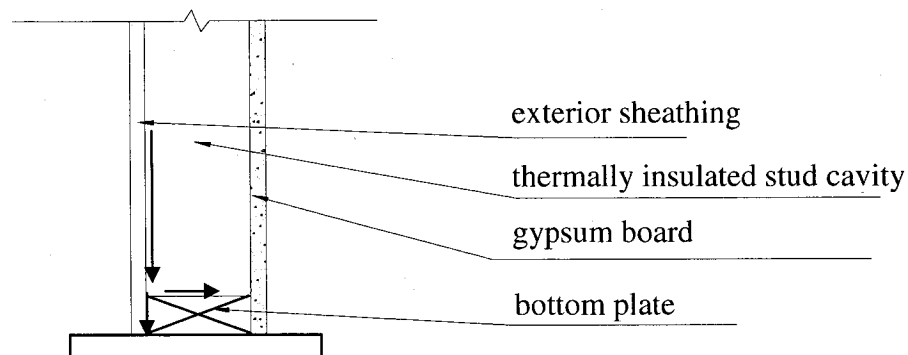


Figure 4.12. Section view showing the expected water flow path at the bottom of the test wall during wetting phase.

4.4.3.1 Gravimetry

Gravimetry is an indirect method of measuring the average moisture content of samples located within a specimen and consists of comparing the weight of a specimen before and after it is oven dried. The determination of the moisture content of a sample by gravimetry entails cutting out a small specimen of the assembly component. It should be recognized that the cut produces a capillary break between the component and the specimen, which alters the capillary moisture migration into the specimen. The significance of this limitation depends on the capillary properties of the material in question and the importance of movement of liquid water within the material, and will be

addressed the next chapter dealing with results and data analysis.

Moisture content can be expressed as a weight fraction or a volume fraction; these are calculated as follows:

$$MC (\%-mass) = \frac{\text{mass of moist sample} - \text{mass of oven-dry sample}}{\text{mass of oven-dry sample}} \quad [4.1]$$

$$MC (\%-volume) = \frac{\text{volume of water within moist sample}}{\text{volume of dry sample}} \quad [4.2]$$

where M is the moisture content. The relation between these two values can be related to the density of the material as follows:

$$MC (\%-mass) = MC (\%-volume) \cdot \rho_w / \rho_{dm} \quad [4.3]$$

where ρ_w and ρ_{dm} are the densities of water and of the dry material, in kg/m^3 , respectively. In each wall, gravimetric samples were installed in the wood studs, bottom plate and in the wall sheathing. These were periodically removed from the test assemblies for gravimetric measurements. The location and number of samples in each component is detailed in Figures 4.8 to 4.11 and Table 4.4.

Table 4.4. Location and number of gravimetric samples and moisture content probes within each wall assembly.

| Wall no. | Number of gravimetric samples | | | Number of Moisture Content Probe Pairs | | |
|----------|-------------------------------|--------------|-----------|--|--------------|-----------|
| | Stud | Bottom Plate | Sheathing | Stud | Bottom Plate | Sheathing |
| 1-16 | 3 | 3 | 9 | 2 | 1 | 2 |
| 17 | 3 | 4 | 9 | 0 | 0 | 0 |
| 18-19 | 3 | 4 | 6 | 2 | 0 | 0 |

Each gravimetric sample in the wood framing was 13 mm in diameter and 13 mm deep, and was accessed during the experiment via the access panels cut from the gypsum finish, as shown in Figures 4.8 to 4.11. A small piece of Velcro was taped to a corner of the gypsum access panels to ensure that the panel remained fully closed during the

experiment, thus reducing the risk of air flow into and out of the panel (see Figure 4.13). Only the sample on the exterior vertical surface of the bottom plate was accessed via a hole in the sheathing cut out for a gravimetric sheathing specimen, as shown in Figure 4.14 and 4.15. The gravimetric specimens in the sheathing were 50 mm in diameter. For the assemblies with exterior extruded polystyrene insulation, a removable piece of insulation was cut in front of the gravimetric samples in order to allow access to these, as demonstrated in the photograph in Figure 4.15.



Figure 4.13. Photo of the interior finish of a typical wall assembly showing the three gypsum access doors.

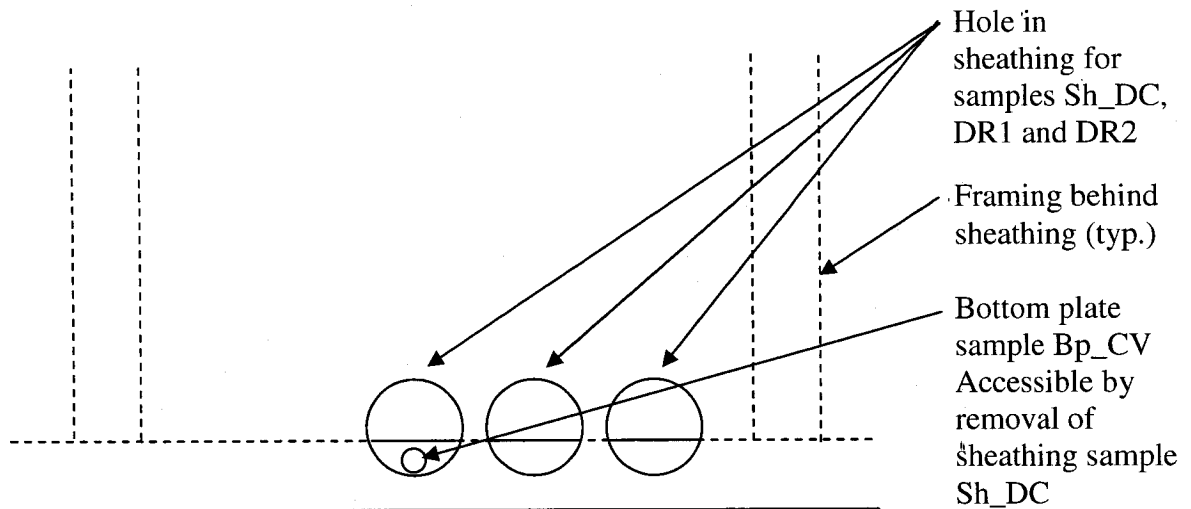


Figure 4.14. A hole for a sheathing gravimetric sample at the bottom center of the sheathing was used as an access panel to reach the sample in the bottom plate.

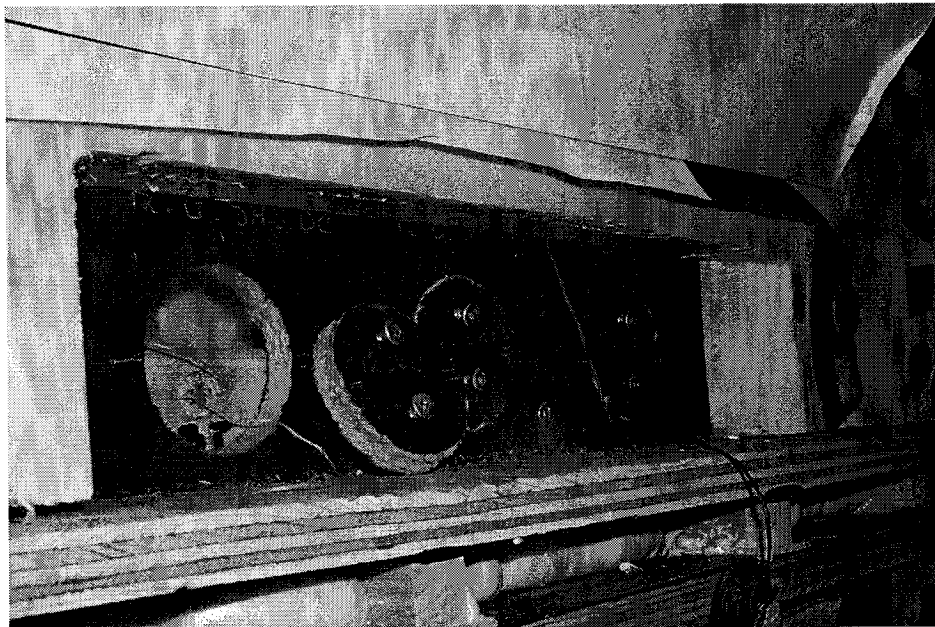


Figure 4.15. Photo from the exterior of assembly 12 showing the access door within the sheathing membrane and exterior insulation, as well a hole made for a sheathing gravimetric sample that enabled access to the bottom plate sample beyond.

The gravimetric samples in the sheathing and in the studs of all walls, as well as in the bottom plate of walls 18 and 19 were removed by using one or two screws which

were installed prior to the beginning of the experiment. No screws were installed in the samples in the bottom of the walls receiving water load because it was felt that the presence of the screw may affect the path of the moisture distribution, especially during the wetting phase of the experiment. Instead, a piece of dental floss was wrapped around each sample to facilitate their extraction, as shown in Figure 4.16 and 4.17. In addition, small notches were made in the access panels of the extruded polystyrene exterior insulation vis-à-vis the screws of the sheathing gravimetric specimens. The notches were made to prevent the sheathing gravimetric samples from being pushed into the insulated space of the wall assembly when the extruded polystyrene access panels were installed after gravimetric measurements. Also, creating access panels in the wood siding for wall no. 14 was necessary to reach the gravimetric samples behind in the sheathing and in the bottom plate.

Gravimetric samples in the bottom plate were painted with two coats of acrylic paint on the unexposed sides. As water ran to the top surface of the bottom plate, it was likely to pool into the hole in the bottom plate in which sits the gravimetric sample. The gravimetric samples were partially painted in order to prevent water absorption into the sample from these sides which would not normally be exposed to water if the bottom plate were intact, as shown in Figures 4.16 and 4.17.

The scale used to weigh the gravimetric samples has an accuracy of 0.1 mg and a maximum capacity of 310 g. The weighing surface upon which the specimens are placed is shielded on all sides to prevent air flows from disturbing the measurements. At the beginning of each weighing series, the scale was calibrated using an internal scale function; periodically, the scale was also calibrated using an external mass.

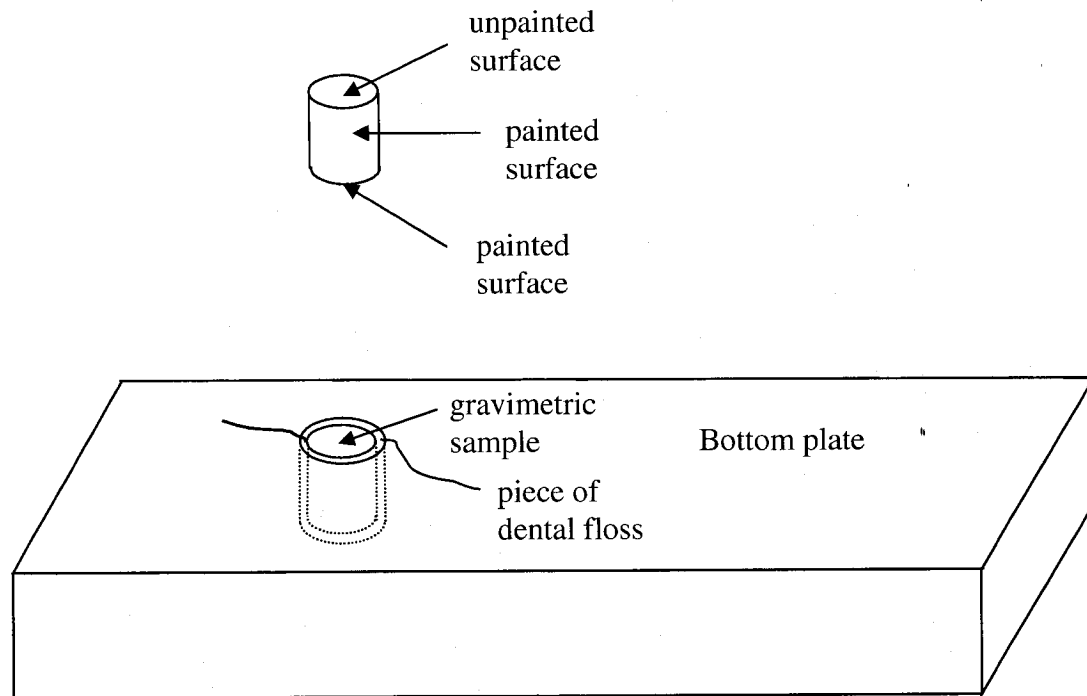


Figure 4.16. Schematic (not to scale) showing the painted surfaces of the gravimetric sample and how it sat within the bottom plate.

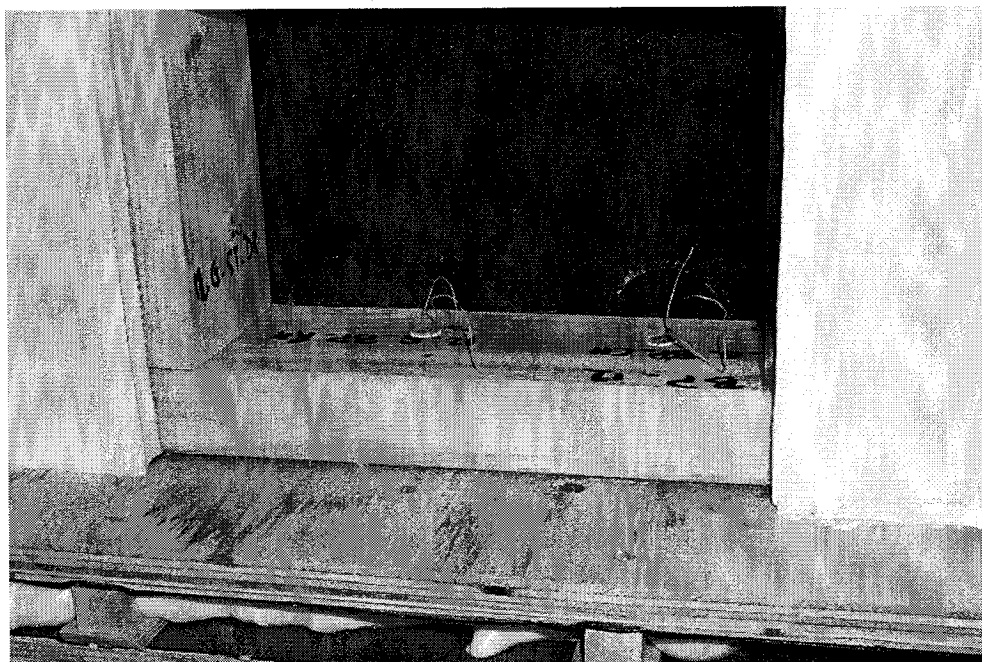


Figure 4.17. Photo of the junction between the wood stud and bottom plate in a typical wall assembly with their gravimetric samples and the dental floss to ease their removal.

The oven used to dry the gravimetric samples was a gravity and forced convection oven with a control sensitivity of $\pm 0.5^{\circ}\text{C}$ and an ability to maintain the temperature throughout the oven at an average uniformity of $\pm 3^{\circ}\text{C}$. The oven was set to 103°C to dry the wood specimens, as recommended by ASTM D4442-92 (ASTM, 1992). However, for the sheathing gravimetric samples, the oven temperature was decreased to prevent the evaporation of possible volatile compounds within the materials.

4.4.3.2 Electrical resistance moisture content measurement

Electrical resistance moisture content probes, also called moisture content pins, were used to measure the local moisture content of wood. The principle for the technique is based on the fact that the electrical resistance of the material decreases with increasing moisture content (Duff, 1968; Skaar, 1988; Derome, 1999). For example, the resistance of wood increases by a factor of roughly 10^7 over the range from fiber saturation point (about 30%) to oven dry state (Lagus, 1994). An electrical resistance moisture measurement system includes a transmitter and probe a pin pair. The transmitter supplies the excitation electrical voltage and converts the measured resistance to analog electronic output. The method involves applying a voltage to the probes, which ionizes the material. The ionization is proportional to the number and the duration of the exposure to the voltage and causes corresponding errors in the readings (Desmarais *et al.*, 1998). A custom electronic set-up designed at the Building Envelope Performance Laboratory switches the direction of the excitation voltage to reduce the polarization effect and maintain the electrical voltage for only a few seconds for each measurement to prevent any electrodeposition on the moisture pins (Fazio *et al.*, 1998). The measured resistances are converted by transmitters to 4 to 20 mA current signals that are read by the data acquisition system. Readings were taken automatically every 5 minutes and were stored to files on the computer hard disk.

In this experiment, moisture probes were installed in the studs, bottom plate and sheathing in assemblies 1 to 16, as shown in Figures 4.8 and 4.9 and Table 4.4. Each moisture content probe consisted of a pair of two metal pins. The shaft of the pins used for the studs and the bottom plates was insulated such that moisture content was

measured only from the tip of the pins. In the studs and the bottom plate, they were inserted from side of the buffer cavity and the bottom of the bottom plate, respectively, such that the tip of the probe was at 6 mm from the surface. Because of the limited thickness of the sheathing, smaller pins, 1 mm in diameter and 7 mm in length, were used. These pins were uninsulated and gold plated to prevent oxidation and corrosion. They were installed in the sheathing from the cold side to a depth of approximately 6 mm from the interior surface.

The accuracy of the electrical resistance readings typically decrease as the moisture content of wood increases, and moisture level readings above the fiber saturation point of wood are only indicative of high moisture content (Derome, 1999; Lagus, 1994; Skaar, 1988). Also, because the electrical resistance of wood decreases with increasing temperature (James, 1975; Lagus, 1994; Forsén and Tarvainen, 2000), temperature corrections must be made. Temperature sensors were installed adjacent to and at the same depth as the moisture content probes for this purpose. The resistance is also affected by the wood species, and more accurate results are obtained if the meter can be calibrated with respect to the wood species' exact place of origin, e.g. pine from Sweden (Forsén and Tarvainen, 2000). Moisture content meter manufacturers typically provide corrections for temperature and wood species, but not for engineered wood products like OSB, plywood and fiberboard.

Calibration curves were developed by Desmarais (2000) based on a method described by Zarr *et al.* (1995) for asphalt-coated sheathing fiberboard to determine moisture content by electrical resistance technique. Five 40 mm by 40 mm fiberboard samples were installed with moisture content resistance sensors and placed in a small conditioning chamber where the temperature and relative humidity were controlled. The temperature was held constant at 17°C and the relative humidity maintained until the specimens reached moisture content equilibrium. The test was conducted at relative humidity of 50%, 75%, 85%, 90%, 95% and 97%. The test was repeated at 4°C and at relative humidity of 50%, 75%, 85% and 92% for temperature-correction purposes. The same type of calibration curves were developed for plywood and OSB, but using different temperatures of 10°C and 20°C and relative humidities of 50%, 75%, 85%, and 92%. The calibration curves will be developed and applied to the experimental data at a later

date. Voltage readings were taken from the moisture content sensors and the samples weighed immediately afterwards. The samples were oven-dried and weighed again at the end of the procedure. The actual moisture contents, determined by gravimetry, were plotted against the voltage readings to find the calibration curve from which the voltage readings taken during the actual experiment are converted into moisture contents, as shown in Figure 4.18 for asphalt-coated fiberboard.

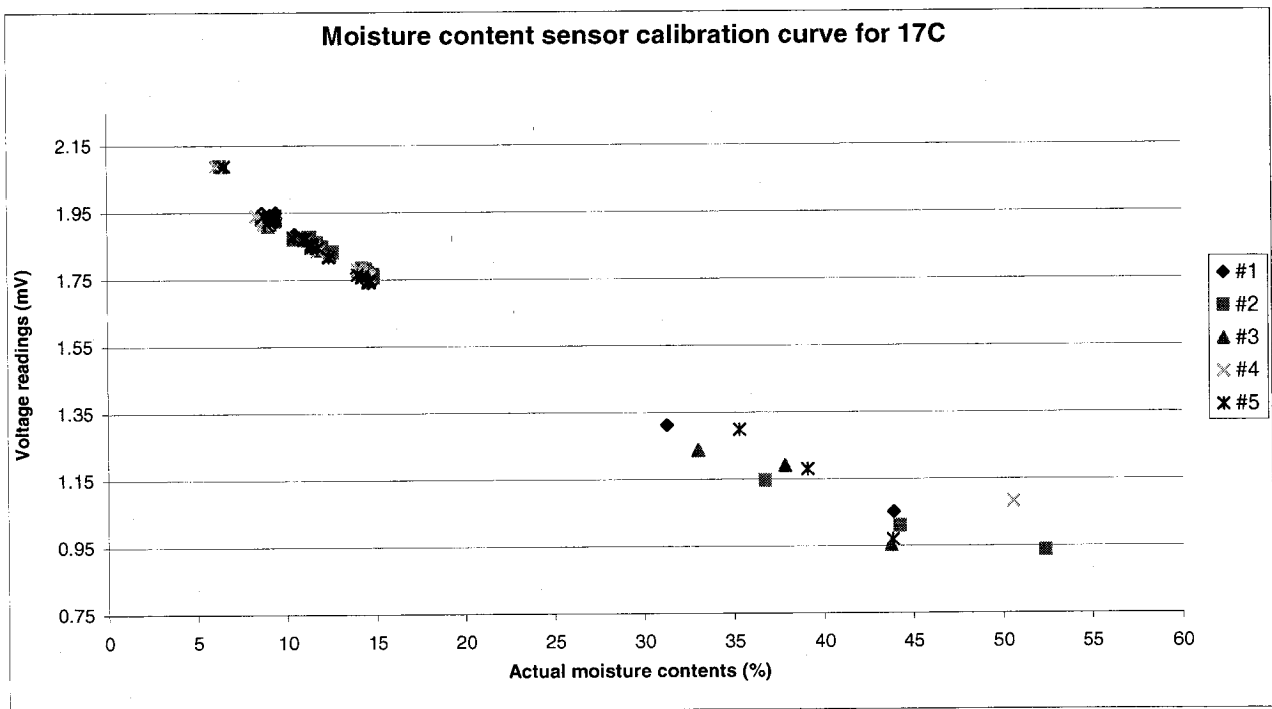


Figure 4.18. Calibration of data points at 17°C for asphalt-coated fiberboard (Desmarais, 2000).

4.4.4 Air pressure

The air pressure differential between the interior of the test hut and the environmental chamber was monitored manually using a micromanometer during the wetting phase and the drying phase. As expected, no pressure difference was observed during the wetting phase. During the drying phase, a small varying pressure difference of 0 to 2 Pa, with the reference pressure inside the test hut, was observed. To increase the airtightness of the test hut and hence minimize the air leakage resulting from this air pressure difference

during the drying phase, more polyurethane foam was sprayed to fill the gaps in the existing polyurethane between wall assemblies at the end the last week of the wetting phase. Latex caulking was applied at the junction of the plywood separator for each wall and the gypsum finish for the same purpose.

4.4.5 Construction and instrumentation

Building the test walls took place first before the construction of the test hut. The test walls were carefully assembled to ensure that the stud members were installed at 90° angle to the top and bottom plate framing members. The construction schedule was carefully planned and controlled such that the assemblies' construction and the installation of sensors took place in tandem. For example, holes for gravimetric samples were drilled into the wood before the framing members were assembled together, a process that greatly facilitated the drilling process. Also, installing the electrical resistance moisture probes and thermocouples from the bottom surface of the bottom plate was executed before the plywood separators were added beneath the bottom plate. Grooves were made into the wood framing members to enable the passage and protect the sensor wiring. During the installation of the wall assemblies into the test hut, 19 mm by 19 mm by 250 mm long spacers were placed between the assemblies to create a space between the assemblies, and shims were used as needed beneath to level the assemblies in all three directions. The leveling was thought to be critical to ensure that the water introduced at the top of the wall during the wetting phase ran vertically down the inside surface of the sheathing along the centerline of the wall.

4.5 Test climate loading

The objective of the testing methodology was to simulate as closely as possible the actual environmental conditions to which walls are exposed in Montreal. In the late fall, winter and early spring, the outer components of the assemblies generally undergo

wetting rather than drying because the temperatures in the sheathing and in the stud space are relatively low and the relative humidities are high. The vapor pressure differential causes diffusion towards the exterior and can result in water vapor absorption and accumulation in the hygroscopic wall components, a process that does not permit drying of wood-based sheathing and wood studs in cold weather conditions. Conversely, drying occurs primarily in the late spring, summer and early fall.

Generally, wetting of envelopes occurs primarily through water vapor diffusion during the cold seasons. Incidental rainwater infiltration due to a defect in the rainwater management components of the envelope can be another important source of moisture. In this work, the effects of wetting by both vapor diffusion and water penetration were combined to provide a worse-case scenario for the hygrothermal performance of wood-frame wall assemblies. To this effect, the walls were subjected to a three-week pre-conditioning phase where wetting by vapor diffusion was induced, followed by a four-week wetting phase where wetting occurred by water insertion directly into the walls at a controlled rate and by vapor diffusion. The last stage of the test was designed to simulate a series of four-week drying phases reflecting spring and summer conditions in Montreal. The premise of the test is of north-facing walls. Therefore, solar effects, and wetting via solar-induced vapor diffusion in particular, were not taken into account. Air migration due to the wind, mechanical ventilation, and stack effect was also not considered.

4.5.1 Pre-conditioning phase

Previous experiments performed at the Environmental Chamber (Derome, 1999; Derome and Desmarais, 2005) have shown that winter absorption of diffusing moisture by wood members within wall assemblies is a slow process. A pre-conditioning phase was devised to reproduce the conditions found at the end of the winter show in Derome and Desmarais's (2005) work, where after three months of exposure to average winter conditions, the average moisture content in the wood and fiberboard components in the airtight wall assemblies had leveled off at approximately 12% by dry weight. It is recognized, however, that in actuality, the moisture content throughout envelope assemblies is not uniform due to various reasons including the presence of a temperature

gradient, moisture gradient, change in indoor and outdoor loading conditions with time, etc.

Derome and Desmarais' (2005) findings served as the basis of the pre-conditioning phase. The adsorption curve of spruce (wood moisture content vs. relative humidity) by Hedlin (1967), reproduced here in Figure 4.19, shows that to obtain a moisture content of 12% by adsorption at a temperature of 21°C, the relative humidity required is approximately 60%. Thus, conditions of 21°C and 60% relative humidity were set throughout the environmental chamber during the three-week pre-conditioning period. During the pre-conditioning phase, the vapor retarder and gypsum board were not yet in place and were only installed at the end of the phase. While a uniform moisture content was sought during the wetting phase, it was recognized that such uniformity is not found in actuality.

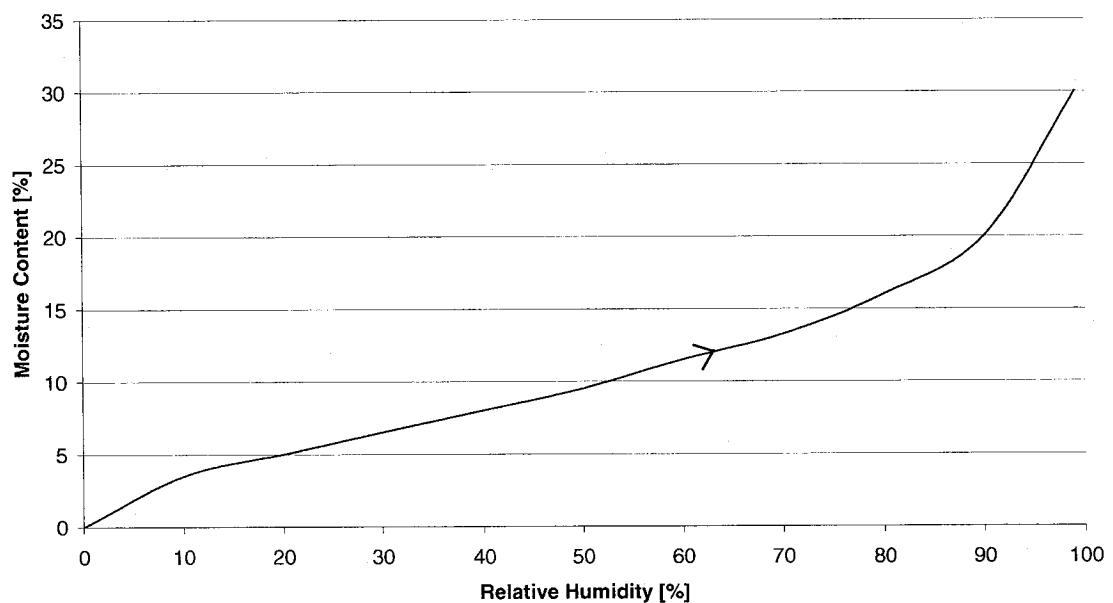


Figure 4.19. Adsorption curve for white spruce at 21°C (Hedlin, 1967).

4.5.2 Wetting phase

The test aimed to reproduce a four-week wetting phase, during which water was introduced into the test assemblies to simulate rain penetration due to a specific example of an envelope defect.

The indoor and outdoor temperatures and relative humidities during the wetting phase were set at 21°C and 50% to 60%, respectively, as in the pre-conditioning phase, to maintain the moisture content levels achieved during the pre-conditioning phase. Setting the same indoor and outdoor temperature and relative humidity conditions also reduced the moisture drive across the test assemblies during the wetting phase. While the indoor relative humidity was perhaps higher than found in homes, it was set to reduce evaporation of the water that was absorbed by the assemblies in the pre-conditioning phase at that introduced into the test wall walls during the wetting phase. From Hedlin's (1967) adsorption curve, it was expected that the equilibrium of the wood would be maintained between 10% and 12 %.

4.5.3 Drying phase

Once the wetting phase was completed, drying conditions were set in the Environmental Chamber and in the test hut, reflecting average spring and summer conditions in Montreal. No water was introduced into the test walls during the drying phase, as if the envelope defect allowed rain leakage into the wall assemblies had been repaired.

The outdoor temperature profile generated in the Environmental Chamber reflected the monthly and the daily temperature variations that exist in reality. For this purpose, average conditions were selected for this study to study the effects of typical rather than extreme moisture loads. Meteorological data from 1981 to 2001 obtained from Environment Canada for Montreal at the Trudeau Airport weather station led to approximate the monthly patterns and daily quasi-sinusoidal variation in temperature and the average daily minimum and maximum temperatures for each month of the drying phase. Hence an outdoor temperature profile was generated for each month.

The outdoor relative humidity was also determined based on actual weather data. However, a daily average was calculated for each period by taking the daily average from the hourly data provided by the meteorological station, and then calculating the mean over the entire period in question.

The typical indoor conditions found on site during the spring and summer were reproduced. The planned indoor and outdoor environmental conditions for both the wetting and drying phases are summarized in Table 4.5.

Table 4.5. Planned indoor and outdoor temperature and relativity conditions for the wetting and drying phases of the experiment.

| Period no. | Duration (days) | Period simulated | Indoor Testing Conditions | | Outdoor Testing Conditions | | | |
|-----------------------|-----------------|--------------------------------------|---------------------------|--------|----------------------------|----------------|-----------------|--------|
| | | | | | Sinusoidal function with: | | | |
| | | | Temp. [°C] | RH [%] | Average Temp. [°C] | Max. Temp [°C] | Min. Temp. [°C] | RH [%] |
| Wetting Phase: | | | | | | | | |
| 1 | 21-28 | Conditions leading to winter wetting | 21 | 50-60 | 21 (constant) | - | - | 50-60 |
| Drying Phase: | | | | | | | | |
| 2 | 28 | April | 21 | 40 | 6.3 | 10.9 | 1.6 | 64 |
| 3 | 28 | May | 21 | 43 | 13.7 | 18.7 | 8.6 | 63 |
| 4 | 30 | June | 23 | 52 | 18.6 | 23.4 | 13.7 | 67 |
| 5 | 31* | July | 23 | 65 | 21.1 | 25.8 | 16.4 | 69 |

* The duration of this period may vary if required.

4.6 Experimental history

The desired interior conditions were set within the test hut; the exterior conditions were reproduced in the environmental chamber. The test was terminated after 63 days, or one week after May conditions were set, because the wetted components dried at a faster rate than expected, and it was deemed that the walls had sufficiently dried at the locations of the gravimetric and moisture content probes.

4.6.1 Climatic conditions

The temperature setpoints that were required in the chamber and inside the test hut during the wetting phase and both drying phases of the experiment were maintained by the HVAC conditioning equipment, as explained in section 4.5. Figures 4.20, 4.21, and 4.22 show the temperature profiles for three typical 24-hour cycles during the wetting phase and the first and second drying phases. Figures 4.20 and 4.21 show that the temperature in the hot box, the cold box and the test hut, respectively, were maintained within a range of approximately $\pm 2^{\circ}\text{C}$ of the setpoints during the wetting and first drying phases, which is considered acceptable given the size of the environmental chamber. For the second drying phase, the temperature is achieved in the cold box as per the desired setpoint with the exception of a small variation between the temperature setpoint in the chamber and the achieved temperature in the hot box toward the peak of the daily cycle (see Figure 4.22). At the bottom of the cyclical curve of this drying phase, the cold box's large 5-ton screw compressor cooling system works in tandem with the smaller cooling unit in the hot box to produce relatively uniform temperatures across the environmental chamber. However, at the top of the cyclical curve, the large cold box screw compressor is turned off and a smaller cooling system switches on to cool the cold box, again working in tandem with the hot box cooling system. At this point in the daily temperature profile, the steady cooling output of the hot box cooling system overcools the hotbox, resulting in a temperature profile at the peak of the curve that is approximately 2.5°C lower than the setpoint.

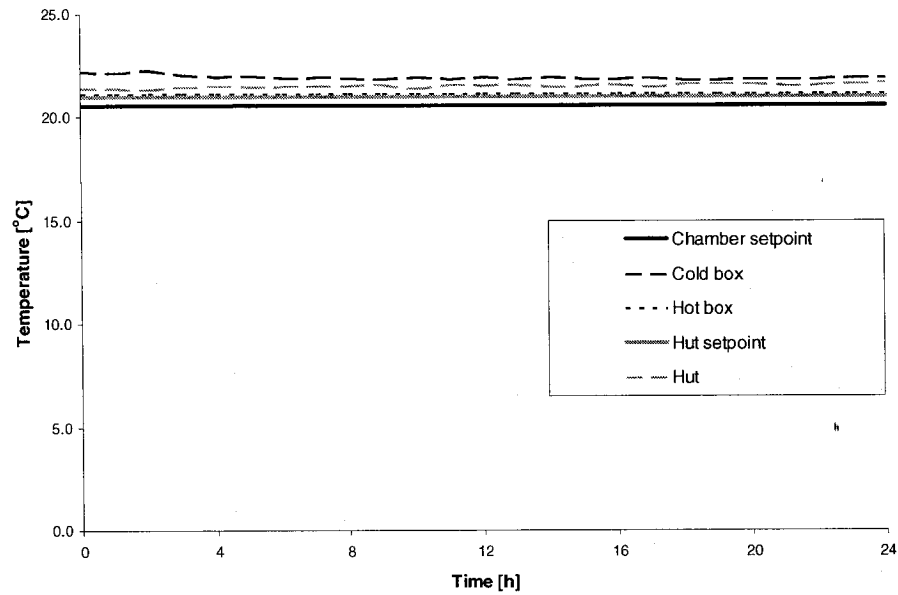


Figure 4.20. Hourly temperature profiles for wetting phase of test 1 showing the average temperatures reproduced in the hot box and cold box of the environmental chamber and inside the test hut vs. the planned temperatures.

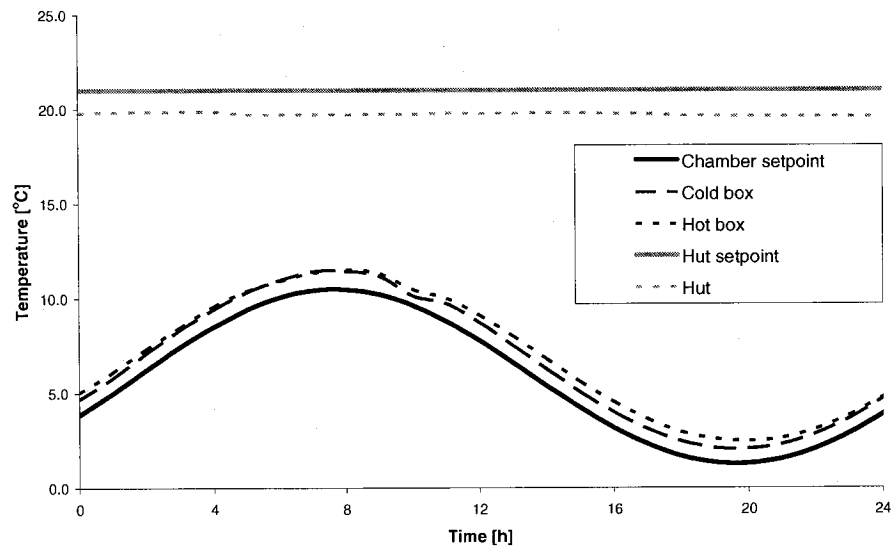


Figure 4.21. Hourly temperature profiles for first drying phase of test 1 showing the average temperatures reproduced in the hot box and cold box of the environmental chamber and inside the test hut vs. the planned temperatures.

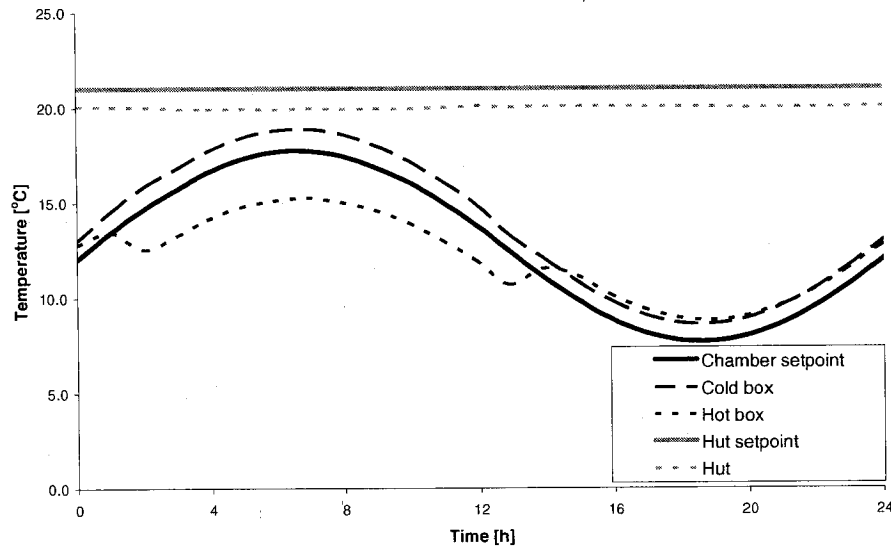


Figure 4.22. Hourly temperature profiles for second drying phase of test 1 showing the average temperatures reproduced in the hot box and cold box of the environmental chamber and inside the test hut vs. the planned temperatures.

The relative humidity in the environmental chamber and inside the test hut was also controlled and monitored during the wetting and drying phases of the test. In the environmental chamber, humidification was achieved by a mist humidifier located above the fan coil unit at the end of the hot box. In the cold box of the environmental chamber, relative humidity was monitored but not controlled. The relative humidity was consistently higher in the hot box. This occurred for two reasons: first, the humidifier was located at the end of the hot box; second, removal of the condensate which formed on the cooling coils in the small and large cooling units in the cold box resulted in dehumidification. This explains why the relative humidity monitored in the hot box was greater than that in the cold box in every phase of the experiment. Inside the test hut, relative humidity control was obtained with the use of a humidifier and a dehumidifier located within a conditioning equipment box located in the middle of the hut.

The desired steady state relative humidity conditions inside the hut were achieved during the wetting phase and both drying phases (see Figures 4.23-4.25). However, there was some difficulty reaching the desired 60% setpoint in the environmental chamber during the wetting phase, and only about 51% relative humidity was obtained, as shown in Figure 4.23. Also, the chamber relative humidity setpoint was difficult to maintain during the drying phases because of the diurnally varying temperature conditions

required in these phases, as shown in Figures 4.24 and 4.25.

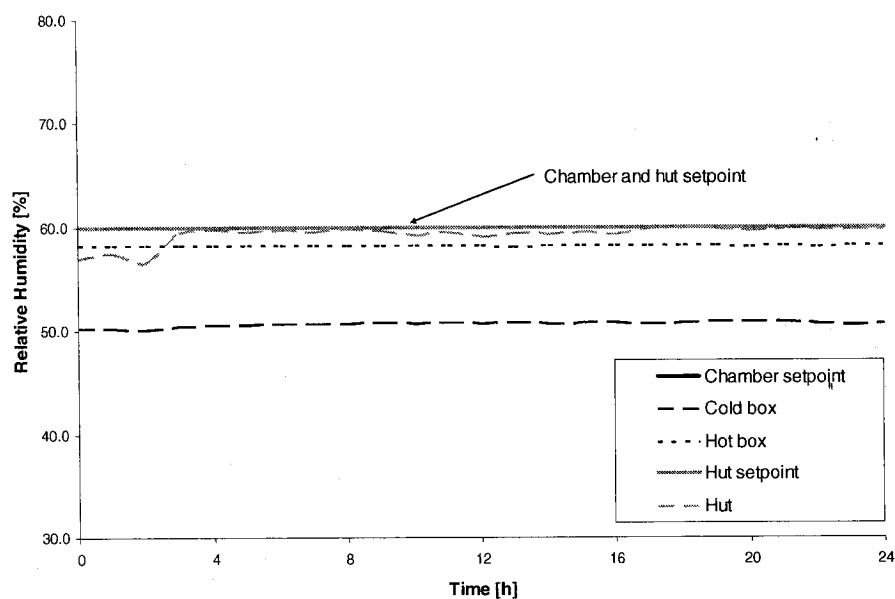


Figure 4.23. Hourly relative humidity profiles for wetting phase of test 1 showing the average relative humidities reproduced in the hot box and cold box of the environmental chamber and inside the test hut vs. the planned relative humidities.

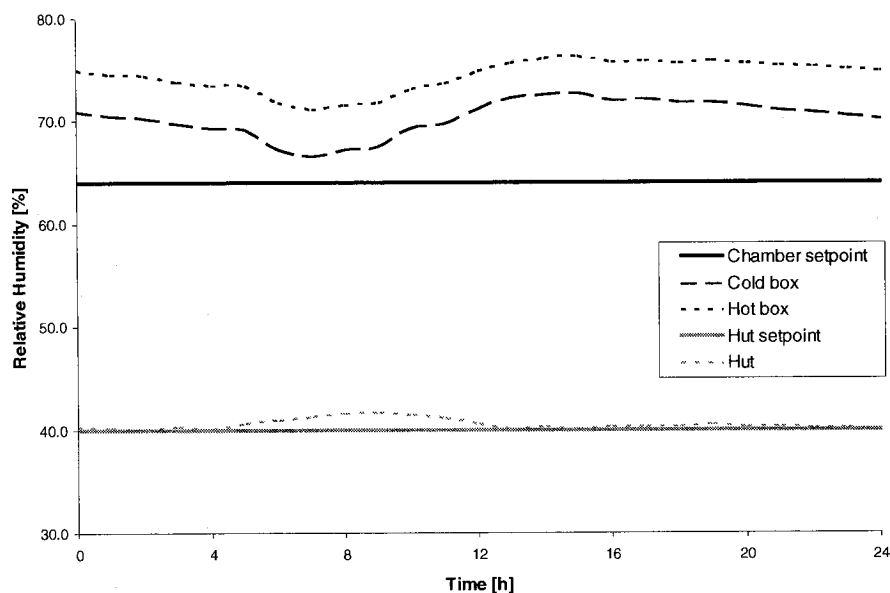


Figure 4.24. Hourly relative humidity profiles for first drying phase of test 1 showing the average temperatures reproduced in the hot box and cold box of the environmental chamber and inside the test hut vs. the planned relative humidities.

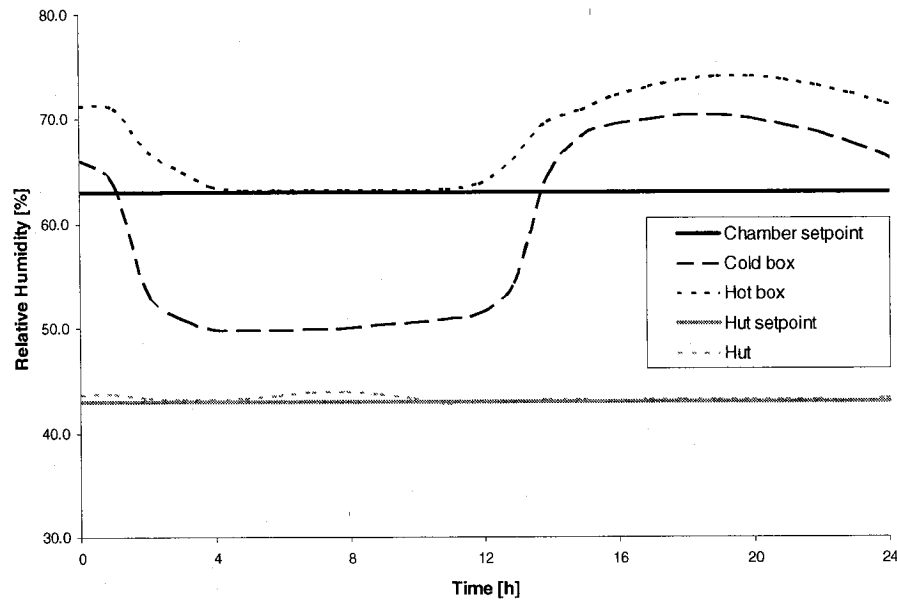


Figure 4.25. Hourly relative humidity profiles for second drying phase of test 1 showing the average relative humidities reproduced in the hot box and cold box of the environmental chamber and inside the test hut vs. the planned relative humidities.

4.6.2 Observations during wetting phase

A different moisture distribution pattern was observed for the plywood-sheathed wall assemblies than for the walls sheathed with OSB and asphalt-coated fiberboard. There was substantial moisture accumulation within the plywood sheathing gravimetric samples in the top two rows of the sheathing board, i.e. in rows 'A' and 'B' (see Figure 4.8 for the location of the sheathing moisture measurements), and in particular within those samples that lay in the path of the water runoff. Water tended to flow through the gap between the sheathing panel and the gravimetric samples by capillarity and wet the samples such that water absorption could be observed on all faces of the samples, as shown for example in Figure 4.26. The wetting patterns and the effect of the sheathing in the various walls are discussed further in the following chapter. As is explained in the next section, the moisture content monitoring in the second test was modified to reduce the effects of gravimetry on the moisture content measurements in the plywood-sheathed walls.

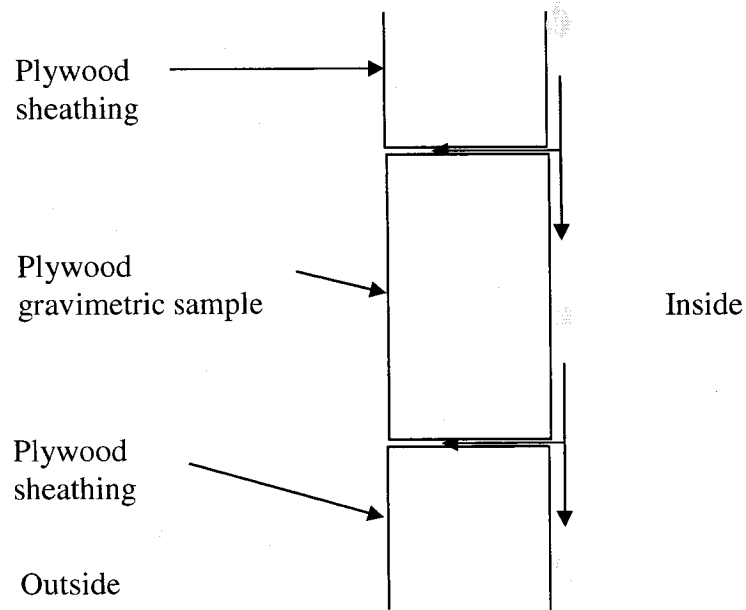


Figure 4.26. Schematic showing path of path of water runoff on the plywood sheathing.

Most of the gravimetric samples that experienced water absorption during the wetting phase swelled to the point that their removal for gravimetric measurement became difficult. Significant swelling was observed for most of the wetted plywood sheathing samples, and particularly those that lay in the path of the water running down the sheathing. Swelling was also observed in the OSB samples located at the bottom of the wall adjacent to the bottom plate, and the samples in absorbed moisture during the wetting phase. To facilitate their later removal and to avoid breaking the samples, the perimeter of the hole within which the samples were placed during the test was sanded during days in the wetting phase where no water was introduced using a Dremel tool. In a few instances, this caused the gap between the specimen and the adjacent wall to widen to a greater extent than desired and resulted in some moisture migration through the gap during the subsequent wetting periods. This occurrence was noted in sheathing sample AC of wall 14, for example.

4.7 Test 2

A second test was conceived and performed for two reasons. First, performing a

second test gave an opportunity to improve the moisture content measurement methodology with respect to the location of each sensor type based on realizations made during the first test. This is explained in more detail below. Second, the exterior sheathing in walls 13 to 19 was changed in test 2 from OSB to plywood to allow comparison of the wetting and drying performance based on a different sheathing type.

The gravimetric measurements obtained during the first test showed that the gravimetric samples in the plywood sheathing that lay in the path of water runoff disturbed the wetting distribution in the plywood boards themselves and in the plywood-sheathed wall assemblies. As was stated earlier, the gravimetric samples at the top of the wall absorbed a much greater amount of water than would normally occur if the samples were not there because of capillarity moisture movement. Their presence may have caused much of the lateral moisture movement during the wetting phase. Therefore, an improved moisture content monitoring method made use of both gravimetric and electrical resistance moisture probes which were both strategically placed such that moisture measurement would not interfere with the water runoff or moisture transfer.

In the following sections, the composition of the wall specimens, the testing parameters, the monitoring methodology, the wetting method and climatic loading conditions, as well as the experimental history are presented.

4.7.1 Composition of the assemblies and testing parameters

The test wall assemblies for the second test were constructed in the same manner as those for the first test with the exception that some walls were sheathed with plywood instead of OSB, which enabled the inclusion of a greater number of experimental variables. Specifically, the sheathing of seven wall assemblies (no. 13, 14, 15, 16, 17, 18 and 19) was changed from OSB to plywood to permit the evaluation of the role of plywood in the hygrothermal performance of the walls.

The test wall configuration and testing parameters for test 2 are summarized in Table 4.6.

Table 4.6. Test wall configuration and testing parameters for test 2.

| No. | Type of Sheathing | Type of vapor retarder | Presence of exterior extruded polystyrene insulation | Presence of Wood Siding | Amount of water* | Other characteristics |
|-----|------------------------|------------------------|--|-------------------------|------------------|-----------------------------|
| 1 | OSB | polyethylene | no | no | X | - |
| 2 | plywood | polyethylene | no | no | X | - |
| 3 | porous wood fiberboard | polyethylene | no | no | X | - |
| 4 | OSB | low permeance paint | no | no | X | - |
| 5 | plywood | low permeance paint | no | no | X | - |
| 6 | porous wood fiberboard | low permeance paint | no | no | X | - |
| 7 | OSB | none | no | no | X | - |
| 8 | plywood | none | no | no | X | - |
| 9 | Porous wood fiberboard | none | no | no | X | - |
| 10 | OSB | polyethylene | yes | no | X | 2"x4" studs |
| 11 | plywood | polyethylene | yes | no | X | 2"x4" studs |
| 12 | porous wood fiberboard | polyethylene | yes | no | X | 2"x4" studs |
| 13 | plywood | polyethylene | No | no | X | full 2.0 m height |
| 14 | plywood | polyethylene | No | Yes | X | - |
| 15 | plywood | polyethylene | No | no | 0.5 X | - |
| 16 | plywood | polyethylene | No | no | 1.5 X | - |
| | plywood | polyethylene | No | no | X | water inserted next to stud |
| 18 | plywood | polyethylene | No | No | none | - |
| 19 | plywood | none | No | No | none | - |

* X denotes the standard amount of water inserted into wall assemblies during wetting phase.

4.7.2 Monitoring protocol

For walls with OSB and asphalt-coated fiberboard sheathing, i.e. walls 1, 3, 4, 6, 7, 9, 10, 12, all instrumentation was the same as per the first test (see Figure 4.8). The instrumentation and placement of the gravimetric samples for walls 18 and 19 were also the same as in the first test since these plywood-sheathed assemblies did not receive a liquid moisture source. The gravimetric and instrumentation schematic is shown in Figure 4.27 for walls 2, 5, 8, 11, 14, 15, and 16, in Figure 4.28 for wall 13 and Figure 4.29 for wall 17.

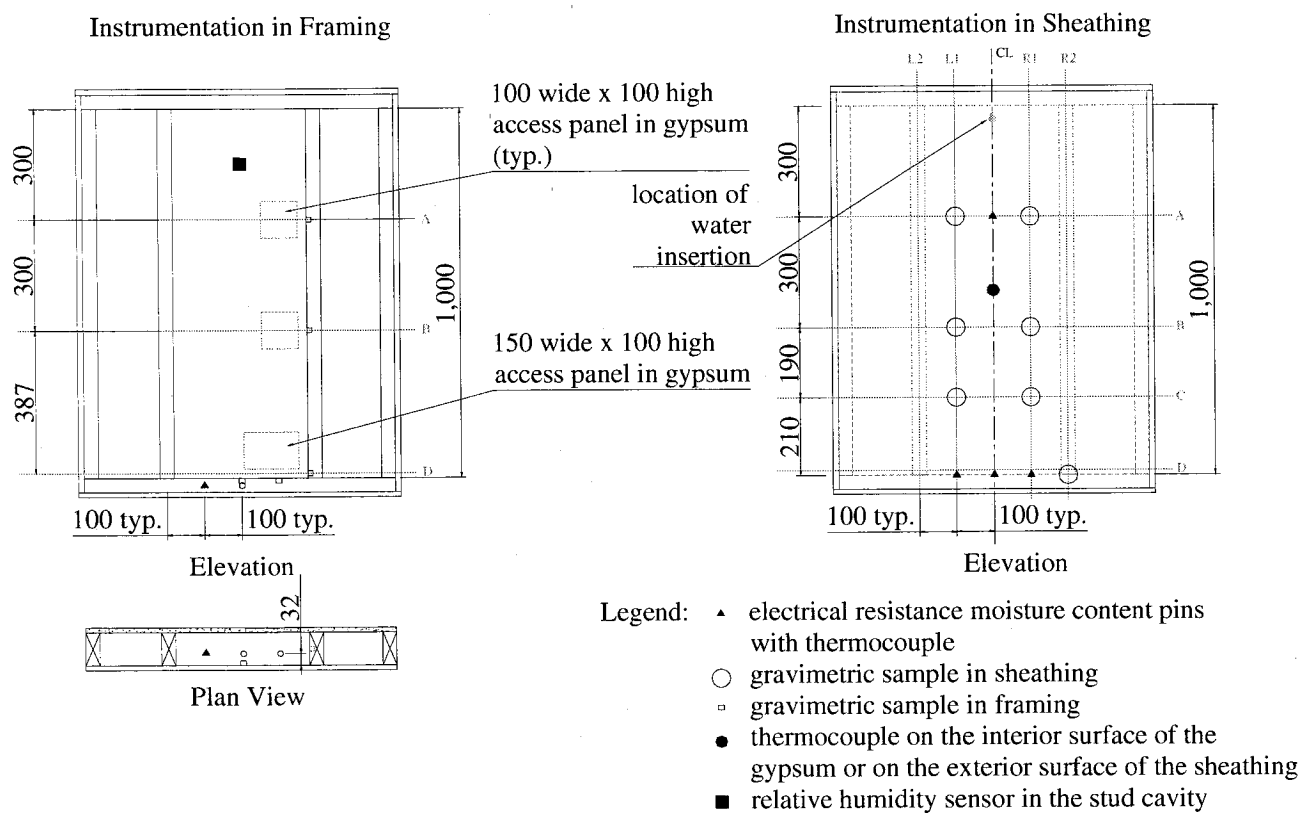


Figure 4.27. Elevation and plan views of the moisture content measurement monitoring protocol in the framing and sheathing of walls 2, 5, 8, 11, 14, 15 and 16 for test 2. The location of the electrical resistance moisture pins with their thermocouple, the gravimetric samples in the sheathing and the framing, the thermocouple on the inside surface of the gypsum and outside surface of the sheathing, and the relative humidity sensor are shown.

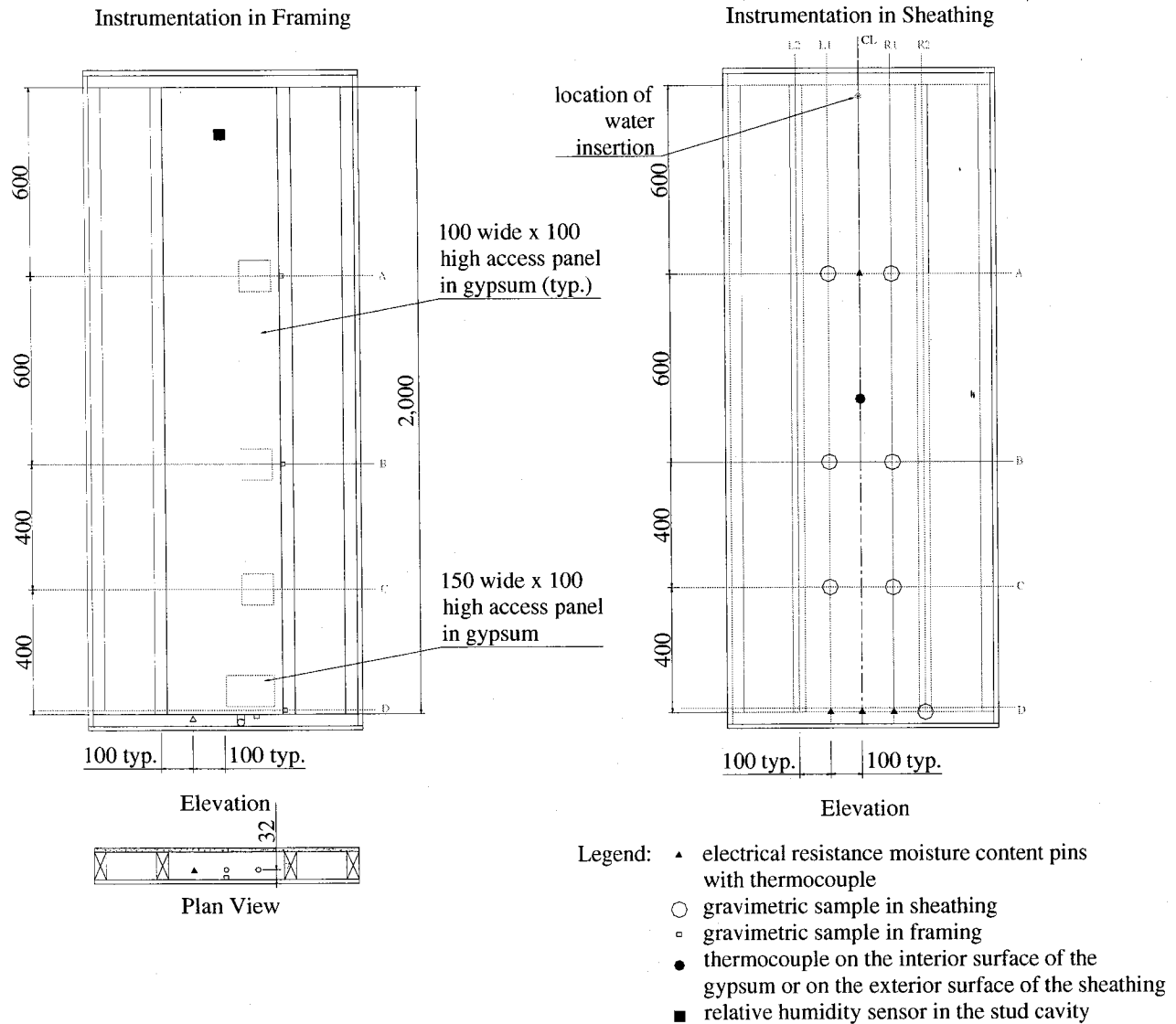


Figure 4.28. Elevation and plan views of the moisture content measurement monitoring protocol in the framing and sheathing of walls 13 for test 2. The location of the electrical resistance moisture pins with their thermocouple, the gravimetric samples in the sheathing and the framing, the thermocouple on the inside surface of the gypsum and outside surface of the sheathing, and the relative humidity sensor are shown.

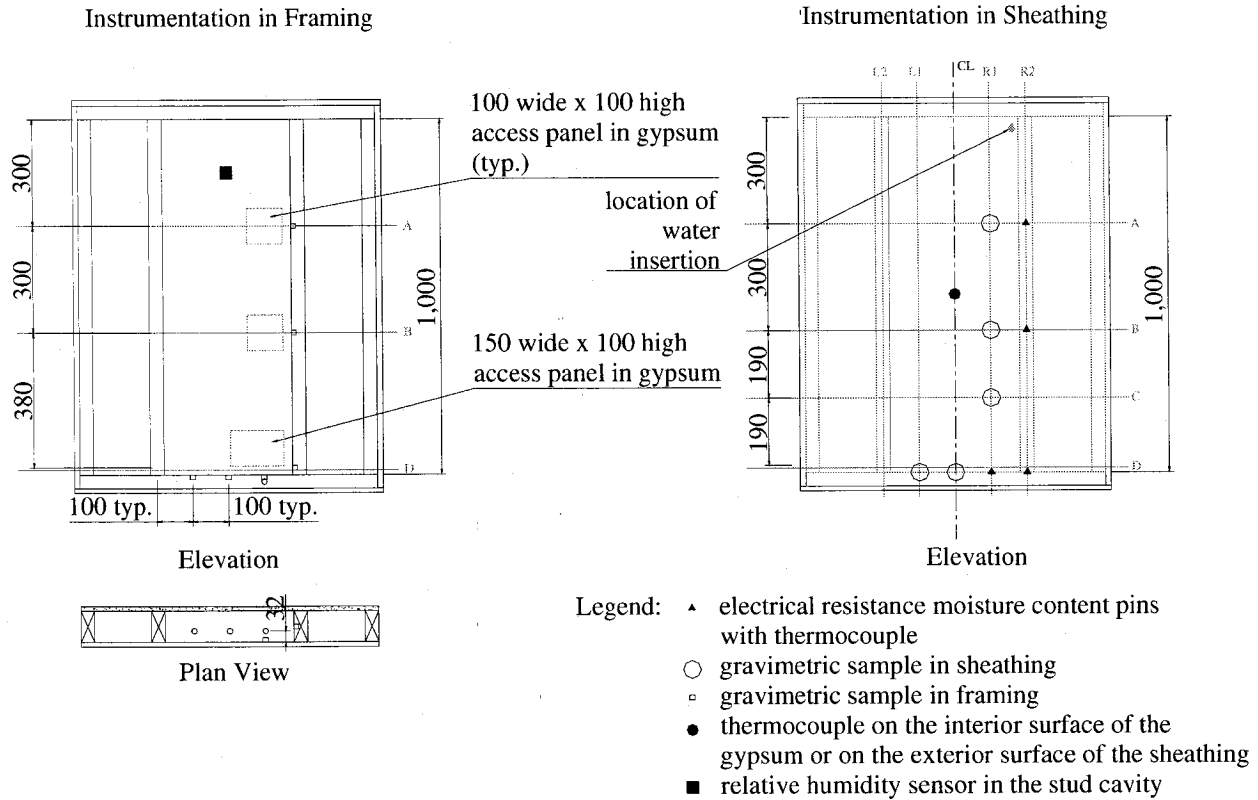


Figure 4.29. Elevation and plan views of the moisture content measurement monitoring protocol in the framing and sheathing of wall 17 for test 2. The location of the electrical resistance moisture pins with their thermocouple, the gravimetric samples in the sheathing and the framing, the thermocouple on the inside surface of the gypsum and outside surface of the sheathing, and the relative humidity sensor are shown.

4.7.3 Wetting methodology and test climate loading

The second test was performed using the same wetting methodology as was used in the first test. With respect to the environmental conditions, they were also similar to that in the first test with the exception of a two-week pre-conditioning phase for the second test. Given the drying rates observed in the first test, it was shortened from four drying phases to one and a half drying phase. Consequently, the drying phase of test 2 was shortened to approximately the same length as the first tests.

4.7.4 Experimental history

As in the first experiment, the second test was terminated after 63 days, or one week after May conditions were set, because it was deemed that the walls had sufficiently dried at the monitored locations. Differences between the planned and actual climatic conditions are explained below, as well as a few observations from the wetting phase of the experiment.

4.7.4.1 Climatic conditions

As was done in the first test, the temperature and relative humidity were monitored inside the Environmental Chamber as well as inside the test hut in order to compare the planned temperature and moisture conditions with those that actually occurred. Figure 4.30 shows the planned and measured temperatures in the Chamber and inside the hut during the wetting phase. The experimental protocol specified a chamber temperature setpoint of 21°C, and yet the figure shows that it was 18°C. It is believed that the discrepancy is due to an error in inputting the setpoint value in the data acquisition system, and that this error did not have a significant impact on the results. Also, during the course of the first wetting phase, the cold box temperature controller that monitors the cold box temperature broke down; however, chamber measurements in the hot box were unaffected and are available for analysis. The temperature monitored in the cold box (Figure 4.30) and in the hot box (Figures 4.30 to 4.32) was typically approximately 1°C greater than the setpoint. During the second drying phase, a small anomaly in the

temperature curve, shown in Figure 4.32, was found, and was due to the mechanical transition of cooling from the cold box's large-capacity 5-ton cooling system when higher cooling loads were required to a smaller unit that provided cooling at the smaller loads in the diurnal cycle. Figures 4.30 to 4.32 also show that the hut temperature shows slight variations which are likely due to opening and closing of the test hut door and human generation of heat within the test hut during the retrieval and installation of gravimetric samples.

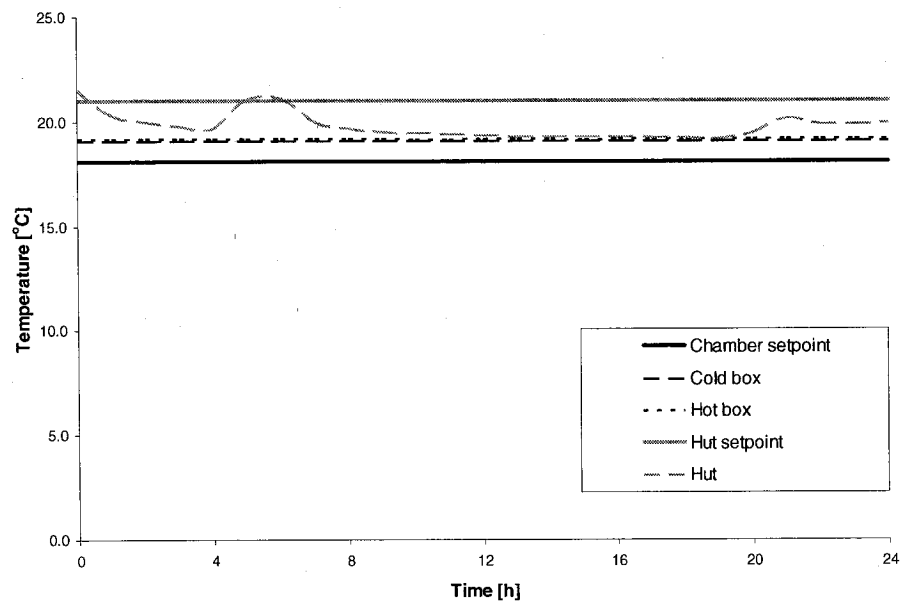


Figure 4.30. Hourly temperature profiles for wetting phase of test 2 showing the average temperatures reproduced in the hot box and cold box of the environmental chamber and inside the test hut vs. the planned temperatures.

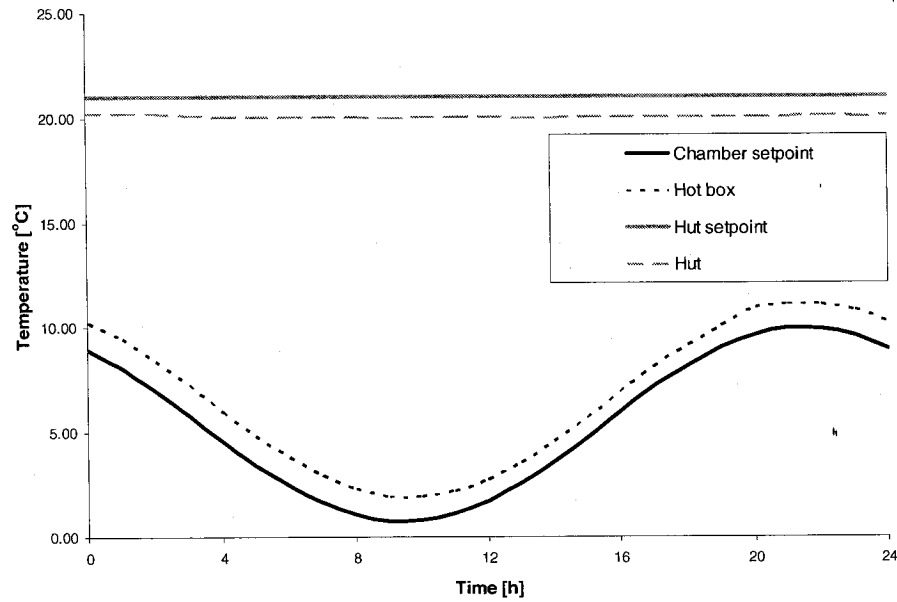


Figure 4.31. Hourly temperature profiles for first drying phase of test 2 showing the average temperatures reproduced in the hot box and cold box of the environmental chamber and inside the test hut vs. the planned temperatures.

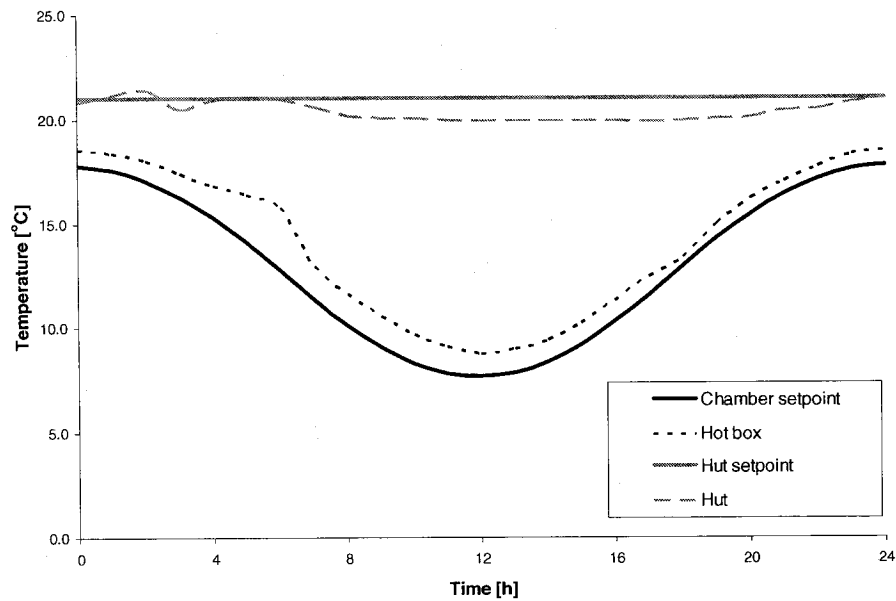


Figure 4.32. Hourly temperature profiles for second drying phase of test 2 showing the average temperatures reproduced in the hot box and cold box of the environmental chamber and inside the test hut vs. the planned temperatures.

It is known that the relative humidity is a parameter that is difficult to control. The wetting phase's setpoint of 60% relative humidity was difficult to achieve both inside the

hut and in the Environmental Chamber (see Figure 4.33). In the first drying phase, the relative humidity was consistently higher in the cold and hot boxes than the setpoint; in the second drying phase, the relative humidity in the cold and hot boxes were higher than the setpoint when the temperature was low and lower when the temperature was high, as expected (Figures 4.34 and 4.35). Similar findings were observed in test 1. The relative humidity inside the test hut was well controlled, and the setpoint of 40% was maintained in the first and second drying phases of the test, as shown in Figures 4.34 and 4.35, respectively.

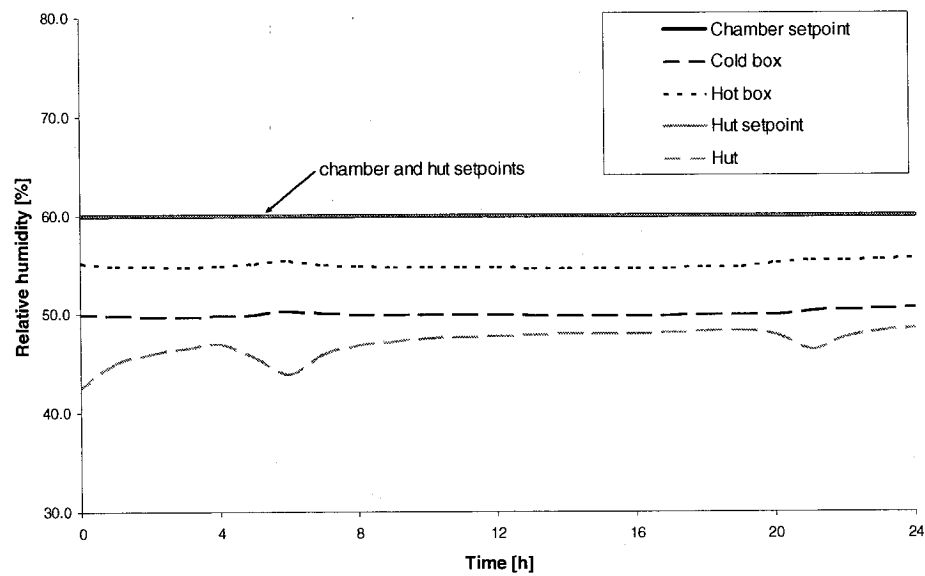


Figure 4.33. Hourly relative humidity profiles for wetting phase of test 2 showing the average relative humidities reproduced in the hot box and cold box of the environmental chamber and inside the test hut vs. the planned relative humidities.

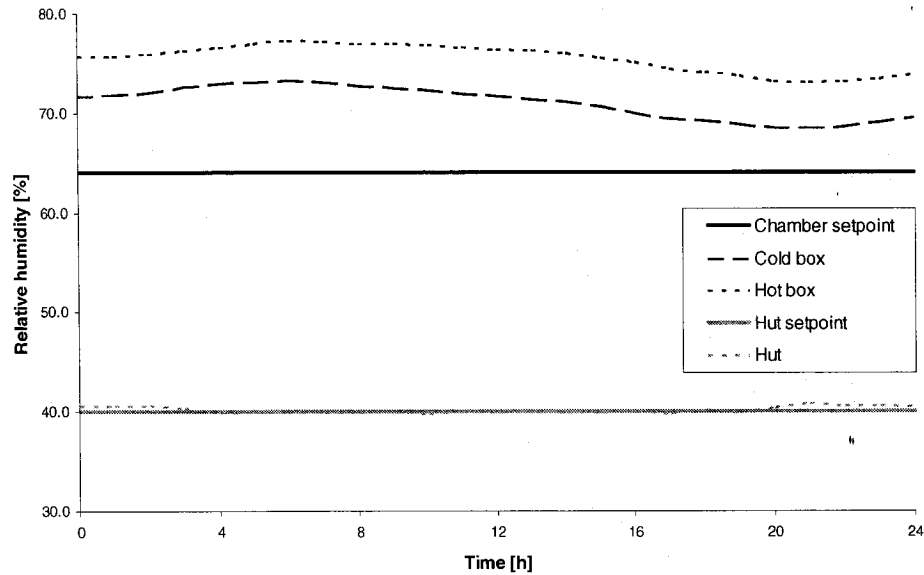


Figure 4.34. Hourly relative humidity profiles for first drying phase of test 2 showing the average relative humidities reproduced in the hot box and cold box of the environmental chamber and inside the test hut vs. the planned relative humidities.

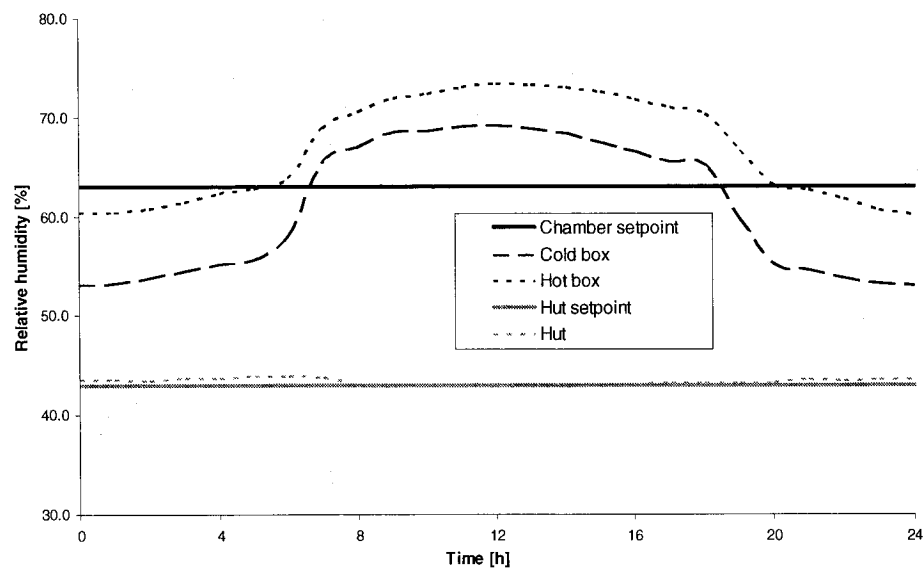


Figure 4.35. Hourly relative humidity profiles for second drying phase of test 2 showing the average relative humidities reproduced in the hot box and cold box of the environmental chamber and inside the test hut vs. the planned relative humidities.

4.7.4.2 Observations during the wetting phase

Problems of capillarity of the plywood sheathing material impacting the gravimetric moisture measurements that occurred in test 1 were largely resolved in test 2 by changing

the instrumentation methodology to electrical resistance moisture probes at sensitive areas in the sheathing.

Both the first and second test showed that the water introduced on the top middle inside surface of the sheathing does not always run vertically downwards to the bottom plate. Rather, the contact between the inside surface of the sheathing and the outside surface of the fiberglass batt insulation strongly influences the trajectory of the water, causing it to veer off to the left or the right instead of flowing down the centerline of the wall. Also, this contact also causes some of the water to be adsorbed by the insulation and released at a later time.

While the wetting method used in tests 1 and 2 is realistic, it was found to result in wetting patterns that vary substantially from wall to wall. The reasons for the differences in the wetting patterns are explained in detail in the following chapter. These differences resulted in different starting moisture boundary conditions at the end of the wetting phase/beginning of the drying phases, which made evaluation of the drying rates due to envelope components and materials difficult.

Because of the disparities in the moisture distributions in the wall assemblies obtained during the wetting phase of tests 1 and 2, there was a need for additional data to permit comparison of the drying performance of the different assemblies. In order to facilitate such an analysis, a third test was conceived where equal or nearly equal initial moisture content conditions were generated. Details pertaining to the wetting methodology of test 3 are addressed in Chapter 3, and the remainder of the experimental methodology is discussed in the following section.

4.8 Test 3

The rationale behind the third test was to provide additional information not available from the first two tests but at the same time be complementary to these. The objective of the third test was to determine the role of the type of wall sheathing and that of the type of vapor barrier on the drying performance of wetted wood-frame walls. The composition of the assemblies, the monitoring protocol, the test climate loading and the

experimental history is presented below.

4.8.1 Composition of the assemblies

The third test was performed on a subset of the walls in tests 1 and 2 that take into consideration two parameters, the sheathing material (OSB, plywood or asphalt-coated fiberboard) and the type of vapor retarder (polyethylene film or low permeance primer paint), as described in detail in Table 4.7 below.

Table 4.7. Types of sheathings and vapor retarders in walls 1 to 6 in test 3.

| Sheathing material | Vapor retarder | |
|-----------------------------|-----------------------|----------------------------|
| | Polyethylene membrane | Low permeance primer paint |
| Oriented strand board (OSB) | wall 1 | wall 4 |
| Plywood | wall 2 | wall 5 |
| Asphalt-coated fiberboard | wall 3 | wall 6 |

4.8.2 Monitoring protocol

The intent of the monitoring plan was to gather data that enables an analysis of the role of sheathing material and vapor retarder in the drying performance of the wall assemblies. Several parameters were monitored including temperature, relative humidity and moisture content. The monitoring protocol for the third test was similar to that used in the previous tests but was modified to meet the objectives of this test. The protocol for the framing and the sheathing can be viewed schematically in Figures 4.36 and 4.37.

4.8.2.1 Temperature

As in tests 1 and 2, thermocouples were used to monitor the temperature on the interior surface of the gypsum board and the exterior surface of the sheathing at their geometric center. In addition, a thermocouple was placed 6 mm from each of the bottom plate gravimetric samples in the bottom plate in order to enable the analysis of the role of temperature in the drying performance of the samples.

4.8.2.2 Relative humidity

A relative humidity sensor was placed in the stud cavity of each wall to monitor the relative humidity induced by the wet sheathing. The sensor, with its thermocouple, was located along the vertical centerline of the wall approximately 50 mm from the top surface of the wetted bottom plate insert.

4.8.2.3 Moisture content by gravimetry

Moisture content monitoring was performed by gravimetry for the main reason that the moisture content was expected to be above the fiber saturation point of wood. The walls were designed such that the entire bottom plate insert could be removed and periodically weighed in order to obtain a global moisture content for the entire piece. In addition, four small gravimetric samples were contained within the bottom plate. Three 13 mm diameter and 13 mm deep holes and one 13 mm diameter and 25 mm deep hole were cut out of the bottom plate and gravimetric samples fitted snugly within. Two of the four samples were located on the top surface of the bottom plate along the centerline of the wall. The first of these, called bottom plate center horizontal 1 (Bp_CH1), was located 32 mm from the gypsum board, and the other, center horizontal 2 (Bp_CH2), was located 32 mm from the edge of the sheathing. These two samples were used to determine if the temperature difference at the two locations has an influence on the drying of the samples. The third bottom plate specimen, center vertical (Bp_CV), was located on the centerline of the wall, on the vertical surface of the bottom plate adjacent to the sheathing. The three samples had all surfaces painted except for the exposed one in order to allow drying only from this exposed surface.

The 25 mm long sample, center horizontal under (Bp_CHU), was placed on the vertical centerline of the wall at the center of the bottom surface of the bottom plate. This sample was not painted to allow the determination of any moisture movement into the bottom plate from the wet surface during the drying phase. The locations of these samples are shown schematically in Figure 4.36.

One sheathing gravimetric sample, called row “D” right 1 (Sh_DR1) was placed on the bottom row of the sheathing adjacent to the bottom plate and served to observe any

moisture transfer from the wetted bottom plate into the sheathing in the drying process. This is shown schematically in Figure 4.37.

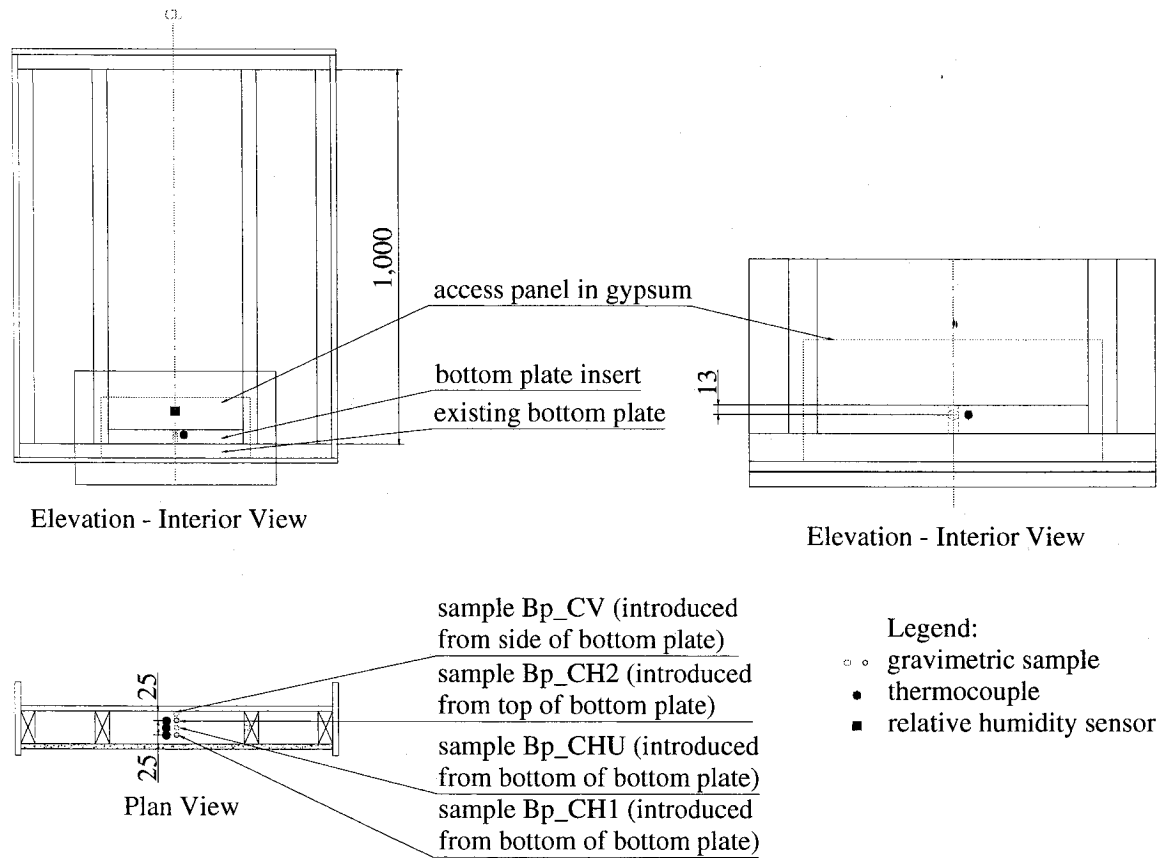
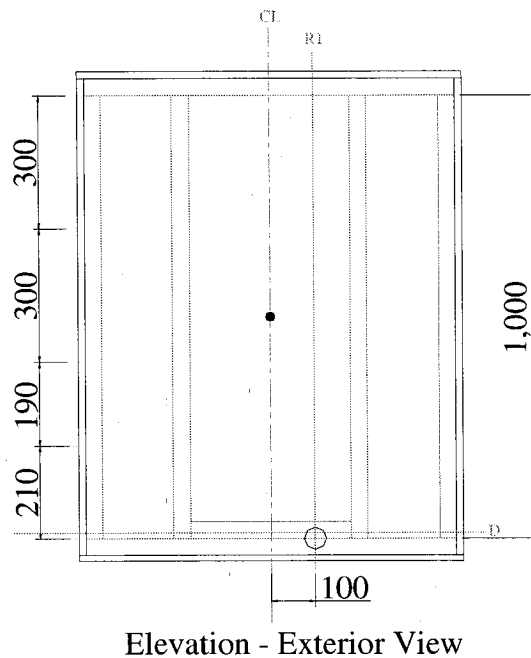


Figure 4.36. Elevation and plan views of the moisture content measurement monitoring protocol in the framing of assemblies 1 to 6 of test 3. The location of the gravimetric samples, the thermocouple on the inside surface of the gypsum, and the relative humidity sensor are shown.

Panels no. 1 to 6
Instrumentation in the Sheathing



- Legend: ○ gravimetric sample
• thermocouple on the interior surface of the gypsum or on the exterior surface of the sheathing

Figure 4.37. Elevation and plan views of the moisture content measurement monitoring protocol in the sheathing of assemblies 1 to 6 for test 3. The location of the gravimetric sample and the thermocouple on the outside surface of the sheathing are shown.

4.8.3 Testing climate loading

As was done in tests 1 and 2, the wall assemblies (except the wetted components) were pre-conditioned in the environmental chamber for a period of two weeks in order to generate moisture content conditions within the walls akin to those resulting from winter diffusion wetting. Specifically, the indoor and outdoor environments were set to 21°C and 60% relative humidity in order to achieve an average moisture content within the walls of approximately 12%. The indoor and outdoor environmental conditions during

the drying phase were identical to those in tests 1 and 2 except that there was no wetting phase, as shown in Table 4.8. With the insertion of a pre-wetted component, no wetting phase was necessary. These diurnally varying conditions reflect those that occur in the springtime months of April and May in Montreal. As in tests 1 and 2, the second month of the drying phase was shortened because rapid drying was observed. Environmental conditions for the pre-conditioning and drying phases are summarized in the table below.

Table 4.8. Planned indoor and outdoor temperature and relativity conditions for the wetting and drying phases of test 3.

| Period no. | Duration (days) | Period simulated | Indoor Testing Conditions | | Outdoor Testing Conditions | | | |
|--------------------------------|-----------------|------------------|---------------------------|--------|----------------------------|-----------------|-----------------|--------|
| | | | | | Sinusoidal function with: | | | |
| | | | Temp. [°C] | RH [%] | Average Temp. [°C] | Max. Temp. [°C] | Min. Temp. [°C] | RH [%] |
| Pre-conditioning Phase: | | | | | | | | |
| 1 | 14 (minimum) | - | 21 | 60 | 21 | - | - | 60 |
| Drying Phase: | | | | | | | | |
| 2 | 28 | April | 21 | 40 | 6.3 | 10.9 | 1.6 | 64 |
| 3 | 31* | May | 21 | 43 | 13.7 | 18.7 | 8.6 | 63 |

* The duration of this period may be shortened if rapid drying is observed.

4.8.4 Experimental history

The experimental history of test 3 including that of the climatic conditions was noted and is described herein. Unfortunately, the controller used to measure the ambient temperature in the cold box broke down during the course of the second experiment. However, the sensor in the Environmental Chamber's hot box still permits evaluation of the performance of the mechanical systems.

The measured temperature in the hot box of the Environmental Chamber during first drying phase was typically slightly higher than the setpoint, the difference ranging from approximately 0.5 to 1.5°C (see Figure 4.38); during second drying phase, the measured temperature in the Environmental Chamber's hot box was slightly higher than the setpoint at the trough of the diurnal cycle and slightly lower than the setpoint at the peak of the diurnal cycle (see Figure 4.39). As was experienced in the second test, a smooth

temperature curve was slightly more difficult to achieve during the second drying phase due to switching of refrigeration systems in the cold box from the large-capacity 5-ton screw compressor system to a smaller water-cooled system. The differences between the setpoint and the measured temperatures were approximately 2.3°C at the peak and 1.5°C at the trough of the cycle, which is acceptable. In the test hut, the measured temperature was consistently approximately 1°C lower than the setpoint, which was deemed acceptable.

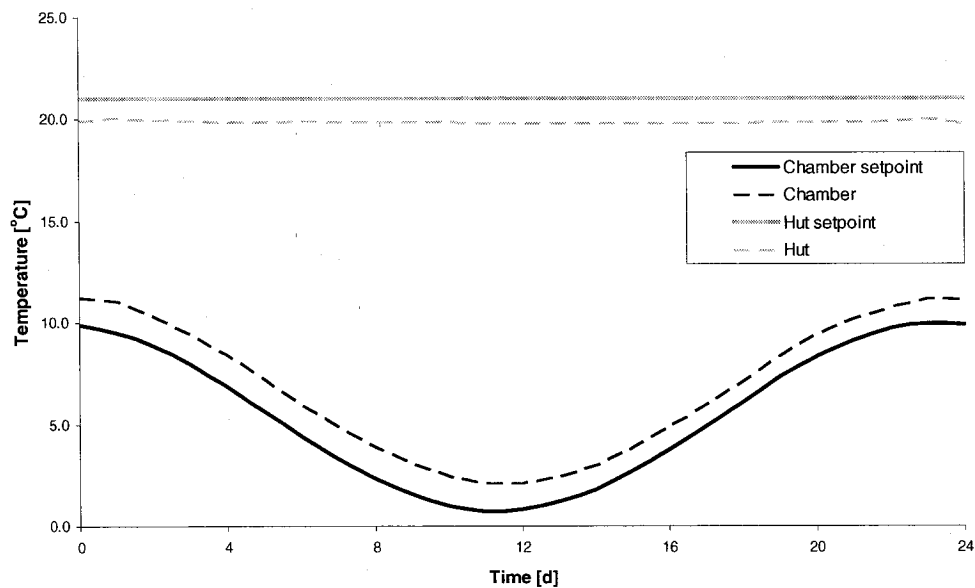


Figure 4.38. Hourly temperature profiles for first drying phase of test 3 showing the average temperatures reproduced in the hot box and cold box of the environmental chamber and inside the test hut vs. the planned temperatures.

As shown in Figure 4.40, the measured relative humidity in the cold and hot boxes of the Environmental Chamber were typically higher than the setpoint during the first drying phase; this was especially true for the cold box relative humidity, and can be explained by the slightly colder temperature attained in the cold box due to its large-capacity refrigeration unit. However, during the second drying phase, the relative humidity in the cold box reached values at the trough of the cycle that were lower than the 63% relative humidity setpoint by approximately 13%. This occurrence is difficult to explain without more information about the cold box temperature. Inside the test hut, the relative humidity was well controlled, with the setpoints of 40% and 43% relative humidity being met in the first and second drying phases, respectively.

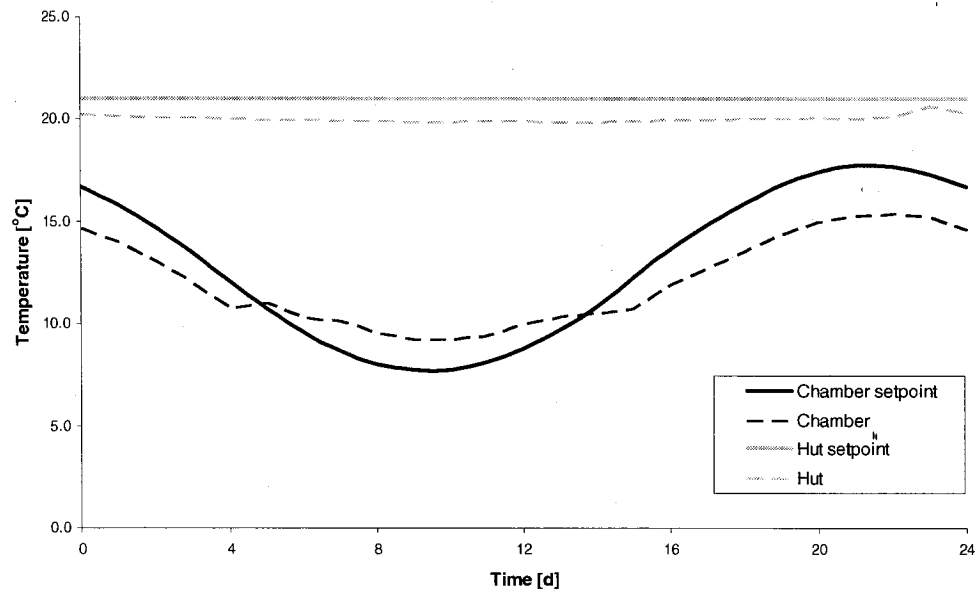


Figure 4.39. Hourly temperature profiles for second drying phase of test 3 showing the average temperatures reproduced in the hot box and cold box of the environmental chamber and inside the test hut vs. the planned temperatures.

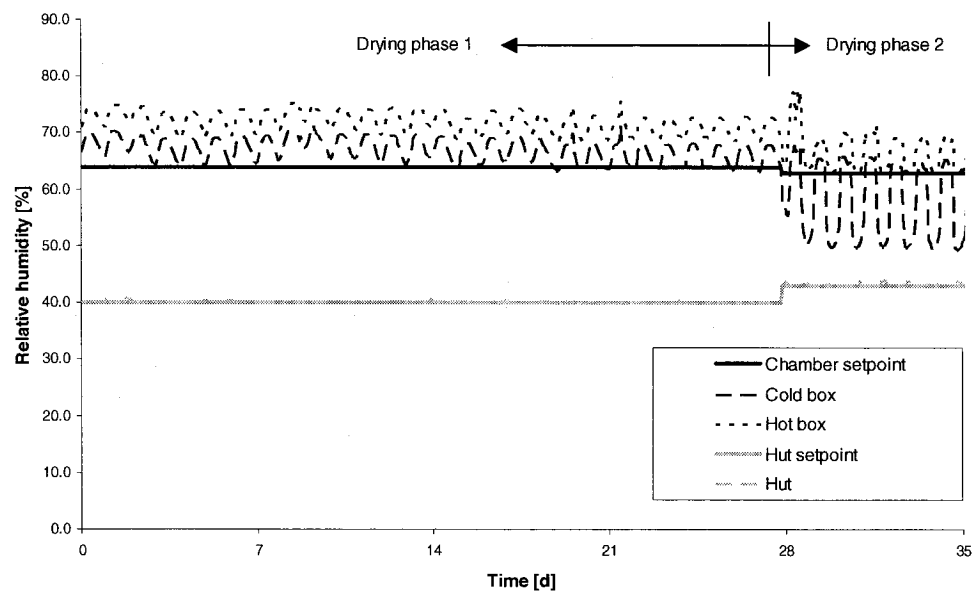


Figure 4.40. Relative humidity profiles for first and second drying phases of test 3 showing the average relative humidities reproduced in the hot box and cold box of the environmental chamber and inside the test hut vs. the planned relative humidities.

4.9 Summary and Conclusion

Three large-scale experiments were performed at the Building Envelope Performance Laboratory at Concordia University. The first two tests included 19 wall assemblies, 17 of which were wetted in a drop-by-drop fashion. The parameters changed from wall to wall included the exterior sheathing, the vapor retarder, the presence of exterior insulation. The experiment also sought to examine the influence of the wall height, the presence of exterior cladding, the rate of water insertion, and the location of water insertion on the hygrothermal wetting and drying performance of the wall assemblies. The assemblies were exposed to 3-week pre-conditioning phase, followed by a 28-day wetting phase, and a drying phase of five to six weeks where April conditions in Montreal were set. The monitoring protocol included sensors to measure the temperature, relative humidity and moisture content within the assemblies; the ambient interior and exterior temperature and relative humidity were also monitored. Test two differed from test 1 in two respects: first, in test 2, walls 13 to 19 used plywood rather than OSB sheathing; second, the moisture content monitoring scheme was improved in test two to take into account the impact of gravimetry on moisture uptake by the plywood sheathing.

The third experiment included six wall assemblies. In this test, the wetting methodology was modified to reduce the level of disparities in initial moisture content at the start of the drying phase that was observed in tests 1 and 2. In test 3, a pre-wetted bottom plate insert was installed into the wall assemblies above the existing bottom plate, and served both as a moisture source and as a gravimetric sample. This five-week test served to provide additional data to permit comparison of the drying performance of the different assemblies, and in particular to investigate the role of the sheathing and the vapor retarder.

The following chapter presents the experimental results for tests 1, 2 and 3. Specifically, observations on the wetting patterns and drying performance in the various walls of tests 1 and 2 are discussed, followed by the role of the sheathing material and the type of vapor retarder in the hygrothermal performance of the wall assemblies in test 3.

5. HYGROTHERMAL PERFORMANCE OF ASSEMBLIES TESTED

In this chapter, the hygrothermal behavior of the walls tested in experiments 1, 2 and 3 is presented by examination of the response of the monitored wood and wood-based components. The wetting patterns observed in the walls of test 1 and 2 are discussed. As explained in Chapters 3 and 4, tests 1 and 2 each included 19 large-scale wood-frame assemblies, 17 of which were wetted by inserting water onto the interior surface of the sheathing in a drop-by-drop fashion where the water insertion rate, frequency and duration reflected actual climate patterns. Rather than measuring the total moisture content of each wall as a whole, the monitoring protocol focused on measuring the moisture content at locations within hygroscopic components where moisture accumulation was expected. A moisture content gravimetric and electrical resistance probe monitoring grid was developed to examine both the wetting and drying behavior at several locations in each of the sheathing, the bottom plate and the studs. The moisture content measurements therefore provide an overall portrait of the moisture content distribution throughout each wall during both the wetting and drying phases, as shown in Figures 4.8 to 4.11 for test 1, 4.27 to 4.29 for test 2, and Figures 4.36 and 4.37 for test 3.

The discussion begins with some observations about the general wetting patterns obtained in the first two experiments, and continues with the rapid effect of the loading on the moisture response of the specimens, the moisture accumulation from day to day and from week to week, general wetting trends in the sheathing and in the bottom plate, lateral migration of water within the assemblies, the repeatability of the wetting pattern, the absorption of water by the insulation, and the occurrence of water leakage. The drying behavior of the assemblies is also presented as a function of the experimental parameters.

To provide more information on two parameters, the sheathing and the vapor retarder, a third experiment was conducted using a different methodology, where the moisture source in each assembly was a pre-wetted component, permitting investigation of the wall components' drying response. An analysis of the role of two parameters from the six large-scale wood-frame wall assemblies in test 3 is presented last.

5.1 Assembly Response to Moisture Load - Tests 1 and 2

5.1.1 General wetting pattern

The moisture content data obtained from the sheathing, stud and bottom plate gravimetric measurements and electrical resistance sensors show that, in general, the water which was introduced at the top inside surface of the sheathing migrated downwards and accumulated at the bottom of the wall, wetting the top surface of the bottom plate and the surfaces at the vertical interface of the sheathing and the bottom plate. Similar observations were made in Lang *et al.*'s (1999) experiment, which used a similar loading methodology. An example of moisture content measurements which show the aforementioned moisture absorption patterns is given in Figures 5.1 and 5.2 for the test 2 wall 1 in the stud and bottom plate, and in the OSB sheathing.

Before continuing, some remarks should be made about the moisture content versus time figures. The curves with markers denote gravimetric measurements while the curves without markers show electrical resistance measurements. The latter are only accurate at moisture contents below the fiber saturation point, or FSP, approximately 28% moisture content. Above that level, the measurements are only indicative of a "high" moisture content.

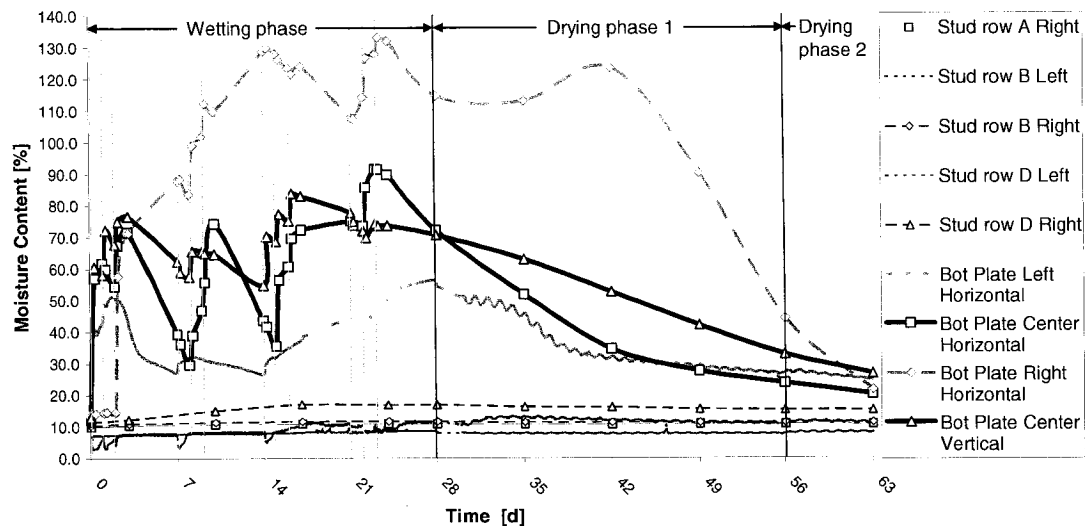


Figure 5.1. Measured moisture content with time at various locations within the studs and bottom plate of OSB-sheathed wall 1, test 2. The missing electronic resistance moisture content data for the bottom plate left horizontal surface is due to a malfunction of the data acquisition system. The curves with markers denote gravimetric measurements while the curves without markers show electrical resistance measurements. The grey vertical lines denote a 3.4 hour wetting event.

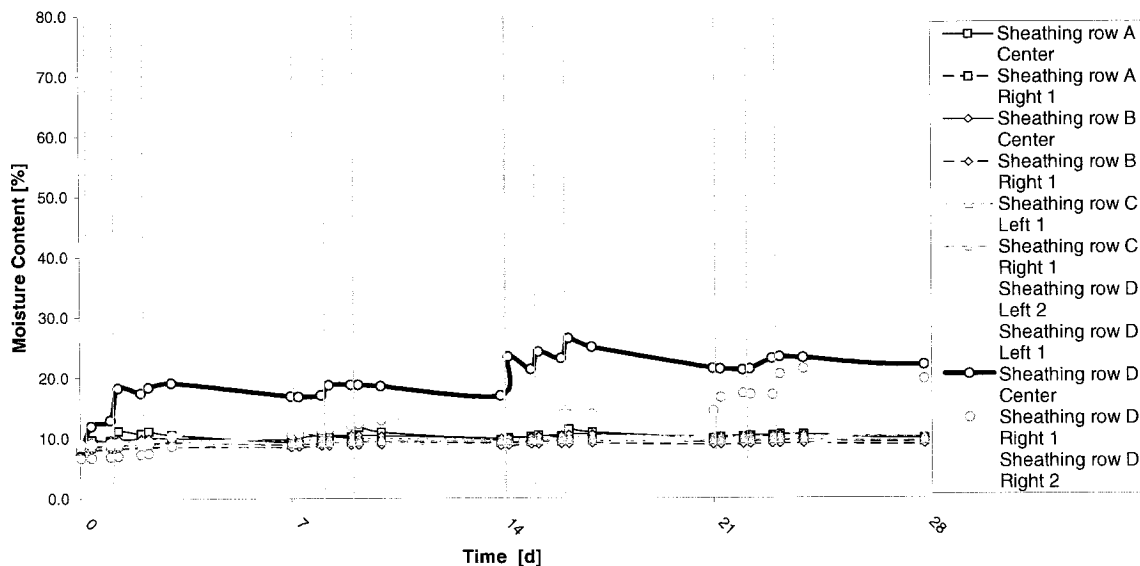


Figure 5.2. Measured moisture content with time at various locations in the OSB sheathing of wall 1 in test 2. The grey vertical lines denote a 3.4 hour wetting event.

The moisture content data show that the small gravimetric specimens in the bottom plate attained the highest moisture contents. For example, the gravimetric specimen located on the Right Horizontal surface of the bottom plate in wall 1 in test 2 reached a peak moisture content of about 133% (see Figure 5.1).

In the sheathing, there was typically little moisture absorption above the bottom plate, although a notable exception in the plywood-sheathed walls is discussed in the next section. The greatest moisture accumulation in the sheathing was generally observed to occur at the center of the bottom row, as illustrated in Figures 5.2, although some lateral migration occurred, as will be explained below.

In comparison with other components, very little if any moisture accumulation was observed in the studs. An exception to this general rule was found in wall 17, where water was introduced on the sheathing surface adjacent to the stud. As shown in Figure 5.3, the moisture content in the bottom row “D” specimen rose to 38.6% at the end of the second week of the wetting phase.

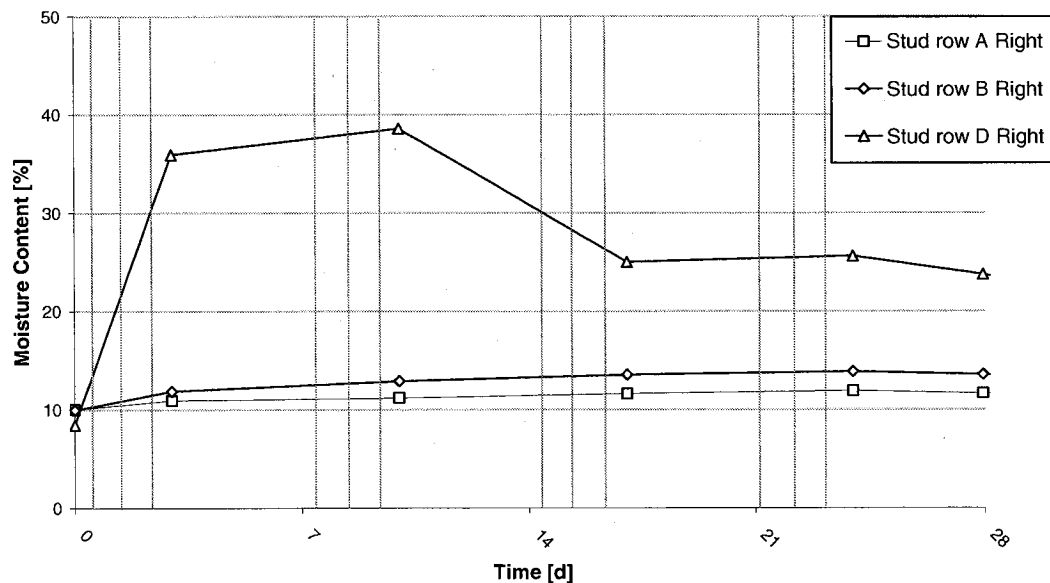


Figure 5.3. Measured moisture content with time at various heights of the spruce stud of wall 17 during the wetting phase of test 1. The grey vertical lines denote a 3.4 hour wetting event.

5.1.2 General wetting trends in the sheathings

As was stated in the previous section, the bottom of the wall was the location where the sheathing experienced the most significant degree of wetting. The exception to this generality occurred in the plywood panels in test 1. In these walls, gravimetric specimens in the plywood were placed along the vertical centerline of the sheathing. It was

observed that water running down the plywood panel was absorbed by the gravimetric samples in the path of the water runoff at the top of the wall. Water entered the narrow gap between the disc-shaped gravimetric specimen and the adjacent sheathing, resulting in water transfer at the perimeter of the sheathing specimen, as shown in Figure 5.4. Because the water absorption rate of plywood is much greater in the plane of the panel rather than across the panel, this effect resulted in high moisture contents measured in the gravimetric samples at the top of the wall, i.e. in rows A and B, as illustrated in Figure 5.5 for the sheathing of plywood wall 2 in test 1. Lateral moisture migration was also observed in these walls. Little moisture made its way to the bottom of the plywood-sheathed walls in test 1. As was stated in the experimental protocol, to reduce the disturbance of the moisture content monitoring protocol on the moisture response of the plywood-sheathed walls, the gravimetric specimens in key locations, including those along the center line of the sheathing, were replaced with electrical resistance probes in test 2.

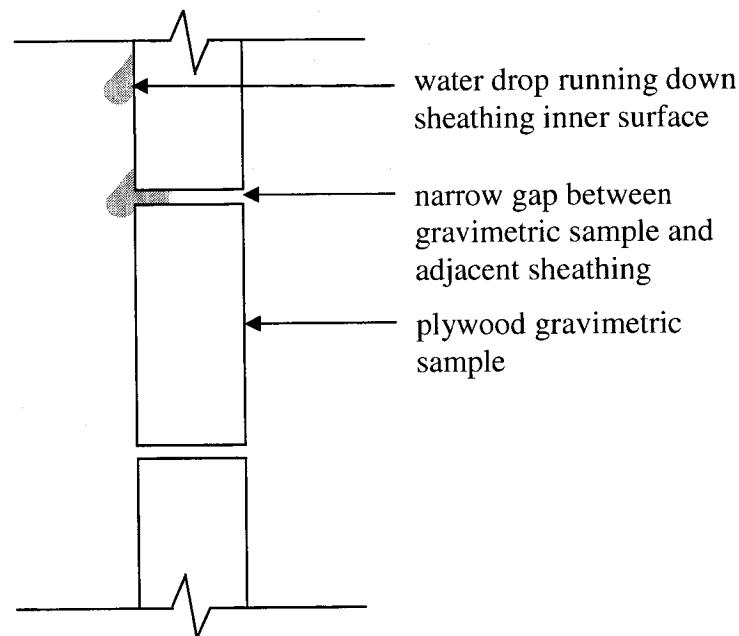


Figure 5.4. Moisture migration path in the plywood gravimetric samples in test 1 which resulted in high moisture accumulation in these gravimetric samples at the top of the walls. The size of the gap between gravimetric sample and adjacent sheathing has been exaggerated for clarity.

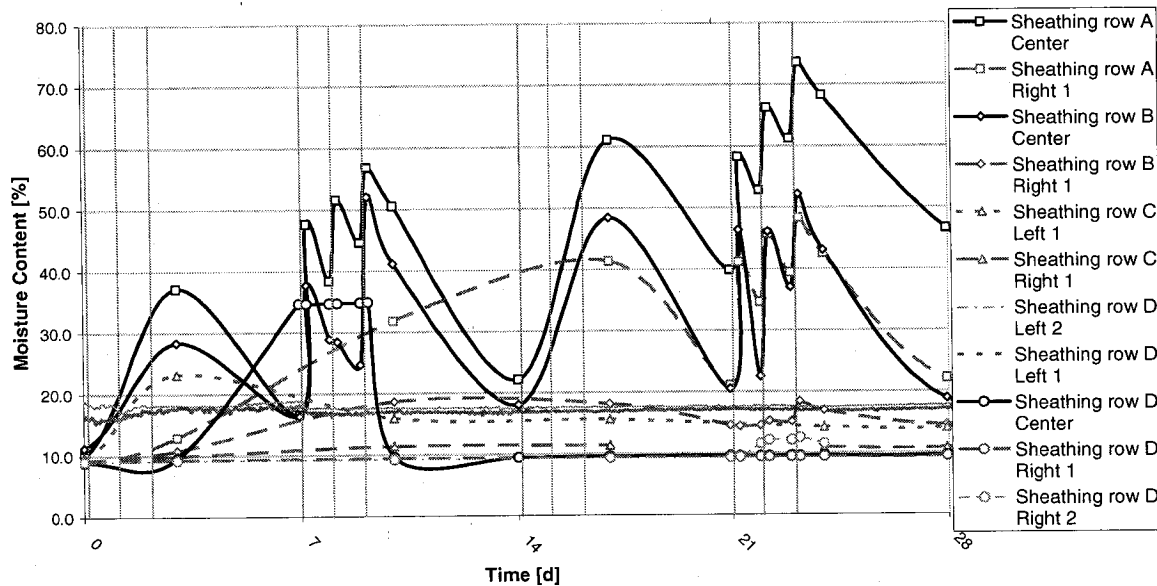


Figure 5.5. Measured moisture content with time at various locations in the plywood sheathing of wall 2 in test 1. The grey vertical lines denote a wetting event. In the first and third weeks, gravimetric measurements were made at the beginning of the first day, and on the fourth day of the week, i.e. before and after the 3-day wetting periods.

Moisture uptake occurred in all three sheathing materials. However, of the three materials, the greatest moisture uptake was generally observed in the plywood sheathing, as shown in Figure 5.6 for test 2. Overall, significantly lower levels of moisture uptake were observed in the OSB and the asphalt-coated fiberboard sheathing, as can be seen, for example, in Figures 5.2 for OSB-sheathed wall 1 in test 1, and Figures 5.7 and 5.8 for fiberboard-sheathed walls 3 and 6 in test 2. In Figure 5.7, one fiberboard gravimetric specimen was observed to reach high moisture content levels, going as high as 50.6% moisture content at the end of week 3. Other such occurrences were found with fiberboard gravimetric samples, e.g. in test 2, wall 12, the sample in row “D”, column right 1. It is suspected that, similarly as with the plywood specimens in test 1, the high moisture content encountered in these fiberboard samples occurred because water migrated within the gap between the fiberboard gravimetric specimen and the adjacent panel, thus circumventing the fiberboard’s asphalt coating and wetting the fiberboard itself. This may likely have happened with some of the OSB samples as well. The disturbance in the moisture response of the sheathing at these locations is disadvantage of the gravimetric method.

The reason for the different moisture content results in the three sheathings can be

explained by their water absorption properties. Tests were performed at the National Research Council Canada (NRCC) to determine the water absorption coefficient of water perpendicular to the plane of various wood-based sheathing panels. This coefficient is determined by measuring the increase in mass of water absorbed in a material as a function of time. The water absorption coefficient is found as the slope of the line of the plotted mass increase against the square root of time during the initial absorption process. The NRCC's water absorption tests show that the water absorption coefficient is highest for plywood, ranging from 0.0031 to 0.0042 for tests done on three specimens, while the water absorption coefficient ranged from 0.0016 to 0.0022 for three OSB specimens and 0.00094 for one asphalt-coated fiberboard specimen (Kumaran *et al.*, 2002b). The NRCC tests show that the asphalt coating surface treatment on the fiberboard panel effectively prevents absorption of water perpendicular to the plane of the panel. As well, the manufacturing process for OSB, which makes use of industrial wax (Forintek 2001), also influences its moisture uptake properties.

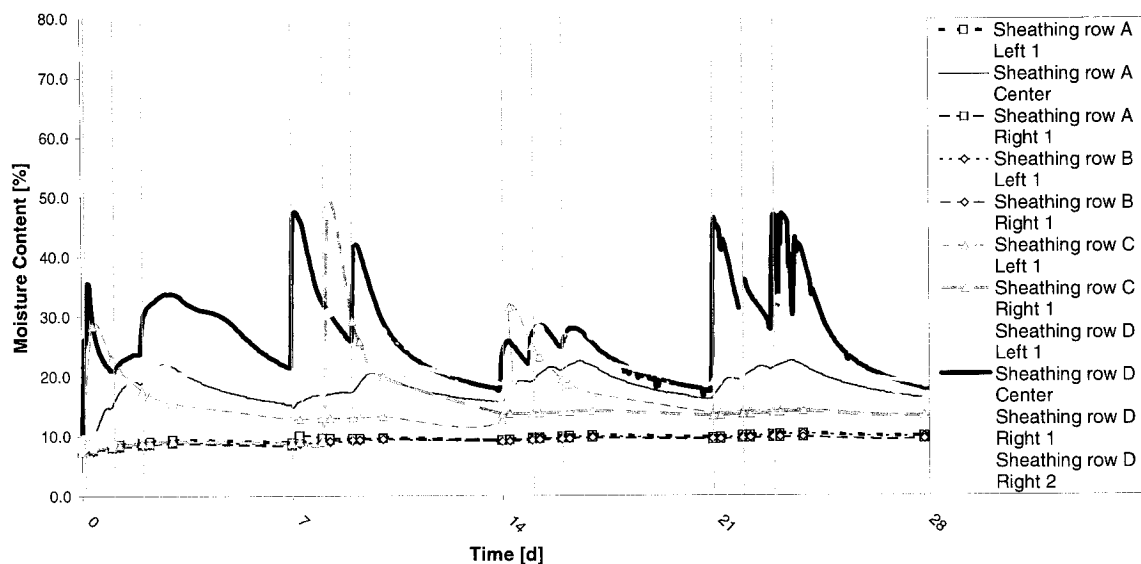


Figure 5.6. Measured moisture content with time at various locations in the plywood sheathing of wall 2 during the wetting phase of test 2. The grey vertical lines denote a 3.4 hour wetting event.

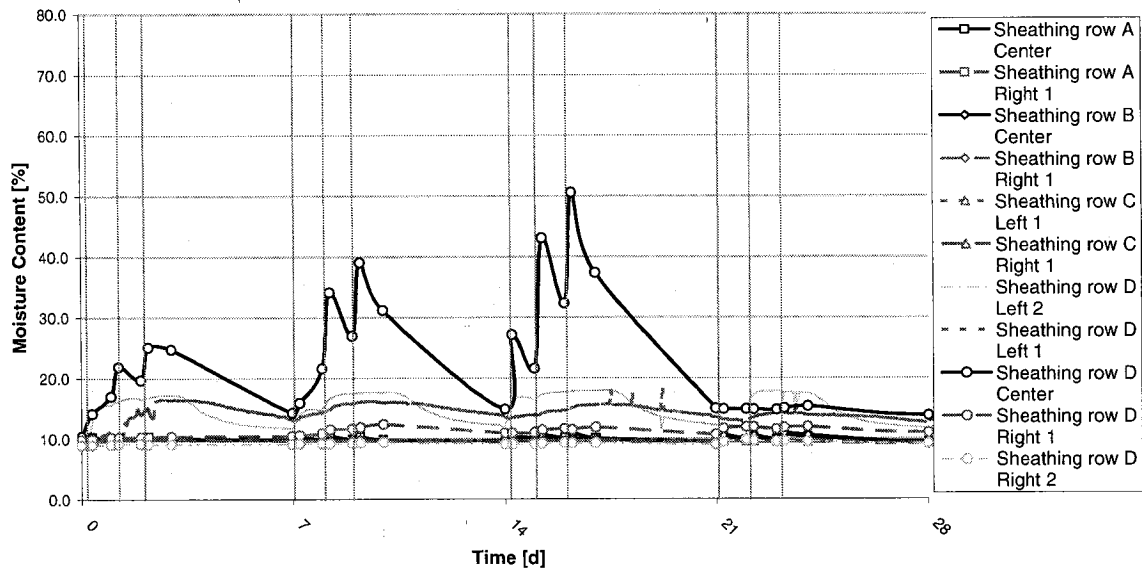


Figure 5.7. Measured moisture content with time at various locations in the fiberboard sheathing of wall 3 during the wetting phase of test 2. The grey vertical lines denote a 3.4 hour wetting event.

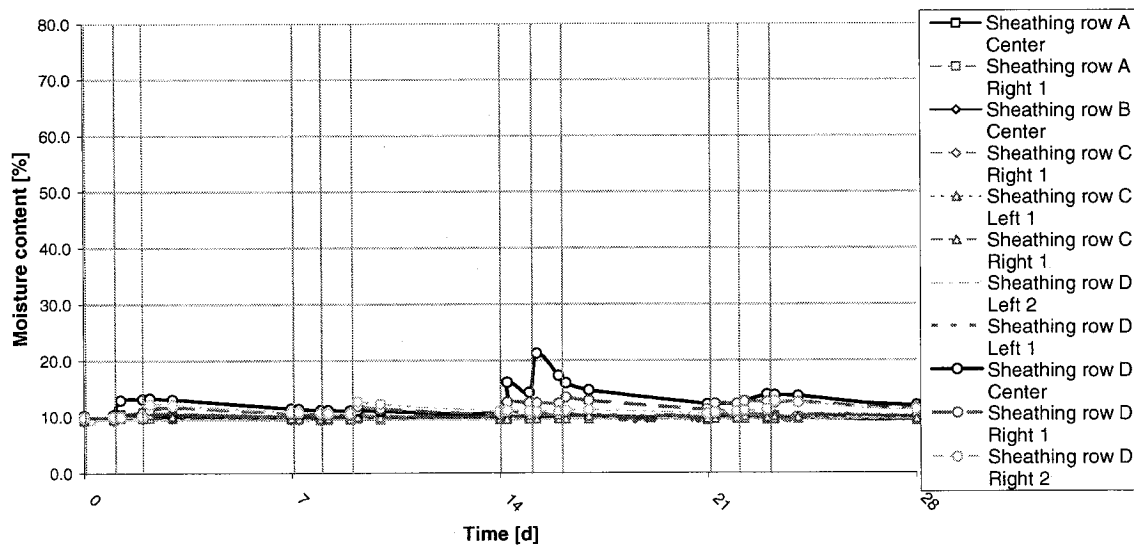


Figure 5.8. Measured moisture content with time at various locations in the fiberboard sheathing of wall 6 during the wetting phase of test 2. The grey vertical lines denote a 3.4 hour wetting event.

Mold growth was observed in both tests on a few OSB sheathing samples located adjacent to the bottom plate (row “D”) 14 days into the wetting phase. It is hypothesized that the industrial wax components used in the OSB manufacturing process limit the water migration within the OSB, causing a high localized moisture content in the wood fibers which favors mold growth.

5.1.3 General wetting trends in the bottom plate

In the bottom plate of the 17 wetted walls of the first two tests, the gravimetric samples facing the center vertical surface in row “D” adjacent to the sheathing were generally exposed to the greatest moisture load overall, an example being shown in Figure 5.9. Figure 5.1 illustrates that there are some cases where the water accumulated in other areas such as on the top horizontal surface.

The wetting patterns in the bottom plates in the walls from tests 1 and 2 were analyzed to attempt to make a qualitative correlation between the zone with the highest moisture uptake and the sheathing material. For both the OSB and the asphalt-coated fiberboard sheathings, a great deal of variability was observed in wetting pattern in the bottom plate, but typically, moisture accumulated at least three of the four monitored locations. However, in the plywood walls, the greatest moisture accumulation was observed at the position of the center vertical sample in every wall and there was little water migration to other surfaces, with a few exceptions. This pattern is likely due to the greater water absorption coefficient and the wettability in the plywood sheathing itself compared to that in OSB and asphalt-coated fiberboard. Independent transient wetting angle tests performed at the Katholieke Universiteit Leuven in Belgium (Derome, 2005) show that the wetting angle of water on a plywood substrate is low, reducing to 0° in just a few minutes. It is significantly smaller than that of OSB. The wetting angle tests on asphalt-coated fiberboard show that the coating causes a high initial wetting angle and as such it is effective in reducing the water absorption. Given the high wettability of plywood, this material absorbed the water running down its surface more than the other sheathings. At the bottom of the wall, once the surface layer of the plywood was saturated, water filled the narrow gap between the sheathing and the bottom plate, thereby wetting the latter. In comparison, in the OSB and asphalt-coated fiberboard-sheathed walls, less water was absorbed by the sheathing, the narrow gap was likely filled more quickly, and water spilled onto the horizontal surface of the bottom plate.

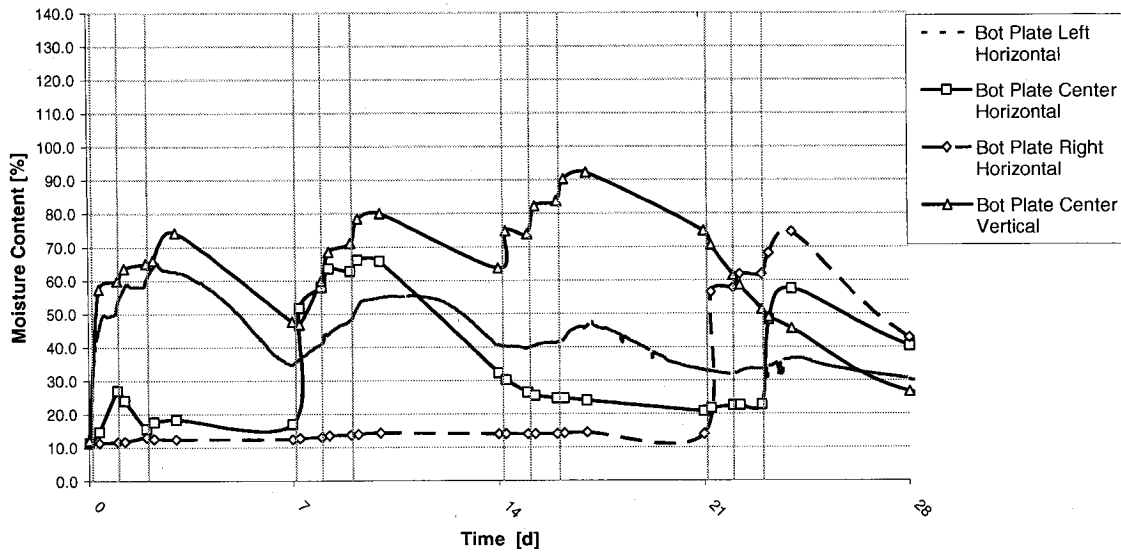


Figure 5.9. Measured moisture content with time at various locations in the bottom plate of the fiberboard-sheathed wall 3 during the wetting phase of test 2. The grey vertical lines denote a 3.4 hour wetting event.

5.1.4 Lateral migration of water.

In both experiments 1 and 2, water was introduced into the wall assemblies at the top center inside surface of the sheathing panel of each wall, except in wall 17 where the water was inserted on the sheathing next to the stud. It was expected that water would run down a vertical path and accumulate at the bottom of the wall about the centerline. In the plywood sheathing, some lateral moisture movement was anticipated due to moisture movement in the grain direction. However, a great deal of lateral migration was seen in the walls, of which only a few cases were observed in the sheathing above the level of the bottom plate. One such example is the plywood gravimetric sample of wall 2 in row C Right 1, located at 100 mm to the right-hand side of the centerline, whose moisture content increased to 49.0% after the second wetting event of the second week (day 8) (see Figure 5.6). In the same wall, lateral migration was also observed during the first wetting event of the second week in the row C left 1 sample, located 100 mm to the left-hand side of the centerline. Plywood is made of rotary peeled veneers from logs which are laid in parallel and cross layers. Liquid transfer can occur more readily in plywood than in solid wood because of the possibility of liquid paths in the more open structure of the veneers

(Forintek 2001). The lateral migration of water observed in these tests may account for the plume wetting patterns seen below leaky windows in the field.

At the level of the bottom plate, a significant number of cases of lateral migration in the bottom plate and in the sheathing have been observed. Some examples are given in the following Table 5.1.

Lateral migration was found to be due to two causes:

1. Physical contact of the sheathing and the fiberglass batt insulation, which altered the trajectory of the water running down the sheathing surface, causing it to move laterally in a more or less random fashion;
2. Capillary movement of water in the gap between the sheathing and the bottom plate, which resulted in a lateral spreading of the moisture. The gap became a small reservoir which wetted the adjacent materials, and dried out slowly when the loading was stopped.

Both of these events were visually confirmed in a separate series of tests performed on small-scale walls using the three different sheathing materials, with and without batt insulation within the stud space.

Table 5.1. Examples of walls where an increase in moisture content was found at the location of sheathing and bottom plate gravimetric samples due to lateral migration of water.

| Wall no. | Test no. | Location of sample | Figure no. |
|------------------------------|----------|--------------------------|------------|
| Examples in the sheathing | | | |
| 1 | 2 | row D Right 1 | 5.2 |
| 3 | 2 | row D Left 2 | 5.7 |
| Examples in the bottom plate | | | |
| 1 | 2 | Right horizontal surface | 5.1 |
| 3 | 2 | Right horizontal surface | 5.9 |

5.1.5 Rapid increase in moisture content due to the wetting events

It can be observed from Figures 5.1 and 5.9 that after only a single wetting event,

rapid increases in moisture content over 40 to 50% in moisture content was experienced by some bottom plate gravimetric samples in the bottom plate. Examples include the center horizontal and the center vertical bottom plate samples in OSB-sheathed wall 1, which were wetted to moisture contents above 55% (see Figure 5.1), and bottom plate gravimetric sample center vertical in wall 3 which was wetted to 57.6% moisture content (Figure 5.9), all following the first wetting event of week 1. The small size of the gravimetric samples in the bottom plate allowed the moisture that reached their location to absorb moisture readily. It is suspected that if the bottom plate were intact, a smaller rate of water absorption at the locations of the gravimetric samples would likely have occurred due to the relatively low rate of moisture absorption in the tangential and radial directions. In addition, the problem may have been exacerbated by the fact that the sample was absorbing moisture via the painted surfaces, whose acrylic coating (see Figure 5.10) failed over the course of the experiment due to the moisture-induced expansion of the sample and friction with the surrounding bottom plate during the frequent removals and re-installations.

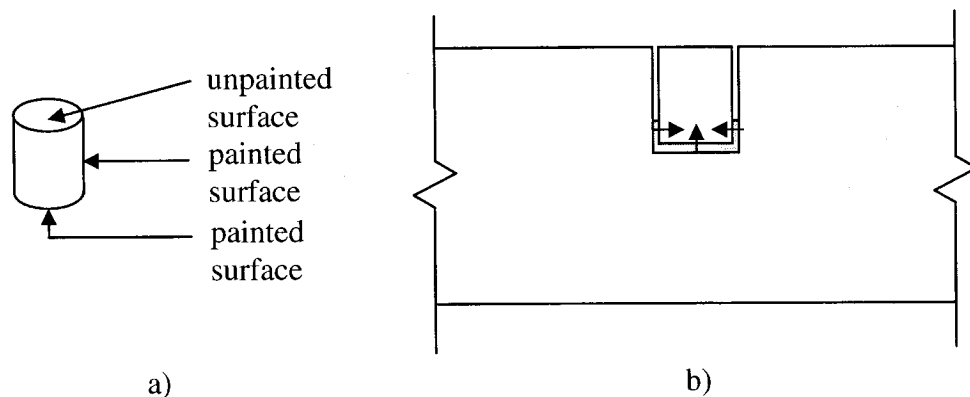


Figure 5.10. a) Bottom plate gravimetric sample showing the painted and the unpainted surfaces. b) Section view of the center horizontal or right horizontal bottom plate gravimetric samples nestled within the bottom plate, showing the direction of moisture flow into the sample.

At the location of the left horizontal moisture content probe in the bottom plate of wall 3 (Figure 5.9), the absorption of water into the top surface of the bottom plate to the depth of the tip of the probes during the first day of the test lead to a peak maximum moisture content of about 50% at about 13 hours after the water insertion started. It is possible that the water absorption rate by the bottom plate was increased by water

migration into drying microcracks in the wood. However, it should be again borne in mind that electrical resistance measurements taken at a moisture content above the fiber saturation point of wood are only a indicative of a “high” moisture content. It is for this reason that the monitoring plan also included gravimetry, and that the electric probes and the gravimetric specimens were located more or less symmetrically about the assemblies’ vertical centerline. However, comparison of both measurement results was made difficult by the fact that the moisture loading proved not to be symmetrical, as will be explained in more detail shortly.

5.1.6 Moisture accumulation from week to week

Where there was continuous or near continuous wetting of the bottom plate and of the sheathing, a moisture accumulation with time occurred over the 4 week wetting phase despite the small 12 ml/h load. Figures 5.11 and 5.12 show the weekly measured moisture content with time at various locations in the bottom plate and sheathing in various wall assemblies in test 2 where moisture accumulation was experienced over the duration of the wetting phase due to repeated moisture loading. It should be noted that few locations experienced repeated loading from day to day and week to week, as will be discussed in the following section.

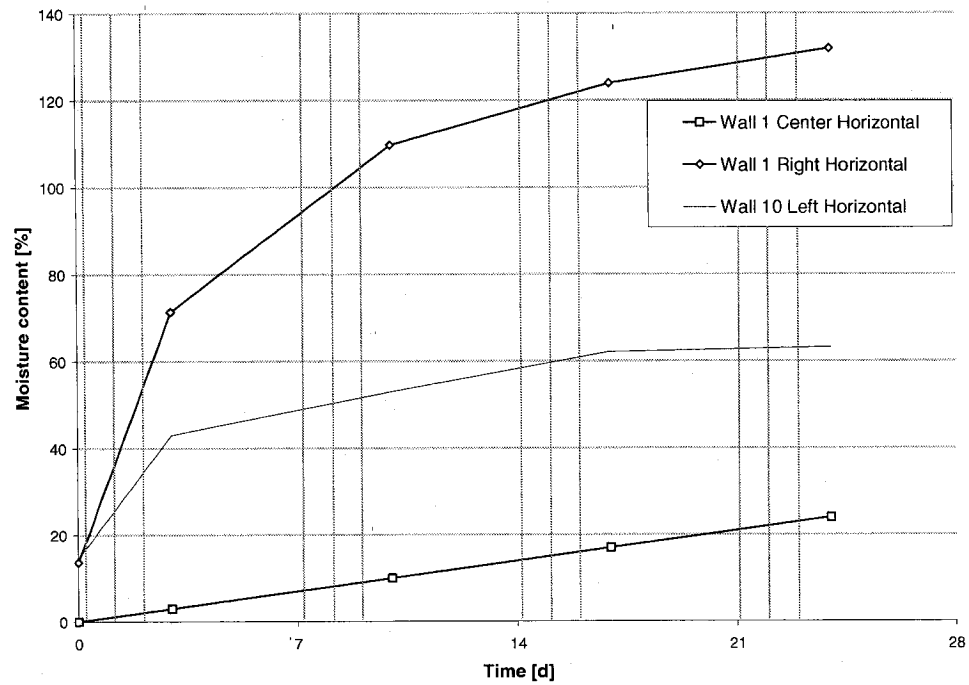


Figure 5.11. Measured moisture content with time in the center horizontal and right horizontal gravimetric specimens of the bottom plate in wall 1, and at the location of the left horizontal electric resistance sensor in wall 10 during the wetting phase of test 2. The grey vertical lines denote a 3.4 wetting event.

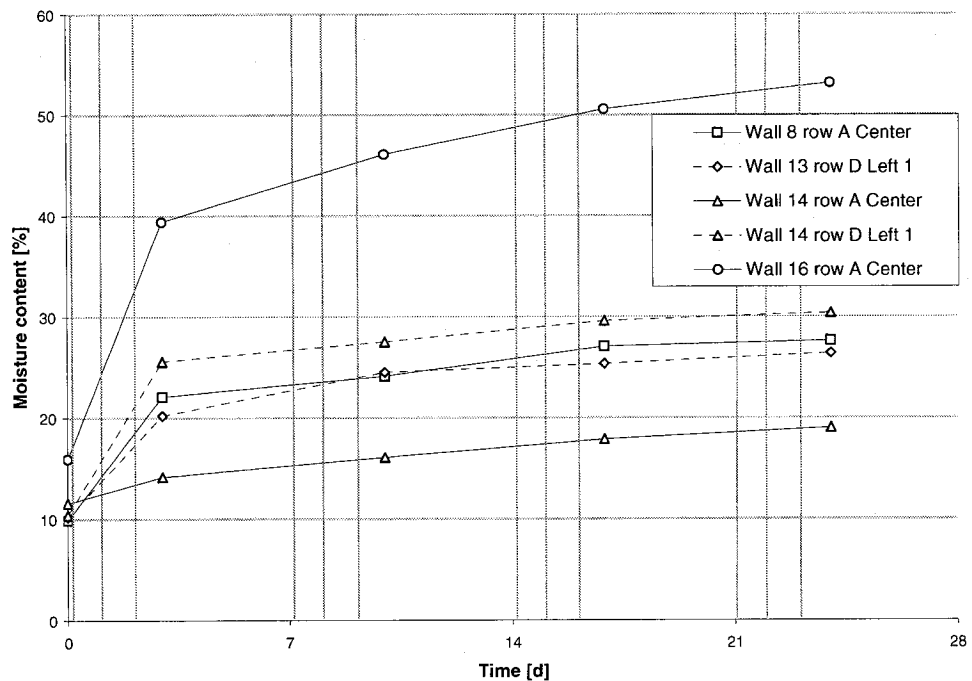


Figure 5.12. Measured moisture content with time at various locations in the plywood sheathings of various wall assemblies during the wetting phase of test 2. The grey

vertical lines denote a 3.4 hour wetting event.

5.1.7 Repeatability of wetting pattern during the course of the tests

One of the significant and unexpected findings of these two experiments was that while the loading was performed according to a well-defined schedule, the wetting of the components at the monitored locations was not necessarily repeated from week to week, or even from one day to the next within a 3-day wetting period. The wetting pattern of the bottom plate sample center horizontal in OSB wall 1 of test 2 (see Figure 5.1) illustrates the point: whereas the sample was wetted to a high moisture content after the first week, it was not wetted in the first event of week 2 or week 3, as shown in Figure 5.1. Another example is the center vertical bottom plate sample in wall 3 (see Figure 5.9) which was repeatedly wetted during over weeks 1 to 3 but not in week 4 of test 2. The lack of repeatability can be attributed to the physical manipulation of the insulation during the test for retrieval of the gravimetric samples, which may have affected the physical contact, or lack thereof, between the insulation and the sheathing.

5.1.8 Adsorption of water by the insulation

An unexpected occurrence was noticed in wall 1 during both tests 1 and 2. In test 1, the moisture content of bottom plate sample on the center horizontal surface (Figure 5.13) shows an increase in the moisture content at these locations after the wetting phase has ended. In test 2, the right horizontal bottom plate sample (Figure 5.1) shows a significant moisture increase during the 4-day “dry” period in between the first and second week, in between the second and third week, and also after the wetting phase has ended. In both walls, the moisture content readings of the left horizontal electrical resistance moisture probe both continue to increase after the last wetting event of the wetting phase. After verifying that there was indeed no unintentional water infiltration into the wall, it was found that water held within the matrix of the fiberglass batt insulation just above the bottom plate specimen by surface tension was released due to the force of gravity, thus

wetting the wood below. However, it should be noted that the continued moisture content increase measured by the electrical resistance probes was likely due to continued moisture transfer deeper into the wood to the uninsulated tips of the probes, which were located at approximately 6 mm from the top surface of the bottom plate.

The adsorption of water by the insulation was also noted in a study by Korsgaard and Rode (1992) in a test done to evaluate the hygrothermal performance of different vapor retarders. These authors noted that condensate did not form on the vapor retarder of walls insulated with glass fiber because the vapor that would have otherwise have condensed on the surface was retained by the glass fiber insulation.

5.1.9 Water leakage

Over the course of the wetting phases of tests 1 and 2, there was evidence of an undetermined amount of water leakage. Water was observed to drip out of the bottom of OSB-sheathed walls 4 and 10 at the junction of the bottom plate and the sheathing. Another separate series of tests run at a later date where the wetting patterns in wood-frame walls with different sheathing types and were studied using a similar methodology showed that the amount of leakage is dependent upon the size of the gap that exists between the bottom plate and the adjacent sheathing board. The moisture absorption of the sheathing also plays a role in the amount of leakage since the moisture absorption properties of the sheathing and its moisture content level affects the amount of water that reaches the bottom of the wall.

A separate series of small-scale tests was conducted to visualize the wetting pattern and measure the moisture absorption and water leakage in simplified 250 mm high wall systems consisting of two studs installed at 400 mm on center, a bottom plate, and a sheathing panel. The tests were conducted using three types of sheathing – OSB, plywood and asphalt-coated fiberboard – and with or without fiberglass batt insulation between the studs. A photo of the set-up of an insulated wall, including the brackets used to maintain the wall in position and the container beneath the wall system to collect the leakage water, is given in Figure 5.13. Figure 5.14 shows a photo of the wetted sheathing

and bottom plate for a disassembled wall system. The photos illustrate the wetting pattern in two plywood panels made with different wood species. The water leakage pattern on both panels shows lateral migration of the water above the bottom plate and also more particularly at the bottom of the sheathing where it was in contact with the bottom plate. Close examination of the photographs also reveals a faint vertical line at the center of the sheathing panels, which is the trace left behind from a similar previous test conducted without insulation. The different wetting patterns in the two plywood panels, and in particular the lateral migration within the plywoods above the bottom plate, is due to the different water absorption coefficients of the two plywoods, which were experimentally determined to be 1.7 and 3.1 for the plywood panels shown in Figures 5.14a and 5.14b, respectively. Tests performed with OSB and asphalt-coated fiberboard showed similar lateral wetting trends as shown in Figure 5.14b. Photographs are not provided because the water leakage path and wetting pattern is more difficult to see with those sheathings.

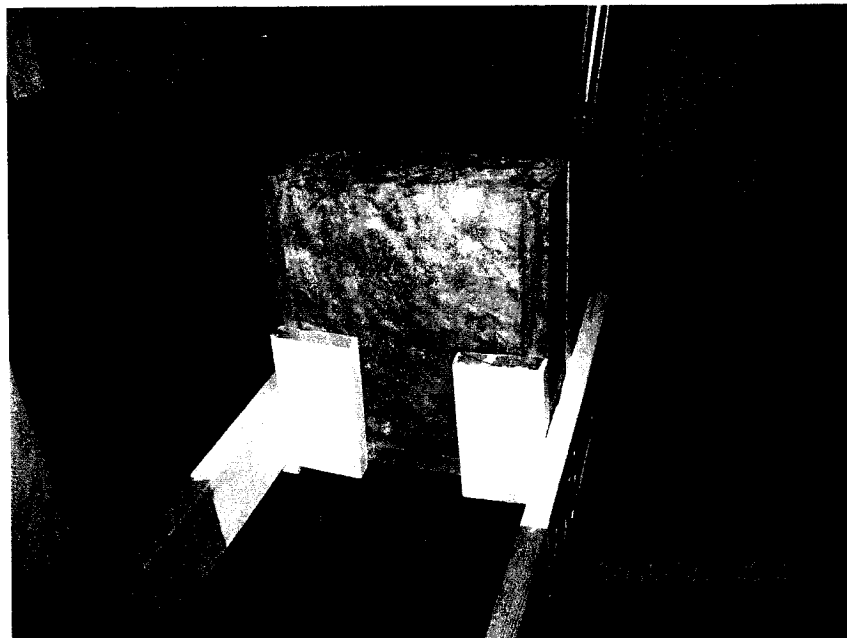
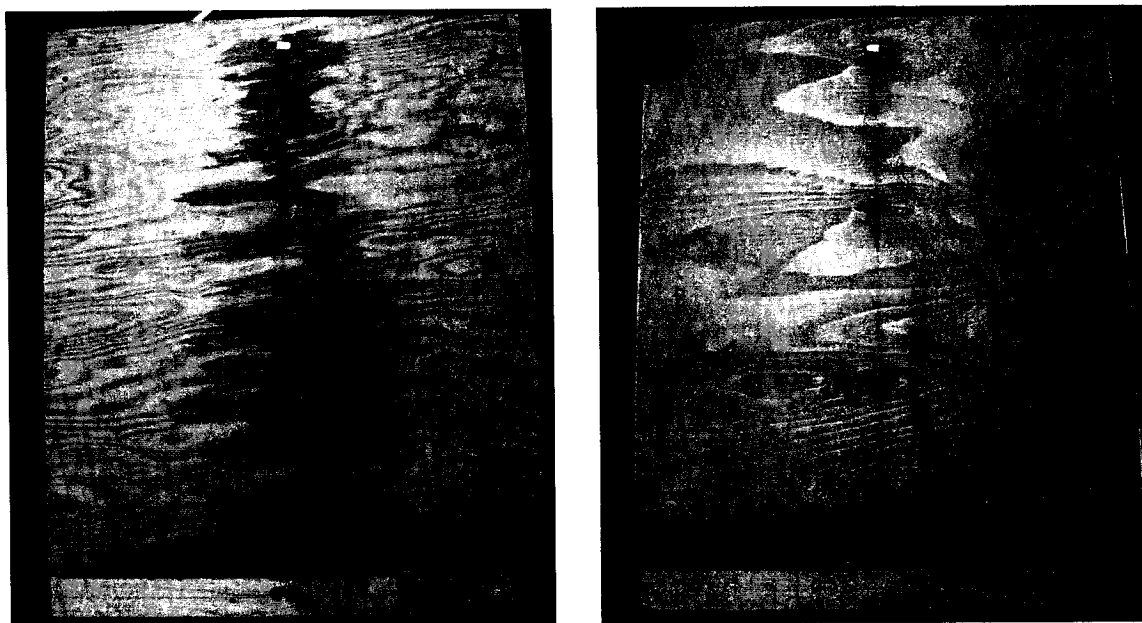


Figure 5.13. Photograph of the test set-up of the wetting pattern obtained on the surface of two plywood sheathings during a separate water infiltration test where, as in tests 1 and 2, water was introduced on the top surface of the sheathing.



a)

b)

Figure 5.14. Photographs of the wetting pattern obtained on the surface of two plywood sheathings, shown in a) and b), during a separate water infiltration test where, as in tests 1 and 2, water was introduced on the top surface of the sheathing. A faint vertical line at the center of the panels shows the trace of a wetting pattern from a previous test where the same test was conducted without insulation between the studs in the stud cavity.

5.1.10 Summary of wetting behavior

To summarize the general wetting behavior of the different wall components due to the different test parameters, the measured peak moisture content at each location during the course the wetting phase in all test 2 wall assemblies was determined, and the average at each location in comparable walls was calculated. For example, in test 2, walls 2, 5, 8 and 11 and 14 all used plywood sheathing. These five walls differed in the type of vapor retarder, the presence of exterior insulation, and of cladding, all of which should not have an impact on the wetting pattern. Figure 5.15 shows the average of the peak moisture contents for the OSB, plywood and fiberboard-sheathed walls. The reader should be cautioned again that electric resistance moisture content readings above the FSP of wood are only an indication of high moisture content. Gravimetric samples in the sheathing are denoted by large circles, and gravimetric samples in the framing are indicated by small

filled circles and squares. Electrical resistance moisture content measurements are indicated by triangles in the figures that follow.

Comparing the average peak moisture content in walls sheathed with OSB, plywood and asphalt-coated fiberboard, the following observations could be made:

- in the sheathing in the zone above the bottom plate, significantly higher moisture contents of 36.7% and 33.7% were found in the plywood in the samples in row C right 1 and row A center, respectively. The high moisture content at row C right 1 is due to lateral migration and absorption by the plywood gravimetric sample. The highest values found in the OSB and the fiberboard sheathing were 15.3% and 11.1% moisture content, respectively.
- significantly higher moisture contents were found in all three sheathings at the level of the bottom plate, again with higher moisture absorption in the plywood than in the other two sheathings: the highest moisture contents in the OSB, plywood and fiberboard were 24.3%, 44.2% and 25.6%, respectively.
- in the bottom plate, there was significant moisture accumulation on the top horizontal surface in the OSB and fiberboard-sheathed walls, and moisture content results showed that for both these types of walls, the highest average peak moisture content was found in the gravimetric sample at the right-hand side of the horizontal surface (66.0% in OSB walls and 64.2% in plywood walls). In the plywood walls, the moisture migration to the top surface was less pronounced, and the moisture accumulation in the bottom plate occurred on the surface adjacent to the bottom plate, with the peak moisture content in the center vertical sample of 48.8% moisture content. The moisture uptake at this location of the bottom plate in the plywood walls was lower than in the other walls because of the greater moisture accumulation in the adjacent plywood than in the OSB or the asphalt-coated fiberboard.

A similar examination of the moisture content results was conducted to see the effect of the height of the assembly on the wetting pattern. The 1-m high plywood sheathed walls 2, 5, 8, 11 and 14, and the 2-m high wall 13 were used for this purpose (see Figure 5.16). The following observations could be made:

- in the sheathing in the zone above the bottom plate, slightly higher average peak values were reached in the 1-m high walls, particularly in row C, with differences in the order of 2% to 6% moisture content, excluding the lateral migration of moisture and subsequent uptake by the gravimetric sample in row C right 1, which reached an average peak of 36.5%.
- in the sheathing at the height of the bottom plate, higher average moisture content levels were reached in the 1-m high wall at 44.2% moisture content, compared to 30.8% in the 2-m high wall.
- in the bottom plate, a comparison of the influence of wall height was difficult because different moisture distributions occurred, with more lateral moisture movement occurring in the 2-m high wall. However, at the center vertical and center horizontal locations, higher average peak moisture contents of 48.8% and 24.8%, occurred in the 1-m high walls compared to 40.9% and 19.9%, respectively.

These findings show that the wall height does have an impact on the wetting pattern for walls subjected to rain infiltration. Therefore, in the framework of research, the size of the wall assembly should be selected to reflect that of the actual wall system under consideration.

The impact of the loading is summarized next. Figure 5.17 shows a) the average of the peak moisture content results in walls 2, 5, 8, 11 and 14; b) the peak moisture contents in wall 15, where the load was halved, and; c) the peak moisture contents in wall 16, where the loading was increased by 50%. The peak moisture content results show that:

- in the sheathing above the level of the bottom plate, the moisture content measurement by electric resistance at row A in the center was affected by the rate of loading, with the highest peak moisture content attained in the wall with the greater load rate (57.1% moisture content), and the lowest moisture content in the wall with half the load (26.1%). Again, the measurement for this method is only indicative above the FSP. Except for a case of lateral migration in the plywood in the base case and in wall 16, there was no significant difference in moisture content at other locations.

- at the level of the bottom plate, the moisture content in the sheathing at the level of the bottom plate was lower in wall 15 (half load), with a peak moisture content of 24.6%; in the base case walls and in the wall with a 50% greater load, the peak moisture contents were approximately the same, indicating that the rate of moisture absorption into the plywood is the governing factor once the gap between the plywood sheathing and the bottom plate is filled with water.
- In the bottom plate, the response of the wood due to the loading rate is more clear: in wall 15, the low rate of loading is reflected in the relatively low peak moisture content of 19.2% found in the center vertical gravimetric sample; at the same location in the base case wall, the average peak moisture content was 48.8%. When the load was increased by 50% (wall 16), the peak moisture content at the same location was measured to be 74.1%. The center horizontal sample in this wall attained a peak moisture content of 80.6%, and it was the only sample in a plywood-sheathed wall that surpassed 30% moisture content. It is thought that when the water infiltration rate was sufficient, the water filled the narrow gap between the sheathing and the bottom plate and, upon reaching the top of the gap, spread over and wetted the top surface of the bottom plate.
- In wall 17, water was inserted at the top of the plywood sheathing next to the stud on the right-hand side of the center cavity rather than in the middle of the stud space. The influence of changing the location of water insertion on the magnitude of the peak moisture content in the sheathing was not significant (see Figure 5.18). The bottom plate gravimetric sample exposed to the vertical surface and facing the sheathing typically absorbed a great deal of moisture, reaching an average peak of 48.8% moisture content in walls 2, 5, 8, 11 and 14 (see Figure 5.18). However, in wall 17, the corresponding sample attained a maximum moisture content of only 24.0%. This may have occurred because, as the water streamed down the surface of the plywood and spread laterally, wicking into the gap at the interface of the sheathing and the stud. Hence, water was absorbed by the sheathing and the adjacent stud, reducing the amount of water that reached the bottom of the wall. Another result of the different location of insertion was the higher peak moisture content in the stud gravimetric sample in row “D” facing the insulated stud cavity: in

wall 17, the sample had a peak moisture content of 25.9%, a condition that may lead to mold and rot growth. On the other hand, the average peak moisture content at that location was 13.3% when a central loading was applied.

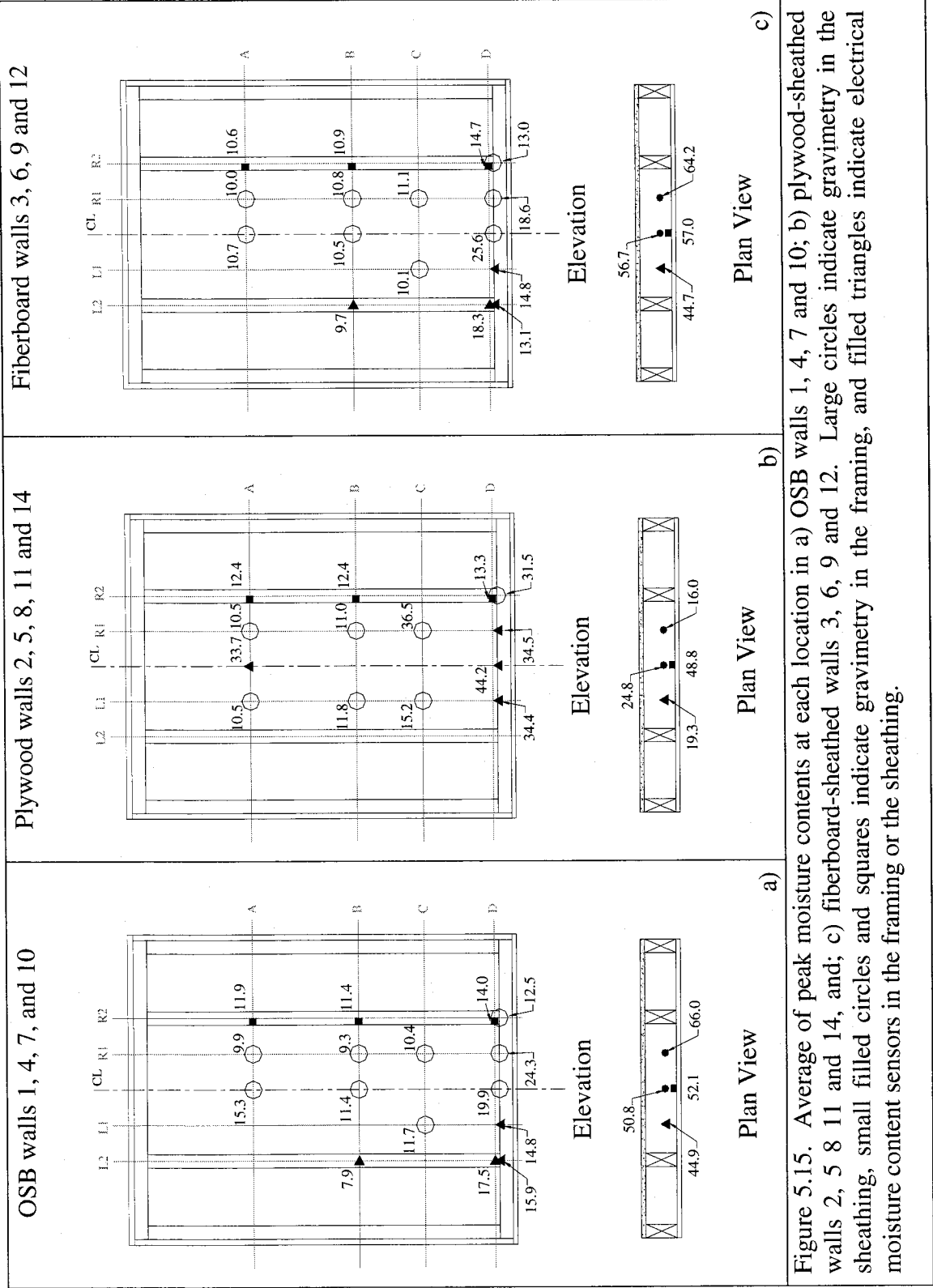
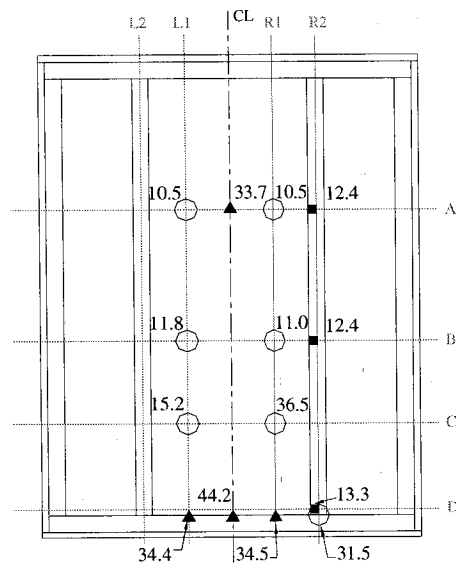
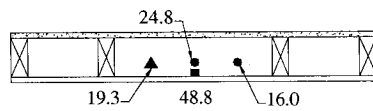


Figure 5.15. Average of peak moisture contents at each location in a) OSB walls 1, 4, 7 and 10; b) plywood-sheathed walls 2, 5 8 11 and 14, and; c) fiberboard-sheathed walls 3, 6, 9 and 12. Large circles indicate gravimetry in the sheathing, small filled circles and squares indicate gravimetry in the framing, and filled triangles indicate electrical moisture content sensors in the framing or the sheathing.

Plywood walls 2, 5, 8, 11 and 14



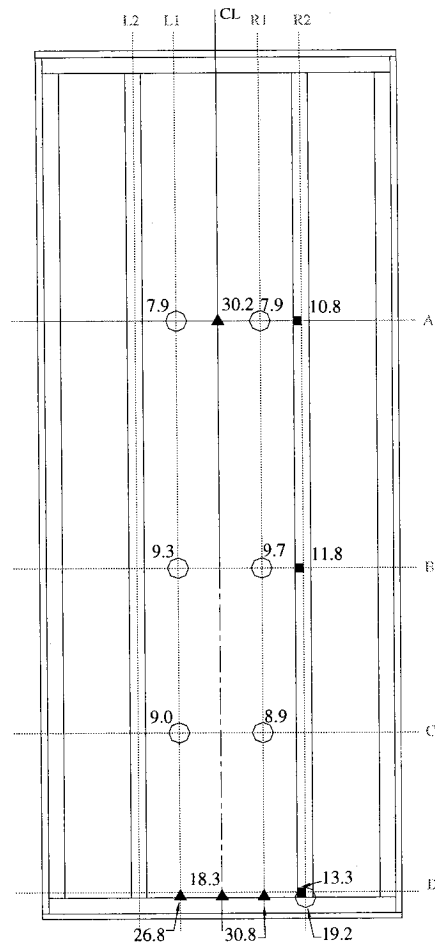
Elevation



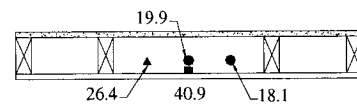
Plan View

a)

Plywood wall no. 13



Elevation



Plan View

b)

Figure 5.16. Average of peak moisture contents at each location in a) 1-m high plywood-sheathed walls 2, 5 8 11 and 14, and; b) 2-m high plywood-sheathed wall 13. Large circles indicate gravimetry in the sheathing, small filled circles and squares indicate gravimetry in the framing, and filled triangles indicate electrical moisture content sensors in the framing or the sheathing.

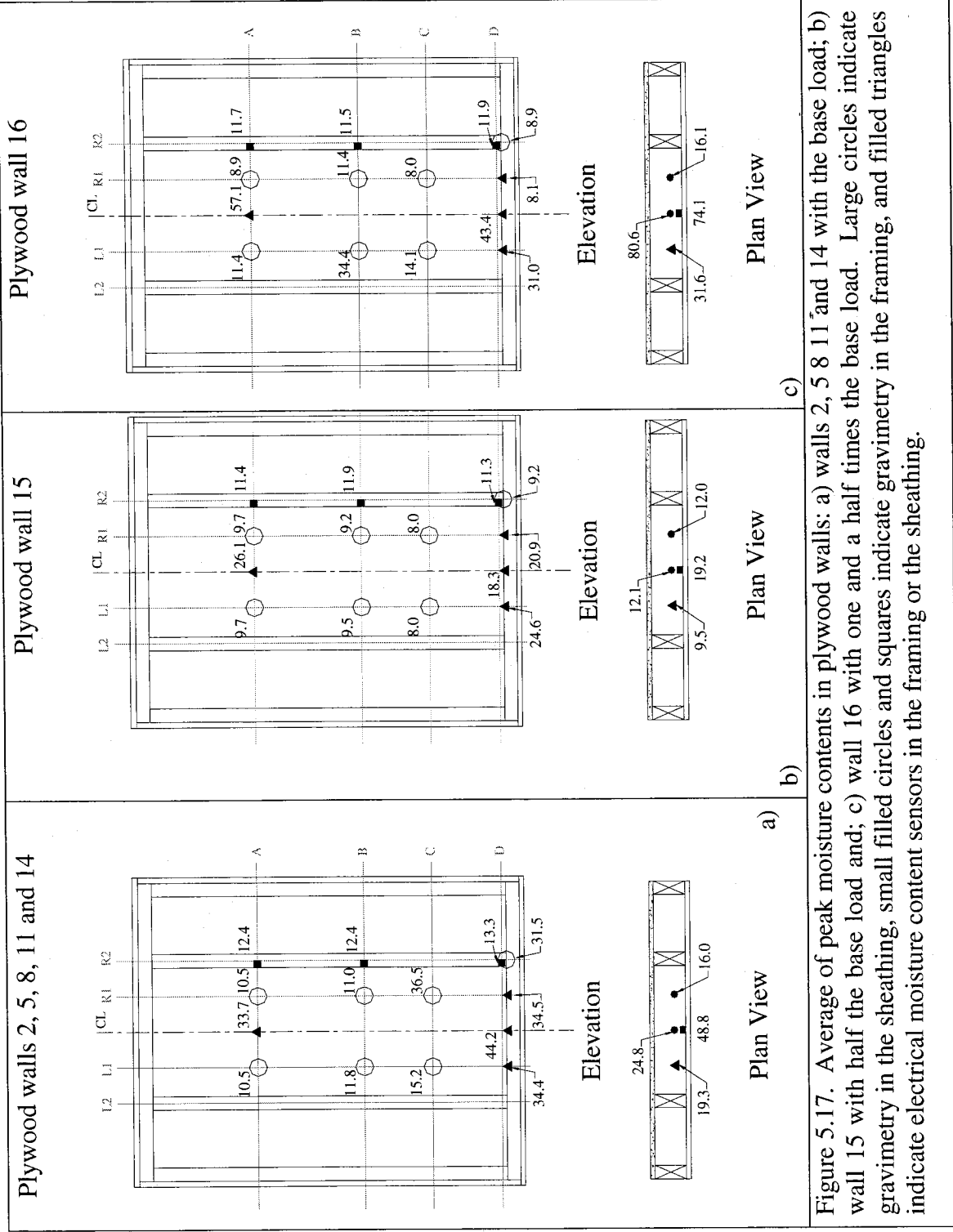
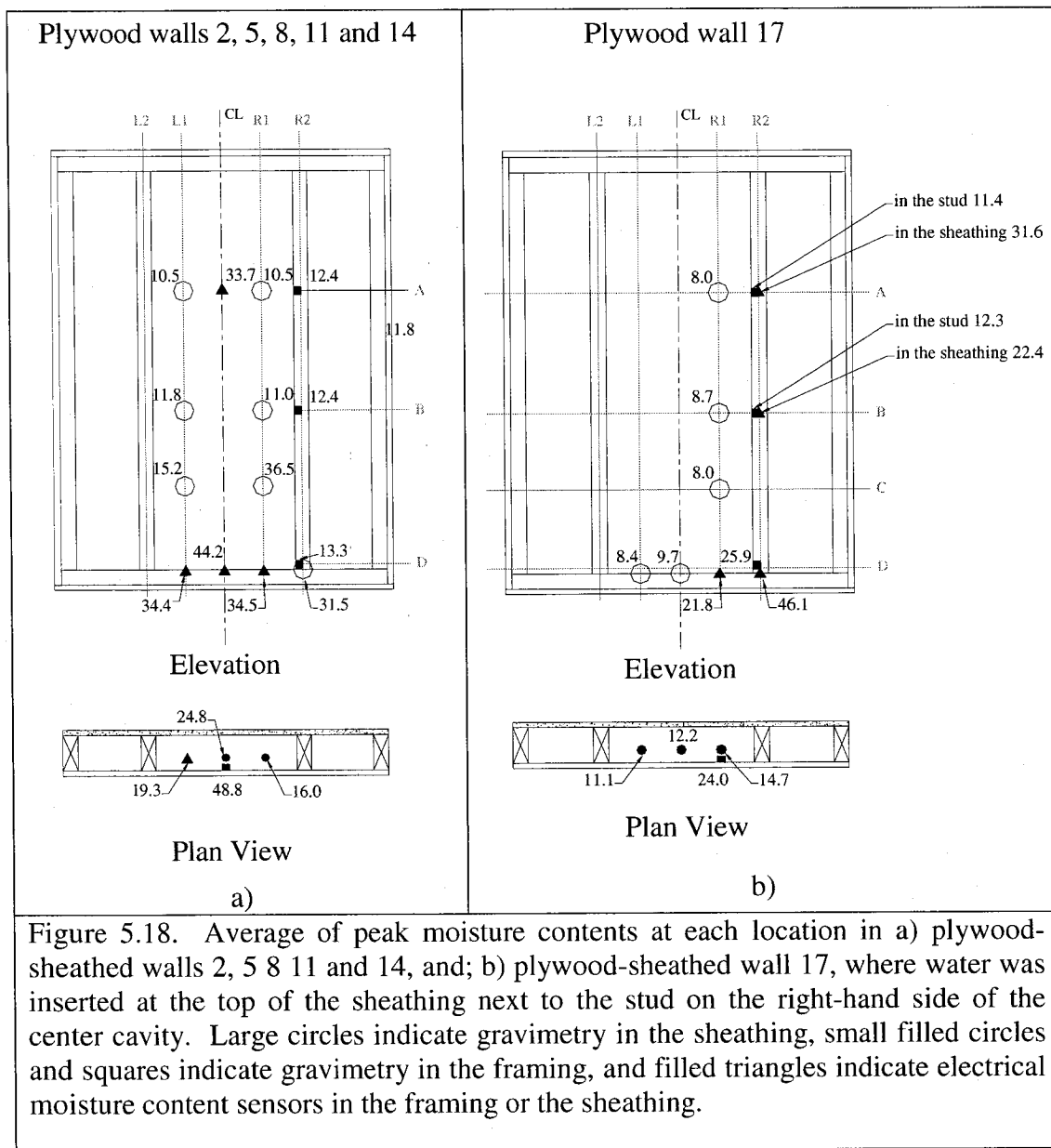


Figure 5.17. Average of peak moisture contents in plywood walls: a) walls 2, 5 8 11 and 14 with the base load; b) wall 15 with half the base load and; c) wall 16 with one and a half times the base load. Large circles indicate gravimetry in the sheathing, small filled circles and squares indicate gravimetry in the framing, and filled triangles indicate electrical moisture content sensors in the framing or the sheathing.



5.2 Role of Wall Components on the Drying Behavior - Tests 1 and 2

While this chapter has so far focused on the wetting behavior of the components, the drying behavior during the wetting phase is now examined. As was explained in Chapter 3, the four-week wetting schedule consisted of three days where water was introduced for

a period of 3.4 hours a day, followed by four “dry” days where no water was inserted. It was generally found that some drying of the wetted gravimetric specimens occurred in the 20.6-hours between wetting events, and even more so during the four-day period in each week. The degree of drying varied from sample to sample due to their different initial moisture contents, the location of the moisture within the sample (i.e. surface or deeper moisture absorption), and the samples’ location within the assembly. The moisture content data was examined to find cases of locations exposed to similar ambient conditions where the moisture content obtained at the end of the start of the weekly four-day “dry” period was similar, permitting comparison of the drying behavior as influenced by the test parameters. For example, Figure 5.19 shows the moisture content values for the center vertical gravimetric samples in walls 1, 2 and 3 of test 2. The circled measurements show those that were taken as initial moisture content for the four-day “dry” period that followed. A plot of the moisture content at the center vertical location for the “dry” period in each of the three walls is shown in Figure 5.20. The relative moisture content of the samples at the start and the end of the four-day “dry” period, relative to the moisture content at the start of the same four-day period, was calculated. An example for the center vertical bottom plate samples of walls 1 to 3 is plotted in Figure 5.21. Therefore, the relative moisture content can range between 0, indicating a moisture content of 0%, to 1.0 for a moisture content equal to that at the start of the four-day period.

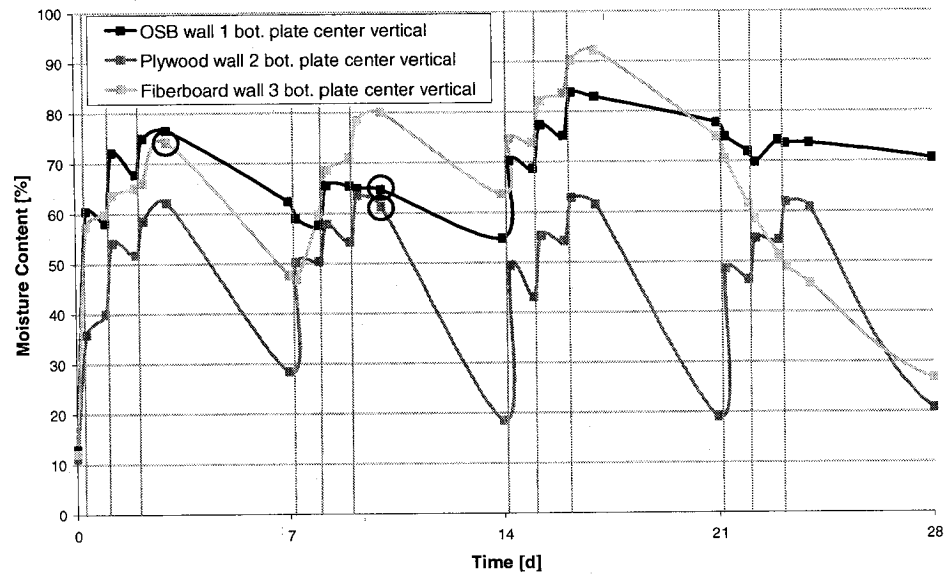


Figure 5.19. Moisture content with time measurements in the center vertical “CV” gravimetric sample in OSB wall 1, plywood wall 2 and fiberboard wall 3 during the wetting phase of test 2. The circled measurements show those that were taken as initial moisture content for the four-day “dry” period that followed. The vertical lines denote a 3.4 hour wetting event.

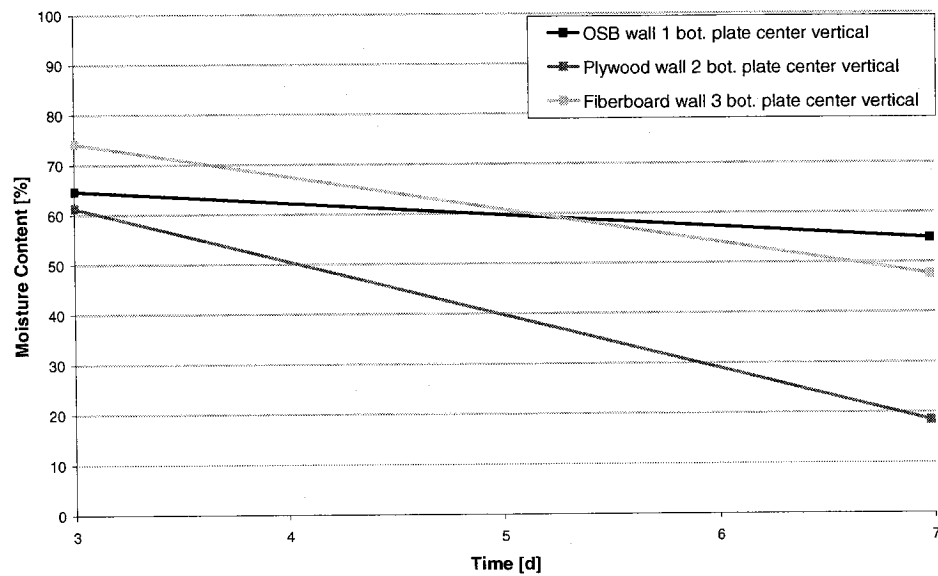


Figure 5.20. Moisture content measured at the start and end of the four-day “dry” period in the center vertical “CV” gravimetric sample in OSB wall 1, plywood wall 2 and fiberboard wall 3 in test 2.

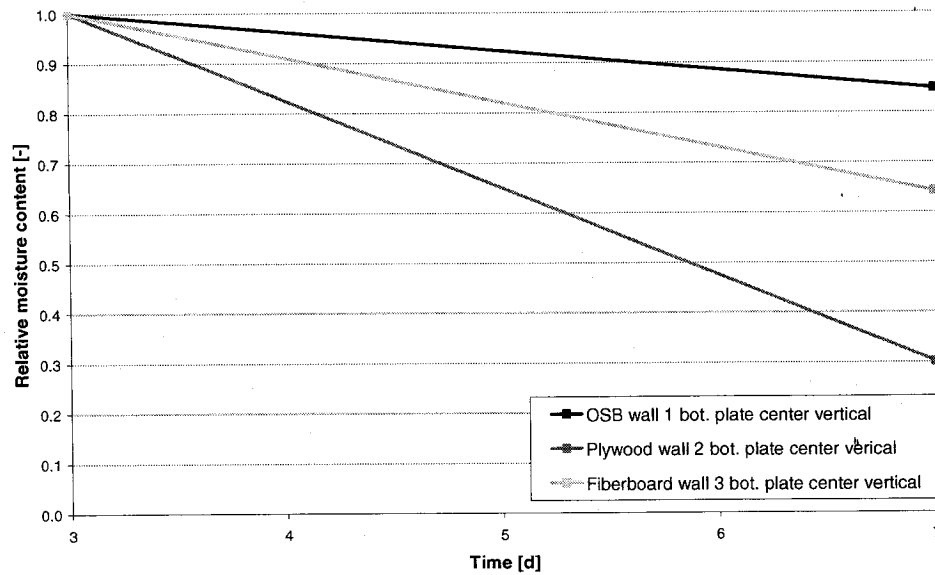


Figure 5.21. Relative moisture content at the beginning and end of the four-day “dry” period, calculated relative to the initial moisture content at the beginning of the same period in the center vertical “CV” gravimetric sample in OSB wall 1, plywood wall 2 and fiberboard wall 3 in test 2.

5.2.1 Role of the sheathing on the drying performance

A summary of the relative moisture content findings for bottom plate and sheathing samples in walls 1 to 9, given in Table 5.2, is used to study the influence of the type of sheathing on the drying behavior of the wall components.

Table 5.2. Relative moisture content at the end of the four-day “dry” period, calculated relative to the initial moisture content at the beginning of the same four-day period at various locations in the bottom plate and the sheathing in walls 1 to 7 of test 2. The moisture content at the start of the four-day period is indicated in parentheses.

| Monitoring location | Bottom plate | | | Sheathing | |
|--|------------------------|-----------------------|----------------------|---------------------|-----------------------|
| | Center horizontal “CH” | Right horizontal “RH” | Center vertical “CV” | Row “D” center “DC” | Row “D” right 1 “DR1” |
| Walls 1-3: Polyethylene vapor retarder | | | | | |
| OSB wall 1 | 0.55 (71.7%) | - | 0.85 (64.7%) | 0.86 (25.0%) | - |
| Plywood wall 2 | 0.32 (59.5%) | - | 0.30 (61.3%) | - | - |
| Fiberboard wall 3 | 0.49 (65.7%) | 0.57 (74.5%) | 0.64 (74.2%) | 0.58 (24.7%) | - |

| Walls 4–6: Low permeance primer paint vapor retarder | | | | | |
|--|-----------------|-----------------|-----------------|---|---|
| OSB wall 4 | - | 0.36 (51.4%) | 0.76 (26.6%) | - | - |
| Plywood wall 5 | - | - | 0.54 (34.9%) | - | - |
| Fiberboard wall 6 | 0.37 (56.6%) | - | 0.59 (36.0%) | - | - |
| Walls 7-9: No vapor retarder | | | | | |
| OSB wall 7 | 0.50 (40.6%) | - | - | - | - |
| Plywood wall 8 | - | - | - | - | - |
| Fiberboard wall 9 | 0.46 (36.2%) | 0.36 (43.4%) | - | - | - |

The relative moisture content values in the center and right horizontal samples at the end of the four-day period in walls 1 to 9 are first compared. In walls 1 to 3, which all had a polyethylene vapor retarder, the lowest relative moisture content of 0.32 is found in the plywood-sheathed wall. The values are similar in the OSB and fiberboard-sheathed walls. In walls 4 to 6, which used a low permeance primer vapor retarder, the relative moisture content values are similar in wall 4 and 6; however, the results for the same samples in walls 7 to 9, which had no vapor retarder, show lower relative moisture contents of 0.36 and 0.46 in the fiberboard wall 9 compared to 0.5 in the OSB-sheathed wall 7. The center vertical samples in walls 1 to 6 show a clear trend, with lowest and highest relative moisture content values in the plywood-sheathed and OSB-sheathed walls, respectively, with the difference more pronounced in walls 1 to 3 with the highest vapor diffusion resistance. It is thought that the asphalt coating on the major surfaces of the fiberboard reduced its liquid uptake, thereby preventing absorption of condensation and of water at the bottom plate-sheathing interface. As a consequence, the rate of drying of the bottom plate was decreased, and moisture egress occurred via the slower process of vapor diffusion.

In the sheathing, the response of the gravimetric samples in the center, “DC”, and the right-hand side, “DR1”, of the bottom row is compared. The relative moisture content results for the OSB sheathing of wall 1 (0.86) in the fiberboard sheathing of wall 3 (0.58) show that the drying response of the fiberboard was faster, which can be attributed to the significantly higher vapor permeability of fiberboard. The role of the sheathing in the drying performance is also examined in section 5.3.1, which

discusses the results of test 3.

5.2.2 Role of the vapor retarder on the drying performance

The results are investigated to examine the effect of the vapor retarder on the drying response of the wall components. Three options of vapor retarders were used: polyethylene membrane (walls 1 to 3), low permeance primer (walls 4 to 6), and no vapor retarder (walls 7 to 9). As was done previously, results of relative moisture contents for samples which showed similar initial moisture contents at the beginning of a weekly four-day “dry” period are tabulated in Table 5.3. Looking first at results in OSB-sheathed walls 1, 4 and 7, the lower relative moisture contents in the center and right horizontal samples in wall 4 indicate that these dried at a faster rate when there was a low permeance primer compared to the samples in wall 7 where the vapor retarder was absent. This finding is unexpected and is not fully understood. In the plywood-sheathed walls 2, 5 and 8 at the center of row “A”, the relative moisture content results show that increasing the permeability of the inner layer increased the drying rate of the samples, although the difference is not significant. Last, in the fiberboard-sheathed walls 3, 6 and 9, increasing the permeability of the vapor retarder reduced the final relative moisture content of the center and right horizontal bottom plate samples. The difference was most pronounced when the polyethylene was removed and replaced by low permeance primer or when no vapor retarder was used. The role of the vapor retarder is revisited when the test 3 results are discussed in section 5.3.2.

Table 5.3. Relative moisture content at the end of the four-day “dry” period, calculated relative to the initial moisture content at the beginning of the same four-day period at various locations in the bottom plate and the sheathing in walls 1 to 7 of test 2. The moisture content at the start of the four-day period is indicated in parentheses.

| Monitoring location | Bottom plate | | Sheathing |
|---|------------------------------------|--------------------------|------------------------|
| | Center horizontal “CH” | Right horizontal “RH” | Row “A” center “AC” |
| Walls 1, 4 and 7: OSB sheathing | | | |
| Polyethylene wall 1 | - | - | - |
| Low permeance primer wall 4 | 0.39 (46.0%) | 0.39 (51.3%) | - |
| No vapor retarder wall 7 | 0.50 (40.6%) | 0.66 (58.8%) | - |
| Walls 2, 5 and 8: plywood sheathing | | | |
| Polyethylene wall 2 | - | - | 0.80 (19.7%)* |
| Low permeance primer wall 5 | - | - | 0.76 (20.9%)* |
| No vapor retarder wall 8 | - | - | 0.71 (25.3%)* |
| Walls 3, 6 and 9: asphalt-coated fiberboard sheathing | | | |
| Polyethylene wall 3 | 0.49 (65.7%) | - | - |
| Low permeance primer wall 6 | 0.27 (64.3%) 0.37 (55.6%) | 0.29 (57.6%) | - |
| No vapor retarder wall 9 | 0.28 (72.9%) | - | - |

*The moisture content at this location was determined using electrical resistance probes.

5.2.3 Role of the exterior insulation on the drying performance

Walls 2 and 11 from tests 2 were used to examine the role of exterior insulation in the drying response of the wall components. Large differences in the moisture distribution in the two walls made the comparison difficult. In the sheathing, only one sample in row “D” right 2 could be compared in terms of the drying. As was done previously, the relative moisture content of the sample at the end of the four-day “dry” period was calculated and is shown in Table 5.4. Again, the relative moisture content is the moisture content at the end of a four-day “dry” period relative to the moisture content at the start

of the same four-day period, and ranges from 0.0 to 1.0. The table shows that the sample in wall 2 reached a lower relative moisture content than the same sample in the wall with exterior insulation. In the bottom plate, the same trend is found: the relative moisture content after the four-day “dry” period, given in Table 5.4, is significantly lower in wall 2, at 0.34, than that in wall 11, at 0.82. The wall 2 sample dried at a much faster rate despite the higher moisture content at the beginning of the four-day period. These findings are likely due to the increased outward vapor resistance provided by the exterior extruded polystyrene. It should be noted here that the interior and exterior ambient conditions were the same during the wetting phase of the test.

The impact of exterior insulation in the presence of a temperature differential is investigated numerically in Chapter 6.

Table 5.4. Relative moisture content at the end of the four-day “dry” period, calculated relative to the initial moisture content at the beginning of the same period in two gravimetric specimens in row “D” right 2 in plywood walls 2 and 11, test 2. The moisture content at the start of the four-day period is indicated in parentheses.

| Monitoring location | Sheathing row “D” right 2 “DR2” | Bottom plate center vertical “CV” |
|------------------------------------|--|--|
| Wall 2 without exterior insulation | 0.58 (26.9%) | 0.34 (60.9%) |
| Wall 11 with exterior insulation | 0.87 (21.9%) | 0.82 (41.0%) |

5.2.4 Role of the cladding on the drying performance

The drying response at two locations in the plywood sheathing – in the center of rows “A” and “D” – are shown in Figures 5.22 and 5.23, respectively. At both locations, the wetting events resulted in higher peak moisture content levels in the plywood of wall 2 than that in wall 14. Despite reaching higher moisture contents, the plywood sheathing in wall 2 dried to lower moisture content levels than at the same location in wall 14 at the end of the wetting phase. Therefore, for exterior and interior conditions of 20°C and 60% relative humidity, the presence of cladding retards drying to the exterior. During the colder drying phases, when April and May conditions were simulated, the moisture content results show a drying trend in the cladded wall, while a trend of moisture increase occurred in the wall without cladding, particularly at the top of the wall, i.e. in row “A”.

It is possible that the bottom plate and the sheathing in wall 2 absorbed a greater amount of moisture than in wall 14 (see Figures 5.22 and 5.23), and as the conditions of the drying phase were applied at day 28, the wetted components began to dry, releasing moisture in the stud cavity which was then redistributed to the upper portions of the sheathing. This explanation is supported by the relative humidity measured in the stud cavity insulation at approximately 150 mm from the water insertion point, which has an upward trend in wall 2 but a downward trend in wall 14 during the drying phases. More analysis on the impact of hygroscopic exterior cladding would require modeling the ventilation in the air cavity, which is beyond the scope of this project.

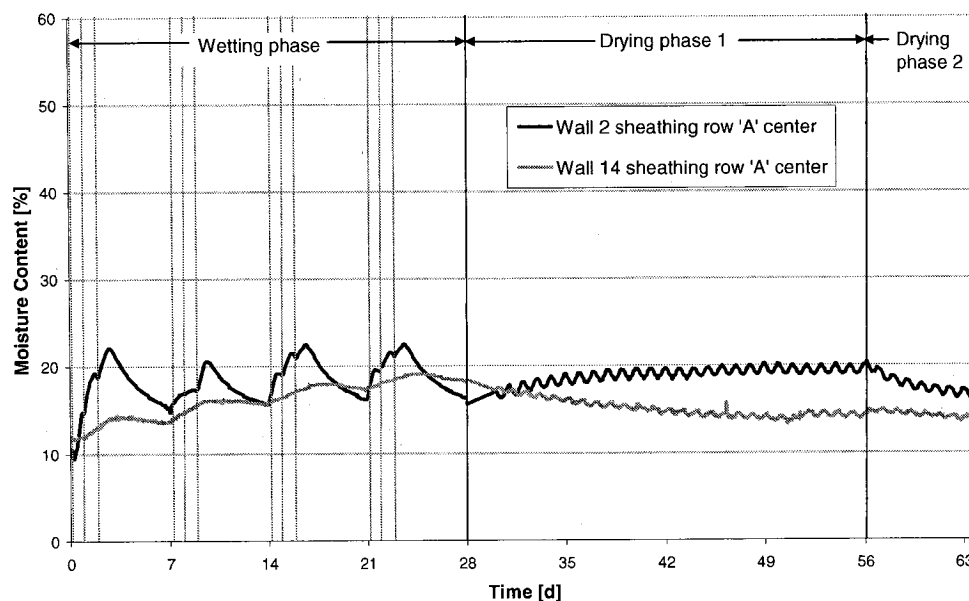


Figure 5.22. Moisture content versus time in the plywood sheathing at row “A” center measured by electrical resistance probes in wall 2 and wall 14 in test 2. Wall 14 has wood siding while wall 2 has no cladding. The grey vertical lines denote a 3.4 hour wetting event.

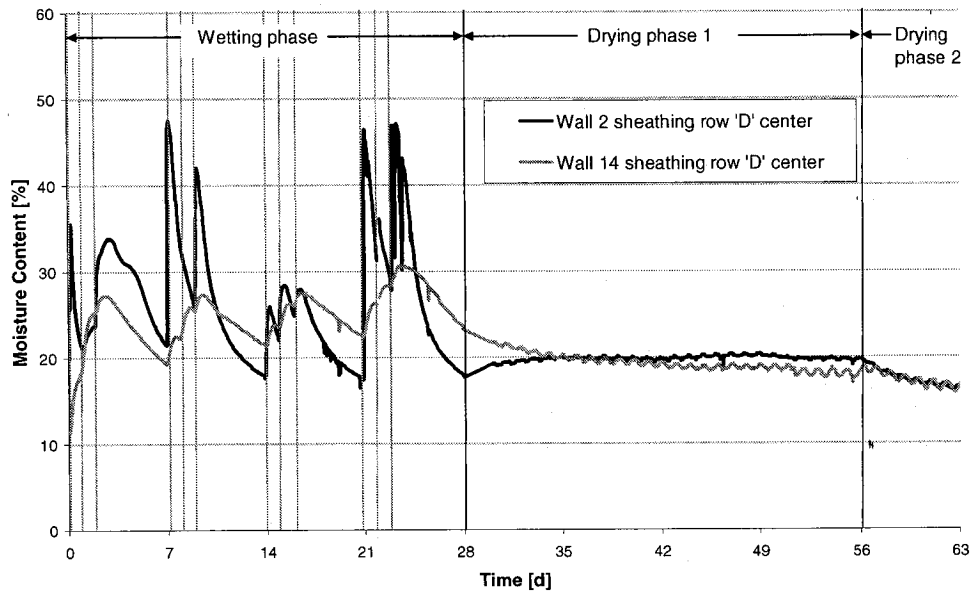


Figure 5.23. Moisture content versus time in the plywood sheathing at row “D” center measured by electrical resistance probes in wall 2 and wall 14 in test 2. Wall 14 has wood siding while wall 2 has no cladding. The grey vertical lines denote a 3.4 hour wetting event.

5.2.5 Role of the assembly height on the drying performance

The role of the height of the assembly on the drying response of the wall components is examined using moisture content results from plywood-sheathed walls 2 and 13. Wall 1 had a height of 1 m while wall 2 was 2 m high. The differences in the wetting distributions and the magnitude of the moisture contents reached during the wetting phase in the two walls renders the comparison difficult. However, the moisture content probes in the sheathing in the center of row “A” recorded moisture absorption in both walls (see Figure 5.24). The moisture content curves for the two walls show similar drying trends in the sheathing in the four “dry” days. In the second week of the test, the drying rate during the four-day “dry” period was higher in wall 13 than in wall 2, but this may have been due to the higher moisture content at the beginning of the four-day period. Chapter 6 will examine the impact of the increased stud cavity height in more detail.

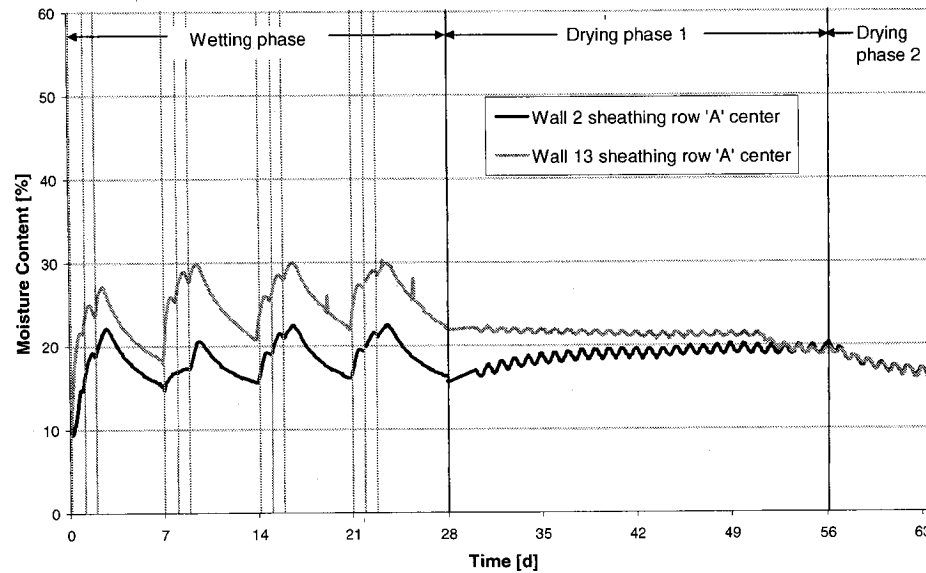


Figure 5.24. Moisture content in time in the plywood sheathing at row “A” center measured by electrical resistance probes in wall 2 and wall 13 in test 2. Wall 2 is 1 m high while wall 13 is 2 m high. The grey vertical lines denote a 3.4 hour wetting event.

Overall, the moisture content results from tests 1 and 2 show that drying occurred in all wall assemblies, and the measured moisture content levels in the sheathing, the bottom plate and the studs generally reached safe levels in terms of fungi growth, i.e. less than 20% moisture content, at the end of the tests. There were five exceptions to this general finding in each of the two tests. However, in these exceptional cases, only in one instance did the final moisture content exceed 23%. The relative humidity, monitored in the fiberglass batt insulation-filled stud cavity, did not exceed 63% in both tests. These findings indicate that the bulk of the moisture load had evacuated the wall assemblies by the end of the experiments.

The next section presents an analysis of the drying response of the various monitored components in the third experiment. Specifically, the section will investigate the role of two wall components on the drying behavior: the type of sheathing, and the type of vapor retarder.

5.3 Global Wetting and Drying Performance in Tests 1 and 2

A moisture performance analysis was conducted in order to obtain a global portrait of the hygrothermal response of the monitored samples in the bottom plates and in the sheathing for selected walls from tests 1 and 2. The analysis included walls 1 to 12, which were exposed to the same moisture load but differed in terms of the type of sheathing material and vapor retarder employed. For each of the 12 walls, the maximum moisture content measured over the course of the tests in the sheathing and in the bottom plate were determined. At that location in the sheathing and the bottom plate, the number of days to which the component was exposed to a moisture content level greater or equal to 20% was calculated. The results are plotted in Figures 5.25 and 5.26 for the sheathing of walls for tests 1 and 2, respectively, in the form of maximum moisture content versus time exposed to a moisture content greater or equal to 20%. The values are grouped with respect to the type of wood-based sheathing. Figure 5.25 shows that in test 1, the plywood sheathing reached greater moisture content levels, and was exposed to high moisture content levels for longer periods of time, thus increasing, for the plywood sheathings, the risk of mold and rot growth. The OSB sheathings were also wetted for significant time durations, but overall, there was less moisture accumulation in the OSB specimens, likely due to the OSB's lower water absorption coefficient. On the other hand, the asphalt coating on the fiberboard surface reduced its liquid moisture uptake; as well, fiberboard was exposed to M conditions above 20% M for a significantly smaller period of time. In test 2, the moisture content monitoring scheme was improved in the plywood-sheathed walls: the plywood gravimetric samples which disturbed the water infiltration path in test 1 were replaced in test 2 by less intrusive electrical resistance moisture probes. As a consequence, the plywood sheathings reached lower moisture content levels in test 2 than in test 1, as illustrated in Figure 5.26. However, the plywood sheathing absorbed more moisture than the other two sheathing materials and stayed wet for a considerable duration of time. Comparably, the OSB sheathings were also wet for a long period of time, despite reaching lower moisture contents. Finally, as in the first experiment, the fiberboard sheathing was the sheathing material that dried at a faster rate.

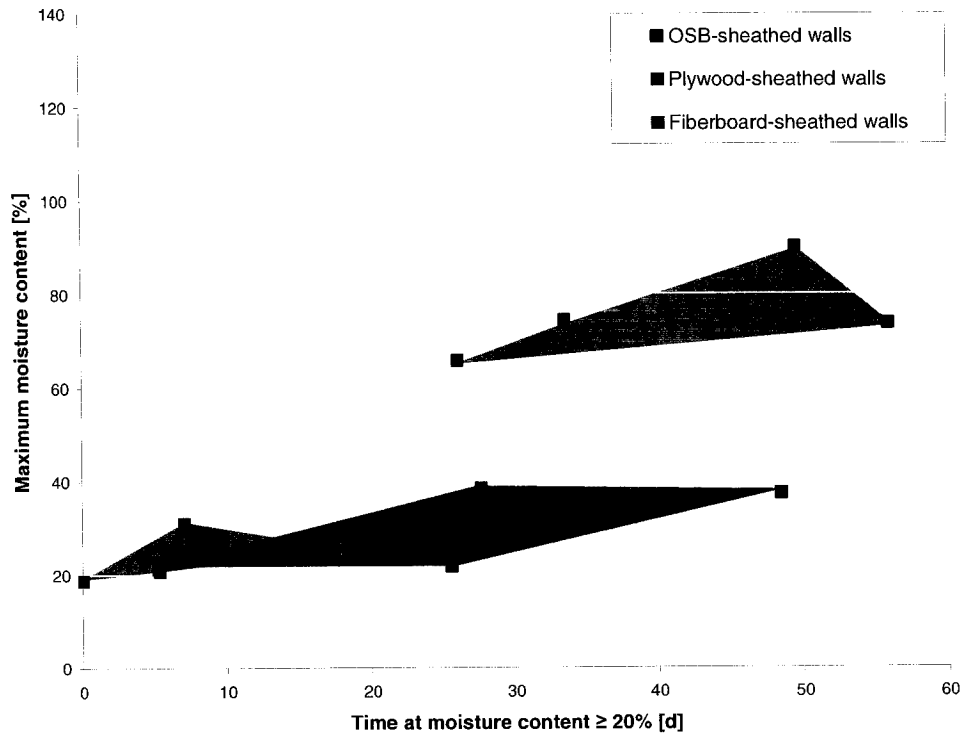


Figure 5.25. Maximum moisture content versus time exposed to moisture content greater or equal to 20% in the OSB, plywood and fiberboard sheathings of walls 1 to 12 in test 1.

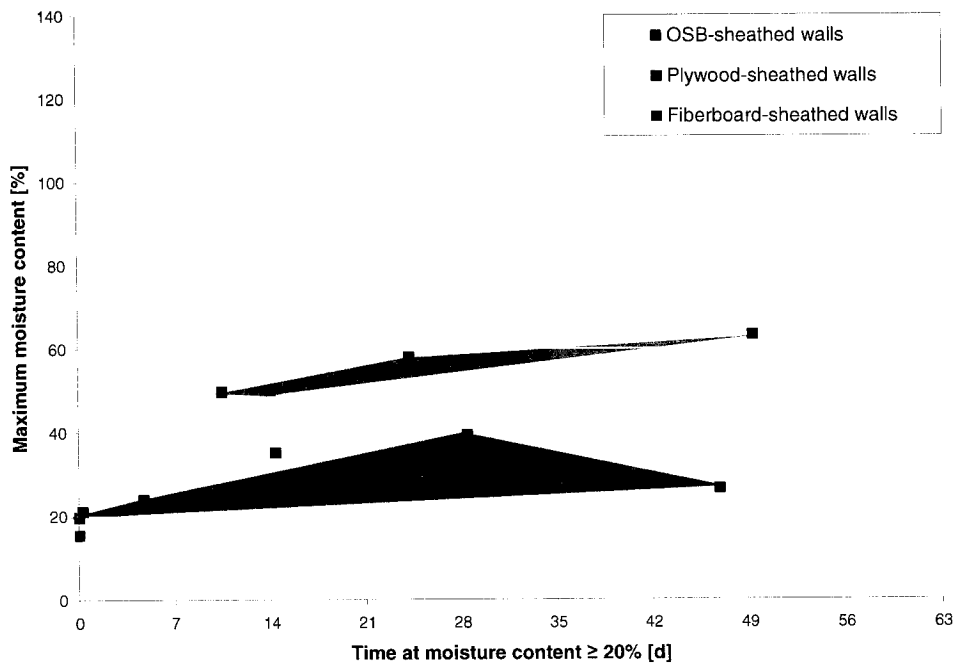


Figure 5.26. Maximum moisture content versus time exposed to moisture content greater or equal to 20% in the OSB, plywood and fiberboard sheathings of walls 1 to 12 in test 2.

A similar analysis was conducted for the bottom plates for walls 1 to 12 of tests 1 and 2, the results of which are illustrated in Figures 5.27 and 5.28, respectively. The bottom plates in the plywood-sheathed walls were not significantly wetted during the first test because the majority of the water was captured by the gravimetric sheathing specimens at the top of the wall. In the OSB and fiberboard-sheathed walls, the bottom plates were wet to moisture contents in the range from about 60 to 100%. However, Figure 5.27 shows that the bottom plate in the OSB walls spent a significantly longer period of time at M greater or equal to 20% compared to the bottom plate in the fiberboard walls, suggesting that the higher vapor permeability of fiberboard increased the walls' drying potential. In test 2, the bottom plate specimens in the OSB and the fiberboard-sheathed walls reached approximately the same level of M , except for the outlier of one OSB-sheathed wall. However, the bottom plates in the OSB walls were again exposed to high moisture contents for considerably longer periods of time, indicating that using OSB reduced the drying ability of the walls, and that the bottom plates were at significantly higher risk of moisture-induced decay when OSB sheathing was employed, particularly as the temperatures during the test were above 0°C. In contrast, the bottom plates in the plywood walls reached lower moisture contents, likely because there was a greater moisture uptake in the plywood. The bottom plates in these walls spent slightly less time at high moisture content levels.

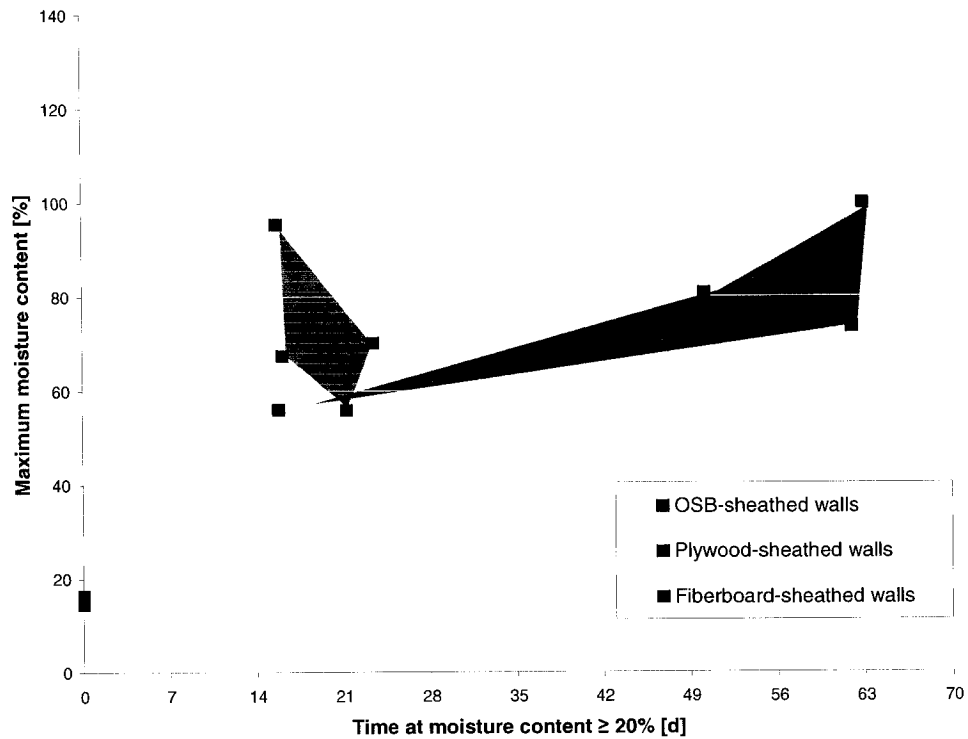


Figure 5.27. Maximum moisture content versus time exposed to moisture content greater or equal to 20% in the bottom plates of walls 1 to 12 of test 1, grouped with respect to the sheathing materials used in each wall.

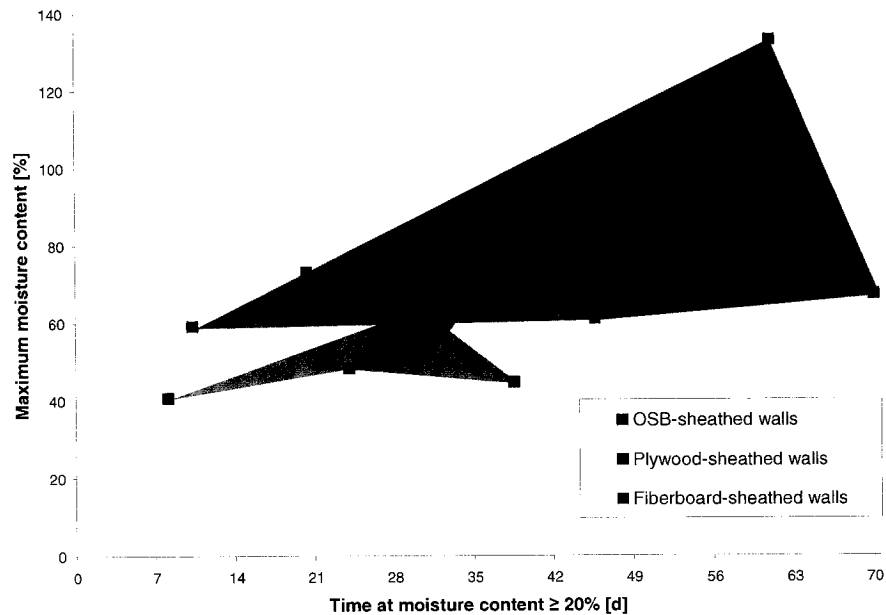


Figure 5.28. Maximum moisture content versus time exposed to moisture content greater or equal to 20% in the bottom plates of walls 1 to 12 of test 1, grouped with respect to the sheathing materials used in each wall.

5.4 Role of Wall Components on the Drying Behavior – Test 3

The following section of the chapter examines the role of two parameters in the drying behavior of the wood-frame wall components. As was stated in the wetting methodology, the moisture source in each wall was a bottom plate insert, measuring 39 mm x 142 mm x approximately 360 mm, which was pre-wetted in a 13 mm deep pool of water for 31 days prior to installation above the existing wall bottom plate at the beginning of the test. Three of the four small gravimetric samples – center horizontal 1 (CH1), center horizontal 2 (CH2) and center vertical (CV) - were also pre-wetted prior to installation into pre-drilled holes in the bottom plate insert just before the experiment started. More details on the monitoring protocol can be found in section 4.8.2. In each wall, the bottom plate insert as well as 4 small gravimetric samples served as moisture content monitors. The hygrothermal response of all but one of these monitors is presented in the following sections. The other sample, which was called “center horizontal under”, or CHU, because it was installed in a pre-drilled hole at the bottom surface of the insert, was intended to monitor transverse moisture migration into the bottom plate. However, its performance is not discussed here because it was not affected by the sheathing.

5.4.1 Role of the exterior sheathing

This section discusses the role of the exterior sheathing in the six walls of test 3. To recap, the six walls were built identically except for two components: the sheathing and the vapor retarder. To examine the role of the sheathing, two series of three walls are compared: walls 1 to 3, which all have a polyethylene vapor retarder, and walls 4 to 6, where the vapor retarder is a low permeance primer paint applied to the gypsum board. The sheathing and vapor retarder used in the six walls is summarized in Table 4.7, which is repeated below for convenience. The investigation begins by looking at the moisture response of the bottom plate inserts.

Table 4.7. Types of sheathings and vapor retarders in walls 1 to 6 in test 3.

| Sheathing material | Vapor retarder | |
|-----------------------------|-----------------------|----------------------------|
| | Polyethylene membrane | Low permeance primer paint |
| Oriented strand board (OSB) | wall 1 | wall 4 |
| Plywood | wall 2 | wall 5 |
| Asphalt-coated fiberboard | wall 3 | wall 6 |

5.4.1.1 Hygrothermal response of the bottom plate inserts

Graphs of gravimetric moisture content as a function of time are examined to investigate the response of the bottom plate inserts to walls constructed with different exterior sheathings.. The initial moisture content of the bottom plate inserts of walls 1, 2 and 3 were 53.0%, 53.1% and 56.8%, respectively; the variation of 3.8% is small enough that the three specimens are deemed to have attained the same level of moisture. It should be noted that during the partial immersion wetting process, the moisture absorption was not the same in all directions (radial, tangential and longitudinal) due to the strong anisotropy of wood: the most significant moisture absorption occurred in the 38 mm x 140 mm surface of the sample because moisture transfer longitudinal is occurs much more readily than in the transverse direction. Hence, the moisture content at the start of the test was not uniform.

Table 5.5 shows the moisture content of each specimen at the start of the test just after being removed from the immersion pool. Relatively uniform starting moisture contents were achieved with moisture content within 3.8% of each other. The table also shows the moisture content at the end of the drying phases. It can be seen that while the insert in wall 3 absorbed the greatest amount of water compared to that in walls 1 and 2 at 56.8% moisture content, its moisture content at the end of the drying period was the lowest at 20.7%. The moisture content lost in the drying process in the inserts of fiberboard-clad wall 3 was 4.4% greater than that lost by the plywood-sheathed wall 2, and 9.8% greater than that in the OSB wall 1.

Table 5.5. Initial and final moisture content and moisture content lost in the drying process for the bottom plate inserts of walls 1 to 3 in test 3.

| Wall no. | Sheathing | Initial moisture content [%] | Final moisture content [%] | Decrease in moisture content in drying process [%] |
|----------|---------------------------|------------------------------|----------------------------|--|
| 1 | OSB | 53.0 | 26.7 | 26.3 |
| 2 | Plywood | 53.1 | 21.4 | 31.7 |
| 3 | Asphalt-coated fiberboard | 56.8 | 20.7 | 36.1 |

The moisture content for the bottom plate inserts of walls 1 to 3 is shown graphically in Figure 5.29. In all three specimens, the moisture content decreased significantly in the first day of the test by 4.3%, 2.9% and 2.6% in OSB-sheathed wall 1, plywood-sheathed wall 2 and fiberboard-sheathed wall 3, respectively. This is due to the evaporation of unbound water on the surface of the bottom plate inserts. The moisture content versus time graph shows that the loss of moisture content for each sample is greatest in the beginning and then tapers off at the end of the test.

Figure 5.29 shows that all specimens dried with time over the 35-day drying period, as expected; however, in all three specimens, the rate of change in moisture content was greatest at the beginning of the drying phase and slowly decreased. The bottom plate insert with the greatest rate of drying was wall 3 with fiberboard sheathing, and although the initial moisture content of the insert in fiberboard-sheathed wall 3 was slightly higher than the other two, the insert reached the lowest moisture content of 20.7% at the end of the test. It is interesting to note that while the initial moisture content of the insert in the plywood-sheathed wall 2 was the same as that in the OSB-sheathed wall 1, the plywood-sheathed wall 2 sample dried to a lower final moisture content of 21.4% compared to that of the OSB-sheathed wall 1 sample of 26.7%. This is likely due to the fact that the vapor permeability of plywood is greater than that of OSB, especially at high relative humidities.

The response of the bottom plate inserts can also be studied by comparing the normalized cumulative mass loss. This parameter allows a direct comparison of the drying response of the sample without taking into account the differences in the initial mass of moisture absorbed by each sample and is calculated as the cumulative moisture

lost at each time step divided by the initial mass of moisture in the sample. Figure 5.30 shows that the normalized cumulative mass loss increases with time for each insert, as anticipated, and is greatest for the fiberboard-sheathed wall 3 insert and lowest for the OSB-sheathed wall 1 insert.

To show the drying rates graphically, curve fitting using polynomial and exponential curves was attempted at first. However, this approach was found to give poor agreement with some of the data series, especially for the data at the beginning of the test. Consequently, a “moving window” approach was adopted. This method consists of finding the linear slope connecting adjacent data points; the derivative at a data point is found by calculating the average of the slopes of the two segments preceding and the two segments following the data point, as shown in Figure 5.31) fiberboard-sheathed walls 3, 6, 9 and 12. Large circles indicated gravimetry in the sheathing, small filled circles. This method is similar to one proposed by Richards (1992) in determining the moisture diffusivity of various porous building materials.

The rate of change of moisture content, or drying rate, versus time, shown using the moving window technique, is shown in Figure 5.32. The graph shows that for all 3 walls, the rate of change of moisture content was greater at the beginning of the drying phase and decreased with time. In the figure, the ordinate is negative, indicating a decreasing moisture content with time. The maximum rate of change of moisture in the bottom plate inserts other than the initial value was greatest in wall 3 at -2.2%-moisture content/day and lowest in the OSB-sheathed wall 1 at -1.0%-moisture content/day.

It should be noted that the initial drying rates, which are typically the highest, are not compared: these rates include drying by evaporation of unbound surface moisture, which may or may not be the same from sample to sample, and therefore does not reflect the drying performance of the bottom plate inserts as a function of the test parameters.

After 35 days of drying, the average rate of change of moisture content was still lower in the wall 1 insert, but the difference was not significant. The average drying rates over the 35-day test were -0.67, -0.85 and -1.01%-moisture content/day in the inserts of 1, 2 and 3, indicating that overall, the inserts in the fiberboard and OSB-sheathed walls experienced the greatest and the lowest rates of drying, respectively.

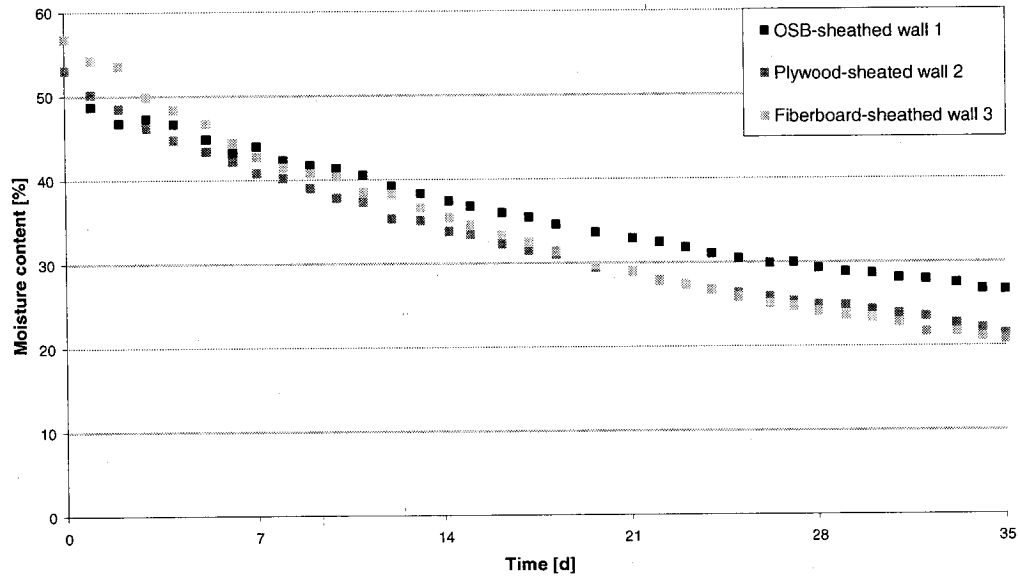


Figure 5.29. Moisture content in the bottom plate inserts versus time for walls 1, 2 and 3 in test 3.

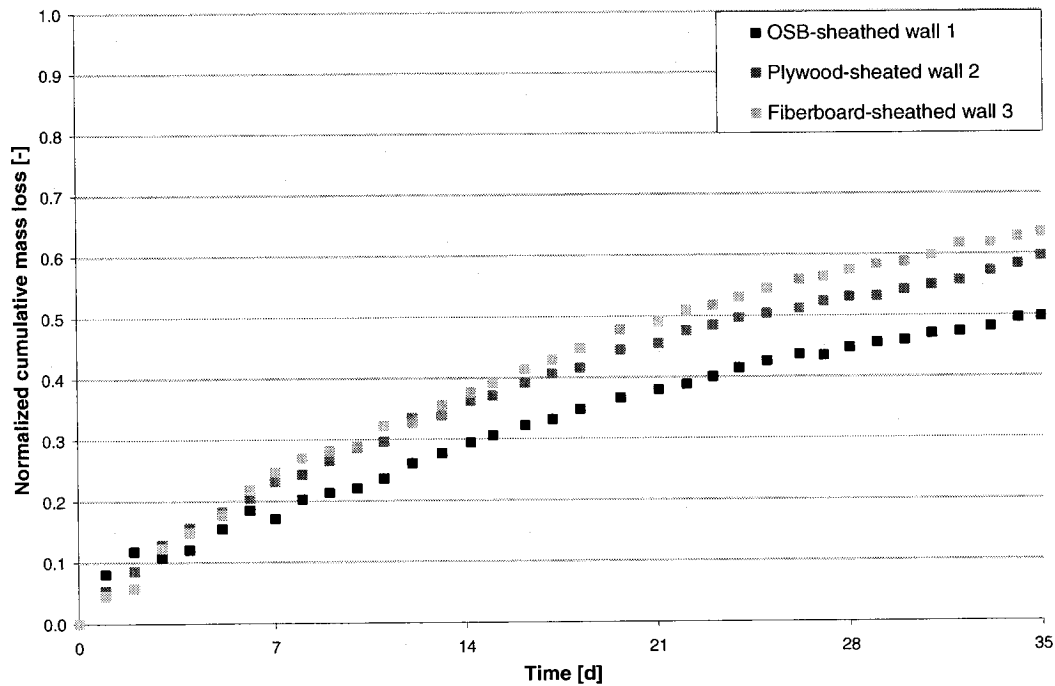


Figure 5.30. Curves of normalized cumulative mass losses with time for the bottom plate inserts in walls 1, 2 and 3 in test 3.

Derivative at $MC(t) = \text{average}(s_{-2}, s_{-1}, s_{+1}, s_{+2})$

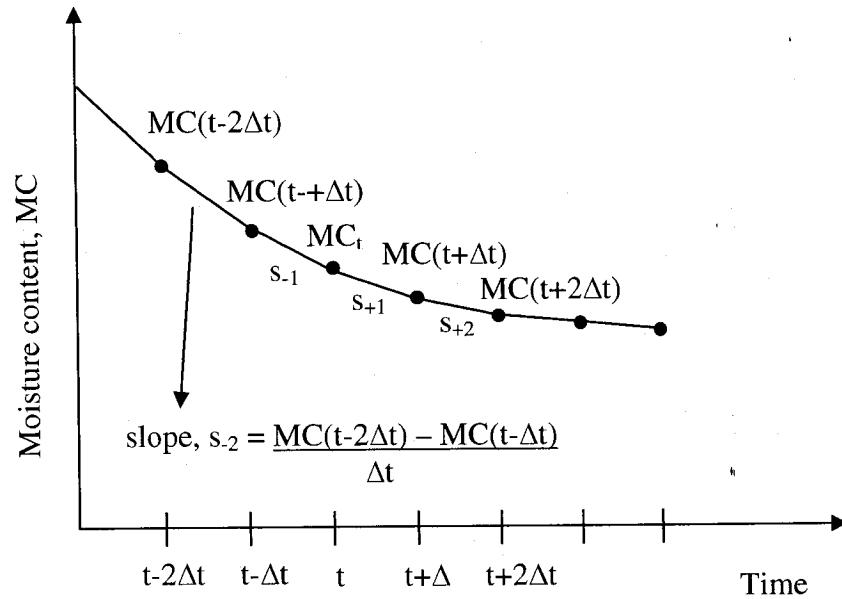


Figure 5.31. Schematic showing the determination of the derivative at point m_t using the moving window approach.

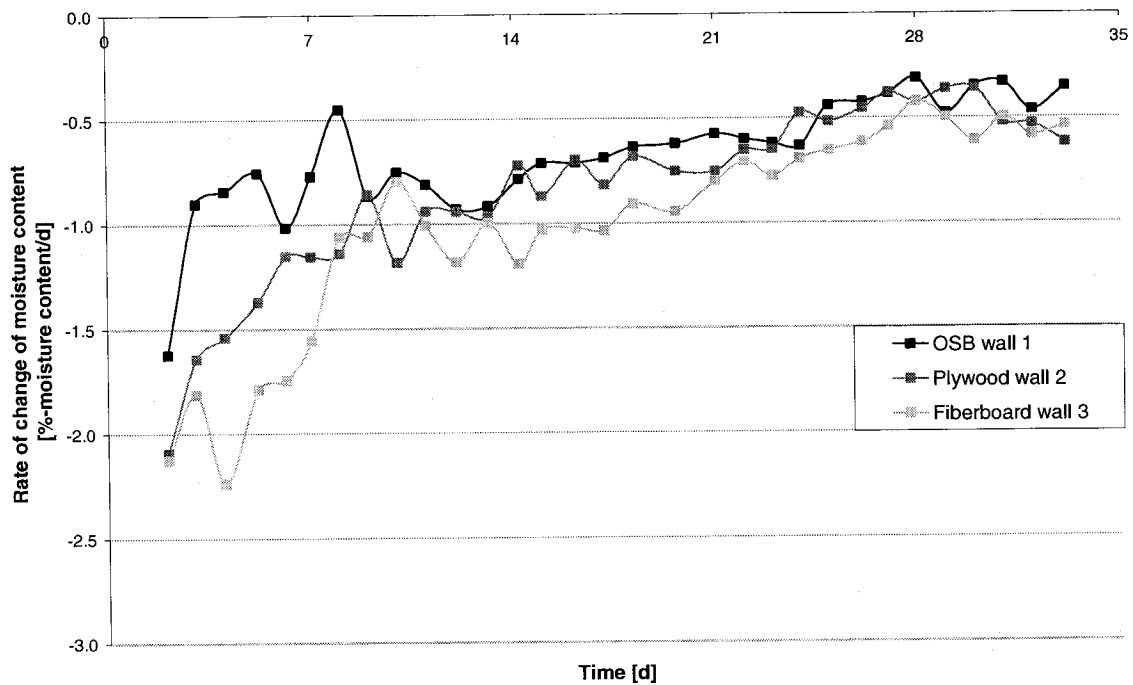


Figure 5.32. Drying rate in the bottom plate inserts versus time for walls 1, 2 and 3 in test 3, found using the moving window technique.

The same form of data analysis was done for the bottom plate inserts for walls 4 to 6, which have the same low permeance primer paint vapor retarder but different sheathings, as shown in Table 5.6. Figure 5.33 shows the moisture content of the bottom plate inserts

for OSB-sheathed wall 4, plywood sheathed wall 5 and asphalt-coated fiberboard-sheathed wall 6. The initial moisture contents varied only slightly from specimen to specimen, representing a total variation of only 2.4% moisture content (see Table 5.29). As was seen in the bottom plate inserts of walls 4 to 6, the unbound water on the surface of the specimen dried out in the first day of the drying phase, reducing the moisture content of the inserts by approximately 2.7% to 3.9% moisture content. Both the moisture content curve and the normalized cumulative mass loss, illustrated in Figure 5.34, confirm that the greatest mass loss occurred in the fiberboard-sheathed wall 6 (see also Table 5.6). The loss of moisture in the inserts of walls 4 and 5 was slower than in wall 6, and there were no significant differences in the response of the inserts in walls 4 and 5. This is confirmed by the average drying rates of the inserts, which were 0.89, 0.91 and 0.96%-moisture content/day in walls 4, 5 and 6 respectively. It is interesting that as the tests enters the second drying phase and the outdoor temperatures increase at day 28, the rate of change of moisture content for the insert in the fiberboard-sheathed wall 6 decreased further, and it reached the lowest moisture content of 17.5%, followed by 21.9% and 22.7% for the samples in the plywood and OSB-sheathed assemblies, respectively.

Figure 5.35 illustrates that the effect of the sheathing properties on the drying rates of the bottom plate inserts were not as significant in this series of walls as they were in walls 1 to 3. At the end of the test, the lowest moisture content was attained by the insert in wall 3 (see Table 5.6). The small differences in the final moisture contents also highlight the small role of the sheathings in the drying response of the insert in walls 4 to 6.

Table 5.6. Initial and final moisture content and moisture content lost in the drying process for the bottom plate inserts of walls 4 to 6 in test 3.

| Wall no. | Sheathing | Initial moisture content [%] | Final moisture content [%] | Decrease in moisture content in drying process [%] |
|----------|---------------------------|------------------------------|----------------------------|--|
| 4 | OSB | 56.0 | 22.7 | 33.3 |
| 5 | Plywood | 54.9 | 21.9 | 33.0 |
| 6 | Asphalt-coated fiberboard | 53.6 | 17.5 | 36.1 |

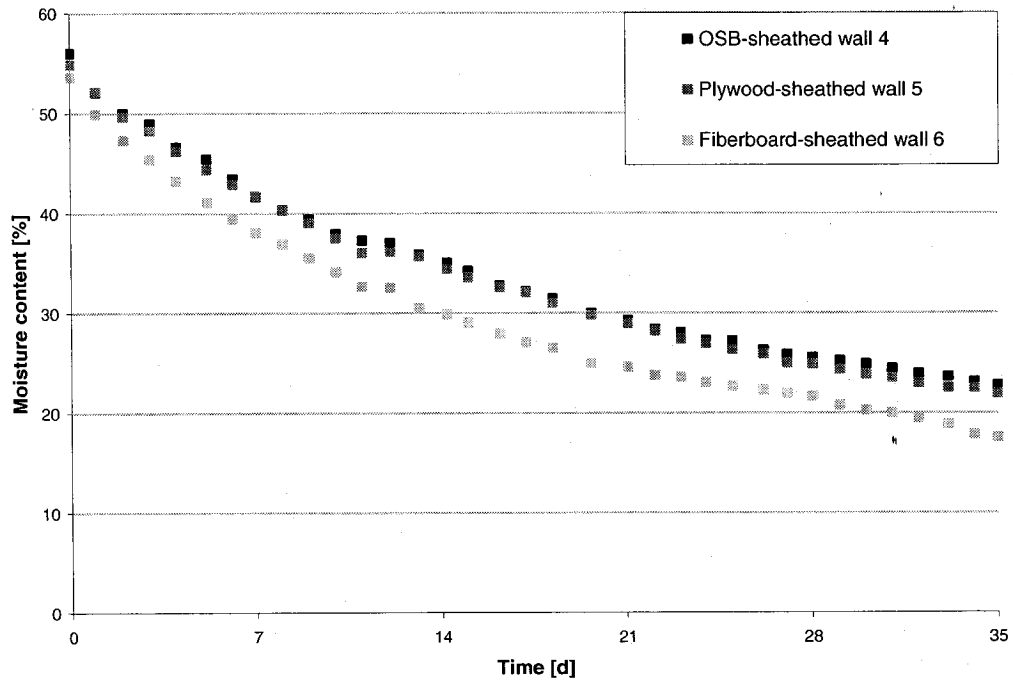


Figure 5.33. Moisture content in the bottom plate inserts versus time for walls 4, 5 and 6 in test 3

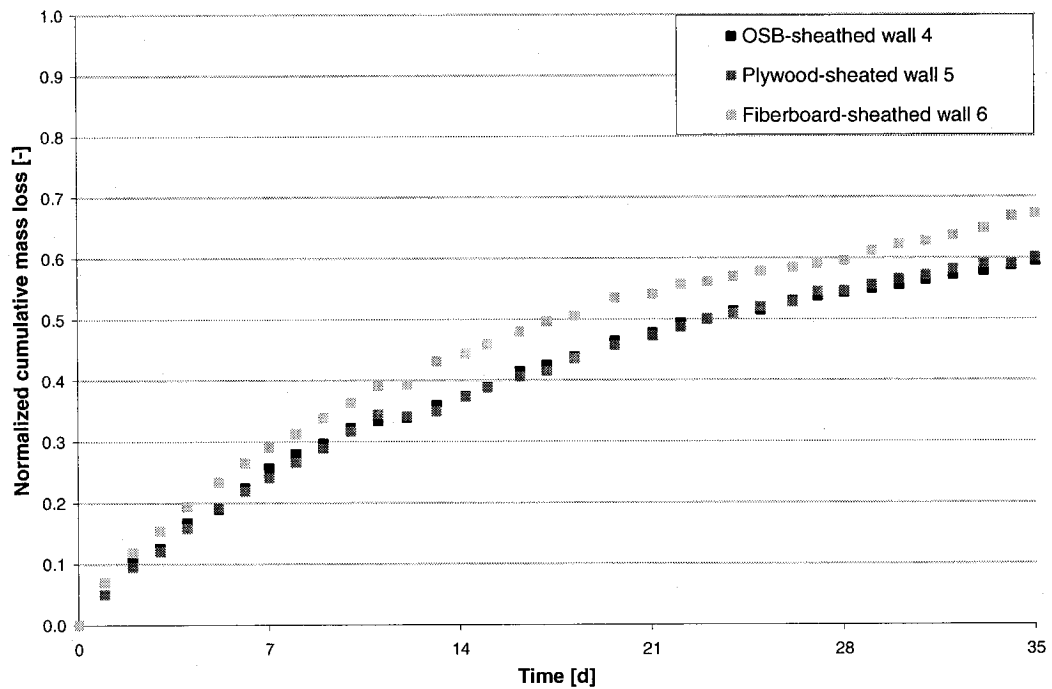


Figure 5.34. Curves of normalized cumulative mass losses with time for the bottom plate inserts in walls 4, 5 and 6 in test 3.

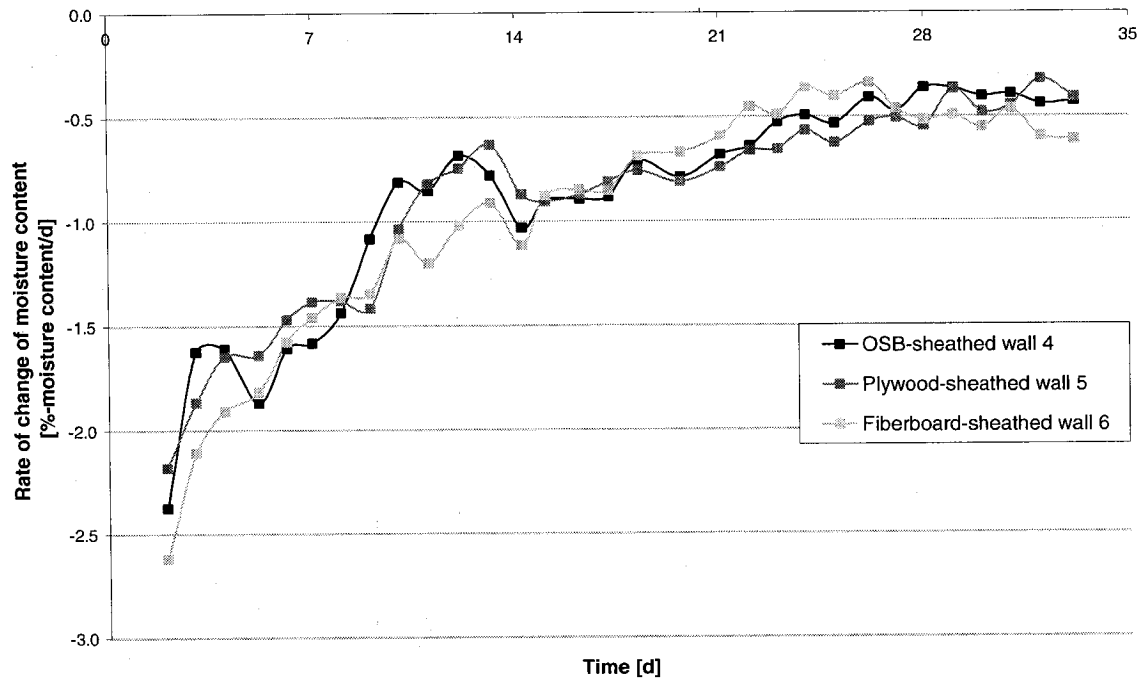


Figure 5.35. Moisture content drying rate in the bottom plate inserts versus time for walls 4, 5 and 6, found using the moving window technique in test 3.

5.4.1.2 Hygrothermal response of the gravimetric specimens Center Horizontal 1

The initial moisture contents of the center horizontal 1 (CH1) samples in walls 1, 2 and 3 were 124.8%, 137.5% and 130.4%, respectively, as shown in Figure 5.36. The location of the CH1 samples is given in section 4.8.2. Given the variation of initial moisture content of 12.7%, comparing the drying response of the specimens should be done with caution. Research has shown that wood specimens with lower initial moisture contents reach lower surface moisture contents faster than specimens with higher initial moisture content, which reduces the drying rates of the former samples because of lower surface hygric conductivities at lower moisture contents. However, in this instance, interestingly enough, the moisture content of all three of the CH1 specimens dropped significantly after just one day and reached about 105% in all three samples. It is suspected that the unbound surface water was not removed from the three samples in the same manner when they were removed from the wetting bath. However, given that their moisture content reached the same level after one day, it is felt that a comparison of their response is possible.

The shape of the moisture content vs. time curves for the CH1 samples is different from that which was found for the large bottom plate insert. Figure 5.36 shows that there was little change in the moisture content of the samples between days 1 to 4 or 5. It is thought that drying trend during this period is due to the boundary conditions surrounding the sample. The top surface of the large bottom plate insert, which was exposed to the fiberglass batt insulation-filled stud cavity, was wet; hence, as the unbound water on the surface of the bottom plate insert evaporated, the relative humidity above the insert in the stud cavity increased, decreasing the vapor drive from the CH1 samples to the stud space and thus decreasing the drying rate. In addition, when a hole was drilled into the bottom plate insert for the placement of sample CH1, the surface of the bottom plate insert was wet; cutting the sample caused moisture on the surface to migrate into the hole to a certain extent. When the sample was placed into the hole, some moisture may have migrated from the sample to the adjacent wood material in the bottom plate; however, this transfer is assumed to be small given the imperfect contact between the rough surfaces of the wood gravimetric sample and the adjacent bottom plate insert.

The drying response of an initially saturated material exposed to constant ambient temperature and relative humidity can be broken down into three drying stages:

- 1) a first drying period where the moisture content decreases at an approximately linear rate with time;
- 2) a second drying period where the drying rate slows down;
- 3) a third stage where the wood in the center dries from fiber saturation point.

The drying in the **first stage** is due to the evaporation of surface moisture from the sample. As drying progresses, the moisture content at the surface decreases and a moisture gradient develops towards the drying surface, initiating liquid moisture flow. During this stage, the drying rate remains constant as long as capillary transport is sufficient to carry liquid to the surface; the average moisture content with time curve is more or less linear, and the slope of the line depends on the boundary conditions just above the drying surface (Hens, 2003; Krus and Holm, 1999). A similar linear trend in the drying moisture content was found in Nabhani *et al.* (2003). As the surface moisture evaporates, heat is absorbed due to latent heat of evaporation and heat of sorption, and the drying specimen's temperature and saturation vapor pressure falls below that in the

ambient atmosphere. In this stage, the heat transfer coefficient at the surface is constant, and surface of the wood behaves like a wet bulb (Nabhani *et al.*, 2003). Small variations in the linear drying trend can occur if the interior or exterior conditions are not constant, which was the case here in test 3.

The moisture content at the surface is said to have become critical when the liquid transported to the surface is not sufficient to maintain the previous drying speed (Krus and Holm, 1999; Hens, 2003). This critical moisture content has been found to be approximately 60% moisture content for wood (Nabhani *et al.*, 2003). Here, the liquid moisture within the pores of the wood no longer has a continuous path to the surface that allows drying. When the wood at the surface has reached reaches the critical moisture content, the mass transfer coefficient decreases due to both the reduction in moisture content at the surface and the change in wood properties at the surface such as roughness and density. The heat transfer coefficient decreases, and at the same time, the surface temperature tends to converge to the dry bulb (Nabhani *et al.*, 2003). The average moisture content in the sample is then called the transition moisture content. In this **second stage**, the dry zone at the surface has reached hygroscopic moisture content, and the liquid diffusivity at the surface becomes zero. A moisture front detaches from the surface and moves into the material. Here, drying by diffusion at the drier zone near the surface controls the drying process for wood (Kollmann and Côté, 1984), with vapor moving within the pores and through the cell walls, and is dependent upon not only the boundary conditions but also the material properties, in particular the vapor permeability. Therefore, the drying rate in the second stage is far smaller than in the first. The second stage of drying continues until the specimen has reached moisture equilibrium with its environment.

In the **third stage**, drying occurs from the center of the wood specimen, slowly decreasing the moisture content from FSP to the equilibrium moisture content for the drying conditions. This is purely a diffusion phenomenon due to the moisture gradients across the wood cell walls (Kollmann and Côté, 1984).

The drying response of the gravimetric samples did not exactly follow the ideal drying scenario described above for a several reasons. The temperature and the ambient vapor pressure in the stud cavity were not constant but varied because of the varying

exterior conditions; in addition, the variation in the vapor pressure in the stud cavity (see Figure 5.37) was due to the release of moisture from the pre-wetted bottom plate insert and gravimetric specimens and also due to the evacuation of the moisture from the stud space to the interior, and even more so, to the exterior of the wall assembly. Nevertheless, the moisture content data for the CH1 samples do show a period where the change in moisture content in time was constant, followed by a period where the moisture loss was significantly reduced.

The drying response of the CH1 samples was analyzed using a line which was fitted to the linear portion of the stage 2 data for each of the three samples. The slope of the line gives the drying rate, which was found to be for -3.8 % moisture content/day wall 1, -6.2 % moisture content/day for wall 2 and -5.8 % moisture content/day for wall 3, the slopes being negative since they represent a loss in moisture content with time. Therefore, the slope of the lines indicate that the greatest rate of drying occurred in the sample within the plywood wall 2, closely followed by that in the fiberboard wall 3. The drying rate of the sample in OSB-sheathed wall 1 was significantly smaller than in the other two walls.

The rate of change of moisture content versus time curves were also found using the moving window method for sample CH1 of walls 1, 2 and 3, and are plotted in Figure 5.38. The graph shows that as expected, all samples experience a high rate of moisture loss at the beginning due to the drying of surface moisture. The drying rates shown in the graph over the first stage confirm those found with the slope of the lines: for the plywood- and fiberboard-sheathed assemblies, the change of rate in moisture content in time are similar and show greater rates of change in moisture content than does the sample in the OSB-sheathed wall from day 3 until day 17; the sample in the plywood wall 2 reaches a peak in rate of moisture loss of 7.1%/day, while the maximum is 6.4 for the specimen in fiberboard-sheathed wall 2 and only 4.5% in OSB-sheathed wall 1 sample. These results are summarized in Table 5.7. After day 17, the trend is reversed and higher rate of moisture loss is seen in the sample in the OSB-sheathed wall. The reversal is likely due to the surface moisture content in the wall 2 and 3 samples reaching the critical moisture content while the average moisture content in sample 1 was still high.

It is interesting to note that towards the end of the drying phase, as the average moisture content in the samples went below the fiber saturation point (FSP), the rate of drying in the sample in the fiberboard-sheathed wall 3 became higher than that in the plywood wall, reaching the lowest final average moisture content (15.2%), followed by the sample in the plywood wall (21.9%) and then the OSB wall (24.7%). This result, and the fact that the vapor pressure in the stud cavity of wall 3 was well below that in walls 1 and 2, is likely due to the high vapor permeability of the asphalt-coated fiberboard sheathing.

Table 5.7. Initial and final moisture contents, drying rate during the period of constant drying, and peak drying rate in the center horizontal 1 (CH1) specimens in walls 1, 2 and 3 in test 3. The highest drying rates are indicated in bold.

| Wall no. | Sheathing material | Initial moisture content [%] | Final moisture content [%] | Period of constant drying rate [%/day] | Peak drying rate [%/day] |
|----------|---------------------------|------------------------------|----------------------------|--|--------------------------|
| 1 | OSB | 124.8 | 24.7 | -3.8 | -4.5 |
| 2 | Plywood | 137.5 | 21.9 | -6.2 | -7.1 |
| 3 | Asphalt-coated fiberboard | 130.4 | 15.2 | -5.8 | -6.4 |

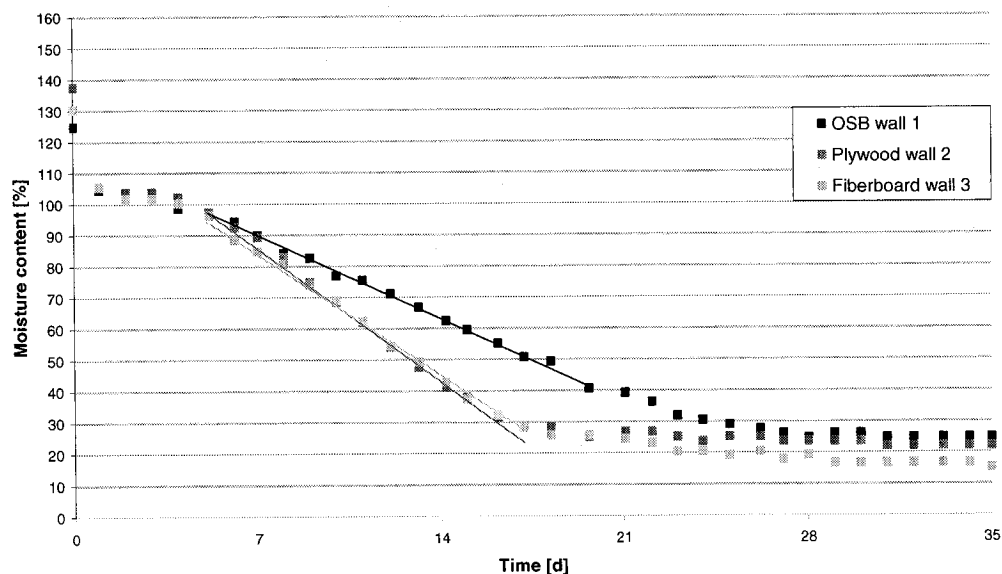


Figure 5.36. Moisture content with time of samples CH1 in OSB-sheathed walls 1, 2 and 3 in test 3. The figure also shows the fitted lines during the first stage of drying, indicating the rates of constant decreasing moisture content for each data series.

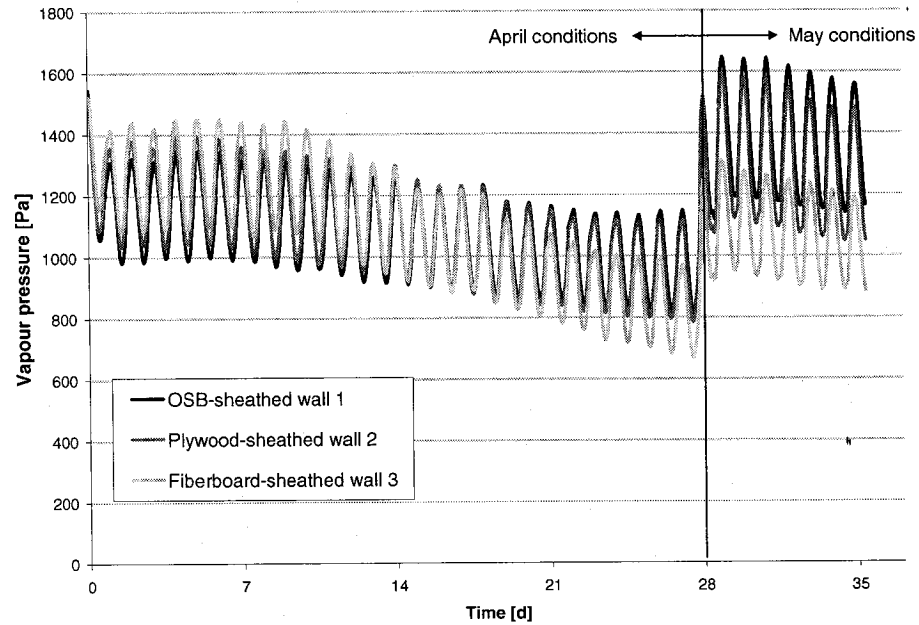


Figure 5.37. Vapor pressure with time in the stud cavity of walls 1, 2 and 3 at approximately 150 mm above the bottom plate inserts in test 3.

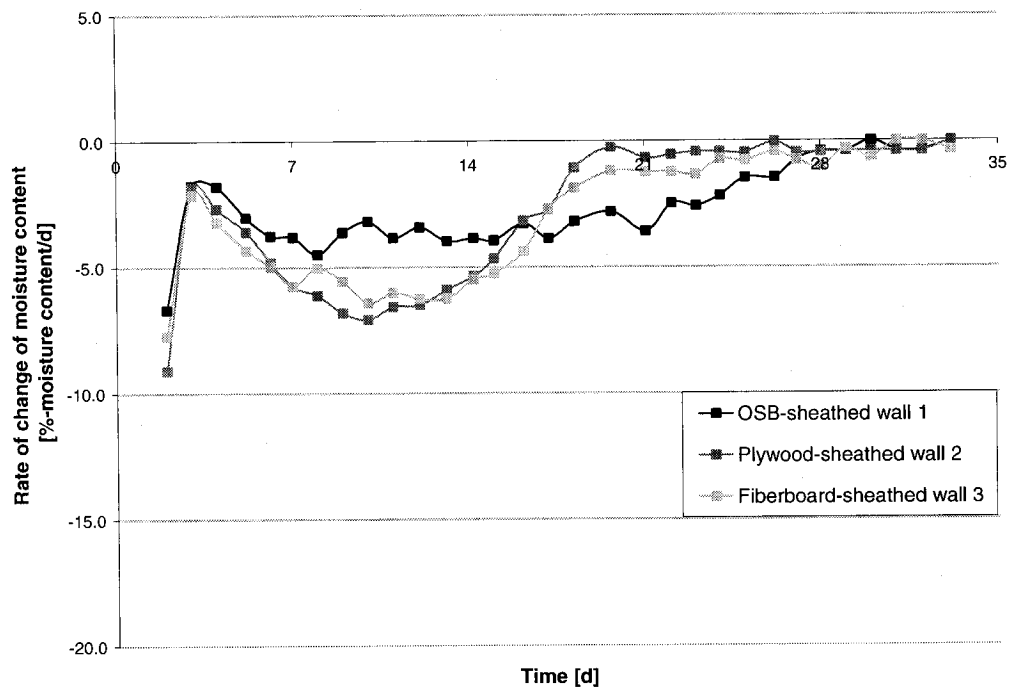


Figure 5.38. Rate of change of moisture content for samples CH1 in walls 1, 2 and 3 in test 3, found using the moving window technique.

The same treatment of data is now performed for the CH1 gravimetric samples in walls 4, 5 and 6. These three walls all have low permeance primer paint as the vapor

retarder, but different sheathing. The initial moisture content of the CH1 samples is 146.8% for the sample in OSB-sheathed wall 4, 119.9% in plywood-sheathed wall 5 and 145.3% in the sample in fiberboard-sheathed wall 6. Given the large difference in the initial moisture content of the wall 2 sample, a comparison of its drying response to that in the other samples is not possible because the moisture content at the start likely affects its subsequent drying performance. However, since the moisture content in the wall 4 and 6 samples are comparable, an analysis is conducted for these.

The samples experience significant drying in the first day and the greatest moisture loss is seen in the sample found in the fiberboard wall at a 27.4% reduction in moisture content), while the smallest moisture loss is found in the sample in the OSB-sheathed wall at a 21% decrease in moisture content. As in the CH1 samples in walls 1-3, the samples in assemblies 4 and 6 experience a slow drying rate after the first day for 4 to 5 days into the test; in the first drying stage, the slope of the moisture content vs. time graph (see Figure 5.39) shows a significant difference in the drying rates during the period of constant drying, with the greatest rate of change in moisture content in fiberboard-sheathed wall 6 sample at -9.4 % moisture content/day, compared to -7.1 % moisture content/day in the OSB-sheathed wall 4 sample. Figure 5.40 and Table 5.8 shows that the peak rate of change of moisture content (not including the initial peak) is also much higher in the sample in the fiberboard-sheathed wall 6, at -10.7%-moisture content/day, compared to -7.6%-moisture content/day for the wall 4 sample. It is interesting that although the wall 4 and wall 6 specimens had similar average initial moisture contents, the wall 6 sample dried significantly faster, reaching the second stage of drying in 16 days compared to about 20 days for the sample in wall 1. Also, while the initial moisture content of the fiberboard-sheathed wall sample was significantly higher than that of that in the plywood-sheathed wall 5, the final moisture content of the former was lower. After three weeks of drying, the drying rates leveled off for all three samples, with the fiberboard wall 3 sample attaining the lowest moisture content of 16.7%, followed by the plywood-sheathed wall 2 sample at 19.4% and finally the OSB-sheathed wall 1 sample at 22.0%.

Table 5.8. Initial and final moisture contents, drying rate during the period of constant drying, and peak drying rate in the center horizontal 1 (CH1) specimens in walls 4, 5 and 6 in test 3. The highest drying rates are indicated in bold. The cells in the table of the samples whose initial moisture content differed significantly from that of the others are shaded in grey.

| Wall no. | Sheathing material | Initial moisture content [%] | Final moisture content [%] | Period of constant drying rate [%/day] | Peak drying rate [%/day] |
|----------|---------------------------|------------------------------|----------------------------|--|--------------------------|
| 4 | OSB | 146.8 | 22.0 | -7.1 | -7.6 |
| 5 | Plywood | 119.9 | 19.4 | -5.7 | -6.3 |
| 6 | Asphalt-coated fiberboard | 145.3 | 16.7 | -9.4 | -10.7 |

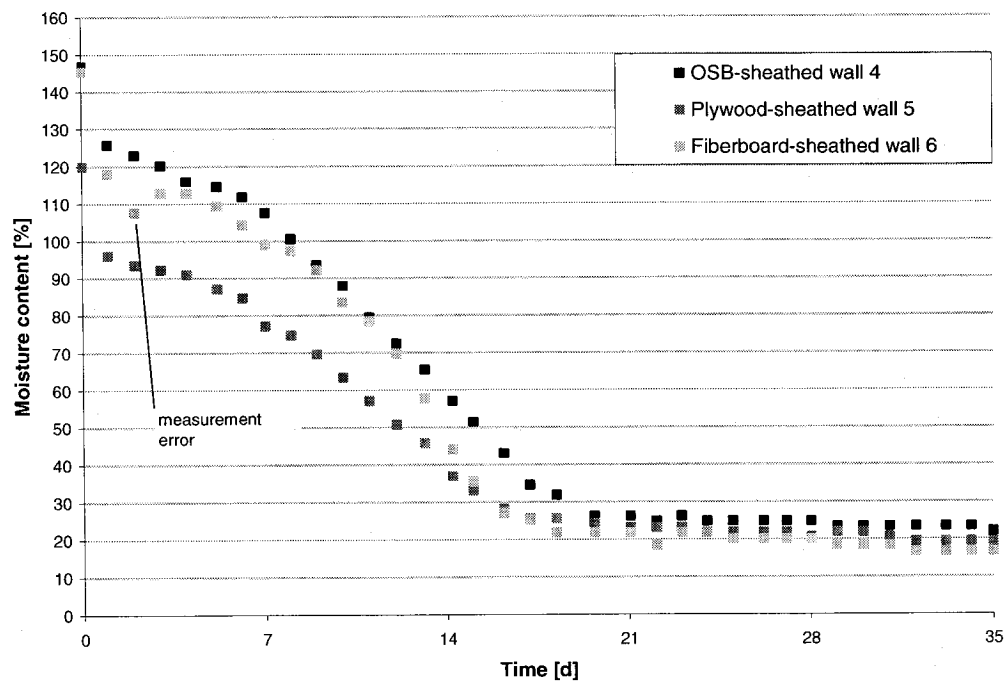


Figure 5.39. Moisture content with time of samples CH1 in walls 4, 5 and 6 in test 3.

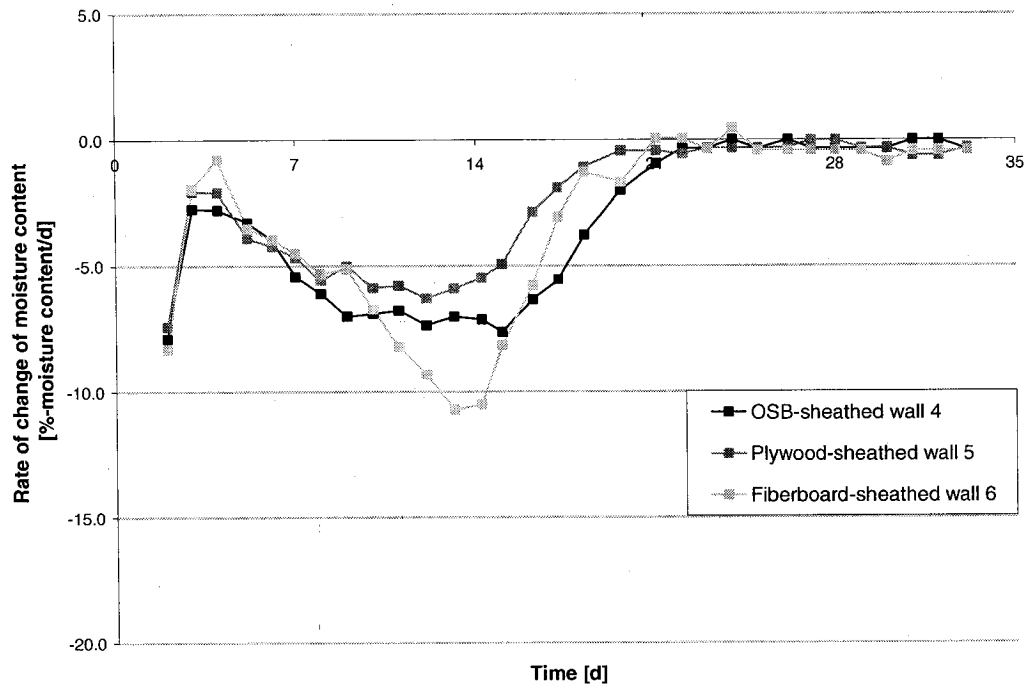


Figure 5.40. Rate of change of moisture content for samples CH1 in walls 4, 5 and 6 in test 3.

5.4.1.3 Hygrothermal response of the gravimetric specimens Center Horizontal 2

The initial moisture content of center horizontal 2 (CH2) samples varied at 126.4% for the sample in the OSB-sheathed wall 1, 135.3% in the plywood-sheathed wall 2 and 138.0% for the fiberboard wall 3 (see Table 5.9). Therefore, a comparison of the responses of the samples in walls 2 and 3 can readily be made, but including the wall 1 sample in the analysis should be done with caution. The location of the CH2 samples is given in section 4.8.2.

The general shape of the moisture content versus time curves for the center horizontal 2 (CH2) samples is different than that for samples CH1, as shown in Figure 5.41. The initial “plateau” that was seen in the CH1 drying curves is absent, likely because the CH2 samples, being closer to the interior gypsum, are exposed to a higher temperature than the CH1 samples and the moisture in the adjacent bottom plate insert dried more rapidly, thus favoring faster drying of the sample itself. As in the CH1 samples, there is a substantial drop in the moisture content after one day of drying, and with the wall 2 sample experiencing the greatest drop at 18.4% moisture content, followed by 24.1% in the wall

3 sample and 18.7% in the wall 1 sample.

It is interesting to note that by the end of the first drying stage, i.e. at day 11 to 12, the moisture content in the plywood-sheathed wall 2 sample was greater than that in the fiberboard-sheathed wall 3 sample. This response is not anticipated, especially given that the vapor resistance of fiberboard is lower than that of plywood. To explain the response, the measured relative humidity in the stud cavity 50 mm above the bottom plate at mid-depth of the insulation is examined. Figure 5.42 shows that the relative humidity in the stud cavity after the insertion of the wetted bottom plate quickly increased in all three walls, as expected. However, the relative humidity in the stud cavity was approximately 12% higher in the fiberboard-sheathed wall than in the other two stud cavities. This finding can be explained as follows: moisture evaporation from the bottom plate inserts raised the relative humidity inside the stud cavities. The outdoor conditions, which varied sinusoidally on a daily basis between approximately 2°C and 11°C, decreased the temperature at the interior surface of the sheathing above the bottom plate insert below the dewpoint, thus causing condensation (RH = 100%) on the interior surface of the sheathing (Figure 5.43). The water absorption of the three materials is not the same. Material testing performed by Kumaran *et al.* (2002b) indicates that of the three sheathings, asphalt-coated fiberboard has the lowest water absorption coefficient and plywood has the highest, as shown in Table 5.10 below. Since the water absorption coefficient of the asphalt-coated fiberboard sheathing is lower than that of OSB and plywood, the condensate was absorbed more readily by the latter sheathings, while in the fiberboard wall, the condensate remained on the inside surface of the sheathing, raising the relative humidity of the stud cavity of this wall relative to that of the other two walls. It is for this reason that the drying rate of the wall 3 sample was slower than in the other two walls. The relative humidity graph in Figure 5.43 also shows that although the stud cavity relative humidity in wall 3 reached the highest peak by far, it also decreased at a faster rate and reached a final value of about 59% compared to 70% in the plywood-sheathed wall 2 and 77% in the OBS-sheathed wall 1.

At day 12, the average moisture content in all three CH2 samples was about the same at 22-24%. The final moisture contents in the samples at the end of the test were 15.2%, 13.5%, and 13.6% in walls 1, 2 and 3, respectively, the slightly higher moisture content

in wall 1 likely due to the higher relative humidity in the stud cavity in the OSB-sheathed wall at the end of the test.

The rate of change of moisture content, was found using the moving window method (see Figure 5.44). The constant stage 1 drying rates show that the greatest drying rate was observed in wall 2 at -13.7 % moisture content/day, followed by that in wall 1 at -11.8% moisture content/day and finally by that of wall 3 at -10.8% moisture content/day. It should also be noted that while the initial moisture content of wall 3's sample was the greatest, it dried to the about the same final moisture content as that in wall 2. The wall 1 sample had a final moisture content approximately 1.6% higher than that in the other two walls.

Table 5.9. Initial and final moisture contents, drying rate during the period of constant drying, and peak drying rate in the center horizontal 2 (CH2) specimens in walls 1, 2 and 3 in test 3. The highest drying rates are indicated in bold. The cells in the table of the samples whose initial moisture content differed significantly from that of the others are shaded in grey.

| Wall no. | Sheathing material | Initial moisture content [%] | Final moisture content [%] | Period of constant drying rate [%/day] | Peak drying rate [%/day] |
|----------|---------------------------|------------------------------|----------------------------|--|--------------------------|
| 1 | OSB | 126.4 | 15.2 | -10.6 | -11.8 |
| 2 | Plywood | 135.3 | 13.5 | -13.2 | -13.7 |
| 3 | Asphalt-coated fiberboard | 138.0 | 13.6 | -9.7 | -10.8 |

Table 5.10. Water absorption coefficients across the major surface for three OSB samples, three plywood samples, and one asphalt-coated wood fiberboard sample (Kumaran *et al.*, 2002b).

| Sheathing materials | Water absorption coefficient [kg/m ² s ^{1/2}] | | |
|--------------------------------|--|----------|----------|
| | Sample 1 | Sample 2 | Sample 3 |
| OSB | 0.0016 | 0.0016 | 0.0022 |
| Plywood | 0.0037 | 0.0042 | 0.0031 |
| Asphalt-coated wood fiberboard | 0.00094 | - | - |

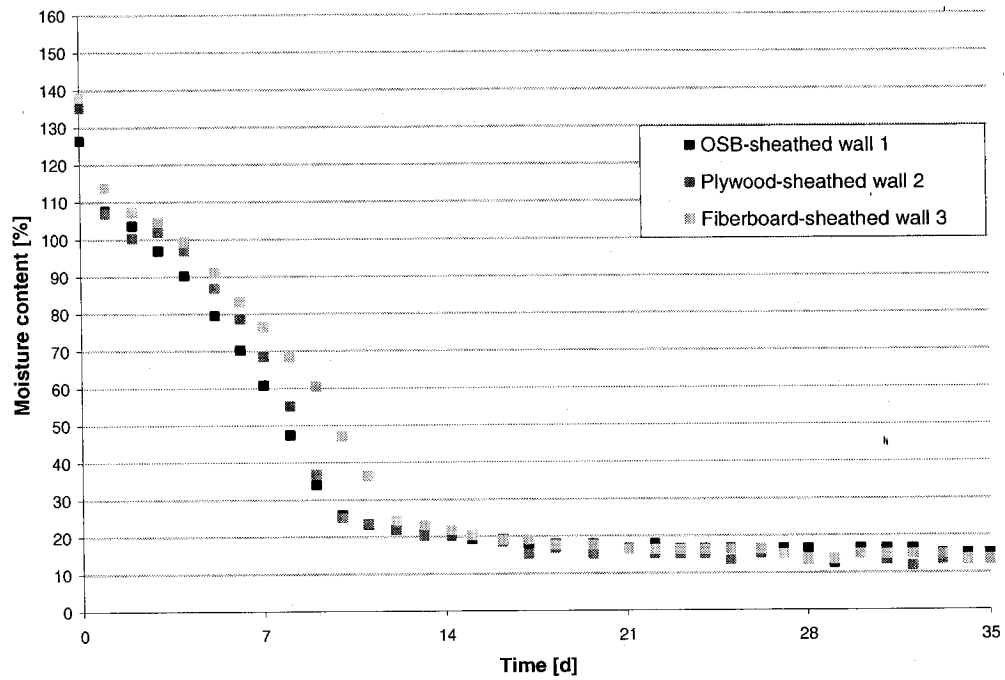


Figure 5.41. Moisture content with time of samples CH2 in walls 1, 2 and 3 in test 3.

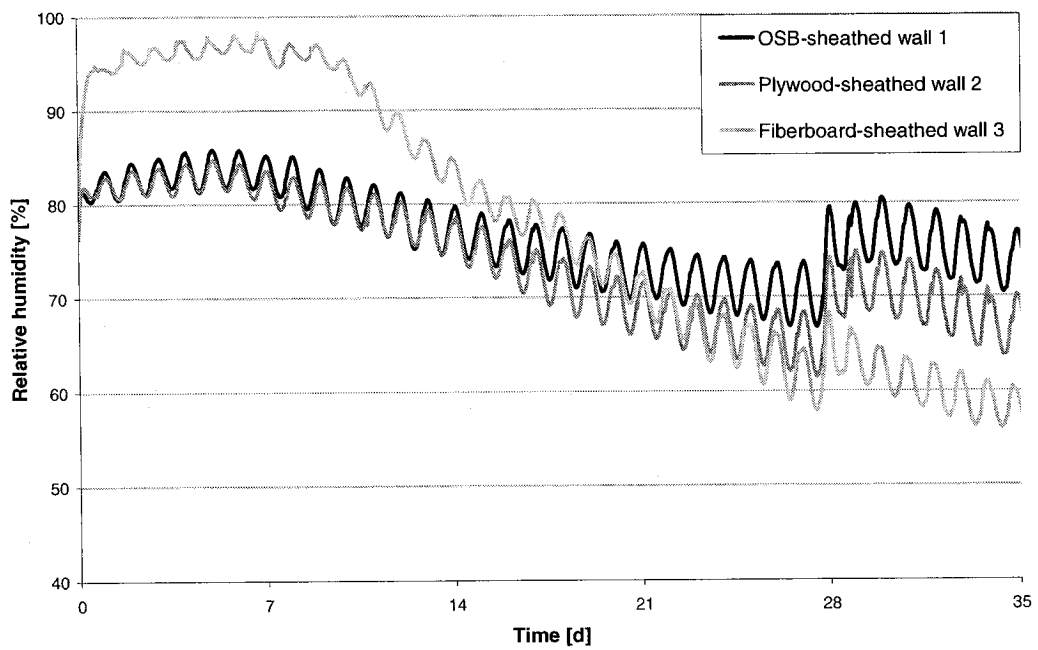


Figure 5.42. Measured relative humidity in the stud cavity of walls 1, 2 and 3 from test 3 at approximately 50 mm above the center of the bottom plate insert.

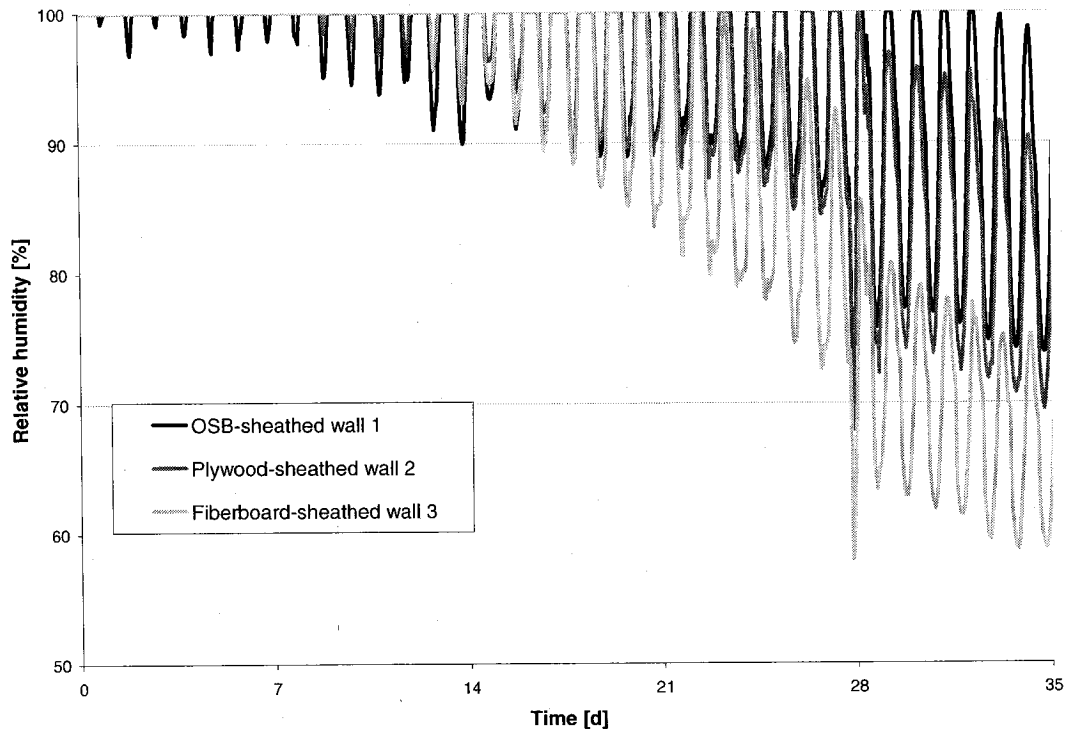


Figure 5.43. Calculated relative humidity in the stud cavity of walls 1, 2 and 3 from test 3 on the interior surface of the sheathing at approximately 50 mm above the center of the bottom plate insert.

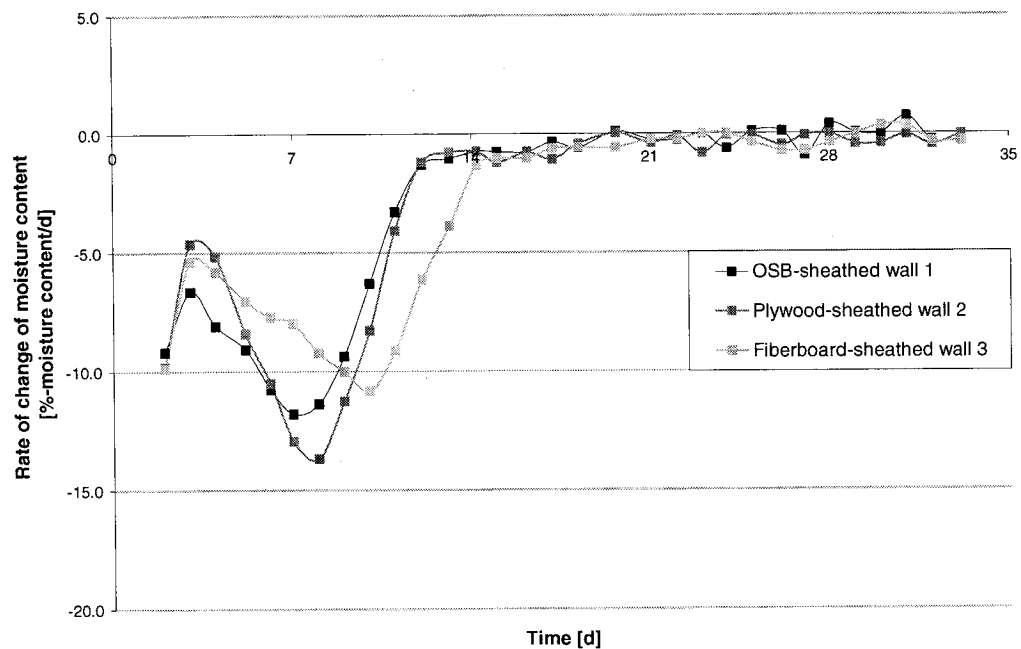


Figure 5.44. Rate of change of moisture content for samples CH2 in OSB wall 1, plywood wall 2 and fiberboard wall 3 in test 3 found using the moving window technique.

A similar data analysis is performed for the CH2 samples in walls 4 to 6. The initially high initial moisture content in the wall 2 sample precludes direct comparison of its hygrothermal response with that of the other two samples (see Table 5.11). The moisture loss after one day of drying is significantly greater in the sample from the fiberboard-sheathed wall 6 at 21.7% moisture content, compared to only 14.8% in the OSB-sheathed wall. In the wall 4 sample, the drying is slow in the first few days, as shown by the “plateau” observed in Figure 5.45 and in the comparatively small drying rate seen at day 3 in Figure 5.46. However, the drying curve for the sample in fiberboard-sheathed wall 6 shows no such “plateau” and the sample dries the faster, which is attributable to the significantly higher water vapor permeability of fiberboard. Experiments performed by Kumaran *et al.* (2002b) on three samples of each OSB and plywood and one sample of asphalt-coated fiberboard found that the water vapor permeance of fiberboard is approximately 2.5 to 6.5 times that of OSB at a relative humidity of 100%, with the ratio increasing with decreasing relative humidity (see Figure 5.47). Also, the average moisture content in the wall 6 sample reached the second stage of drying in less than five days, whereas the sample in walls 4 required about 9 days to reach that moisture content.

It is interesting that the samples in the OSB-sheathed wall 4 and plywood-sheathed wall 5 reached the same moisture content at day 10 despite the greater initial moisture content of the wall 5 sample, which was initially 18.2% greater. At the end of the test, all three samples dried to a moisture content of about 13%.

Table 5.11. Initial and final moisture contents, drying rate during the period of constant drying, and peak drying rate in the center horizontal 2 (CH2) specimens in walls 4, 5 and 6 in test 3. The highest drying rates are indicated in bold. The cells in the table of the samples whose initial moisture content differed significantly from that of the others are shaded in grey.

| Wall no. | Sheathing material | Initial moisture content [%] | Final moisture content [%] | Period of constant drying rate [%/day] | Peak drying rate [%/day] |
|----------|---------------------------|------------------------------|----------------------------|--|--------------------------|
| 4 | OSB | 112.4 | 13.6 | -16.2 | -14.3 |
| 5 | Plywood | 130.6 | 13.3 | -14.2 | -14.0 |
| 6 | Asphalt-coated fiberboard | 118.5 | 13.1 | -20.6 | -17.4 |

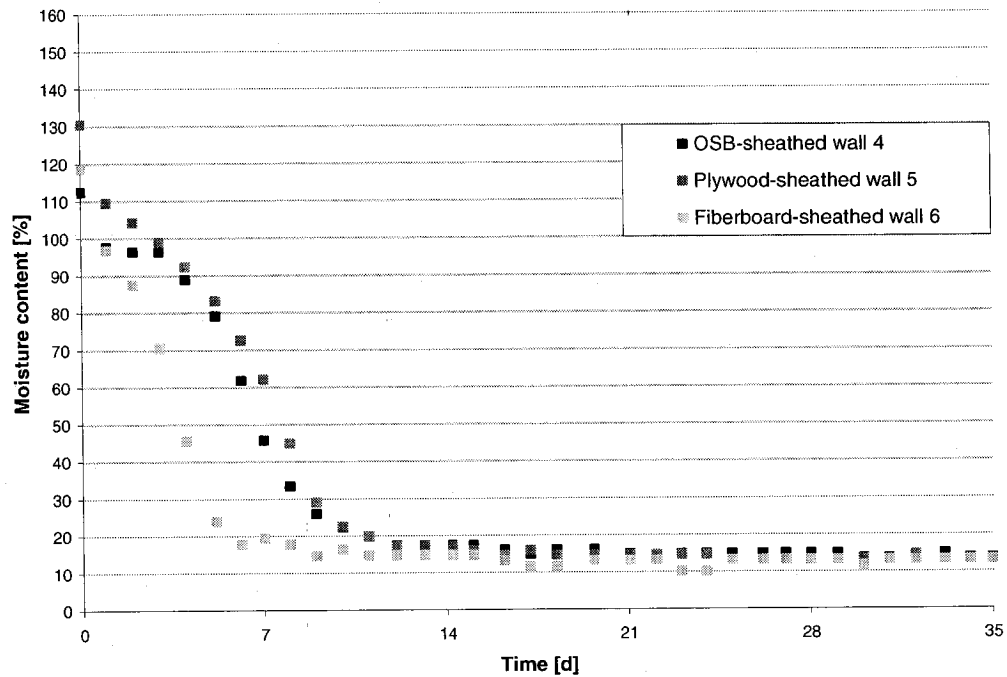


Figure 5.45. Moisture content with time of samples CH2 in OSB-sheathed wall 4, plywood-sheathed wall 5 and fiberboard-sheathed wall 6 in test 3.

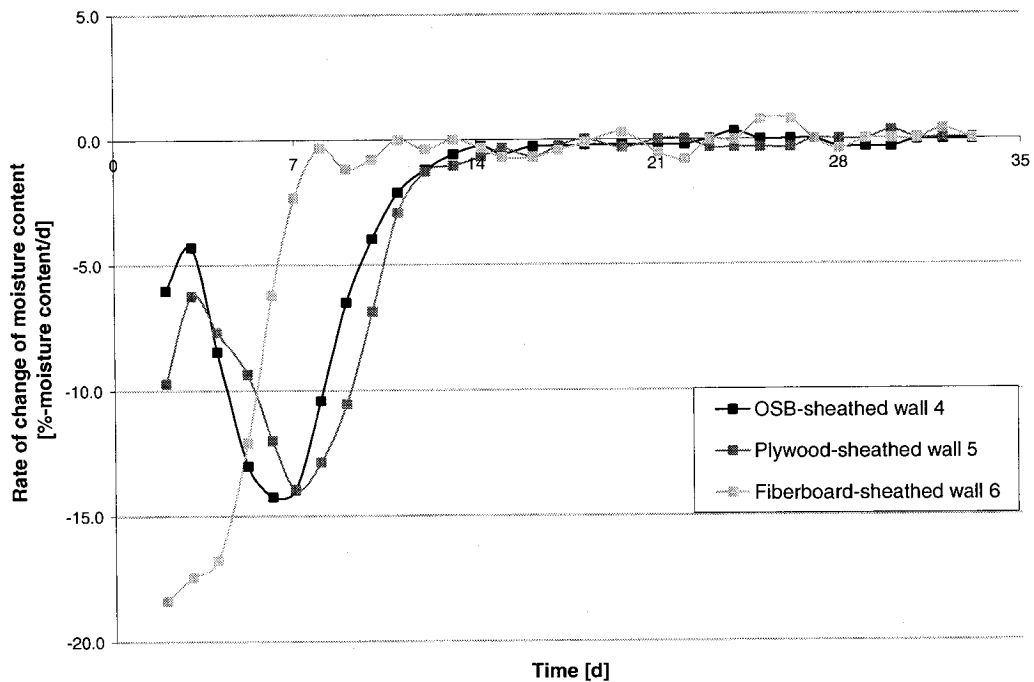


Figure 5.46. Rate of change of moisture content for samples CH2 in walls 4, 5 and 6 from test 3, found using the moving window technique.

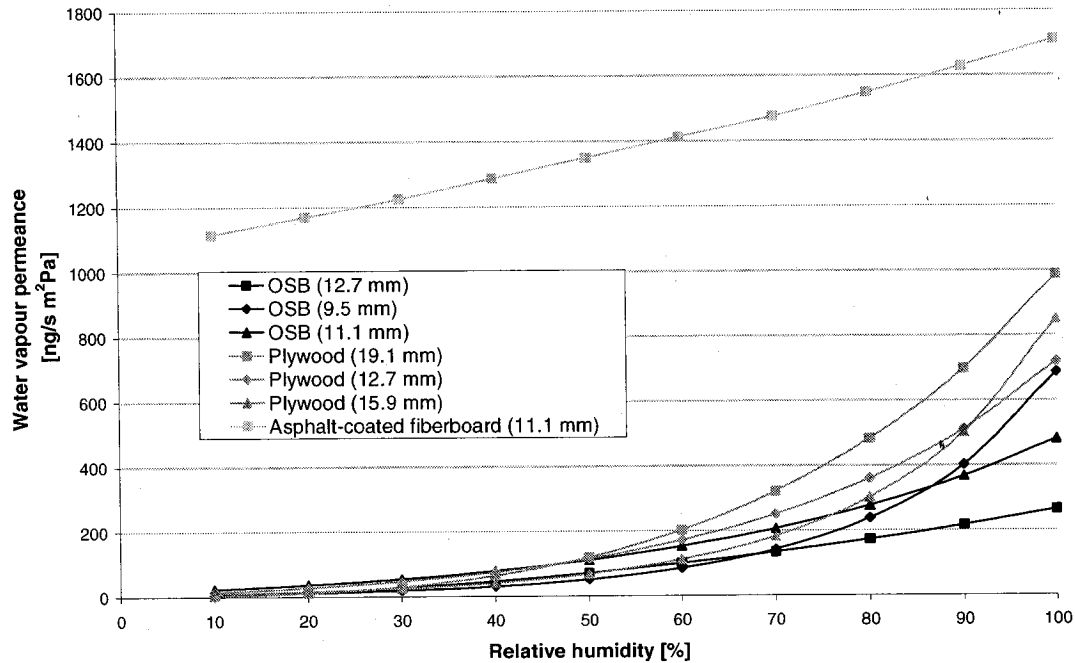


Figure 5.47. Water vapor permeance in OSB, plywood and asphalt-coated fiberboard (data extracted from Kumaran *et al.*, 2002b).

5.4.1.4 Hygrothermal response of the gravimetric specimens Center Vertical

Unlike specimens CH1 and CH2, the center vertical (CV) gravimetric samples were installed in a hole drilled on the vertical surface of the bottom plate insert and faced the sheathing board. Therefore, also unlike the other two samples, the CV samples were not exposed to the conditions in the stud cavity, and their response can be directly linked to that of the sheathing.

There was a significant difference in the initial moisture contents of the CV samples in walls 1 to 3, ranging from 152.9%, 119.6% and 152.2% in walls 1, 2 and 3, respectively, as shown in Figure 5.48 and Table 5.12; therefore, only the performance of the wall 1 and wall 3 samples is investigated.

The greatest loss in moisture after the first day of drying occurs in the sample in the fiberboard wall at 30.5%, while it was significantly lower in the OSB wall at 24.4% and the sample in the plywood wall is the lowest at 23.7%. The initial “plateaus” that were seen in the moisture content with time curves of samples CH1 are observed here in the sample in OSB wall 1 for a duration of 4 days; however, the plateau does not occur in the

wall 3 sample. Since the initial drying is a function of the conditions at the surface of the specimen, as was explained previously, the difference in behavior may be due to the greater water vapor permeability of the asphalt-coated sheathing compared to the OSB sheathing which permits greater drying capability. Hence, the greater water vapor permeability of the asphalt-coated fiberboard promoted the drying of the CV specimen in wall 3.

The samples in the OSB wall 1 and the fiberboard wall 3 both started at the same initial moisture content. However, the moisture content in the fiberboard sample decreased at a much faster rate, as shown in Figures 5.48 and 5.49, and this continued until for the first 13 days until sample the second stage of drying. This result is confirmed by the slope of the line during the first stage of drying (Figure 5.49 and Table 5.12): wall 3 has the greatest slope by far, at -6.4% moisture content/day, compared to that in wall 1 at -4.2% moisture content/day in wall 1. In addition, sample 3 took 20 days to reach the second drying stage, while sample 1 required 29 days.

The CV sample in plywood-sheathed wall 2 started with a lower moisture content of about 120% and decreased to 95.9% after the first day. It is interesting that despite the differences in initial moisture content, the sample in the fiberboard wall reached the same moisture content as that in the plywood-sheathed wall 18 days after the start of the test. The specimen in the fiberboard-sheathed wall dried to the lowest moisture content of all three samples at 15.1%, followed by 21.6% for the sample in the plywood wall and 27.3 for the sample in the OSB-sheathed wall.

Table 5.12. Initial and final moisture contents, drying rate during the period of constant drying, and peak drying rate in the center vertical (CV) specimens in walls 1, 2 and 3 from test 3. The highest drying rates are indicated in bold. The cells in the table of the samples whose initial moisture content differed significantly from that of the others are shaded in grey.

| Wall no. | Sheathing material | Initial moisture content [%] | Final moisture content [%] | Period of constant drying rate [%/day] | Peak drying rate [%/day] |
|----------|---------------------------|------------------------------|----------------------------|--|--------------------------|
| 1 | OSB | 152.9 | 27.3 | -4.2 | -5.0 |
| 2 | Plywood | 119.6 | 21.6 | -6.1 | -6.5 |
| 3 | Asphalt-coated fiberboard | 152.2 | 15.1 | -6.4 | -7.3 |

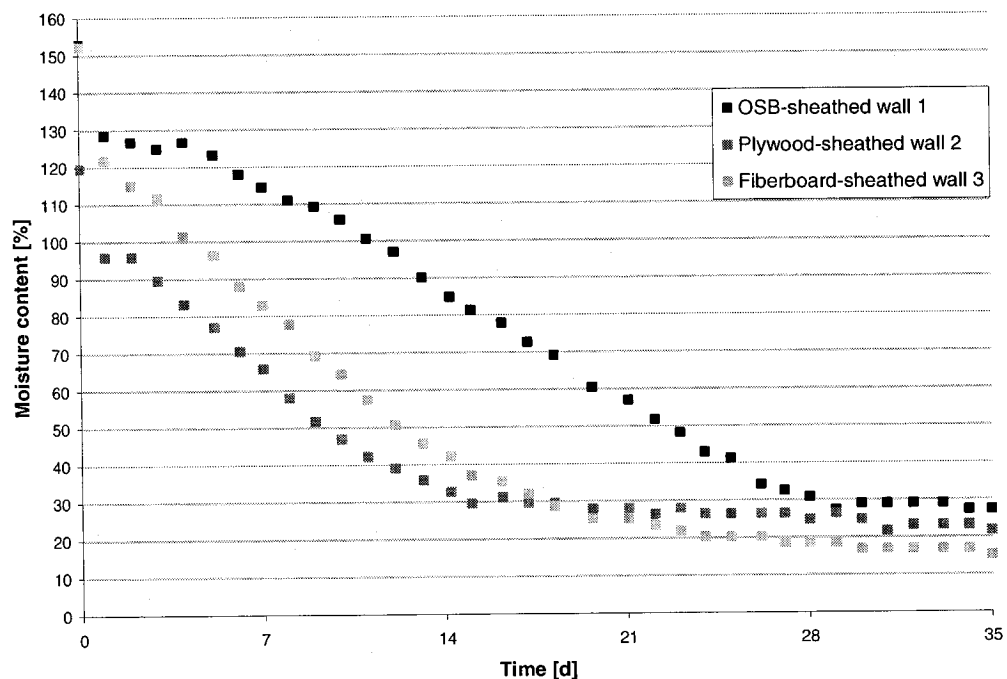


Figure 5.48. Moisture content with time of samples CV in walls 1, 2 and 3 from test 3.

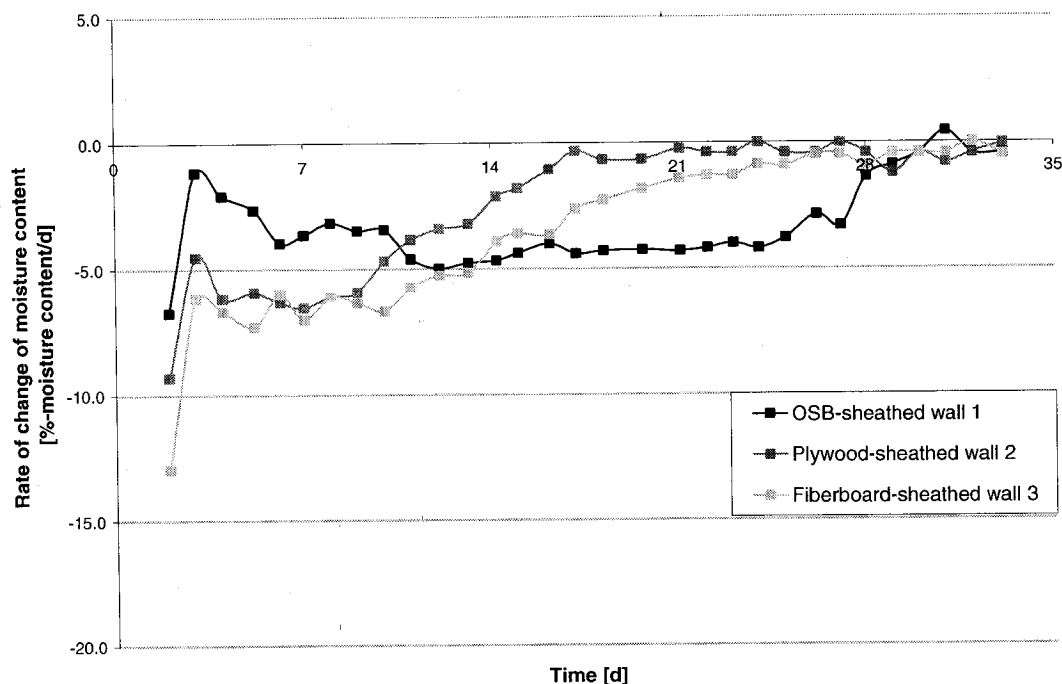


Figure 5.49. Rate of change of moisture content for samples CV in walls 1, 2 and 3 in test 3, found using the moving window technique.

In walls 4 to 6, the initial moisture contents in the CV samples, shown in Table 5.13 varied by 13.4%. However, as Figure 5.50 illustrates, this difference was reduced to 3.7% after one day, and therefore, as was the case with the wall 1-3 CH1 samples, it is felt that a performance comparison of all three samples is appropriate.

It is clear from Figures 5.50 and 5.51 that the sample in the fiberboard wall 6 dried at a significantly greater rate at the beginning of the test, with an average constant drying rate of -9.8% moisture content/day, compared to a rate of -5.5% moisture content/day for the wall 5 sample and -4.5% moisture content/day for the wall 4 sample. The peak drying rate was also significantly higher in the wall 6 sample (see Table 5.13). The average moisture content in sample 6 reached the second drying stage at day 11 whereas this occurred at days 20 and 24 for the plywood and OSB-sheathed wall 5 and 6 samples, respectively; the CV specimen in wall 6 reached the lowest moisture content by far at the end of the test (see Figure 5.50 and Table 5.13).

The drying rate with time curves in Figure 5.51, found using the moving window technique, show that the drying rates were greater in the fiberboard-sheathed wall 6 sample up to the 11th day of drying; as the moisture content in the sample reached the

second stage of drying, the rate of drying significantly decreased. The same general trend can be seen in the wall 5 sample, which did not reach the second drying stage until about day 18.

There is a significant difference in the final average moisture content of the three samples: 25.7% in wall 1, 32.6% in wall 2 and 15.8% in wall 3. The data discussed herein all show that the positive effect of the water vapor permeability of the sheathing on the drying response of the adjacent materials.

Table 5.13. Initial and final moisture contents, drying rate during the period of constant drying, and peak drying rate in the center vertical (CV) specimens in walls 4, 5 and 6 from test 3. The highest drying rates are indicated in bold.

| Wall no. | Sheathing material | Initial moisture content [%] | Final moisture content [%] | Period of constant drying rate [%/day] | Peak drying rate [%/day] |
|----------|---------------------------|------------------------------|----------------------------|--|--------------------------|
| 4 | OSB | 142.2 | 25.7 | -4.5 | -5.1 |
| 5 | Plywood | 128.1 | 21.6 | -5.5 | -6.0 |
| 6 | Asphalt-coated fiberboard | 131.5 | 15.8 | -9.8 | -10.0 |

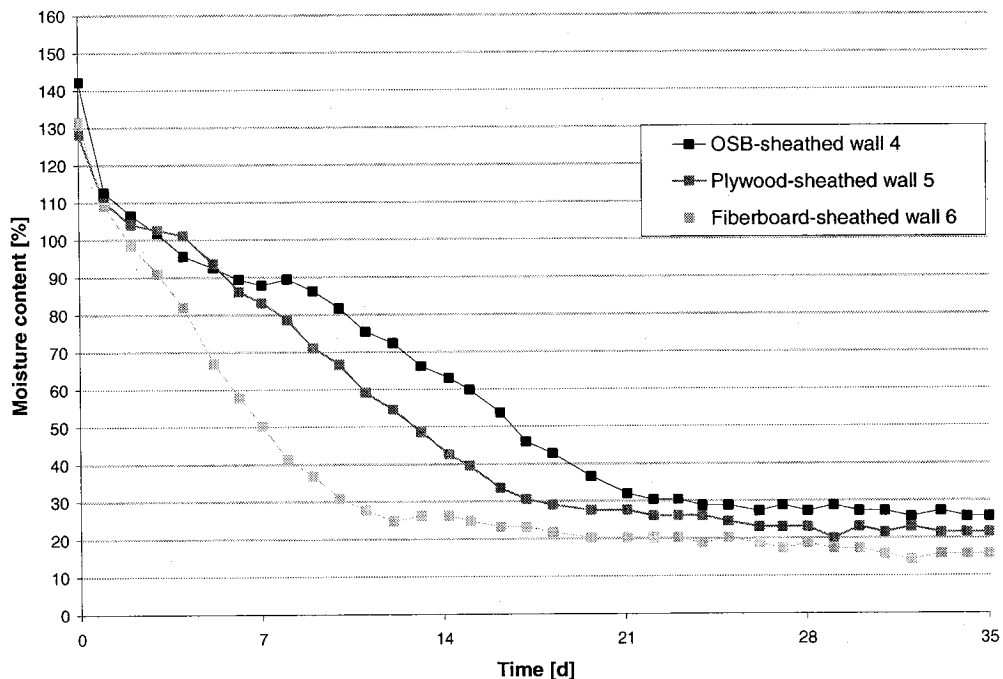


Figure 5.50. Moisture content with time of samples CV in OSB-sheathed walls 4, 5 and 6 from test 3.

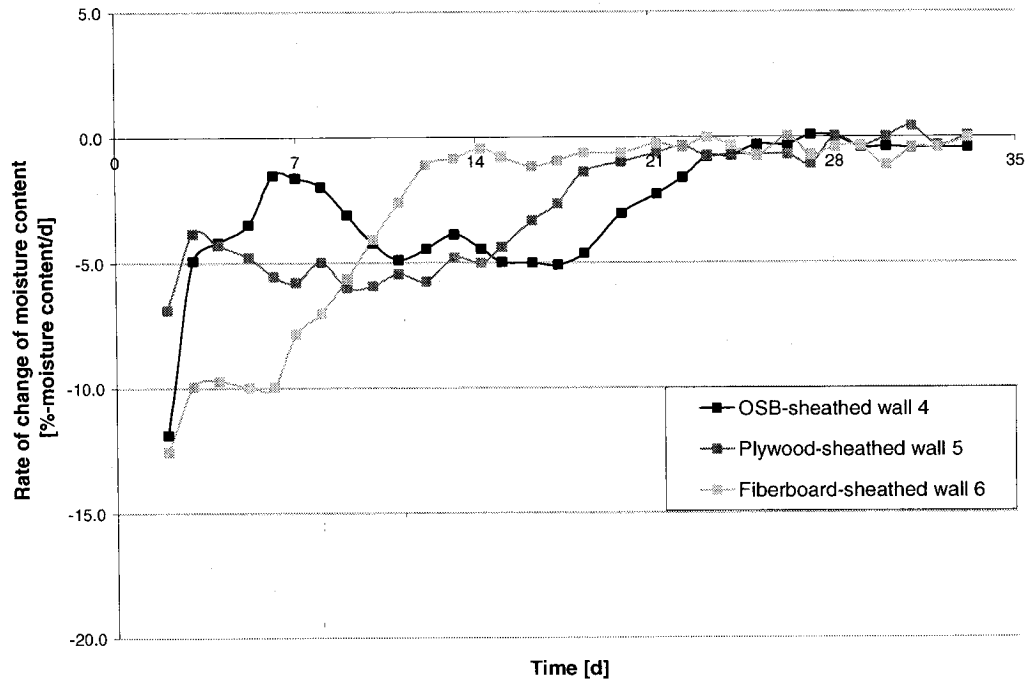


Figure 5.51. Rate of change of moisture content for samples CV in walls 4, 5 and 6 in test 3, found using the moving window technique.

5.4.1.5 Hygrothermal response of the sheathing gravimetric specimens row D right 1 (DR1)

The moisture content in the sheathing was monitored gravimetrically in each wall with one specimen located at the height of the bottom plate insert. A graph of the moisture content versus time of the sheathing sample in the three walls (Figure 5.52) shows that while the samples had a relatively similar moisture content at the beginning of the test, varying between 11.0% and 13.3% (also see Table 5.14), the response of the specimens differed. The moisture content of all the sheathing samples increased at the beginning of the test as moisture was released from the bottom plate inserts and redistributed to the sheathing and the other hygroscopic components enveloping the insulation-filled stud cavity.

The moisture content of the OSB specimen in wall 1 increased steadily up to the end of the first drying phase at day 28, when the outdoor temperature increased, after which time the sample slowly dried. The plywood sample in wall 2 also increased steadily in moisture content, obtaining the highest moisture content of all three sheathing materials

at 19.4 %, but its moisture content leveled off about 15 days into the first drying phase and then dried during the second drying phase. The fiberboard sample shows the least moisture absorption of all three specimens, reaching an early peak moisture content of less than 15% moisture content. A drying trend occurred during the last week of the test, as the walls were exposed to warmer May conditions, with the final moisture content in the OSB, plywood and fiberboard sheathings reaching 16.6%, 16.9% and 11.6%, respectively, as shown in Table 5.14.

The differences in the moisture behavior of the sheathing materials can be explained by their different capillary water absorption coefficient and their water vapor permeabilities. Plywood, which has the greatest capillary water absorption coefficient of the three sheathings (see Table 5.10), absorbed water readily; however, since plywood also has a high water vapor permeance at high relative humidities (see Figure 5.47), the plywood sample dried quickly. The asphalt coating on the fiberboard significantly gives it a low capillary water absorption coefficient, which explains its low moisture content during the test, as does its high water vapor permeance. OSB has both a lower capillary water absorption coefficient and a lower water vapor permeability than plywood, and therefore absorbed moisture at a slower rate and dried more slowly than plywood.

Table 5.14. Initial and final moisture content and drying rate in the sheathing DR1 specimens in walls 1, 2 and 3 from test 3. The lowest final moisture content is indicated in bold.

| Wall no. | Sheathing material | Initial moisture content* [% mass] | Final moisture content [% mass] | Maximum moisture content [% mass] |
|--|---------------------------|---------------------------------------|------------------------------------|--------------------------------------|
| Polyethylene vapor retarder | | | | |
| 1 | OSB | 11.0 | 16.6 | 17.7 |
| 2 | Plywood | 12.3 | 16.9 | 19.4 |
| 3 | Asphalt-coated fiberboard | 13.3 | 11.6 | 14.6 |
| Low permeance primer paint vapor retarder | | | | |
| 4 | OSB | 10.8 | 17.9 | 20.0 |
| 5 | Plywood | 12.7 | 17.1 | 19.5 |
| 6 | Asphalt-coated fiberboard | 12.1 | 11.8 | 15.3 |

*The initial moisture content was measured one day after the test started.

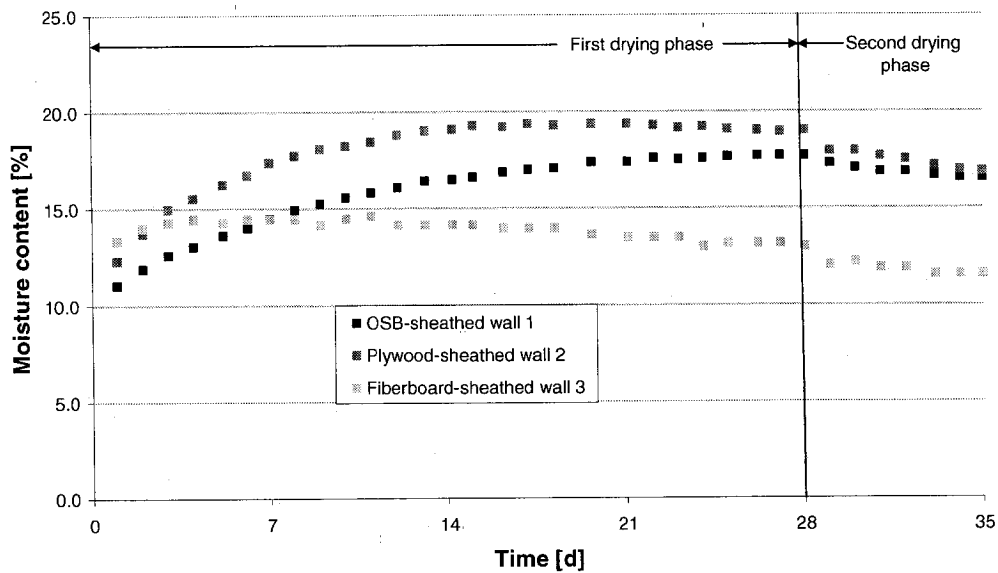


Figure 5.52. Moisture content with time of sheathing samples DR1 in walls 1, 2 and 3 from test 3.

Similar hygrothermal responses can be observed in the sheathing specimens in walls 4 to 6, as shown in Figure 5.53. One small difference is that the OSB specimen in wall 4 reached a higher moisture content during the first drying phase and at the end of the test. This may be attributed to a greater physical contact with the moist bottom plate insert. Again, in this series of walls, the final moisture content was significantly lower in the fiberboard sample.

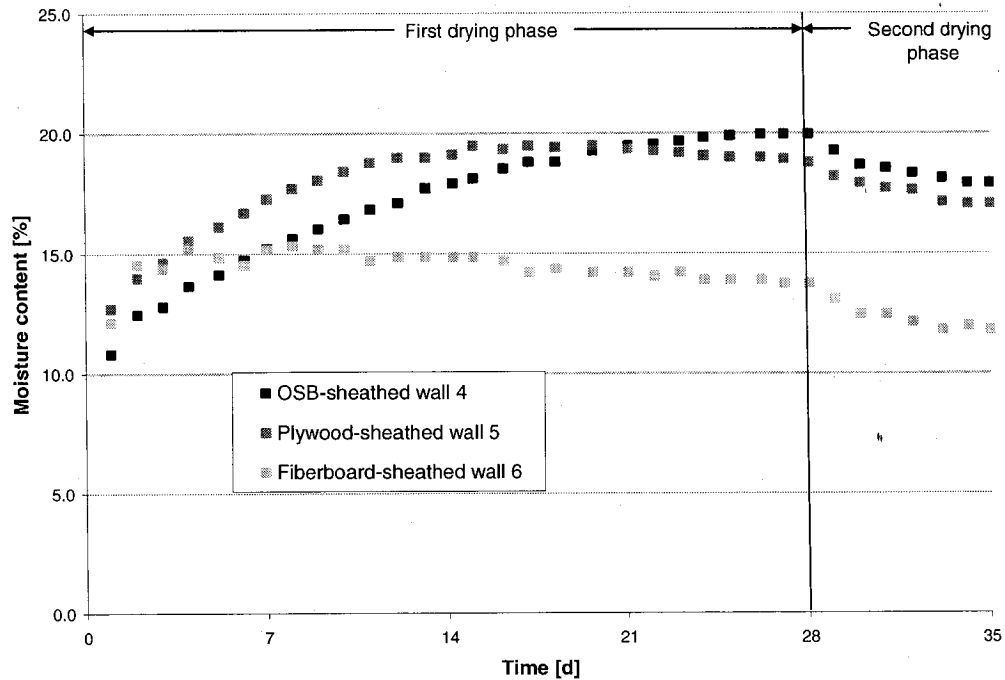


Figure 5.53. Moisture content with time of sheathing samples DR1 in wall 4, 5 and 6 from test 3.

5.4.1.6 Summary of the role of the sheathing on the hygrothermal response of the bottom plate and of the sheathing

Bottom plate insert

Overall, in both wall series 1 to 3 and 4 to 6, it was found that the bottom plate inserts dried at a faster average rate in the walls with the asphalt-coated fiberboard, and that the inserts in these walls also achieved the lowest average moisture content at the end of the test. In both wall series, the inserts in the walls sheathed with OSB dried at the lowest rate and had the highest final moisture content. However, the differences observed in the hygrothermal response of the inserts were more pronounced in the walls 1 to 3 with a polyethylene vapor retarder.

CH1 and CH2 samples

Analysis of the hygrothermal performance of the center horizontal 1 and 2 samples is complicated at times because of significant variations in initial moisture content in the small gravimetric samples, which could in themselves influence their behavior. Table

5.15 summarizes the constant rates of drying during the first drying stage and the peak drying rates in the CH1 and the CH2 samples of series. The table shows that in walls 1 to 3, both the rates of constant drying and the peak drying rate for samples CH1 and CH2 were greatest in the plywood-sheathed wall 2. However, in the walls 4 to 6, the CH1 and CH2 samples in wall 5 both experienced significantly different initial moisture contents that preclude a performance comparison. In these walls, the CH1 and CH2 samples experienced the greatest drying rate in the fiberboard-sheathed walls. Table 5.16 summarizes the final moisture contents in the CH1 and CH2 samples in walls 1 to 6. The table shows that despite the differing initial moisture contents, the samples in the fiberboard-sheathed walls 3 and 6 typically have the lowest final moisture contents; this is especially true at the colder location, CH1. The CH1 and CH2 samples in the OSB-sheathed walls 1 and 4, on the other hand, have the highest final moisture contents, which were higher than 20% in both cases. The drying rates of the CH1 samples in both OSB-sheathed walls were not significant at the end of the test despite the higher outdoor temperatures during the second phase of drying starting at day 28. This suggests that there is a risk of moisture-induced damage of the bottom plate near the sheathing when the sheathing permeance is low.

Table 5.15. Constant rates and peak rates of change of moisture content for samples CH1 and CH2 in walls 1 to 6 in test 3, sorted in terms of the level of drying – low, medium and high. The cells in the table of the samples whose initial moisture content differed significantly from that of the others are shaded in grey.

| Level of drying rate | Wall no./ sheathing material | Constant drying rate [%/day] | Peak rate of drying [%/day] | Wall no./ sheathing material | Constant drying rate [%/day] | Peak rate of drying [%/day] |
|----------------------|------------------------------|------------------------------|-----------------------------|------------------------------|------------------------------|-----------------------------|
| | Walls 1 to 3, sample CH1 | | | Wall 4 to 6, sample CH1 | | |
| Low | 1/OSB | -3.8 | -4.5 | 5/plywood | -5.7 | -6.3 |
| Medium | 3/fiberboard | -5.8 | -6.4 | 4/OSB | -7.1 | -7.6 |
| High | 2/plywood | -6.2 | -7.1 | 6/fiberboard | -9.4 | -10.7 |
| Level of drying rate | Walls 1 to 3, sample CH2 | | | Walls 4 to 6, sample CH2 | | |
| Low | 3/fiberboard | -9.7 | -10.8 | 5/plywood | -14.2 | -14.0 |
| Medium | 1/OSB | -10.6 | -11.8 | 4/OSB | -16.2 | -14.3 |

| | | | | | | |
|------|-----------|-------|-------|--------------|-------|-------|
| High | 2/plywood | -13.2 | -13.7 | 6/fiberboard | -20.6 | -17.4 |
|------|-----------|-------|-------|--------------|-------|-------|

Table 5.16. Final moisture content in samples CH1 and CH2 from walls 1 to 6 in test 3. The lowest final moisture contents in each series are indicated in bold. The cells in the table of the samples whose initial moisture content differed significantly from that of the others are shaded in grey.

| Wall no. | Sheathing material | CH1 [% mass] | CH2 [% mass] |
|--|---------------------------|-----------------|-----------------|
| Polyethylene vapor retarder | | | |
| 1 | OSB | 24.7 | 15.2 |
| 2 | Plywood | 21.9 | 13.5 |
| 3 | Asphalt-coated fiberboard | 15.2 | 13.6 |
| Low permeance primer paint vapor retarder | | | |
| 4 | OSB | 22.0 | 13.6 |
| 5 | Plywood | 19.4 | 13.3 |
| 6 | Asphalt-coated fiberboard | 16.7 | 13.1 |

CV samples

The gravimetric samples located on the center vertical (CV) surface of the bottom plate insert revealed drying patterns that clearly illustrate the role of the sheathing on the response of the drying performance. In both series of walls 1 to 3 and 4 to 6, the highest constant and peak rates of drying were experienced in the walls 3 and 6, which are both sheathed with fiberboard. In these walls, the CV samples had the lowest moisture content, by far. In contrast, the slowest constant and peak rates of drying occurred in the samples in the OSB-sheathed walls 1 and 4. These samples also had the highest final moisture contents, by far, at more than 25% moisture content at the end of the 35-day test. These results demonstrate that the sheathing properties have a considerable impact on the bottom plate at this location, and also that the bottom plate may potentially be vulnerable to moisture-induced problems at this location.

Sheathing sample DR1

The hygrothermal response of the sheathing specimens installed in row "D" of the sheathing, adjacent to the bottom plate insert, was discussed. Overall, in both series of walls, the general behavior of the OSB and of the plywood sheathing specimens was similar. The difference in the maximum moisture content reached in the OSB and

plywood samples was less than 2% moisture content. The two sheathings also reached similar final moisture contents. It is believed that the small differences in their response are due to the differences in physical contact between the sheathing and the wet bottom plate insert. In both series of walls, the fiberboard sheathing specimens reached the lowest peak moisture content and also the lowest final moisture content by far. This finding is attributed to the fiberboard's asphalt coating which reduced liquid water absorption at the surface. During the last week of the test, the moisture content of all of the sheathing specimens was steadily decreasing, reaching final moisture content levels below 20%. These moisture content results, in tandem with the moisture content values in the bottom plate inserts and the other gravimetric samples installed within the bottom plate inserts, suggest that moisture egress in the wall as a whole was taking place at the end of the test.

In hindsight, it would have been beneficial to install a sheathing gravimetric sample at a level above the bottom plate insert to compare the response of the different sheathings exposed to the stud cavity environments.

5.4.2 Role of the vapor retarder

The drying performance of the pre-wetted bottom plate inserts and the smaller gravimetric samples in the six walls of test 3 are studied to investigate the role of the vapor retarder. Walls 1, 2 and 3 used a polyethylene membrane as the vapor retarder, whereas in walls 4, 5 and 6, a coat of low permeance primer which was painted on the inside surface of the gypsum carried out this function. The response of the bottom plate inserts, followed by that of the sheathing samples is compared for walls 1 and 4, both sheathed with OSB; in walls 2 and 5, both sheathed with plywood; and last in walls 3 and 6, which use asphalt-coated fiberboard. Unfortunately, the initial moisture content of the center horizontal 1 (CH1), center horizontal 2 (CH2) and the center vertical (CV) differ significantly in all cases but one, which precludes comparison of the drying behavior of these samples. In addition, the sheathing specimens, which were installed at the bottom of the wall at the height of the sheathing, were not effective in showing the effect of the vapor retarder, given their location. As was said earlier, sheathing samples should have

been installed above the bottom plate to compare the response of the different sheathings as the bottom plate inserts dried out.

5.4.2.1 Hygrothermal response of the bottom plate inserts

A comparison is performed of the drying response of the bottom plate inserts in walls 1 (polyethylene vapor retarder) and 4 (low permeance primer paint), both built with OSB sheathing. As shown in Figure 5.54 and Table 5.17, the initial moisture content of both bottom plate inserts were very similar: 53.0% in wall 1 and 56.0% in wall 4. The moisture content of both specimens decreased by about 4% after one day of drying, likely attributed to the loss of unbound surface water. It can be seen that the insert in the wall having a low permeance primer paint (wall 4) dried at a faster rate than that in the wall having a polyethylene vapor retarder. The difference in the moisture performance is shown advantageously when the normalized mass losses are compared (see Figure 5.55): these show that the moisture evaporation occurred more readily in the wall 4 insert than that in wall 1, particularly during the first seven days of the test.

The rate of change of moisture content with time was determined using the previously described moving window technique (Figure 5.56). The graph illustrates that the drying rate is higher in the wall 4 insert, with the difference in drying rate being greatest over the first week of the test and diminishing as the drying progresses. The average drying rate was higher in wall 4 at 0.89%-moisture content/day compared to 0.67%-moisture content/day in wall 1. The peak drying rate in the wall 4 insert was almost double that of wall 1, with -1.9%-moisture content/day in wall 4 and -1.0%-moisture content/day in wall 1. Notwithstanding the initial moisture content of the specimen in wall 4 was 3.0% greater, it dried to a moisture content at the end of the test that was 4.0% lower than that of the specimen in wall 1. Moreover, the total moisture content lost in the insert in wall 4 was significantly greater than that in wall 1 (see Table 5.17).

Table 5.17. Initial and final moisture content and moisture content lost in the drying process for the bottom plate inserts of walls 1 to 6 in test 3.

| Wall no. | Vapor retarder | Initial moisture content [%] | Final moisture content [%] | Moisture content lost in drying process [%] |
|------------------------------|------------------------|------------------------------|----------------------------|---|
| Sheathing: OSB | | | | |
| 1 | Polyethylene | 53.0 | 26.7 | 26.3 |
| 4 | Low perm. primer paint | 56.0 | 22.7 | 33.3 |
| Sheathing: plywood | | | | |
| 2 | Polyethylene | 53.1 | 21.4 | 31.7 |
| 5 | Low perm. primer paint | 54.9 | 21.9 | 33.0 |
| Sheathing: fiberboard | | | | |
| 3 | Polyethylene | 56.8 | 20.7 | 36.1 |
| 6 | Low perm. primer paint | 53.6 | 17.5 | 36.1 |

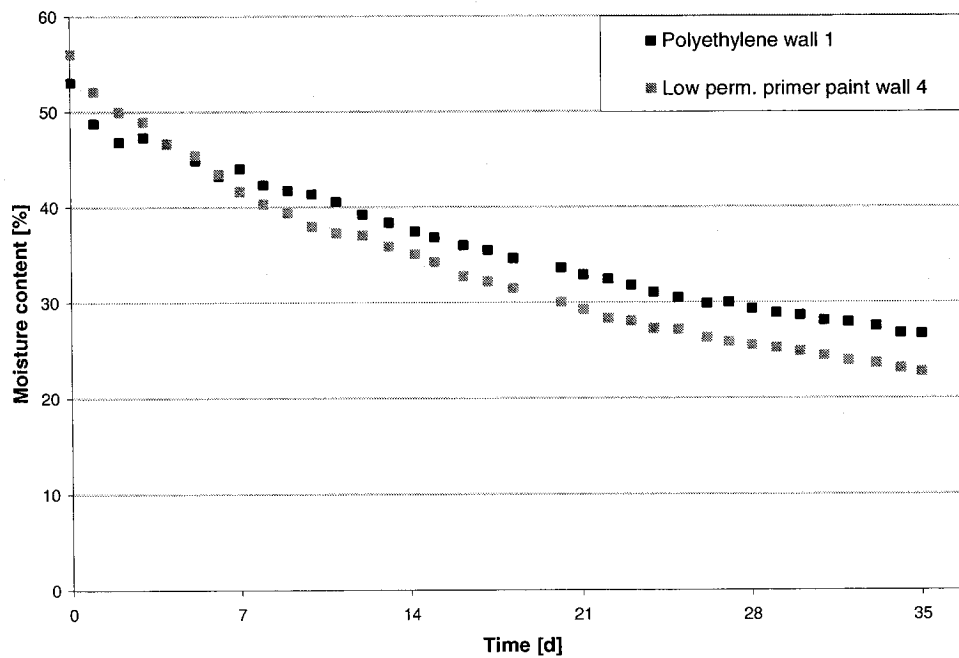


Figure 5.54. Moisture content in the bottom plate inserts versus time for walls 1 and 4 in test 3. Both walls are sheathed with OSB.

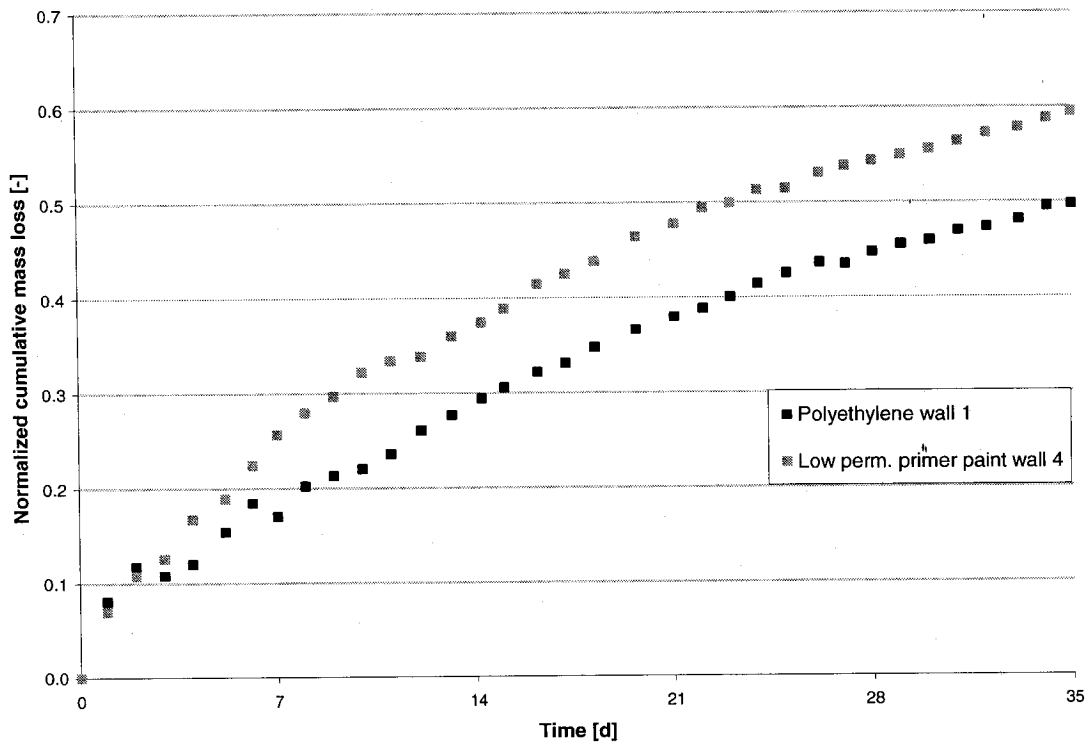


Figure 5.55. Normalized cumulative moisture loss in the bottom plate inserts versus time for walls 1 and 4 in test 3. Both walls are sheathed with OSB.

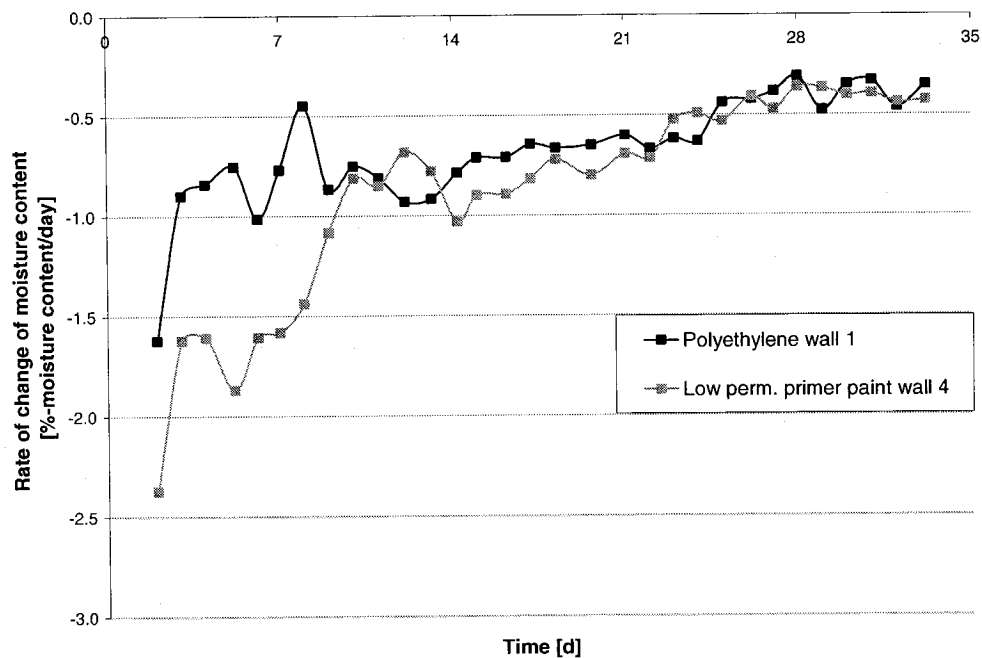


Figure 5.56. Rate of change of moisture content for bottom plate inserts in walls 1 and 4 in test 3, found using the moving window technique. Both are sheathed with OSB.

The same treatment of data was undertaken for the bottom plate inserts for the

plywood-sheathed walls 2 and 5. Wall 2 used a polyethylene vapor retarder whereas wall 5 had a low-permeance primer paint. The moisture content versus time curves shown in Figure 5.57 illustrates that the initial moisture contents were almost the same: 53.1% in wall 2 and 54.9% in wall 5, and that the moisture response was very similar. The average drying rates were also similar, at -0.85%-moisture content/day in wall 2 and -0.91%-moisture content/day in wall 5. However, as seen in Figures 5.58 and 5.59, in the first seven days of the test, the moisture loss and the drying rate were slightly higher in wall 5 than in wall 2. This is confirmed by the peak drying rate, which was -1.9%-moisture content/day in the wall 5 insert and -1.6%-moisture content/day in that in wall 2. The final moisture contents were 21.4% and 21.9% in the inserts of walls 2 and 5, respectively, with a slightly greater overall moisture loss in the wall 5 insert (Table 5.17). These differences are not significant and may be attributed to the fact that the initial moisture content in the wall 5 specimen was slightly higher.

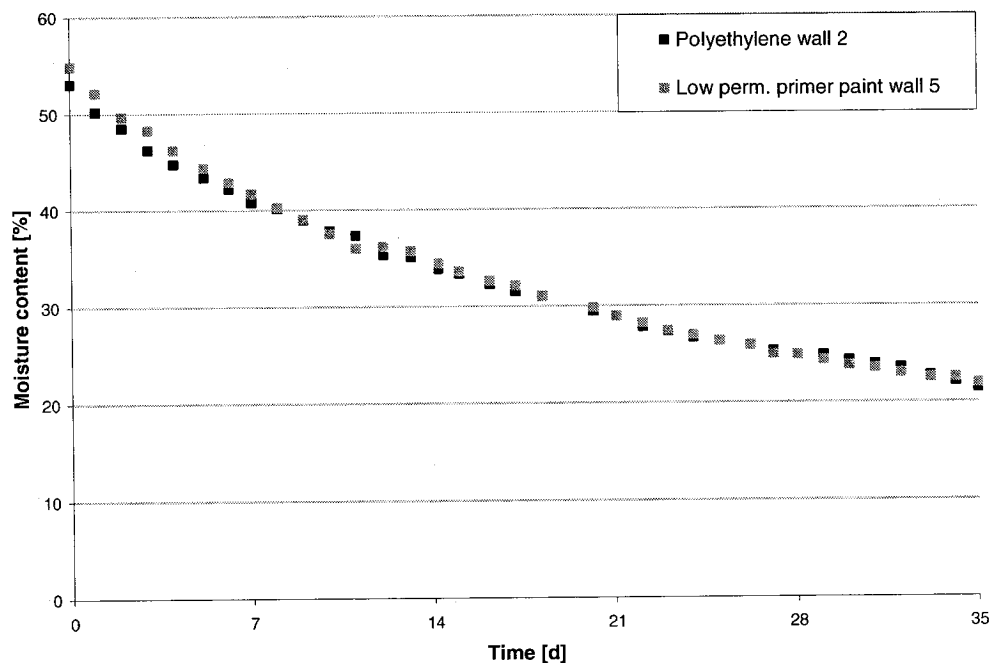


Figure 5.57. Moisture content in the bottom plate inserts versus time for walls 2 and 5 in test 3. Both walls are sheathed with plywood.

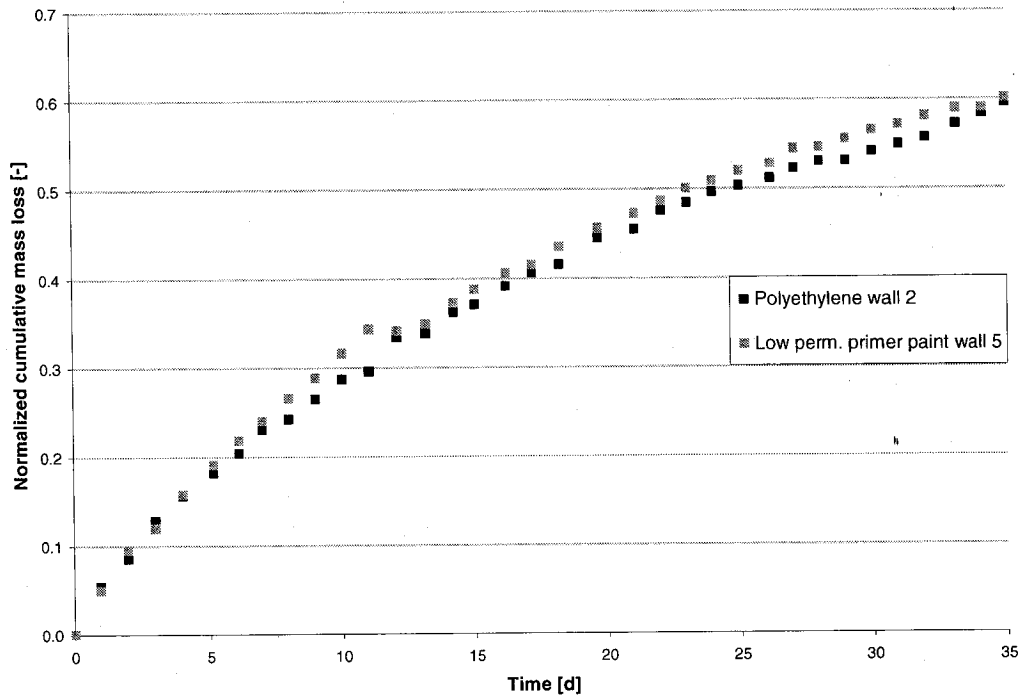


Figure 5.58. Normalized cumulative moisture loss in the bottom plate inserts versus time for walls 2 and 5 in test 3. Both walls are sheathed with plywood.

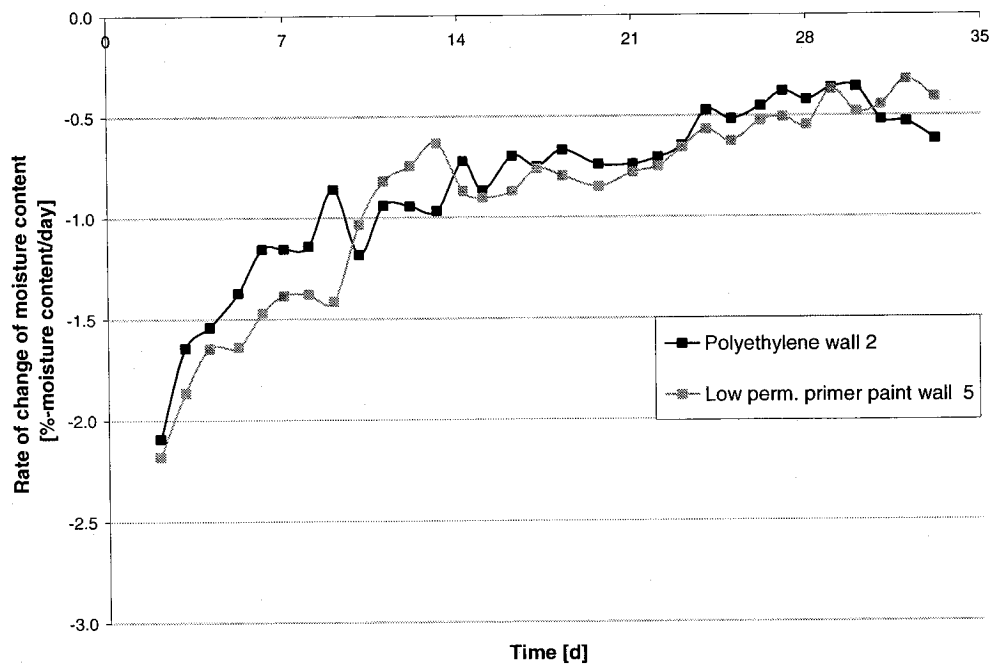


Figure 5.59. Rate of change of moisture content for bottom plate inserts in wall 2 and 5 from test 3, found using the moving window technique. Both walls are sheathed with plywood.

Similarly, the moisture response versus time was also examined for the bottom plate

insert specimens in fiberboard-sheathed walls 3 and 6, shown in Figure 5.60. Wall 3 had a polyethylene vapor retarder whereas wall 6 a low permeance primer paint. The initial moisture contents of the bottom plate inserts were similar at 56.8% and 53.6%, a variation of only 3.2% (Table 5.17). The difference in the moisture content in the two bottom plate inserts increased from that point, reaching a maximum over days 10 to 13, with the moisture content of the insert in wall 3 approximately 6% greater than that in wall 3. This general trend in the moisture response can also be seen in the normalized cumulative moisture loss curves in Figure 5.61. The average drying rate was slightly greater in wall 6 at -1.01%-moisture content/day, compared to -0.96%-moisture content/day in wall 3. The peak rates of change of moisture content (other than the initial values) were similar, at -2.2 and -2.1 in walls 3 and 6, respectively, as illustrated in Figure 5.62. The figure also shows that the rate of change of moisture content for the wall 6 insert decreases relative to that in wall 3 as of day 14 of the test. This may be due to the wetted portions of the wall 3 insert reaching the second drying stage faster, likely because of its slightly lower initial moisture content. Upon reaching this stage, moisture transfer by diffusion dominated and the drying rate decreased. However, the drying rate in both inserts increased slightly and become more or less equal from day 28, when the outdoor temperature was increased. The final average moisture content in the two specimens was lower in the bottom plate specimen from the low permeance primer paint assembly at 17.5%, compared to a 20.7% moisture content in the polyethylene wall specimen.

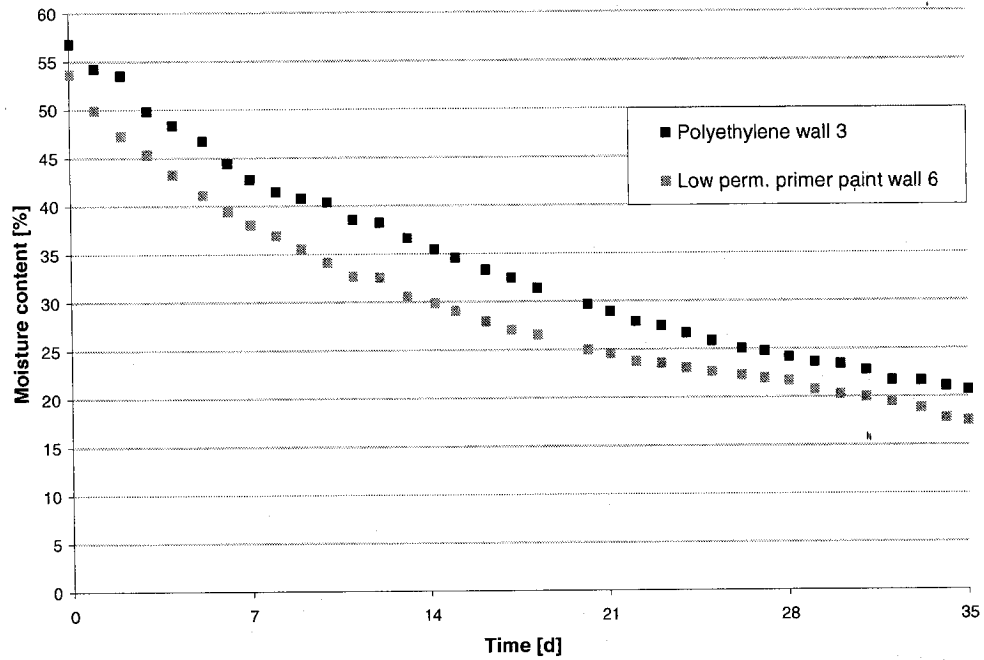


Figure 5.60. Moisture content in the bottom plate inserts versus time for walls 3 and 6 in test 3. Both walls are sheathed with asphalt-coated fiberboard.

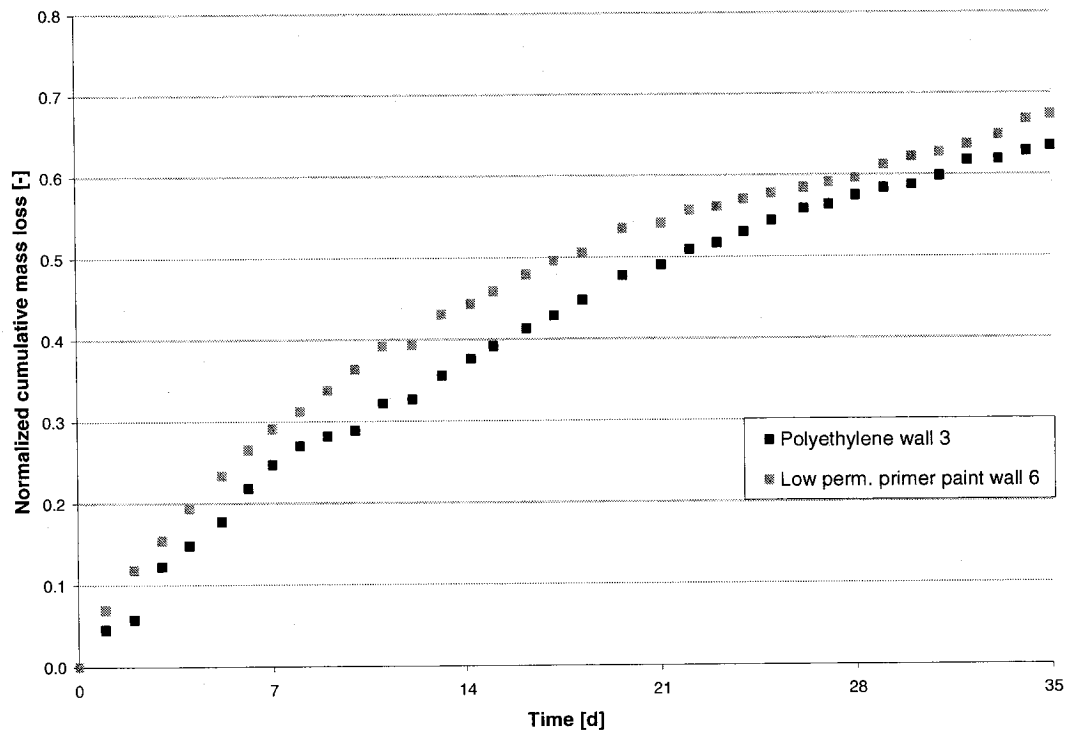


Figure 5.61. Normalized cumulative moisture loss in the bottom plate inserts versus time for walls 3 and 6 in test 3. Both walls are sheathed with asphalt-coated fiberboard.

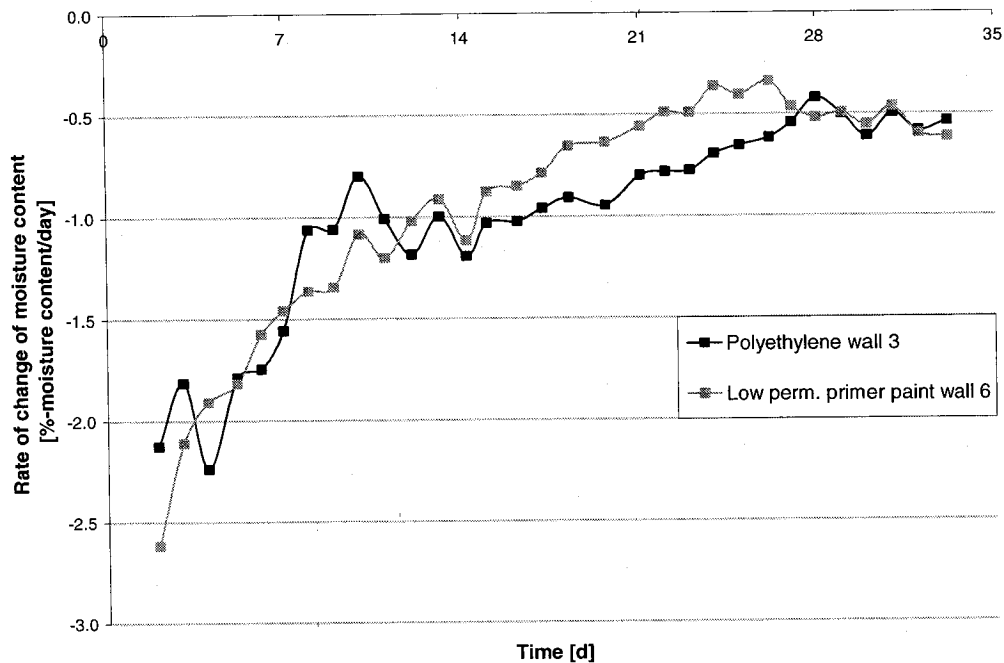


Figure 5.62. Rate of change of moisture content for bottom plate insets in walls 3 and 6 in test 3 using the moving window technique. Both walls are sheathed with fiberboard.

5.4.2.2 Summary of the role of the vapor retarder on the hygrothermal response of the bottom plate and of the sheathing

Results show that the influence of the vapor retarder on the performance of the wall components depends on the type of sheathing used. For the walls sheathed with OSB, the vapor retarder played a role in the drying of the bottom plate insert: the peak drying rate of the insert in the wall with low permeance paint (wall 4) was -1.9% -moisture content/day compared to -1.0% moisture content/day in the wall with polyethylene (wall 1). The insert in the wall with low permeance primer dried to a lower moisture content at the end of the test than the one in the polyethylene wall despite the fact that its initial moisture content was slightly greater. In walls having either plywood sheathing or asphalt-coated fiberboard as sheathing board, the effect of the vapor retarder was insignificant. In the latter case, the moisture content profiles showed similar drying rates throughout the test despite the different permeance of the vapor retarder. In general, these findings show that when the permeance of the sheathing is low, as it is for OSB, then the effect of the permeance of the vapor retarder is more critical, and the

permeability of the vapor retarder should be increased up to a value allowed by the building code to promote drying of the assembly towards the interior. The test results demonstrate that the average moisture content of the monitored components in walls with both types of vapor retarders were below the fiber saturation point of wood at the end of the 35-day test exposed to April and May conditions and were continuing to dry, and would therefore be expected to reach acceptable levels of moisture content, i.e. 20% moisture content, thus mitigating the risk of moisture induced damage.

5.5 Summary and Conclusions

Three experiments were conducted to examine the wetting and drying behavior of several hygroscopic components in wood-frame walls wetted by simulated wind-driven rain infiltration. In tests 1 and 2, the walls were wetted by water penetration simulating wind-driven rain infiltration at a specific building envelope failure, i.e. a defect at a windowsill. In the two experiments, water was inserted in a drop-by-drop fashion on the top interior surface of the sheathing at a rate, frequency and duration reflecting average wind-driven rain events in April in Montréal, Québec. Water was introduced in this manner in 17 of the 19 walls in both tests 1 and 2. The wall specimens had no cladding, as a ventilated air space behind an eventual cladding would permit exchange of air between the air space and the exterior environment.

The moisture content monitoring protocol included localized rather than global wall measurements in order to measure the wetting and drying response of the walls at locations susceptible to moisture accumulation. The test set-up reflected a north-facing wall, and thus did not consider solar effects. Air leakage due to wind, mechanical ventilation and stack effects was also not taken into account. Steady state climatic conditions were generated in the pre-conditioning and wetting phases of tests 1 and 2 to increase the moisture content reflecting wetting due to winter diffusion. The walls were exposed to cyclic exterior conditions reflecting April and May Montreal conditions in the first and second drying phases.

Results from experiments 1 and 2 show that, in general, the water which was

introduced at the top of the wall migrated and accumulated at the bottom of the wall, wetting the bottom plate and the adjacent sheathing. Little moisture absorption occurred in the sheathing above the bottom plate, except in test 1, where the presence of gravimetric samples in the plywood sheathing disturbed the path of water as it ran down the surface of the sheathing. In the bottom plate, the small gravimetric specimens that incurred the highest moisture content were those facing the exterior sheathing. Little moisture absorption occurred in the wood studs.

Moisture content results from the tests 1 and 2 show that of the three sheathings, the greatest moisture uptake was found to occur in the plywood, as was attributed to its higher water absorption coefficient. The results also showed that the asphalt-coating on the surfaces of the fiberboard effectively reduces its water absorption, as reflected by its low water absorption coefficient.

The moisture content results in the sheathing and the bottom plate showed a stochastic wetting pattern, with different moisture distributions from wall to wall, and from one wetting event to another within the same wall. Lateral migration of water was observed. Above the bottom plate, the lateral migration was attributed to physical contact between the sheathing and the fiberglass batt insulation, which altered the trajectory of the water running down the sheathing surface. Lateral migration of water has been reported in the field in cases of water infiltration due to a leaky window, for example. At the level of the bottom plate, lateral migration was due to capillary movement in the gap between the sheathing and the bottom plate. Generally, the wetting pattern in time was stochastic, resulting in wetting patterns that are not necessarily repeated at a given location from one wetting event to the next. However, it was found that when a location was exposed to repeated wettings, significant moisture accumulation was observed, creating a risk for moisture-induced damage. The variability in the moisture content results at the end of the wetting phase precluded an analysis on the subsequent drying behavior during the drying phase.

The “dry” periods when the water insertion was stopped typically allowed significant drying, particularly during the 4-day “dry” period in each week. Comparing the response of the bottom plate samples in walls with different sheathings, the plywood generally afforded faster drying rates, and the OSB the lowest drying rates; it is hypothesized that

the asphalt-coating in the fiberboard, which reduces its moisture uptake, slows the drying rate of the bottom plate despite the fiberboard's higher vapor permeability. In the sheathing itself, the fiberboard shows the highest drying rate.

The role of the vapor retarder was also examined, with results indicating that increasing the vapor permeability of the vapor retarder increased the drying response of the plywood and, even more so, in the fiberboard-sheathed walls. In the OSB-sheathed walls, the results showed that drying rate was unexpectedly faster when low permeance primer was added, compared to the wall without a vapor retarder.

The experimental results indicated that adding exterior insulation decelerated the drying rate the bottom plate and the sheathing due to the greater exterior vapor diffusion resistance provided by the extruded polystyrene. However, it should be noted that the exterior and interior ambient conditions were similar when the measurements were taken, and the benefit of adding exterior insulation in terms of increasing the wall's thermal resistance cannot be appreciated based on the data presented. The role of exterior insulation is examined in the next chapter.

Analysis of the role of exterior cladding and of the wall height was complicated by the different moisture accumulation and distribution in the walls, and no conclusions could be made based on the experimental data. Chapter 6 examines the impact of wall height on the drying performance using a hygrothermal simulation tool. Analysis on the impact of hygroscopic exterior cladding, however, would require modeling the ventilation in the air cavity, which is beyond the scope of this project.

The moisture content results of the six walls in test 3 were used to examine the role of the exterior sheathing and the vapor retarder on the drying response of the different wall assembly components. In this test, the primary moisture source was a pre-wetted bottom plate insert, which also served as a gravimetric sample during the course of the test. A comparison of the moisture content results in the bottom plate inserts showed that the inserts in the asphalt-coated fiberboard-sheathed walls had the highest drying rate and achieved the lowest final moisture content. Conversely, the lowest drying rate and the highest final moisture content were observed in the OSB-sheathed walls. These findings were more pronounced in the walls with the less vapor permeable polyethylene membrane. In the small "center vertical" bottom plate gravimetric specimens facing the

sheathing, the highest and lowest drying rates occurred in the walls with asphalt-coated fiberboard sheathing and OSB, respectively. In the sheathing, the moisture content in the gravimetric sample facing the bottom plate was similar in the OSB and plywood specimens. However, the moisture uptake in the fiberboard was significantly lower, again likely due to its asphalt coating.

The effect of two different vapor retarders – polyethylene and low permeance primer paint – was also examined using the moisture content results from test 3. The findings indicate that the influence of the vapor retarder on the drying performance of the monitored components depends on the type of sheathing used. The effect of the vapor retarder was greater in the OSB-sheathed walls. In these walls, the higher vapor resistance of the OSB reduced the outward vapor flux; inward vapor flux was greater in the walls with the low permeance primer due to its lower vapor permeability compared to that of polyethylene. The effect of the vapor retarder was not significant in the plywood and asphalt-coated fiberboard walls. As was stated earlier, these findings show that when the permeance of the sheathing is low, then the vapor permeability of the vapor retarder should be increased up to a value allowed by the building code to promote drying of the assembly towards the interior. Finally, the moisture content levels at all locations in the sheathing, bottom plate and stud, except at a few locations in the bottom plate, were below 20% moisture content at the end of the tests, indicating that each wall system as a whole had dried.

6. HYGROTHERMAL SIMULATIONS AND PARAMETRIC ANALYSES

This chapter presents modeling work conducted to simulate the experimental set-up of six wood-frame assemblies as per the third experiment. The experimental and numerical results are compared, and possible explanations for the differences between these are provided. Subsequently the results of parametric analyses are presented that give additional insight into the response of the wall systems wetted by weekly simulated wind-driven rain infiltration.

The chapter begins by a review of heat, air and moisture modeling, including a presentation of its advantages and limitations. This is followed by a series of numerical simulations that were done to recreate the set-up of the third experiment and to examine the potential of a simulation tool to predict the hygrothermal response of wall assemblies exposed to a simulated wind-driven rain infiltration load. The simulations were conducted using an existing two-dimensional hygrothermal tool, WUFI-2D, on the six wall assemblies from the third experiment. Finally the results of parametric analyses that complement those of experiments 1 and 2 are given to illustrate the impact of varying several wall components on the hygrothermal drying response of the wall systems.

6.1 Overview of Heat, Air and Moisture Modeling

Models with transient capabilities have been developed in recent years to simulate the heat and moisture flow through the building envelope under varying environmental conditions, on a daily basis or on a yearly basis. Current one-dimensional tools are available today to general practitioners include WUFI, MATCH (Moisture and Temperature Calculations for Constructions of Hygroscopic Materials), hygIRC-ID; two-dimensional versions of WUFI and DELPHIN are also available.

The models typically use numerical methods to solve equations of heat and moisture

transfer and accumulation. DELPHIN also considers salt transport. Few tools exist, like hygIRC, that consider air transport using uniformly distributed air flow. The mechanisms of heat, air, moisture and salt transport are coupled; in other words, they occur interdependently of each other. Most material properties are not constant: for example, both water vapor permeability and liquid water diffusivity have been shown to be strongly dependent on moisture content, and thermal conductivity is dependent on moisture content. The ability of models to predict the response of single materials and more complex envelope systems has improved dramatically due in part to their ability to consider complex material functions. However, modern tools do have limitations, as will be discussed below. Annex C presents the different transport mechanisms and material properties as used in five HAM models.

The use of numerical models is limited because of:

1. the lack of availability of material properties in general; the difficulty in obtaining accurate materials properties that cover the entire moisture content range, especially in the liquid water uptake range; and the difficulty in simulating three-dimensional moisture transport in materials like wood, which are highly anisotropic;
2. the simulation of mass transfer by local air exfiltration/infiltration and other complex geometric problems require three-dimension representation;
3. the difficulty to study problems that include liquid water, as to how to represent the flow of water and define proper contact time between water and material;
4. the difficulty to include in the model the actual transport at the interfaces between building materials. An apparent resistance at the boundary from one material to the other can be added. Also, the air and liquid flow at these interstices is not included;
5. the possibility that the assumption of instantaneous equilibrium using sorption curves at each time step does not represent reality accurately. However, as most models have been validated against experimental data, it seems that the combination of the sorption curves with appropriate moisture transfer

properties, such as vapor permeability or moisture diffusivity, yields good results.

Despite their shortcomings, simulation models are practical tools because, when validated, they allow rapid investigations of the hygrothermal response of envelope assemblies, and comparative analyses of the impact of varying materials, components, exposure conditions, etc. The next section presents numerical work done to recreate the test set-up of the six walls in experiment 3 using WUFI-2D.

6.2 Numerical Simulation of Test 3 using WUFI 2D

A series of modeling simulations were conducted to compare the data obtained from test 3 of the experimental work presented in chapters 3, 4 and 5 with computer simulations conducted with the hygrothermal model WUFI-2D. This hygrothermal tool was selected because of its availability, its ability to model building envelope performance in a two-dimensional framework, and its user-friendly interface. As such, the simulations sought to recreate the physical geometry, material properties and interior and exterior boundary from test 3. The test and the simulations included six large-scale wood-frame walls with three different sheathings, OSB, plywood and asphalt-coated fiberboard, and two vapor retarders, polyethylene membrane and low permeance primer. As explained in chapter 3, in this test, a pre-wetted piece of lumber called the bottom plate insert was installed on top of the existing bottom plate at the start of the test and was allowed to dry. The bottom plate inserts had an initial moisture content which diminished as the test progressed (see Figure 5.25). While the experiment lasted 35 days in total, the WUFI 2D simulations were conducted for the first 28 days only, i.e. for the April conditions in Montreal. The heat and moisture transport governing equations in WUFI 2D are discussed next, followed by a brief description of the assemblies for the numerical simulations, the output data, the climate loading, surface transfer and initial conditions, and finally the simulation results.

6.2.1 Governing heat and moisture transport equations in WUFI-2D

WUFI is a building envelope heat and moisture transport tool that was developed at the German Fraunhofer Institute for Building Physics in Germany. The acronym WUFI stands for Wärme- und Feuchtetransport instationärzweidimensional, or transient one or two-dimensional heat and moisture transport. The governing equations used in WUFI are described below.

The balance equation for heat transport is given by:

$$\frac{\partial H}{\partial t} = -\nabla \cdot q + S_h \quad [6.1]$$

where H is the total enthalpy [J/m^3],

q is the heat flux density [W/m^2], and

S_h is the heat source or sink [W/m^3].

The total enthalpy, H , is equal to the sum of the enthalpy of the dry building material, H_{dm} , and of the building material moisture, H_w , both in J/m^3 :

$$H = H_{dm} + H_w \quad [6.2]$$

The heat flux density q can be found using:

$$q = -k_w \nabla T \quad [6.3]$$

where k_w is the moisture-dependent thermal conductivity in W/m , and T is the temperature in degrees C. In this model, the enthalpy flows are taken into account in the form of source terms in the heat balance equation:

$$S_h = h_v \nabla \cdot g_v \quad [6.4]$$

where S_h is the heat source or sink due to condensation and evaporation [W/m^3],

h_v is the latent heat of phase change [J/kg], and

g_v is the vapor diffusion flux density [$\text{kg}/\text{m}^2\text{s}$].

The latent heat of phase change consists of the heat of evaporation of pure water, $h_v = 2500 \text{ kJ}/\text{kg}$, and the enthalpy of the sorbed moisture within the building material, which is dependent on the building material, and is considered negligible compared to the evaporation heat.

The law of continuity, when expressed for moisture, is given by:

$$\frac{\partial w}{\partial t} = -\nabla \cdot (g_w + g_v) + S_w \quad [6.5]$$

where w is the moisture content of the building material [kg/m^3],

g_w is the liquid transport density [$\text{kg/m}^2\text{s}$],

g_v is the vapor diffusion flux density [$\text{kg/m}^2\text{s}$], and

S_w is the moisture source or sink [$\text{kg/m}^3\text{s}$].

The liquid transport density, g_w , is a function of the moisture content gradient:

$$g_w = -D_w(w)\nabla w \quad [6.6]$$

where D_w is the capillary transport coefficient, also called the liquid diffusivity, with units m^2/s , and w is the moisture content in kg/m^3 . This equation can also be stated using relative humidity as the moisture transport potential:

$$g_w = -D_\phi \nabla \phi \quad [6.7]$$

where D_ϕ is the liquid conduction coefficient [$\text{kg/m}\cdot\text{s}$], and ϕ is the relative humidity [-].

The advantage of this second equation relates to the fact that it contains a material-independent moisture transport potential that is also continuous at the layer boundaries.

The two transport coefficients, D_w and D_ϕ , can be connected as follows:

$$D_\phi = D_w \cdot \frac{dw}{d\phi} \quad [6.8]$$

where $dw/d\phi$ is often referred to as the moisture capacity of the material.

The vapor diffusion flux, g_v , is found using:

$$g_v = -\delta \nabla p \quad [6.9]$$

Other than the moisture absorbed and released by hygroscopic materials, moisture sources and sinks are not treated in WUFI.

The heat and moisture balance equations [6.2] and [6.6] are coupled due to the moisture dependence of the total enthalpy, the thermal conductivity, the heat of evaporation/condensation and of the temperature dependence of the moisture flows. The following are the equations for simultaneous heat and moisture transport:

$$\frac{dH}{dT} \cdot \frac{\partial T}{\partial t} = \nabla \cdot (k_w \nabla T) + h_v \nabla \cdot (\mu \nabla (\phi p_o)) \quad [6.10]$$

$$\frac{dw}{D\phi} \cdot \frac{\partial \phi}{\partial t} = \nabla \cdot (D_\phi \nabla \phi) + \mu \nabla (\phi p_o) \quad [6.11]$$

where dH/dT is the heat storage capacity of the moist building material [J/m^3K],

$dw/d\phi$ is the moisture storage capacity of the building material [kg/m^3],

t is time,

p_o is the saturation water vapor pressure [Pa],

μ is the vapor diffusion resistance factor of a material, which shows how many times the vapor permeability of a material is smaller than that of air, at the same conditions of temperature and total pressure (see Appendix C), and the other terms have been defined previously. The water vapor saturation pressure can be calculated using an empirical relation, which is a function of temperature:

$$p_o = 611 \cdot \exp\left(\frac{a \cdot T}{T_o + T}\right) \quad [6.12]$$

with $a = 22.44$ and $T_o = 272.44^\circ C$ for $T < 0^\circ C$,

and $a = 17.08$ and $T_o = 234.18^\circ C$ for $T \geq 0^\circ C$.

The coupled equations are discretized in time and space and solved numerically using the finite volume technique iteratively and by solving the individual equations repeatedly and successively. More information about the discretization and the solving method can be found in Künzeli (1995).

6.2.2 Description of the assemblies

The six wall assemblies simulated in the modeling work are identical in dimension, configuration and material types as was described in the experimental protocol for test no. 3 in section 4.8 of the thesis. The materials, their thicknesses, material properties and material functions are described in Appendix D. Figure 6.1 below shows a section view of the wall assembly. The material property data, given in Appendix D, was obtained from several sources, including the WUFI-2D and WUFI Pro databases, Kumaran (1996) and Kumaran *et al.* (2002b).

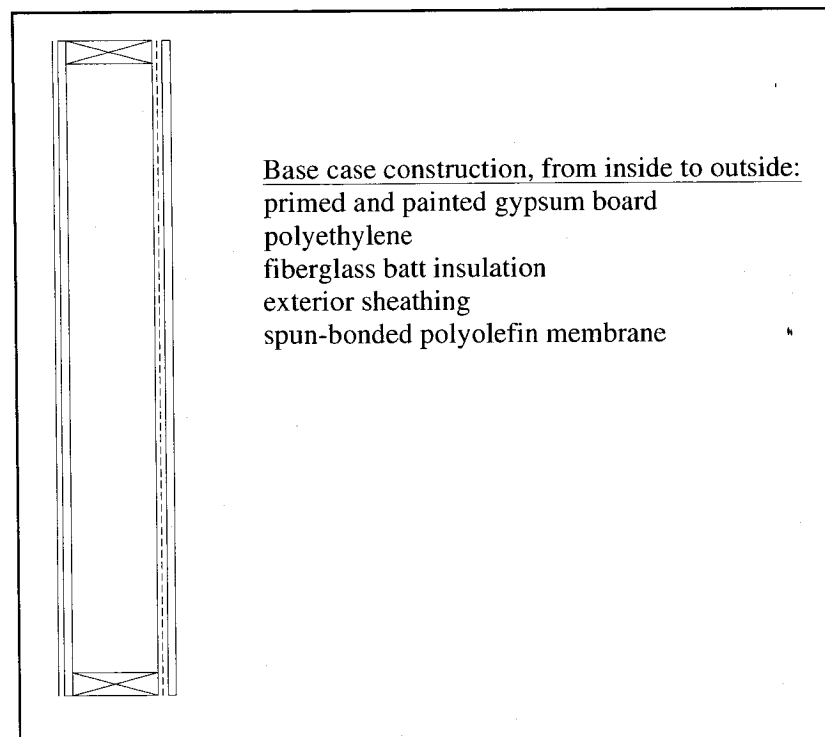


Figure 6.1. Section view of the wall assemblies 1 to 6. Walls 4, 5 and 6 employ low permeance primer paint as a vapor retarder rather than polyethylene.

6.2.3 Output data

In WUFI-2D, output data includes moisture content in individual components. In addition, specific points, if desired, can be selected by the user to monitor temperature, relative humidity and moisture content. Each component is divided into a user-determined number of elements both in the x- and the y-directions for the purpose of the discretization scheme, and monitoring points can be set in the center of any element. A sensor was installed in the middle of the stud cavity in the element just above the bottom plate to serve as a comparison for the measured temperature and relative humidity at that location at 50 mm above the bottom plate in the experiment.

6.2.4 Climate loading, surface transfer and initial conditions

Climate

The interior and exterior conditions that were set for the simulation were the same as the temperature and relative humidity setpoints measured during test no. 3. WUFI-2D allows the setting of an exterior climate that varies on a periodic-sinusoidal manner on a yearly as well as on a daily basis. To this effect, the first four weeks – those reflecting average Montreal April conditions – out of the total five weeks of test no. 3 were simulated. However, it was observed during the experiment that the monitored interior temperature was 20°C rather than 21°C, and therefore an interior temperature of 20°C was set for the simulation. Along the same lines, the exterior relative humidity during the test was difficult to control and varied in a sinusoidal fashion because of the exterior temperature which also changed in a similar fashion. The measured exterior relative humidity varied from approximately 70% to 73.5% during the first drying phase of the experiment (April conditions), and therefore this approximate range was set in the simulation. These conditions are summarized in Table 6.1.

Table 6.1. Interior and exterior conditions set in test no. 3 and in the WUFI2D simulations.

simulations.

| Duration (days) | Period simulated | Steady state indoor testing conditions | | Outdoor testing conditions | | | | | |
|--|---------------------|--|-----------|----------------------------|------|------|--------------------------|------|-----|
| | | | | Temperature [°C] | | | Relative humidity [%] | | |
| | | Temp. [°C] | RH [%] | Mean | Max. | Min. | Mean | Max. | Min |
| Monitored experimental test conditions | | | | | | | | | |
| 28 | April 1 - 30 | 20 | 40 | 6.3 | 10.9 | 1.6 | 71.75 | 73.5 | 70 |
| Numerical test conditions | | | | | | | | | |
| 28 | April 1 - 30 | 20 | 40 | 6 | 11 | 1 | 72 | 74 | 70 |

Surface transfer

Exterior heat transfer film coefficient: The exterior heat transfer film coefficient, h_{ext} , is a function of the speed of the air in contact with the outer surface of the building envelope and of the surface radiation emittance. The value of $h_{ext} = 22.7 \text{ W/m}^2\cdot\text{K}$ suggested by ASHRAE (2001) for a wind speed of 3.4 m/s and an exterior surface emittance of 0.9 was

used. In the chamber; air was mixed with fans inducing air velocities of approximately 0.2 to 1.1 m/s. It is recognized that the value selected for the exterior heat transfer film coefficient may overestimate the heat transfer in the simulations, although the effect is expected to be small. This issue is revisited in the following section.

Interior heat transfer film coefficient: The value of the interior heat transfer film coefficient, h_{int} , of $8.3 \text{ W/m}^2\cdot\text{K}$ for still air and a surface emissivity of 0.9 was used (ASHRAE, 2001).

Radiation: One of the premises upon which the third test was based was that of north-facing wall assemblies, thus not considering the effects of direct solar radiation. The laboratory set-up reflected this assumption. Given the small temperature difference between the exterior surface of the wall assemblies and the surrounding surfaces within the Environmental Chamber, the contribution of radiation heat transfer to the total was negligible and is already taken into account by the surface coefficient determined previously.

Vapor diffusion thickness, s_d : Here, the software allows the user to input a value for the vapor diffusion thickness of a coating such as a water repellent paint that may be applied to the exterior cladding or the interior sheathing. The vapor diffusion thickness is described as the thickness of a stagnant air layer with the same diffusion resistance as that of the material. Therefore, the greater the vapor resistance of a material, the greater the s_d -value, and vice-versa. In this test, no exterior coating has been applied per se, but the weather resistant membrane, the spun-bonded polyolefin membrane applied to the exterior surface, is treated as a coating, and is given a vapor diffusion thickness, s_d , of 0.043. A coating has been laid on the interior surface of the gypsum in the form of primer and paint. In walls 1, 2 and 3, this takes the form of one coat of latex paint and two coats of latex paint. These layers have a combined permeance of $69.4 \text{ ng/m}^2\cdot\text{s}\cdot\text{Pa}$, or a vapor diffusion thickness of 2.83 m for the estimated thickness. In walls 4, 5 and 6, the latex primer has been changed to a low permeance primer, for a combined permeance of $24.9 \text{ ng/m}^2\cdot\text{s}\cdot\text{Pa}$, or a vapor diffusion thickness of approximately 5 m.

Short-wave absorptivity: The short-wave solar absorptivity of the outer-most envelope component in the experiment, the white spun-bonded polyolefin membrane, was set to 0.3, which is the lower limit for light surfaces, as given by ASHRAE (2001).

Long-wave radiation emissivity: The long-wave emissivity of both the outer layer and inner layers was assumed to be 0.9, as suggested by ASHRAE (2001).

Rain: WUFI-2D assumes that the layer exposed to the exterior ambient environment is saturated every time rain falls. This assumption can lead to errors for materials with a high moisture absorption capacity. Therefore, WUFI-2D allows the user to “disregard rain below” a user-defined rainfall rate, in mm/h. Since the experiment did not involve rain impinging onto the cladding, this was reflected in the simulation, and a high limit of 1000 mm/h was arbitrarily selected.

The surface transfer conditions for each of the four faces, i.e. the exterior and interior surface and the top and bottom of the wall are summarized in Table 6.2.

Table 6.2. Surface transfer conditions for wall assemblies.

| Surface transfer characteristic | Exterior | Interior | Top of wall | Bottom of wall |
|--|----------|---|-------------|----------------|
| Total exterior heat transfer coefficient [W/m ² ·K] | 22.7 | 8.3 | 0 | 0 |
| Radiation | 0 | 0 | 0 | 0 |
| Vapor diffusion thickness [m] | 0.043 | Walls 1 to 3: 2.83 Walls 4 to 6: 5.0 | 10000 | 10000 |
| Short-wave absorptivity | 0.3 | 0 | 0.3 | 0.3 |
| Long-wave radiation emissivity: | 0.9 | 0.9 | 0.9 | 0.9 |
| Disregard rain below [mm/h] | 1000 | 1000 | 1000 | 1000 |

Initial conditions

The initial temperature was set for each material, as shown in Table 6.3. Generally,

components facing the exterior were given a temperature of 6.0°C, components facing the interior environment were given an initial temperature of 20.0°C, and components in the middle of the assembly were given a temperature of 13.0°C, reflecting the average of the exterior and interior temperatures.

For the purpose of the simulations, the initial moisture distribution within the bottom plate inserts was determined based on an estimate of the moisture uptake by the bottom plate inserts in the pre-wetting process in test 3. The estimate assumed that a steep moisture front occurred within the wood due to water uptake by the surfaces which were exposed to water during the pre-wetting process in test 3. The initial moisture content within the saturated zones was given as 600 kg/m³, and within the non-wetted zones, the measured moisture content of 55% of the inserts before the wetting process was used. Appendix E presents the development of the assessment of the depth of the wetted fronts in the transverse and longitudinal directions. A diagram showing the section of the wall assemblies at the level of the bottom plate is shown in Figure 6.2, and includes the vapor and liquid moisture fluxes g_v and g_w , respectively, from the wall components and in the various zones in the bottom plate, as well as the heat flux, q , from the interior to the exterior of the wall assembly.

The initial moisture content of other components was assumed to be uniformly distributed throughout each component. In the hygroscopic components where moisture content measurements were not taken, i.e. the spruce top plate and the gypsum, the initial moisture content was assumed using sorption data (see Appendix D), for equilibrium at a relative humidity of approximately 60%. Polyethylene, a non-hygroscopic material, was assumed to have an initial moisture content of zero. Fiberglass batt insulation, which is also usually considered to be non-hygroscopic, was also given an initial moisture content of zero. The assigned initial moisture contents for each material are shown in Table 6.4.

Table 6.3. The initial temperature assigned to each wall component.

| Component | Initial temperature [°C] |
|------------------------------|--------------------------|
| Gypsum | 20.0 |
| Polyethylene membrane | 20.0 |
| Spruce top and bottom plates | 13.0 |
| Fiberglass batt insulation | 13.0 |
| Sheathing | 6.0 |

Table 6.4. The initial moisture content assigned to each wall component.

| Component | Initial moisture content [% / kg/m ³] |
|---|---|
| Gypsum | 0.5 / 3.24 |
| Polyethylene membrane | 0 / 0 |
| Spruce top plate | 13.3 / 53.0 ¹ |
| Spruce bottom plates, saturated zones | 175.3 / 600.00 |
| Spruce bottom plates, non-saturated zones | 16.1 / 55.00 |
| Fiberglass batt insulation | 0 / 0 |
| Sheathing | OSB: 10.0 / 65.00 plywood: 11.0 / 51.67 fiberboard: 4.1 / 13.01 |

¹ The initial moisture content in kg/m³ is determined assuming a spruce density of 400 kg/m³ since the density of the top plates was not measured.

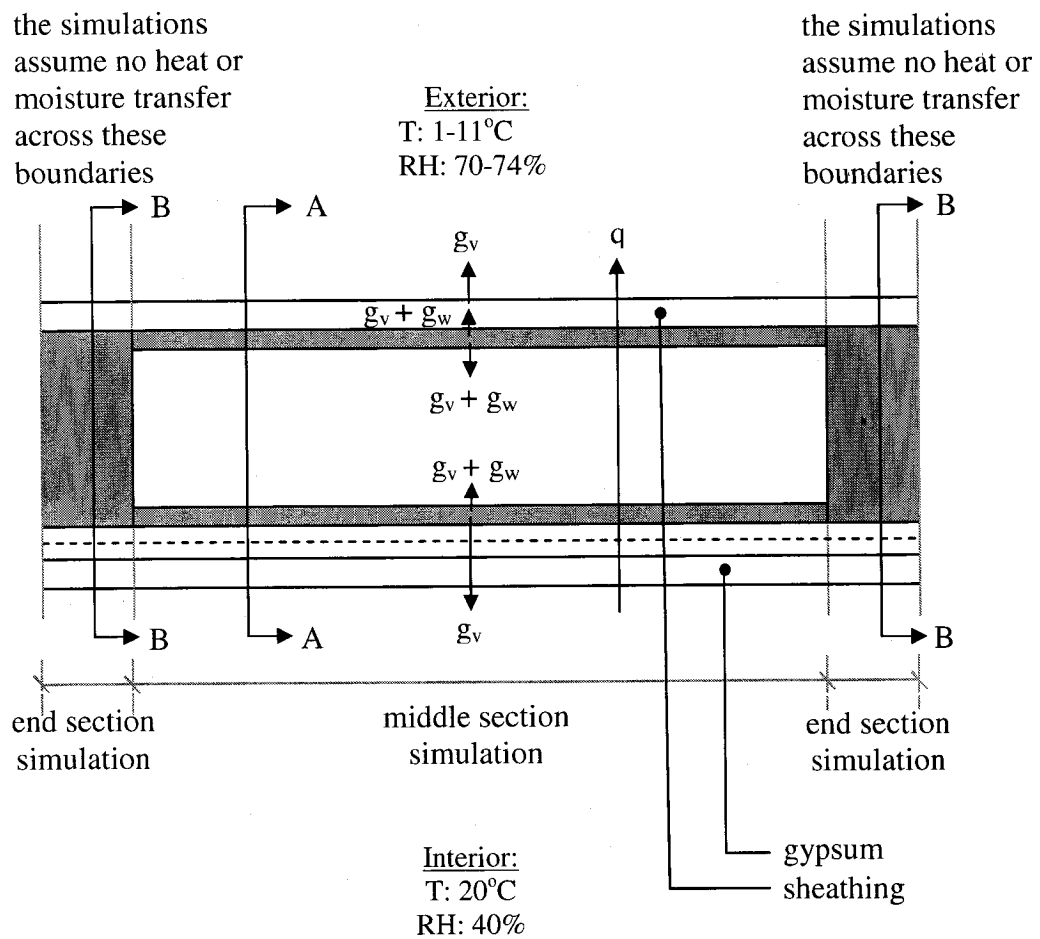


Figure 6.2 a) Horizontal wall cross-section.

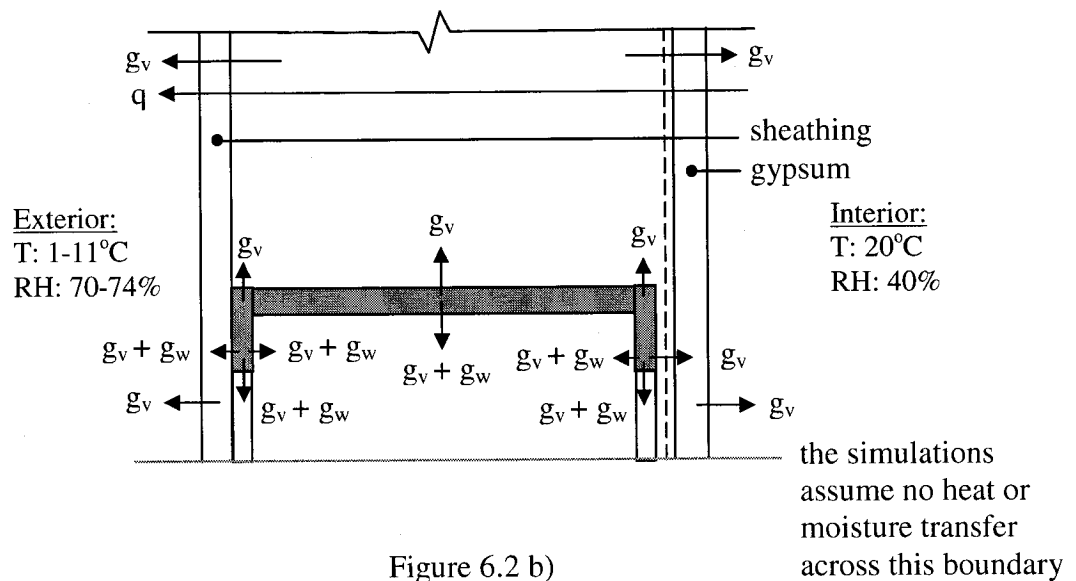


Figure 6.2 b)
Middle section simulations
(section A-A)

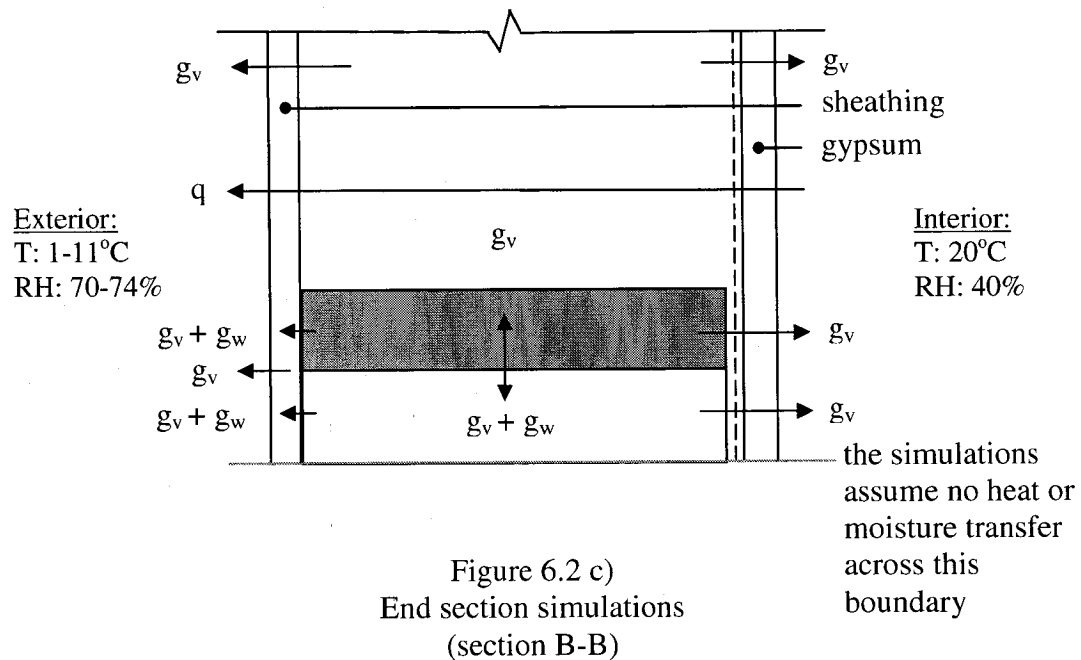


Figure 6.2 Horizontal wall cross section (a) and vertical wall cross-section for the middle (b) and end (c) sections (see Figure 6.2 c) for at the level of the bottom plate for a wall with a polyethylene vapor retarder showing the localized vapor and liquid moisture fluxes, g_v and g_w , respectively, from the wall components and in the various zones in the bottom plate, as well as the general heat flux, q , from the interior to the exterior. The bottom plate zones shaded in grey were initially saturated.

6.2.5. Simulation results

The experimental and simulation moisture content results for the bottom plate moisture content of walls 1 to 6 are shown graphically in Figure 6.3, with markers identifying the experimental measurements, typically taken at one-day intervals, and curves showing the simulation results. Both the experimental and simulation results show a similar drying trend in the bottom plate inserts. However, the moisture contents measured experimentally in all six walls show greater drying rates than do the simulations. The difference between the final moisture contents obtained experimentally and numerically ranges from 7.4% (in wall 1) to 13.32% moisture content (in wall 6).

The general effect of the sheathing on the drying behavior of the bottom plate insert is similar in both the experimental and the simulation work: the drying rate is highest in the wall with fiberboard sheathing, and lowest in the OSB-sheathed wall. The curves in Figure 6.3, and the final moisture contents obtained from the experiment and the simulations does not permit an accurate portrayal of the hygrothermal behavior of the inserts because of the slightly different initial moisture contents obtained in the experiment. In order to obtain a global portrait of the drying rate over the course of the test, the average of the slopes between the discrete experimental moisture content data points was calculated to represent the average rate of drying. The same was done for the simulation results using the moisture contents at the same point in time as the gravimetric measurements. The average drying rates are summarized in Table 6.5.

Comparing the response in walls 1, 2 and 3 with different sheathings, both the experiment and the simulations show that the average drying rate was lowest in OSB-sheathed wall 1. The drying rate in fiberboard-sheathed wall 3 given by the experimental data is significantly higher, while in the numerical work, the average drying rate for wall 3 is about the same as that for plywood-sheathed wall 2. In walls 4, 5, and 6, also with different sheathings, the experimental data indicates the same drying rate for the OSB and plywood-sheathed walls 4 and 5, and a higher drying rate for wall 6 with the more vapor permeable sheathing. The average drying rates from the simulations are lower for the OSB-sheathed wall 4 and about the same for plywood- and fiberboard sheathed walls 5 and 6, as was the case in walls 1 to 3.

The simulation results show repeatable trend in the walls with different sheathings – low drying rate in the OSB-sheathed wall and higher similar drying rates in the plywood and fiberboard-sheathed walls for both series of walls. This suggests that in the simulations, the hygrothermal response of the bottom plates are due to different moisture transport in the sheathing. It is hypothesized that the both the sheathings' vapor permeance (Figure 6.4) and liquid diffusivity (Figure 6.5) play a role in the drying response of the wall. OSB has both a low vapor permeance and a low liquid diffusivity, which explains why the drying rate in the OSB-sheathed walls 1 and 4 is low. Plywood, in comparison, also has a relatively low vapor permeability but a high liquid diffusivity, that latter of the two being the likely reason for the higher drying rate of the insert in the

plywood-sheathed walls 2 and 5. Fiberboard, on the other hand, has both a high vapor permeance and a high vapor liquid diffusivity, which explains why the simulation results shows that the insert in the fiberboard-sheathed walls have a lower drying rate. However, given that the vapor permeance of fiberboard is significantly higher than that of OSB and plywood, a higher drying rate than that given by the simulation would be expected.

Two numerical sensitivity analyses were done to see the effects of artificially increasing the water vapor permeability of the OSB by a factor of 100 (up to a maximum vapor permeability of water vapor in air), and increasing the liquid diffusivity of the OSB by a factor of 100. Increasing the vapor permeability increased the average drying rate from 0.66 to 0.76; increasing the liquid diffusivity increased the average drying rate to 0.73 (see Figure 6.6). Therefore, a high sheathing permeability and a high liquid diffusivity increases the drying potential of the wall. Both these tests indicate that the use of fiberboard, which has both a high vapor permeability and a high liquid diffusivity, should significantly promote drying of the bottom plate insert. Based on these results, another calculation was run to see the impact of another material property, sheathing sorption, on the wall response. The OSB-sheathed wall 1 was used again, with an increased vapor permeability as before, but using the sorption curve of fiberboard, which has a comparably low moisture absorption capacity per unit volume, particularly at low relative humidities (Figure 6.7). Changing the sorption curve resulted in decreasing the average drying rate from 0.76 to 0.73. Therefore, the results showed that the sheathing moisture absorption capacity has an impact on the wall behavior.

The simulations also showed that changing the vapor retarder from the traditional polyethylene film to low permeance primer consistently increased the average drying rate of the bottom plate insert by 0.02. However, the experimental results showed that the effect of the type of vapor retarder varied depending on the type of sheathing used: in the OSB walls, the drying rate increased by 0.27 when low permeance primer was used; in the plywood-sheathed walls, the increase was smaller at 0.09; and in the fiberboard-sheathed walls, changing the vapor retarder had no effect.

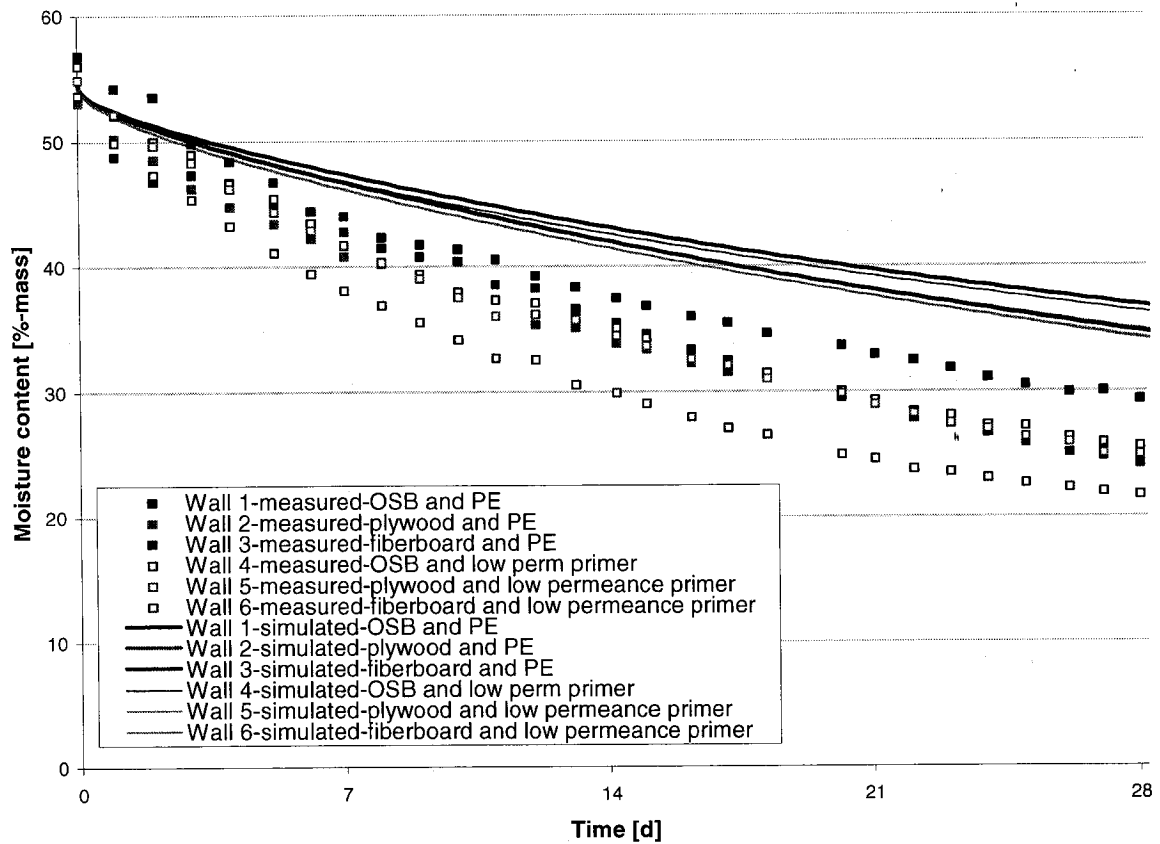


Figure 6.3. Moisture content in the bottom plate inserts in walls 1 to 6 from the first 28 days of the third experiment and from the simulations. The markers show gravimetric moisture content measurements from test 3, and the curves show simulation results.

Table 6.5. Average drying rate of the bottom plate inserts, calculated from the results of experiment 3 and the WUFI 2D simulations.

| Wall number | Sheathing | Vapor retarder | Average drying rate | |
|-------------|------------|----------------------------|---------------------|------------|
| | | | Experiment | Simulation |
| 1 | OSB | Polyethylene membrane | 0.83 | 0.66 |
| 2 | plywood | | 1.01 | 0.73 |
| 3 | fiberboard | | 1.16 | 0.74 |
| 4 | OSB | Low permeance primer paint | 1.10 | 0.68 |
| 5 | plywood | | 1.10 | 0.75 |
| 6 | fiberboard | | 1.16 | 0.76 |

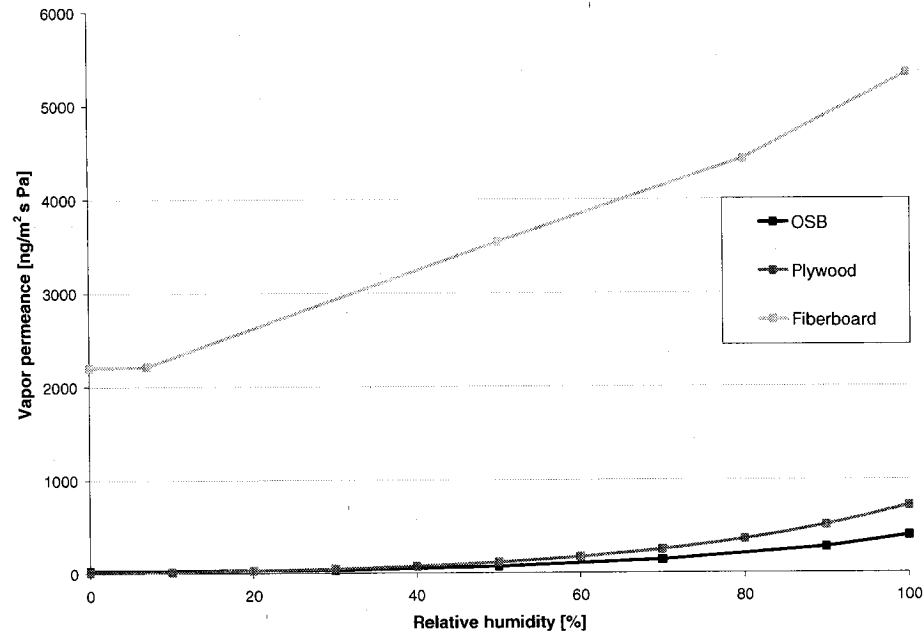


Figure 6.4. Vapor permeance of OSB, plywood and fiberboard. The data for OSB is derived from the WUFI Pro database for a density of 600 kg/m^3 ; the data for plywood is taken from Kumaran *et al.* (2002b) for plywood with a density of 470 kg/m^3 and a thickness of 12.7 mm, and; the data for fiberboard is taken from the WUFI Pro database for fiberboard with a density of 300 kg/m^3 .

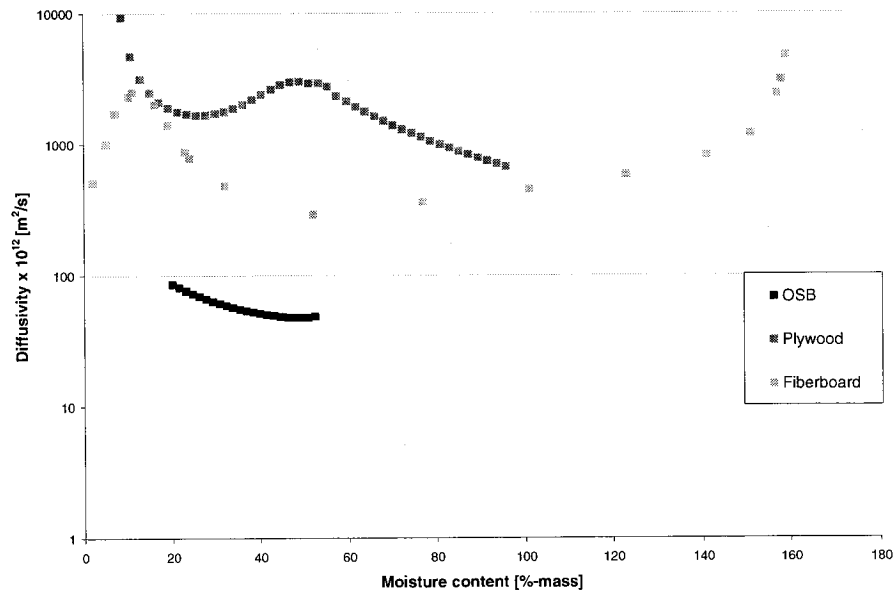


Figure 6.5. Liquid diffusivity of OSB, plywood and fiberboard. The data for OSB is derived from Kumaran *et al.* (2002) for OSB with a density of 650 kg/m^3 and a thickness of 12.7 mm; the data for plywood is taken from Kumaran *et al.* (2002b) for plywood with a density of 470 kg/m^3 and a thickness of 19 mm, and; the data for fiberboard is taken from NRCC data published in Kumaran (1996b) for fiberboard with a density of 243

kg/m³.

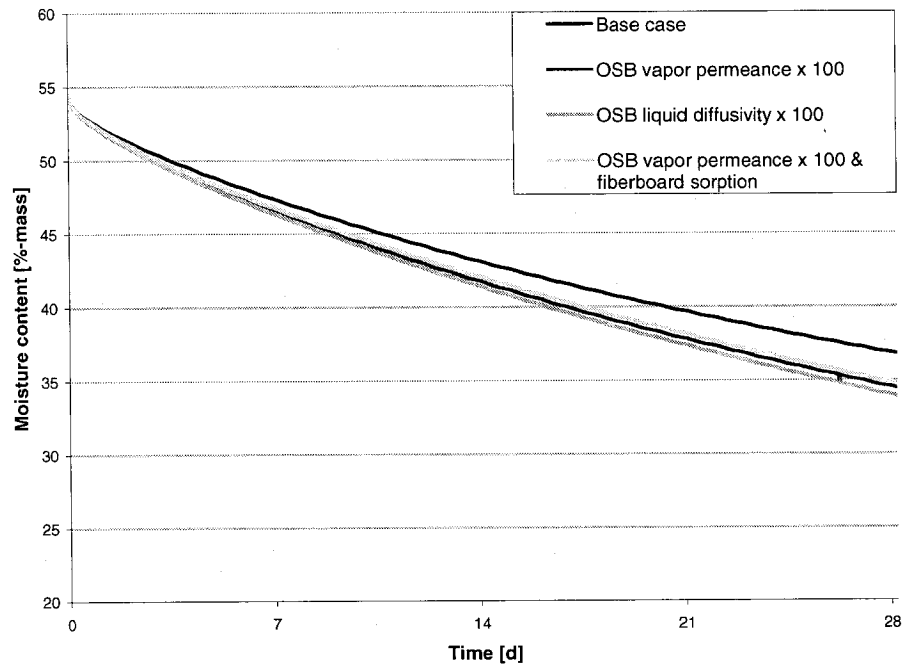


Figure 6.6. Moisture content in the bottom plate inserts in wall 1 for the base case, when the OSB permeance is increased by a factor of 100, and when the OSB liquid diffusivity is increased by a factor of 100.

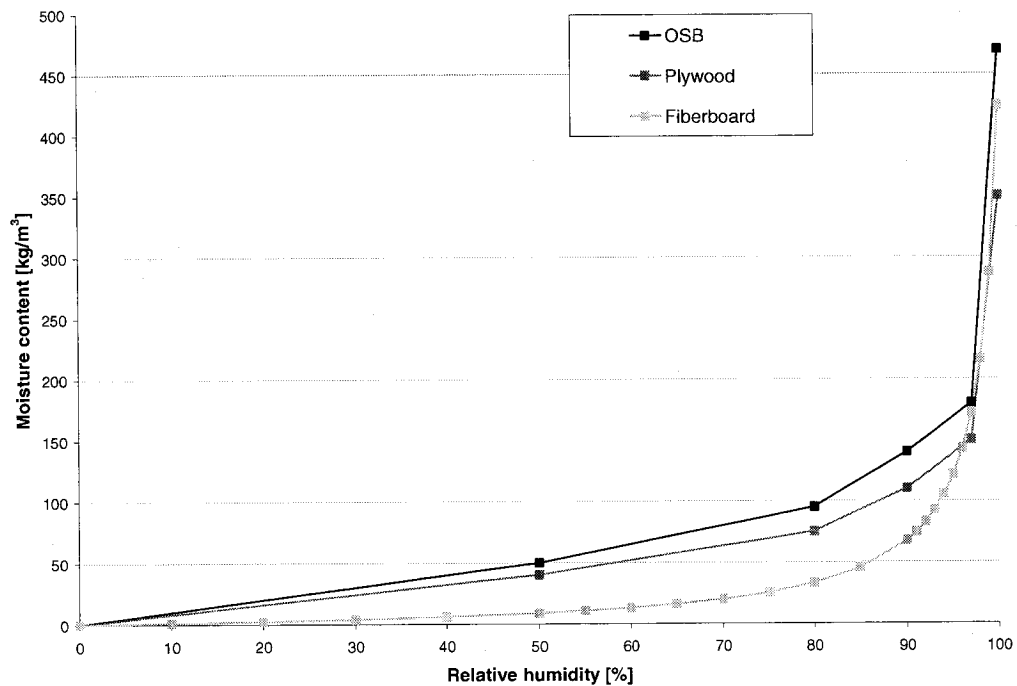


Figure 6.7. Sorption curves for OSB, plywood and fiberboard based on volumetric moisture content. The data for OSB, plywood and fiberboard are taken from the WUFI

Pro material database for OSB with a density of 630 kg/m^3 , plywood, 500 kg/m^3 , and fiberboard, 300 kg/m^3 .

In the following section, the simulation results and those from the third experiment are compared and reasons for the differences between the two are given.

6.3 Comparison of simulation results and results from test 3

As was said earlier, the drying rates found using the experimental moisture content results were significantly higher than those derived from the simulations. This could be an indication of one or more phenomena occurring during the experiment that is not taken into account by the model. Explanations or possible reasons for the difference between experimental and numerical results are given below.

1. Numerical tools typically do not take into consideration mass transfer with envelopes in the form of air convection. Thermally-driven convection loops form in cavities such as sealed cavities in glazing systems, and in stud cavities insulated with porous insulation materials when these are exposed to a temperature differential on each side, as was the case in the experiment. The convection loops carry not only heat and air, but also water vapor. Air movement within the fiberglass batt insulation-filled stud cavity was not monitored in the experiment. It is expected that a convection loop in the cavity would carry the moisture evaporating from the wet bottom plate on an upward path along the interior surface of the stud space, depositing the moisture in the hygroscopic materials at the boundary of the stud space, as shown in the schematic in Figure 6.8. The presence of air movement in the stud cavity decreases the water vapor gradient within the stud space and the relative humidity above the wetted bottom plate insert, thus promoting vapor evaporation at the surface of the insert.
2. The occurrence of unintentional air leakage in the wall assemblies during the experiment could also have affected the moisture response of the bottom plate inserts. Air leakage through the wall assemblies was not monitored, although the measured air pressure difference across the walls of the test hut was on the order

of ± 2 Pa.. The six walls were located near the cold box's recirculation fan which created a zone of high turbulence, which could have resulted in a zone of negative pressure at the exterior wall surface, thereby promoting exfiltration. Both the interior gypsum board and the sheathing were not airtight due to the presence of an access door in the gypsum and to gravimetric samples in the sheathing. The presence of air leakage could explain why the average rate of drying is the same for both fiberboard-sheathed walls and is higher than in any other wall: the air permeability of fiberboard sheathing is two to four orders of magnitude that of OSB and plywood (Kumaran *et al.*, 2002b), thereby facilitating air migration.

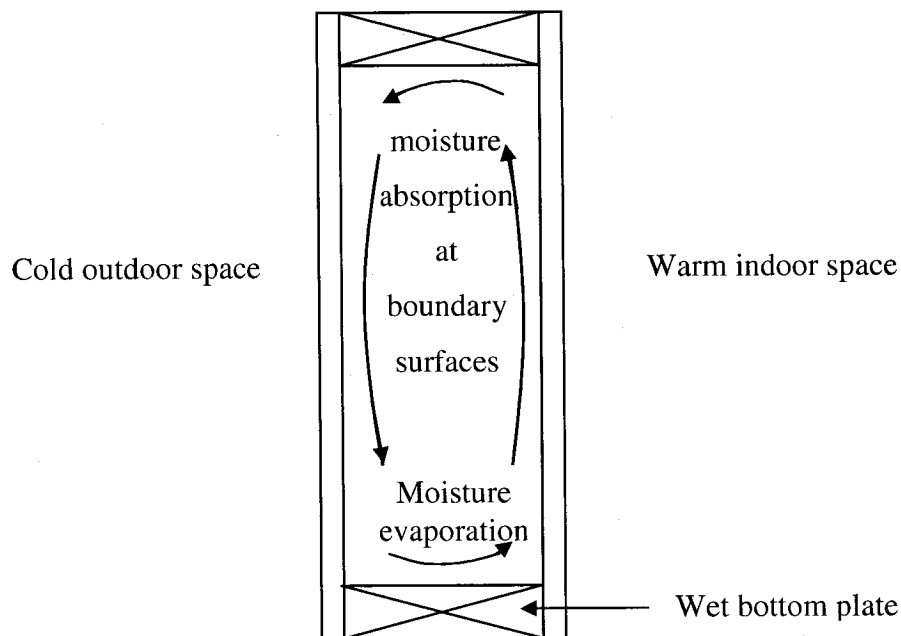


Figure 6.8. Schematic showing the moisture laden air convection loop within an insulated stud cavity.

3. The difficulties of using a two-dimensional domain of calculation to simulate three-dimensional wall systems with highly anisotropic materials properties and with three-dimensional moisture profile in the bottom plate inserts – and in particular, in this case, the assumed initial moisture distribution within the bottom plate. The simplified moisture content distribution in the bottom plate insert to determine the depth of the moisture front in the transverse and the radial directions assumed a steep moisture front where the exterior zones were saturated

and the non-saturated zones were not wetted at all. In reality, a more gradual moisture content gradient would result from the wetting process (Derome *et al.*, 2005), and therefore the assumed steep moisture front decreases the accuracy of the simulation results. The initial moisture content in the materials other than the bottom plate was not measured, and as such, initial moisture content values were taken as the equilibrium moisture content of each hygroscopic material with an environment of 60% relative humidity. This assumption may have reduced the accuracy of the simulations.

4. In addition, the material properties used for the various wall components were obtained from a variety of sources and may or may not reflect the actual properties of the materials tested. Moreover, the material properties found did not cover the entire moisture content range and did not take into account the anisotropic material properties of wood and wood-based materials. This is particularly true for the liquid diffusivities at high moisture contents for wood components like spruce top and bottom plates and the wood-based sheathings, and could have an impact on the simulation results. In hindsight, material property testing of the materials used in the experiment should ideally have been conducted to increase the accuracy of the simulations. In addition, the homogenization of the material properties of asphalt-coated fiberboard may also have contributed to the difference between experimental and numerical results. In fact, the asphalt coating on both major surfaces effectively reduces liquid flux into the material, but is difficult to model numerically mainly for the complete lack of material property data;
5. In simulation work, wall assemblies are modeled in such a way that interface transport resistances are neglected, an oversimplification which may result in errors in the calculation of heat and moisture fluxes. The presence of small air gaps between components, e.g. at the interface of the bottom plate insert and the sheathing, may in fact increase the drying rate of the wet materials at these surfaces. In the experiment, the presence of small air gaps at the interface of the 38 x 140 mm ends of the bottom plate inserts and the adjacent studs likely promoted moisture evaporation from the insert, thus increasing the overall drying

rate of the inserts. However, the two-dimensional model does not take moisture transport in the plane of the wall into account. Hence, neglecting the interface resistance in the simulations likely underestimated the drying response of the bottom plate insert. In addition, simplifications made in the simulation assumed no heat or moisture transfer from the bottom surface of the bottom plate insert, while in reality a small moisture flux may have occurred between the bottom plate insert and the bottom plate below.

6. The selected value of the exterior heat transfer film coefficient, h_{ext} , of 22.7 W/m²K, which is suggested by ASHRAE (2001) for a wind speed of 3.4 m/s, likely overestimated the heat transfer at the exterior surface of the wall, thereby reducing the temperature of the exterior sheathing and of the adjacent components. An additional simulation was conducted to investigate the effect of the exterior heat transfer film coefficient on the moisture response of the bottom plate insert in OSB-sheathed/polyethylene wall 1. A convective heat transfer coefficient, h_{conv} , for the measured air velocity of 1.1 m/s was calculated based on a simplified equation from McAdams (1954), given in ASHRAE (2001) for heat transfer over a plane surface and air velocities less than 5 m/s:

$$h_{conv} = 5.62 + 3.9V = 5.62 + 3.9(1.1) = 9.9 \text{ W/m}^2\text{K} \quad [6.13]$$

The coefficient for the radiative heat transfer, h_{rad} , between the wall assemblies and the Environmental Chamber was based on a measured temperature on the exterior of the wall surfaces of 20.9°C and on the interior surface of the Environmental Chamber of 19.0°C. To determine the angle factors, the two surfaces were assumed to be parallel and at a distance of 450 mm, and for simplicity, of both surfaces were given the dimensions of wall assembly. A graph to determine the angle factors is given in ASHRAE (2001). The emissivity of the exterior wall surfaces and of the interior Environmental Chamber wall surface were taken as 0.9 and 0.2, respectively, and were used to calculate the emissivity factor. The coefficient of radiation heat transfer, h_{rad} , was calculated as 0.47 W/m²K. The exterior heat transfer film coefficient, h_{ext} , determined as the sum of the convective and radiative components, was 10.4 W/m²K. A comparison of the WUFI-2D moisture content simulation results for wall 1 using the exterior heat

transfer film coefficients of $22.7 \text{ W/m}^2\text{K}$ and $10.4 \text{ W/m}^2\text{K}$, yielded an insignificant difference for the moisture content values, as expected.

The following section makes use of the general wall set-up of OSB-sheathed wall 1 from the above-described simulation to conduct parametric analyses on the role of exterior insulation and on the stud cavity height on the hygrothermal performance of wood-frame walls, as well as the impact of wind-driven rain loading on the response of the walls.

6.4 Parametric Analyses and Effect of Duration of Exposure

Parametric analyses were conducted using WUFI 2D to compliment the analysis of the hygrothermal performance of wall assemblies in tests 1 and 2. The goal of the parametric analyses was to provide additional information to examine in more detail the impact of the following parameters:

- adding exterior insulation;
- increasing the stud cavity height;
- increasing the moisture loading in terms of the wetted surface area, and;
- increasing the frequency of the moisture loading.

A last test was conducted to examine the wall's response as a function of the duration of exposure, where the series of simulations were run from April to October. The wall configuration and moisture loading for the parametric analyses were based on the wall set-up of tests 1 and 2 and the tests' ensued moisture distribution results. The tests were conducted for a wall sheathed with OSB and with a polyethylene vapor retarder. The results of the numerical simulation re-creating the experimental set-up for this wall, shown graphically in Figure 6.3, showed experimental and simulation results to be within 7.4% moisture content, or 14% error, for this wall. The following sections describe the simulation set-up including the description of the assemblies, the wetting approach and schedule, and the climate loading, surface transfer and initial conditions for the simulation work.

6.4.1 Description of test set-up

This section highlights details of the assemblies' description, wetting and drying schedule, and climate loading, surface transfer and initial conditions.

6.4.2 Description of the assemblies

The wall assemblies simulated in the modeling work are the same in dimension, configuration and material types as was described in the experimental protocol for test no. 3 in section 4.8 of the thesis and in the above work, with the exception that the wall assemblies used a stud cavity height of 1000, reflecting the wall set-up in experiments 1 and 2. A vertical section view of the wall assembly is shown in Figure 6.1. The wall's materials, their thicknesses, material properties and material functions are described in Appendix D.

6.4.3 Wetting method and schedule

In the simulations, the wetting method was performed in a way that reflected the findings of experiments 1 and 2. As such, the sheathing and the bottom plate were wetted at the interface of these two; in addition, the top surface of the bottom plate was wetted, as shown in Figure 6.9. As the figure shows, the width of the saturated surface on the top of the bottom plate was 20 mm. A set of simulations was also done for OSB-sheathed wall 1 where the width was doubled to 40 mm to investigate the impact of the loading on the response of the wall.

While simulation models like WUFI do consider impinging wind-driven rain as an input variable, they do not permit water *infiltration* loading into a wall assembly. Therefore, a wetting schedule was adopted to simulate periodic water infiltration loading. The four week simulation tests were broken down into weekly intervals where the wetted zones in the bottom plate and sheathing components were initially saturated each week, reflecting a weekly wind-driven rain infiltration event. For non-wetted components, the

final moisture content of the component at the end of each week was used as the initial moisture content at the start of the following week.

One of the parametric analyses was also performed where the wetted components of the sheathing and the bottom plate were initially saturated on days 1, 2 and 3 of each week, and then allowed to dry from day 3 to day 7. This process was repeated for four weeks. This method reflects the general wetting protocol employed in experiments 1 and 2.

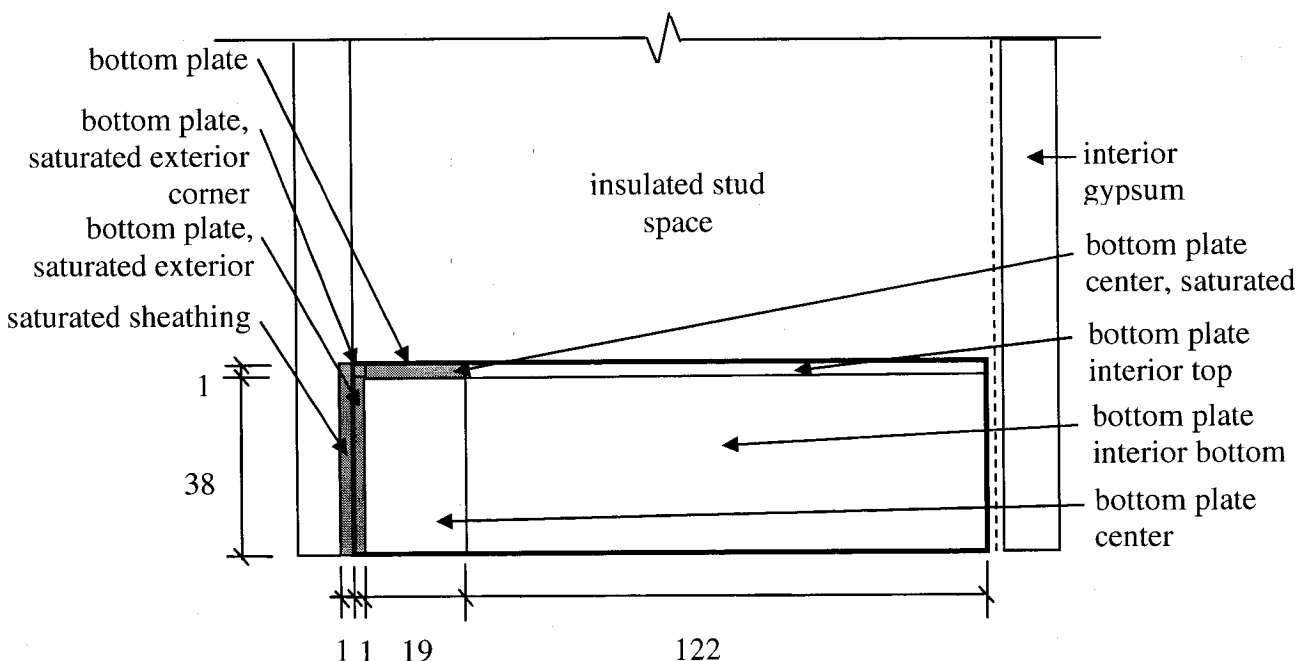


Figure 6.9. Vertical section view of the bottom of the wall assembly insert showing the areas in the sheathing and in the bottom depth that are saturated at each wetting event. Zones that are saturated on a weekly basis are shaded.

6.4.4 Climate loading, surface transfer and initial conditions

Climate

The exterior conditions that were set for the simulation were those stipulated as setpoints for the month of April in the experimental work, as determined by statistical analysis of a 20-year weather database provided by Environment Canada. In the simulations, however, sinusoidal values were used for the exterior relative humidity as well as the temperature, as shown in Table 6.6.

One series of simulations was run for the OSB-sheathed wall 1 to examine the impact of longer-term wetting and drying cycles on the drying performance. For this purpose,

the simulations were performed from April to October; the exterior temperatures and relative humidities for these months are detailed in Table 6.6. Constant indoor conditions were also set, as stipulated in the experimental work (see Table 6.6).

Table 6.6. Interior and exterior conditions set in test no. 3 and in the WUFI2D simulations.

| Period simulated | Duration (days) | Steady state indoor testing conditions | | Outdoor testing conditions | | | | | |
|------------------|-----------------|--|--------|----------------------------|------|-----|-----------------------|------|------|
| | | | | Temperature [°C] | | | Relative humidity [%] | | |
| | | Temp. [°C] | RH [%] | Mean | Min. | Max | Mean | Min. | Max. |
| April | 28 | 21 | 40 | 6 | 1 | 11 | 64 | 46 | 82 |
| May | 28 | 21 | 43 | 14 | 9 | 19 | 63 | 43 | 83 |
| June | 28 | 23 | 52 | 19 | 14 | 24 | 68 | 49 | 87 |
| July | 28 | 23 | 65 | 21 | 16 | 26 | 69 | 50 | 88 |
| August | 28 | 23 | 65 | 20 | 15 | 25 | 72 | 53 | 91 |
| September | 28 | 21 | 43 | 15 | 10 | 20 | 75 | 57 | 93 |
| October | 28 | 21 | 40 | 9 | 5 | 13 | 74 | 57 | 91 |

Surface transfer

Values and premises set for the exterior surface film heat transfer coefficient, radiation, surface vapor diffusion thickness, short and long-wave absorptivity at the exterior surface and impinging wind-driven rain are the same as those set for the above work. See section 6.2.4.

Initial conditions

The initial temperature was set for each material, as shown in the table below. Generally, components facing the exterior were given a temperature of 6.0°C, components facing the interior environment were given an initial temperature of 21.0°C, and components in the middle of the assembly were given a temperature of 13.5°C, reflecting the average of the exterior and interior temperatures.

Initial moisture content values were also set assuming moisture equilibrium with an environment at 60% relative humidity. Sorption moisture content data given in Appendix D were used for this purpose. For example, the bottom plate insert zones in the non-wetted zones start at with an initial moisture content of 13% moisture content. Polyethylene, a non-hygroscopic material, was assumed to have an initial moisture

content of zero. The same assumption was used for extruded polystyrene. The assigned initial temperatures and moisture contents for each material are shown in Table 6.7 and 6.8, respectively. It should be noted that the initial moisture contents described were only used at the beginning of the series of simulations. After the first week-long simulation, the moisture contents obtained at the end of a week, i.e. week 1, were used as initial conditions for the following week, i.e. week 2. However, the zones in the bottom plate and the sheathing that were wetted were assigned a saturation moisture content (as shown in Table 6.8) at each wetting event, i.e. at the beginning of each week.

Table 6.7. The initial temperature assigned to each wall component.

| Component | Initial temperature [°C] |
|------------------------------|--------------------------|
| Gypsum | 20.0 |
| Polyethylene membrane | 20.0 |
| Spruce top and bottom plates | 10.5 |
| Fiberglass batt insulation | 10.5 |
| Sheathing | 1.0 |

Table 6.8. The initial moisture content assigned to each wall component.

| Component | Initial moisture content [kg/m ³] |
|---|---|
| Gypsum, homogeneous | 3.24 |
| Polyethylene membrane | 0 |
| Spruce top and bottom plates, non-saturated zones | 53.00 |
| Spruce bottom plates, saturated zones | 600.00 |
| Fiberglass batt insulation | 0.03 |
| OSB, non-saturated zone | 65.00 |
| OSB, saturated zone | 470.00 |
| Extruded polystyrene | 0 |

6.4.5 Role of exterior insulation on the hygrothermal performance

Adding exterior insulation is a popular retrofit measure to increase the total thermal resistance of exterior wall assemblies. A simulation was run in order to see the impact of adding extruded polystyrene on the cold side of the sheathing. To this end, the materials and wall configuration of wall 1 were used, and a 38 mm panel of extruded polystyrene was added, on the exterior side of the exterior sheathing. The properties of the extruded polystyrene can be found in Appendix D. The new wall is sheathed with OSB and is

called wall 10, as it was in experiments 1 and 2.

The total moisture content of the bottom plates, plotted in Figure 6.10, shows that overall, adding the exterior insulation had a slight negative effect on the drying response of the bottom plate as a whole. The moisture content of the different zones within the bottom plate was also examined. Figure 6.11 shows the moisture content within the saturated exterior corner and saturated exterior zones of the bottom plate, both zones facing the saturated sheathing. The figure shows that the drying of the bottom plate within these zones is faster in the exterior insulated wall 10 than in wall 1, and is likely due to the higher temperatures experienced at those locations in wall 10, as illustrated in Figure 6.12 which gives the temperature at the geometric center of the saturated exterior zone in the bottom plate. This is also true for the saturated center and center zones, but to a lesser extent. While the saturated zones dry at a faster rate when exterior insulation is present, the relative humidity in the insulated stud space is higher (Figure 6.13), which causes a slightly higher moisture content in the top and bottom interior zones in wall 10 compared to wall 1. To summarize, the wetted zones in the bottom plate do exhibit more rapid drying when exterior insulation is applied to the wall because of the higher temperatures achieved within the stud cavity for the given exterior climate. However, a more detailed investigation in terms of risk of mold and fungal growth for longer exposure periods would be needed to determine whether or not the more rapid drying in wall 10 is sufficient to preclude biological damage.

The OSB sheathings in the two walls behave quite similarly, as shown in Figure 6.14, although it should be noted that while the sheathing moisture content in wall 10 is lower than that in wall 1 at the first and second weeks, the sheathing moisture content in wall 10 rises to surpass that in wall 1 at the end of the test. This is likely due to the greater outbound vapor diffusion caused by the presence of the exterior extruded polystyrene in wall 10. The saturated zone of the sheathing demonstrates a slightly more rapid drying response in wall 10 than in wall 1, shown in Figure 6.15, although the difference is not significant, and the warmer temperatures experienced by the saturated OSB in the exterior insulated wall 10 do not allow it to dry fast enough to preclude the risk of moisture-induced damage.

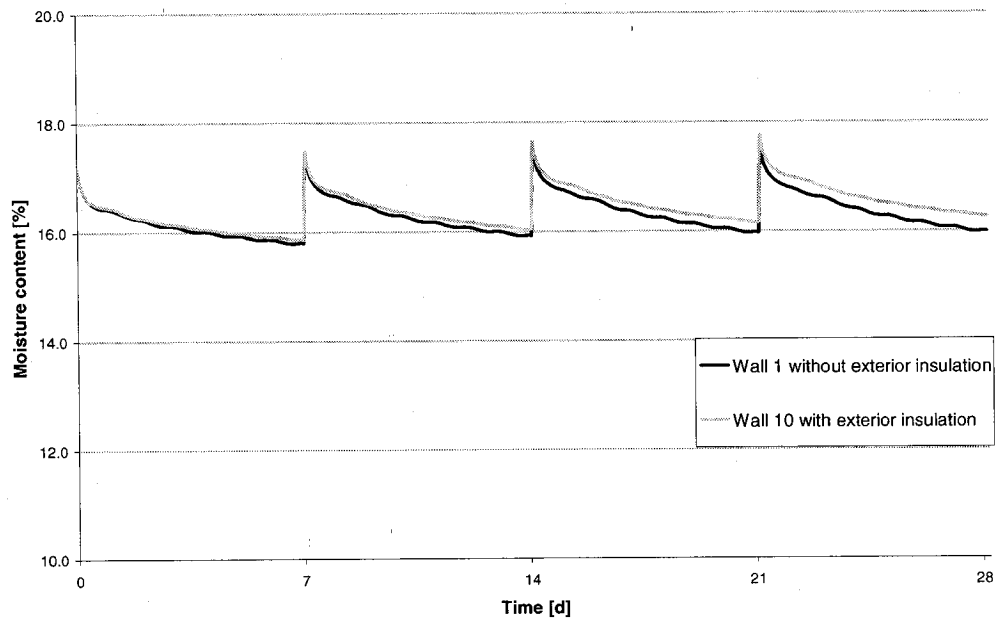


Figure 6.10. Total moisture content simulation results for the bottom plate of OSB-sheathed walls 1 and 10. Wall 10 has exterior extruded polystyrene insulation, while wall 1 does not. Refer to Figure 6.9 for the location of the components.

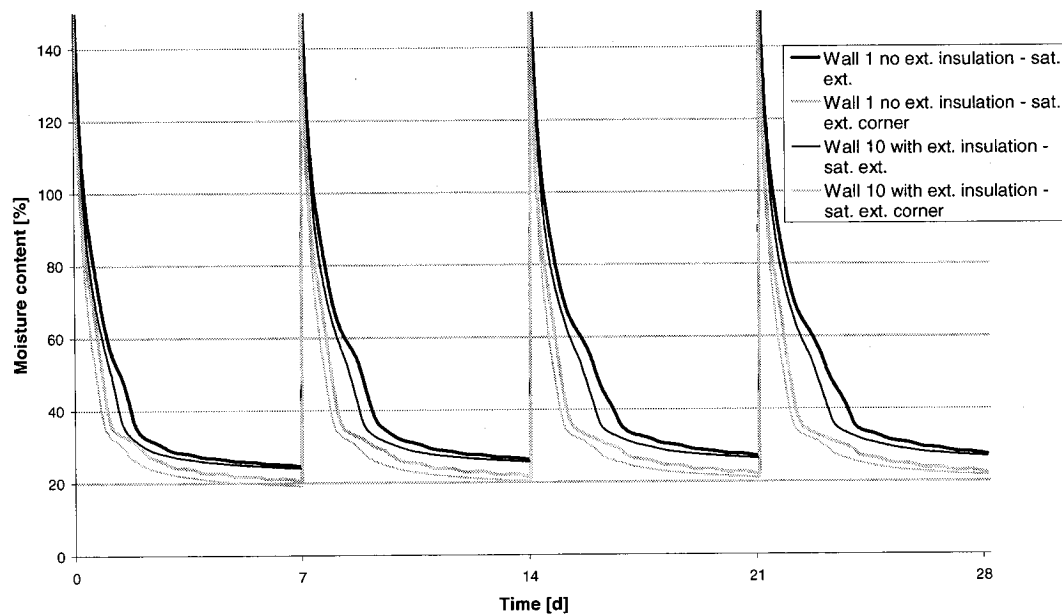


Figure 6.11. Moisture content simulation results in the saturated exterior and saturated exterior corner zones of the bottom plate for OSB-sheathed walls 1 and 10. Wall 10 has exterior extruded polystyrene insulation, while wall 1 does not. Refer to Figure 6.9 for the location of the zones within the bottom plate.

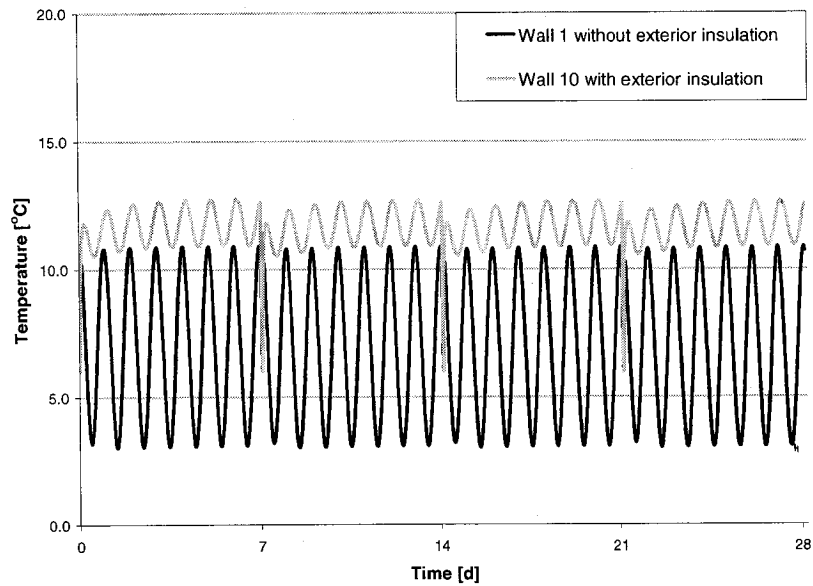


Figure 6.12. Temperature simulation results at the geometric center of the saturated exterior zone of the bottom plate OSB-sheathed walls 1 and 10. Wall 10 has exterior extruded polystyrene insulation, while wall 1 does not. Refer to Figure 6.9 for the location of the zones within the bottom plate.

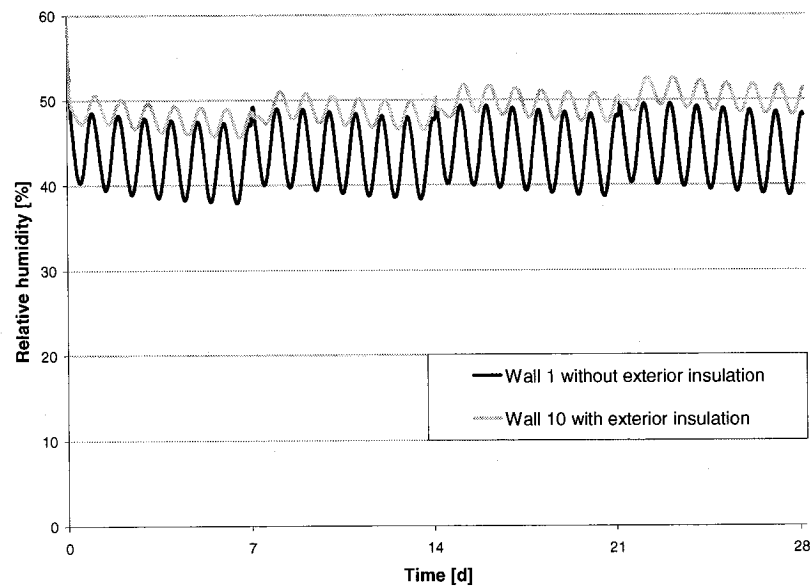


Figure 6.13. Relative humidity simulation results in the insulated stud space above the bottom plate in OSB-sheathed walls 1 and 10. Wall 10 has exterior extruded polystyrene insulation, while wall 1 does not. Refer to Figure 6.9 for the location of the zones within the sheathing.

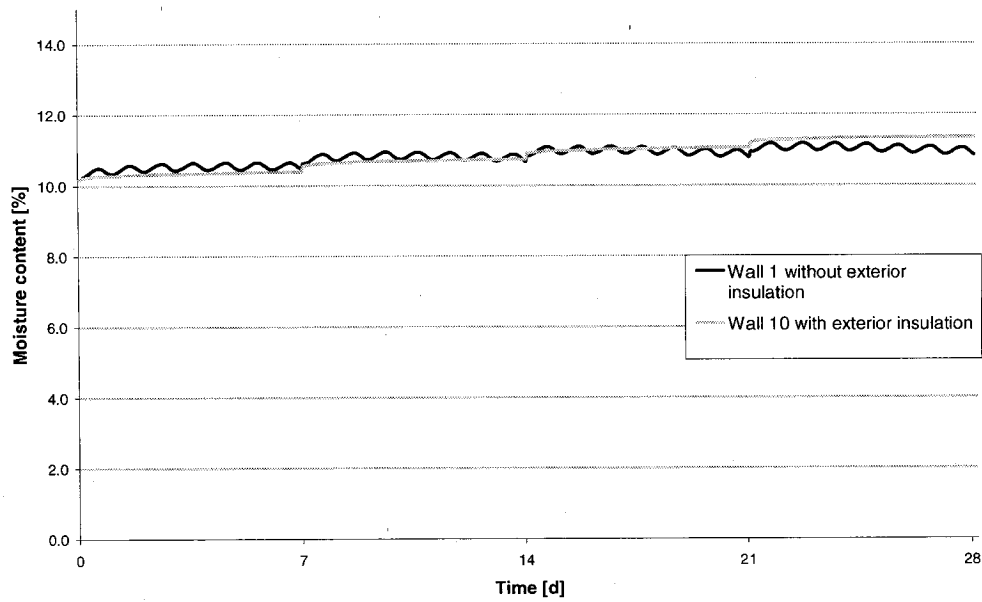


Figure 6.14. Total moisture content simulation results in the OSB sheathing for OSB-sheathed walls 1 and 10. Wall 10 has exterior extruded polystyrene insulation, while wall 1 does not. Refer to Figure 6.9 for the location of the wall components.

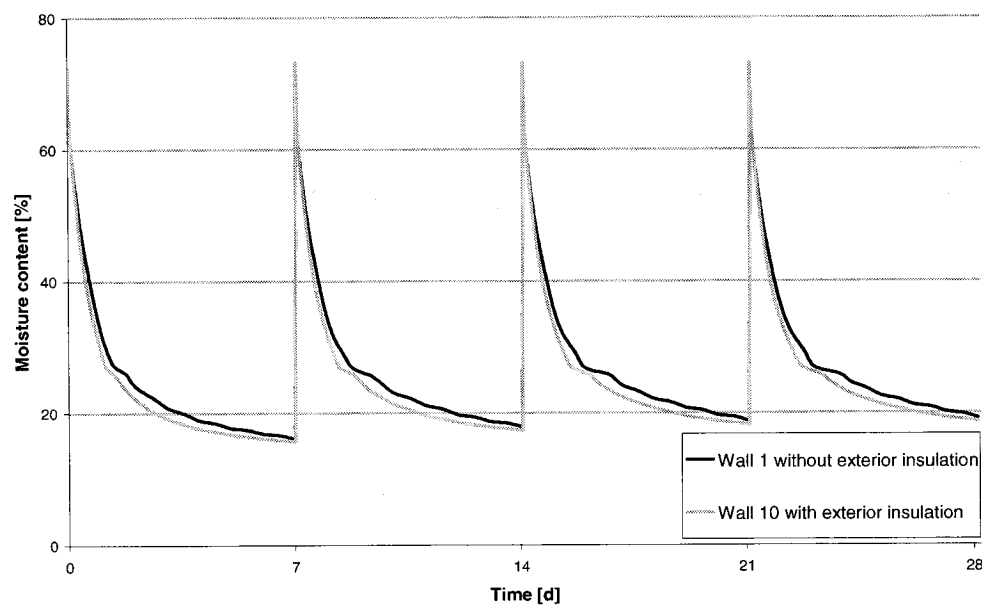


Figure 6.15. Moisture content simulation results in the saturated zone of the OSB sheathing for OSB-sheathed walls 1 and 10. Wall 10 has exterior extruded polystyrene insulation, while wall 1 does not. Refer to Figure 6.9 for the location of the zones within the sheathing.

A note should be made here about the impact of exterior insulation on the hygrothermal performance of wall systems, and the accuracy of the numerical results in

perspective of what could occur in actual walls. Adding exterior insulation in the form of extruded polystyrene could have an impact on the wall performance in terms of air transport. Extruded polystyrene board that fit together in a tongue and groove fashion with taped joints, or more so, sprayed polyurethane insulation, could reduce the likelihood for air leakage through the envelope, thereby decreasing the drying potential of the wetted components. It is recognized that air leakage is also a mechanism for moisture accumulation in the heating season. Using exterior insulation could also reduce potential for thermally induced convection since the thermal differential is decreased, thereby also reducing the potential for drying of wetted components. Numerically simulating the impact of exterior insulation should ideally take air transport into account in order to increase the accuracy of the predicted hygrothermal response.

6.4.6 Effect of stud cavity height on the hygrothermal performance

The simulation for the OSB-sheathed wall 1 described above in section 6.3.1 was repeated, this time doubling the height of the stud cavity to 2000 mm. The new wall is called wall 13, as it was in experiments 1 and 2. It was expected that increasing the height of the wall would increase the drying rate of the bottom plate inserts by the virtue that the surface area of the hygroscopic materials at the boundary of the stud cavity is doubled, thereby increasing their moisture absorption and at the same time decreasing the moisture content within the stud space. Figure 6.16 shows the simulation results of the case for the 1000 mm high stud cavity and the simulation with the increased stud cavity height of 2000 mm. The graph shows that increasing the stud cavity height has a negligible effect on the moisture performance of the bottom plate insert. However, the OSB sheathing in wall 13 is slightly lower, likely due to the fact that a greater sheathing surface area is available to absorb the moisture evaporating from the wetted insert, and therefore the mass of moisture on a basis of unit mass of sheathing is smaller.

As discussed earlier, numerical tools typically do not yet take into consideration mass transfer with envelopes in the form of air convection. Thermally-driven convection loops form in cavities such as sealed cavities in glazing systems, and in stud cavities insulated with porous insulation materials when these are exposed to a temperature differential on

each side, as was the case in the experiment. It is anticipated that increasing the height of the stud cavity should provide a greater volume of air within the porous fiberglass batt insulation and within the hygroscopic materials that envelop the stud cavity to absorb the moisture released from the wetted bottom plates, therefore possibly reducing the moisture content within the insulation above the bottom plate and increasing the bottom plate inserts' potential for evaporation.

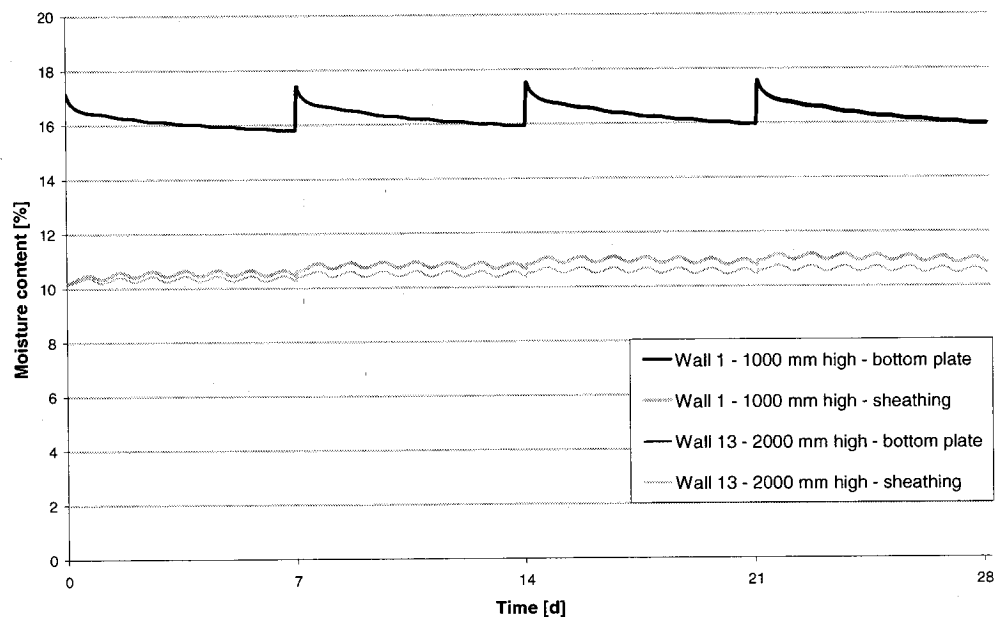


Figure 6.16. Global moisture content simulation results in the bottom plate and the OSB sheathing for walls 1 and 13, with a 1000-mm and 2000-mm high stud cavity, respectively. The total bottom plate moisture content curves for both walls are congruent. Refer to Figure 6.9 for the location of the components.

6.4.7 Impact of wind-driven rain infiltration loading on hygrothermal performance

Two simulations were run to investigate the impact of increased loading and increased frequency of wind-driven rain infiltration loading on the hygrothermal performance of the wall. In the first exercise, a simulation was performed for OSB-sheathed wall 1, where the wetted surface area on the top surface of the bottom plate was increased. In the second exercise, the frequency of the water infiltration loading was increased. In both sets of simulations, April exterior and interior loads were used, as before. Details of the moisture loading and results are presented below.

6.4.7.1 Impact of increased loading

A series of simulations were run for OSB-sheathed wall 1, where the total wetted width on the top surface of the bottom plate was increased from 20 mm to 40 mm, as shown in Figure 6.17. This simple simulation reflects what could occur if the rate of wind-driven rainwater infiltration increased, and the water which has made its way to the bottom plate spreads out on the top surface.

Moisture content results for the bottom plate and the sheathing were obtained for the case of increased loading in the OSB-sheathed walls. In the bottom plate, the total moisture content shows a significant difference in the case of the wall with a 40-mm wetted width, as shown in Figure 6.18. However, examining the moisture content of the different zones within the bottom plate indicates that there is little difference in the moisture content in these zones for both wetting schemes. The difference in the total moisture content of the bottom plate lies in the relative size of the two center zones and the two interior zones, and the moisture contribution that each brings to the total bottom plate. Total sheathing moisture content results due to the different loadings show little difference, as illustrated in Figure 6.18.

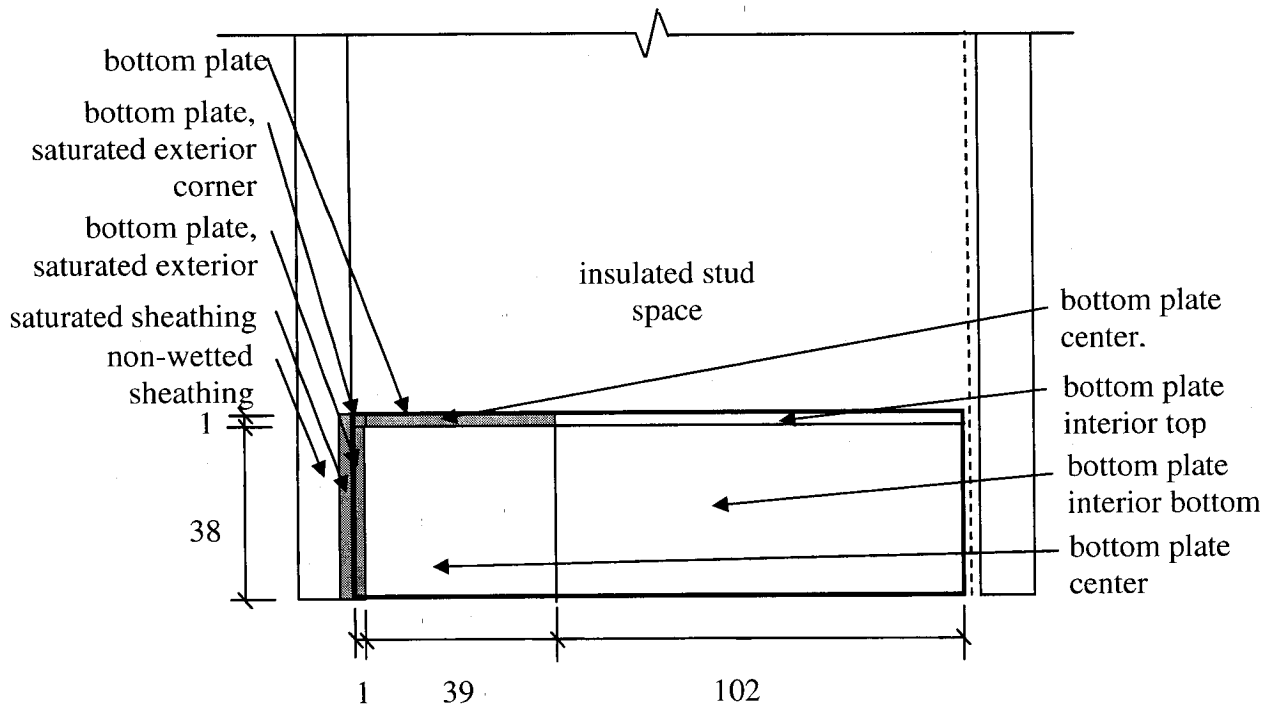


Figure 6.17. Vertical section view of the bottom of the wall assembly bottom plate showing the areas in the sheathing and in the bottom depth that are saturated at each wetting event. Zones that are saturated are shaded.

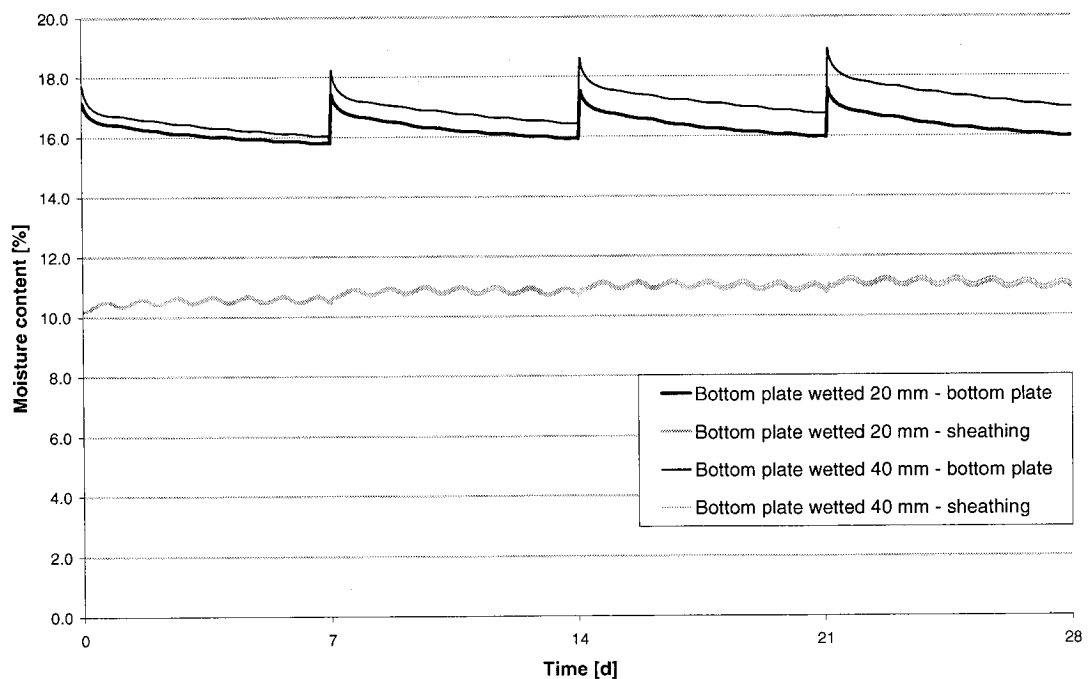


Figure 6.18. Global moisture content simulation results in the bottom plate and in the sheathing of the two OSB-sheathed walls, one with a bottom plate wetted width of 20

mm and the other with a width of 40 mm. Refer to Figure 6.17 for the location of the components.

6.4.7.2 Impact of increased frequency of loading

The impact of increased frequency of wind-driven rain infiltration was examined for the same OSB-sheathed wall 1, where the frequency of the water infiltration loading was increased from a weekly load to an infiltration event on three consecutive days per week for four weeks, reflecting the wetting methodology employed in experiments 1 and 2.

Figure 6.19 shows the total moisture content in the bottom plate in wall 1. As expected, increasing the wetting frequency resulted in a significant rise in the total bottom plate moisture content with time. The moisture content in all saturated zones of the bottom plate shows slower drying rates when the wetting load is increased. All zones exhibit higher final moisture contents when the wetting load is increased. Table 6.9 shows that the difference in the final moisture content in the bottom plate zones for wall wetted at different frequencies varied from 1.2% to 8.69% moisture content. More importantly, increasing the wetting frequency maintains the saturated zones in the bottom plate at moisture content levels greater than 20% for significantly longer periods of time (see Figure 6.20 for an example of the saturated center zone). In addition, the average moisture content within the core of the bottom plate, i.e. in the center zone, steadily increases with time from approximately 15.5% at the beginning of the month to 32% after just 28 days, as shown in Figure 6.20, due to moisture migration from both the saturated exterior and the saturated center zones. In the OSB sheathings, while the panels' global moisture content remain at acceptable moisture content levels well below 20%, the moisture content in the saturated zone of the frequently wetted wall stays at moisture contents well above safe levels for a longer duration of time, although the moisture contents in the saturated zone rises steadily with time in both cases, indicating that the saturated zone is at risk of moisture-induced decay even with a weekly rain infiltration event (Figure 6.21).

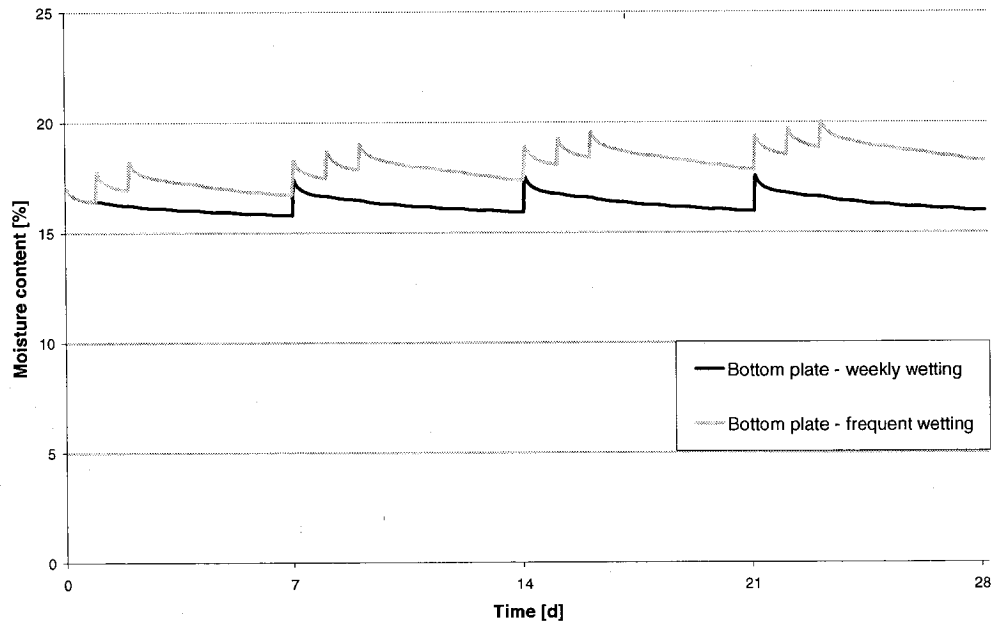


Figure 6.19. Total moisture content simulation results in the bottom plate of two OSB-sheathed walls, one which is wetted once a week, and the other three times a week. Refer to Figure 6.9 for the location of the components.

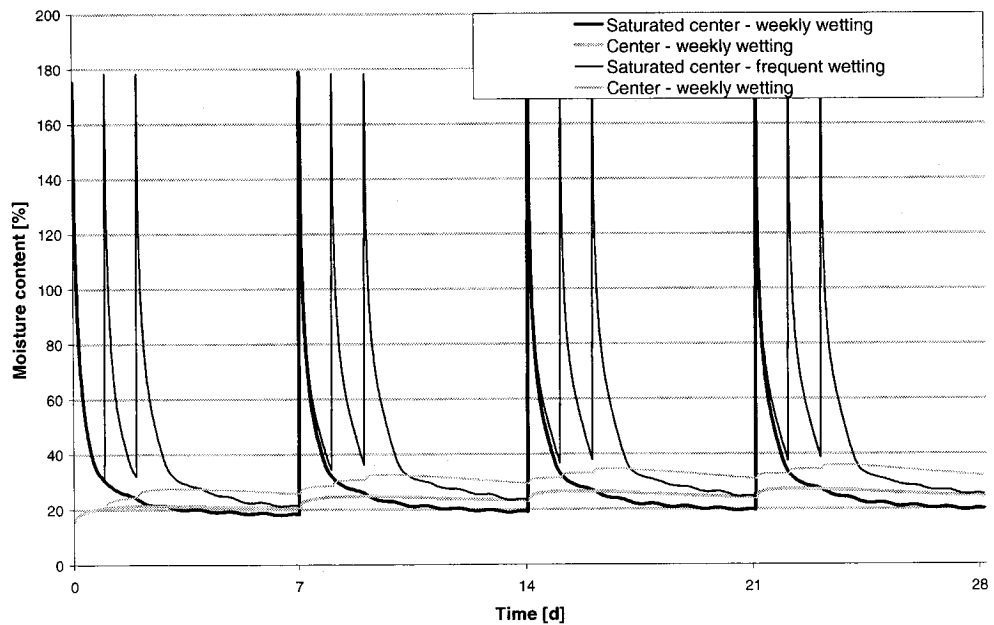


Figure 6.20. Moisture content simulation results in the saturated center and (non-saturated) center zones of the bottom plate for two OSB-sheathed walls, one which is wetted once a week, and the other three times a week. Refer to Figure 6.9 for the location of the bottom plate zones.

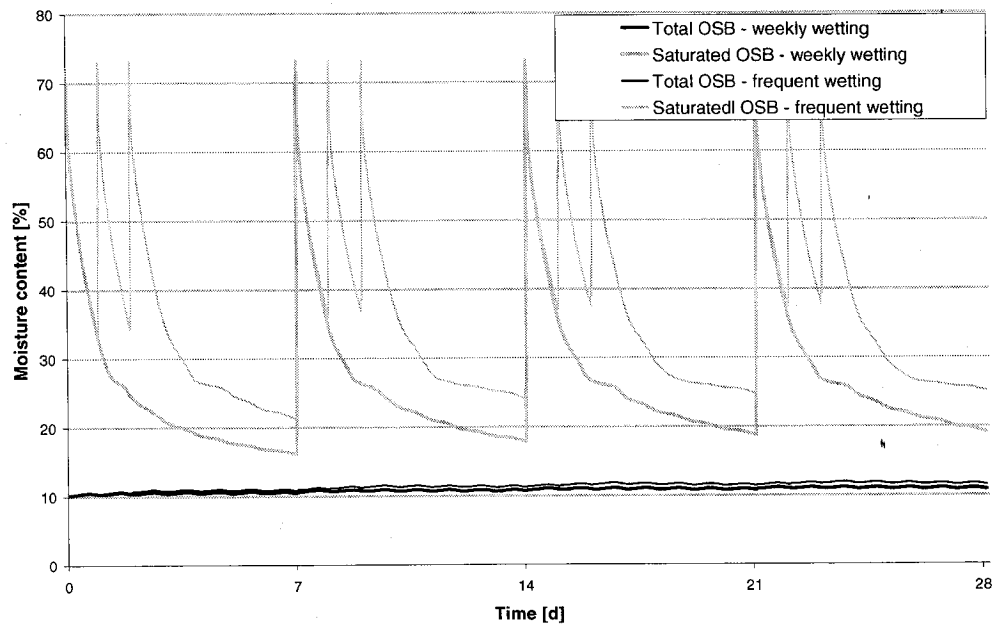


Figure 6.21. Moisture content simulation results in the sheathing as a whole and in the saturated zone of the sheathing for two OSB-sheathed walls, one which is wetted once a week, and the other three times a week. Refer to Figure 6.9 for the location of the bottom plate zones.

Table 6.9. Final moisture content simulation results in the bottom plate zones for two wall systems, one which is wetted once a week, and the other three times a week.

| Bottom plate zone | Final moisture content | | |
|---------------------------|------------------------|------------------|--------------------------------------|
| | Weekly wetting | Frequent wetting | Difference in final moisture content |
| Saturated exterior | 22.3% | 28.6% | 6.3% |
| Saturated exterior corner | 27.4% | 36.1% | 8.7% |
| Saturated center | 20.0% | 25.3% | 5.3% |
| Center | 24.6% | 31.9% | 7.3% |
| Top interior | 13.4% | 14.7% | 1.2% |
| Bottom interior | 14.6% | 16.0% | 1.4% |
| Total bottom plate | 16.0% | 18.3% | 2.3% |

6.4.8 Effect of Duration of Exposure on hygrothermal performance

A last series of simulations were run using the configuration of wall 1 to examine the impact of a prolonged exposure to a weekly rain infiltration load. It was hypothesized that the moisture accumulation in the bottom plate and the sheathing may be slowed or even reversed when the wall is exposed to warmer summer temperatures. As such, the

simulation was run with a weekly rain infiltration event for the months from April to October. Moisture content results for the bottom plate and the OSB sheathing are shown in Figure 6.22. The bottom plate shows a trend of increasing moisture content that continues throughout the warm summer months and slows down unexpectedly in the month of October. To explain this unanticipated finding, the moisture content in each zone of the bottom plate was examined, and it was found that the moisture content in all but two zones – the saturated center and the center zones – decreased in the last month of the simulation. A calculation was done to determine the amount of moisture contained in each zone which showed that the moisture gained in these two zones was offset by the loss in the other four zones. In addition to the continued simulated rain infiltration loading, the overall increase in moisture content in the bottom plate during the summer months can be explained by diffusive wetting of the wall system due to high exterior and interior relative humidities, and hence vapor pressures. Conversely, the drop in the total moisture content in the bottom plate during October is the result of the lower relative humidity in the stud cavity at that time, as seen in Figure 6.23, which is in itself due to lower exterior, and to a lesser extent, interior relative humidities.

As shown in Figure 6.24, the moisture content response of the sheathing increases during the course of the 7-month simulation, as anticipated. In the saturated zone, however, a steady increase is observed, but the rate of moisture accumulation is lower in the summer months, likely because the warmer exterior temperatures at that time permit the wetted zone in the sheathing to dry faster.

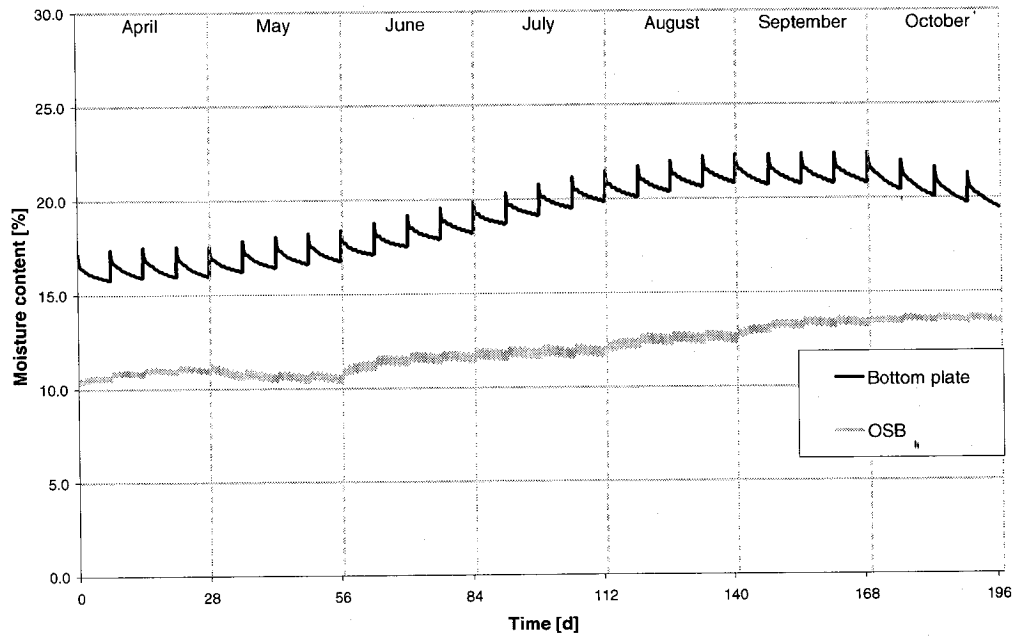


Figure 6.22. Global moisture content simulation results in the bottom plate and in the sheathing of OSB-sheathed wall 1. Refer to Figure 6.8 for the location of the components.

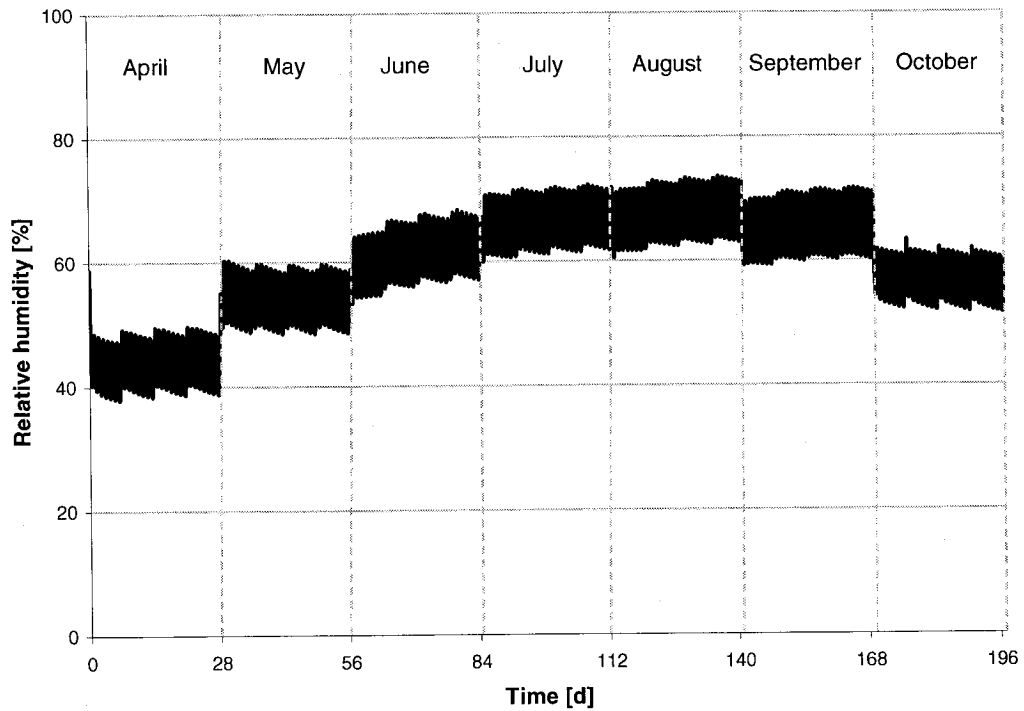


Figure 6.23. Relative humidity simulation results at the center of the insulated stud cavity above the bottom plate in OSB-sheathed wall 1.

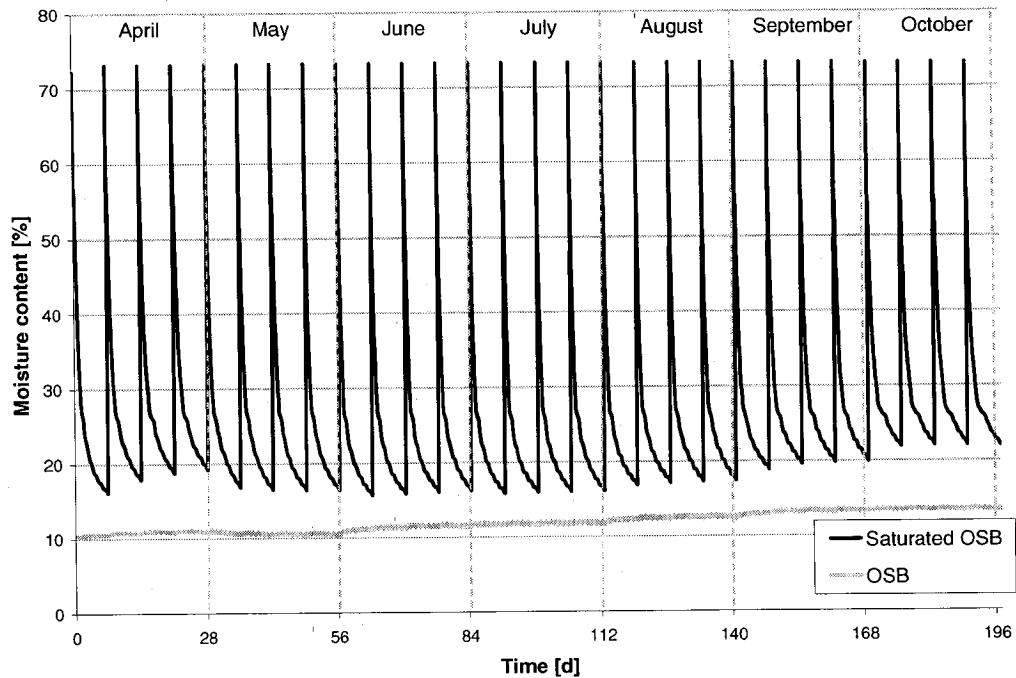


Figure 6.24. Global moisture content simulation results in the OSB-sheathed and in the saturated sheathing zone of wall 1. The wall is exposed to a weekly rain infiltration event. Refer to Figure 6.9 for the location of the saturated OSB zone.

6.5 Summary and Conclusions

A series of numerical simulations were conducted using assumptions and simplifications to recreate the test wall configurations, boundary conditions and initial conditions for the third experiment that was performed in the Building Envelope Performance Laboratory as part of this thesis. One of the difficulties found involved simplifying a three-dimensional heat and mass transfer problem for application in a two-dimensional heat and moisture transport tool. The assumptions that were made explain some of the differences between the experimental and simulation results. The assumptions include the non-uniform moisture distribution within the partially wetted bottom plate, the depth of the wetting front on all surfaces, the uniform distribution within the non-wetted bottom plate core, and the material properties – including the sorption curves, vapor permeances and liquid diffusivities for the hygroscopic materials –

which were taken from a variety of sources and may or may not reflect the actual properties of the materials tested. Also with respect to material properties, the two-dimensional domain of calculation does not take into consideration the anisotropic nature of wood and its greater vapor permeability and liquid diffusivity in the longitudinal direction. In addition, while air transport is not included in WUFI, it likely played a role in the walls' response in experiment 3. In the experiment, air transport was likely present both in the form of convection loops within the insulated stud cavity and unintentional air flow through the assemblies, the latter case being especially true for the walls sheathed with highly air permeable fiberboard. Air movement was not monitored in the experiment. In addition, the model does not account for interface transport resistance between components. In the experiment, the presence of narrow gaps between the components, i.e. between the sheathing and the bottom plate, likely increased the rate of moisture evaporation of the wet bottom plate insert in the experiment. While differences were observed between the absolute experimental and numerical results, similar trends were found when comparing the moisture content response of the bottom plates in the walls with different sheathings and vapor retarders. Despite their shortcomings, numerical HAM models are useful tools that allow insight into the behavior of building envelope systems and investigation of the effect of various parameters on the performance of the assemblies.

Parametric analyses were conducted to complement the results obtained in tests 1 and 2 which involved a drop-by-drop water infiltration wetting method. Because rain infiltration events cannot be simulated directly by numerical tools like WUFI, weekly initial conditions of saturation at specific locations within the bottom plate and sheathing simulated the result of a weekly event of wind-driven rain infiltration into the wall assemblies. The parametric analyses were based on the wall configuration and materials of wall 1, which included OSB sheathing and a polyethylene vapor retarder. The previously described exercise illustrated graphically in Figure 6.3 showed experimental and simulation moisture content results for the bottom plate inserts to be within 14% difference for this wall, and the same range of difference between numerical and experimental results as was shown in Figure 6.2. Parametric analyses were conducted to examine the influence of adding exterior insulation, increasing the stud cavity height, and

increasing the rain infiltration load.

Adding exterior insulation has two effects on the performance of a wall: 1) it increases the thermal resistance of the assembly, and therefore all inboard materials including the sheathing and the bottom plate experience warmer temperatures when the exterior insulation is present. Adding exterior insulation also increases the vapor diffusion resistance of the assembly, therefore decreasing the rate of outbound vapor flux. The results from the numerical exercise showed that for the specific wall configuration, wall materials, climate and wind-driven rain infiltration loads, the benefit provided by adding exterior insulation outweighs the negative effect of increasing the vapor resistance by increasing the temperature of the wetted zones within the bottom plate and the sheathing, thus accelerating their drying response (see Figures 6.11 and 6.15). However, more work is required to determine whether the drying rate is sufficient to preclude biological attack altogether. In reality, adding exterior insulation may increase the airtightness of a wall assembly, thereby changing its HAM response. Therefore, a tool that also takes air transport into account is necessary to increase the accuracy of the moisture performance prediction.

The effect of doubling the height of the wall was also investigated. Contrary to expectations, it was found that the wall height had a negligible impact on the drying response of the wetted bottom plate, but that the overall moisture content per unit mass within the sheathing was slightly reduced due to the larger exposed surface area in the 2-m high wall in the moisture redistribution process (Figure 6.16). It should be noted that the numerical tool does not take air transport phenomena into account, and therefore the simulation results should be interpreted carefully. In reality, increasing the wall height is expected to increase the magnitude of the thermally-induced convection loop forming within the highly porous insulation, thus reducing the moisture content gradient within the insulation and the relative humidity above the bottom plate, thereby increasing the potential for the bottom plate to dry.

Two investigations were conducted to examine the impact of water infiltration loading on the walls' response. First, the loading was increased by doubling the wetted area on the top horizontal surface of the bottom plate for OSB-sheathed wall 1. This test resulted in increasing the total moisture content of the bottom plate, as expected (Figure

6.18). However, there was no difference in the moisture content of the different zones within the bottom plate and of the sheathing behaved similarly in both cases. The impact of the loading on the OSB sheathing was negligible.

A parametric study was also done to look at the effect of increasing the frequency of the rain infiltration events from once a week to three consecutive days a week. As anticipated, the bottom plate demonstrated a steady and significant increase in moisture content when the loading frequency was increased (Figure 6.19), particularly in the zones that were wetted directly, but also in the zones within the core of the bottom plate (Figure 6.20). The results showed that frequent wetting over just four weeks 'could result in moisture conditions that could foster mold and fungal decay. The overall impact on the sheathing was small; however, when the loading frequency is increased, the saturated sheathing zone experienced higher moisture content levels for longer time durations (Figure 6.21), exposing it to higher risk of biological attack.

The weekly wetting and drying simulations were continued from April to October for the OSB-sheathed wall to investigate the performance of the wall when exposed to a longer period of time. It was hypothesized that exposure to warmer temperatures during the summer may promote drying. The results showed that, on the contrary, moisture accumulation occurred at a faster rate in the summer months despite the warmer exterior temperatures, likely because of high exterior and interior vapor pressures, which reduced the drying potential (Figure 6.22). In addition, the warmer summer temperatures are expected to increase the risk of moisture-induced decay.

It is reiterated here that the ability of simulation tools to accurately predict the hygrothermal performance of envelope systems depends strongly on the selection of input variables such as material properties, boundary conditions, and initial conditions that represent those in actual assemblies, as well as the inclusion of heat and mass transport phenomena that reflect those occurring in the actual physical system.

7. CONCLUSION

7.1 Summary

Field observations over the last two decades have shown that water infiltration through building envelope defects and into wall assemblies can cause serious damage, especially if water can accumulate within the back wall. If exposed to high moisture content and appropriate temperature levels for sufficient time, wall components such as wood framing or wood-based sheathing are vulnerable to mold growth and biodegradation.

An extensive review of the literature has shown that little research and development work has been done to investigate the behavior of hygroscopic components in wood-frame wall systems exposed to wind-driven rain infiltration. Of those studies that did consider liquid moisture loads, none have rationalized the liquid moisture loading using real climatic data and estimates of water infiltration proportions. In addition, few studies examined the impact of the sheathing and of the vapor retarder in the wetting and drying response of large-scale wood-frame wall assemblies under realistic loading conditions.

To this effect, three experiments were conducted to study the hygrothermal performance of different wood or wood-based wall components in large-scale wood-frame walls wetted by simulated wind-driven rain infiltration using two different wetting methodologies. The primary objectives of the research project were:

- To investigate the wetting and drying performance of hygroscopic components in wood-frame wall systems wetted by simulated rain infiltration through a building envelope defect;
- To determine the locations within the wall that are most susceptible to moisture accumulation, and;

- To examine the impact of several parameters including the sheathing, the vapor retarder, and the presence of exterior foam insulation and of exterior cladding on the hygrothermal behavior of the wetted components.

A novel experimental wetting protocol based on actual climatic parameters for Montreal was developed and utilized in the first and second tests for the simulation of wind-driven rain infiltration through a wall defect. The steps of the wetting methodology included:

1. Statistically analyzing the horizontal rainfall and wind speed using a long-term Montreal weather database to determine the hourly rate, frequency and duration of wind-driven rain occurrence;
2. Calculating the amount of water impinging on a given façade location of a one-storey building using results of driving rain CFD analysis and local climatic data, and;
3. Determining the ratio of water that infiltrates through a given envelope defect to the total amount of water impinging on the envelope surface.

The drop-by-drop wetting methodology consisted of introducing water through a small tube to the top center of the interior surface of the sheathing panel, recreating a water leak through a defective wall-window junction above. Water was inserted at a rate of 12 ml/h for 3.4 hours a day over three consecutive days in a week for four weeks, and was applied to 17 of the 19 walls in each of the first two experiments.

A third experiment was conducted to supplement the results of tests 1 and 2, this time employing a different wetting methodology in order to generate more repeatable initial moisture content loads in one of the wall assembly components, the bottom plate insert. The moisture content results of the first and second test indicated that significant moisture absorption occurred at the bottom of the wall, particularly in the bottom plate. To reflect this finding, the approach used in the third test involved pre-wetting the bottom plate inserts in a pool of water 13 mm deep and installing them on top of the existing bottom plate at the start of the test. The bottom plate inserts thus performed two functions: they served both as a moisture source in the wall assemblies and as a gravimetric specimen for the monitoring of moisture content in each wall throughout the test. The wetting methodology was applied to six walls in test 3.

The experimental methodology was comprised of the wall design, which reflected wood-frame residential construction. All but one wall in tests 1 and 2 were constructed without cladding. For all three experiments, the experimental protocol also included setting an environmental protocol for the simulation of daily and monthly temperature and relative humidity conditions for Montreal for the pre-conditioning phase, the four week wetting phase (in tests 1 and 2 only) and the two drying phases, which lasted a total of five weeks. As well, a monitoring scheme was developed for the local measurement of temperature, relative humidity and moisture content in the various hygroscopic components of the wall assemblies. The moisture content findings from the first experiment highlighted the limitations of gravimetry in monitoring the moisture response of highly hygroscopic sheathings like plywood when these are exposed to liquid water loads, and served to refine the monitoring plan for experiment 2.

Numerical work was also undertaken using an existing two-dimensional heat and moisture tool, WUFI-2D. Six walls were set-up to recreate the wall design, test conditions and the bottom plate inserts' initial moisture content data from the third experiment.

While similar drying trends were found, the simulation moisture content curves yielded higher final moisture contents and slower drying rates than were achieved in the experiment. There are possible reasons for the difference between the experimental and the numerical results, including the estimated initial moisture distribution within the bottom plate inserts, the material properties which did not cover the entire moisture content range, the inherent difficulties in simulating a three-dimensional problem in a two-dimensional framework, particularly with respect to modeling moisture transport in highly anisotropic materials. In addition, while air transport is not included in WUFI, it likely played some role in the wall components' response in experiment 3 in the form of a thermally-induced convection loop within the porous fiberglass batt stud cavity insulation and as air migration through the assemblies, especially for the walls sheathed with highly air permeable fiberboard. The work showed the importance of modeling all relevant heat and mass transport phenomena to increase the accuracy of the simulation results.

Parametric analyses were performed numerically based on the configuration of a wall with OSB sheathing and a polyethylene vapor retarder to complement the results from

tests 1 and 2. The parameters investigated were the addition of exterior insulation, stud cavity height, and infiltration loading on the hygrothermal response of bottom plate and of the sheathing. The liquid moisture load was applied once a week for four weeks to the materials at the interface of the bottom plate and the sheathing, and on the top surface of the bottom plate. At these locations, the surfaces of the OSB sheathing and of the bottom plate were saturated to a moisture content of 175% and 72%, respectively, to a depth of 1 mm. Exterior and interior environments were set to reflect April conditions in Montreal. A last test was carried out from April to October to see the effect of the climate conditions for long-term infiltration.

7.2 Scope and Limitations of the Work

This study aimed to investigate the hygrothermal performance of wood-frame walls wetted by simulated wind-driven rain infiltration once a building envelope failure had occurred. The failure case examined an example of water infiltration through a windowsill, although other possible failure locations are possible. The failure permits rain infiltration into the back wall, thus wetting the components to the inside of the sheathing. This failure represents a worst-case scenario because envelopes are not designed nor built to manage water infiltration into the back wall.

The first step in the development of the drop-by-drop wetting methodology consisted of determining the rate of water infiltration loading by conducting a statistical analysis of a Montreal weather database. Average values of horizontal rainfall and wind speed were sought in order to investigate the impact of frequently-occurring wind-driven rain, although different values of rainfall and wind speed would be justified if a more extreme rain infiltration loading was sought. For the sake of simplicity, the wind direction was not considered in the determination of wind speed frequencies or for determining the rate of wind-driven rain on building façades, which may have reduced the accuracy of the rate of impinging wind-driven rain. The second step of the methodology was to determine the rate of impinging rain on a given area of a building façade. For this purpose, the rate of impinging rain was found in a central zone at approximately one-third the height of a

one-story building. It is recognized that greater rates of impinging wind-driven rain would be expected in the zones at the sides of the façade, and also at the top of the façade for a building without overhangs. The third and final step in the development of the methodology consisted of establishing the ratio of water leakage through the windowsill defects. The determination of the ratio was based on the prescribed requirements of ASTM E331-00 (ASTM, 2000a). The large spray rate and air pressure differential prescribed by the ASTM standard test method may have produced a larger water proportion of water leakage than a smaller rate. This would have to be verified with measurements since the openings used were quite small and saturation of the opening area may even occur at lower rates. Finally, although the wetting methodology mimics reality, the moisture content results from tests 1 and 2 show that the resulting wetting pattern was random, and was not repeatable from wall to wall, or from one wetting event to another.

The second methodology, developed and applied in test 3, showed that pre-wetting the bottom plate inserts provided curves of moisture content versus time that could be compared with that of numerical simulations. However, the immersion takes a relatively long time (31 days to reach approximately 55% moisture content. The initial moisture content in the bottom plate inserts varied from 53.0 to 56.8%, a difference of only 3.8% moisture content, or 7%. The bottom plate inserts thus served both as a moisture source, which decreased with time, and a moisture content monitor.

The premise of the wall design and climatic conditions were that of a north-facing wall with a ventilated rainscreen cavity, where air movement between the exterior environment and the air space behind the cladding would reduce the differentials in temperature and moist air pressure across the cladding. Based on this assumption, all but one of the walls in experiments 1 and 2 were constructed without cladding. In addition, the impact of solar radiation, and solar-driven water vapor diffusion in particular, were not examined. Local monitoring of temperature, relative humidity and moisture content was performed. Localized moisture content monitoring was preferred in order to obtain an overall distribution within the hygroscopic wall components and throughout the walls. Access to the gravimetric samples within the walls was obtained via access doors in the gypsum interior sheathing, which may or may not have disturbed the environment within

the wall. In addition, disturbance of the fiberglass batt insulation to retrieve the gravimetric samples within the wall possibly affected the path of the water infiltration within the wall.

The climatic conditions simulated during the pre-conditioning phases of tests 1 and 2 sought to simulate moisture contents resulting from winter diffusion. The conditions set during the drying phases of tests 1 to 3 simulated exterior and interior conditions in April and May. Air migration due to the wind, mechanical ventilation, and stack effect was not explicitly considered or simulated, although air movement generated by the recirculation fans in the Environmental Chamber did occur. Last, while the air pressure difference across the test hut was measured, air leakage through the walls and air movement within the fiberglass batt insulation in the stud cavity were not monitored.

7.3 Summary of experimental and Simulation Findings

In terms of the wetting behavior, the experimental results from tests 1 and 2 have shown that:

- Water introduced at the top of the assembly made its way down to the bottom of the wall. As a result, the most significant moisture accumulation was seen in the materials at the interface of the bottom plate and the sheathing, and also on the top surface of the sheathing.
- Lateral redistribution of water was observed in many walls.
- The greatest moisture uptake occurred in the plywood sheathing, and the lowest in the fiberboard sheathing, the latter likely due to the asphalt-coating which effectively prevented water uptake by the fiberboard. Visual signs of mold growth were found on the OSB sheathing samples facing the bottom plate, indicating that the sheathing at this location was susceptible to moisture accumulation.
- The wetting methodology in experiments 1 and 2 resulted in variations in the wetting patterns of the sheathing and the bottom plates, from one wall to another

and even from one wetting event to another within the same wall. However, the locations in the bottom plate and the sheathing that were exposed to repeated wetting experienced steady increases in moisture content, and to conditions that could lead to mold and fungal growth.

In terms of the drying response of the wall components, the moisture content data from all tests 2 and 3 were analyzed to assess the role of the test parameters, including the sheathing material, the type of vapor retarder, the presence of exterior insulation, the stud cavity height, and the presence of hygroscopic cladding. The impact of three sheathings commonly used in North America was investigated: OSB, plywood and asphalt-coated fiberboard. The rate of drying results show that the selection of the sheathing material has the strongest influence with respect to the drying response of the wall components. Moisture content data from the 35-day test 3 show that the bottom plate inserts in the fiberboard-sheathed walls dried most rapidly and attained the lowest final moisture contents; on the other hand, the lowest drying rates and highest final moisture contents were found to occur in the OSB-sheathed walls. The same drying response patterns were found in the bottom plate's center vertical (CV) spruce samples facing the sheathings. The differences in the results have been attributed to the different vapor permeability characteristics of the three sheathings. In tests 2 and 3, the small gravimetric samples installed in the bottom plate facing the insulated stud cavity showed that the highest drying rates were found in the gravimetric samples in the plywood-sheathed walls. These results are likely due to the plywood sheathing's higher liquid moisture absorption capacity, which causes it to absorb surface condensation more readily than OSB and asphalt-coated fiberboard, thus reducing the moisture content within the stud cavity. The sheathing moisture content data shows that the fiberboard's asphalt coating is effective in reducing the liquid water intake and keeping the sheathing dry.

The experimental results show that generally, increasing the permeability of the vapor retarder increases the drying rate of the wetted components within the wall. The influence of the vapor retarder, however, is dependent upon the type of sheathing used, as is indicated by the test 3 data. In test 3, the vapor retarder played a significant role in the OSB-sheathed walls: the bottom plate insert in the wall with the low permeance primer paint had a greater drying rate and a lower final moisture content than the one in the

polyethylene wall. However, the effect of the vapor retarder was not as significant in the walls sheathed with plywood and fiberboard. In the latter case, the moisture content profiles showed similar drying rates throughout the test despite the different permeance of the vapor retarder. In general, the moisture content data show that when the permeance of the sheathing is low, as it is for OSB, then the influence of the permeance of the vapor retarder is more critical, and the permeability of the vapor retarder should be increased up to a value allowed by the building code to promote drying of the assembly towards the interior.

The moisture content result from the third experiment indicate that the average total moisture content of the monitored components in all the walls were below the fiber saturation point (FSP) of wood at the end of the 35-day test, which experimentally recreated April and May conditions. The moisture content distribution within the bottom plate inserts was not measured; it is likely that the moisture content at certain locations within the pre-wetted bottom plate inserts in test 3 was greater than the FSP. However, in general, the drying process was on-going within all samples at the end of the test, and would therefore be anticipated to reach acceptable levels of moisture content, i.e. 20% moisture content, thus mitigating the risk of moisture induced damage. However, the moisture content data in the OSB-sheathed walls also indicate that some locations on the bottom plate, i.e. on the vertical surface adjacent to the sheathing and on the horizontal surface facing the stud cavity near the sheathing, exhibited low drying rates and relatively high final moisture contents despite the higher outdoor temperatures during the second drying phase. These findings suggest that there is a risk of moisture-induced damage of the bottom plate near the sheathing when the sheathing permeance is low.

Simulations conducted using WUFI-2D showed that adding exterior insulation to upgrade the thermal performance of the OSB-sheathed wall system resulted in slightly increasing the drying capacity of the wetted components despite the higher outboard water vapor diffusion resistance provided by the extruded polystyrene. The impact of increasing the stud cavity height on the response of the bottom plate and the sheathing was negligible. It should be noted that adding exterior insulation and increasing the stud cavity height in actual walls may affect the air transport within the walls, reducing the likelihood of air leakage in the first case, and reducing thermally-induced convection

loops in the second case. Neglecting air transport in the model may reduce the accuracy of the predicted heat and moisture behavior.

The impact of the wetting loading scheme was also investigated numerically. It was found that increasing the wetting load by increasing the wetted surface area on the top of the bottom plate for the OSB-sheathed wall had almost no impact on the response of the wall components. However, increasing the frequency of loading from once to three times a week had a significant effect on the OSB-sheathed wall by increasing the duration of time that the wetted component were exposed to high moisture contents, thereby increasing the risk of biological attack. Last, the simulations were conducted from April to October to investigate the effect of climate and long-term exposure. The results showed that moisture accumulation occurred at a faster rate in the summer months despite the warmer exterior temperatures, likely because of high indoor and outdoor vapor pressures, which reduced the diffusion drying potential. In addition, the warmer summer temperatures are expected to increase the risk of moisture-induced decay.

7.4 Contributions of the research

The experimental work in this thesis has advanced the field of study of moisture movement in the building envelope through the following contributions:

- A state-of-the-art literature review describing both undisturbed wind-driven rain and impinging wind-driven rain on building façades, as well as a comprehensive summary of previous methods employed to physically simulate wind-driven rain on building façades and wind-driven rain infiltration into building envelopes.
- The development of a rationalized approach to estimate and apply wind-driven rain infiltration loading for a building envelope failure. This methodology is based on statistical analysis of local precipitation, wind speed and wind direction, as well as the application of the results of a wind-driven rain numerical model (developed by others), to quantify the driving rain impinging on a façade. The wetting protocol also applies the results of a rain leakage test to determine the

proportion of the impinging water that penetrates through a building envelope defect;

- The development and refining of a moisture content monitoring protocol, including the establishing the advantages and limitations of the available method for measurement of hygroscopic materials exposed to liquid moisture loads;
- The production of a unique set of data on the wetting patterns of wood-frame wall systems exposed to realistic wind-driven rain infiltration loads, and;
- The investigation of the role of exterior wall sheathing material, type of vapor barrier, and the addition of exterior insulation on the drying performance of several hygroscopic component in wood-frame wall assemblies wetted by simulated wind-driven rain infiltration, and identification of those wall parameters that promote drying.

The numerical work has lead to the following contributions:

- The investigation of the some of the benefits and practical limitations of an hygrothermal computer tools for the prediction of the hygrothermal performance of building envelopes, and;
- The application of an existing 2-dimensional model to study the hygrothermal response of wood-frame wall components subjected to repeated simulated wind-driven rain infiltration, and numerical investigation of the role of the exterior insulation, wall height, water infiltration loading and duration of loading on the drying response of a wall system.

7.5 Suggestions to Improve the Experimental Protocol and Recommendations for Future Work

The implementation of the developed experimental protocols, including the two wetting methodologies, and the analysis of the ensued results, has brought forth suggestions to improve the protocol:

- The drop-by-drop methodology could be improved by including the direction of the wind in the determination of impinging wind-driven rain;
- The drop-by-drop wetting methodology, which resulted in random wetting patterns as implemented, could be improved by using a wick to direct the stream of water running down the sheathing surface and installing a blotting paper at the bottom plate-sheathing interface and on the top surface of the bottom plate to distribute the water uniformly from wall to wall.

The findings from this work have highlighted the need for future work in the following areas:

- Application of an improved drop-by-drop wetting methodology and the overall experimental protocol to longer periods (all rainy months) using actual cold and hot-humid climate conditions to establish levels of rain infiltration in the back wall that may lead to conditions that favor mold and rot growth. The impact of solar radiation on the hygrothermal response of the walls should also be investigated.
- Experimental studies on the influence of initial moisture content on the drying rate of wood such as spruce;
- Further development of numerical modeling to allow the simulation of wind-driven rain infiltration into the back wall of a envelope assemblies;
- Expanding the capabilities of existing numerical tools to include air transport in the form of, for example, air leakage due to air pressure differentials across envelope assemblies and buoyancy-induced air movement within cavity spaces, and;
- The development of a large-scale testing framework which would serve to compare the relative performance of different wall systems and which would move the design of the building envelope toward an engineering approach;
- The development of a standard test method akin to E331-00 (ASTM, 2000a) and E547-00 (ASTM, 2000b) for determining impinging wind-driven rain loads on building facades that takes into consideration climate parameters.

7.6 Related Publications

Teasdale-St-Hilaire, A. and Derome, D. Methodology and application of simulated wind-driven rain infiltration in building envelope experimental testing. Accepted for publication in *ASHRAE Transactions*, Québec City, Québec, June 24-28, 2006.

Teasdale-St-Hilaire, A. and Derome, D. 2005. State-of-the-art review of simulated rain infiltration and environmental loading for large-scale building envelope testing. *ASHRAE Transactions*, Denver, Colorado, June 25-29, vol. 111, part 2, pp. 389-401.

Teasdale-St-Hilaire, A., Derome, D. and Fazio, P. 2005. Investigating the role of the vapor retarder in the drying response of wood-frame walls wetted by simulated rain infiltration. *Proceedings of the 10th Canadian Conference on Building Science and Technology*, Ottawa, Ont., May 12-13, 13 p.

Teasdale-St-Hilaire, A., Derome, D. and Fazio, P. 2004. Behavior of wall assemblies with different wood sheathings wetted by simulated rain infiltration. *Performance of the Exterior Envelopes of Whole Buildings IX, Conference Proceedings*, ASHRAE, Clearwater Beach, Florida, Dec. 5-10, 15 p.

Teasdale-St-Hilaire, A., Derome, D. and Fazio, P. 2003. Development of an experimental methodology for the simulation of wetting due to rain infiltration for building envelope testing. *Proceedings of the 2nd International Building Physics Conference*, Balkema, Leuven, Belgium, Sept. 14-18, pp. 455-462.

Teasdale-St-Hilaire, A., Derome, D., Fazio, P. 2003. Approach for the simulation of wetting due to rain infiltration for building envelope testing. *Proceedings of the 9th Canadian Conference on Building Science and Technology*, National Building Envelope Council, February 26-27, Vancouver, B.C., 15 p.

Derome, D., Teasdale-St-Hilaire, A. and Fazio, P. 2001. Methods for the Assessment of Moisture Content of Envelope Assemblies. *Performance of the Exterior Envelopes of Whole Buildings VIII, Conference Proceedings*, ASHRAE, Clearwater Beach, Florida, December 2-6, 13 p.

Derome, D., Teasdale-St-Hilaire, A., Fazio, P. 2001. Comparaison entre la gravimétrie et les sondes de teneur en humidité pour le monitoring du transfert de l'humidité dans les essais à grande échelle sur l'enveloppe du bâtiment. *Ve Colloque interuniversitaire Franco-Québécois*, Lyon, France, May 28-30, 2001, pp. 353-360.

REFERENCES

AAMA. 2002. AAMA 502-02 Voluntary specification for field testing of windows and sliding doors. American Architectural Manufacturers Association, Schaumburg, Illinois, 7 p.

AAMA. 2003. AAMA 501.2-03 Quality assurance and diagnostic water leakage field check of installed storefronts, curtain walls, and sloped glazing systems. American Architectural Manufacturers Association, Schaumburg, Illinois, 5 p.

Addleson, L. 1972. *Materials for building*. Vol. 2, Iliffe, London, 168 p.

ASHRAE. 2001. *2001 ASHRAE Handbook, Fundamentals*. American Society of Heating, Refrigerating and Air Conditioning Engineers, Atlanta, GA.

ASTM, 1984. ASTM E283-84 Standard test method for rate of air leakage through exterior windows, curtain walls, and doors. American Society for Testing and Materials, West Conshohocken, PA, 4 p.

ASTM, 1990. ASTM E514-90 Standard test method for water penetration and leakage through masonry. American Society for Testing and Materials, West Conshohocken, PA, 4 p.

ASTM. 1992. ASTM D4442-92 Standard test method for direct moisture content measurement of wood and wood-base materials. American Society for Testing and Materials, West Conshohocken, PA, 5 p.

ASTM, 2000a. ASTM E331-00 Standard test method for water penetration of exterior windows, curtain walls, and doors by uniform static air pressure difference. American Society for Testing and Materials, West Conshohocken, PA, 4 p.

ASTM, 2000b. ASTM E547-00 Standard test method for water penetration of exterior windows, curtain walls, and doors by cyclic static air pressure differential. American Society for Testing and Materials, West Conshohocken, PA, 4 p.

ASTM, 2002. ASTM E2128-01a Standard guide for evaluating water leakage of building walls. American Society for Testing and Materials, West Conshohocken, PA, 35 p.

Barrett, D. 1998. *The renewal of trust in residential construction. Commission of enquiry into the quality of condominium construction in British Columbia*. Report submitted to the Lieutenant Governor in Council of the Government of British Columbia. June.

<http://www.qp.gov.bc.ca/condo/> Website accessed December 20, 2003.

Beaulieu, P., Bomberg, M., Cornick, S., Dalglish, A., Desmarais, G., Djebbar, R., Kumaran, K., Lacasse, M., Lackey, J., Maref, W., Mukhopadhyaya, P., Nofal, M., Normandin, N., Nicholls, M., O'Connor, T., Quirt, J., Rousseau, M., Said, M., Swinton, M., Tariku, F., and van Reenen, D. 2002. *Final report from task 8 of MEWS project (T8-03) - Hygrothermal response of exterior wall systems to climate loading: Methodology and interpretation of results for stucco, EIFS, masonry and siding clad wood-frame walls*. National Research Council of Canada, Institute for Research in Construction, Ottawa, RR-118, Nov., 184 p.

Beers, P. E. and Smith, W. D. 1998. Repair method for common water leaks at operable windows and siding glass doors. *Water Leakage Through Building Façades*, ASTM STP 1314, R. J. Kudder and J. L. Erdly, Eds., American Society for Testing and Materials, West Conshohocken, PA, pp. 105-114.

Bell, G. R. 2001. A framework for quantifying the water-penetration resistance of exterior wall cladding. *Proceedings of the International Conference on Building Envelope Systems and Technologies* (ICBEST), National Research Council of Canada, Institute of Research in Construction, Ottawa, Ont., pp. 95-100.

Best, A.C. 1950. The size distribution of raindrops. *Quarterly Journal of the Royal Meteorological Society*, Bracknell Royal Meteorological Society, vol. 76, pp. 16-36.

Blocken, B., Carmeliet, J. 2000. Driving rain on building envelopes – I. Numerical estimation and full-scale experimental verification. *Journal of Thermal Envelopes and Building Science*, Technomic Publishing, Lancaster, PA, vol. 24, July, pp. 61-85.

Blocken, B., and Carmeliet, J. 2001a. Estimating driving rain load on buildings: A 3D numerical and an experimental approach. *International Conference on Building Envelope Systems and Technologies* (ICBEST), National Research Council, Ottawa, Ont., pp. 181-185.

Blocken, B., and Carmeliet, J. 2001b. Spatial and temporal distribution of driving rain on buildings: Numerical simulation and experimental verification. *Performance of Exterior Envelopes of Whole Buildings VIII: Integration of Building Envelopes, Conference Proceedings*, ASHRAE, Clearwater Beach, Florida, Dec. 2-7, 11 p.

Blocken, B., and Carmeliet, J. 2002a. Spatial and temporal distribution of driving rain on a low-rise building. *Wind & Structures: An International Journal*, Techno-Press, Taejeon, Korea, vol. 5, no. 5, pp. 441-462.

Blocken, B., Janssen, H., and Carmeliet, J. 2002b. On the modelling of runoff of driving rain on a capillary active surface. *Proceedings 11th Symposium for Building Physics*, Dresden, Germany, 26-30 September, 2002, pp. 400-408.

Blocken, B. and Carmeliet, J. 2005. On the accuracy of wind-driven rain measurements on buildings. Accepted for publication in *Building and Environment*, Elsevier, July, 13 p.

Bomberg, M. and Brown, W. 1993. Building envelope: Heat, air and moisture interactions. *Journal of Thermal Insulation and Building Envelopes*, Technomic Publishing, Mancaster, PA, vol. 16, April, pp. 306-311.

Bomberg, M.T.; Rousseau, M.Z.; Desmarais, G.; Nicholls, M.; Lacasse, M.A. 2002. *Report from task 2 of MEWS Project - Description of 17 large scale wall specimens built for water entry investigation in IRC dynamic wall testing facility*. National Research Council, Institute in Construction, Ottawa, Oct., RR-111, 142 pp.
<http://irc.nrc-cnrc.gc.ca/fulltext/rr111/>

Brown, W.C., Bomberg, M. T., Ullett, J.M. 1993. Measure thermal resistance of frame Walls with defects in the installation of mineral fiber insulation. *Journal of Thermal Insulation and Building Environment.*, vol. 16, pp.318-339.

Brown, W., Adams, P., Tonyan, T. and Ullett, J. 1997. Exterior management in exterior wall claddings. *Journal of Thermal Insulation and Building Envelopes*, Technomic Publishing, Mancaster, PA, vol. 21, July, pp. 23-43.

Burch, D. M, and Thomas, W. C. 1992. An analysis of moisture accumulation in a wood-frame wall subjected to winter climate. *Thermal Performance of the Exterior Envelopes of Buildings V, Conference Proceedings*, ASHRAE, Clearwater Beach, Florida, Dec. 7-10, pp. 467-479.

CAN/CSA-A440-M00. 2000. Windows. Canadian Standards Association, Toronto, 96 p.

Carmeliet, J. and Blocken, B. 2004. Driving rain, rain absorption and rainwater runoff for evaluating water leakage risks in building envelopes. *Performance of Exterior Envelopes of Whole Buildings IX, Conference Proceedings*, ASHRAE, Clearwater Beach, Florida, Dec. 5-10, pp. 24 p.

Carmeliet, J., Rychtáriková, M. and Blocken, B. 2005. Numerical modeling of impact, runoff and drying of wind-driven rain on a window glass surface. Submitted to the International Building Physics Conference, 8 p.

Chebil S., Galanis N. and Zmeureanu R., 2003. Computer simulation of thermal impact of air infiltration through multilayered exterior walls. *eSim2003 Conference*, Eindhoven, pp.97-104.

Choi, E.C.C. 1991. Numerical simulation of wind-driven rain falling onto a 2-D building. *Computational Mechanics*, Balkema, Rotterdam, pp. 1721-1727.

- Choi, E.C.C. 1992. Simulation of wind-driven rain around a building. *Journal of Wind Engineering*, Elsevier Science, Amsterdam, vol. 52, August, pp. 60-65.
- Choi, E.C.C. 1993. Simulation of wind-driven rain around a building. *Journal of Wind Engineering and Industrial Aerodynamics*, Elsevier, vol. 46 & 47, pp. 721-729.
- Choi, E.C.C. 1994. Parameters affecting the intensity of wind-driven rain on the front face of a building. *Journal of Wind Engineering and Industrial Aerodynamics*, Elsevier Science, Amsterdam, vol. 53, pp. 1-17.
- Choi, E. C. C. 1998. Criteria for water penetration testing. *Water Leakage Through Building Façades*, ASTM STP 1314, R. J. Kudder and J. L. Erdly, Eds., American Society for Testing and Materials, West Conshohocken, PA, STP 1314, pp. 3-16.
- Choi, E. C. C. 1999. Wind-driven rain on building faces and the driving-rain index. *Journal of Wind Engineering and Industrial Aerodynamics*, Elsevier, vol. 79, pp. 105-122.
- Choi, E.C.C. 2000. Variation of wind-driven rain intensity with building orientation. *Journal of Architectural Engineering*, American Society of Civil Engineers, New York, vol. 6 no. 4, December, pp. 122-128.
- Claridge, D.E., Liu, M. 1996. The measured energy impact of infiltration in an outdoor test cell. *Transactions of the ASME*, American Society of Mechanical Engineering, vol. 118, pp.162-167.
- CMHC. 1988. *Canadian Wood-Frame House Construction*. CMHC, Ottawa, Ont., 2nd metric ed., 231 p.
- CMHC. 1999. *Séminaire: Détails de construction avancés*, Montréal, Qué. Oct. 19.
- Cornick, S., Dalglish, A., Said, N., Djebbar, R., Tariku, F., and Kumaran, M.K. 2002. *Report from task 4 of MEWS project - Task 4-Environmental conditions final report*. National Research Council, Institute for Research in Construction, Ottawa, Report RR-113, Oct. 112 p. <http://irc.nrc-cnrc.gc.ca/fulltext/rr113/>
- Culyer, P. and Edgar, J. 1998. The downpour in B.C. *Construction Canada*, Kenilworth Publishing, Richmond Hill, Ont., vol. 40 no. 5, Sept., pp. 14-19.
- Derome, D. 1999. *Moisture occurrence in roof assemblies containing moisture storing insulation and its Impact on the durability of building envelope*. Ph.D. Thesis, Concordia University, Montreal, Qué., 207 p.
- Derome, D. 2005. Unpublished wetting angle data.

- Derome, D., Roels, S., Carmeliet, J. 2005. "Qualitative work to study water movement in wood", Proceedings of the 7th Symposium on Building Physics in the Nordic Countries, vol. 1, The Icelandic Building Research Institute, Reykjavik Iceland 2005, pp. 173-180.
- Derome, D. and Desmarais, G. 2005. Exposure to condensation moisture of sheathing in retrofitted leaky wall assemblies. Accepted for publication in *ASCE Journal of Architectural Engineering*, American Society of Civil Engineers, Reston, Virginia, 28 p.
- Derome, D. and Fazio, P. 2000. Large-scale testing of two flat roof assemblies insulated with cellulose. *Journal of Architectural Engineering*, American Society of Civil Engineers, New York, vol. 6no. 1, March, pp. 12-23.
- Desjarlais, A. O., Christian, J. E., Kyle, D. M., and Rode, C. 1993. Moisture: Its effects on the thermal performance of a low-slope roof system. *ASHRAE Transactions*, American Society of Heating, Refrigerating and Air-Conditioning Engineers, Atlanta, vol. 99, pt. 2, pp. 1004-1012.
- Desjarlais, A. O., Petrie, T. W., Childs, P. W., and Atchley, J. A. 1998. Moisture studies of a self-drying roof: Tests in the large-scale climate simulator and results from thermal and hygric models. *Thermal Performance of the Exterior Envelopes of Buildings VII, Conference Proceedings*, ASHRAE, Clearwater Beach, Florida, Dec. 6-10, pp. 41-54.
- Desmarais, G., Derome, D., Fazio, P. 1998. Experimental setup for the study of air leakage patterns. *Thermal Performance of the Exterior Envelopes of Buildings VII, Conference Proceedings*, ASHRAE, Clearwater Beach, Florida, Dec. 6-10, pp. 99-108.
- Desmarais, G. 2000. *Impact of Added Insulation on the Hygrothermal Performance of Leaky Exterior Wall Assemblies*. M. A. Sc. Thesis, Concordia University, Montreal, Québec, Canada, 213 p.
- DeWit, M. H. 2004. Heat and moisture in building envelopes. Faculteit Bouwkunde Capaciteitgroep FAGO, Technische Universiteit Eindhoven, Dec., 136 p.
- DIN EN 1027. 2000. Windows and doors – Watertightness, Deutsches Institut für Normung, Berlin.
- Dingle, A. N and Lee, Y. 1972. Terminal fallspeeds of raindrops. *Journal of Applied Meteorology*, American Meteorological Society, Boston, MS, vol. 11, Aug., pp 877-879.
- Djebbar, R., van Reenen, D. and Kumaran, M. K. 2001. Environmental boundary conditions for long-term hygrothermal calculations. *Performance of Exterior Envelopes of Whole Buildings VIII, Conference Proceedings*, Clearwater Beach, FL: American Society of Heating, Refrigerating and Air Conditioning Engineers, Dec. 2-7, 13 p.

Doshi, H. 2005. Rain water on building cladding: Two case studies. *Proceedings of the 10th Canadian Conference on Building Science and Technology*, Ottawa, Ont., May 12-13, vol. 1, pp. 116-126.

Duff, J. E. 1968. Moisture distribution in wood-frame walls in winter. *Forest Products Journal*, Forest Products Research Society, Madison, Wisconsin, vol. 18, no. 1, pp. 60-64.

Dupont, 2002. *Tyvek – Providing protection in construction*, product literature. May.

Edgar, J. 1998. Blueprint for building trust. *Construction Canada*, Kenilworth Publishing, Richmond Hill, Ont., vol. 40 no. 5, Sept., pp. 20-23.

Environment Canada website: http://www.msc-smc.ec.gc.ca/climate/index_e.cfm

Fazio, P., Mallidi, S. R. and Zhu, D. 1995. A quantitative study for the measurement of driving rain exposure in the Montreal region. *Building and Environment*, vol. 30 no. 1, Pergamon Press, Oxford, pp. 1-11.

Fazio, P., Athienitis, A., Marsh, C. and Rao, J. 1997. Environmental chamber for investigation of building envelope performance. *Journal of Architectural Engineering*, American Society of Civil Engineers, New York, vol. 3, no.2, June, pp. 97-102.

Fazio, P., Derome, D., Gerbasi, D., Athienitis, A. and Depani, S. 1998. Testing of flat roofs insulated with cellulose insulation. *Thermal Performance of the Exterior Envelopes of Building VII, Conference Proceedings*, ASHRAE, Clearwater Beach, Florida, Dec. 6-10, pp. 3-13.

Forsén, H. and Tarvainen, V. 2000. *Accuracy and functionality of hand held wood moisture content meters*. Rev. ed. Technical Research Center of Finland, Espoo, Finland, 102 p.

Galitz, C. L. and Whitlock A. R. 1998. The application of local weather data to the simulation of wind-driven rain. *Water Leakage Through Building Façades*, ASTM STP 1314, R. J. Kudder and J. L. Erdly, Eds., American Society for Testing and Materials, West Conshohocken, PA, pp. 17-32.

Geving, S. 1997. Moisture design of building constructions: Hygrothermal analysis using simulation models, Part I. Doctoral thesis. Trondheim, Norway: The Norwegian University of Science and Technology, 138 p.

Geving, S., Karagiozis, A. and Salonvaara, M. 1997. Measurements and two-dimensional computer simulations of the hygrothermal performance of a wood frame wall. *Journal of Thermal Insulation and Building Envelopes*, Technomic Publishing, vol. 20, April, pp. 301-318.

- Handegord, G.O. 1982. Air leakage, ventilation, and moisture control in buildings. *Moisture Migration in Buildings*, ASTM STP 779. M. Lieff and H. R. Trechsel, Eds., American Society for Testing and Materials, pp. 223-233.
- Hagentoft, C.-E. and Harderup, E. 1993. Reference years for moisture calculations. Report T2-S-93/01, IEA Annex 24, HAMTIE, 20 p.
- Hagentoft, C.-E. and Harderup, E. 1996. Climatic influences on the building envelope using the Π factor. IEA Annex 24, HAMTIE, Task 2: Environmental conditions, closing seminar, Finland, September, pp. 15-22.
- Hangan, H. 1999. Wind-driven rain studies. A C-FD-E approach. *Journal of Wind Engineering and Industrial Dynamics*, Elsevier Science, vol. 81, pp. 323-331.
- Hangan, H. and Inculet, D. 2001. Wind-driven rain. Numerical and physical modeling. *International Conference on Building Envelope Systems and Technologies (ICBEST)*, National Research Council, Ottawa, Ont., pp. 151-155.
- Hazleden, D.G. and Morris, P. I. 1999. Designing for durable wood construction: The 4 Ds. *Durability of Building Materials and Components 8*, edited by M.A. Lacasse and D.J. Vanier, Institute for Research in Construction division of the National Research Council, Ottawa, Ont., pp. 734-745.
- Hazleden, D. 2001. *Envelope drying rates analysis - Final Report*. Canada Mortgage and Housing Corporation, Ottawa, Ont., 87 p.
- Hazleden, D. G. and Morris, P.I. 2001. The influence of design on drying of wood-frame walls under controlled conditions. *Performance of Exterior Envelopes of Whole Buildings VIII: Integration of Building Envelopes, Conference Proceedings*, ASHRAE, Clearwater Beach, Florida, Dec. 2-7, 18 p.
- Hedlin, C.P. 1967. Sorption isotherms of twelve woods at subfreezing temperatures. *Forest Products Journal*, Forest Products Research Society, Madison, Wisconsin, Dec., vol. 17 no. 12, pp. 43-48.
- Henriques, F. M. A. 1992. Quantification of wind driven rain – An experimental approach. *Building Research and Information*, E. & F. N. Spon, London, vol. 20, pp. 295-297.
- Hens, H. 1996. *Final report, Task 1: Modelling, volume 1*. International Energy Agency (IEA) Annex 24, Heat, Air and Moisture Transfer Through New and Retrofitted Insulated Envelope Parts (HAMTIE), Katholieke Universiteit Leuven, Leuven, Belgium, 90 p.
- Hens, H. 2003. *Building Physics. Heat and Mass Transfer*. 6th edition, English-language draft, Katholieke Universiteit Leuven, Belgium, 265 p.

- Hens, H. and Fatin, A. M. 1995. Heat-air-moisture design of masonry cavity walls: Theoretical and experimental results and practice. *ASHRAE Transactions*, ASHRAE, Atlanta, GA, vol. 101 pt. 1, pp. 607-626.
- Hens, H., and Janssens, A. 1999. Heat and moisture response of vented and compact cathedral ceilings: A test house evaluation. *ASHRAE Transactions: Symposia*, vol. 105, ASHRAE, Atlanta, GA, pp. 837-850.
- Houghton, E. L. and Carruthers, N. B. 1976. *Wind forces on buildings and structures: an introduction*. John Wiley, New York, 243 p.
- Hutcheon, N. B. 1963. *Requirements for exterior walls*. *Canadian Building Digest No. 48*. National Research Council, Division for Building Research, Ottawa.
<http://irc.nrc-cnrc.gc.ca/cbd/cbd048e.html>
- Hutcheon, N. B. and Handegord, G. O. P. 1995. *Building Science for a Cold Climate*. National Research Council Canada, Division of Building Research, Ottawa, 439 p.
- ICI Paints, Technical Service Department. 2003. *Technical specifications of ICI Paints for moisture vapor transmission*, Concord, Ont., received on Nov. 19, 2003.
- James, W. 1975. *Electrical moisture meters for wood*. Forest Products Laboratory, General Technical Report FPL-6, U. S. Department of Agriculture Forest Service, Madison, Wisconsin, 27 p.
- Janssens, A. 1998. *Reliable control of interstitial condensation in lightweight roof systems*. Ph.D. thesis, Departement Burgerlijke Bouwkunde, Katholieke Universiteit Leuven, Leuven, Belgium, 213 p.
- Jones, D.C., Ober, D.G., Goodrow, J.T. 1995. Thermal performance characterization of residential wall systems using a calibrated hot box with airflow induced by differential pressures. *Airflow Performance of Building Envelopes, Components and Systems, ASTM STP 1255*, American Society for Testing and Materials, Philadelphia, pp.197-228.
- Kalamees, T. and Vinha, J. 2004. Estonian climate analysis for selecting moisture reference years for hygrothermal calculations. *Journal of Thermal Insulation and Building Science*, Technomic Publishing, Lancaster, Penn., vol. 27, no. 3, pp. 199-220.
- Karagiozis, A. 2004a. Application of advanced tools to develop energy efficient building envelopes that are durable. *Performance of Exterior Envelopes of Whole Buildings VIII, Conference Proceedings*, ASHRAE, Clearwater Beach, Florida, Dec. 5-10, 12 p.
- Karagiozis, A. 2004b. Private communication, April 1.

Karagiozis, A. and Hadjisophocleous, G. 1995. Wind-driven rain on high-rise buildings. *Thermal Performance of the Exterior Envelopes of Building VI, Conference Proceedings*, ASHRAE, Clearwater Beach, Florida, Dec. 4-8, pp. 480-490.

Karagiozis, A., Salonvaara, M. and Kumaran, K. 1996. Numerical simulation of experimental freeze conditions in glass-fiber insulation. *Proceedings of the 4th Symposium on Building Physics in the Nordic Countries*, VTT Building Technology, Espoo, Finland, Sept. 9-10, pp. 455-465.

Karagiozis, A. and Hadjisophocleous, G. 1997. Wind-driven distribution on two buildings. *Journal of Wind Engineering and Industrial Aerodynamics*, Elsevier Science, vol. 67 & 68, pp. 559-572.

Karagiozis, A., Serino, R. and Salonvaara, M. 2004. Development of wall assembly system properties used to model performance of various wall claddings. *Performance of Exterior Envelopes of Whole Buildings VIII: Integration of Building Envelopes, Conference Proceedings*, ASHRAE, Clearwater Beach, Florida, Dec. 2-7, 9 p.

Kim, S.-E., Choudhury, D. and Patel, B. 1997. Computations of complex turbulent flows using the commercial code FLUENT. *Proceedings of the ICASE/LaRC/AFOSR Symposium on Modeling Complex Turbulent Flows*. Kluwers Academic Publishers, Hampton, Virginia, pp. 259-276.

Kollmann, F. F. P. and Côté, W. A. 1984. *Principles of Wood Science and Technology, Volume 1: Solid Wood*. Springer-Verlag, Berlin, 592 p.

Kontopidis, T., Srinivasa Reddy, M. and Fazio, P. 1993. Potential of rain screen walls to prevent rain penetration: pressurized cavity principle. *Building Research and Information*, E. & F. N. Spon, London, vol. 21, no. 3, pp. 176-186.

Korsgaard, V. and Rode, C. 1992. Laboratory and practical experience with a novel water-permeable vapor retarder. *Thermal Performance of the Exterior Envelopes of Building V, Conference Proceedings*, ASHRAE, Clearwater Beach, Florida, Dec. 7-10, pp. 480-490.

Krarti, M. 1994. Effect of air flow on heat transfer in walls. *Journal of Solar Energy*, vol. 116, pp. 35-42.

Krischer, O., and Kast, W. 1978. Die wissenschaftlichen Grundlagen der Trocknungstechnik, 3. Auflage, Springer-Verlag, Berlin., as found in Krus, M. and Holm, A. 1999.

Krus, M. and Holm, A. 1999. Simple methods to approximate the liquid transport coefficients describing the absorption and drying. *Proceedings of the 5th Symposium, Building Physics in the Nordic Countries*, Chalmers University of Technology, Göteborg, Sweden, April 24-26, pp. 241-248.

- Kumaran, K. 1996a. Taking the guess work out of placing air/vapor barriers. *Canadian Consulting Engineer*, Southam Business Publications, March/April, pp. 32-34.
- Kumaran, M. K. 1996b. *Final Report, Volume 3, Task 3:Material Properties*, International Energy Agency Annex 24 Report, Published by Katholieke Universiteit–Leuven Belgium.
- Kumaran, M. K. 1999. Moisture diffusivity of building materials from water absorption measurements. *Journal of Thermal Envelopes and Building Science*, Technomic Publishing, vol, 22, April, pp. 349-355.
- Kumaran, M.K., Lackey, J., Normandin, N., van Reenen, D., and Tariku, F. 2002a. *Summary report from task 3 of MEWS Project: Hygrothermal properties of several building materials*. Institute for Research in Construction, National Research Council, Ottawa, NRCC-45369, 68 p.
- Kumaran, M. K., Lackey, J. C., Normandin, N., Tariku, F. and van Reenen, D. 2002b. *A thermal and moisture transport property database for common building and insulating materials, Final report from ASHRAE research project 1018-RP*. National Research Council, Ottawa, July 4, 229 p.
- Künzel, H. M., 1993. Averaging climatic data and its effect on the results of heat and moisture transfer calculation. Report T1-D-93/05, IEA Annex 24, HAMTIE, 7 p.
- Künzel, H. M. 1995. *Simultaneous heat and moisture transport in building components. One- and two-dimensional calculation using simple parameters*. Ph.D. thesis, Fraunhofer Institute for Building Physics, Stuttgart, Germany, 65 p.
- Künzel, H. M. 1999. Flexible vapor control solves moisture problems of building assemblies – Smart retarder to replace the conventional PE-film. *Journal of Thermal Envelopes and Building Science*, Technomic Publishing, Publishing, Lancaster, PA, vol. 23, July, pp. 95-102.
- Lacasse, M.A., O'Connor, T.J., Nunes, S., and Beaulieu, P. 2003. *Report from task 6 of MEWS project : Experimental assessment of water penetration and entry into wood-frame wall specimens - Final report*. National Research Council of Canada, Institute for Research in Construction, Ottawa, RR-133, Feb., 308 p.
- Lacy, R. E. 1965. Driving-rain maps and the onslaught of rain on buildings. *Proceedings of the RILEM/CIB Symposium on Moisture Problems in Buildings*, Helsinki, Aug. 16-19, vol. 3, 29 p.
- Lagus, P. L. in Trechsel, Heinz R., ed. 1994. *Moisture Control in Buildings*. American Society for Testing and Materials, Philadelphia, Pa., 234 p.

Lang, A., Lawton, M. and Brown, W.C. 1999. *Stucco-clad wall drying experiment*. Canadian Mortgage and Housing Corporation, Vancouver, B.C., Research report no. 5972204.00, April.

Lawton, M. and Scott, D. 1995. Envelope durability problems in high-humidity buildings. *Thermal Performance of the Exterior Envelopes of Building VI, Conference Proceedings*, ASHRAE, Clearwater Beach, Florida, Dec. 4-8, pp. 197-205.

Lies, K. M. and B. A. Faith. 1998. Window detailing considerations for leakage prevention. *Water Leakage Through Building Façades*, ASTM STP 1314, R. J Kudder and J. L. Erdly, eds, American Society for Testing and Materials, West Conshohocken, Pa, pp. 33-46.

Lund, H. and Mathis, K. 1991. The design reference year. Report T2-CH-91/02, IEA Annex 24, HAMTIE.

Maerker, B. 1983. Erzeugung eines künstlichen Schlagregens für die Bauteilprüfung. Ph.D. thesis, Technischen Universität Berlin, Berlin, 97 p.

Maref, W., Lacasse, M.A. and Booth, D.G. 2002a. *Executive summary of research contributions related to moisture management of exterior wall systems (MEWS) - Modeling, experiments, and benchmarking*. National Research Council of Canada, Institute for Research in Construction, Ottawa, Report RR-127, Dec., 15 p. <http://irc.nrc-cnrc.gc.ca/fulltext/rr127/>

Maref, W.; Lacasse, M.A.; Booth, D.G. 2002b. *Benchmarking of IRC's advanced hygrothermal model - hygIRC using mid- and large-scale experiments*. National Research Council of Canada, Institute for Research in Construction, Ottawa, Dec., Report RR-126, 46 pp. <http://irc.nrc-cnrc.gc.ca/fulltext/rr126/>

Marsh, P. H. 1977. *Air and rain penetration of buildings*. Construction Press, New York, 174 p.

McAdams, W. H. 1954. *Heat transmission*. 3rd ed., McGraw-Hill, New York.

Mualem, Y. and Assouline, S. 1986. Mathematical model for rain drop distribution and rainfall kinetic energy. *Transactions of the American Society of Agricultural Engineers*, vol. 29, no. 2, pp. 494-500.

Mukhopadhyaya, P., Kumaran, K., Tariku, F. and van Reenen, D. 2003. *Long-term performance: Predict the moisture management performance of wall systems as a function of climate, material properties, etc. through mathematical modelling*. National Research Council of Canada, Institute for Research in Construction, Ottawa, RR-132, Feb., 146 p. <http://irc.nrc-cnrc.gc.ca/fulltext/rr132/>

- Nabhani, M., Tremblay, C. and Fortin, Y. 2003. "Experimental determination of convective heat and mass transfer coefficients during wood drying", 8th international IUFRO Wood Drying Conference, Brasov, Romania, Aug. 24-29, pp. 225-230.
- National Research Council of Canada (NRCC). 1995. *National Building Code of Canada*. Ottawa, Ont.
- Newman, A. J., Whiteside, D., Kloss, P.B. and Willis, W. 1980. Full-scale water penetration tests on twelve cavity fills – Part 1. Nine retrofit fills. *Building and Environment*, Pergamon Press, Oxford, vol. 15, no. 3, pp. 175-191.
- Nordic Innovation Center. 1993. NT BUILD 421. Watertightness under pulsating Air pressure. Nordtest, Espoo, Finland, 8 p.
- Nordic Innovation Center. 1980. NT BUILD 116 Windows, window-doors, external doors, façades: Pulsating air pressure test, approved 03-80, Oslo, 10 p.
- Ogle, R. and O'Connor, J. 1995. Failure of the building envelope: Two case studies. *Thermal Performance of the Exterior Envelopes of Buildings VI, Conference Proceedings*, ASHRAE, Clearwater Beach, Florida, Dec. 4-8, pp. 55-66.
- Ojanen, T., Salonvaara, M., Kohonen, R., and Nieminen, J. 1989. *Moisture transfer in building structures: numerical methods / Kosteuden siirtyminen rakenteissa Laskentamenetelmät*. Technical Research Center of Finland, report no. 595, 113 p. (english translation by Institute for Research in Construction, National Research Council of Canada)
- Ojanen, T. 1998. Improving the drying efficiency of timber frame walls in cold climates by using exterior insulation. *Thermal Performance of the Exterior Envelopes of Building VII, Conference Proceedings*, ASHRAE, Clearwater Beach, Florida, Dec. 6-10, pp. 155-164.
- Onysko, D. M. and Jones, S. K. 1989. Airtightness of wall sheathing as a function of lumber drying. *Thermal Performance of the Exterior Envelopes of Building IV, Conference Proceedings*, ASHRAE, Clearwater Beach, Florida, Dec. 4-7, pp. 458-472.
- Poirier, G. F. 1993. Notes from NRC Canada. NRC facility aids wall system design. *Journal of Thermal Insulation and Building Envelopes*, Technomic Publishing, Mancaster, PA, vol. 16, April, pp. 312-317.
- Powell, F., Krarti, M. and Tuluca, A. 1989. Air movement influence on the effective thermal resistance of porous insulation: A literature survey. *Journal of Thermal Insulation*, vol. 12, pp. 239-251.

Quirouette, R. L. 1985. The difference between a vapour barrier and an air barrier. *Building Practice Note No. 54*, National Research Council, Division of Building Research, 13 p.

Regulation respecting energy conservation in new buildings. 1992. Éditeur officiel du Québec, Québec City.

Richards, R. F. 1992. Measurement of moisture diffusivity for porous building materials. *Thermal Performance of the Exterior Envelopes of Buildings V, Conference Proceedings*, ASHRAE, Clearwater Beach, Florida, Dec. 7-10, pp. 501-511.

Ricketts, D. R. and Lovatt, J.E. 1996. *Survey of building envelope failures in the coastal Climate of British Columbia*. Canadian Mortgage and Housing Corporation, Vancouver, B. C., 43 p.

Rode, C. 1993. Reference years for moisture calculations. IEA Annex 24, HAMTIE, Report T2-DK-93/02, April 16, 8p.

Roels, S., Carmeliet, J., Hens, H., Adan, O., Brocken, H., Cerny, R., Pavlik, Z., Hall, C., Kumaran, K., Pel, L. and Plagge, R. 2004. Interlaboratory comparison of hygric properties of porous building materials. *Journal of Thermal Envelope and Building Science*, Technomic Publishing, vol. 27, no. 4, April, pp. 307-325.

Roels, S. and Carmeliet, J. 2005. Water vapor permeability and sorption isotherm of coated gypsum board. *Proceedings of the 7th Symposium on Building Physics in the Nordic Countries*, Reykjavic, Iceland, June 13-15, pp. 609-616.

Rose, W. 1995. The history of attic ventilation regulation and research. *Thermal Performance of the Exterior Envelopes of Buildings VI, Conference Proceedings*, ASHRAE, Clearwater Beach, Florida, Dec. 4-8, pp. 125-134.

Salonvaara, M., Ojanen, T., Kokko, E., and Karagiozis, A. 1998. Drying capabilities of wood frame walls with wood siding. *Thermal Performance of the Exterior Envelopes of Buildings VII, Conference Proceedings*, ASHRAE, Clearwater Beach, Florida, Dec. 6-10, pp. 165-177.

Salonvaara, M., and Karagiozis, A. 1998. EIFS hygrothermal performance due to initial construction moisture as a function of air leakage, interior cavity insulation, and climate conditions. *Thermal Performance of the Exterior Envelopes of Buildings VII, Conference Proceedings*, ASHRAE, Clearwater Beach, Florida, Dec. 6-10, pp. 179-188.

Sanders, C. 1996. Final report - Task 2: Environmental conditions, IEA - Annex 24 HAMTIE, Belgium: Catholic University of Leuven, vol. 2, 96 p.

- Sankaran, R. and Paterson, D.A. 1995. Computation of rain falling on a tall rectangular building. *9th International Conference on Wind Engineering*, Wiley Eastern Ltd., New Delhi, pp. 2127-2137.
- Schumacher, C., Shi, X., Davidovic, D., Burnett, E. and Straube, J. 2003. Ventilation drying in wall systems. *Proceedings of the Second International Building Physics Conference: Research in Building Physics*, A.A. Balkema Publishers, Leuven, Belgium, September 14-18, pp. 479-486.
- Segerholm, I. 2005. Moisture conditions in wooden elements exposed to artificial precipitation. *Proceedings of the 7th Symposium on Building Physics in the Nordic Countries*, Reykjavic, Iceland, June 13-15, pp. 141-148.
- Shih, T.-H., Liou, W. W., Shabbir, A. and Zhu, J. 1995. A new k- ϵ eddy-viscosity model for high Reynolds number turbulent flows- Model development and validation. *Computers and Fluids*, Pergamon, vol. 24, no. 3, pp. 227-238.
- Siau, J. F. 1984. *Transport processes in wood*. Springer Verlag, Berlin, 245 p.
- Simiu, E. and Scanlan, R.H. 1996. *Wind Effects on Structures: Fundamentals and Applications to Design*, John Wiley & Sons, 3rd ed.
- Skaar, C. 1988. *Wood-Water Relations*. Springer-Verlag, Berlin Heidelberg, Germany, 274 p.
- Straube, J. F. 2000. *Driving rain measurement – Draft final report for MEWS*, Institute for Research in Construction, National Research Council, April.
- Straube, J. F. 2001. The influence of low-permeance vapor barriers on roof and wall performance. *Performance of Exterior Envelopes of Whole Buildings VIII: Integration of Building Envelopes, Conference Proceedings*, ASHRAE, Clearwater Beach, Florida, Dec. 2-7, 12 p.
- Straube, J. F. and Burnett, E. F. P. 1998a. Driving rain and masonry veneer. *Water Leakage Through Building Façades*, ASTM STP 1314, R. J. Kudder and J. L. Erdly, Eds., American Society for Testing and Materials, West Conshohocken, PA, pp. 73-87.
- Straube, J. F. and Burnett, E. F. P. 1998b. Drainage, ventilation drying and enclosure performance. *Thermal Performance of the Exterior Envelopes of Building VII, Conference Proceedings*, ASHRAE, Clearwater Beach, Florida, Dec. 6-10, pp. 189-198.
- Straube, J. F. and Burnett, E. F. P. 2000a. Simplified prediction of driving rain on buildings. *Proceedings of the International Building Physics Conference*, Eindhoven University of Technology, Eindhoven, the Netherlands, pp. 375-382.

- Straube, J. F. and Burnett, E. F. P. 2000b. Pressure moderation and rain control for multiwythe masonry walls. *Proceedings of the International Building Physics Conference*, Eindhoven University of Technology, Eindhoven, the Netherlands, pp. 179-186.
- Straube, J. F. and Burnett, E. F. P. 2005. *Building Science for Building Enclosures*, Building Science Press, Westford, MA, 549 p.
- Svendsen, Sven D. 1955. *Driving rain: Experimental research on the resistance of external Walls against rain penetration*. Norwegian Building Research Institute, Oslo, Report no. 20, 19 p.
- TenWolde, A., Rose, W. 1999. Issues related to venting of attics and cathedral ceilings. *ASHRAE Transactions: Symposia*, ASHRAE, Atlanta, GA, pp. 851-857.
- Thomson, W. 1871. *Phil. Mag. J. Sci*, vol. 42, p. 448.
- Tsongas, G. A., Govan, D. P., and McGillis, J. A. 1998. Field observations and laboratory tests of water migration in walls with shiplap hardboard siding. *Thermal Performance of the Exterior Envelopes of Buildings VII, Conference Proceedings*, ASHRAE, Clearwater Beach, Florida, Dec. 6-10, pp. 469-483.
- van Mook, F. J. R., de Wit, M.H. and Wisse, J.A. 1997. Computer simulation of driving rain on building envelopes. *Proceedings of the 2nd European and African Conference on Wind Engineering*, University of Genova, Italy, pp. 1059-1066.
- van Mook, F. J. R. 1999a. Measurement and simulations of driving rain on the Main Building of the TUE. *Proceedings of the 5th Symposium on Building Physics in the Nordic Countries*, Chalmers University of Technology, Goteborg, Sweden, August 24-26, pp. 377-384.
- van Mook, F. J. R. 1999b. Full-scale measurements and numeric simulations of driving rain on a building. *Proceedings of the 10th International Conference on Wind Engineering*, Larsen, Larose and Livesey, eds., Balkema, Kobenhavn, Denmark, June 21-24, pp. 1145-1152.
- Viitanen, H. 1996. *Factors affecting the development of mold and brown rot decay in wooden material and wooden structures. Effect of humidity, temperature and exposure time*. Dissertation, the Swedish University of Agricultural Sciences, Uppsala, Sweden.
- Wahlgren, P. 1998. Convection in loose-fill attic insulation – Simulations and large-scale measurements. *Performance of Exterior Envelopes of Whole Buildings VIII: Integration of Building Envelopes, Conference Proceedings*, ASHRAE, Clearwater Beach, Florida, 8 p.

Waldvogel, A. 1974. The N_0 jump of raindrop spectra. *Journal of the Atmospheric Sciences*, American Meteorological Society, Boston, MA, vol. 31, May, pp. 1067-1078.

Whiteside, D., Newman, A. J., Kloss, P.B. and Willis, W. 1980. Full-scale testing of the resistance to water penetration of seven cavity fills. *Building and Environment*, Pergamon Press, Oxford, vol. 15, pp. 109-118.

Zarr, R. R., Burch, D. M., and Fanne, A. H. 1995. Heat and moisture transfer in wood-based wall construction: Measured versus predicted. *NIST Building Science Series 173*, National Institute of Standards and Technology, Gaithersburg, MD, 72 p.

Zhu, D., Reddy Mallidi, S., and Fazio, P. 1995. Approach for urban driving rain index by using climatological data recorded at suburban meteorological station. *Building and Environment*, vol. 30 no. 2, Pergamon Press, Oxford, pp. 229-236.

Zwayer, G. L., Cook, D. F. and Crowe, J. P. 1998. Criteria for water penetration testing. *Water Leakage Through Building Façades*, ASTM STP 1314, R. J. Kudde and J. L. Erdly, Eds., American Society for Testing and Materials, West Conshohocken, PA, pp. 142-154.

APPENDIX A. STATISTICAL ANALYSIS OF TRUDEAU INTERNATIONAL AIRPORT WEATHER STATION PRECIPITATION DATA FOR EXPERIMENTAL PROTOCOL

Table 3.2 in section 3.1.1.1 shows the results of a statistical analysis for determining: a) the average hourly horizontal rainfall; b) the average daily number of hours of rain; c) and the average number of rainy days, as well as d) average monthly horizontal rainfall for the months from April to October. The raw data was taken from Environment Canada climatic data for the Pierre-Elliott Trudeau International Airport weather station for the years 1981 to 2001. This appendix describes how the analysis was performed.

a) Average hourly horizontal rainfall over 20 years

To determine the hourly horizontal rainfall for each month over a period of 20 years, the total monthly rainfall was calculated from the hourly rainfall data for each month over the 20-year period. As well, the total number of hours of rain was calculated for every month. Then, to determine the average hourly rainfall over 20 years, the sum of the total monthly rainfall was taken over the 20-year period, and divided by the sum of the total number of hours of rain over the same period for each month in question. The equation is given below:

$$\text{Average hourly rainfall over 20 years} = \frac{\sum R_h}{\sum n_H} \quad [\text{A.1}]$$

where R_h is the monthly horizontal rainfall for a specific month and n_H is the number of hours of rain over that month. The summation is carried out for a specific month, e.g. April, over 20 years.

b) Average daily number of hours of rain

To determine the average daily number hours of rain, the total number of hours of

rainfall is determined for each month over the 20 year span, as well as the number of rainy days. Then, the sum over 20 years of the total number of hours of rainfall for the month in question (e.g. April) is divided by the sum over 20 years of the number of rainy days for the month in question. The equation is given below:

$$\text{Average daily number of hours of rain} = \frac{\sum n_H}{n_M} \quad [\text{A.2}]$$

where n_H is the number of hours of rain over a specific month, and n_M is the number of months under consideration, 20 in this case. The summation is carried out for a specific month, e.g. April, over 20 years.

c) Average number of rainy days in a month [days]

To find the average number of rainy days in a month, the number of rainy days is determined for each month in question (e.g. April) over the 20 year span, and then the sum of these is taken and then divided by the number of years being considered.

$$\text{Average number of rainy days in a month} = \frac{\sum n_D}{n_M} \quad [\text{A.3}]$$

where n_D is the number of rainy days for a specific month, and n_M is the number of months under consideration, 20 in this case. The summation is carried out for a specific month, e.g. April, over 20 years.

d) Average monthly horizontal rainfall over 20 years [mm]

The average monthly horizontal rainfall over 20 years is found by first calculating the total rainfall for each month in question over the 20 year span, taking a sum of these and then dividing this sum by the number of years under consideration. The equation is given below:

$$\text{Average monthly horizontal rainfall over 20 years} = \frac{\sum R_h}{n_M} \quad [\text{A.4}]$$

where R_h is the monthly horizontal rainfall for a specific month and n_M is the number of months under consideration, 20 in this case. The summation is carried out for a specific month, e.g. April, over 20 years.

APPENDIX B. DETERMINATION OF WATER IMPINGING THE TOP CORNER OF A LOW-RISE BUILDING

In Blocken and Carmeliet's numerical model, the wind-driven rain striking a building envelope is calculated using computational fluid dynamics, with the realizable k- ϵ model as the wall function to determine the wind flow pattern around buildings and the raindrop trajectory in the airflow. The authors determined the specific catch ratio, $\eta_a(a)$, which is a function of the raindrop radius, a , and is defined as the ratio of the intensity of rainfall with raindrops of radius a landing on a specific zone on the building face to the intensity of the rainfall on a horizontal plane away from the local effects of the building:

$$\eta(a) = \frac{R_{bv}(a)}{R_h(a)} \quad [\text{B.1}]$$

R_{bv} is the rate of rain deposition on a vertical building surface and R_h is the rate of horizontal rainfall. The catch ratio for a zone, η , is the integral product of the specific catch ratio and the raindrop size distribution, in m^{-1} , over all raindrop diameters:

$$\eta = \int_a f_h(a) \eta_a(a) da \quad [\text{B.2}]$$

In their analysis, Blocken and Carmeliet chose the raindrop size distribution developed by Best, a pioneer in this research area who carried out an extensive experimental study of rain droplet size distributions and developed mathematical expressions to determine the cumulative probability distribution of raindrops. Best's model has been utilized by many wind-driven rain numerical models (Choi, 1991, 1992, 1994, 1999; Blocken and Carmeliet, 2000, 2001a, 2001b, 2002a, 2002b; Karagiozis and Hadjisophocleous, 1995, 1997; Hangan and Incelet, 2001).

Blocken and Carmeliet have performed numerical evaluations to determine the catch ratio at several locations on a building façade, and have validated the model using field data. Their catch ratio results are reproduced here in Figure B.1 for a location at approximately 1/3 of the height of a one-story building with a flat roof (shown as rain gauge no. 6 in Figure B.2). The wind direction is perpendicular to the surface of the

façade. Required local meteorological data for the graph are the horizontal rainfall, R_h , and the wind speed at a 10 m height above ground, V_{10} .

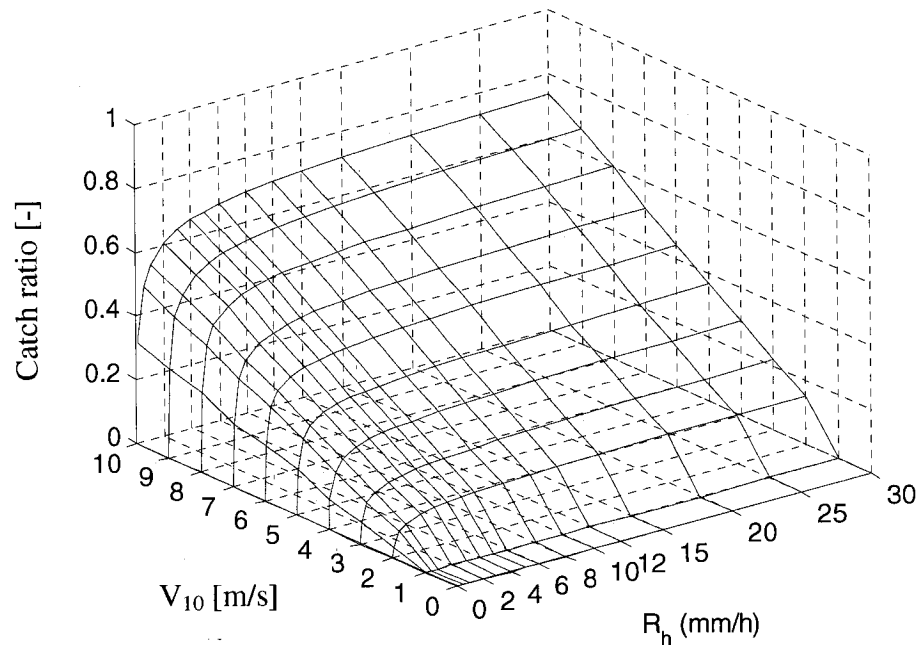


Figure B.1. Numerical results of specific catch ratio as a function of wind speed at 10 m height and horizontal rainfall intensity (Blocken and Carmeliet, 2001b).

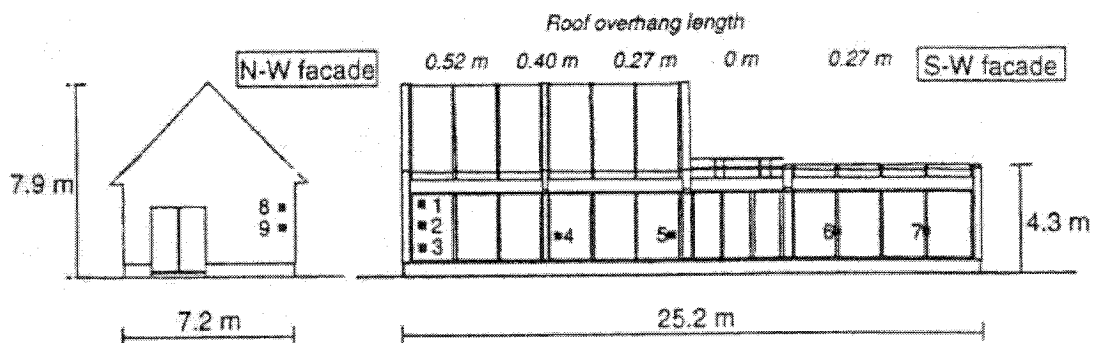


Figure B.2. Test building: north-west and south-west facades and position of driving rain gauges 1 to 9 at the façade (Blocken and Carmeliet, 2001a).

The present study aims to establish the amount of wind-driven rain for a low-rise residential building, and specifically, on the lower central level of the building. The wind is assumed to strike normally to the surface of the façade, and hence no correction will be necessary in this respect. As well, the upstream wind flow is assumed to be unaffected

by surrounding buildings, trees and other structures. The calculations for rain load have been completed for the month of August.

As was stated earlier, the horizontal rainfall is required to determine the catch ratio. To this effect, the above-mentioned meteorological database for Montreal's Pierre Elliott Trudeau International Airport climatic station was utilized, and the mean hourly rainfall for the months of April to October was found and is repeated here for convenience (see Table B.1). The highest mean monthly rainfall was found for the month of August. Thus, August was selected for the purpose of this study, yielding a mean hourly horizontal rainfall of 1.93 l/m^2 , as seen in Table B.2

Table B.1. Mean precipitation data for Montreal's Trudeau International Airport weather station for years 1941 to 1990 (Environment Canada website).

| Month | April | May | June | July | August | September | October |
|----------------------|-------|------|------|------|--------|-----------|---------|
| Rainfall [mm] | 62.6 | 66.7 | 82.5 | 85.6 | 100.3 | 86.5 | 72.8 |

Table B.2. Data showing the average horizontal hourly rainfall and total rainfall for the months from April to October, taken from analysis of Environment Canada hourly climatic data for the Trudeau International Airport climatic station for the years 1981 to 2001.

| | April | May | June | July | August | September | October |
|---|-------|------|------|------|--------|-----------|---------|
| Average hourly horizontal rainfall over 20 years [mm] | 1.06 | 1.21 | 1.63 | 2.02 | 1.93 | 1.56 | 1.23 |
| Average monthly horizontal rainfall over 20 years [mm] | 66.4 | 75.4 | 82.3 | 82.0 | 89.7 | 84.4 | 74.2 |

*Data for 2001 were not available when the analysis was done.

The other input required to find the catch ratio from Figure B.1 is the local wind speed. For this purpose, a database of hourly climatic data from the Trudeau meteorological station for 1981 to 2001 was obtained for this purpose, and a frequency distribution of hourly wind speed during rainfall for the month of August was made (see Figure B.3). The most commonly occurring wind speed during rainfall was initially selected. It was found to range between 1.50 and 2.0 m/s and to occur 13.5% of the time. Hence, the median, 1.75 m/s, was initially used. Since the geographical location of interest is in a suburban terrain, the wind speed measured at a height of 10 m in the open country airport station must be converted for the greater terrain roughness provided by

the suburbs. This can be done using the Power Law from wind engineering.

The Power Law, a well-known relation used in wind engineering, can be used to make the conversion, and is expressed as follows:

$$\frac{V_{z1}}{V_{z2}} = \left(\frac{z_1}{z_2} \right)^\alpha \quad [\text{B.3}]$$

where V_{z1} and V_{z2} are the wind velocities at a height of z_1 and z_2 , respectively, and α depends on the upstream roughness of the terrain. In this instance, the wind speed measured at a height of 10 m at the Trudeau International Airport meteorological station, in an open country terrain, shown in Figure B.3, must be converted to the 10 m height wind speed in a suburban-type terrain. This is done in two steps. First, the wind speed at a height above ground of 10 m measured by the Trudeau meteorological station is converted to the gradient wind speed at the open country boundary layer thickness, $V_{g, oc}$, as follows:

$$V_{g, oc} = V_{10, oc} \left(\frac{\delta_{g, oc}}{10} \right)^{\alpha_1} \quad [\text{B.4}]$$

where $V_{10, oc}$ is the 10 m velocity given by the Trudeau meteorological station, $\delta_{g, oc}$, the boundary layer thickness for an open terrain, is 275 m, and α_1 is 0.16 for an open terrain. Since V_g remains unchanged for an open country terrain and a suburban terrain, it can now be used to calculate the wind speed at 10 m height, $V_{10, sub}$, in the suburban terrain:

$$V_{10, sub} = V_{g, sub} \left(\frac{10}{\delta_{g, sub}} \right)^{\alpha_2} \quad [\text{B.5}]$$

where $V_{g, sub}$ is the suburban boundary layer wind velocity. $\delta_{g, sub}$, the boundary layer thickness of the suburban terrain, is equal to 400 m and α_2 is 0.28. The values for the boundary layer thicknesses and α are given by Simiu and Scanlan (1996) and recommended in the American National Standard A58.1-1982.

The wind speed conversion from open country terrain to suburban terrain results in a corrected suburban wind speed of 1.06 m/s. This low wind speed, when inputted into Figure B.1, yields a catch ratio that would indicate an insignificant amount of wind-driven rain on the building façade. Recognizing that higher wind speeds produce higher driving rain rates on building surfaces, a wind speed in the range of 3.0 to 3.5 m/s,

occurring 9.6% of the time, was selected. The median value, when corrected for suburban terrain roughness, is 2.0 m/s.

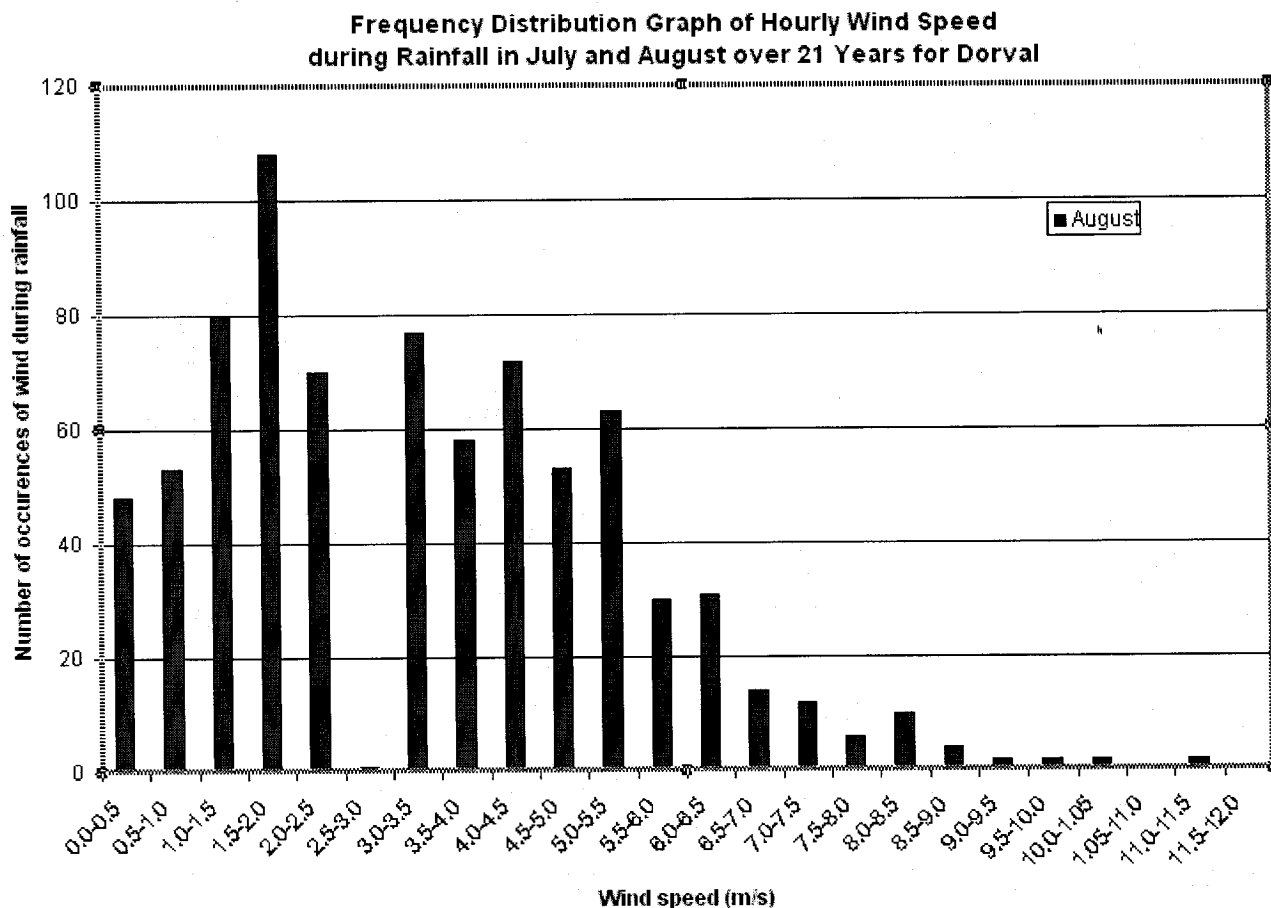


Figure B.3. Frequency distribution of hourly wind speed during rainfall in August (1981-2001).

Now that the 10 m wind speed and the hourly rate of horizontal rainfall are known, the catch ratio can be determined. For this purpose, the results of Blocken and Carmeliet's research (2001b), which is based on Best's raindrop size distribution, are used. Figure B.1 shows that for a wind speed V_{10} of 2.0 m/s and an August hourly horizontal precipitation rate of 1.93 l/m^2 , the catch ratio is approximately 0.12. This catch ratio, multiplied by the horizontal precipitation rate, results in 0.23 l/m^2 per hour of rain impinging on specified location on the building envelope.

APPENDIX C. TRANSPORT MECHANISMS AND MATERIAL PROPERTIES AS USED IN FOUR HYGROTHERMAL MODELS

Basic material properties required by heat, air and moisture (HAM) models include the bulk density of the dry materials, the open porosity and the specific heat capacity. Calculating the heat transfer involves determination of sensible heat transfer using the thermal conductivity of the dry materials, but some models such as WUFI and DELPHIN also consider the influence of moisture content on the material's thermal conductivity and the latent heat of evaporation.

Few hygrothermal tools consider air movement through an assembly as a mode of heat and mass transfer. Air movement can occur through a porous material, as is the case with wind washing, when wind infiltrates into the assembly and moves through porous insulation such as glass fiber insulation. hygIRC does consider air leakage over the total envelope surface area.

Moisture transfer can occur in the vapor form, in the liquid form, or as a combination of both. Models typically utilize vapor permeability or permeance to determine the vapor flux where vapor pressure is the driving force. In Europe, the vapor diffusion resistance factor or the vapor diffusion thickness are often used. The vapor diffusion resistance factor of a material, μ , shows how many times the water vapor permeability of a air is greater than that of the material, at the same conditions of temperature and total pressure:

$$\mu = \frac{\delta_a}{\delta} \quad [C.1]$$

where δ_a and δ are the water vapor permeabilities of the air and of the material, respectively, both with units of $\text{kg/m}\cdot\text{s}\cdot\text{Pa}$, or s. The value of δ_a can be determined from (Hens, 2003):

$$\delta_a = \frac{D_{vl}}{R_v \Phi} \quad [C.2]$$

Here, R_v is the gas constant of water vapor, and D_{vl} is the binary diffusion coefficient

between water vapor and air, in m²/s, which is given by:

$$D_{v1} = \frac{2.26173}{p_a} \left(\frac{\Phi}{273.16} \right)^{1.81} \quad [C.3]$$

where Φ is the temperature in K and p_a is the atmospheric pressure. Equation [6.2] simplifies to:

$$\delta_a = \frac{2.0 \cdot 10^{-7} \cdot \Phi^{0.81}}{p_a} \quad [C.4]$$

The vapor diffusion thickness, s_d , represents the equivalent diffusion air layer thickness in meters. In other words, the s_d value describes the thickness of a stagnant air layer with the same diffusion resistance as the material or air layer in the case of a surface air film.

For liquid transfer, transport coefficients such as the liquid diffusivity, also called the liquid transport coefficient, and the liquid conductivity are used. It should be noted that in hygroscopic materials, all of the aforementioned moisture transport coefficients are a function of moisture content. These vapor and liquid transport coefficients are defined in the literature review chapter.

The two-dimensional version of hygIRC and its predecessor, LATENITE, also consider liquid moisture permeability which is defined for these two tools as gravity-driven liquid flow through porous media.

Advanced models also take moisture storage into account. This is usually given by a sorption curve, but can also be found in the form of a moisture retention characteristic, which is divided into the sorption curve in the hygroscopic range and the water retention characteristic in the capillary range.

Table C.1 shows a summary of the material parameters and the material functions considered by the two-dimensional HAM models LATENITE and its successor, hygIRC, DELPHIN4 and WUFI2D. Table C.2 shows the transport mechanisms and Table C.3 the driving potentials used by the three hygrothermal models.

Table C.1. Material parameters and material functions used in hygrothermal models.

| | Description | LATENITE/ hygIRC | DELPHIN 2-D | WUFI 2-D | MATCH |
|---|---|---------------------|----------------|-------------|-------|
| Material parameters | | | | | |
| Bulk density of dry material [kg/m ³] | - | Y | Y | Y | Y |
| Open porosity [-], or open pore volume [$m_{\text{pore}}^3/m_{\text{bulk mat}}^3$], or kg/m ³ bulk mat | - | | Y | Y | |
| Specific heat capacity [J/kg·K] | - | Y | Y | Y | Y |
| Material functions | | | | | |
| Thermal conductivity, moisture-dependent [W/m ² ·K] | Heat flux due to a temperature gradient (moisture dependent) | Y | Y | Y | Y |
| Sorption curve or moisture retention curve (moisture storage) | Moisture content as a function of capillary pressure; combination of sorption isotherm (hygroscopic) and water retention characteristic (capillary) | Y | Y | Y | Y |
| Water vapor permeability [ng/m·s·Pa] | Mass of vapor flux due to vapor gradient per unit area and unit time | Y | | | Y |
| Vapor diffusion resistance factor [-] | A factor indicating how many times the water vapor permeability of a air is greater than that of the material | | Y | Y | |
| Water vapor diffusivity [m ² /s] | Vapor diffusion flux due to a water vapor gradient | | Y | | |
| Hygroscopic | Total moisture flux | | Y | | |

| | | | | | |
|--|--|---|---|---|---|
| moisture conductivity [kg/s·m·Pa = s] | due to a vapor pressure gradient (hygroscopic range) | | | | |
| Liquid water conductivity [kg/s·m·Pa = s] | Liquid water flux due to capillary pressure gradient | | Y | | Y |
| Liquid water or liquid moisture diffusivity [m ² /s] | Liquid water flux due to a moisture content gradient | Y | Y | Y | |
| Capillary moisture conductivity [kg/s·m·Pa = s] | Total moisture flux due to a capillary pressure gradient (capillary range) | | Y | | |
| Liquid moisture permeability [kg/s·m·Pa = s] | Gravity-driven liquid flow through porous media (see Karagiozis <i>et al.</i> , 1996; Meref <i>et al.</i> , 2002b) | Y | | | |

*salt transport coefficients are neglected

Table C.2. Transport mechanisms considered by hygrothermal models.

| | LATENITE/ hygIRC | DELPHIN | WUFI 2-D | MATCH |
|--|---------------------|---|---|--------------------------|
| Moisture transport | | | | |
| Vapor diffusion | Y | Y | Y | Y |
| Liquid transport | Y | Y | Y | Y |
| Liquid gravity flow | Y | N | N | N |
| Thermal transport | | | | |
| Conduction | Y | Y | Y | Y |
| Convection (heat flow through air transport) | Y | N (surface film coefficients included in model) | N (surface film coefficients included in model) | N |
| Heat of evaporation | Y | Y | Y | Y |
| Heat of freeze/thaw | Y | N | N | Y (taken into account by |

| | | | | |
|--|---|---|---|---------------------------------|
| | | | | modification of c_p value) |
| Air transport | | | | |
| Vapor flow through air transport | Y | N | N | N |

Table C.3. Moisture and thermal potentials used in several hygrothermal models.

| | LATENITE/ hygIRC | DELPHIN 2-D | WUFI 2-D | MATCH |
|--------------------------|---------------------------------|--|----------------------|---------------------------------|
| Thermal transport | | | | |
| | Temperature | Temperature | Temperature | Temperature |
| Thermal transport | | | | |
| Vapor transport | Vapor pressure difference | Capillary pressure | Relative humidity | Vapor pressure difference |
| Liquid transport | Moisture content | RH, or the derived capillary pressure (hygroscopic range) and capillary pressure (capillary range), or moisture content | Relative humidity | Capillary pressure |
| Air transport | | | | |
| | Air velocity vector | - | - | - |

APPENDIX D. BASIC MATERIAL PROPERTIES AND MATERIAL PROPERTY FUNCTIONS AS USED IN THE WUFI SIMULATIONS

Numerical simulations require many material properties as input data. Some of the material properties are constants, such as the bulk density, the porosity, the specific heat capacity and the thermal conductivity of the dry material. Other material properties are functions that depend on another parameter, such as:

- the sorption, which is the moisture content of a hygroscopic material as a function of the relative humidity;
- the liquid diffusivity, which is a function of the moisture content;
- the thermal conductivity, which, in hygroscopic materials, is a function of the moisture content, and;
- the vapor transport coefficient, expressed either the vapor permeability, the permeance, or the vapor diffusion resistance factor.

The following tables give the values for the material properties used in the numerical simulations: OSB, plywood, fiberboard, spruce, fiberglass batt insulation, polyethylene, gypsum board and extruded polystyrene.

Table D.1. Materials and basic material properties used in the simulations.

| Material and thickness | Bulk density [kg/m ³] | Porosity [-] | Specific heat capacity [J/kg·K] | Thermal conductivity of dry material [W/m·K] | Permeance [ng/s·m ² ·Pa] or permeability [ng/s·m·Pa], vapor/ diffusion resistance factor [-] of dry material |
|----------------------------|--|--------------------|------------------------------------|---|---|
| OSB sheathing, 12.7 mm | 650 (Kumaran <i>et al.</i> , 2002b) | 0.60 (WUFI Pro) | 1880 (Kumaran, 1996b) | 0.101 (Kumaran <i>et al.</i> , 2002b) | 0.044 ng/s·m·Pa (Kumaran <i>et al.</i> , 2002b), 650 [-] |
| Plywood sheathing, 12.5 mm | 470 (Kumaran <i>et al.</i> , 2002b) | 0.80 (WUFI Pro) | 1880 (Kumaran, 1996b) | 0.1 WUFI Pro | 1220 [-] (derived from Kumaran <i>et al.</i> , 2002b) |

| | | | | | |
|--|---|-----------------------------------|--------------------------|---|---|
| Asphalt-coated fiberboard sheathing, 11 mm | 320 (Kumaran <i>et al.</i> , 2002b) | 0.80 | 1880 (Kumaran, 1996b) | 0.048 (WUFI Pro) | 1470 ng/s·m·Pa (derived from Kumaran <i>et al.</i> , 2002b); 7.80 [-] |
| Spruce top and bottom plates, 142 mm (radial/tangential) | 342.3 | 0.76 ¹ | 1880 (Kumaran, 1996b) | 0.082 (WUFI Pro) | 928.5 (WUFI Pro) |
| Fiberglass batt insulation, 140 mm | 11.5 (Kumaran <i>et al.</i> , 2002b) | 0.99 (WUFI Pro) | 840 (Kumaran, 1996b) | 0.035 (WUFI Pro) | 1.3 |
| Polyethylene, 0.15 mm | 130 (WUFI Pro) | 0.001 (WUFI Pro) Negligible | 2300 (WUFI Pro) | 2.3 (WUFI Pro) | 3.4 ng/s·m ² ·Pa (ASHRAE, 2001), 385650 [-] (57847 for 1 mm at 20°C [-]) |
| Gypsum, 12.5 mm | 625 (Kumaran <i>et al.</i> , 2002b) | 0.65 (WUFI Pro) | 870 (Kumaran, 1996b) | 0.163 (WUFI Pro) | 6.0 [-] (WUFI Pro) |
| Extruded polystyrene, 38 mm | 28.6 (Kumaran <i>et al.</i> , 2002b) | 0.95 (WUFI Pro) | 1470 (WUFI Pro) | 0.0239 (Kumaran <i>et al.</i> , 2002b) | 1.22 ng/s·m ² ·Pa (Kumaran <i>et al.</i> , 2002b), 155 [-] |

¹ Derived from the density of the solid wood substance (1500 kg/m³, from Kollmann and Côté (1984)) and the calculated density of the bottom plate inserts, approximately 360 kg/m³.

Table D.2. Material functions for OSB.

Table D.2a. Moisture storage function (sorption).

| RH [%] | Moisture content [kg/m ³]* |
|--------|--|
| 0 | 0 |
| 50 | 0.077*650=50.0 |
| 80 | 0.146*650=95.0 |
| 90 | 0.215*650=140.0 |
| 97 | 0.277*650=180.0 |
| 100 | 0.723*650=470.0 |

Source: WUFI Pro database for OSB with a density of 650 kg/m³.

*Units of moisture content, in kg_{moisture}/kg_{dry material}, multiplied by density, in kg/m³, yields moisture content in kg/m³.

Table D.2b. Liquid transport coefficient, D_w.

| Moisture content [kg/m ³] | D _w [m ² /s] |
|---------------------------------------|------------------------------------|
| 0.200*650=130.0 | 8.55E-11 |
| 0.215*650=139.8 | 8.05E-11 |
| 0.231*650=150.2 | 7.61E-11 |
| 0.246*650=159.9 | 7.23E-11 |
| 0.262*650=170.3 | 6.89E-11 |
| 0.277*650=180.1 | 6.60E-11 |
| 0.292*650=189.8 | 6.33E-11 |
| 0.308*650=200.2 | 6.09E-11 |
| 0.323*650=210.0 | 5.88E-11 |
| 0.338*650=219.7 | 5.69E-11 |
| 0.354*650=230.1 | 5.52E-11 |
| 0.369*650=239.9 | 5.37E-11 |
| 0.385*650=250.3 | 5.23E-11 |
| 0.400*650=260.0 | 5.12E-11 |
| 0.415*650=269.8 | 5.01E-11 |
| 0.431*650=280.2 | 4.93E-11 |
| 0.446*650=289.9 | 4.86E-11 |
| 0.462*650=300.3 | 4.81E-11 |
| 0.477*650=310.1 | 4.78E-11 |
| 0.492*650=319.8 | 4.77E-11 |
| 0.508*650=330.2 | 5.08E-11 |
| 0.523*650=340.0 | 4.85E-11 |

Source: Kumaran *et al.* (2002b).

Table D.2c. Heat conductivity as a function of moisture content.

| Moisture content [kg/m ³] | Thermal conductivity [W/m·K] |
|---------------------------------------|------------------------------|
| 0 | 0.101 |
| 600 | 0.253 |

Source: WUFI Pro.

Table D.2d. Vapor diffusion resistance factor as a function of relative humidity.

| RH [%] | μ [-] |
|--------|-------|
| 0 | 650.0 |
| 30 | 485.0 |
| 50 | 220.0 |
| 70 | 107.0 |
| 90 | 55.0 |
| 100 | 38.0 |

Source: WUFI Pro for OSB with density 600 kg/m³.

Table D.3. Material functions of plywood.

Table D.3a. Moisture storage function.

| RH [%] | Moisture content [kg/m ³]* |
|--------|---|
| 0 | 0 |
| 50 | 0.085*470=40.0 |
| 80 | 0.160*470=75.0 |
| 90 | 0.234*470=110.0 |
| 97 | 0.319*470=150.0 |
| 100 | 0.745*470=350.0 |

Source: WUFI Pro database for plywood with a density of 470 kg/m³.

*Units of moisture content, in kg_{moisture}/kg_{dry material}, multiplied by density, in kg/m³, yields moisture content in kg/m³.

Table D.3b. Liquid transport coefficient, D_w.

| Moisture content [kg/m ³] | D _w [m ² /s] |
|--|---------------------------------------|
| 0.085*470=40.0 | 9.32E-9 |
| 0.106*470=49.8 | 4.70E-9 |
| 0.128*470=60.2 | 3.16E-9 |
| 0.149*470=70.0 | 2.47E-9 |
| 0.170*470=79.9 | 2.10E-9 |
| 0.191*470=89.8 | 1.89E-9 |
| 0.213*470=100.1 | 1.76E-9 |
| 0.234*470=110.0 | 1.69E-9 |
| 0.255*470=119.9 | 1.66E-9 |
| 0.277*470=130.2 | 1.67E-9 |
| 0.298*470=140.1 | 1.71E-9 |
| 0.319*470=149.9 | 1.77E-9 |
| 0.340*470=159.8 | 1.87E-9 |
| 0.362*470=170.1 | 2.01E-9 |
| 0.383*470=180.0 | 2.18E-9 |
| 0.404*470=189.9 | 2.39E-9 |
| 0.426*470=200.2 | 2.62E-9 |
| 0.447*470=210.1 | 2.84E-9 |
| 0.468*470=220.0 | 2.98E-9 |
| 0.489*470=229.8 | 3.01E-9 |
| 0.511*470=240.2 | 2.92E-9 |
| 0.532*470=250.0 | 2.75E-9 |
| 0.553*470=259.9 | 2.53E-9 |
| 0.574*470=269.8 | 2.32E-9 |
| 0.596*470=280.1 | 2.12E-9 |
| 0.617*470=290.0 | 1.93E-9 |
| 0.638*470=300.0 | 1.77E-9 |
| 0.660*470=310.2 | 1.63E-9 |
| 0.681*470=320.1 | 1.50E-9 |
| 0.702*470=329.9 | 1.39E-9 |
| 0.723*470=339.8 | 1.29E-9 |
| 0.745*470=350.2 | 1.21E-9 |
| 0.766*470=360.0 | 1.13E-9 |
| 0.787*470=369.9 | 1.05E-9 |
| 0.809*470=380.2 | 9.90E-10 |
| 0.830*470=390.1 | 9.32E-10 |
| 0.851*470=400.0 | 8.78E-10 |
| 0.872*470=409.8 | 8.30E-10 |
| 0.894*470=420.2 | 7.85E-10 |

| | | | |
|--|---|-----------------|----------|
| | | 0.915*470=430.1 | 7.44E-10 |
| | | 0.936*470=439.9 | 7.06E-10 |
| | | 0.957*470=449.8 | 6.71E-10 |
| | Source: Kumaran <i>et al.</i> (2002b) for plywood with a density of 470 kg/m ³ . | | |

| | | | |
|--|------------------------------|---|-------------------|
| Table D.3c. Heat conductivity as a function of moisture content. | | Table D.3d. Vapor diffusion resistance factor as a function of relative humidity. | |
| Moisture content [kg/m ³] | Thermal conductivity [W/m·K] | RH [%] | μ [-] |
| 0 | 0.1 | 0 | 1200 ¹ |
| 500 | 0.25 | 10 | 979.47 |
| | | 20 | 538.57 |
| | | 30 | 318.78 |
| | | 40 | 199.41 |
| | | 50 | 129.48 |
| | | 60 | 86.71 |
| | | 70 | 59.26 |
| | | 80 | 41.27 |
| | | 90 | 29.08 |
| | | 100 | 20.71 |

| | | | |
|----------------------------|--|--|--|
| Source: WUFI Pro database. | | ¹ Derived from fitted function. Source: Kumaran <i>et al.</i> (2002b). | |
|----------------------------|--|--|--|

Table D.4. Material functions of asphalt-coated fiberboard.

Table D.4a. Moisture storage function.

| RH [%] | Moisture content [kg/m ³]* |
|--------|---|
| 0 | 0 |
| 10 | 0.003*320= 0.99 |
| 20 | 0.007*320=2.22 |
| 30 | 0.012*320=3.8 |
| 40 | 0.018*320=5.88 |
| 50 | 0.027*320=8.76 |
| 55 | 0.033*320=10.66 |
| 60 | 0.041*320=13.01 |
| 65 | 0.050*320=15.99 |
| 70 | 0.062*320=19.9 |
| 75 | 0.079*320=25.24 |
| 80 | 0.103*320=33.0 |
| 85 | 0.142*320=45.28 |
| 90 | 0.211*320=67.67 |
| 91 | 0.233*320=74.55 |
| 92 | 0.259*320=82.79 |
| 93 | 0.290*320=92.83 |
| 94 | 0.329*320=105.34 |
| 95 | 0.379*320=121.34 |
| 96 | 0.445*320=142.53 |
| 97 | 0.537*320=171.95 |
| 98 | 0.674*320=215.53 |
| 99 | 0.896*320=286.73 |
| 100 | 1.325*320=424.00 |

Source: WUFI Pro database for fiberboard with a density of 320 kg/m³.

*Units of moisture content, in kg_{moisture}/kg_{dry material}, multiplied by density, in kg/m³, yields moisture content in kg/m³.

Table D.4b. Liquid transport coefficient, D_w.

| Moisture content [kg/m ³] | D _w [m ² /s] |
|---------------------------------------|---------------------------------------|
| 4.86 | 5.1*10 ⁻¹⁰ |
| 12.15 | 1.0*10 ⁻⁹ |
| 17.01 | 1.7*10 ⁻⁹ |
| 24.3 | 2.3*10 ⁻⁹ |
| 26.73 | 2.5*10 ⁻⁹ |
| 38.88 | 2.0*10 ⁻⁹ |
| 46.17 | 1.4*10 ⁻⁹ |
| 55.89 | 8.7*10 ⁻¹⁰ |
| 58.32 | 7.48*10 ⁻¹⁰ |
| 77.76 | 4.8*10 ⁻¹⁰ |
| 126.36 | 2.9*10 ⁻¹⁰ |
| 187.11 | 3.6*10 ⁻¹⁰ |
| 245.43 | 4.5*10 ⁻¹⁰ |
| 298.89 | 5.8*10 ⁻¹⁰ |
| 342.63 | 8.1*10 ⁻¹⁰ |

Source: Kumaran (1996b).

Table D.4c. Heat conductivity as a function of moisture content.

| Moisture content [kg/m ³] | Thermal conductivity [W/m·K] |
|---------------------------------------|---------------------------------|
| 0 | 0.048 |
| 800 | 0.264 |

Source: WUFI Pro.

Table D.4d. Vapor diffusion resistance factor as a function of relative humidity.

| RH [%] | μ [-] |
|--------|----------|
| 0 | 7.80 |
| 7 | 7.76 |
| 50 | 4.85 |
| 80 | 3.88 |
| 100 | 3.22 |

Source: WUFI Pro.

Table D.5. Material functions of spruce.

Table D.5a. Moisture storage function.

| RH [%] | Moisture content [kg/m ³]* |
|--------|---|
| 0 | 0 |
| 20 | 0.075*400=30.0 |
| 50 | 0.113*400=45.0 |
| 65 | 0.143*400=57.0 |
| 80 | 0.200*400=80.0 |
| 90 | 0.250*400=100.0 |
| 96 | 0.313*400=125 |
| 99 | 0.825*400=330 |
| 99.6 | 0.875*400=350 |
| 99.9 | 0.975*400=390 |
| 99.96 | 1.075*400=430 |
| 99.99 | 1.275*400=510 |
| 1.0 | 1.500*400=600 |

Source: WUFI Pro database for spruce with a density of 455 kg/m³.

*Units of moisture content, in kg_{moisture}/kg_{dry material}, multiplied by density, in kg/m³, yields moisture content in kg/m³.

Table D.5b. Liquid transport coefficient D_w, in the radial direction.

| Moisture content [kg/m ³] | D _w [m ² /s] |
|---------------------------------------|---------------------------------------|
| 0 | 0 |
| 20 | 3.2*10 ⁻¹³ |
| 600 | 9.2*10 ⁻¹² |

Source: WUFI Pro for spruce with a density of 455 kg/m³.

Table D.5c. Heat conductivity as a function of moisture content.

| Moisture content [kg/m ³] | Thermal conductivity [W/m·K] |
|--|---------------------------------|
| 0 | 0.082 |
| 730 | 0.277 |

Source: WUFI Pro for spruce with a density of 400 kg/m³.

Table D.5d. Vapor diffusion resistance factor as a function of relative humidity.

| RH [%] | μ [-] |
|--------|----------|
| 0 | 928.53 |
| 10 | 507.96 |
| 20 | 300.16 |
| 30 | 177.32 |
| 40 | 104.08 |
| 50 | 61.18 |
| 60 | 35.73 |
| 70 | 20.66 |
| 80 | 11.75 |
| 90 | 6.49 |
| 100 | 3.37 |

Source: Kumaran *et al.* (2002b).

Table D.6. Material functions of interior gypsum.

Table D.6a. Moisture storage function (sorption) ($\rho_{\text{dry}} = 625 \text{ kg/m}^3$).

| RH [%] | Moisture content [kg/m ³]* |
|--------|--|
| 0 | 0 |
| 50.5 | 0.0040*625=2.50 |
| 70.5 | 0.0065*625=4.06 |
| 90.8 | 0.0180*625=11.25 |
| 94.0 | 0.0420*625=26.25 |
| 100.0 | 1.130*625=706.25 |

Source: Kumaran *et al.* (2002b).

*Units of moisture content, in kg_{moisture}/kg_{dry material}, multiplied by density, in kg/m³, yields moisture content in kg/m³.

Table D.6b. Liquid transport coefficient, D_w .

| Moisture content [kg/m ³] | D_w [m ² /s] |
|---------------------------------------|---------------------------|
| 0.032*625=20 | 2.09E-8 |
| 0.064*625=40 | 3.81E-8 |
| 0.096*625=60 | 5.36E-8 |
| 0.128*625=80 | 6.98E-8 |
| 0.160*625=100 | 8.82E-8 |
| 0.192*625=120 | 1.10E-7 |
| 0.224*625=140 | 1.34E-7 |
| 0.256*625=160 | 1.60E-7 |
| 0.288*625=180 | 1.87E-7 |
| 0.320*625=200 | 2.13E-7 |
| 0.352*625=220 | 2.44E-7 |
| 0.384*625=240 | 2.91E-7 |
| 0.400*625=250 | 3.30E-7 |
| 0.416*625=260 | 3.91E-7 |
| 0.432*625=270 | 5.07E-7 |
| 0.448*625=280 | 8.22E-7 |
| 0.464*625=290 | 4.13E-6 |
| 0.480*625=300 | 1.47E-6 |
| 0.496*625=310 | 8.46E-7 |
| 0.528*625=330 | 3.35E-7 |
| 0.544*625=340 | 2.84E-7 |
| 0.560*625=350 | 2.54E-7 |
| 0.576*625=360 | 2.36E-7 |
| 0.592*625=370 | 2.24E-7 |
| 0.608*625=380 | 2.17E-7 |
| 0.624*625=390 | 2.13E-7 |
| 0.640*625=400 | 2.12E-7 |
| 0.656*625=410 | 2.15E-7 |
| 0.672*625=420 | 2.20E-7 |
| 0.688*625=430 | 2.29E-7 |
| 0.704*625=440 | 2.42E-7 |
| 0.720*625=450 | 2.63E-7 |
| 0.736*625=460 | 2.94E-7 |
| 0.752*625=470 | 3.46E-7 |
| 0.768*625=480 | 4.45E-7 |
| 0.784*625=490 | 7.11E-7 |
| 0.800*625=500 | 2.55E-6 |

Source: Kumaran *et al.* (2002b).

Table D.6c. Heat conductivity as a function of moisture content.

| Moisture content [kg/m ³] | Thermal conductivity [W/m·K] |
|---------------------------------------|------------------------------|
| 0 | 0.163 |
| 650.0 | 1.160 |

Source: WUFI Pro.

Table D.6d. Vapor diffusion resistance factor as a function of relative humidity.

| RH [%] | μ [-] |
|--------|-----------|
| 0 | 6.00 |
| 10 | 6.08 |
| 60 | 5.80 |
| 100 | 3.21 |

Source: WUFI Pro.

APPENDIX E. APPROXIMATION OF THE MOISTURE CONTENT DISTRIBUTION IN THE BOTTOM PLATE INSERTS IN WALLS 1 TO 6

The initial moisture content distribution with the bottom plate inserts was estimated for the purpose of the WUFI 2D numerical simulations. The determination of the moisture content distribution was based on calculation of moisture uptake from the wetting methodology used in test 3. As was explained in the wetting methodology in Chapter 3, the bottom plate inserts were wetted by partially immersing them in a pool of water approximately 13 mm deep over a period of 31 days. Since the water uptake occurs more readily in the longitudinal direction than in the radial or tangential directions, it was logical to assume that the water penetration depth occurring at the 38 x 140 mm faces at either ends of the inserts was greater than that on the other wetted surfaces, as shown in Figure E.1. Therefore, two simulations were performed: the first was done reflecting the moisture distribution at the middle transverse section of the bottom plate insert, while the second simulation took into account the water absorbed at the 38 x 140 mm ends, as shown in Figure E.1.

The wetting of the bottom plate inserts was first approximated by determining a water penetration depth, x , at each surface of the bottom plate insert at which the wood was saturated. It was also necessary to determine the area on each surface of the bottom plate insert that was wetted.

The equation given by de Wit (2004) was used as a starting point to determine the water penetration depth, x , at the various wetted surfaces:

$$x = B\sqrt{t} \quad [\text{E.1}]$$

where x is in m, B is the water penetration coefficient, in $\text{m/s}^{1/2}$, and t is time, in seconds. The water penetration coefficient, B , can be determined as follows (deWit, 2004):

$$B = \frac{A_c}{w_c - w_i} \quad [\text{E.2}]$$

where A_c is the capillary water absorption coefficient, in $\text{kg/m}^2\text{s}^{1/2}$, w_c is the capillary

moisture content, and w_i is the initial moisture content before the wetting process, both in kg/m^3 . The capillary absorption coefficient for spruce was determined using the results of water absorption tests of spruce in the longitudinal and in the transverse (radial/tangential) directions. These were found to be $7.25 \text{ g/m}^2\text{s}^{1/2}$ in the longitudinal direction and $1.93 \text{ g/m}^2\text{s}^{1/2}$ in the transverse direction. The capillary saturation moisture content of spruce is approximately 600 kg/m^3 (WUFI Pro database, 1999). This value was divided by the dry density of each bottom plate insert, and then multiplied by 100% to find the capillary saturation moisture content in %-mass. The water penetration depth, which was calculated for each bottom plate inserts, was found to be approximately 22 mm in the longitudinal direction and approximately 5.8 mm in the transverse direction, as shown in Table E.1. It will be seen shortly how these values were revisited.

During the wetting process, it was observed that wicking up the side of the vertical surfaces occurred due to the high wettability of wood, thereby increasing the wetted area. It was assumed that on the transverse faces, the wicking reached a height approximately 2 mm above the surface of the water pool. However, the wetting on the longitudinal face was different, with water wicking upward following the annual growth rings. The average wetted height was assumed to be approximately 4 mm higher than the water surface, for a wetted height of 17 mm, as shown in the Figures E.1 and E.2.

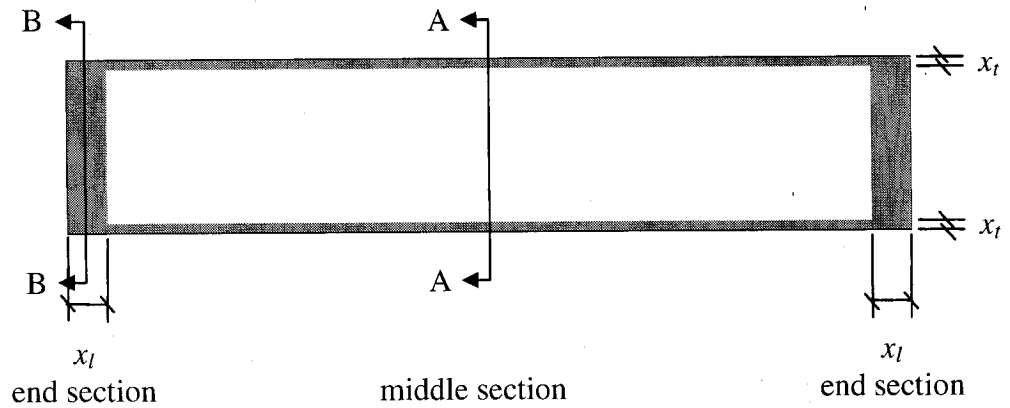
The initial moisture content of the volumes within the wetted bottom plate insert that were assumed not to be wetted was then determined using the measured total initial moisture content within each bottom plate insert, the wetted surface areas, the water penetration depths on each wetted surface, mass of moisture contained within the wetted and the “non-wetted” volumes, the capillary moisture content, and the measured total initial moisture content of the bottom plate insert.

In the calculation of the initial moisture content of the bottom plate with non-uniform moisture distribution, the wetted volumes were assumed to contain 600 kg/m^3 of moisture. A simple calculation was performed to determine the moisture content in kg/m^3 of the non-wetted volume. The volume of the wetted portion of each bottom plate was determined to be approximately $4.0 \cdot 10^{-4} \text{ m}^3$ and from this volume, the mass of moisture contained within this wetted portion was found by multiplying this volume by the saturation moisture content, in kg/m^3 , for each bottom plate insert. Then, this mass of

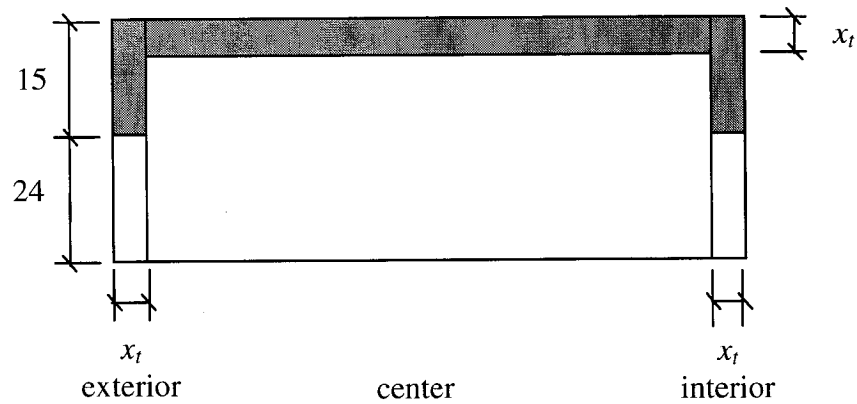
moisture was subtracted from the total mass of moisture contained within the bottom plate at the end of the wetting process to give the mass of moisture contained within the non-wetted portion. The latter mass, when divided by the volume of the non-wetted portion of the bottom plate, approximately $1.6 \cdot 10^{-3} \text{ m}^3$, resulted in the moisture content in the non-wetted volume, in kg/m^3 . Table E.1 shows that these moisture content values ranged greatly from 73.29 to 105.99 kg/m^3 .

In order to reduce the variability in moisture content from one insert to another in the initially non-wetted zones of the inserts, the procedure was modified. The determination of the depth of the wetted fronts was determined for all six inserts using average values of the initial moisture content within the inserts as well as of density. The longitudinal and transverse water penetration depth was calculated by multiplying the depth of the water front obtained using de Wit's equations [E.1] and [E.2] by a constant factor such that the moisture content within the non-wetted core zones was the same as that measured in the inserts before the wetting process, 16.0%-mass, or 55.0 kg/m^3 . The resulting final transverse water penetration depth and initial moisture content in the non-wetted zones are shown in Table E.1. This second method for determining the depth of the longitudinal and transverse water fronts provided a unique moisture content distribution for all six bottom plate inserts, therefore facilitating the comparison of the subsequent drying response of each insert.

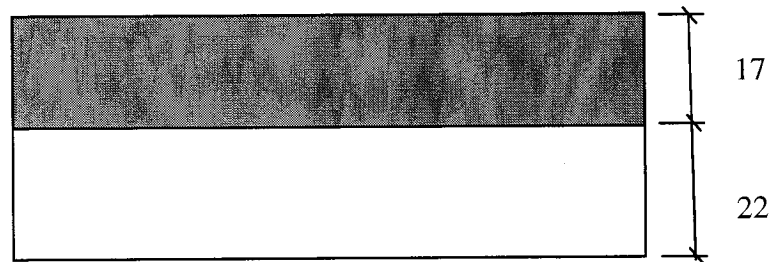
In the simulation post-processing, the moisture content of each entire bottom plate insert was determined in $\% \text{ kg}_{\text{moisture}}/\text{kg}_{\text{dry wood}}$ by taking the sum of the mass of moisture contained within the "middle" and "end" volumes, as these are depicted in Figure E.1, and then dividing the sum by the dry mass of each of the whole bottom plate inserts.



Plan view of the bottom plate insert



Section A-A



Section B-B

Figure E.1. Plan view of the bottom plate insert showing the depth of the water penetration at the height of the pool of water, and wetted surfaces in section A-A, called the “middle section” and section B-B, called the “end section”. The initially saturated zones are shaded. “ x_t ” and “ x_l ” are the transverse and longitudinal depths of the wetted fronts, respectively.

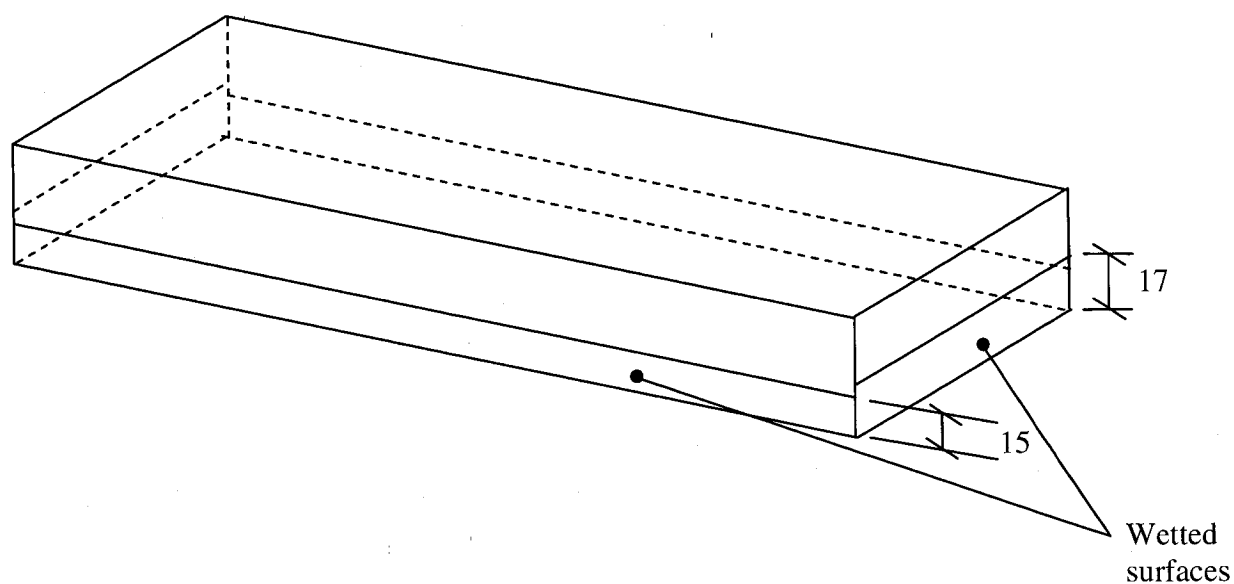


Figure E.2. Bottom plate insert showing the wetted surfaces during the partial immersion.

Table E.1. Measured dry density and mass measurements of the bottom plate inserts, and calculations for determination of the initial average moisture content of the wood within the bottom plate.

| Parameter | Wall 1 | Wall 2 | Wall 3 | Wall 4 | Wall 5 | Wall 6 |
|---|--------|--------|--------|--------|--------|--------|
| Measured dry density [kg/m^3] (a) | 336.6 | 341.4 | 360.8 | 344.8 | 337.3 | 334.6 |
| Moisture content at capillary saturation [kg/m^3] (b) | 600 | 600 | 600 | 600 | 600 | 600 |
| Measured oven-dry mass of bottom plate [kg] (c) | 0.667 | 0.671 | 0.719 | 0.686 | 0.671 | 0.663 |
| Measured initial moisture content of bottom plate insert prior to wetting [kg/m^3] (d) | 54.36 | 52.54 | 55.64 | 56.13 | 56.22 | 52.36 |
| Measured mass of bottom plate after wetting [g] (e) | 1.021 | 1.027 | 1.128 | 1.070 | 1.038 | 1.019 |
| Total mass of moisture in bottom plate after wetting [kg] (f) | 0.354 | 0.356 | 0.409 | 0.384 | 0.368 | 0.356 |
| Depth of initial longitudinal wetting front [mm] (g) | 22 | 22 | 22 | 22 | 22 | 22 |

| | | | | | | |
|---|-----------------------|-----------------------|-----------------------|-----------------------|-----------------------|-----------------------|
| Initial trial for depth of transverse wetting front [mm] (h) | 5.8 | 5.8 | 5.8 | 5.8 | 5.8 | 5.8 |
| Initially wetted volume [m³] (i) | $3.965 \cdot 10^{-4}$ | $3.926 \cdot 10^{-4}$ | $3.992 \cdot 10^{-4}$ | $3.989 \cdot 10^{-4}$ | $3.986 \cdot 10^{-4}$ | $3.953 \cdot 10^{-4}$ |
| Mass of moisture in initially wetted volume [kg] (j) | 0.240 | 0.236 | 0.240 | 0.239 | 0.239 | 0.237 |
| Mass of moisture in non-wetted volume in bottom plate [kg] (k) | 0.116 | 0.121 | 0.169 | 0.145 | 0.129 | 0.119 |
| Non-wetted volume [m³] (l) | $1.586 \cdot 10^{-3}$ | $1.573 \cdot 10^{-3}$ | $1.594 \cdot 10^{-3}$ | $1.590 \cdot 10^{-3}$ | $1.590 \cdot 10^{-3}$ | $1.587 \cdot 10^{-3}$ |
| Initial trial for moisture content of “unwetted” wood in bottom plate [kg/m³] (m) | 73.19 | 76.65 | 105.99 | 91.39 | 81.02 | 74.75 |
| Final value of depth of transverse wetting front [mm] (n) | 7.3 | 7.3 | 7.3 | 7.3 | 7.3 | 7.3 |
| Final value of moisture content of “unwetted” wood in bottom plate [kg/m³] (o) | 55.00 | 55.00 | 55.00 | 55.00 | 55.00 | 55.00 |

$$(b) = 2 \cdot (a)$$

$$(f) = (e) - (c)$$

$$(g) = (A / ((b) - (d))) \cdot t^{1/2}, \text{ where } A \text{ is the transverse capillary absorption coefficient, } 0.00193 \text{ kg/m}^2\text{s}^{1/2}, \text{ and } t \text{ is time, in this case 30.9 days, or 2669760 s.}$$

$$(j) = (b) \cdot (i)$$

$$(k) = (f) - (j)$$

$$(m) = (k) / (l)$$

(n) and (o) were determined by using an average value of the density and the moisture content in the wetted bottom plate inserts, increasing the depth of the longitudinal (g) and transverse (h) water penetration fronts by a factor of 1.26, and also assuming that the moisture content in the non-wetted zone in all inserts was equal at 55.0 kg/m³.